

Max-Planck-Institut für Molekulare Pflanzenphysiologie
Research group: Applied Metabolome Analysis, Dr. Joachim Kopka
The University of Melbourne
Research group: Roessner Lab, Prof. Dr. Ute Roessner

Ribosome Heterogeneity and Specialization during Temperature Acclimation in Plants

by

Federico Martínez Seidel

[ORCID: 0000-0002-1410-2492](https://orcid.org/0000-0002-1410-2492)

Student ID: 1021290 (UoM), 811758 (UP)
fmartinezsei@student.unimelb.edu.au

A cumulative thesis (Potsdam University) / thesis by publication (The University of Melbourne) submitted in total fulfillment of the requirements for a jointly awarded degree of

Doctor of Philosophy
at the Faculty of Science, School of Biosciences
The University of Melbourne

and

“doctor rerum naturalium” (Dr. rer. nat.)
at the Faculty of Science, Institute of Biochemistry and Biology
Discipline “Plant Physiology”
University of Potsdam

Potsdam, Melbourne, February 2023

Doctoral Research and Thesis Supervisors:

The University of Melbourne:

Hauptbetreuer*in/Principal Supervisor: Prof. Dr. Ute Roessner

Betreuer*innen/Second Supervisor: Assoc. Prof. Berin Alain Boughton

University of Potsdam:

Hauptbetreuer*in/Principal Supervisor: Prof. Dr. Lothar Willmitzer

Betreuer*innen/Second Supervisor: Dr. Joachim Kopka

Unless otherwise indicated, this work is licensed under a Creative Commons License Attribution – NonCommercial – ShareAlike 4.0 International.

This does not apply to quoted content and works based on other permissions.

To view a copy of this licence visit:

<https://creativecommons.org/licenses/by-nc-sa/4.0>

Published online on the

Publication Server of the University of Potsdam:

<https://doi.org/10.25932/publishup-58072>

<https://nbn-resolving.org/urn:nbn:de:kobv:517-opus4-580724>

Abstract

by [Federico Martínez Seidel](#)

[ORCID: 0000-0002-1410-2492](#)

Ribosomes decode mRNA to synthesize proteins. Ribosomes, once considered static, executing machines, are now viewed as dynamic modulators of translation. Increasingly detailed analyses of structural ribosome heterogeneity led to a paradigm shift toward ribosome specialization for selective translation. As sessile organisms, plants cannot escape harmful environments and evolved strategies to withstand. Plant cytosolic ribosomes are in some respects more diverse than those of other metazoans. This diversity may contribute to plant stress acclimation. The goal of this thesis was to determine whether plants use ribosome heterogeneity to regulate protein synthesis through specialized translation. I focused on temperature acclimation, specifically on shifts to low temperatures. During cold acclimation, *Arabidopsis* ceases growth for seven days while establishing the responses required to resume growth. Earlier results indicate that ribosome biogenesis is essential for cold acclimation. REIL mutants (*reil-dkos*) lacking a 60S maturation factor do not acclimate successfully and do not resume growth. Using these genotypes, I ascribed cold-induced defects of ribosome biogenesis to the assembly of the polypeptide exit tunnel (PET) by performing spatial statistics of rProtein changes mapped onto the plant 80S structure. I discovered that growth cessation and PET remodeling also occurs in barley, suggesting a general cold response in plants. Cold triggered PET remodeling is consistent with the function of Rei-1, a REIL homolog of yeast, which performs PET quality control. Using seminal data of ribosome specialization, I show that yeast remodels the tRNA entry site of ribosomes upon change of carbon sources and demonstrate that spatially constrained remodeling of ribosomes in metazoans may modulate protein synthesis. I argue that regional remodeling may be a form of ribosome specialization and show that heterogeneous cytosolic polysomes accumulate after cold acclimation, leading to shifts in the translational output that differs between wild-type and *reil-dkos*. I found that heterogeneous complexes consist of newly synthesized and reused proteins. I propose that tailored ribosome complexes enable free 60S subunits to select specific 48S initiation complexes for translation. Cold acclimated ribosomes through ribosome remodeling synthesize a novel proteome consistent with known mechanisms of cold acclimation. The main hypothesis arising from my thesis is that heterogeneous/ specialized ribosomes alter translation preferences, adjust the proteome and thereby activate plant programs for successful cold acclimation.

Zusammenfassung

Ribosomen dekodieren mRNA, um Proteine zu synthetisieren. Ribosomen, früher als statische, ausführende Maschinen betrachtet, werden heute als dynamische Modulatoren der Translation angesehen. Zunehmend detailliertere Analysen der Strukturheterogenität von Ribosomen führte zu einem Paradigmenwechsel hin zu einer Spezialisierung von Ribosomen für eine selektive Translation. Als sessile Organismen können Pflanzen schädlichen Umwelteinflüssen nicht ausweichen und haben Strategien entwickelt, um diesen zu widerstehen. Zytoplasmatische Ribosomen von Pflanzen sind in mancher Hinsicht vielfältiger, als die von anderen Metazoen. Diese Vielfalt könnte zur Stressakklimatisierung der Pflanzen beitragen. Ziel dieser Arbeit war es, festzustellen, ob Pflanzen die Heterogenität der Ribosomen nutzen, um die Proteinsynthese durch spezialisierte Translation zu regulieren. Ich habe mich auf die Temperaturakklimatisierung konzentriert, insbesondere auf den Wechsel zu niedrigen Temperaturen. Im Verlauf der Kälteakklimatisierung stellt Arabidopsis das Wachstum für sieben Tage ein. Währenddessen etabliert sie die für die Wiederaufnahme des Wachstums erforderlichen Anpassungen. Vorherige Ergebnisse deuten darauf hin, dass Ribosomenbiogenese für die Kälteakklimatisierung essentiell ist. REIL-Mutanten (*reil-dkos*), denen ein 60S-Reifungsfaktor fehlt, akklimatisieren sich nicht erfolgreich und nehmen das Wachstum nicht wieder auf. Anhand dieser Genotypen habe ich kältebedingte Defekte der Ribosomenbiogenese auf den Aufbau des Polypeptidaustritts-Tunnels (PET) zurückgeführt, indem ich räumliche statistische Analysen von rProtein-Veränderungen auf die pflanzliche 80S-Struktur abgebildet habe. Ich habe entdeckt, dass Wachstumsstillstand und PET-Umbau auch in Gerste auftreten, was auf eine allgemeine Kältereaktion in Pflanzen hindeutet. Der durch Kälte ausgelöste PET-Umbau stimmt über ein mit der Funktion von Rei-1, einem REIL-homologen Protein aus Hefe, in der Rei-1 die PET-Qualitätskontrolle durchführt. Anhand bahnbrechender Daten zur Ribosomenspezialisierung zeige ich, dass Hefe die tRNA-Eintrittsstelle von Ribosomen bei einem Wechsel von Kohlenstoffquellen umbaut, und demonstriere, dass ein räumlich begrenzter Umbau von Ribosomen in Metazoen die Proteinsynthese modulieren kann. Ich argumentiere, dass die regionale Umgestaltung eine Form der Ribosomenspezialisierung sein kann, und zeige, dass nach einer Kälteakklimatisierung heterogene zytoplasmatische Polysomen akkumulieren, was zu Verschiebungen im Translationsoutput führt, der sich zwischen Wildtyp und *reil-dkos* unterscheidet. Ich habe festgestellt, dass die heterogenen Komplexe aus neu synthetisierten und wiederverwendeten Proteinen bestehen. Ich schlage vor, dass maßgeschneiderte Ribosomenkomplexe freie 60S-Untereinheiten in die Lage versetzen, spezifische 48S-Initiationskomplexe für die Translation auszuwählen. Kälte-akklimatisierte Ribosomen synthetisieren durch Ribosomenumbau ein neues Proteom, das mit bekannten Mechanismen der Kälteakklimatisierung übereinstimmt. Die Haupthypothese, die sich aus meiner Arbeit ergibt, ist, dass heterogene/spezialisierte Ribosomen ihre Translationspräferenzen verändern, das Proteom anpassen und dadurch Pflanzenprogramme für eine erfolgreiche Kälteakklimatisierung aktivieren.

Declaration of Authorship

I, Federico Martínez Seidel, declare that this thesis titled, ‘Ribosome Heterogeneity and Specialization during Temperature Acclimation in Plants’ and the work presented in it are my own. I confirm that:

- The thesis comprises only my original work towards the Doctor of Philosophy degree at The University of Melbourne and the Dr. rer. nat. degree at Potsdam University except where indicated in the preface;
- The work described in this thesis was performed in the Max Planck Institute of Molecular Plant Physiology, in the School of Biosciences at The University of Melbourne and the Institute of Biochemistry and Biology, Faculty of Science at the University of Potsdam between September 2018 year and August 2022;
- This thesis is submitted to The University of Melbourne and the Faculty of Science at the University of Potsdam in the frame of a joint doctoral degree procedure. No part of this thesis has been submitted to any other University, for any other degree or diploma;
- due acknowledgement has been made in the text to all other material used; and
- the thesis is fewer than the maximum word limit in length, exclusive of tables, figures, bibliographies and appendices as specified by both Potsdam University and The University of Melbourne guidelines.

Signed:

Date:

Preface

This document has been written to the best of my knowledge as a synergy of the structures for doctoral dissertations at The University of Melbourne and Potsdam University. The structure combines the requirements of both universities by merging sections that are common to both and adding elements that are unique to each of them to comprehensively include all the required information. In the body of the thesis, chapters were used to define each section. Each chapter displayed as a scientific paper meets the necessary open access and copyright requirements to be displayed in its entirety in this thesis. Accordingly, each scientific publication as a chapter includes its own bibliography section. The sections Introduction (Chapter 1), Methodology (Chapter 3), and Discussion (Chapter 9) also each contain their own bibliography.

Chapters 2, 4, 5, and 6 are all publicly available as original research manuscripts, and the respective supplementary materials can be found via the embedded links in the respective manuscripts. Chapter 7 is publicly available as a bioRxiv preprint and has been submitted for publication, and chapter 8 represents two unpublished papers that have not yet been submitted and one manuscript publicly available as a bioRxiv preprint. Therefore, all supplementary materials for the last two chapters have been deposited in File S5 and S6, respectively. The details, nature, and proportion of the collaborations and contributions, as well as my own work, are explained here:

- no thesis work has been submitted for other qualifications;
- no thesis work has been completed prior to enrollment in the degree program;
- no third-party editorial assistance was provided in the preparation of the thesis;
- All of the work in this thesis has been done in collaboration with others, and is presented in the form of multi-author publications or articles in preparation included in the thesis. The nature and proportion of the contribution of others and, in general terms, the parts of the work that I claim as original are presented below (for the specifics, please refer to the respective 'Declaration for publications' duly signed by my principal supervisors and incorporated in this thesis as File S7) along with the publication status of all chapters presented in article format.

First Author / Corresponding Author publications that comprise my main contributions to scientific advance in my field:

-
- **Systematic review of plant ribosome heterogeneity and specialization** by Martinez-Seidel, F., Beine-Golovchuk, O., Hsieh, Y. C., and Kopka, J. Published by Frontiers in Plant Sciences (doi:10.3389/fpls.2020.00948) on June 25th 2020. More than 51% of the work was done by me. For specifics please see the 'author contributions' section of the published manuscript.
Personal Contribution: My own contributions include being the corresponding author of the manuscript, writing and editing the manuscript according to feedback from my supervisors, creating and modifying the figures, conceptualizing them in the context of the current literature, and creating the main tables and meta-analyses presented in the publication.

 - **Membrane-enriched proteomics link ribosome accumulation and proteome reprogramming with cold acclimation in barley root meristems** by Martinez-Seidel, F., Suwanchaikasem, P., Nie, S., Leeming, M. G., Pereira Firmino, A. A., Williamson, N. A., Kopka, J., Roessner, U., and Boughton, B. A. Published by Frontiers in Plant Sciences (doi:10.3389/fpls.2021.656683) on April 30th 2021. More than 51% of the work was done by me. For specifics please see the 'author contributions' section of the published manuscript.
Personal Contribution: My own contributions include being the corresponding author of the manuscript, writing and editing the manuscript according to feedback from my supervisors. Performing the LC-MS/MS related experimental work in collaboration with another PhD student. Stabilization of protein extraction and purification procedures. Conceptualization and creation of *in silico* resources. Experiment design, figure design and statistics.

 - **COSNet_i: ComplexOme-Structural Network Interpreter used to study spatial enrichment in metazoan ribosomes** by Martinez-Seidel, F., Hsieh, Y. C., Walther, D., Kopka, J., and Pereira Firmino, A. A. (2021). Published by BMC Bioinformatics (doi:10.1186/s12859-021-04510-z) on December 20th 2021. More than 51% of the work was done by me. For specifics please see the 'author contributions' section of the published manuscript.
Personal Contribution: My own contributions include being the corresponding author of the manuscript, writing and editing the manuscript according to feedback from my supervisors. Conceptualizing, writing and executing the bioinformatics pipeline into a Python module, figure design and statistics. The code was written in collaboration with a master student conducting an

internship under my supervision.

- **Spatially enriched paralog rearrangements argue functionally diverse ribosomes arise during cold acclimation in Arabidopsis** by Martinez-Seidel, F., Beine-golovchuk, O., Hsieh, Y. C., El Eshraky, K., Gorka, M., Cheong, B. E., Jimenez-posada, E. V., Walther, D., Skiryecz, A., Roessner, U., Kopka, J., and Pereira Firmino, A. A. Published by International Journal of Molecular Sciences (doi:10.3390/ijms22116160) on June 7th 2021. More than 51% of the work was done by me. For specifics please see the 'author contributions' section of the published manuscript.

Personal Contribution: My own contributions include being the corresponding author of the manuscript, writing and editing the manuscript according to feedback from my supervisors. Literature review, optimization of the cytosolic ribosomal proteome measurements, growth method optimization, dry weight measurements, R-scripting for proteome and transcriptome data analyses, figure design, statistics, phylogenetic tree construction, ribosomal structural analysis development, structural analysis, formatting, manuscript writing.

- **Remodelled Ribosomes Synthesise a Specific Proteome in Proliferating Plant Tissue during Cold** by Martinez-Seidel, F., Suwanchaikasem, P., Gentry-Torfer, D., Rajarathinam, Y., Ebert, A., Erban, A., Pereira Firmino, A. A., Nie, S., Leeming, M. G., Williamson, N. A., Roessner, U., Kopka, J., and Boughton, B. A. Published by bioRxiv not yet peer-reviewed (doi:10.1101/2022.11.28.518201) on November 29th 2022. More than 51% of the work was done by me. For specifics please see the 'author contributions' section of the published manuscript.

Personal Contribution: My own contributions include being the corresponding author of the manuscript, writing and editing the manuscript according to feedback from my supervisors. Literature review, optimization of the cytosolic ribosomal proteome measurements, growth method optimization, dry weight measurements, R-scripting for labelled proteome and protein synthesis data analyses, figure design, statistics, ribosomal structural analysis development, structural analysis, formatting, manuscript writing.

- **KineticMSI, an R-based framework for relative quantification of spatial isotopic incorporation in mass spectrometry imaging experiments** by *Farzana, F., & *Martinez-Seidel, F., Hannan, A., Hatters, D., and Boughton, B. A. Published by bioRxiv not yet peer-reviewed (doi:

10.1101/2022.08.31.505954) on September 3rd 2022. *co-first authorship, 50% of the work was done by me.

Personal Contribution: My own contributions include being co-corresponding author of the manuscript, writing and editing the manuscript. Literature review, R-scripting, figure design, statistics, formatting, manuscript writing.

Co-Author publications that comprise a methodological framework, both in the wet and dry laboratory, for my main studies (directly related to ribosome structure and function):

- **Arabidopsis REI-LIKE proteins activate ribosome biogenesis during cold acclimation** by Cheong, B. E., Beine-Golovchuk, O., Gorka, M., Ho, W. W. H., Martinez-Seidel, F., Firmino, A. A. P., Skiryecz, A., Roessner, U., and Kopka, J. Published by Scientific Reports (doi:10.1038/s41598-021-81610-z) on January 28th 2021.

Personal Contribution: My own contributions to this manuscript included the analysis of proteomic data that yielded ribosomal protein candidate paralogs that were further investigated using reverse genetics approaches.

- **Separation and paired proteome profiling of plant chloroplast and cytoplasmic ribosomes** by Firmino, A. A. P., Gorka, M., Graf, A., Skiryecz, A., Martinez-Seidel, F., Zander, K., Kopka, J., and Beine-Golovchuk, O. Published by Plants (doi:10.3390/plants9070892) on July 14th 2020.

Personal Contribution: My own contribution to this work includes analysis of cytosolic ribosomal proteome data (R-scripting), editing and assistance with manuscript writing, and optimization of detergent removal from freshly separated and fractionated ribosomal fractions. This publication includes the core methodological workflow I used for separating non-translational and translational complexes (Figure 2 of the manuscript). The current method I use for ribosomal proteomics differs from what is described in this manuscript and was also optimized and developed by me.

Co-Author publications that comprise a methodological framework, in the dry laboratory, needed to analyse in a comprehensive manner the large omics datasets generated during my studies (indirectly related but fundamental for the study of ribosome structure and function):

- **Multiplexed Profiling and Data Processing Methods to Identify Temperature-Regulated Primary Metabolites Using Gas Chromatography Coupled to Mass Spectrometry.** by Erban, A., Martinez-Seidel,

F., Rajarathinam, Y., Dethloff, F., Orf, I., Fehrle, I., Alpers, J., Beine-Golovchuk, O., and Kopka, J. Published by Springer US (10.1007/978-1-0716-0660-5_15) In *Methods in Molecular Biology* (ed. Hinch, D. K.) and Zuther, E.) 2020.

Personal Contribution: My contributions to this Book chapter include: Section 3.1 (Plant Cultivation and Labelling) Including Figure 1. Section 3.2 (Sampling and Gravimetric determination of the Sample amount) including Figure 2. Section 3.14 (Non-targeted Data Mining of Relevant Mass Features).

In the following set of publications, my main contributions are related to the quality control, data analysis and statistics of mass spectrometry data. In more detail, I used Section 3.14 (Non-targeted Data Mining of Relevant Mass Features) of the previous manuscript to develop [RandoDiStats](#), a publically available R package that has multiple citations and can be installed using devtools. The package is permanently on development with help of users and collaborators and has been used extensively in most of the publications referenced in this section.

Class Comparison

- **Univariate statistical analysis of gas chromatography–mass spectrometry fingerprints analyses** by Melo, T. O., Franciscon, L., Brown, G., Kopka, J., Cunha, L., Martinez-Seidel, F., dos Santos Madureira, L. A., Hansel, F. A., and Network, T. P. I. Published by Chemical Data Collections (doi:10.1016/j.cdc.2021.100719) on May 24th 2021.

Personal Contribution: More specifically my work includes preparation, optimization, conceptualization and editing in collaboration with the main authors of Figures 1, 2 and 3.

Class Prediction

- **Discovery of food identity markers by metabolomics and machine learning technology** by Erban, A., Fehrle, I., Martinez-Seidel, F., Brigante, F., Más, A. L., Baroni, V., Wunderlin, D., and Kopka, J. Published by Scientific Reports (doi:10.1038/s41598-019-46113-y) on July 4th 2019.

&

-
- **Authenticity assessment of commercial bakery products with chia, flax and sesame seeds: Application of targeted and untargeted metabolomics results from seeds and lab-scale cookies** Brigante, F., Más, A. L., Erban, A., Fehrle, I., Martinez-Seidel, F., Kopka, J., Wunderlin, D., and Baroni, V. Published by Food Control (10.1016/j.foodcont.2022.109114) version of record on May 25th 2022.

Personal Contribution: More specifically my work includes preparation, optimization, conceptualization and editing in collaboration with the main authors of Figures 3, 7, 8 and 9 from the first manuscript and discussion and utilization of algorithms, statistical analyses and interpretation for both manuscripts.

Class Discovery

- **Unravelling the metabolic and hormonal machinery during key steps of somatic embryogenesis: A case study in coffee** by Awada, R., Campa, C., Gibault, E., Déchamp, E., Georget, F., Lepelley, M., Abdallah, C., Erban, A., Martinez-Seidel, F., Kopka, J., Legendre, L., Lérant, S., Conéjéro, G., Verdeil, J. L., Crouzillat, D., Breton, D., Bertrand, B., and Etienne, Hervé. Published by International Journal of Molecular Sciences (doi:10.3390/ijms20194665) on September 20th 2019.
&
- **Global transcriptome profiling reveals differential regulatory, metabolic and hormonal networks during somatic embryogenesis in Coffea arabica** by Awada, R., Lepelley, M., Breton, D., Charpagne, A., Campa, C., Berry, V., Georget, F., Breitler, J.C., Lérant, S., Djerrab, D., Martinez-Seidel, F., Descombes, P., Crouzillat, D., Bertrand, B., and Etienne, Hervé. Accepted by BMC Genomics (doi:10.21203/rs.3.rs-2109047/v1) on December 22nd 2022.
Personal Contribution: More specifically my work includes statistics, data analyses, preparation, optimization, conceptualization and editing in collaboration with the main authors of Figures 3 and 6 of the first manuscript and Figure 1 and 5 of the second manuscript.
- **Gone wild: Integration of antioxidative, physicochemical, volatilomic and sensorial profiles ratify rustic relatives of cherry tomato as ideal mating partners** by Londoño-Giraldo, L. M., Baena-Pedroza, A. M., Martinez-Seidel, F., Corpas-Iguarán, E., and Taborda-Ocampo, G. Published

by *Scientia Horticulturae* (doi:10.1016/j.scienta.2020.109814) on November 5th 2020.

Personal Contribution: More specifically my work includes preparation, optimization, conceptualization and editing in collaboration with the main authors of Figures 2 and 3.

- **The Metabolic Response of Brachypodium Roots to the Interaction with Beneficial Bacteria Is Affected by the Plant Nutritional Status** by Schillaci, M., Kehelpannala, C., Martinez-Seidel, F., Smith, P., Arsova, B., Watt, M., and Roessner, U. Published by *Metabolites* (doi:10.3390/metabo11060358) on June 3rd 2021.

Personal Contribution: More specifically my work includes preparation, optimization, conceptualization and editing in collaboration with the main authors of Figure 4.

- **The Effect of Cold Stress on the Root-Specific Lipidome of Two Wheat Varieties with Contrasting Cold Tolerance** Cheong, B.E., Yu, D., Martinez-Seidel, F., Ho, W.W.H., Rupasinghe, T.W., Dolferus, R. and Roessner, U., 2022. Published by *Plants* (10.3390/plants11101364) on May 20th 2022.

Personal Contribution: More specifically my work includes preparation, optimization, conceptualization and editing in collaboration with the main authors of Figures 4.

Confirmation of Principal Supervisors:

Lothar Willmitzer:

Ute Roessner:

Acknowledgements

I would like to thank all the wonderful people who have made the development of this work possible and have supported me in one way or another over the years.

I would like to thank my parents Cristina Seidel Arango and Andrés Fernando Martínez Jimenez, who have encouraged me all these years. Despite the great distance, I feel every day how close you are to me through your love and support. I would also like to thank my uncle Santiago and my aunt Angela for sharing with me their scientifically oriented, inquisitive minds and precise insights during my life that have helped me advance in the academic world. I would also like to thank Lucas and Isabella for the wonderful hours we spent playing and having fun during school vacations, and Ada and Lucia for being my supportive sisters and accomplices throughout my life. A very special thank you to the rest of my family, who opened the door to my curiosity and allowed me to develop without bias; without this foundation, this would not have been possible. I would especially like to mention my great-aunt Dora Seidel and my grandmother Gloria Jimenez, both of whom always showed me unconditional love.

I would like to thank my supervisor and mentor Joachim Kopka for every second you devoted to developing my project with scientific soundness, as well as my supervisor Lothar Willmitzer for his support over the years. Likewise, my admiration and gratitude goes to my supervisors Ute Roessner and Berin A. Boughton. The projects, the scientific discussions, and the personal and academic encounters I experienced with all of you will remain in my memory for a lifetime.

I would also like to thank my PhD Advisory Board in Australia: Joshua Heazlewood and Mike Haydon, and in Germany: Mark Stitt, Aleksandra Skiryecz and Zoran Nikoloski for the fruitful discussions and the opportunity to benefit from your scientific experience. A very special thanks to the two research groups that hosted me. From AG Kopka: Ines, Paula, Alina, Yoga, Alex E, Susi, Kheloud, Olga, Yin, Alex F, Florian, Luisa and Bernhard. From the Roessner lab: Rob, Bo Eng, Allene, Carl, Cheka, Lisa, Martino, Pipob, Sibel, Sneha, Tannaz. Another very special thank you goes to all the collaborators with whom I share a deep love of science and an eagerness to solve problems: Farheen Farzana, Anna Siodmak, Heribert Hirt, Mike Ting, Mastoureh Sedaghatmehr, Salma Balazadeh, Reimo Zoschke, Alban Mariette, Berit Ebert, Ester Murillo Villuendas, Sara Rosa Téllez, Michael Leeming, Shuai Nie, Nicholas Williamson, Dirk Walther, Ewelina Sokolowska.

Interactions with so many talented, dedicated, and passionate scientists, listed here or not, have truly shaped my perspective on the day-to-day work in my scientific endeavor,

and without all of these interactions, the depth that my project has reached would have been impossible.

My extended gratitude goes to all the support services that make possible our daily reasearch, green team, media kitchen with a special mention to Dietlind Witzger. Finally I would like to acknowledge the Max-Planck Society (Max Planck Institute of Molecular Plant Physiology) and The University of Melbourne for funding my research via the Melbourne-Potsdam PhD Programme (MelPoPP) and Ina Talke for her immeasurable help in navigating the program.

I would also like to thank all my friends around the world with whom I have shared unforgettable moments that were absolutely necessary to inspire scientific curiosity, but also in times of uncertainty and doubt.

Finally, I would like to thank the love of my life and my wife, Dione Gentry, for her unparalleled support. The journey of my life has been an adventure of joy alongside you, and I thank you for how incredibly selfless and caring you are, I truly admire every day what a beautiful person you are, always striving to make things better.

Contents

Supervisors	i
Abstract	ii
Zusammenfassung	iii
Declaration of Authorship	iv
Preface	v
Acknowledgements	xii
List of Figures	xv
List of Tables	xvi
Abbreviations	xvii
1 Introduction	1
1.1 Origin, Function and Diversification of Cytosolic Ribosomes	1
1.2 Ribosome Heterogeneity and Specialization	2
1.3 Plant Cytosolic Ribosomes	3
1.4 Aim of This Thesis	4
1.5 Statement of Organization	5
2 Systematic Review of Plant Ribosome Heterogeneity and Specialization	15
2.1 Introduction	17
2.2 Assembly of Heterogeneous Ribosomes	17
2.2.1 Variation of Ribosomal RNA	18
2.2.2 Alternative Pre-Ribosome Processing	18
2.2.3 Variation of Ribosome Associated Proteins	20
2.3 Protein Composition of the Cytosolic Ribosome	22
2.3.1 Deviation From Canonical Compositions	22
2.3.2 Post-Translational Modifications	24

2.4	Functional Heterogeneity of RP Paralogs	25
2.4.1	Cytosolic Ribosomal Proteins	25
2.4.2	Plastid Ribosomal Proteins	25
2.4.3	Mitochondrial Ribosomal Proteins	27
2.5	Transcriptomic Evidence of Plant Ribosome Specialization: A Testcase	27
2.6	Future Perspectives	30
2.7	Summary	31
2.8	Data Availability Statement	32
2.9	Author Contributions	32
2.10	Funding	32
2.11	Acknowledgements	32
2.12	Supplementary Material	32
2.13	References	32
3	Materials and Methods	39
3.1	Wet Laboratory	40
3.1.1	Experimental Design	40
3.1.2	Plant Growth Systems	40
3.1.3	Profiling of the Plant Cytosolic Ribosomal Proteome	42
3.1.3.1	Purification of Ribosomes	42
3.1.3.2	Translation-related Omics Biochemical Assays	46
3.1.4	Molecular Biology	46
3.1.5	Cloning Approaches	46
3.1.6	T-DNA Lines	48
3.2	Dry Laboratory	48
3.2.1	Preprocessing	49
3.2.2	Class Comparison	50
3.2.3	Class Discovery	51
3.2.4	Class Prediction	52
3.2.5	GitHub Repositories	57
3.3	Extended Methods	59
4	Membrane-Enriched Proteomics Link Ribosome Accumulation and Proteome Reprogramming With Cold Acclimation in Barley Root Meristems	62
4.1	Introduction	64
4.2	Materials and Methods	65
4.2.1	Growth Conditions	65
4.2.2	Proteomics Profiling	65
4.2.2.1	Protein Extraction	65
4.2.2.2	Ribosomal Protein Content	65
4.2.2.3	Protein Digestion	65
4.2.2.4	Tandem Mass Tag Labeling	66
4.2.2.5	LC-MS/MS Analyses	66
4.2.3	Data Acquisition and Interpretation	66
4.2.3.1	Barley Proteome	66
4.2.3.2	Homology Alignments	66

4.2.3.3	Protein Contents	67
4.2.3.4	Shotgun Proteomics	67
4.3	Results	67
4.3.1	Sampling the Barley Root Proteome	68
4.3.2	Induced Changes of the Root Proteome	69
4.3.2.1	Total Protein Contents	69
4.3.2.2	Individual Protein Abundances	71
4.3.3	Biological Context of Induced Protein Changes	72
4.3.4	Adjusting the Ribosomal Proteome During Cold Acclimation	75
4.4	Discussion	76
4.4.1	Translational Reprogramming	76
4.4.2	Acquired Cold Tolerance	78
4.4.3	Summary	79
4.5	Data Availability Statement	79
4.6	Author Contributions	80
4.7	Funding	80
4.8	Acknowledgements	80
4.9	Supplementary Material	80
4.10	References	80
5	COSNet_i: ComplexOme-Structural Network Interpreter Used to Study Spatial Enrichment in Metazoan Ribosomes	84
5.1	Background	86
5.2	Implementation	88
5.2.1	Structural Data Preprocessing	88
5.2.2	Proximity Network Building	89
5.2.3	Structural Region Definition	90
5.2.4	Testing of Enriched Relative Changes Within Regions	91
5.2.5	Test Case Datasets	92
5.3	Results	93
5.3.1	Translating Structures Into Graphs	93
5.3.2	Defining Spatial Regions	95
5.3.3	Building a Ribosomal Protein Network	98
5.3.4	Testing the Spatial Constraints of Ribosome Specialization	101
5.4	Discussion	103
5.4.1	Structure Quality Requirements	104
5.4.2	Optimization of Region Definition	104
5.4.3	Ribosomal Networks	106
5.4.4	Spatially Enriched Ribosomal Protein Substoichiometry	107
5.5	Conclusion	109
5.6	Availability and Requirements	109
5.6.1	Abbreviations	110
5.7	Supplementary Information	110
5.7.1	Acknowledgements	110
5.7.2	Authors' Contributions	110
5.7.3	Funding	110
5.7.4	Availability of Data and Materials	111

5.8	Declarations	111
5.8.1	Competing Interests	111
5.8.2	Author Details	111
5.9	References	111
5.10	Publisher's Note	113
6	Spatially Enriched Paralog Rearrangements Argue Functionally Diverse Ribosomes Arise during Cold Acclimation in Arabidopsis	114
6.1	Introduction	116
6.2	Results	118
6.2.1	Early Temperature Acclimation Effects on Plant Growth	118
6.2.2	Cytosolic Ribosomal Transcriptome Reprogramming	119
6.2.3	Cytosolic Ribosomal Proteome Reprogramming	122
6.2.4	Substoichiometry in Non-Translating Versus Translating Ribosome Complexes	123
6.2.5	Cold-Induced Changes in Active Translating Polysomes	125
6.2.6	Spatially Constrained Cold-Triggered Ribosome Heterogeneity	126
6.2.7	Paralog Specific Cold Responses—uL30 Family	129
6.3	Discussion	130
6.3.1	Different Types of RAP Transcripts Mediate the Initial and Long-Term Responses to Temperature Acclimation	130
6.3.2	Cold-Triggered Reprogramming Indicates That Spatial Constraints Adjust the Ribosomal Proteome	130
6.3.3	Cold Ribosomal Protein Changes during Early Biogenesis	132
6.3.4	Cold Dynamics of Ribosomal Protein Assembly	132
6.3.5	Cold-Induced Ribosomal Protein Substoichiometry Co-Localizes With Rei1 Binding Site	133
6.3.6	Cold Dynamics of uL30 Paralogs Could Orchestrate Spatially Constrained Rearrangements in Ribosomes	133
6.3.7	REIL Concomitant Ribosome Reprogramming Argues Potential Specialization	134
6.4	Materials and Methods	134
6.4.1	Plant Material	134
6.4.2	Growth Conditions	135
6.4.3	Dry Weight Measurements	135
6.4.4	Microarray-Based Transcriptome Analysis	135
6.4.5	Transcriptome Data Analyses	136
6.4.6	Cytosolic Ribosomal Proteome Preparation	136
6.4.7	Proteome Analysis by Liquid Chromatography—Tandem Mass Spectrometry (LC-MS/MS)	137
6.4.8	Proteome Data Analyses	137
6.4.9	Structural Analysis of Changes in Ribosome Protein or Transcript Abundance	138
6.4.10	Sequence Alignments	139
6.4.11	Software	139
6.5	Conclusions	140
6.6	Supplementary Materials	140
6.7	Author Contributions	140

6.8	Funding	140
6.9	Data Availability Statement	140
6.10	Acknowledgments	140
6.11	Conflicts of Interest	140
6.12	References	141
7	Remodelled Ribosomes Synthesise a Specific Proteome in Proliferating Plant Tissue during Cold	147
7.1	Introduction	148
7.2	Results	150
7.2.1	Experimental design	150
7.2.2	Root growth dynamics	152
7.2.3	Reprogramming of the Primary Metabolome	154
7.2.4	Tracer Dynamics in Soluble Amino Acid Pools	156
7.2.5	Protein Synthesis during Transition from a Physiological Steady State	157
7.2.6	Cold Shifts in Protein Synthesis across Plant Cellular Complexes	160
7.2.7	Recycled and Remodelled Ribosomes during Cold Acclimation	163
7.3	Discussion	166
7.3.1	Phenotype during Sub-optimal Low Temperature Germination in Barley Roots	166
7.3.2	Metabolic Phenotype as a Potential Translational Response	167
7.3.3	Amino Acid Metabolism and ^{15}N Isotopic Flux	168
7.3.4	Ribozyme-mediated ^{15}N Incorporation Into Protein	169
7.3.5	Structurally Divergent Ribosomes and Translational Dynamics	169
7.3.6	Translation Initiation: Newly Synthesized Complexes	170
7.3.7	Ribosome Biogenesis: Assembled and Remodelled Ribosomes	171
7.3.8	Translational Outcome of Heterogenous Ribosomes: A Proteome Shift	172
7.3.9	Considerations of Barley Cultivar Keel and Its Responses to Cold	173
7.4	Conclusions	173
7.5	Methods and Materials	174
7.5.1	Experimental Setup	174
7.5.2	Plant rearing	174
7.5.2.1	Surface Seed Sterilisation and Imbibition	174
7.5.2.2	Seedling Germination and Treatment	174
7.5.3	Plant Harvest and Phenotyping	175
7.5.4	Morphometric Image Processing	175
7.5.5	Primary Metabolome Analysis	175
7.5.6	Ribosome Enriched Proteomics	176
7.5.6.1	Protease Considerations	176
7.5.6.2	Ribosomal Protein Purification and Processing	176
7.5.6.3	LC-MS/MS Analysis	177
7.5.7	Data Analyses	178
7.5.7.1	Phenotyping	178
7.5.7.2	Primary Metabolome	179
7.5.7.3	Plant Protein Synthesis Rates (K_s)	179

7.5.7.4	Ribosome Enriched Proteome	181
7.6	Acknowledgements	182
7.7	References	182
8	Functional Translational Regulation during Cold Acclimation in Plants	199
8.1	uL30 Ribosomal Protein Family	200
8.2	Transcript Translational Control During Cold Acclimation	202
8.3	¹⁵ Nitrogen Enrichment Characterizes Functionally Divergent Active Ribosomes during Cold Acclimation in Arabidopsis	209
8.3.1	Summary	209
8.3.2	Results	210
8.3.3	Reaching a Steady State Rate of ¹⁵ N Incorporation	211
8.3.4	Tailoring a Customized ¹⁵ N Labelling Strategy	214
8.3.5	Incorporation of ¹⁵ N Labelled Serine and Glycine into Ribosomal Proteins	216
8.3.6	Accumulation of Actively Translating Polysomes during Cold Acclimation	218
8.3.7	Future steps: Towards Physiological Validation of the Glycine-Serine Labelling Strategy	220
8.4	Using kinetic Mass Spectrometry Imaging to Unravel Spatial Translational Dynamics in Roots	221
9	Discussion	230
9.1	Plant Phenotype during Cold Acclimation	230
9.2	Transcriptional Response of Translation-Related Genes during Cold Acclimation	231
9.3	Ribosome Biogenesis as a Fundamental Process to Start Cold Acclimation	232
9.4	Origin and Spatial Constraints of Cold-Triggered Ribosome Heterogeneity	233
9.5	Modulation of the Translational Machinery and Consequences for Protein Synthesis	234
9.6	Proteome Shifts and Other Triggered Mechanisms during Cold Acclimation Suggesting Ribosome Specialization	237
9.7	Functional Aspects Linking Translational Regulation to Cold-Proteome Shifts	238
9.7.1	uL30 Ribosomal Protein Family: On the Origin of PET Rearrangements	238
9.7.2	REIL 60S Maturation Factor: On the Need For PET Quality Control	239
9.7.3	Polysomes: On the Accumulation of Translating Ribosomes and Their Control of Translation	240
9.8	Conclusions, Working Model and Outlook	241
	SciVal Author Metrics	253
A	Molecular Cloning	264
B	T-DNA Lines	288

C Extended Methods

307

List of Figures

2.1	Simplified scheme of plant cytosolic ribosome biogenesis highlighting the potential steps at which structural heterogeneity may occur and can be controlled.	19
2.2	Localization of RPs (top) or rRNAs (bottom) within the translating wheat 80S ribosome visualized by PyMOL.	21
2.3	Differential expression in response to temperature stress of Arabidopsis genes encoding structural ribosomal proteins of the 60S subunit.	29
2.4	RP remodeling potential of Arabidopsis 80S ribosomes upon 4°C cold stress (A, B) or 38°C heat stress (C, D).	30
3.1	Simplified schematic of the experimental design used in this work to study acclimation to low suboptimal temperatures in the cultivar Keel of <i>Hordeum vulgare</i> and the ecotype Col-0 of <i>Arabidopsis thaliana</i>	41
3.2	Hydroponic plant cultivation.	42
3.3	Schematic workflow of paired proteome profiling of non-translating and translating plant ribosome complexes.	44
3.4	Sucrose density gradient analyses of ribosome complexes in the upper panel and Log ₂ -fold changes relative to Col-0 at several cold acclimation time points of selected cytosolic RP families in the lower panel.	47
3.5	Random response variables with specific distribution shapes, as determined by kurtosis and square of skewness parameters, were used to determine the regression family model for a GLM evaluating both N dose response (A, n = 7617) and comparative Amazonian soils (B, n = 3393) datasets.	54
3.6	RF based selection of seed identity markers from mass features of non-targeted metabolite profiles of experimental bakery products that were prepared with or without additions of chia, linseed, or sesame seeds.	55
3.7	Profiling primary and secondary metabolites during 14 key sampled stages of the Arabica somatic embryogenesis process.	56
3.8	Bootstrapped hierarchical clustering analysis (HCA) of lipid autoscaled intensities from all the root samples (control and subjected to cold stress for three developmental root zones) of cold-sensitive Wyalkatchem and cold-tolerant Young varieties.	57
3.9	Profile of lipid species identified in Azospirillum-inoculated and non-inoculated samples harvested at 7, 14, and 21 DAI using K-means clustering.	58
3.10	Differences among profiles of ten wild cherry tomato accessions obtained by HS-SPME/GC/MS and sensory analysis.	59
4.1	Methodological workflow to achieve measurements of total protein content and individual protein abundances in barley root tips.	68

4.2	Comparison of unique and shared obtained barley proteome using two extraction methods.	69
4.3	Protein content boxplots from <i>Hordeum vulgare</i> roots treated during germination with cold temperature, or additions to the germination solution (chitin or chitosan).	70
4.4	Summary log ₂ -heatmap of statistical methods applied for class comparison, class discovery, and class prediction in LC-MS.	71
4.5	Gene ontology (GO) enrichment test of proteins from relevant clusters 3 and 1 of <i>Hordeum vulgare</i> roots.	73
4.6	Status of the translational machinery in <i>Hordeum vulgare</i> roots after a shift to 4°C during 5 days of germination.	77
5.1	COSNet _i step-by-step detailed workflow.	89
5.2	COSNet _i workflow emphasizing the novelties within our consensus random walk sampling procedure.	90
5.3	Ribosomal protein networks at different distance thresholds (d_t) between amino acid residues in contact.	94
5.4	Overlap between obtained PET regions of yeast and rabbit at varying iteration number for consensus.	96
5.5	Optimized yeast and rabbit ribosomal protein networks.	98
5.6	Spatial confinement during ribosome specialization: a test case of the COSNet _i workflow.	103
5.7	Violin plots of rProtein sequence percentage coverage in interpreted Cryo-EM densities of cytosolic ribosomes.	105
5.8	Histograms summarizing the node degree statistics of the optimized rabbit and yeast ribosomal protein networks.	108
6.1	Arabidopsis Col-0 arrests biomass accumulation after shift to suboptimal temperatures.	119
6.2	Changes of gene expression of cytosolic structural ribosome proteins in roots of <i>Arabidopsis thaliana</i> acclimating to suboptimal temperature.	121
6.3	Differentially expressed ribosomal paralog genes from RP families of <i>Arabidopsis thaliana</i> root.	122
6.4	Substoichiometry of 60S proteome LSU-RPs 7 days after shifting from 20°C to 10°C in <i>Arabidopsis thaliana</i> Col-0 roots (left panel) and at the same time point in two double knockouts (<i>dkos</i>) genotypes of REIL proteins (right panel).	124
6.5	RP candidates of temperature-induced rearrangements in active translating ribosomes.	126
6.6	Significantly altered ribosomal regions during cold acclimation in <i>Arabidopsis thaliana</i> roots measured in three independent genotypes and four biological replicates in total.	127
6.7	Phylogenetic tree resulting from the Bayesian analysis of the uL30 ribosomal protein gene family found in <i>Arabidopsis thaliana</i> , <i>Homo sapiens</i> , and <i>Saccharomyces cerevisiae</i>	129
7.1	Experimental setup.	151
7.2	Root growth dynamics of barley seedlings reared at optimal and cold suboptimal temperatures.	153

7.3	Primary metabolome dynamics of barley seedlings reared at optimal and cold suboptimal temperatures.	155
7.4	Mean isotopic enrichment of amino acid soluble pools in barley root tips from seedlings germinated at suboptimal and optimal temperatures.	156
7.5	Bioinformatics pipeline written as a python function and an R package that jointly enable to calculate stable isotope tracer incorporation into peptides from LC-MS/MS data and derive fractional protein synthesis rates in the organismal physiological context.	159
7.6	Characterization of cold heterogeneous barley ribosomes, their ribosomal protein (rProtein) composition, fractional synthesis rates and induced substoichiometry.	164
8.1	Compendium of evidence arguing that uL30 ribosomal protein paralogs are functionally divergent in plants and contribute to cold induced ribosomal protein heterogeneity.	201
8.2	General results of a Ribo-Seq experiment performed on cold acclimated Arabidopsis seedlings using Col-0 as wild-type and <i>reil-dkos</i> as a negative control to stop ribosome biogenesis during cold.	203
8.3	Polysome accumulation dynamics during cold acclimation in Arabidopsis wild-type and <i>reil-dkos</i>	205
8.4	GO ontology categories that are enriched due to transcript translational control potentially leading to shifts in the translated cellular machinery during cold acclimation in Arabidopsis wild-type and <i>reil-dkos</i>	206
8.5	Standard quality controls for the Ribo-Seq experiment.	208
8.6	¹⁵ N tracer incorporation dynamics into amino acid soluble pools from Arabidopsis plants reared in a hydroponic system.	212
8.7	Differential label incorporation into Arabidopsis roots among diverse labelling strategies.	215
8.8	¹⁵ N enrichment percentages selectively incorporated into the soluble pools of serine and glycine in the optimized enrichment strategy that allowed minimal technical variation during the study of plant acclimation to suboptimal low temperature.	216
8.9	Exemplary isotopolog shift, peptide and protein enrichment percentages in a ribosomal protein from 60S large subunits purified from plant shoot systems reared at suboptimal low or high temperature.	217
8.10	Relative abundance of free and actively translating ribosomal complexes purified from roots of Arabidopsis seedlings reared at different temperatures.	219
8.11	Summary of the methodological workflow to achieve measurements of protein synthesis, abundance and distribution across barley root tips.	222
8.12	Simplified schematic diagram of the KineticMSI workflow for pre-processing and analysis of kMSI datasets.	224
9.1	Proposal for a mechanistic model of the translational processes triggered when plants perceive cold, enabling them to adapt successfully to low suboptimal temperatures.	242

List of Tables

2.1	Plant studies with supporting evidence for and major conclusions regarding cytosolic ribosome heterogeneity and specialization in chronological order.	23
2.2	Studies of structural ribosomal protein mutant lines of <i>Arabidopsis thaliana</i> , <i>Oryza sativa</i> , <i>Nicotiana tabacum</i> , and <i>Nicotiana benthamiana</i> sorted by RP family.	26
3.1	Composition, preparation and storage of mass spectrometry friendly cytosolic ribosome extraction buffer.	43
3.2	Composition, preparation and storage of sucrose cushion solution.	45
4.1	Median protein intensity (\log_2 transformed, pooled-normalized) per ontology functional group sorted according to molecular function (clusters 1 and 3) or biological process (cluster 2).	74
4.2	Statistics of cold acclimated and homology alignments of significantly changed- <i>Arabidopsis thaliana</i> (AT) and <i>Hordeum vulgare</i> (HORVU) RP and RAP paralogs outlined in Figure 6.	78
5.1	Compromise between connectivity and coverage among networks fitted at varying distance (\AA) thresholds.	95
5.2	Tuning the walking length enables yielding region sizes needed for specific biological questions.	97
5.3	Matching of coherent regions with biologically known network topologies.	100
6.1	Paralogs of RP families that showed altered stoichiometry in 60S and polysome fractions.	124
6.2	Paralog abundance changes that imply significantly modulated regions during cold acclimation in plants.	128
7.1	Relative growth rates calculated from multiple root growth proxies from germinating barley seedlings.	154
7.2	Accumulation and origin of protein components from detected multi-protein complexes in barley root tips.	160
8.1	^{15}N enrichment percentage of soluble amino acid pools of <i>Arabidopsis</i> root and shoot.	213

Abbreviations

Å	Ångströms
AU-P	Approximately Unbiased Probability-values
BS	Background Significance
BSA	Bovine Serum Albumin
COSNet_i	ComplexOme-Structural Network Interpreter
CRP	Cytosolic Ribosomal Proteome
Cryo-EM	Cryogenic-Electron Microscopy
d_t	distance threshold
DW	Dry Weight
ES	Expansion Segments
FDR	False Discovery Rate
FW	Fresh Weight
GLM	Generalized Linear Model
LB	Lysis Buffer
LSU	Large Subunit
ORF	Open Reading Frame
PET	Polypeptide Exit Tunnel
PSRP	Plastid-Specific Ribosomal Proteins
PTM	Post-Translational Modification
RAP	Ribosome Associated Proteins
RAS	Region Average Size
RBF	Ribosome Biogenesis Factors
REB	Ribosome Extraction Buffer
<i>reil-dkos</i>	<i>reil1-1 reil2-1</i> AND <i>reil1-1 reil2-2</i>
ROS	Reactive Oxygen Species

RP	R ibosomal P rotein
rProteome	ribosomal-structural P roteome
rRNA	ribosomal R NA
SC	S ucrose C ushion
S-GSH	S - G lutathionylation
SSU	S mall S ubunit
TMT	T andem M ass T ag
TOL	T ree O f L ife
UGSL	U niversal G ene S et of L ife
WGD	W hole G enome D uplication
WL	W alking L engths

Chapter 1

Introduction

This section provides an overarching introduction to the topic of protein biosynthesis and how it may be regulated in plants according to the evolutionary history of ribosomes in higher metazoans. This introduction covers the entirety of the included manuscript-
s/published articles and explains the general question and aim of the thesis by illustrating the general importance and universality of the protein translation machinery and its possible evolution in extremely plastic plant organisms. Chapter 2, on the other hand, provides a more specific introduction focusing on a systematic assessment of all relevant and current scientific literature contributing to the topic of ribosome heterogeneity and specialization in plants.

1.1 Origin, Function and Diversification of Cytosolic Ribosomes

Ribosomes decode mRNA to synthesize all proteins throughout the tree of life (TOL) [3]. In fact, the most accurate versions of the TOL achieved to date were generated using aligned genomic sequences of both ribosomal RNA (rRNA) and ribosomal proteins (rProteins) [8, 13, 51, 52]. Because of this centrality, many of the ribosomal components are part of and dominate the universal gene set of life (UGSL) [2], which refers to the set of orthologous genes that are conserved throughout the phylogenetic TOL and have changed only by speciation, retaining most of their common functions [7, 21, 26].

Accordingly, the ribosomal core, which is conserved throughout the TOL, cannot diverge beyond certain thresholds in cytosolic ribosomes without making life untenable. However, organellar ribosomes and ribosomes of eukaryotic obligate pathogens and symbionts are an exception in that they can be evolutionarily stretched beyond the limit set by the ribosomal core in the UGSL [19, 36, 42, 49]. Despite their limited modifiability by evolutionary forces, cytosolic ribosomes have acquired rRNA via the accretion model [2, 22, 28, 43], and rProteins have increased in size and number and diversified [10, 37, 39–41]. Accelerated accretion has happened logarithmically, based on rRNA, over the last two billion years in metazoans [2, 3, 40], suggesting functional diversification and malleability of the translational machinery in these organisms. As expected, this finding, accompanied by an ever-expanding body of literature, has drawn considerable attention over the past decade to the conceptual field of ribosome heterogeneity and functional specialization, where many mechanisms uncovered serve to address the most pressing challenges we face, such as cancer, neurological diseases, food safety, and, more generally, the adaptation of organisms to unforeseen conditions.

1.2 Ribosome Heterogeneity and Specialization

Ribosomes, once considered static, executing machines, are now considered dynamic modulators of the mRNA-to-protein translation process. This paradigm shift was driven by the discovery of ribosome heterogeneity *in vivo*, a property that alters the ribosome biochemical function and endows ribosomes with selective translational capabilities, which is the very definition of ribosome specialization [54]. In nature, evolution has produced successful and very clear examples of structure-dependent functional specialization of ribosomes. The most prominent example is mitochondrial ribosomes, whose structure has changed greatly compared to their bacterial predecessors, leading to specialization for the biosynthesis of mitochondrial membrane proteins [19]. Similarly, many examples in ribosomes from metazoans have documented structural changes that ribosomes undergo in different contexts to become selective and produce only the proteins they need. The instances in which ribosome heterogeneity can alter translational output have been documented in several recent review publications [11, 14, 15, 35, 38] and mostly include sequence variations in rRNAs [24, 29], modulation of expression or post-transcriptional modifications in rRNA [20] or rProtein transcripts [50], post-translational

modifications in rProteins [23], rProtein substoichiometry [5, 12, 45], rProtein paralog exchange [16, 34], and tRNA expression programs [17]. Each of these cases of ribosome heterogeneity is more or less important for the study of ribosome specialization, depending on the taxa studied and the specific features evolutionarily acquired by their cytosolic ribosomes.

1.3 Plant Cytosolic Ribosomes

Cytosolic ribosomes in plants have very specific and distinctive features as compared to those from other higher metazoans and even more if one moves further away from higher eukaryotes. Plants as sessile organisms cannot escape harmful environments and plant-specific ribosomal features may be a reflection of this lifestyle. Consequently, the study of a ribosomal code in plants needs to account for plant-specific features in the protein biosynthesis apparatus.

The most diversifying aspect of plant evolution are whole genome duplication events (WGD), which have occurred independently many times in the plant lineage compared to all other organisms. It is generally assumed that most, if not all, seed plants have remnants of at least one round of polyploidization in their evolutionary history [18, 25, 46, 47], and that genome sizes return to diploidy in the long term [9, 53]. Thus, WGDs may have shaped plant evolution by providing redundant, dispensable genes that are not constrained by selection pressure and do not incur additional long-term costs from larger polyploid genomes. This aspect of plant evolutionary history leads to many plant-specific mechanisms by reinforcing functional divergence between duplicated paralog genes [4]. As expected, plant ribosomes are particularly heterogeneous due to the presence of many paralog genes encoding ribosomal components in general and rProteins in particular. The rProtein paralogs are mostly products of WGD events and tandem duplications, leading in many cases to a short-lived existence of the additional gene copies [30]. As a result, the number of rProtein paralogs is variable, with 2-7 genes encoding each protein family [1], and a greater or lesser divergence within the gene sequences of each family.

In terms of general aspects of rProteins, compared to Archaea and Bacteria, metazoans have increased rProtein number and size, as well as rProtein basicity and number of nuclear localization signals/export motifs [3, 40]. This last feature may be a consequence

of compartmentalization, as metazoans must import ribosomal proteins into the nucleus more efficiently for ribosome assembly, and this occurs through counterionic carriers that perform their function selectively based on the size and sequence of basic amino acid clusters [44, 48]. Plants share with higher metazoans the increase in number and size of rProteins, while their basicity and increase in nuclear localization signals are still present but significantly reduced, closer to the level of lower eukaryotes [40]. Nevertheless, plants have evolved very specific, diverse, and unpredictable mechanisms for importing proteins into the nucleolus [6], compensating for the apparent lack of common nuclear localization signals in metazoans. Regarding rRNA, higher metazoans accreted significantly more rRNA segments compared to plants and lower metazoans [3]. This accumulation in higher eukaryotes is not thought to be beneficial [31, 32], but rather a product of genome colonization by weakly beneficial or even transiently detrimental phenotypes [33] in organisms with small populations, slow replication, and large cells, characteristics that make these organisms inefficient at eliminating untranslated sequences [27]. On the other hand, plants have a similar rRNA size to lower metazoans, in which the logarithmic accretion of rRNA expansion segments has not occurred.

Thus, based on the particular evolutionary history of plants, it seems likely that their cytosolic ribosomes have greater potential for the evolution of specialized translational mechanisms associated with the use and functional divergence of rProteins and rProtein paralogs.

1.4 Aim of This Thesis

The aim of this thesis was to determine whether and how the potential of cytosolic ribosomal heterogeneity, particularly at the level of rProteins and their paralogs, is exploited by plants to control protein synthesis through specialized translation, thus enabling successful acclimation to sub-optimal low temperatures. The details of this endeavor are presented in the following section, "Statement of Organization."

1.5 Statement of Organization

This work includes six original papers - four published, two prepared to be submitted - that demonstrate the physiological importance to plants of ribosome heterogeneity, which has long been thought to be redundant and to serve only to generate a constant supply of ribosomes. However, the chapters of this thesis conclusively demonstrate that in many cases this heterogeneity is far from redundant and has important functional implications for protein biosynthesis.

Chapter 2 provides an introduction to the main topic by presenting the main concepts in the field of translation, ribosome heterogeneity and specialization. This is followed by a systematic assessment of all relevant literature related to functional ribosome heterogeneity in plants, and concludes with a proposal of a methodological framework at the wet and dry laboratory levels for assessing the extent of the ribosomal code in plants.

In Chapter 3, the materials and methods section, I describe all the collaborative projects that led to the development of the methodological framework explained in Chapter 2 and used in this thesis. These methods form the experimental basis for all other chapters.

Together, the first three chapters form a solid and integrated introduction to how we have turned this thesis into an innovative attempt to show how plastic and evolutionarily malleable the ribosomal code can actually be in extremely plastic organisms such as plants.

Chapter 4 presents a case study of one of the major cereal crops, barley (*Hordeum vulgare*, cv Keel), and characterizes the emergence of ribosome heterogeneity induced by suboptimal low temperatures. Two very important aspects are highlighted in this study. First, plants acclimated to cold accumulate complexes associated with protein biosynthesis beyond the level of control plants. Second, the mechanisms driving translational regulation can be expanded by examining actively proliferating plant tissues such as root meristems.

In Chapter 5, I present a bioinformatic method aimed at ordering the chaos of complex ribosomal proteome datasets, where each ribosome in plants contains 80 accessory proteins and it is therefore quite complicated to derive unified conclusions about translational dynamics. To address this problem for the specific case of acclimation to low

temperatures, the starting point was the fact that ribosome biogenesis, as shown by my research groups, is crucial for successful acclimation, and is a stepwise process in which groups of juxtaposed proteins are permanently incorporated into ribosomal complexes. Thus, if heterogeneity arises during biogenesis, or if it nevertheless has a spatial component, it can be found by using spatial statistical analysis of the dispersion of this heterogeneity. To validate the method, my research group and I applied it to known published data from other metazoans where ribosomal protein heterogeneity has already been linked to specialization in response to environmental factors, and we found that ribosomal protein-dependent specialization can indeed occur as a spatial restructuring of ribosomes in yeast, where the 40S subunit becomes heterogeneous in the ribosomal region that forms the entry for tRNAs. Thus, in this chapter we were able to confirm the idea that spatial constraints are an important aspect for the functional heterogeneity of ribosomes.

In Chapter 6, I applied the method from Chapter 5 to transcriptomic and ribosomal proteomic data sets of *Arabidopsis thaliana* to establish a link between cold acclimation and spatial adjustment of the ribosomal proteome or the expression of its coding genes. The researchers involved in this work and I found that at the level of gene expression, ribosome biogenesis is crucial at the beginning of the acclimation period, whereas ribosomal protein-coding genes are differentially regulated toward the end of this period. With respect to ribosome structure, we found that three regions are significantly affected by ribosomal protein heterogeneity. The polypeptide exit tunnel (PET) at the protein level and the P-stalk, as well as a region between subunits at the transcriptional level. In addition, we combined ribosomal proteomic analyses of *reil-dkos* with those of the Col-0 wild type because *reil-dkos* block ribosome biogenesis during cold, and we conclude that the triggered heterogeneity may have arisen during biogenesis. Therefore, altered PET assembly during cold is suggested as a possible mechanistic link that results in REIL factors having to insert their C-terminus into the PET to verify its integrity, which is phenotypically limiting in plants only during cold. Efforts to provide mechanistic evidence of this process based on the cold dynamics of the uL30 ribosomal protein family have begun in this Chapter and are discussed further in Chapter 8 and 9.

In Chapter 7, I used the barley experimental system described in Chapter 4 to elucidate the origin of ribosomal protein heterogeneity and its potential regulatory capabilities in the synthesis of the proteome from macromolecular complexes. The researchers involved

in this work and I show that ribosomes produced during cold are composed of both newly synthesized and recycled protein components, and that these heterogeneous complexes in turn directly or indirectly translate a cold-induced complexome proteome. Furthermore, the translational dynamics uncovered allow us to propose a model for how selective translation might operate during cold acclimation in plants.

In Chapter 8, I show clear evidence for actively intact translating polysomes that preferentially accumulate at the end of the cold acclimation period in plants. At the same time, as in Chapter 7, The researchers involved in this work and I evaluate the origin of ribosomal proteins incorporated into ribosomal complexes and clarify the changing dynamics of translational output based on sequencing of footprints translated by ribosomes over the acclimation period. In addition, in this chapter we list other results that have not yet been published but form an important part of the mechanistic model proposed in this thesis to be functional during cold acclimation. We conclude that the unambiguous accumulation of functional ribosomal complexes during the cold period leads to successful acclimation through targeted translation of a cold-specific proteome.

Chapter 9 contains the general discussion of our results and the proposed translational model that we hypothesize operates in plants during acclimation to suboptimal low temperatures, based on the results outlined in all the other chapters. Finally, we draw conclusions and a summary about which parts of the model have been sufficiently substantiated and which are still incompletely understood and require future research.

Bibliography

- [1] A Barakat, K Szick-Miranda, I F Chang, R Guyot, G Blanc, R Cooke, M Delseny, and J Bailey-Serres. The organization of cytoplasmic ribosomal protein genes in the Arabidopsis genome. *Plant physiology*, 127(2):398–415, 2001. ISSN 0032-0889. doi: 10.1104/pp.010265.398.
- [2] Chad R. Bernier, Anton S. Petrov, Nicholas A. Kovacs, Petar I. Penev, and Loren Dean Williams. Translation: The universal structural core of life. *Molecular Biology and Evolution*, 35(8):2065–2076, 2018. ISSN 15371719. doi: 10.1093/molbev/msy101.

- [3] Jessica C. Bowman, Anton S. Petrov, Moran Frenkel-Pinter, Petar I. Penev, and Loren Dean Williams. Root of the Tree: The Significance, Evolution, and Origins of the Ribosome. *Chemical Reviews*, 120(11):4848–4878, 2020. ISSN 15206890. doi: 10.1021/acs.chemrev.9b00742.
- [4] Ingo Braasch, Julien Bobe, Yann Guiguen, and John H. Postlethwait. Reply to: 'Subfunctionalization versus neofunctionalization after whole-genome duplication'. *Nature Genetics*, 50(7):910–911, 2018. ISSN 15461718. doi: 10.1038/s41588-018-0163-3.
- [5] Joseph W. Briggs and Jonathan D. Dinman. Subtractional Heterogeneity: A Crucial Step toward Defining Specialized Ribosomes. *Molecular Cell*, 67(1):3–4, 2017. ISSN 10974164. doi: 10.1016/j.molcel.2017.06.022.
- [6] Chiung Wen Chang, Rafael Miguez Couñago, Simon J. Williams, Mikael Boden, and Bostjan Kobe. The distribution of different classes of nuclear localization signals (NLSs) in diverse organisms and the utilization of the minor NLS-binding site in plant nuclear import factor importin- α . *Plant Signaling and Behavior*, 8(10):5074–5088, 2013. ISSN 15592316. doi: 10.4161/psb.25976.
- [7] Robert L. Charlebois and W. Ford Doolittle. Computing prokaryotic gene ubiquity: Rescuing the core from extinction. *Genome Research*, 14(12):2469–2477, 2004. ISSN 10889051. doi: 10.1101/gr.3024704.
- [8] Francesca D. Ciccarelli, Tobias Doerks, Christian Von Mering, Christopher J. Creevey, Berend Snel, and Peer Bork. Toward automatic reconstruction of a highly resolved tree of life. *Science*, 311(5765):1283–1287, 2006. ISSN 00368075. doi: 10.1126/science.1123061.
- [9] Steven Dodsworth, Mark W. Chase, and Andrew R. Leitch. Is post-polyploidization diploidization the key to the evolutionary success of angiosperms? *Botanical Journal of the Linnean Society*, 180(1):1–5, 2016. ISSN 10958339. doi: 10.1111/boj.12357.
- [10] Annette M. Evangelisti and Gavin C. Conant. Nonrandom survival of gene conversions among yeast ribosomal proteins duplicated through genome doubling. *Genome biology and evolution*, 2:826–834, 2010. ISSN 17596653. doi: 10.1093/gbe/evq067.

- [11] Max B. Ferretti and Katrin Karbstein. Does functional specialization of ribosomes really exist? *Rna*, 25(5):521–538, 2019. ISSN 14699001. doi: 10.1261/rna.069823.118.
- [12] Max B. Ferretti, Homa Ghalei, Ethan A. Ward, Elizabeth L. Potts, and Katrin Karbstein. Rps26 directs mRNA-specific translation by recognition of Kozak sequence elements. *Nature Structural and Molecular Biology*, 24(9):700–707, 2017. ISSN 15459985. doi: 10.1038/nsmb.3442.
- [13] Gregory P. Fournier and J. Peter Gogarten. Rooting the ribosomal tree of life. *Molecular Biology and Evolution*, 27(8):1792–1801, 2010. ISSN 15371719. doi: 10.1093/molbev/msq057.
- [14] David M. Gay, Anders H. Lund, and Martin D. Jansson. Translational control through ribosome heterogeneity and functional specialization. *Trends in Biochemical Sciences*, 47(1):66–81, 2022. ISSN 13624326. doi: 10.1016/j.tibs.2021.07.001.
- [15] Naomi R. Genuth and Maria Barna. Heterogeneity and specialized functions of translation machinery: From genes to organisms. *Nature Reviews Genetics*, 19(7):431–452, 2018. ISSN 14710064. doi: 10.1038/s41576-018-0008-z.
- [16] Jeffrey E. Gerst. Pimp My Ribosome: Ribosomal Protein Paralogs Specify Translational Control. *Trends in Genetics*, 34(11):832–845, 2018. ISSN 13624555. doi: 10.1016/j.tig.2018.08.004.
- [17] Hila Gingold, Disa Tehler, Nanna R. Christoffersen, Morten M. Nielsen, Fazila Asmar, Susanne M. Kooistra, Nicolaj S. Christophersen, Lise Lotte Christensen, Michael Borre, Karina D. Sørensen, Lars D. Andersen, Claus L. Andersen, Esther Hulleman, Tom Wurdinger, Elisabeth Ralfkiær, Kristian Helin, Kirsten Grønbæk, Torben Orntoft, Sebastian M. Waszak, Orna Dahan, Jakob Skou Pedersen, Anders H. Lund, and Yitzhak Pilpel. A dual program for translation regulation in cellular proliferation and differentiation. *Cell*, 158(6):1281–1292, 2014. ISSN 10974172. doi: 10.1016/j.cell.2014.08.011.
- [18] Natasha M. Glover, Henning Redestig, and Christophe Dessimoz. Homoeologs: What Are They and How Do We Infer Them? *Trends in Plant Science*, 21(7):609–621, 2016. ISSN 13601385. doi: 10.1016/j.tplants.2016.02.005.

- [19] Basil J. Greber and Nenad Ban. Structure and Function of the Mitochondrial Ribosome. *Annual Review of Biochemistry*, 85:103–132, 2016. ISSN 15454509. doi: 10.1146/annurev-biochem-060815-014343.
- [20] Pulkit Gupta, Shanmugapriya Sothiselvam, Nora Vázquez-Laslop, and Alexander S. Mankin. Deregulation of translation due to post-transcriptional modification of rRNA explains why erm genes are inducible. *Nature Communications*, 4:1–9, 2013. ISSN 20411723. doi: 10.1038/ncomms2984.
- [21] J. Kirk Harris, Scott T. Kelley, George B. Spiegelman, and Norman R. Pace. The genetic core of the universal ancestor. *Genome Research*, 13(3):407–412, 2003. ISSN 10889051. doi: 10.1101/gr.652803.
- [22] Chiaolong Hsiao, Srividya Mohan, Benson K. Kalahar, and Loren Dean Williams. Peeling the onion: Ribosomes are ancient molecular fossils. *Molecular Biology and Evolution*, 26(11):2415–2425, 2009. ISSN 07374038. doi: 10.1093/molbev/msp163.
- [23] Koshi Imami, Miha Milek, Boris Bogdanow, Tomoharu Yasuda, Nicolai Kastelic, Henrik Zauber, Yasushi Ishihama, Markus Landthaler, and Matthias Selbach. Phosphorylation of the Ribosomal Protein RPL12/uL11 Affects Translation during Mitosis. *Molecular Cell*, 72(1):84–98, 2018. ISSN 10974164. doi: 10.1016/j.molcel.2018.08.019.
- [24] Martin D. Jansson, Sophia J. Häfner, Kübra Altinel, Disa Tehler, Nicolai Krogh, Emil Jakobsen, Jens V. Andersen, Kasper L. Andersen, Erwin M. Schoof, Patrice Ménard, Henrik Nielsen, and Anders H. Lund. Regulation of translation by site-specific ribosomal RNA methylation. *Nature Structural and Molecular Biology*, 28(11):889–899, 2021. ISSN 15459985. doi: 10.1038/s41594-021-00669-4.
- [25] Yuannian Jiao, Norman J. Wickett, Saravanaraj Ayyampalayam, André S. Chandrabali, Lena Landherr, Paula E. Ralph, Lynn P. Tomsho, Yi Hu, Haiying Liang, Pamela S. Soltis, Douglas E. Soltis, Sandra W. Clifton, Scott E. Schlarbaum, Stephan C. Schuster, Hong Ma, Jim Leebens-Mack, and Claude W. Depamphilis. Ancestral polyploidy in seed plants and angiosperms. *Nature*, 473(7345):97–100, 2011. ISSN 00280836. doi: 10.1038/nature09916.

- [26] Eugene V. Koonin. Comparative genomics, minimal gene-sets and the last universal common ancestor. *Nature Reviews Microbiology*, 1(2):127–136, 2003. ISSN 17401534. doi: 10.1038/nrmicro751.
- [27] Eugene V. Koonin. Energetics and population genetics at the root of eukaryotic cellular and genomic complexity. *Proceedings of the National Academy of Sciences*, 112(52):15777–15778, 2015. ISSN 10916490. doi: 10.1073/pnas.1520869112.
- [28] Nicholas A. Kovacs, Anton S. Petrov, Kathryn A. Lanier, and Loren Dean Williams. Frozen in Time: The History of Proteins. *Molecular Biology and Evolution*, 34(5): 1252–1260, 2017. ISSN 15371719. doi: 10.1093/molbev/msx086.
- [29] Chad M. Kurylo, Matthew M. Parks, Manuel F. Juette, Boris Zinshteyn, Roger B. Altman, Jordana K. Thibado, C. Theresa Vincent, and Scott C. Blanchard. Endogenous rRNA Sequence Variation Can Regulate Stress Response Gene Expression and Phenotype. *Cell Reports*, 25(1):236–248, 2018. ISSN 22111247. doi: 10.1016/j.celrep.2018.08.093.
- [30] Ting Lan, Wei Xiong, Xuemei Chen, Beixin Mo, and Guiliang Tang. Plant cytoplasmic ribosomal proteins: an update on classification, nomenclature, evolution and resources. *Plant Journal*, 110(1):292–318, 2022. ISSN 1365313X. doi: 10.1111/tpj.15667.
- [31] Michael Lynch. The frailty of adaptive hypotheses for the origins of organismal complexity. *Proceedings of the National Academy of Sciences of the United States of America*, 104(SUPPL. 1):8597–8604, 2007. ISSN 00278424. doi: 10.1073/pnas.0702207104.
- [32] Michael Lynch and John S. Conery. The Origins of Genome Complexity. *Science*, 302(5649):1401–1404, 2003. ISSN 00368075. doi: 10.1126/science.1089370.
- [33] Michael Lynch and Georgi K. Marinov. The bioenergetic costs of a gene. *Proceedings of the National Academy of Sciences of the United States of America*, 112(51): 15690–15695, 2015. ISSN 10916490. doi: 10.1073/pnas.1514974112.
- [34] Catherine M. Mageehey and Vassie C. Ware. Specialized eRpL22 paralogue-specific ribosomes regulate specific mRNA translation in spermatogenesis in *Drosophila melanogaster*. *Molecular Biology of the Cell*, 30(17):2240–2253, 2019. ISSN 19394586. doi: 10.1091/mbc.E19-02-0086.

- [35] Federico Martinez-Seidel, Olga Beine-Golovchuk, Yin Chen Hsieh, and Joachim Kopka. Systematic review of plant ribosome heterogeneity and specialization. *Frontiers in Plant Science*, 11:948, 2020. ISSN 1664462X. doi: 10.3389/fpls.2020.00948.
- [36] Sergey Melnikov, Adam Ben-Shem, Nicolas Garreau De Loubresse, Lasse Jenner, Gulnara Yusupova, and Marat Yusupov. One core, two shells: Bacterial and eukaryotic ribosomes. *Nature Structural and Molecular Biology*, 19(6):560–567, 2012. ISSN 15459993. doi: 10.1038/nsmb.2313.
- [37] Sergey Melnikov, Kasidet Manakongtreecheep, and Dieter Söll. Revising the structural diversity of ribosomal proteins across the three domains of life. *Molecular Biology and Evolution*, 35(7):1588–1598, 2018. ISSN 15371719. doi: 10.1093/molbev/msy021.
- [38] Karl Norris, Tayah Hopes, and Julie Louise Aspden. Ribosome heterogeneity and specialization in development. *Wiley Interdisciplinary Reviews: RNA*, 12(4):e1644, 2021. ISSN 17577012. doi: 10.1002/wrna.1644.
- [39] Michael S. Parker, Ambikaipakan Balasubramaniam, and Steven L. Parker. On the segregation of protein ionic residues by charge type. *Amino Acids*, 43(6):2231–2247, 2012. ISSN 09394451. doi: 10.1007/s00726-012-1418-4.
- [40] Michael S. Parker, Renu Sah, Ambikaipakan Balasubramaniam, Floyd R. Sallee, Edwards A. Park, and Steven L. Parker. On the expansion of ribosomal proteins and RNAs in eukaryotes. *Amino Acids*, 46(7):1589–1604, 2014. ISSN 14382199. doi: 10.1007/s00726-014-1704-4.
- [41] Cyrielle Petibon, Julie Parenteau, Mathieu Catala, and Sherif Abou Elela. Introns regulate the production of ribosomal proteins by modulating splicing of duplicated ribosomal protein genes. *Nucleic Acids Research*, 44(8):3878–3891, 2016. ISSN 13624962. doi: 10.1093/nar/gkw140.
- [42] Anton S. Petrov, Chad R. Bernier, Chiaolong Hsiao, Ashlyn M. Norris, Nicholas A. Kovacs, Chris C. Waterbury, Victor G. Stepanov, Stephen C. Harvey, George E. Fox, Roger M. Wartell, Nicholas V. Hud, and Loren Dean Williams. Evolution of the ribosome at atomic resolution. *Proceedings of the National Academy of Sciences of the United States of America*, 111(28):10251–10256, 2014. ISSN 10916490. doi: 10.1073/pnas.1407205111.

- [43] Anton S. Petrov, Burak Gulen, Ashlyn M. Norris, Nicholas A. Kovacs, Chad R. Bernier, Kathryn A. Lanier, George E. Fox, Stephen C. Harvey, Roger M. Wartell, Nicholas V. Hud, and Loren Dean Williams. History of the ribosome and the origin of translation. *Proceedings of the National Academy of Sciences of the United States of America*, 112(50):15396–15401, 2015. ISSN 10916490. doi: 10.1073/pnas.1509761112.
- [44] Scott M. Plafker and Ian G. Macara. Ribosomal Protein L12 Uses a Distinct Nuclear Import Pathway Mediated by Importin 11. *Molecular and Cellular Biology*, 22(4):1266–1275, 2002. ISSN 0270-7306. doi: 10.1128/mcb.22.4.1266-1275.2002.
- [45] Zhen Shi, Kotaro Fujii, Kyle M. Kovary, Naomi R. Genuth, Hannes L. Röst, Mary N. Teruel, and Maria Barna. Heterogeneous Ribosomes Preferentially Translate Distinct Subpools of mRNAs Genome-wide. *Molecular Cell*, 67(1):71–83, 2017. ISSN 10974164. doi: 10.1016/j.molcel.2017.05.021.
- [46] Douglas E. Soltis, Victor A. Albert, Jim Leebens-Mack, Charles D. Bell, Andrew H. Paterson, Chunfang Zheng, David Sankoff, Claude W. DePamphilis, P. Kerr Wall, and Pamela S. Soltis. Polyploidy and angiosperm diversification. *American Journal of Botany*, 96(1):336–348, 2009. ISSN 00029122. doi: 10.3732/ajb.0800079.
- [47] Pamela S. Soltis, D. Blaine Marchant, Yves Van de Peer, and Douglas E. Soltis. Polyploidy and genome evolution in plants. *Current Opinion in Genetics and Development*, 35:119–125, 2015. ISSN 18790380. doi: 10.1016/j.gde.2015.11.003.
- [48] Lin Ru Tai, Chang Wei Chou, I. Fang Lee, Ralph Kirby, and Alan Lin. The quantitative assessment of the role played by basic amino acid clusters in the nuclear uptake of human ribosomal protein L7. *Experimental Cell Research*, 319(4):367–375, 2013. ISSN 10902422. doi: 10.1016/j.yexcr.2012.12.007.
- [49] Florent Waltz, Tan Trung Nguyen, Mathilde Arrivé, Anthony Bochler, Johana Chicher, Philippe Hammann, Lauriane Kuhn, Martine Quadrado, Hakim Mireau, Yaser Hashem, and Philippe Giegé. Small is big in Arabidopsis mitochondrial ribosome. *Nature Plants*, 5(1):106–117, 2019. ISSN 20550278. doi: 10.1038/s41477-018-0339-y.
- [50] Carrie A. Whittle and Joan E. Krochko. Transcript profiling provides evidence of functional divergence and expression networks among ribosomal protein gene

- paralogs in brassica napus. *Plant Cell*, 21(8):2203–2219, 2009. ISSN 10404651. doi: 10.1105/tpc.109.068411.
- [51] C. R. Woese and G. E. Fox. Phylogenetic structure of the prokaryotic domain: The primary kingdoms. *Proceedings of the National Academy of Sciences of the United States of America*, 74(11):5088–5090, 1977. ISSN 00278424. doi: 10.1073/pnas.74.11.5088.
- [52] C. R. Woese, O. Kandler, and M. L. Wheelis. Towards a natural system of organisms: Proposal for the domains Archaea, Bacteria, and Eucarya. *Proceedings of the National Academy of Sciences of the United States of America*, 87(12):4576–4579, 1990. ISSN 00278424. doi: 10.1073/pnas.87.12.4576.
- [53] Kenneth H. Wolfe. Yesterday’s polyploids and the mystery of diploidization. *Nature Reviews Genetics*, 2(5):333–341, 2001. ISSN 14710056. doi: 10.1038/35072009.
- [54] Shifeng Xue and Maria Barna. Specialized ribosomes: A new frontier in gene regulation and organismal biology. *Nature Reviews Molecular Cell Biology*, 13(6): 355–369, 2012. ISSN 14710072. doi: 10.1038/nrm3359.

Chapter 2

Systematic Review of Plant Ribosome Heterogeneity and Specialization



Systematic Review of Plant Ribosome Heterogeneity and Specialization

Federico Martinez-Seidel^{1,2*}, Olga Beine-Golovchuk³, Yin-Chen Hsieh⁴ and Joachim Kopka¹

¹ Willmitzer Department, Max Planck-Institute of Molecular Plant Physiology, Potsdam, Germany, ² School of BioSciences, University of Melbourne, Parkville, VIC, Australia, ³ Biochemie-Zentrum, Universitaet Heidelberg (BZH), Heidelberg, Germany, ⁴ Bioinformatics Subdivision, Wageningen University, Wageningen, Netherlands

OPEN ACCESS

Edited by:

Anna N. Stepanova,
North Carolina State University,
United States

Reviewed by:

Johannes Hanson,
Umeå University, Sweden
Hideji Yoshida,
Osaka Medical College, Japan
Catharina Merchante,
University of Malaga, Spain

*Correspondence:

Federico Martinez-Seidel
mseidel@mpimp-golm.mpg.de

Specialty section:

This article was submitted to
Plant Abiotic Stress,
a section of the journal
Frontiers in Plant Science

Received: 13 June 2019

Accepted: 10 June 2020

Published: 25 June 2020

Citation:

Martinez-Seidel F,
Beine-Golovchuk O, Hsieh Y-C and
Kopka J (2020) Systematic Review of
Plant Ribosome Heterogeneity
and Specialization.
Front. Plant Sci. 11:948.
doi: 10.3389/fpls.2020.00948

Plants dedicate a high amount of energy and resources to the production of ribosomes. Historically, these multi-protein ribosome complexes have been considered static protein synthesis machines that are not subject to extensive regulation but only read mRNA and produce polypeptides accordingly. New and increasing evidence across various model organisms demonstrated the heterogeneous nature of ribosomes. This heterogeneity can constitute specialized ribosomes that regulate mRNA translation and control protein synthesis. A prominent example of ribosome heterogeneity is seen in the model plant, *Arabidopsis thaliana*, which, due to genome duplications, has multiple paralogs of each ribosomal protein (RP) gene. We support the notion of plant evolution directing high RP paralog divergence toward functional heterogeneity, underpinned in part by a vast resource of ribosome mutants that suggest specialization extends beyond the pleiotropic effects of single structural RPs or RP paralogs. Thus, *Arabidopsis* is a highly suitable model to study this phenomenon. *Arabidopsis* enables reverse genetics approaches that could provide evidence of ribosome specialization. In this review, we critically assess evidence of plant ribosome specialization and highlight steps along ribosome biogenesis in which heterogeneity may arise, filling the knowledge gaps in plant science by providing advanced insights from the human or yeast fields. We propose a data analysis pipeline that infers the heterogeneity of ribosome complexes and deviations from canonical structural compositions linked to stress events. This analysis pipeline can be extrapolated and enhanced by combination with other high-throughput methodologies, such as proteomics. Technologies, such as kinetic mass spectrometry and ribosome profiling, will be necessary to resolve the temporal and spatial aspects of translational regulation while the functional features of ribosomal subpopulations will become clear with the combination of reverse genetics and systems biology approaches.

Keywords: functional heterogeneity, substoichiometry, specialized ribosome, ribosomal code, remodeling

INTRODUCTION

Historically, ribosomes have been considered passive mediators of the central dogma of molecular biology. Nonetheless, the first concept of the role of ribosomes in molecular information flow proposed in 1958 (Crick, 1958; Crick, 1970), was based on the “one gene one ribosome one protein” hypothesis. This notion implied an extreme degree of ribosome specialization. Later, in 1961, the discovery of mRNA as a carrier of open reading frames (ORFs) that code for protein synthesis marginalized the ribosome as a passive bystander of translation (Brenner et al., 1961). The role of ribosomes started to be reconsidered between 1985 and 1995, when independent studies supported the view that the heterogeneity of ribosome composition is likely an additional layer of translational regulation. In 1987, two divergent 18S rRNA sequences were found to be dominant during distinct stages of the rodent malaria life cycle (Gundersen et al., 1987). In 1990, ribosomal protein (RP) expression and posttranslational modification (PTM) were found to change in *Dictyostelium discoideum* upon transition from a unicellular to a multicellular lifestyle (Ramagopal, 1990). In 1995, the model plant *Arabidopsis thaliana* revealed tissue-specific expression of the many RP paralogs that exist in plants (Williams and Sussex, 1995). Nowadays, among many examples, well-studied global translational regulators in plants couple external stimuli to translation, arguing for deeper investigation of translational control (Urquidí Camacho et al., 2020) upon environmental cues.

The altered composition of the translation machinery at any level is a phenomenon called ribosome heterogeneity (Horiguchi et al., 2012; Shi et al., 2017; Gerst, 2018). Ribosome heterogeneity includes sequence variation of rRNAs, absence of specific RPs from the canonical ribosome structure, which causes substoichiometric ribosomes, exchange of RP paralogs, posttranscriptional or posttranslational modifications of rRNA or RPs and possibly additional variations of the ribosome-associated proteome. The difference between heterogeneity and specialization resides in the functional role assigned to sub-ribosomal populations. Thus, specialized ribosomes are defined as a subset of heterogeneous ribosomes that constrain translation to specific mRNAs or may have other specific functions. Functional subpopulations of ribosomes would appear for example after an environmental cue to shape the acclimated proteome. These definitions have previously been proposed (Emmott et al., 2018; Genuth and Barna, 2018) and reflect controversial opinions in the field as yet.

Currently, there is a dualism of hypotheses. The first hypothesis states that heterogeneous ribosomes translate mRNA subsets using mechanisms linked to the diverse aspects of structural ribosome heterogeneity. The second suggests that preference of translation toward transcript subsets is a consequence of insufficient amounts of functional ribosomes. The insufficiency hypothesis considers ribosomes as static machines and assigns selective properties of

preferred translation to transcripts. Highly translated mRNAs are thought to out-compete less readily translated but required transcripts when availability of functional ribosomes limits translation. A similar dualism of hypotheses prevails among explanations of phenotypes linked to *rp*-paralogs where the term of ribosome insufficiency was coined for plants (Horiguchi et al., 2012). In this context, paralog mutant abnormalities are attributed to insufficient functional ribosomes and not to specialized functions of heterogeneous ribosomes. The lack of information on the highly resolved spatiotemporal ribosome composition and the ribo-interactome limits our ability to distinguish between these alternative hypotheses. To fully understand what constitutes functional ribosome heterogeneity, technical obstacles must be surpassed.

RP substoichiometry is likely to assist specialization (Slavov et al., 2015). In yeast, the central role of RPs during translational regulation supports the existence of a ribosomal code (Komili et al., 2007), i.e., the concept of an additional level of complexity attributed to ribosomes that regulate protein translation, and is paralleled by the concept of a histone code that contributes to the regulation of the transcriptional status of a gene. Specialization may entail the remodeling of existing ribosomes where the core structure of the ribosome will be reused and the surface and solvent-exposed proteins are exchanged by *de novo* synthesized paralogs. Alternatively, new ribosomal populations may be *de novo* synthesized. These processes may give rise to substoichiometric ribosome populations in the cell. In plants, where each RP family contains several paralogs, we suggest extending and generalizing the term substoichiometric ribosome population to include ribosomes with exchanged RP paralogs. Currently, analytical methods capable of monitoring specialization are scarce. Therefore, claims of new findings in the field are technology dependent and must be interpreted carefully.

In this review, we distinguish and discuss ribosome heterogeneity according to structural components starting with interacting factors during ribosome biogenesis. Ribosome synthesis represents a compendium of steps by which specialized ribosomes may become assembled. Additionally, we review the methods used for generating insights into ribosome specialization. Our biological focus is on the adaptive benefit of potential functional heterogeneity of cytosolic ribosomes modulating stress responses of sessile organisms, such as plants. Our technical focus defines suitable methodological strategies that will approximate or even allow the acceptance or rejection of ribosome specialization. In all these aspects, we use plants as potentially important but neglected models of ribosome function.

ASSEMBLY OF HETEROGENEOUS RIBOSOMES

Cytosolic ribosomes in eukaryotes consist of a 60S large subunit (LSU) and a 40S small subunit (SSU). The latter decodes mRNA, and the former catalyzes the peptidyl transferase reaction that leads to the peptide bond formation of the newly synthesized proteins. The subunits are composed of rRNA and accessory ribosomal proteins (RPs). The large subunit is composed of 5S, 5.8S, and

Abbreviations: RP, Ribosomal Protein; ORF, Open Reading Frame; PTM, Posttranslational Modifications; GLM, Generalized Linear Model; FDR, False Discovery Rate; LSU, Large Subunit; SSU, Small Subunit; RAP, Ribosome Associated Proteins; RBF, Ribosome Biogenesis Factors; CRP, Cytosolic Ribosomal Proteome; PSRP, Plastid-Specific Ribosomal Proteins; Cryo-EM, cryogenic electron microscopy.

25S rRNA, which ranges between 25S and 26S in plants but is 28S in mammals (Chang et al., 2005). In contrast, the small subunit contains only a single 18S rRNA. At the protein level, the plant 60S and 40S subunits contain at least 47 and 33 RPs, respectively (Wilson and Cate, 2012), with each RP encoded by two to seven paralogs (Barakat et al., 2001; Browning and Bailey-Serres, 2015) (**Supplemental Table S1**). Thus, the 80 RP families may comprise 10^{34} different potential ribosome structural conformations that, considering paralog number, could theoretically serve as a source of heterogeneity (Hummel et al., 2012) and may be the basis of functional specialization or functional divergence within RP families. Given this, specialized ribosomes seem more likely than ribosome heterogeneity seen as a purely stochastic non-functional phenomenon. Important unresolved questions need to be answered: If heterogeneity is basis of a functional mechanism in plant cells, how is it controlled and when is it triggered? A first indication of heterogeneity as a non-stochastic process may be considered from the observation that core ribosomal proteins are assembled by a controlled and highly sequential biogenesis process. Hence, if the assembly line is better understood, then we could improve our current knowledge of ribosome specialization.

Ribosome biogenesis has previously been reviewed both for plants (Weis et al., 2015a; Sáez-Vásquez and Delseny, 2019) and yeast (Woolford and Baserga, 2013). This review provides detailed insights into known and currently unknown plant ribosome biogenesis aspects and is focused on highlighting the processing steps and structures, which may contribute to the assembly of heterogeneous ribosomal populations. Cytosolic ribosome biogenesis starts in the nucleolus and finalizes in the cytoplasm where the last maturation steps take place (**Figure 1**). The main steps at which ribosome heterogeneity may be introduced and specialized functions may be controlled are: 1) 45S and 5S rDNA transcription, 2) pre-ribosomal RNA (pre-rRNA) processing, 3) transcription of RPs and ribosome-associated proteins (RAPs) such as plant ribosome biogenesis factors (RBFs) (Weis et al., 2015a; Palm et al., 2019) or translation factors (Browning and Bailey-Serres, 2015), 4) RP and RAP translation and reallocation to the nucleus, and finally, 5) successive RP and RAP assembly during ribosomal subunit maturation. These key processing steps throughout biogenesis may serve as points of control for the generation of specific ribosome populations (**Figure 1**).

Variation of Ribosomal RNA

Cytosolic ribosomes comprise four mature rRNAs, i.e., 5S, 5.8S, 25S, and 18S. The process to obtain the mature RNAs starts with:

RNA polymerase III mediated synthesis of 5S rRNA (**Figure 1** Step 1A). In *Arabidopsis*, 5S genes are encoded by over 2000 copies distributed over three locations on chromosomes 3, 4, and 5 (Murata et al., 1997). Loci in different chromosomes encode rRNAs of varying lengths (Murata et al., 1997; Poczai et al., 2014), and are differentially enriched by epigenetic marks promoting specific chromatin states. The balance between euchromatin and heterochromatin impacts which 5S rRNAs get transcribed (Vaillant et al., 2007). A locus on chromosome 5 gives rise to an atypically long 5S splicing variant due to aberrant transcription termination, which is also expressed in several

mutants deficient in chromatin remodeling processes (Vaillant et al., 2006; Blevins et al., 2009). 5S rRNA genes from this locus translocated in *Arabidopsis* ecotype Ler, impacting chromatin status and ultimately the selected 5S loci that get transcribed (Simon et al., 2018). Similarly, if 5S rDNA chromatin gets remodeled following stress cues (Asensi-Fabado et al., 2017), a transition could be initiated to modulate ribosome subpopulations. Moreover, the translocation events have increased the exchange frequency among 5S rDNA loci (Simon et al., 2018), increasing the possibilities of coupling the right locus with the right environmental stimulus, ultimately converging at a functionally advantageous ribosome.

In parallel, RNA polymerase I mediated synthesis of a polycistronic rRNA transcript, the precursor of 18S, 5.8S and 25S rRNA (**Figure 1** Step 1B), from highly duplicated 45S rDNA genomic repeats (Sáez-Vásquez and Echeverría, 2007). The tandem-repeated units are arranged into nucleolar organizer regions (NORs) on the short arms of chromosomes 2 and 4 of *Arabidopsis thaliana* (Copenhaver and Pikaard, 1996; Poczai et al., 2014; Browning and Bailey-Serres, 2015). Both NORs contain 45S rDNA variants, with those on chromosome two being tightly regulated during plant development (Chen and Pikaard, 1997; Fransz et al., 2002; Mohannath et al., 2016; Sáez-Vásquez and Delseny, 2019). The short arms of human 21 and 22 NOR-containing chromosomes are physically embedded in the nucleolus (Dunham, 2005).

Remodeling of pre-existing ribosomes by exchanging rRNA seems unlikely, since this process would require fundamental ribosome disassembly and reassembly. Hence, specialized rRNAs may be introduced by *de novo* ribosome synthesis upon an environmental challenge. For example, a controlled mechanism of *Vibrio vulnificus* Gram-negative bacteria upon temperature or nutrient shifts, synthesizes divergent rRNAs that ultimately direct translation of specific mRNAs (Song et al., 2019). Similarly, variation of the rRNA nucleotide sequence modulates the stress responses of *Escherichia coli* in the newly synthesized active translating fractions of ribosomes (Kurylo et al., 2018). An alternative non-plant example from *Escherichia coli* and human studies, are posttranscriptional modifications of rRNA (Popova and Williamson, 2014; Natchiar et al., 2017), which are concomitant to RP stoichiometry (Popova and Williamson, 2014). These modifications can confer selectivity to ribosomes. In plants, these mechanisms remain to be found. However, examples of rRNA heterogeneity harboring functional potential exist both at rDNA level, as outlined in the two previous paragraphs, and during rRNA pre-processing, as detailed in the following section.

Alternative Pre-Ribosome Processing

The 5S rRNA transcript is processed in the nucleoplasm (**Figure 1** Step 2). In contrast, the initial steps of polycistronic rRNA processing take place in the nucleolus. After 45S rDNA transcription, the resulting transcript, designated as 35S pre-rRNA in yeast, associates with a larger ribonucleoprotein complex forming the 90S pre-ribosome and commences processing steps in the nucleolus (**Figure 1** Step 2). The 90S pre-ribosome complex contains similar components as the SSU processome (Grandi et al., 2002). This initial ribosome

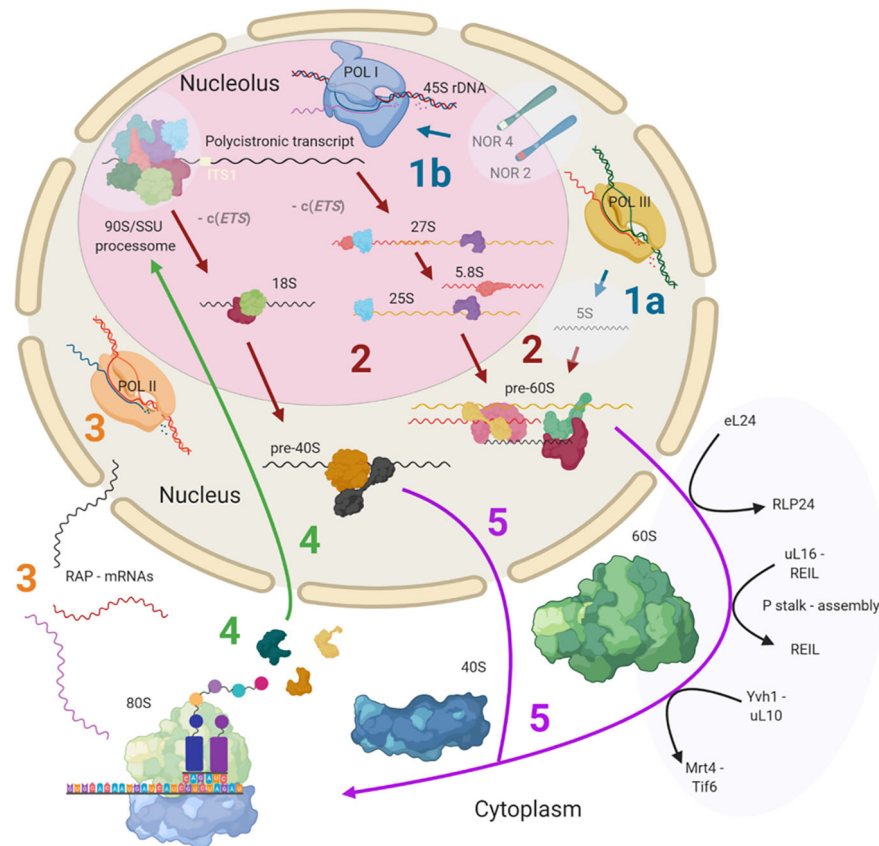


FIGURE 1 | Simplified scheme of plant cytosolic ribosome biogenesis highlighting the potential steps at which structural heterogeneity may occur and can be controlled. Biogenesis is complex and involves at least three cell compartments, the nucleolus, the nucleoplasm, and the cytoplasm. (Step 1A) 5S rRNA is transcribed by RNA polymerase III (POL III) in the nucleus. (Step 1B) The 45S rDNA, localized in the nucleolus, is transcribed into a polycistronic transcript containing 18S, 5.8S and 25S rRNAs by RNA polymerase I (POL I). Heterogeneity may rise from rDNA loci coding for different rRNA species. (Step 2) The large pre-rRNA transcript forms the 90S pre-ribosome/SSU processome, a large ribonucleoprotein complex, which is processed into pre-40S and pre-60S subunits after the splicing event on ITS1. Biogenesis factors are temporarily recruited and ribosomal proteins (RPs) are permanently assembled while rRNA is successively processed. Heterogeneity may result from the recruitment of different rRNAs and ribosome-associated proteins (RAPs), including RPs and RP paralogs. (Step 3) The RAPs are transcribed by RNA polymerase II (POL II). Heterogeneity can result from the changed availability of transcripts for subsequent translation or the presence of different splicing variants. (Step 4) RPs and other RAPs are translated in the cytoplasm and imported into the nucleus where they are assembled or assist the assembly process. Heterogeneity may be caused by availability of divergent RAP and RP paralogs at the time and location of assembly within the nucleus. (Step 5) The nuclear ribosomal pre-subunits are exported to the cytoplasm where they undergo the final maturation steps that render the subunits translationally competent (black arrows). Heterogeneity may arise from the last steps of ribosome biogenesis mediated by RAPs. Posttranscriptional or posttranslational modifications of all components may occur at any stage during or post ribosome biogenesis. Note that some processes and or structure-derived insights have yet to be described in plants (light blue transparencies highlights), and these gaps have been filled with knowledge from other model eukaryotes. The figure was created with BioRender (www.biorender.com) and exported under a paid subscription. 5' or 3' external transcribed spacer c(ETS), internal transcribed spacer (ITS), nucleolar organizer regions (NORs).

maturation complex was purified from other eukaryotes and provided structural insights into the initial pre-rRNA processing steps (Kressler et al., 2017). While it remains to be structurally characterized in plants, most protein orthologs within the complex are encoded in the plant genome (Sáez-Vásquez and Delseny, 2019). The 90S/SSU-processome, also designated as U3 snoRNP (Sáez-Vásquez et al., 2004), likely exchanges RBFs and assembles RPs, since 22 homologues of *Arabidopsis thaliana* SSU RPs co-purified with the BoU3 complex of *Brassica oleracea* as was determined by mass spectrometry of 1D SDS-PAGE purified bands (Samaha et al., 2010). Hence, specialized RPs or paralogs may already be assembled at an early stage of ribosome

biogenesis. In plants, the complex is thought to cleave the internal transcribed spacer (ITS), ITS1, facilitated by previous trimming and cleavage at the P site (Zakrzewska-Placzek et al., 2010), that is, the primary endonucleolytic cleavage site located in the 5' external transcribed spacer (ETS). ITS1 cleavage splices the polycistronic transcript into 27S rRNA, containing the immature 25S and 5.8S rRNAs, and 18S rRNA, thereby splitting the processing into a pre-60S and pre-40S branch. Most unprocessed *Arabidopsis* 35S-type transcripts contain a non-conserved insertion of 1,083-bp that is absent from other cruciferous species (Sáez-Vásquez et al., 2004). This feature supports the notion of unique features of *Arabidopsis*

ribosome biogenesis as compared to other plant species. Such unique aspects should be taken into account when interpreting and generalizing studies of 35S-type transcript pre-processing in *Arabidopsis*.

Pre-rRNA processing of the polycistronic transcript follows two independent pathways in plants (Weis et al., 2015b). This process has been regarded as a redundancy that may secure ribosome abundance under varying conditions. The convergence point of the alternative processing paths is the 27SB_{S/L} rRNA, which is the 27S pre-rRNA spliced from any 5' or 3' ETS or -c(ETS) as depicted in **Figure 1**. At this convergence point, the pre-60S subunits are released into the nucleoplasm (Gadal et al., 2002) for further processing. The small subunit 18S rRNA processing may converge at a barely detectable 20S pre-rRNA that is produced after the excision of 5.8S by MTR4 (Lange et al., 2011) and a similar ETS splicing as aforementioned for pre-60S. rRNA processing involves plant-specific RBFs (Palm et al., 2019), suggesting that specialized features of ribosome biogenesis are to be found in plants. This supports the view that RBFs and RPs have specialized functions in alternative pre-rRNA processing routes in plants. Examples indicate that mutations in *Arabidopsis* AtBRX1-1 and AtBRX1-2 orthologs of the yeast RBF, Brx-1, affect only one of the alternative pre-rRNA processing routes (Weis et al., 2015b). In yeast, Brx-1 associates with RBFs Tif6 and Ebp2 to form the Rpf2 complex (Talkish et al., 2012), which also contains structural proteins uL18 (ScRPL5) and eL18 (ScRPL11). In *Arabidopsis*, *tif6* and *brx1-1* transcripts are differentially accumulated compared to wild type (WT) in mutant lines of the RBF REIL that are likely impaired in late cytosolic ribosome maturation and during cold acclimation (Beine-Golovchuk et al., 2018). Similarly, heat stress could decrease the abundance of pre-rRNAs belonging to one of the alternative processing pathways (Weis et al., 2015a). More generally, plant responses to abiotic stress include altered expression patterns of pre-rRNA processing factors. Such expression changes occur mainly during cold, heat and UV-B light stresses (Sáez-Vásquez and Delseny, 2019). In summary, beyond securing ribosome abundance by redundant factors, evidence points toward effective subfunctionalization and specialized mechanisms that act during stress and enable pre-rRNA processing.

Following nucleolar and nuclear processing, pre-60S LSU and pre-40S SSU complexes are exported into the cytoplasm. Pre-LSU is aided by RBFs to undergo final maturation steps (**Figure 1** Step 5). The associated factors have been elucidated and reviewed in yeast (Woolford and Baserga, 2013; Greber et al., 2016; Ma et al., 2017). The cytosolic steps in plants are thought to be mediated by cytosolic RBF homologs, amongst them REIL1 and REIL2 (Beine-Golovchuk et al., 2018). REIL proteins are *Arabidopsis* RBFs homologous of yeast Rei1. In yeast, Rei1 has a structural proofreading function of the 60S LSU subunit (Meyer et al., 2010; Greber et al., 2016). During cytosolic LSU maturation in yeast, a RLP24 placeholder protein is replaced by RP eL24, then RP uL16 is added and P-stalk assembly is initiated in parallel to or after Rei1 action (Meyer et al., 2010). The P-Stalk is a pentameric uL10-(P1-P2)₂ complex in yeast (Wawiórka et al., 2017), with additional P3 components in plants, that

assists translation associated GTPases. For P-stalk assembly, Yvh1 mediates the release of Mrt4, a placeholder for uL10, and enables substitution by functional uL10 (Zhou et al., 2019). In rice blast fungus *Magnaporthe oryzae*, MoYvh1 is translocated to the nucleus upon oxidative stress where it interacts with MoMrt4 in a process that ultimately subverts the production of proteins needed for plant immunity (Liu et al., 2018), implying that these maturation factors could guide biogenesis of specialized ribosomes to filter immunity-related proteins. After final quality control checks, ScTif6, the anti-SSU-LSU association factor (Basu et al., 2001), is released, and the 60S subunit is rendered translationally competent.

Variation of Ribosome Associated Proteins

During the whole biogenesis process, ribosome associated proteins or RAPs are either transiently (i.e., proteins assisting the process) or in the case of RPs, permanently (i.e., proteins comprising structural constituents of translationally competent complexes) bound to the pre-ribosomes. The RP and other RAP coding genes are transcribed and spliced in the nucleus (**Figure 1** Step 3), the mRNAs are exported and translated in the cytoplasm and finally, most of the RAPs are imported into the nucleus and nucleolus for ribosome assembly (**Figure 1** Step 4).

All RPs have specific entry points during ribosome biogenesis. Therefore, the main processing steps of ribosome biogenesis may determine when RP-specialized ribosomes can be assembled based on selection of specific RPs or paralogs instead of a non-controlled stochastic choice. Controlled assembly would mean that adjacently located RPs, if co-assembled, might be co-dependent on each other or on specific biogenesis factors. Consequently, defined ribosomal regions might be modulated by specialization mechanisms that rely on a sequential assembly line to construct functionally divergent complexes. In line with the previous idea, systematic analyses of individual ribosomal protein mutants (*rp*), compiled in a literature review of yeast ribosome biogenesis (Woolford and Baserga, 2013), have shown a correlation between localization of RPs (**Figures 2A, B**) relative to rRNA domains (**Figures 2C, D**) and the impairment of pre-rRNA maturation. For example, SSU proteins can be attached near the 5' or 3' domains of 18S rRNA, which are located at the body and head of the SSU, respectively. RPs near the 5' end are important during the early stages of pre-rRNA processing, while those near the 3' end are incorporated in later maturation steps. Similarly, LSU RPs are docked to three rRNA regions. 1) Domains I and II, approximately surrounding the equator of the solvent-exposed face of the LSU, are near the 5' ends of 25S rRNA and 5.8S rRNA, respectively. The RPs binding near these ribosomal regions are necessary for 27SA₂ and 27SA₃ pre-rRNA processing. 2) Domains I and III are located near the polypeptide exit tunnel and the RPs binding nearby are necessary for 27SB pre-rRNA cleavage. 3) Finally, the third docking area is located near the central protuberance on the interface side of the LSU. The nearby bound RPs are necessary for 7S pre-rRNA processing and nuclear export. Whether plant-RPs conserve these sequential and spatial dependencies, remains to be tested.

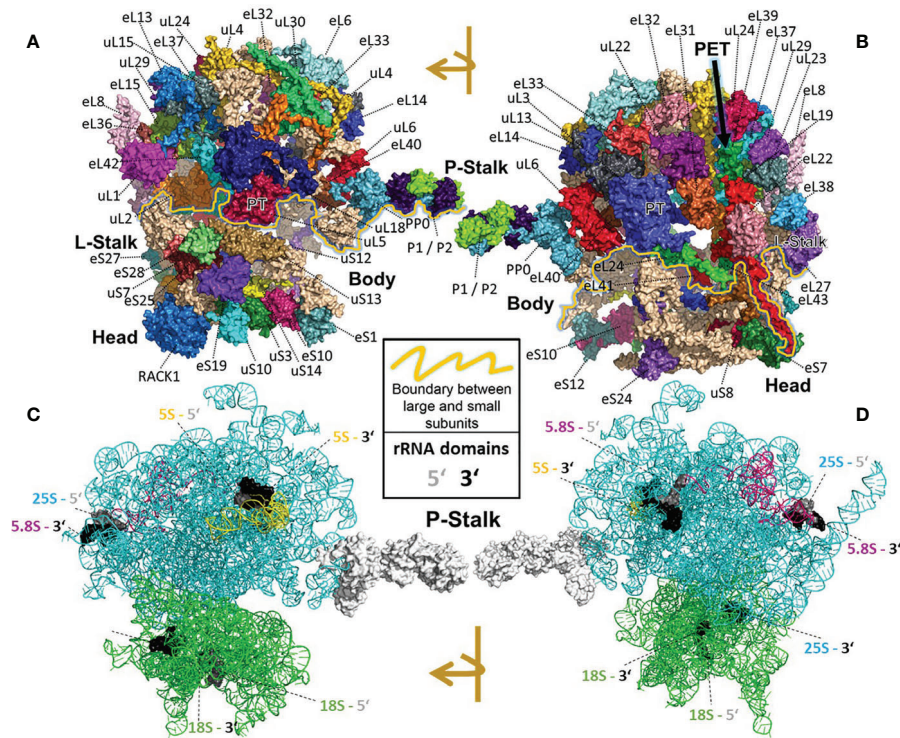


FIGURE 2 | Localization of RPs (top) or rRNAs (bottom) within the translating wheat 80S ribosome (Armache et al., 2010a; Armache et al., 2010b; Ben-Shem et al., 2011; Gamalinda et al., 2013) visualized by PyMOL (PyMOL, RRID : SCR_000305). RP localization was modeled at 5.5 Å resolution by combining structural data of wheat and yeast according to (Ben-Shem et al., 2010). rRNA chains are omitted from top panels (A, B) and are shown separately in bottom panels (C, D) without RP decorations except the P-Stalk that was added as a white surface outline for orientation. Each colored amino acid chain represents the position of a ribosomal protein family within the 40S SSU (lower part of the 80S ribosome) or in the 60S LSU (upper part). (A) Ribosome solvent surface. The main topological characteristics, P-stalk, L-stalk, head and body, and the 40S SSU to 60S LSU interface are indicated (yellow line). (B) Rotated ribosome. The interface and location of the polypeptide exit tunnel (PET, arrow) are indicated. (C, D) Rotated ribosome solvent and interface positions featuring the rRNA chains distinguished by colors. Positions of the four 5' (grey) and four 3' (black) ends of the 18S, 25S, 5.8S and 5S rRNAs are indicated by highlighting of the last ten nucleotide residues.

Transiently bound RAPs assist the translational machinery at every step, from ribosomes biogenesis, through translation, to ribosome recycling. All of these RAPs comprise the ribo-interactome that is highly complex and includes multiple RAP paralogs. Presence of RAP paralogs in plants implies that sub- or neofunctionalized RAPs may mediate cell responses by selective translation as was demonstrated for the mammalian ribo-interactome (Simsek et al., 2017). RAPs, such as the subset of RBFs, can have a wide range of functions during assembly and processing. For example, the mammalian ribo-interactome contains RAPs such as mRNA binding proteins, mRNA/tRNA modifiers, RNA helicases, and potential regulators of metabolism and the cell cycle (Simsek et al., 2017). In plants, numerous examples indicate specific or specialized RAPs. The presence of plant-specific factors, such as the additional eIFiso4F cap-binding complex (Browning et al., 1992; Browning and Bailey-Serres, 2015), which has functionally divergent isoforms (Gallie, 2016), may serve as the first indicator. For example, mutations of the rice eIFiso4F homolog confer resistance to yellow mottle virus (RYMV) (Albar et al., 2006), suggesting that functional divergence of this factor is readily adaptable to generate selective translation constrains. A second

indication is the absence of 25% of yeast RBF orthologs from the plant genome (Weis et al., 2015a). The missing RBFs were likely replaced during plant evolution. A third indication is the duplication of conserved RBFs in plants, such as BRX1-1/1-2, Lsg-1/2, NUC1/2, XRN2/XRN3, and REIL1/2 (Weis et al., 2015a) that are, as was explained above, involved in multiple stress responses of pre-ribosome processing. Clearly, the ribo-interactome of plants is more complex than in other model eukaryotes. This complexity has already resulted in subfunctionalization as may be exemplified by the two REIL biogenesis factor paralogs that act in the cytosol. Only REIL2 but not REIL1 is required for successful cold acclimation. Absence of both paralogs, however, enhances the defect and halts *Arabidopsis* development and growth at low temperature (Schmidt et al., 2013; Beine-Golovchuk et al., 2018). REIL proteins affect accumulation of non-translational ribosomal complexes (Cheong et al., 2020), that is, free pools of 60S LSUs and single 80S monosomes, and in the case of REIL2 are linked to the cold induced C-repeat-binding factor (CBF) regulon (Yu et al., 2020), which is a compendium of more than 100 genes with altered expressions due to the action of CBF transcription factors and enhances freezing tolerance. Whether REIL functions include

contributions to ribosome specialization and cold-acclimated ribosome biogenesis are hypotheses that remain to be validated.

PROTEIN COMPOSITION OF THE CYTOSOLIC RIBOSOME

An early attempt to characterize an eukaryotic, cytosolic ribosomal proteome (CRP) was conducted with rat liver ribosomes (Wool et al., 1995). The 79 RP families that were characterized had homologs in yeast and plants (Wilson and Cate, 2012). Each yeast protein is encoded by two paralogs. Only 64 of the yeast RPs are essential for growth (Steffen et al., 2012). There is an additional 80th plant-specific RP family (Carroll, 2013), namely, the acidic stalk protein P3 (Barakat et al., 2001; Chang et al., 2005; Carroll, 2013). The other 79 plant families represent yeast homologs with high fidelity. Despite the high similarity between the eukaryotic CRPs, in plants, duplication led to structural divergence between RP paralogs (Wool et al., 1995; Barakat et al., 2001). Attempts to verify plant RP families that were predicted at the genome level through proteomic approaches have produced a range of answers. For example, a proteomic study found representatives of all 80 plant RP families, with specific identifications of 87 family members (Carroll et al., 2008). A more recently published data set mapped 70 RP families and 165 RP family members to the CRP (Hummel et al., 2015). The striking difference in the detected paralogs per RP family in both studies may be explained by technical variation of the complex CRP preparation and proteomic analysis but may equally likely originate from changes of ribosome heterogeneity between the two investigated ribosome populations. The most recent study that refined the compositions of the Arabidopsis cytosolic ribosome mapped 76 RP families and 184 members using a label-assisted proteomics approach (Salih et al., 2019).

Deviation From Canonical Compositions

If substoichiometric complexes arise from a non-random specialized ribosome biogenesis, and RPs get affected as co-assembled groups, we need to be able to map the changes of RPs or RP paralogs onto an accurate plant ribosome structure in order to understand the spatial boundaries of these modulatory mechanisms. The currently best localization of RPs within a cytosolic plant ribosome was generated through modelling of known ribosomal protein structures (using archaeal and bacterial templates) into a bread wheat *Triticum aestivum* cryogenic electron microscopy (cryo-EM) map that was reported at 5.5 Å resolution (Armache et al., 2010b). Simultaneously, the rRNA backbone structures were elucidated at 5.5 Å resolution and comprehensively modeled (Armache et al., 2010a), thus completing the current structure model of the wheat 80S ribosome. We coupled RP localization with a comprehensive mapping of RP and RP paralogs (**Supplemental Table S1**) to ribosome complexes (**Figure 2**), compiled based on model organisms, such as yeast (Ben-Shem et al., 2011; Gamalinda et al., 2013). **Figure 2** summarizes the main structural domains and location of RPs by rotated 2D projections of the 3D wheat 80S translating ribosome model. The *Triticum aestivum*

structure contains 80 ribosomal proteins, 47 of the 60S subunit and 33 of the 40S subunit, as well as 4 rRNA structures. Given that a high resolution structure of the mature, translating Arabidopsis cytosolic ribosome has yet to be made publically available, the *Triticum aestivum* 80S ribosomal structure published by Armache et al. (2011) was used as reference for our visualizations (PDB ID 4v7e). Using protein BLAST comparisons, we verified the RP identity of Arabidopsis RP homologs of the protein entries linked to the macromolecular Crystallographic Information Files (mmCIF) of the wheat 80S structure model. We concluded that Arabidopsis RPs (**Supplemental Table S1**) are adequately matched to the wheat RPs mapped in the 80S structure model. To the best of our knowledge, the wheat structure is the currently most complete and adequate, high-resolution plant cytosolic ribosome structure in the PDB database and represents the current canonical structure model of plant 80S ribosomes.

Several lines of evidence indicate that deviations from the canonical 80S structure of plant ribosomes exist, that is, incomplete, substoichiometric ribosomes lacking RPs or ribosomes with varied RP paralog composition (**Table 1**). RP-dependent ribosome structural divergence was deduced by shifts in mass or charge among 25% of the Arabidopsis RPs analyzed (Chang et al., 2005). These observations can be caused by paralog exchanges or by PTMs. Paralog exchanges are likely considering independent reports showing that paired transcript translation and protein degradation rates of cytosolic-RPs from tomato *Solanum lycopersicum* are high (Belouah et al., 2019) and cytosolic RPs of Arabidopsis have a high standard deviation of the protein degradation rates (Li et al., 2017a). These studies suggest that a potential mechanism of ribosome remodeling exists even though RPs are in general stable and long-lived (Li et al., 2017a). Ribosomal complexes of Arabidopsis have a mean-RP half-life of 3–4 days (Salih et al., 2019). Considering the general stability of ribosomes, it seems likely that the high variation among RPs results from induced translation targeted to specific RPs or RP paralogs and remodeling of pre-existing ribosome complexes by RP exchange.

Induced accumulation of RPs and RP paralogs exist in Arabidopsis. Label-free proteomics generated evidence of differential paralog use in response to changing physiological conditions. Phosphorous and iron deficiencies trigger differential accumulation of RPs in plant roots (Wang et al., 2013). UV-B treatment modulates the uL16 paralogs by increasing AtRPL10C and decreasing AtRPL10B (Ferreya et al., 2010). This process is modulated by CKB1, i.e., the regulatory subunit of plastid Casein kinase2 (Zhang et al., 2020). Mutants of the cold-specific Arabidopsis RBF, REIL, indicated that ribosome biogenesis can alter RP paralog accumulation in non-translational ribosome complexes (Cheong et al., 2020). The abundance of specific paralogs, namely, eL28 (AtRPL28A) and eS7 (AtRPS7C), changed upon sucrose feeding (Hummel et al., 2012), and importantly, this effect of sucrose is concomitant to selective mRNA translation (Gamm et al., 2014). The causal link between both observations remains to be elucidated. When linking altered translation of RP paralogs to RP substoichiometry, claims of dosage compensation among plant paralogs within the respective RP family need to be

TABLE 1 | Plant studies with supporting evidence for and major conclusions regarding cytosolic ribosome heterogeneity and specialization in chronological order.

Study	Species	Evidence	Major Conclusions
(Chang et al., 2005)	<i>Arabidopsis thaliana</i> —Cell culture	Proteomics	25% of the cytosolic RPs vary in terms of mass or charge, affecting the overall composition of the 80S monosome.
(Degenhardt and Bonham-Smith, 2008a; Degenhardt and Bonham-Smith, 2008b)	<i>Arabidopsis thaliana</i>	Reverse genetics, live cell imaging, RNA interference, transcript profiling	RP paralog AtRPL23aA (uL23) is targeted to the nucleolus. Loss of the paralog causes pleiotropic effects associated with an <i>rp</i> plant mutant. AtRPL23aB is targeted to the nucleus but its absence does not cause developmental or growth abnormalities. Dosage compensation does not apply to paralog loss in uL23.
(Guo and Chen, 2008)	<i>Arabidopsis thaliana</i>	Reverse genetics, mutant complementation	AtRACK1B and AtRACK1C loss of function mutants do not have the growth and developmental abnormalities that AtRACK1A has. Multiple AtRACK1 mutants exacerbate the abnormalities. The B and C paralogs complement loss of function of paralog A.
(Whittle and Krochko, 2009)	<i>Brassica napus</i> —Microspores, ovules, pollen, microspore-derived embryos, and <i>in vitro</i> pollen	Transcriptome co-expression networks	<i>Brassica napus</i> has a tissue-specific RP paralog composition, which is likely associated with tissue differentiation and/or specialization.
(Falcone Ferreyra et al., 2010)	<i>Arabidopsis thaliana</i> —Shoots	Label-free proteomics	UV-B stress differentially regulates paralogs from the uL16 family of Arabidopsis. RPL10C is upregulated by UV-B in all studied organs, while AtRPL10B is downregulated and RPL10A does not change upon a UV-B stimulus.
(Szick-Miranda et al., 2010)	<i>Arabidopsis thaliana</i>	Reverse genetics, RT-qPCR, phenotyping	Type II uS8 RP paralogs are plant specific and evolutionarily divergent. RPS15aB and RPS15aE are differentially expressed. RPS15aE mutant has larger leaves, roots, and cells.
(Rosado et al., 2010)	<i>Arabidopsis thaliana</i>	Reporter gene microscopy	Subpopulations of RPL4-containing heterogeneous ribosomes co-exist featuring paralog A or D.
(Sormani et al., 2011b)	<i>Arabidopsis thaliana</i>	Transcriptomic data	Subgroups of RPs corresponding to specific paralogs are transcriptionally regulated during stress, leading to “ribosome diversity”. The authors propose a model that controls heterogeneity during biogenesis.
(Hummel et al., 2012)	<i>Arabidopsis thaliana</i> —Shoots	Transcriptomic data and label-free proteomics	Sucrose feeding induces abundance changes in specific paralogs, among them eL28 (AtRPL28A) and eS7 (AtRPS7C). Additionally, at transcript level, many RP genes become upregulated.
(Falcone Ferreyra et al., 2013)	<i>Arabidopsis thaliana</i> —Shoots	Proteomics, subcellular localization, yeast complementation	Non-redundant functional roles of uL16 RPs are indicated. RPL10C expression is restricted to pollen grains. RPL10B localization to the nuclei increases after UV-B stress. The three isoforms complement a yeast <i>uL16</i> mutant.
(Wang et al., 2013)	<i>Arabidopsis thaliana</i> —Roots	Transcriptomic & label free proteomics	Specialized paralogs are associated with Pi-deficiency, uL11 (AtRPL12B) regulated at protein level, eL33, eL39, uS9 (AtRPL35aC, AtRPL39B and AtRPS16B) regulated at transcript level, or with Fe-deficiency, eL22 (AtRPL22B and AtRPL22C) regulated at protein level.
(Gamm et al., 2014)	<i>Arabidopsis thaliana</i> —seedlings	Polysome profiling	Sucrose feeding to Arabidopsis seedling induces selective mRNA translation events, which include numerous RP transcripts.
(Simm et al., 2015)	<i>Solanum lycopersicum</i> —Young leaves and anthers	Next generation sequencing, Quantitative real-time PCR (qRT-PCR)	Co-regulated clusters containing RBFs and RPs exert their functions preferentially in different tissues of <i>Solanum lycopersicum</i> .
(Moin et al., 2016)	<i>Oryza sativa</i> —Roots, shoots, leaves, root-shoot transition region, flowers, grains and panicles	Quantitative real-time PCR (qRT-PCR)	RP transcripts of the LSU are responsive to stress in <i>Oryza sativa</i> , suggesting that proteins encoded by these transcripts could play a specialized role responding to stress.
(Li et al., 2017a)	<i>Arabidopsis thaliana</i>	Labeled proteomics	Structural proteins of the LSU and SSU are stable and long-lived compared to other major protein complexes. Relative degradation rates of RPs had higher standard deviation, suggesting active remodeling takes place.
(Merret et al., 2017)	<i>Arabidopsis thaliana</i> —Seedlings	Polysome profiling, ¹⁵ N elemental analysis mass spectrometry	Transcripts of uS12 (AtRPS23B), uS14 (AtRPS29B) and eL37 (AtRPL37B) are preferentially stored during heat shock and subsequently released and translated in an HSP101-dependent manner during recovery.
(Saha et al., 2017)	<i>Oryza sativa</i> —Plumules, radicles, shoot, and leaf	Quantitative real-time PCR (qRT-PCR)	RP transcripts of the SSU (RPS4, RPS13a, RPS18a and RPS4a) are upregulated during several abiotic stresses in <i>Oryza sativa</i> . RPS4 is also responsive to biotic stress.
(Belouah et al., 2019)	<i>Solanum lycopersicum</i> —Fruits	Transcriptome—proteome paired modelling	RP transcript translation (k_t) and protein degradation rates (k_d) are amongst the highest in all transcript-protein paired measurements of <i>Solanum lycopersicum</i> indicating flexible remodeling of cytosolic ribosomes.
(Sáez-Vásquez and Delseny, 2019)	Plants—review	Transcriptome data meta-analyses	Transcripts related to cytosolic ribosomes either of RAPs or of RPs are induced at transcriptome level by three major stresses, namely, cold, heat, and UV-B stress.
(Salih et al., 2019)	<i>Arabidopsis thaliana</i>	Labeled proteomics	Cytosolic ribosomal populations are replaced every 3–4 days according to the half-life of constituent RPs. RPs featuring significantly shorter turnover were POD (RPP0D), 0.5 days and RACK1B and C, 1.2 days.

(Continued)

TABLE 1 | Continued

Study	Species	Evidence	Major Conclusions
(Zhang et al., 2020)	<i>Arabidopsis thaliana</i>	Proteomics, Quantitative real-time PCR (qRT-PCR), reverse genetics	CKB1 functions in UV-B stress possibly by modulating the responses of the uL16 RP family paralogs of Arabidopsis.
(Cheong et al., 2020)	<i>Arabidopsis thaliana</i>	Transcriptome data, sucrose density ribosome purification, proteomics, reverse genetics	REIL proteins affect paralog composition of cytosolic ribosomes of Arabidopsis. The accumulation of non-translating and translating complexes, as well as their constituent RP transcript or proteoforms differ in REIL mutants.

carefully considered and dissected from potential paralog-specific functions. Examples indicate that subfunctionalization of RP paralogs exists. Arabidopsis paralogs of RP families uL16 (Falcone Ferreyra et al., 2013), uL23 (Degenhardt and Bonham-Smith, 2008a; Degenhardt and Bonham-Smith, 2008b), RACK1 (Guo and Chen, 2008) and uS8 (Szick-Miranda et al., 2010) are non-redundant in function, while other families, such as uL4, contain paralogs that can be linked to co-existing, potentially divergent populations of ribosomes (Rosado et al., 2010). Our compiled list of references implies the existence of translation bias mechanisms. Specialized ribosomes customized to environmental cues can contribute to such mechanisms (Table 1).

The influence of environmental and developmental cues on transcripts of plant cytosolic RP and RBF transcripts becomes increasingly evident. For Arabidopsis, a regulatory model that triggers ribosome heterogeneity was proposed based on transcriptome *in silico* analyses (Sormani et al., 2011b). Such a model assumes that plant ribosome heterogeneity plays a major role for the modulation and reprogramming of the translome. In *Solanum lycopersicum* and *Brassica napus* clusters of RAPs determine tissue identity (Whittle and Krochko, 2009; Simm et al., 2015) and plant organ- or development-specific ribosomes are a well-known plant feature (Horiguchi et al., 2012). In *Oryza sativa* RP transcripts respond to abiotic stresses (Moin et al., 2016; Saha et al., 2017). The differential expression of RAP and specifically RP paralog genes implies that transcriptional reprogramming of the translome mediates responses of the protein composition of ribosomes to environmental stimuli (Figure 1 Step 3) but the contribution and interplay of transcription with additional layers of control of the protein composition of ribosomes require further research.

Post-Translational Modifications

PTMs of RPs generate heterogeneous ribosomes without requiring *de novo* synthesis of complete ribosome complexes or synthesis of RPs followed by ribosome remodeling. In short, PTMs can create heterogeneity on a shorter time scale than possible by ribosome or RP turnover. Arabidopsis RPs undergo a great variety of covalent modifications, such as initiator methionine removal, N-terminal acetylation, N-terminal methylation, lysine N-methylation, phosphorylation and S-cyanation (Carroll et al., 2008; Turkina et al., 2011; García et al., 2019). Non-targeted analysis of the CRP revealed more than one protein spot in a 2D gel proteomics analysis for half of the identified RPs and suggested the presence of multiple RP isoforms (Giavalisco et al., 2005). Presence of a variety of RP PTMs is further supported by proteomic studies where

consideration of expected PTM mass shifts enhances peptide matching per RP family and even RP paralogs (Carroll et al., 2008).

In other eukaryotes, PTMs are involved in translational control (Simsek and Barna, 2017). The likely best investigated functional PTM of a plant RP is the TOR-mediated phosphorylation of the eS6 protein (AtRPS6). TOR is a eukaryotic master regulator complex that integrates energy and nutrient signaling at many system levels ranging from protein synthesis to the control of cell growth and proliferation (Xiong and Sheen, 2014; Chowdhury and Köhler, 2015). In plants, auxin is one of the main signals that affect TOR-mediated translational control (Schepetilnikov and Ryabova, 2017). Phosphorylation of the 40S ribosomal protein S6 kinase 1 (S6K1) is modulated by auxin upstream of TOR (Schepetilnikov et al., 2013) and in turn, leads to eS6 phosphorylation. Next to auxin, S6K1 is modulated by stimuli like glucose and light signals (Li et al., 2017b). The phosphorylation status of eS6 affects pre-18S rRNA synthesis at the rDNA level (Kim et al., 2014). Dephosphorylated eS6 directly binds to a plant-specific histone deacetylase that represses rDNA transcription by altering the chromatin structure. Additionally, translation reinitiation of specific ORFs relies on TOR/S6K1 activity (Schepetilnikov et al., 2011). In essence, eS6 phosphorylation and its upstream signaling cascade regulates translation at multiple levels by a direct link to a cellular master switch. Other plant examples include structural RPs that are differentially phosphorylated during the day and night cycle and modulate diurnal protein synthesis (Turkina et al., 2011), or P-stalk proteins that are phosphorylated and are thought to regulate translation initiation (Szick et al., 1998). Phosphorylation sites are known, e.g. Ser-103 of P1/P2 paralogs, RPP1A, 1B, and 1C, and Ser-305 of uL10 paralog, RPP0A (Reiland et al., 2009). Phosphorylation events at these sites may regulate selective translation in plants, as it appears to link an integrated stress response in mammalian models through the interaction with General control nonderepressible2 (GCN2) global translational regulator (Inglis et al., 2019).

In summary, diverse evidence of structural ribosome heterogeneity challenges the view of ribosomes as mere executing bystanders of protein synthesis. Observations of translational regulation by changes of translation initiation factors (eIFs) need to consider the multiple modes of ribosome heterogeneity. We think that there is reasonable doubt that ribosome heterogeneity is a mere consequence of stochastic ribosome assembly and that heterogeneity has the sole function of engineering redundancy to ensure a secure supply of the essential ribosome machinery. We support the view that evolution molded the ample structural diversity of plant ribosomes toward functionally specialized ribosomes, where

PTM mechanisms act rapidly on slowly turned-over ribosome populations and *de novo* synthesis of ribosome complexes or RPs coupled to ribosome remodeling supports long-term acclimation to environmental changes.

FUNCTIONAL HETEROGENEITY OF RP PARALOGS

For heterogeneous ribosomes to be functional, the translated proteome must be shaped by selective transcript recruiting according to external stimuli. Means of selective translation by structural changes to the ribosome at the RP level that became apparent in other organisms (Ferretti et al., 2017; Shi et al., 2017) remain to be proven in plants. One of the means that plants use to select subsets of transcripts for translation are cis-regulatory elements of mRNAs (Von Arnim et al., 2014; Van Der Horst et al., 2020). Ribosomes decode cis-regulatory elements. For instance, in Arabidopsis, RPL24B regulates uORF-mediated translation reinitiation at the 5'UTR (Nishimura et al., 2005). Through this mechanism, RPL24B modulates the auxin pathway during development, directing translation of auxin response factors (ARFs) (Rosado et al., 2012). Another example of how ribosomes rely on RPs to target subsets of mRNA is the RACK1 protein family. In yeast RACK1 affects translation in a length-dependent manner and promotes translation of short mRNAs (Thompson et al., 2016). The three Arabidopsis RACK1 paralogs proved to be functionally unequal (Guo and Chen, 2008). Although complementation studies and multi-paralog mutants indicate partial genetic redundancies, due to differential expression of the three paralogs, RACK1 factors have differential contributions to plant development and translation (Table 2). Thus, if selective translation is conserved, the paralogs might show distinct mRNA recruiting abilities. Remarkably, the knowledge gathered on this RP family by plant ribosome structural and functional research (Islas-Flores et al., 2015) contributed to the discovery of how poxviruses can achieve trans-kingdom mimicry by inducing a plant-like status of human RACK1 to translate their own RNA (Jha et al., 2017). These examples show that plant RP paralogs can functionally diversify. In the following, we surveyed further evidence of functional heterogeneity of plant RPs that may reach beyond cytosolic ribosomes (Table 2).

Cytosolic Ribosomal Proteins

Many RP genes have been mutated to enable a deeper functional understanding of their gene products. These studies focus on the developmental role of single or few RP paralogs (Horiguchi et al., 2011; Horiguchi et al., 2012). A summary of studies that target the functions of single RPs tell a story of common themes and diversity (Table 2). Diversity becomes apparent, for example, by observations that distinct developmental stages need specific RP paralogs, e.g., the uL23 (AtRPL23) paralogs, which are not equivalent for plant development (Degenhardt and Bonham-Smith, 2008a). In addition, the loss of single RP paralogs often causes phenotypes of varying severity, questioning claims of full functional RP paralog redundancy.

On the other hand, common phenotypes are apparent (Table 2). The *rp* mutants share typical features, for example, altered leaf polarity establishment, cell proliferation and shape determination (Byrne, 2009; Horiguchi et al., 2011; Roy and Arnim, 2013) and the frequent occurrence of embryo-lethality. The latter observation is in agreement with the essential function of ribosomes. Early embryo development is achieved through the use of inherited ribosomes, but the embryo cannot advance further because ribosome *de novo* synthesis is necessary. Where the mutation is not embryo lethal, a pointed leaf phenotype is frequently found. The shared *rp* phenotypes can be explained by ribosome insufficiency, i.e., the limited availability of translationally competent ribosomes, or alternatively by the lack of developmentally specialized ribosome subpopulations. In the plant field, however, the extra ribosomal, or so-called moonlighting functions of RPs, such as detailed for human pathogenesis mechanisms (Wang et al., 2015), are frequently considered explanations for *rp* mutant phenotypes (Gerst, 2018). These non-structural functions of RPs are just beginning to be unveiled and may be independent of ribosome specialization (Segev and Gerst, 2018). Systematic functional analyses of *rp* paralog mutants need to account for such extra-ribosomal functions of RPs. For instance, uL23 recruits a nascent protein to its future localization in the chloroplast by coupling with its receptor (Kim et al., 2015). Whether the differential uL23 paralog phenotypes are influenced by both moonlighting and ribosomal functions remains an open discussion.

In summary, the unambiguous experimental dissection of the three basic functional explanations of RP deficiencies, namely, ribosome specialization, ribosome insufficiency, or moonlighting of single RPs with functions that are linked to ribosome biogenesis or translation, is the grand challenge of the field of plant ribosome physiology.

Plastid Ribosomal Proteins

The cyanobacterial origin of chloroplasts determines the nature of their 70S bacterial-type ribosomes. Part of the chloroplast proteome comprising ~3000 proteins, is nuclear encoded (Jensen and Leister, 2014), while only 100 ORFs remain chloroplast encoded (Jarvis and López-Juez, 2013). Consequently, final protein abundances in the chloroplast are mostly determined posttranscriptionally, translationally, and posttranslationally (Sun and Zerges, 2015). Recent years have observed increasing interest in the plastid translational apparatus. The first structure of the spinach chloroplast ribosome was made available in 2016 using cryo-EM (Bieri et al., 2017). Insights into ribosome-associated factors were rapidly facilitated by the structure modeling capabilities of cryo-EM technology (Ahmed et al., 2017; Bieri et al., 2017; Graf et al., 2017; Boerema et al., 2018).

Plastid-specific ribosomal proteins (PSRPs) are split between nuclear and plastid encoded and can be divided in the model plant Arabidopsis into essential and nonessential components (Tiller et al., 2012). By definition, the nonessential components of chloroplast ribosomes are a subset of proteins that can be removed without an obvious phenotype. These nonessential accessory proteins may represent specialized factors that are needed beyond optimized *in vitro* or controlled greenhouse

TABLE 2 | Studies of structural ribosomal protein mutant lines of *Arabidopsis thaliana*, *Oryza sativa*, *Nicotiana tabacum*, and *Nicotiana benthamiana* sorted by RP family.

Gene code	Paralog	Family	Phenotype
Cytosolic ribosome			
Os03g0725000	RPL6— OsRPL6	eL6	Two mutants with high water-use efficiency in rice (Moin et al., 2017).
AT4G27090	RPL14B	eL14	Heterozygous female gametophytes from <i>rp14b</i> /RPL14B ovules are impaired for cell fate specification resulting in pollen tube defects (Luo et al., 2020).
AT5G27850	RPL18C	eL18	Pointed leaves (Horiguchi et al., 2011) and reduced leaf area (Wang et al., 2018).
AT1G02780	RPL19A	eL19	Embryo lethal (Tzafrir et al., 2004).
AT3G16780	RPL19B— NbRPL19	eL19	Decreased non-host disease resistance against bacterial pathogens (Nagaraj et al., 2016).
AT2G34480	RPL18aB	eL20	Required for both male gametophyte function and embryo development (Yan et al., 2016).
AT2G36620	RPL24A	eL24	Suppresses proline accumulation of the parental <i>Arabidopsis thaliana</i> ring zinc finger 1 (<i>atrzf1</i>) mutant (Park et al., 2017).
AT3G53020	RPL24B	eL24	Pale leaf-color (Yao et al., 2008), defects in gynoecium apical-basal patterning, RP paralogs with different translational status (Nishimura et al., 2005; Tiruneh et al., 2013).
AT2G19730	RPL28A	eL28	Serrated-pointed leaves (Horiguchi et al., 2011), pale leaf color (Yao et al., 2008).
AT3G59540	RPL38B	eL38	Larger palisade mesophyll cells coupled with serrated-pointed leaves (Horiguchi et al., 2011).
AT4G31985	RPL39C	eL39	Pointed leaves (Horiguchi et al., 2011).
AT3G52590	RPL40B	eL40	Embryo lethal (Tzafrir et al., 2004).
AT3G23390	RPL36aA	eL42	Serrated-pointed leaves (Casanova-Sáez et al., 2014).
AT4G14320	RPL36aB	eL42	Serrated-pointed leaves (Casanova-Sáez et al., 2014).
AT2G27530	RPL10aB	uL1	Serrated-pointed leaves (Pinon et al., 2008) (Horiguchi et al., 2011).
AT2G18020	RPL8A	uL2	Embryo lethal (Tzafrir et al., 2004).
AT1G43170	RPL3A	uL3	Embryo lethal (Tzafrir et al., 2004), silencing uL3 genes in <i>Nicotiana tabacum</i> affects growth (Popescu and Tumer, 2004).
Os11g0168200	RPL3B	uL3	Paralog A does not compensate mutation in paralog B, reduction in free 60S subunits and polysomes, aberrant leaf morphology (Zheng et al., 2016), silencing uL3 genes in <i>Nicotiana tabacum</i> affects growth (Popescu and Tumer, 2004).
AT3G09630	RPL4A	uL4	Aberrant auxin responses and developmental phenotypes (Rosado et al., 2010; Rosado et al., 2012).
AT5G02870	RPL4D	uL4	Abaxialized leaves with larger palisade mesophyll cells (Horiguchi et al., 2011), defects in vacuole trafficking and development, downregulation of genes implicated in lipid metabolism (Li et al., 2015), uORF-mediated translation repression of SAC51 by <i>sac52-d</i> (<i>AtRPL10A</i>), <i>sac53-d</i> (<i>AtRACK1A</i>), <i>sac56-d</i> (<i>AtRPL4D</i>), and thermospermine (Kakehi et al., 2015).
AT1G33140	RPL9C	uL6	Serrated-pointed leaves with laminar outgrowths (Pinon et al., 2008), delayed growth, paralogs C and D have redundant functions (Devis et al., 2015).
AT4G10450	RPL9D	uL6	Delayed growth, paralogs C and D have redundant functions (Devis et al., 2015).
AT5G60670	RPL12C— NbRPL12	uL11	Decreased non-host disease resistance against bacterial pathogens (Nagaraj et al., 2016).
Os01g0348700	RPL23A— OsRPL23A	uL14	Two mutants with high water-use efficiency in rice (Moin et al., 2017).
AT3G04400	RPL23C	uL14	Embryo lethal (Tzafrir et al., 2004).
AT2G47110	RPL27aB	uL15	Female gametogenesis less strongly affected than in aC paralog mutant (Zsögön et al., 2014).
AT1G70600	RPL27aC	uL15	Serrated-pointed leaves, embryo and plant shoot developmental defects (Szakonyi and Byrne, 2011), female sterility (Zsögön et al., 2014).
AT1G14320	RPL10A	uL16	Female gametophyte lethality (Imai et al., 2008), embryo lethal (Ferreira et al., 2010), uORF-mediated translation repression of SAC51 by <i>sac52-d</i> (<i>AtRPL10A</i>), <i>sac53-d</i> (<i>AtRACK1A</i>), <i>sac56-d</i> (<i>AtRPL4D</i>) and thermospermine (Kakehi et al., 2015).
At1G26910	RPL10B	uL16	knock down mutant, reduced growth in all measured physiological parameters (Ferreira et al., 2010).
AT3G25520	RPL5A	uL18	Reduced female/male transmission (Fujikura et al., 2009), serrated-pointed leaves and reduced leaf development (Wang et al., 2018). Abnormal, similar to abaxialized leaves when combined with <i>as1</i> (Pinon et al., 2008) or <i>as2</i> , otherwise wild-type like (Yao et al., 2008).
AT5G39740	RPL5B	uL18	Abnormal, similar to abaxialized leaves when combined with <i>as2</i> , otherwise pale coloring (Yao et al., 2008). Reduced female/male transmission (Fujikura et al., 2009), functionally redundant to RPL5A paralog and decreased leaf width (Van Minnebruggen et al., 2010).
AT2G39460	RPL23aA	uL23	RNAi line, pointed and fused leaves, delayed flowering, retarded plant growth, apical dominance loss, lethal double-mutant with paralog aB (Degenhardt and Bonham-Smith, 2008a), low levels of RPL23A amiRNA result in an albino phenotype (Kim et al., 2015).
AT3G55280	RPL23aB	uL23	No phenotype reported, lethal double-mutant with paralog aA (Degenhardt and Bonham-Smith, 2008a), low levels of RPL23A amiRNA result in an albino phenotype (Kim et al., 2015).
AT1G80750	RPL7A	uL30	Pointed leaves and reduced leaf area (Wang et al., 2018).
AT2G01250	RPL7B	uL30	Serrated-pointed leaves (Horiguchi et al., 2011) and reduced leaf area and development (Wang et al., 2018).
AT4G31700	RPS6A	eS6	Strongest phenotype within eS6 family, has been combined with <i>as1</i> and <i>as2</i> mutants (Horiguchi et al., 2011), reduced leaf area and enhanced <i>var2</i> -mediated leaf variegation (Wang et al., 2018), slow growth (haplodeficiency) in paralog A-B double mutant (Creff et al., 2010).
AT5G10360	RPS6B	eS6	Defective phyllotaxy, apical dominance loss (Morimoto et al., 2002), slow growth (haplodeficiency) in paralog A-B double mutant (Creff et al., 2010).
AT5G41520	RPS10B	eS10	Affects the formation and separation of shoot lateral organs, including the shoot axillary meristems (Stirnberg et al., 2012)
AT3G53890	RPS21B	eS21	Serrated-pointed leaves, reduced leaf area (Wang et al., 2018) and cell size in shoot (Horiguchi et al., 2011).
AT5G27700	RPS21C	eS21	Functionally redundant to B paralog, reduced leaf area (Wang et al., 2018).

(Continued)

TABLE 2 | Continued

Gene code	Paralog	Family	Phenotype
AT5G28060	RPS24B	eS24	Serrated-pointed leaves, reduced leaf area (Wang et al., 2018).
AT3G61110	RPS27A	eS27	Increased sensitivity to UV-B and methyl methanesulfonate (Revenkova et al., 1999).
AT5G03850	RPS28B	eS28	Decreased cell proliferation, has been combined with <i>as1</i> and <i>as2</i> mutations (Horiguchi et al., 2011).
AT3G11940	RPS5A	uS7	Cell-division perturbed when heterozygous, embryo lethal when homozygous (Weijers et al., 2001).
AT2G19720	RPS15aB	uS8	Pointed leaves, a double mutant with RPL28A was investigated (Horiguchi et al., 2011), type II uS8, evolutionarily divergent and plant specific paralog (Szick-Miranda et al., 2010).
AT4G29430	RPS15aE	uS8	Type II uS8, evolutionarily divergent and plant specific paralog, larger leaf surface, root, and cells (Szick-Miranda et al., 2010).
AT1G22780	RPS18A	uS13	Pointed leaves and reduced growth (Van Lijsebettens et al., 1994).
AT4G00100	RPS13A	uS15	Defects of leaf and trichome morphology, retarded flowering and root growth (Ito et al., 2000).
AT3G48930	RPS11A	uS17	Embryo lethal (Tzafrir et al., 2004).
AT1G18080	RACK1A	RACK1	Pointed leaf phenotype and partial genetic redundancy of paralogs by complementation studies (Guo and Chen, 2008), ATRPL4D restored by <i>sac52-d</i> (ATRPL10A), <i>sac53-d</i> (ATRACK1A), <i>sac56-d</i> and thermospermine (Kakehi et al., 2015).
AT1G48630	RACK1B	RACK1	No phenotype reported, exacerbates RACK1A mutation defects (Guo and Chen, 2008).
AT3G18130	RACK1C	RACK1	No phenotype reported, exacerbates RACK1A mutation defects (Guo and Chen, 2008).
Plastid ribosome			
Os01g0662300	RPL12	bL12c	Albino lethal phenotype at seedling stage (Zhao et al., 2016).
Os02g0259600	RPL21/CL21	bL21c	Chloroplast developmental defects and seedling death in rice, the synonymous mutant name is <i>asl2</i> (<i>albino seedling lethality 2</i>) (Lin et al., 2015).
Os01g0749200	RPL13A	uL13c	Single-base substitution affects chloroplast development in rice grown under low temperature conditions (Song et al., 2014), albino lethal-seedlings of T-DNA insertion mutant (Lee et al., 2019).
AT3G25920	RPL15	uL15c	Decreased levels of uL15c lead to chlorosis and reduced leaf photosynthetic capacity, the null mutant is embryo lethal (Bobik et al., 2019).
AT5G54600	RPL24	uL24c	Reductions in growth, leaf pigments and photosynthesis (Romani et al., 2012).
AT5G30510	RPS1	bS1c	Reductions in growth, leaf pigments and photosynthesis (Romani et al., 2012).
Os12g0563200	RPS6	bS6c	Albino phenotype at low temperature (Wang et al., 2018), pale leaves and defective thylakoid architecture (Sun et al., 2016).
Os01g0678600	RPS20	bS20c	Albino lethal phenotype at seedling stage (Gong et al., 2013).
AT2G38140	PSRP-4	bTHXc	Putative role in light-dependent regulation of translation (Tiller et al., 2012).
AT3G52150	PSRP-2	cS22	Putative role in light-dependent regulation of translation (Tiller et al., 2012).
AT1G68590	PSRP-3	cS23	Putative role in light-dependent regulation of translation (Tiller et al., 2012).
AT2G33800	RPS5	uS5c	Smaller rosettes, photosystem I and II components, and many PRPs are suppressed, involved in plant development and cold stress (Zhang et al., 2016).
Os03g0769100	RPS9	uS9c	Embryo lethal in maize (Ma and Dooner, 2004), albino at three leaf stage in rice (Qiu et al., 2018).
AT1G79850	RPS17	uS17c	Reductions in growth, leaf pigments and photosynthesis (Romani et al., 2012), embryo-lethal in maize (Schultes et al., 2000).

To reduce ambiguity of interpretation, we avoided to report mutants of multiple defective loci where unique RP mutant lines were available; information of combined mutants is indicated.

conditions. The severity of the *psrp* mutant phenotypes does not strictly correlate with their orthologous prokaryotic counterparts (Romani et al., 2012). This observation suggests plant-specific features of plastid ribosome biogenesis and translation. The functional studies reported in **Table 2** are selections of snapshots that highlight plant-specific aspects of plastid ribosomes. PSRP families are typically smaller than cytosolic RP families, and some PSRPs appear to be single copies. Future research will determine whether concepts of ribosome heterogeneity, specialization, and insufficiency or PSRP moonlighting may apply to plastid ribosomes that acclimate to environmental stress, such as cold stress. Plants appear to modify plastid ribosomes at suboptimal temperatures. In *Arabidopsis*, tolerance to cold can be achieved by overexpression of plastid ribosomal proteins, e.g., uS5c (PRSP5) (Zhang et al., 2016). PRPS5 and PRPS1 interact indirectly with the CHLOROPLAST RIBOSOME ASSOCIATED (CRASS) protein to support translation during cold stress (Pulido et al., 2018). In rice, uL13c is important for plastid development during cold (Song et al., 2014).

Mitochondrial Ribosomal Proteins

The number of plant mito-*rp* studies is small as compared to those analyzing genes of the cytosolic or plastidic ribosomes. Nevertheless, the already existing body of literature, reviewed elsewhere (Robles

and Quesada, 2017), points toward mito-RP families with functionally divergent members across plant species. Moreover, mito-RPs have particular roles during development (Robles and Quesada, 2017) that still need to be linked to either moonlighting functions or to their translational context. Interestingly, single-particle cryo-EM images in combination with proteomic analyses of enriched *Arabidopsis* mitochondrial ribosome fractions have shown substantial structural divergence from their prokaryote and eukaryote counterparts (Rugen et al., 2019; Waltz et al., 2019). The current body of studies suggests plant-specific features of mitochondrial translation.

TRANSCRIPTOMIC EVIDENCE OF PLANT RIBOSOME SPECIALIZATION: A TEST-CASE

This section exemplifies and critically assesses instances of differential paralog usage that can be observed at the transcript level. Final protein abundance is shaped at several control points ranging from chromatin modifications to transcription, translation and PTMs (Vogel and Marcotte, 2012). Hence, transcript levels

cannot predict the final active protein concentration or nature and extent of PTMs. Nevertheless, transcript changes are arguably a crucial component of the translational response to environmental cues in plants (see *Deviation From Canonical Compositions* and **Table 1**). In yeast, a mechanism that remains to be probed in plants relies on regulating the transcription of RPs in response to arrested ribosome biogenesis (Albert et al., 2019). Hence, we argue that changes in RP transcript levels provide one line of evidence—in the sense of a translation potential (**Figure 1** Step 3) or feedback mechanisms—that supports the search for ribosome specialization in the context of stress acclimation.

To substantiate this claim, we chose temperature stress acclimation as a test case and show that differential gene expression may indicate changes of ribosome paralog composition as one mechanism of generating functional heterogeneity adjusted to environmental cues (**Figure 3**). Exploring temperature stress was the obvious choice in view of the increasingly visible effects of global warming. We propose a meta-analysis of the dynamics of RP family transcripts following opposing temperature shifts. In our case study, we compare *Arabidopsis thaliana* Col-0 root exposed to heat shock (38°C) and cold (4°C) stress with the respective control at 20°C optimized temperature. The experiment is identified as entry AT-00120 in the Genevestigator repository (organism: *Arabidopsis thaliana*, selection: AT-8, type: Gene). We based our test-case on a compiled list of 376 *Arabidopsis* genes that have been annotated as members of the cytosolic ribosomal proteome. As to the procedures, the background-subtracted microarray signals of experiment AT-00120 were retrieved and imported into the R statistical programming environment. All initial matrix related transformations, object conversions and data handling were performed with the R packages *stringi* (version 1.4.6—<https://cran.r-project.org/web/packages/stringi/index.html>), *reshape* (Wickham, 2007), and *Tidyverse* (version 1.0.0—<https://github.com/hadley/tidyverse>). Only the signals belonging to heat or cold stress subset of AT-00120 were further processed, because suboptimal temperature was reported to impact significantly RBF and RP transcripts (Sáez-Vásquez and Delseny, 2019). The resulting matrix was quantile normalized using the R package *preprocessCore* (version 1.46.0 - <https://github.com/bmbolstad/preprocessCore>). Afterwards the distribution of the data within treatments and genes was evaluated with density plots for treatments using the R package *ggplot2* (Ginestet, 2011), and a Cullen and Frey graph for ATGs using the R package *fitdistrplus* (Delignette-Muller and Dutang, 2015). Analysis of the distribution patterns determined that a generalized linear model (GLM) was the appropriate statistical test. Accordingly, GLMs were fitted with different link functions to parametrize the mean and variances. Gamma, Lognormal and Gaussian functions were applied. The ranking and significances of resulting *P* values did not differ among link functions, showing the robustness of quantile normalization of data. Significance values were corrected for multiple testing using the false discovery rate (FDR) approach (Benjamini and Hochberg, 1995) and a significance threshold of $P < 0.05$ applied to all analyses.

We selected a test case of RP gene expression in root tissue because this tissue is often neglected in temperature studies, even though root systems of crops are frequently exposed to

temperature extremes (Kaspar and Bland, 1992). Normalized gene expression intensities were divided in 60S and 40S subunit coding genes according to a curated list of the *Arabidopsis* cytosolic ribosomal proteome (**Supplemental Table S1**). Abundances were auto-scaled in order to plot them in a heatmap with equal means and variances (Gu et al., 2014; Gu et al., 2016) (**Figure 3A**). The *Arabidopsis* RP names were used as identifiers in the heatmap to highlight paralog-specific behavior of transcripts. Each ribosomal protein family was scored to belong to one of three response groups. Group (1) was defined as “increased”, if transcripts of one or more paralogs within a RP family were significantly increased. Group (2) was defined as “decreased”, if transcripts of one or more paralogs within a RP family were significantly decreased. Finally, group (3) was defined as “inversely regulated”, if a transcript of at least one paralog was significantly increased and in parallel another paralog of the same RP family was significantly decreased, either under heat or under cold stress (**Figures 3A–C**). To visualize the spatial distribution and location within the 80S ribosome, the increased, decreased, and inversely regulated RP families were mapped onto the previously outlined 3D representation of the 80S wheat monosome (**Figure 2**), applying different color codes to the significantly changed RP families (**Figure 4**). For the mapping PyMOL visualization software (RRID : SCR_000305) was used to obtain a surface representation and to highlight proteins with significant changes. By choice of 2D rotations, emphasis was given to the proteins that are visible from either the interface- or solvent-sides. In the interest of simplifying the image, rRNAs were excluded from the structural representation. The expression patterns were reduced from paralogs in **Figure 3** to RP-family level in **Figure 4** for the sake of visualization and reflect the RP paralog specific behaviors reported in **Supplemental Table S2**.

This meta-analysis adds the new aspect of differential RP paralog usage to the plethora of insights gathered on plant system reprogramming during temperature acclimation at metabolic, transcript or protein levels, e.g. (Scharf and Nover, 1982; Merret et al., 2017; Calixto et al., 2018; Beine-Golovchuk et al., 2018). Considering the significant observations only from this exemplary study, heat shock may induce more changes than cold acclimation (**Figure 3**). The results indicate fundamental temperature-specific reprogramming of RP gene transcription (**Figures 3A, B**) and differential responses among cytosolic RP families under opposing conditions of temperature stress. Focusing on the changes that occur within RP families, we encountered instances of potential temperature-specialized RP paralogs, and, as exemplified by the inversely regulated P1/P2 P-stalk components AtRPP1D and AtRPP1A, even indications of paralog preference under heat stress (**Figures 3C and 4C, D**).

Some of the significant gene expression changes from our test case have been reported and investigated previously. For example, the transcript encoding for eL37 (AtRPL37B) is sequestered into stress granules upon heat stress to be quickly released during stress deacclimation to resume cytosolic ribosome synthesis (Merret et al., 2017). This process limits availability of eL37 (AtRPL37B) transcripts for translation under heat stress. Sequestration into stress granules stores and recycles transcripts and therefore does

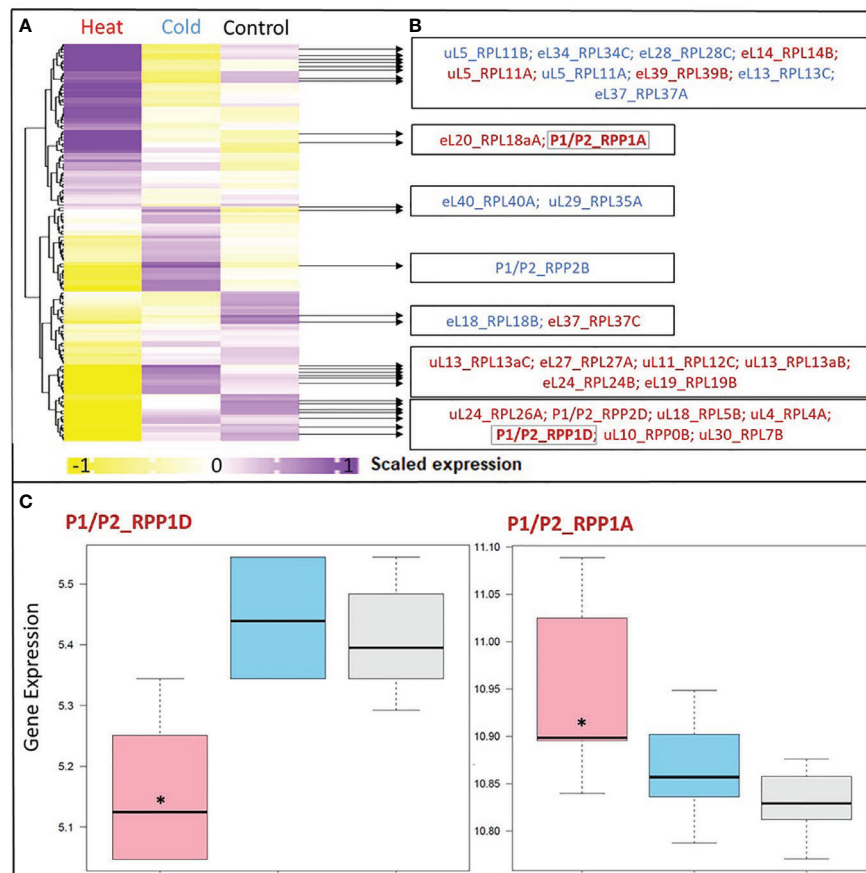


FIGURE 3 | Differential expression in response to temperature stress of Arabidopsis genes encoding structural ribosomal proteins of the 60S subunit. Expression values of 96 40S and 136 60S RPs and RP paralogs were retrieved from Genevestigator experiment AT-00120 of root tissue ($n = 30$) exposed to 38°C heat shock ($n = 6$) or 4°C cold stress ($n = 12$) compared to 20°C control conditions [$n = 12$]. Transcriptome data processing and analysis was carried out in the R programming language and environment for statistical computing, <https://www.R-project.org/> (Ihaka and Gentleman, 1996), using the R project for statistical computing (RRID : SCR_001905). Gene intensities were background subtracted and quantile normalized. **(A)** Heatmap of autoscaled and treatment-scaled abundances ranging from -1 (yellow) to +1 (purple), mean centering was performed by the function `colMeans` with the R package `timeSeries` (version 3042.102; <https://CRAN.R-project.org/package=timeSeries>). Correlation and Euclidean distance produced equivalent heatmaps due to the mode of scaling. R packages `ComplexHeatmap` (Gu et al., 2016), `circlize` (Gu et al., 2014) and `fBasics` (version 3042.89; <https://CRAN.R-project.org/package=fBasics>) were used to transform data and create the Heatmap. The statistical significance of changed gene expression relative to the control was evaluated by a generalized linear model (GLM). **(B)** False discovery rate (FDR)-corrected, significant temperature-responsive transcripts following heat shock (red, 20 genes) or cold stress (blue, 10 genes). One example of inversely regulated expression of two members of a single RP family, i.e., P-stalk components, during heat is highlighted in bold and by a gray outline (*) in panel **C**. **(C)** Boxplots of the highlighted inversely heat responsive transcript abundances of the P1/P2 paralogs RPP1D and RPP1A. Data are \log_2 -transformed, background subtracted, quantile normalized, and non-scaled.

not require changes of total mRNA. Our meta-analysis indicates an additional regulation of the eL37 family at total mRNA level. Significant transcript changes of two different eL37 paralogs, AtRPL37a and AtRPL37c, occur following heat stress and are also part of cold acclimation (Figures 3 and 4).

RP transcript levels of Arabidopsis roots are, however, not necessarily associated with compositional changes of the non-translating ribo-proteome (Cheong et al., 2020). Ribosomes are stable complexes and have a longer half-life as compared to average protein half-lives. Ribosomes may share this property with other multi-protein complexes as plant enzymes embedded in complexes have a significantly longer half-life than free enzymes (Nelson et al., 2013). Mammalian RPs have a longer half-life in the cytoplasm,

where RPs can be considered to be enriched in the ribosome-bound state, as compared to RPs of the nucleolus, where higher fractions of free RPs are expected to support the assembly process (Boisvert et al., 2012). A ribosome half-life range of ~ 72-178 h is reported for normal and regenerating rat liver (Hirsch and Hiatt, 1966; Nikolov et al., 1983). A similar range of 3-4 days was determined for Arabidopsis ribosomes (Salih et al., 2019). Therefore, it can be argued that transcript changes will need to extend over long periods to alter overall RP or RP paralog abundances or, alternatively, transcript changes will only affect the subpopulation of newly synthesized ribosomes. Cytosolic ribosomes may remodel surface accessible RPs upon environmental cues, e.g., by paralog loss and addition or by exchange processes. Such variation may explain why

improvements relative to RNA-seq partly rely on excluding mRNA that is part of inactive transcript pools. Examples of excluded transcripts include those sequestered in stress granules for transient storage or associated with processing bodies and subject to catabolism (Chantarachot and Bailey-Serres, 2018; Lee and Seydoux, 2019), as well as the contribution of the nuclear transcriptome and incompletely spliced pre-mature mRNAs (Lee and Bailey-Serres, 2018). Ultimately, transcript complexity is reduced by more than 50% when polysomal-bound mRNAs are sequenced (Zhang et al., 2015). In essence, Ribosome profiling, aka Ribo-Seq, provides improved insight into the translated transcriptome (Wang and Sachs, 1997; Seidelt et al., 2009; Ishimura et al., 2014; Hou et al., 2016; Matsuo et al., 2017; Yamashita et al., 2017; Zhang et al., 2017).

Additional information that is required to link the actively translated transcriptome to the proteome may be obtained by measuring *de novo* protein synthesis through label-assisted proteomics. Label-assisted proteomic studies monitor the kinetics of label incorporation into proteins, allowing for calculations of protein synthesis and degradation rates at biological steady states (Nelson and Millar, 2015). Under optimized conditions, label incorporation can be used as direct evidence of *de novo* ribosome biosynthesis or remodeling by condition-specific RP paralogs. In the first case, the tracer incorporation into total ribosome complexes can be measured after amino acid hydrolysis and isotope enrichment analysis. These measurements can be used to calculate rates of *de novo* ribosome biosynthesis. In the latter case, calculations of individual RP paralog turnover (Salih et al., 2019) indicate which RPs and RP paralogs are *de novo* synthesized and which paralogs are recycled from pre-existing ribosomes.

Moving beyond biological steady states will be required to reveal whether environmental cues trigger ribosome heterogeneity. To do so, current turnover studies using a metabolic tracer to label RP paralogs have to be refined. The limitations that need to be overcome include intrinsic properties of plant cytosolic ribosomes. First, the unusually high variance of degradation RP rates (Li et al., 2017a) suggests that the stoichiometry of the ribosome complexes or paralog composition may change. Consequently, controls are necessary that verify or detect remodeling and deviations of ribosome complexes from the canonical structure (**Figures 2 and 4**). Second, paralog-resolved ^{15}N -dependent turnover analysis of RPs is possible (Salih et al., 2019; Salih et al., 2020), but the dynamics of label incorporation into soluble amino acids pools need to be taken into account. Environmental stresses including temperature stress affect metabolites and change pool sizes of free amino acids, e.g., (Kaplan et al., 2004). The rate of label incorporation into amino acid monomers will change in response to environmental cues. If the free amino acid pools are not carefully considered, observed differential label incorporation rates into RPs or RP paralogs may be misinterpreted. Third, non-translating and translating fractions of ribosome complexes exist that may harbor different quantities of pre-existing and *de novo* synthesized ribosome. Separation of the diverse pools of ribosome complexes, e.g. (Beine-Golovchuk et al., 2018), will enhance our insight and answer questions on complex

specific or non-specific label incorporation by calculating protein turnover of plant RPs in the non-translating compared to translating ribosomal fractions.

Finally and as a general consideration, functional ribosome heterogeneity research in plants will enhance sustainability in agriculture. Rice and maize are plant models and crops in which ribosome biology is already well understood. In rice, the paralog OsL23A, homolog of AtRPL23A, was shown to positively affect the drought and salt stress responses (Moin et al., 2017). Moreover, ribosome heterogeneity is apparently triggered by environmental stress in rice (Moin et al., 2016; Moin et al., 2017). This observation indicates that ribosome heterogeneity may be generalized. Crops engineered at ribosome level may be of utmost importance for future food security. In maize, the tool box of ribosome profiling has been refined (Chotewutmontri et al., 2018), and insights into translational regulation during drought stress (Lei et al., 2015) and viral infection (Xu et al., 2019) have been gained. RP abundance and phosphorylation status change during germination in maize (Hernández-Hermenegildo et al., 2018) and provide the potential of selective mRNA translation by heterogeneous ribosome populations during seedling development. Similarly, specific clusters of tomato RBFs and RPs are differentially expressed and are characteristics of tissue identity (Simm et al., 2015). These studies indicate the importance of future functional RP studies for diminishing the effects of climate stress on crop production.

SUMMARY

Given the highly variable nature of the plant ribosomal proteome and the availability of many experimental tools in the plant field (Merchante et al., 2017), plants may have extraordinary potential for the study of structural and functional ribosome heterogeneity at RP level. The high number of plant paralogs per RP family compared to other eukaryote models warrants explanation and in depth analysis of potential paralog specialization that can contribute to a plant ribosomal code. Current research indicates that plant ribosome populations are heterogeneous at multiple levels. Deviations of the canonical ribosome structure by substoichiometry, additional interacting proteins, PTMs of rRNA and RPs, or rRNA variants, and by multiple RP paralogs are known. The functional consequence of ribosome heterogeneity, however, is in many cases a matter of debate, but ribosome specialization has been proven in some cases, for instance in the case of the TOR-mediated control of ribosome function by secondary modification of the RPS6 structural protein (Kim et al., 2014; Chowdhury and Köhler, 2015; Dobrenel et al., 2016). A wealth of functional analyses of plant RPs indicates that the structural variation potential of the multiple RPs or paralogs may have functions in plant development and physiology. The involvement of RP paralogs in plant stress physiology is supported by current literature (**Table 2**). Differential gene expression analysis of high versus low temperature responses, where RP gene expression is largely inverted and the balance

between paralogs of RP families can be changed (Figures 3 and 4) supports the notion of plant ribosome specialization.

Ribosomes must translate specific subsets of mRNA species to be considered functionally specialized. The intrinsic potential of ribosome remodeling and *de novo* synthesis to produce ribosome populations adapted to control translation of mRNA subsets needs to be further investigated. Such research has been applied to developmental biology as well as to stress physiology across many model organisms (Bailey-Serres, 1999; Kawaguchi et al., 2004; Branco-Price et al., 2005; Nicolai et al., 2006; Branco-Price et al., 2008; Mustroph et al., 2009; Matsuura et al., 2010; Sormani et al., 2011a; Juntawong and Bailey-Serres, 2012; Moeller et al., 2012; Ueda et al., 2012; Wu et al., 2012; Xue and Barna, 2012; Browning and Bailey-Serres, 2015; Thompson et al., 2016; Jha et al., 2017; Shi et al., 2017; Simsek et al., 2017; Bates et al., 2018; Genuth and Barna, 2018; Guo, 2018; Emmott et al., 2019; Magee and Ware, 2019; Sulima and Dinman, 2019; Yu et al., 2019). However, questions of functional conservation, convergence, or speciation across organism kingdoms remain largely unanswered. Full explanation of a ribosomal code will likely reveal synergies of mechanisms and may require concomitant exchanges of RPs, involvement of ribosome associated factors, changes of rRNA status, PTMs, and ribosome biogenesis or ribosome remodeling. All in all, we hypothesize that all ribosome functions, i.e., ribosome biogenesis, translation initiation, elongation, termination, and recycling, may be affected by ribosome heterogeneity.

DATA AVAILABILITY STATEMENT

Publicly available datasets were analyzed in this study. This data can be found here: Genevestigator, AT-00120.

REFERENCES

- Ahmed, T., Shi, J., and Bhushan, S. (2017). Unique localization of the plastid-specific ribosomal proteins in the chloroplast ribosome small subunit provides mechanistic insights into the chloroplastic translation. *Nucleic Acids Res.* 45, 8581–8595. doi: 10.1093/nar/gkx499
- Albar, L., Bangratz-Reyser, M., Hébrard, E., Ndjondjop, M. N., Jones, M., and Ghesquière, A. (2006). Mutations in the eIF(iso)4G translation initiation factor confer high resistance of rice to Rice yellow mottle virus. *Plant J.* 47, 417–426. doi: 10.1111/j.1365-3113X.2006.02792.x
- Albert, B., Kos-Braun, I. C., Henras, A. K., Dez, C., Rueda, M. P., Zhang, X., et al. (2019). A ribosome assembly stress response regulates transcription to maintain proteome homeostasis. *Elife* 8. doi: 10.7554/eLife.45002
- Armache, J. P., Jarasch, A., Anger, A. M., Villa, E., Becker, T., Bhushan, S., et al. (2010a). Cryo-EM structure and rRNA model of a translating eukaryotic 80S ribosome at 5.5-Å resolution. *Proc. Natl. Acad. Sci. U. S. A.* 107, 19748–19753. doi: 10.1073/pnas.1009999107
- Armache, J. P., Jarasch, A., Anger, A. M., Villa, E., Becker, T., Bhushan, S., et al. (2010b). Localization of eukaryote-specific ribosomal proteins in a 5.5-Å cryo-EM map of the 80S eukaryotic ribosome. *Proc. Natl. Acad. Sci. U. S. A.* 107, 19754–19759. doi: 10.1073/pnas.1010005107
- Armache, J. (2011). *5.5 Å Structure of the Eukaryotic Ribosome* (Ludwig-Maximilians-Universität München).
- Asensi-Fabado, M. A., Amtmann, A., and Perrella, G. (2017). Plant responses to abiotic stress: The chromatin context of transcriptional regulation. *Biochim. Biophys. Acta Gene Regul. Mech.* 1860, 106–122. doi: 10.1016/j.bbagr.2016.07.015

AUTHOR CONTRIBUTIONS

FM-S: Conceptualization, literature research, figure shaping, statistical analyses, structural analysis and mapping, manuscript writing. OB-G: Ribosomal proteome supplement, literature research, figure shaping. Y-CH: Figure shaping, structural analysis and mapping. JK: Conceptualization, literature research, figure shaping, manuscript writing.

FUNDING

We acknowledge the Max-Planck Society (Max Planck Institute of Molecular Plant Physiology) and the University of Melbourne for funding this research via the Melbourne-Potsdam PhD Programme (MelPoPP).

ACKNOWLEDGMENTS

We acknowledge the long-standing support by Prof. Dr. L. Willmitzer, Prof. Dr. M. Stitt, and Prof. Dr. R. Bock (Max-Planck-Institute of Molecular Plant Physiology, Potsdam, Germany).

SUPPLEMENTARY MATERIAL

The Supplementary Material for this article can be found online at: <https://www.frontiersin.org/articles/10.3389/fpls.2020.00948/full#supplementary-material>

- Bailey-Serres, J. (1999). Selective translation of cytoplasmic mRNAs in plants. *Trends Plant Sci.* 4, 142–148. doi: 10.1016/S1360-1385(99)01386-2
- Ban, N., Beckmann, R., Cate, J. H. D., Dinman, J. D., Dragon, F., Ellis, S. R., et al. (2014). A new system for naming ribosomal proteins. *Curr. Opin. Struct. Biol.* 24, 165–169. doi: 10.1016/j.sbi.2014.01.002
- Barakat, A., Szick-Miranda, K., Chang, I. F., Guyot, R., Blanc, G., Cooke, R., et al. (2001). The organization of cytoplasmic ribosomal protein genes in the Arabidopsis genome. *Plant Physiol.* 127, 398–415. doi: 10.1104/pp.010265.398
- Basu, U., Si, K., Warner, J. R., and Maitra, U. (2001). The Saccharomyces cerevisiae TIF6 Gene Encoding Translation Initiation Factor 6 Is Required for 60S Ribosomal Subunit Biogenesis. *Mol. Cell. Biol.* 21, 1453–1462. doi: 10.1128/mcb.21.5.1453-1462.2001
- Bates, C., Hubbard, S. J., and Ashe, M. P. (2018). Ribosomal flavours: An acquired taste for specific mRNAs? *Biochem. Soc Trans.* 46, 1529–1539. doi: 10.1042/BST20180160
- Belouah, I., Nazaret, C., Pétriacq, P., Prigent, S., Bénard, C., Mengin, V., et al. (2019). Modeling protein destiny in developing fruit. *Plant Physiol.* 180, 1709–1724. doi: 10.1104/pp.19.00086
- Benjamini, Y., and Hochberg, Y. (1995). Controlling the False Discovery Rate: A Practical and Powerful Approach to Multiple Testing. *J. R. Stat. Soc. Ser. B* 57, 289–300. doi: 10.1111/j.2517-6161.1995.tb02031.x
- Ben-Shem, A., Jenner, L., Yusupova, G., and Yusupov, M. (2010). Crystal structure of the eukaryotic ribosome. *Science (80-)* 330, 1203–1209. doi: 10.1126/science.1194294
- Ben-Shem, A., De Loubresse, N. G., Melnikov, S., Jenner, L., Yusupova, G., and Yusupov, M. (2011). The structure of the eukaryotic ribosome at 3.0 Å resolution. *Science (80-)* 334, 1524–1529. doi: 10.1126/science.1212642

- Beine-Golovchuk, O., Firmino, A. A. P., Dąbrowska, A., Schmidt, S., Erban, A., Walther, D., et al. (2018). Plant temperature acclimation and growth rely on cytosolic ribosome biogenesis factor homologs. *Plant Physiol.* 176, 2251–2276. doi: 10.1104/pp.17.01448
- Bieri, P., Leibundgut, M., Saurer, M., Boehringer, D., and Ban, N. (2017). The complete structure of the chloroplast 70S ribosome in complex with translation factor pY. *EMBO J.* 36, 475–486. doi: 10.15252/embj.201695959
- Blevins, T., Pontes, O., Pikaard, C. S., and Meins, F. (2009). Heterochromatic siRNAs and DDM1 independently silence aberrant 5S rDNA transcripts in Arabidopsis. *PLoS One* 4. doi: 10.1371/journal.pone.0005932
- Bobik, K., Fernandez, J. C., Hardin, S. R., Ernest, B., Ganusova, E. E., Staton, M. E., et al. (2019). The essential chloroplast ribosomal protein uL15c interacts with the chloroplast RNA helicase ISE2 and affects intercellular trafficking through plasmodesmata. *New Phytol.* 221, 850–865. doi: 10.1111/nph.15427
- Boerema, A. P., Aibara, S., Paul, B., Tobiasson, V., Kimanius, D., Forsberg, B. O., et al. (2018). Structure of the chloroplast ribosome with chl-RRF and hibernation-promoting factor. *Nat. Plants* 4, 212–217. doi: 10.1038/s41477-018-0129-6
- Boisvert, F. M., Ahmad, Y., Gierliński, M., Charrière, F., Lamont, D., Scott, M., et al. (2012). A quantitative spatial proteomics analysis of proteome turnover in human cells. *Mol. Cell. Proteomics* 11. doi: 10.1074/mcp.M111.011429
- Branco-Price, C., Kawaguchi, R., Ferreira, R. B., and Bailey-Serres, J. (2005). Genome-wide analysis of transcript abundance and translation in Arabidopsis seedlings subjected to oxygen deprivation. *Ann. Bot.* 96, 647–660. doi: 10.1093/aob/mci217
- Branco-Price, C., Kaiser, K. A., Jang, C. J. H., Larive, C. K., and Bailey-Serres, J. (2008). Selective mRNA translation coordinates energetic and metabolic adjustments to cellular oxygen deprivation and reoxygenation in Arabidopsis thaliana. *Plant J.* 56, 743–755. doi: 10.1111/j.1365-313X.2008.03642.x
- Brenner, S., Jacob, F., and Meselson, M. (1961). An unstable intermediate carrying information from genes to ribosomes for protein synthesis. *Nature* 190, 576–581. doi: 10.1038/190576a0
- Browning, K. S., and Bailey-Serres, J. (2015). Mechanism of Cytoplasmic mRNA Translation. *Arab. B.* 13, e0176. doi: 10.1199/tab.0176
- Browning, K. S., Webster, C., Roberts, J. K. M., and Ravel, J. M. (1992). Identification of an isozyme form of protein synthesis initiation factor 4F in plants. *J. Biol. Chem.* 267, 10096–10100.
- Byrne, M. E. (2009). A role for the ribosome in development. *Trends Plant Sci.* 14, 512–519. doi: 10.1016/j.tplants.2009.06.009
- Calixto, C. P. G., Guo, W., James, A. B., Tzioutziou, N. A., Entizne, J. C., Panter, P. E., et al. (2018). Rapid and dynamic alternative splicing impacts the Arabidopsis cold response transcriptome[CC-BY]. *Plant Cell* 30, 1424–1444. doi: 10.1105/tpc.18.00177
- Carroll, A. J., Heazlewood, J. L., Ito, J., and Millar, A. H. (2008). Analysis of the Arabidopsis cytosolic ribosome proteome provides detailed insights into its components and their post-translational modification. *Mol. Cell. Proteomics* 7, 347–369. doi: 10.1074/mcp.M700052-MCP200
- Carroll, A. J. (2013). The Arabidopsis cytosolic ribosomal proteome: From form to function. *Front. Plant Sci.* 4, 1–14. doi: 10.3389/fpls.2013.00032
- Casanova-Sáez, R., Candela, H., and Micol, J. L. (2014). Combined haploinsufficiency and purifying selection drive retention of RPL36a paralogs in Arabidopsis. *Sci. Rep.* 4. doi: 10.1038/srep04122
- Chang, I. F., Szick-Miranda, K., Pan, S., and Bailey-Serres, J. (2005). Proteomic characterization of evolutionarily conserved and variable proteins of Arabidopsis cytosolic ribosomes. *Plant Physiol.* 137, 848–862. doi: 10.1104/pp.104.053637
- Chantarachot, T., and Bailey-Serres, J. (2018). Polysomes, stress granules, and processing bodies: A dynamic triumvirate controlling cytoplasmic mRNA fate and function. *Plant Physiol.* 176, 254–269. doi: 10.1104/pp.17.01468
- Chen, Z. J., and Pikaard, C. S. (1997). Epigenetic silencing of RNA polymerase I transcription: A role for DNA methylation and histone modification in nucleolar dominance. *Genes Dev.* 11, 2124–2136. doi: 10.1101/gad.11.16.2124
- Cheong, B. E., Beine-Golovchuk, O., Gorka, M., Ho, W. W. H., Martinez-Seidel, F., Firmino, A. A. P., et al. (2020). Arabidopsis REI-LIKE proteins activate ribosome biogenesis during cold acclimation. *bioRxiv* 2020. doi: 10.1101/2020.02.18.954396
- Chotewutmontri, P., Stiffler, N., Watkins, K. P., and Barkan, A. (2018). “Ribosome profiling in Maize,” in *Methods Mol. Biol.* 1676, 165–183. doi: 10.1007/978-1-4939-7315-6_10
- Chowdhury, T., and Köhler, J. R. (2015). Ribosomal protein S6 phosphorylation is controlled by TOR and modulated by PKA in *Candida albicans*. *Mol. Microbiol.* 98, 384–402. doi: 10.1111/mmi.13130
- Copenhaver, G. P., and Pikaard, C. S. (1996). Two-dimensional RFLP analyses reveal megabase-sized clusters of rRNA gene variants in *Arabidopsis thaliana*, suggesting local spreading of variants as the mode for gene homogenization during concerted evolution. *Plant J.* 9, 273–282. doi: 10.1046/j.1365-313X.1996.09020273.x
- Creff, A., Sormani, R., and Desnos, T. (2010). The two Arabidopsis RPS6 genes, encoding for cytoplasmic ribosomal proteins S6, are functionally equivalent. *Plant Mol. Biol.* 73, 533–546. doi: 10.1007/s11103-010-9639-y
- Crick, F. H. (1958). On protein synthesis. *Symp. Soc. Exp. Biol.* 12, 138–163.
- Crick, F. (1970). Central dogma of molecular biology. *Nature* 227, 561–563. doi: 10.1038/227561a0
- Degenhardt, R. F., and Bonham-Smith, P. C. (2008a). Arabidopsis ribosomal proteins RPL23aA and RPL23aB are differentially targeted to the nucleolus and are separately required for normal development. *Plant Physiol.* 147, 128–142. doi: 10.1104/pp.107.111799
- Degenhardt, R. F., and Bonham-Smith, P. C. (2008b). Transcript profiling demonstrates absence of dosage compensation in Arabidopsis following loss of a single RPL23a paralog. *Planta* 228, 627–640. doi: 10.1007/s00425-008-0765-6
- Delignette-Muller, M. L., and Dutang, C. (2015). fitdistrplus: An R package for fitting distributions. *J. Stat. Software* 64, 1–34. doi: 10.18637/jss.v064.i04
- Devis, D., Firth, S. M., Liang, Z., and Byrne, M. E. (2015). Dosage sensitivity of RPL9 and concerted evolution of ribosomal protein genes in plants. *Front. Plant Sci.* 6, 1102. doi: 10.3389/fpls.2015.01102
- Dobrenel, T., Mancera-Martinez, E., Forzani, C., Azzopardi, M., Davanture, M., Moreau, M., et al. (2016). The Arabidopsis TOR kinase specifically regulates the expression of nuclear genes coding for plastidic ribosomal proteins and the phosphorylation of the cytosolic ribosomal protein S6. *Front. Plant Sci.* 7, 1611. doi: 10.3389/fpls.2016.01611
- Dunham, I. (2005). Chromosomes 21 and 22: Comparisons. *Encycl. Life Sci.* doi: 10.1038/npg.els.0005015
- Emmott, E., Jovanovic, M., and Slavov, N. (2019). Approaches for Studying Ribosome Specialization. *Trends Biochem. Sci.* 44, 478–479. doi: 10.1016/j.tibs.2019.01.008
- Emmott, E., Jovanovic, M., and Slavov, N. (2018). Ribosome stoichiometry: from form to function. *Peer J Prepr.* 141. doi: 10.1111/evo.13504
- Falcone Ferreyra, M. L., Casadevall, R., Luciani, M. D., Pezza, A., and Casati, P. (2013). New evidence for differential roles of L10 ribosomal proteins from Arabidopsis. *Plant Physiol.* 163, 378–391. doi: 10.1104/pp.113.223222
- Ferretti, M. B., and Karbstein, K. (2019). Does functional specialization of ribosomes really exist? *Rna* 25, 521–538. doi: 10.1261/rna.069823.118
- Ferretti, M. B., Ghalei, H., Ward, E. A., Potts, E. L., and Karbstein, K. (2017). Rps26 directs mRNA-specific translation by recognition of Kozak sequence elements. *Nat. Struct. Mol. Biol.* 24, 700–707. doi: 10.1038/nsmb.3442
- Ferreyra, M. L. F., Pezza, A., Biarc, J., Burlingame, A. L., and Casati, P. (2010). Plant L10 ribosomal proteins have different roles during development and translation under ultraviolet-B stress. *Plant Physiol.* 153, 1878–1894. doi: 10.1104/pp.110.157057
- Fransz, P., De Jong, J. H., Lysak, M., Castiglione, M. R., and Schubert, I. (2002). Interphase chromosomes in Arabidopsis are organized as well defined chromocenters from which euchromatin loops emanate. *Proc. Natl. Acad. Sci. U. S. A.* 99, 14584–14589. doi: 10.1073/pnas.212325299
- Fujikura, U., Horiguchi, G., Ponce, M. R., Micol, J. L., and Tsukaya, H. (2009). Coordination of cell proliferation and cell expansion mediated by ribosome-related processes in the leaves of Arabidopsis thaliana. *Plant J.* 59, 499–508. doi: 10.1111/j.1365-313X.2009.03886.x
- Gadal, O., Strauss, D., Petfalski, E., Gleizes, P. E., Gas, N., Tollervey, D., et al. (2002). Rlp7p is associated with 60S preribosomes, restricted to the granular component of the nucleolus, and required for pre-rRNA processing. *J. Cell Biol.* 157, 941–951. doi: 10.1083/jcb.200111039

- Gallie, D. R. (2016). Eukaryotic initiation factor eIFiso4G1 and eIFiso4G2 are isoforms exhibiting distinct functional differences in supporting translation in Arabidopsis. *J. Biol. Chem.* 291, 1501–1513. doi: 10.1074/jbc.M115.692939
- Gamalinda, M., Jakovljevic, J., Babiano, R., Talkish, J., De La Cruz, J., and Woolford, J. L. (2013). Yeast polypeptide exit tunnel ribosomal proteins L17, L35 and L37 are necessary to recruit late-assembling factors required for 27SB pre-rRNA processing. *Nucleic Acids Res.* 41, 1965–1983. doi: 10.1093/nar/gks1272
- Gamm, M., Peviani, A., Honsel, A., Snel, B., Smeekens, S., and Hanson, J. (2014). Increased sucrose levels mediate selective mRNA translation in Arabidopsis. *BMC Plant Biol.* 14, 306. doi: 10.1186/s12870-014-0306-3
- Garcia, I., Arenas-Alfonseca, L., Moreno, I., Gotor, C., and Romero, L. C. (2019). HCN regulates cellular processes through posttranslational modification of proteins by s-cyanylation. *Plant Physiol.* 179, 107–123. doi: 10.1104/pp.18.01083
- Genuth, N. R., and Barna, M. (2018). Heterogeneity and specialized functions of translation machinery: From genes to organisms. *Nat. Rev. Genet.* 19, 431–452. doi: 10.1038/s41576-018-0008-z
- Gerst, J. E. (2018). Pimp My Ribosome: Ribosomal Protein Paralogs Specify Translational Control. *Trends Genet.* 34, 832–845. doi: 10.1016/j.tig.2018.08.004
- Giavalisco, P., Wilson, D., Kreitler, T., Lehrach, H., Klose, J., Gobom, J., et al. (2005). High heterogeneity within the ribosomal proteins of the Arabidopsis thaliana 80S ribosome. *Plant Mol. Biol.* 57, 577–591. doi: 10.1007/s11103-005-0699-3
- Ginestet, C. (2011). ggplot2: Elegant Graphics for Data Analysis. *J. R. Stat. Soc. Ser. A (Statistics Soc)* 174, 245–246. doi: 10.1111/j.1467-985x.2010.00676_9.x
- Gong, X., Jiang, Q., Xu, J., Zhang, J., Teng, S., Lin, D., et al. (2013). Disruption of the rice plastid ribosomal protein S20 leads to chloroplast developmental defects and seedling lethality. *G3 Genes Genomes Genet.* 3, 1769–1777. doi: 10.1534/g3.113.007856
- Graf, M., Arenz, S., Huter, P., Dönhöfer, A., Nováček, J., and Wilson, D. N. (2017). Cryo-EM structure of the spinach chloroplast ribosome reveals the location of plastid-specific ribosomal proteins and extensions. *Nucleic Acids Res.* 45, 2887–2896. doi: 10.1093/nar/gkx1272
- Grandi, P., Rybin, V., Baßler, J., Pefalski, E., Strauß, D., Marzioch, M., et al. (2002). 90S pre-ribosomes include the 35S pre-rRNA, the U3 snoRNP, and 40S subunit processing factors but predominantly lack 60S synthesis factors. *Mol. Cell* 10, 105–115. doi: 10.1016/S1097-2765(02)00579-8
- Greber, B. J., Gerhardt, S., Leitner, A., Leibundgut, M., Salem, M., Boehringer, D., et al. (2016). Insertion of the Biogenesis Factor Rei1 Probes the Ribosomal Tunnel during 60S Maturation. *Cell* 164, 91–102. doi: 10.1016/j.cell.2015.11.027
- Gu, Z., Gu, L., Eils, R., Schlesner, M., and Brors, B. (2014). Circize implements and enhances circular visualization in R. *Bioinformatics* 30, 2811–2812. doi: 10.1093/bioinformatics/btu393
- Gu, Z., Eils, R., and Schlesner, M. (2016). Complex heatmaps reveal patterns and correlations in multidimensional genomic data. *Bioinformatics* 32, 2847–2849. doi: 10.1093/bioinformatics/btw313
- Gunderson, J. H., Sogin, M. L., Wollett, G., Hollingdale, M., De La Cruz, V. F., Waters, A. P., et al. (1987). Structurally distinct, stage-specific ribosomes occur in Plasmodium. *Science (80-)* 238, 933–937. doi: 10.1126/science.3672135
- Guo, J., and Chen, J. G. (2008). RACK1 genes regulate plant development with unequal genetic redundancy in Arabidopsis. *BMC Plant Biol.* 8, 108. doi: 10.1186/1471-2229-8-108
- Guo, H. (2018). Specialized ribosomes and the control of translation. *Biochem. Soc Trans.* 46, 855–869. doi: 10.1042/BST20160426
- Haag, E. S., and Dinman, J. D. (2019). Still Searching for Specialized Ribosomes. *Dev. Cell* 48, 744–746. doi: 10.1016/j.devcel.2019.03.005
- Hernández-Hermenegildo, R. A., Bernal, L., Jiménez-Pérez, L. V., Bernal-Lugo, I., and de Jiménez, E. S. (2018). Ribosomal Heterogeneity of Maize Tissues: Insights of Biological Relevance. *Plant Mol. Biol. Rep.* 36, 491–499. doi: 10.1007/s11105-018-1080-4
- Hirsch, C. A., and Hiatt, H. H. (1966). Turnover of liver ribosomes in fed and in fasted rats. *J. Biol. Chem.* 241, 5936–5940.
- Horiguchi, G., Mollá-Morales, A., Pérez-Pérez, J. M., Kojima, K., Robles, P., Ponce, M. R., et al. (2011). Differential contributions of ribosomal protein genes to Arabidopsis thaliana leaf development. *Plant J.* 65, 724–736. doi: 10.1111/j.1365-313X.2010.04457.x
- Horiguchi, G., Van Lijsebettens, M., Candela, H., Micol, J. L., and Tsukaya, H. (2012). Ribosomes and translation in plant developmental control. *Plant Sci.* 191–192, 24–34. doi: 10.1016/j.plantsci.2012.04.008
- Hou, C. Y., Lee, W. C., Chou, H. C., Chen, A. P., Chou, S. J., and Chen, H. M. (2016). Global analysis of truncated RNA ends reveals new insights into Ribosome Stalling in plants. *Plant Cell* 28, 2398–2416. doi: 10.1105/tpc.16.00295
- Hsu, P. Y., Calviello, L., Wu, H. Y. L., Li, F. W., Rothfels, C. J., Ohler, U., et al. (2016). Super-resolution ribosome profiling reveals unannotated translation events in Arabidopsis. *Proc. Natl. Acad. Sci. U. S. A.* 113, E7126–E7135. doi: 10.1073/pnas.1614788113
- Hummel, M., Cordewener, J. H. G., de Groot, J. C. M., Smeekens, S., America, A. H. P., and Hanson, J. (2012). Dynamic protein composition of Arabidopsis thaliana cytosolic ribosomes in response to sucrose feeding as revealed by label free MS E proteomics. *Proteomics* 12, 1024–1038. doi: 10.1002/pmic.201100413
- Hummel, M., Dobrenel, T., Cordewener, J. H. G., Davanture, M., Meyer, C., Smeekens, S. J. C. M., et al. (2015). Proteomic LC-MS analysis of Arabidopsis cytosolic ribosomes: Identification of ribosomal protein paralogs and re-annotation of the ribosomal protein genes. *J. Proteomics* 128, 436–449. doi: 10.1016/j.jprot.2015.07.004
- Ihaka, R., and Gentleman, R. (1996). R: A Language for Data Analysis and Graphics. *J. Comput. Graph. Stat.* 5, 299–314. doi: 10.1080/10618600.1996.10474713
- Imai, A., Komura, M., Kawano, E., Kuwashiro, Y., and Takahashi, T. (2008). A semi-dominant mutation in the ribosomal protein L10 gene suppresses the dwarf phenotype of the ac15 mutant in Arabidopsis thaliana. *Plant J.* 56, 881–890. doi: 10.1111/j.1365-313X.2008.03647.x
- Inglis, A. J., Masson, G. R., Shao, S., Perisic, O., McLaughlin, S. H., Hegde, R. S., et al. (2019). Activation of GCN2 by the ribosomal P-stalk. *Proc. Natl. Acad. Sci. U. S. A.* 116, 4946–4954. doi: 10.1073/pnas.1813352116
- Ingolia, N. T., Ghaemmaghami, S., Newman, J. R. S., and Weissman, J. S. (2009). Genome-wide analysis in vivo of translation with nucleotide resolution using ribosome profiling. *Science (80-)* 324, 218–223. doi: 10.1126/science.1168978
- Ingolia, N. T., Hussmann, J. A., and Weissman, J. S. (2019). Ribosome profiling: Global views of translation. *Cold Spring Harb. Perspect. Biol.* 11, 1–20. doi: 10.1101/cshperspect.a032698
- Ishimura, R., Nagy, G., Dotu, I., Zhou, H., Yang, X. L., Schimmel, P., et al. (2014). Ribosome stalling induced by mutation of a CNS-specific tRNA causes neurodegeneration. *Science (80-)* 345, 455–459. doi: 10.1126/science.1249749
- Islas-Flores, T., Rahman, A., Ullah, H., and Villanueva, M. A. (2015). The receptor for activated C kinase in plant signaling: Tale of a promiscuous little molecule. *Front. Plant Sci.* 6, 1090. doi: 10.3389/fpls.2015.01090
- Ito, T., Kim, G. T., and Shinozaki, K. (2000). Disruption of an Arabidopsis cytoplasmic ribosomal protein S13-homologous gene by transposon-mediated mutagenesis causes aberrant growth and development. *Plant J.* 22, 257–264. doi: 10.1046/j.1365-313X.2000.00728.x
- Jarvis, P., and López-Juez, E. (2013). Biogenesis and homeostasis of chloroplasts and other plastids. *Nat. Rev. Mol. Cell Biol.* 14, 787–802. doi: 10.1038/nrm3702
- Jensen, P. E., and Leister, D. (2014). Chloroplast evolution, structure and functions. *F1000Prime Rep.* 6. doi: 10.12703/P6-40
- Jha, S., Rollins, M. G., Fuchs, G., Procter, D. J., Hall, E. A., Cozzolino, K., et al. (2017). Trans-kingdom mimicry underlies ribosome customization by a poxvirus kinase. *Nature* 546, 651–655. doi: 10.1038/nature22814
- Juntawong, P., and Bailey-Serres, J. (2012). Dynamic light regulation of translation status in Arabidopsis thaliana. *Front. Plant Sci.* 3, 66. doi: 10.3389/fpls.2012.00066
- Juntawong, P., Hummel, M., Bazin, J., and Bailey-Serres, J. (2015). “Ribosome profiling: a tool for quantitative evaluation of dynamics in mRNA translation,” in *Methods Mol. Biol. (Clifton N.J.)* 1284, 139–173. doi: 10.1007/978-1-4939-2444-8_7
- Takehi, J.II, Kawano, E., Yoshimoto, K., Cai, Q., Imai, A., and Takahashi, T. (2015). Mutations in ribosomal proteins, RPL4 and RACK1, suppress the phenotype of a thermopermine-deficient mutant of Arabidopsis thaliana. *PLoS One* 10. doi: 10.1371/journal.pone.0117309

- Kaplan, F., Kopka, J., Haskell, D. W., Zhao, W., Schiller, K. C., Gatzke, N., et al. (2004). Exploring the temperature-stress metabolome of Arabidopsis. *Plant Physiol.* 136, 4159–4168. doi: 10.1104/pp.104.052142
- Kaspar, T. C., and Bland, W. L. (1992). Soil temperature and root growth. *Soil Sci.* 154, 290–299. doi: 10.1097/00010694-199210000-00005
- Kawaguchi, R., Girke, T., Bray, E. A., and Bailey-Serres, J. (2004). Differential mRNA translation contributes to gene regulation under non-stress and dehydration stress conditions in Arabidopsis thaliana. *Plant J.* 38, 823–839. doi: 10.1111/j.1365-313X.2004.02090.x
- Kim, Y. K., Kim, S., Shin, Y. J., Hur, Y. S., Kim, W. Y., Lee, M. S., et al. (2014). Ribosomal protein s6, a target of rapamycin, is involved in the regulation of rRNA genes by possible epigenetic changes in Arabidopsis. *J. Biol. Chem.* 289, 3901–3912. doi: 10.1074/jbc.M113.515015
- Kim, D. H., Lee, J. E., Xu, Z. Y., Geem, K. R., Kwon, Y., Park, J. W., et al. (2015). Cytosolic targeting factor AKR2A captures chloroplast outer membrane-localized client proteins at the ribosome during translation. *Nat. Commun.* 6, 1–13. doi: 10.1038/ncomms7843
- Komili, S., Farny, N. G., Roth, F. P., and Silver, P. A. (2007). Functional Specificity among Ribosomal Proteins Regulates Gene Expression. *Cell* 131, 557–571. doi: 10.1016/j.cell.2007.08.037
- Kressler, D., Hurt, E., and Baßler, J. (2017). A Puzzle of Life: Crafting Ribosomal Subunits. *Trends Biochem. Sci.* 42, 640–654. doi: 10.1016/j.tibs.2017.05.005
- Kurylo, C. M., Parks, M. M., Juette, M. F., Zinshteyn, B., Altman, R. B., Thibado, J. K., et al. (2018). Endogenous rRNA Sequence Variation Can Regulate Stress Response Gene Expression and Phenotype. *Cell Rep.* 25, 236–248.e6. doi: 10.1016/j.celrep.2018.08.093
- Kyritsis, K. A., Angelis, L., Ouzounis, C., and Vizirianakis, I. (2019). “Understanding Specialized Ribosomal Protein Functions and Associated Ribosomopathies by Navigating Across Sequence, Literature, and Phenotype Information Resources.” in *Leveraging Biomed. Healthc. Data* 1284, 35–51. doi: 10.1016/b978-0-12-809556-0.00003-4
- Lange, H., Sement, F. M., and Gagliardi, D. (2011). MTR4, a putative RNA helicase and exosome co-factor, is required for proper rRNA biogenesis and development in Arabidopsis thaliana. *Plant J.* 68, 51–63. doi: 10.1111/j.1365-313X.2011.04675.x
- Lee, T. A., and Bailey-Serres, J. (2018). Lighting the shadows: methods that expose nuclear and cytoplasmic gene regulatory control. *Curr. Opin. Biotechnol.* 49, 29–34. doi: 10.1016/j.copbio.2017.07.010
- Lee, C. Y., and Seydoux, G. (2019). Dynamics of mRNA entry into stress granules. *Nat. Cell Biol.* 21, 116–117. doi: 10.1038/s41556-019-0278-5
- Lee, J., Jang, S., Ryu, S., Lee, S., Park, J., Lee, S., et al. (2019). Mutation of plastid ribosomal protein L13 results in an albino seedling-lethal phenotype in rice. *Plant Breed. Biotechnol.* 7, 395–404. doi: 10.9787/PBB.2019.7.4.395
- Lei, L., Shi, J., Chen, J., Zhang, M., Sun, S., Xie, S., et al. (2015). Ribosome profiling reveals dynamic translational landscape in maize seedlings under drought stress. *Plant J.* 84, 1206–1208. doi: 10.1111/tj.13073
- Li, R., Sun, R., Hicks, G. R., and Raikhel, N. V. (2015). Arabidopsis ribosomal proteins control vacuole trafficking and developmental programs through the regulation of lipid metabolism. *Proc. Natl. Acad. Sci. U. S. A.* 112, E89–E98. doi: 10.1073/pnas.1422656112
- Li, L., Nelson, C. J., Trösch, J., Castleden, I., Huang, S., and Millar, A. H. (2017a). Protein degradation rate in Arabidopsis thaliana leaf growth and development. *Plant Cell* 29, 207–228. doi: 10.1105/tpc.16.00768
- Li, X., Cai, W., Liu, Y., Li, H., Fu, L., Liu, Z., et al. (2017b). Differential TOR activation and cell proliferation in Arabidopsis root and shoot apices. *Proc. Natl. Acad. Sci. U. S. A.* 114, 2765–2770. doi: 10.1073/pnas.1618782114
- Lin, D., Jiang, Q., Zheng, K., Chen, S., Zhou, H., Gong, X., et al. (2015). Mutation of the rice ASL2 gene encoding plastid ribosomal protein L21 causes chloroplast developmental defects and seedling death. *Plant Biol.* 17, 599–607. doi: 10.1111/plb.12271
- Liu, X., Yang, J., Qian, B., Cai, Y., Zou, X., Zhang, H., et al. (2018). MoYvh1 subverts rice defense through functions of ribosomal protein MoMrt4 in Magnaporthe oryzae. *PLoS Pathog.* 14, doi: 10.1371/journal.ppat.1007016
- Luo, A., Zhan, H., Zhang, X., Du, H., Zhang, Y., and Peng, X. (2020). Cytoplasmic ribosomal protein L14B is essential for fertilization in Arabidopsis. *Plant Sci.* 292, 110394. doi: 10.1016/j.plantsci.2019.110394
- Ma, Z., and Dooner, H. K. (2004). A mutation in the nuclear-encoded plastid ribosomal protein S9 leads to early embryo lethality in maize. *Plant J.* 37, 92–103. doi: 10.1046/j.1365-313X.2003.01942.x
- Ma, C., Wu, S., Li, N., Chen, Y., Yan, K., Li, Z., et al. (2017). Structural snapshot of cytoplasmic pre-60S ribosomal particles bound by Nmd3, Lsg1, Tif6 and Reh1. *Nat. Struct. Mol. Biol.* 24, 214–220. doi: 10.1038/nsmb.3364
- Magee, C. M., and Ware, V. C. (2019). Specialized eRPL22 paralogue-specific ribosomes regulate specific mRNA translation in spermatogenesis in Drosophila melanogaster. *Mol. Biol. Cell* 30, 2240–2253. doi: 10.1091/mbc.E19-02-0086
- Matsuo, Y., Ikeuchi, K., Saeki, Y., Iwasaki, S., Schmidt, C., Udagawa, T., et al. (2017). Ubiquitination of stalled ribosome triggers ribosome-associated quality control. *Nat. Commun.* 8, 1–13. doi: 10.1038/s41467-017-00188-1
- Matsuura, H., Ishibashi, Y., Shinmyo, A., Kanaya, S., and Kato, K. (2010). Genome-wide analyses of early translational responses to elevated temperature and high salinity in Arabidopsis thaliana. *Plant Cell Physiol.* 51, 448–462. doi: 10.1093/pcp/pcq010
- Merchante, C., Stepanova, A. N., and Alonso, J. M. (2017). Translation regulation in plants: an interesting past, an exciting present and a promising future. *Plant J.* 90, 628–653. doi: 10.1111/tj.13520
- Merret, R., Carpentier, M. C., Favory, J. J., Picart, C., Descombin, J., Bousquet-Antonelli, C., et al. (2017). Heat shock protein HSP101 affects the release of ribosomal protein mRNAs for recovery after heat shock. *Plant Physiol.* 174, 1216–1225. doi: 10.1104/pp.17.00269
- Meyer, A. E., Hoover, L. A., and Craig, E. A. (2010). The cytosolic J-protein, Jjj1, and Re1 function in the removal of the Pre-60 S subunit factor Arx1. *J. Biol. Chem.* 285, 961–968. doi: 10.1074/jbc.M109.038349
- Moeller, J. R., Moscou, M. J., Bancroft, T., Skadsen, R. W., Wise, R. P., and Whitham, S. A. (2012). Differential accumulation of host mRNAs on polyribosomes during obligate pathogen-plant interactions. *Mol. Biosyst.* 8, 2153–2165. doi: 10.1039/c2mb25014d
- Mohannath, G., Pontvianne, F., and Pikaard, C. S. (2016). Selective nucleolus organizer inactivation in Arabidopsis is a chromosome position-effect phenomenon. *Proc. Natl. Acad. Sci. U. S. A.* 113, 13426–13431. doi: 10.1073/pnas.1608140113
- Moin, M., Bakshi, A., Saha, A., Dutta, M., Madhav, S. M., and Kirti, P. B. (2016). Rice ribosomal protein large subunit genes and their spatio-temporal and stress regulation. *Front. Plant Sci.* 7, 1284. doi: 10.3389/fpls.2016.01284
- Moin, M., Bakshi, A., Madhav, M. S., and Kirti, P. B. (2017). Expression profiling of ribosomal protein gene family in dehydration stress responses and characterization of transgenic rice plants overexpressing RPL23A for water-use efficiency and tolerance to drought and salt stresses. *Front. Chem.* 5, 97. doi: 10.3389/fchem.2017.00097
- Morimoto, T., Suzuki, Y., and Yamaguchi, I. (2002). Effects of partial suppression of ribosomal protein S6 on organ formation in Arabidopsis. *Biosci. Biotechnol. Biochem.* 66, 2437–2443. doi: 10.1271/bbb.66.2437
- Murata, M., Heslop-Harrison, J. S., and Motoyoshi, F. (1997). Physical mapping of the 5S ribosomal RNA genes in Arabidopsis thaliana by multi-color fluorescence in situ hybridization with cosmid clones. *Plant J.* 12, 31–37. doi: 10.1046/j.1365-313X.1997.12010031.x
- Mustroph, A., Zanetti, M. E., Jang, C. J. H., Holtan, H. E., Repetti, P. P., Galbraith, D. W., et al. (2009). Profiling translomes of discrete cell populations resolves altered cellular priorities during hypoxia in Arabidopsis. *Proc. Natl. Acad. Sci. U. S. A.* 106, 18843–18848. doi: 10.1073/pnas.0906131106
- Nagaraj, S., Senthil-Kumar, M., Ramu, V. S., Wang, K., and Mysore, K. S. (2016). Plant ribosomal proteins, RPL12 and RPL19, play a role in nonhost disease resistance against bacterial pathogens. *Front. Plant Sci.* 6, 1192. doi: 10.3389/fpls.2015.01192
- Natchiar, S. K., Myasnikov, A. G., Kratzat, H., Hazemann, I., and Klaholz, B. P. (2017). Visualization of chemical modifications in the human 80S ribosome structure. *Nature* 551, 472–477. doi: 10.1038/nature24482
- Nelson, C. J., and Millar, A. H. (2015). Protein turnover in plant biology. *Nat. Plants* 1, 1–7. doi: 10.1038/nplants.2015.17
- Nelson, C. J., Li, L., Jacoby, R. P., and Millar, A. H. (2013). Degradation rate of mitochondrial proteins in Arabidopsis thaliana cells. *J. Proteome Res.* 12, 3449–3459. doi: 10.1021/pr400304r
- Nicolaï, M., Roncato, M. A., Canoy, A. S., Rouquié, D., Sarda, X., Freyssinet, G., et al. (2006). Large-scale analysis of mRNA translation states during sucrose

- starvation in Arabidopsis cells identifies cell proliferation and chromatin structure as targets of translational control. *Plant Physiol.* 141, 663–673. doi: 10.1104/pp.106.079418
- Nikolov, E. N., Dabeva, M. D., and Nikolov, T. K. (1983). Turnover of ribosomes in regenerating rat liver. *Int. J. Biochem.* 15, 1255–1260. doi: 10.1016/0020-711X(83)90215-X
- Nishimura, T., Wada, T., Yamamoto, K. T., and Okada, K. (2005). The Arabidopsis STV1 protein, responsible for translation reinitiation, is required for auxin-mediated gynoecium patterning. *Plant Cell* 17, 2940–2953. doi: 10.1105/tpc.105.036533
- Palm, D., Streit, D., Shanmugam, T., Weis, B. L., Ruprecht, M., Simm, S., et al. (2019). Plant-specific ribosome biogenesis factors in Arabidopsis thaliana with essential function in rRNA processing. *Nucleic Acids Res.* 47, 1880–1895. doi: 10.1093/nar/gky1261
- Park, S. H., Chung, M. S., Lee, S., Lee, K. H., and Kim, C. S. (2017). Loss of Ribosomal Protein L24A (RPL24A) suppresses proline accumulation of Arabidopsis thaliana ring zinc finger 1 (atrzf1) mutant in response to osmotic stress. *Biochem. Biophys. Res. Commun.* 494, 499–503. doi: 10.1016/j.bbrc.2017.10.092
- Pinon, V., Etschells, J. P., Rossignol, P., Collier, S. A., Arroyo, J. M., Martienssen, R. A., et al. (2008). Three PIGGYBACK genes that specifically influence leaf patterning encode ribosomal proteins. *Development* 135, 1315–1324. doi: 10.1242/dev.016469
- Pocza, P., Cernák, I., Varga, I., and Hyvönen, J. (2014). Analysis of the genome sequence of the flowering plant Arabidopsis thaliana. *Genet. Resour. Crop Evol.* 61, 796–815. doi: 10.1134/S1022795411020074
- Popescu, S. C., and Tumer, N. E. (2004). Silencing of ribosomal protein L3 genes in *N. tabacum* reveals coordinate expression and significant alterations in plant growth, development and ribosome biogenesis. *Plant J.* 39, 29–44. doi: 10.1111/j.1365-313X.2004.02109.x
- Popova, A. M., and Williamson, J. R. (2014). Quantitative analysis of rRNA modifications using stable isotope labeling and mass spectrometry. *J. Am. Chem. Soc.* 136, 2058–2069. doi: 10.1021/ja412084b
- Pulido, P., Zagari, N., Manavski, N., Gawroński, P., Matthes, A., Scharff, L. B., et al. (2018). CHLOROPLAST RIBOSOME ASSOCIATED supports translation under stress and interacts with the ribosomal 30S subunit. *Plant Physiol.* 177, 1539–1554. doi: 10.1104/pp.18.00602
- Qiu, Z., Chen, D., He, L., Zhang, S., Yang, Z., Zhang, Y., et al. (2018). The rice white green leaf 2 gene causes defects in chloroplast development and affects the plastid ribosomal protein S9. *Rice* 11, 1–12. doi: 10.1186/s12284-018-0233-2
- Ramagopal, S. (1990). Induction of cell-specific ribosomal proteins in aggregation-competent nonmorphogenetic Dictyostelium discoideum. *Biochem. Cell Biol.* 68, 1281–1287. doi: 10.1139/o90-190
- Reiland, S., Messerli, G., Baerenfaller, K., Gerrits, B., Endler, A., Grossmann, J., et al. (2009). Large-scale Arabidopsis phosphoproteome profiling reveals novel chloroplast kinase substrates and phosphorylation networks [w]. *Plant Physiol.* 150, 889–903. doi: 10.1104/pp.109.138677
- Revenkova, E., Masson, J., Koncz, C., Afsar, K., Jakovleva, L., and Paszkowski, J. (1999). Involvement of Arabidopsis thaliana ribosomal protein S27 in mRNA degradation triggered by genotoxic stress. *EMBO J.* 18, 490–499. doi: 10.1093/emboj/18.2.490
- Robles, P., and Quesada, V. (2017). Emerging roles of mitochondrial ribosomal proteins in plant development. *Int. J. Mol. Sci.* 18, 2595. doi: 10.3390/ijms18122595
- Romani, I., Tadini, L., Rossi, F., Masiero, S., Pribil, M., Jahns, P., et al. (2012). Versatile roles of Arabidopsis plastid ribosomal proteins in plant growth and development. *Plant J.* 72, 922–934. doi: 10.1111/tpj.12000
- Rosado, A., Sohn, E. J., Drakakaki, G., Pan, S., Swidergal, A., Xiong, Y., et al. (2010). Auxin-mediated ribosome biogenesis regulates vacuolar trafficking in Arabidopsis. *Plant Cell* 22, 143–158. doi: 10.1105/tpc.109.068320
- Rosado, A., Li, R., Van De Ven, W., Hsu, E., and Raikhel, N. V. (2012). Arabidopsis ribosomal proteins control developmental programs through translational regulation of auxin response factors. *Proc. Natl. Acad. Sci. U. S. A.* 109, 19537–19544. doi: 10.1073/pnas.1214774109
- Roy, B., and von Arnim, A. G. (2013). Translational Regulation of Cytoplasmic mRNAs. *Arab. B.* 11, e0165. doi: 10.1199/tab.0165
- Rugen, N., Straube, H., Franken, L. E., Braun, H. P., and Eubel, H. (2019). Complexome profiling reveals association of PPR proteins with ribosomes in the mitochondria of plants. *Mol. Cell. Proteomics* 18, 1345–1362. doi: 10.1074/mcp.RA119.001396
- Sáez-Vásquez, J., and Delseny, M. (2019). Ribosome biogenesis in plants: From functional 45S ribosomal DNA organization to ribosome assembly factors. *Plant Cell* 31, 1945–1967. doi: 10.1105/TPC.18.00874
- Sáez-Vásquez, J., and Echeverría, M. (2007). “Polymerase I Transcription,” in *Regul. Transcription Plants* 29, 162–183. doi: 10.1002/9780470988886.ch7
- Sáez-Vásquez, J., Caparros-Ruiz, D., Barneche, F., and Echeverría, M. (2004). A Plant snoRNP Complex Containing snoRNAs, Fibrillarin, and Nucleolin-Like Proteins Is Competent for both rRNA Gene Binding and Pre-rRNA Processing In Vitro. *Mol. Cell. Biol.* 24, 7284–7297. doi: 10.1128/mcb.24.16.7284-7297.2004
- Saha, A., Das, S., Moin, M., Dutta, M., Bakshi, A., Madhav, M. S., et al. (2017). Genome-wide identification and comprehensive expression profiling of ribosomal protein small subunit (RPS) genes and their comparative analysis with the large subunit (RPL) genes in rice. *Front. Plant Sci.* 8, 1553. doi: 10.3389/fpls.2017.01553
- Salih, K. J., Duncan, O., Li, L., Troesch, J., and Millar, A. H. (2019). Refining the composition of the Arabidopsis thaliana 80S cytosolic ribosome. *bioRxiv*, 764316. doi: 10.1101/764316
- Salih, K. J., Duncan, O., Li, L., O’Leary, B., Fenske, R., Trösch, J., et al. (2020). Impact of oxidative stress on the function, abundance, and turnover of the Arabidopsis 80S cytosolic ribosome. *Plant J.* doi: 10.1111/tpj.14713
- Samaha, H., Delorme, V., Pontvianne, F., Cooke, R., Delalande, F., Van Dorselaer, A., et al. (2010). Identification of protein factors and U3 snoRNAs from a Brassica oleracea RNP complex involved in the processing of pre-rRNA. *Plant J.* 61, 383–398. doi: 10.1111/j.1365-313X.2009.04061.x
- Scharf, K. D., and Nover, L. (1982). Heat-shock-induced alterations of ribosomal protein phosphorylation in plant cell cultures. *Cell* 30, 427–437. doi: 10.1016/0092-8674(82)90240-9
- Schepetilnikov, M., and Ryabova, L. A. (2017). Auxin signaling in regulation of plant translation reinitiation. *Front. Plant Sci.* 8, 1014. doi: 10.3389/fpls.2017.01014
- Schepetilnikov, M., Kobayashi, K., Geldreich, A., Caranta, C., Robaglia, C., Keller, M., et al. (2011). Viral factor TAV recruits TOR/S6K1 signalling to activate reinitiation after long ORF translation. *EMBO J.* 30, 1343–1356. doi: 10.1038/emboj.2011.39
- Schepetilnikov, M., Dimitrova, M., Mancera-Martínez, E., Geldreich, A., Keller, M., and Ryabova, L. A. (2013). TOR and S6K1 promote translation reinitiation of uORF-containing mRNAs via phosphorylation of eIF3h. *EMBO J.* 32, 1087–1102. doi: 10.1038/emboj.2013.61
- Schmidt, S., Dethloff, F., Beine-Golovchuk, O., and Kopka, J. (2013). The REIL1 and REIL2 proteins of Arabidopsis thaliana are required for leaf growth in the cold. *Plant Physiol.* 163, 1623–1639. doi: 10.1104/pp.113.223925
- Schultes, N. P., Sawers, R. J. H., Brutnell, T. P., and Krueger, R. W. (2000). Maize high chlorophyll fluorescent 60 mutation is caused by an Ac disruption of the gene encoding the chloroplast ribosomal small subunit protein 17. *Plant J.* 21, 317–327. doi: 10.1046/j.1365-313X.2000.00676.x
- Segev, N., and Gerst, J. E. (2018). Specialized ribosomes and specific ribosomal protein paralogs control translation of mitochondrial proteins. *J. Cell Biol.* 217, 117–126. doi: 10.1083/jcb.201706059
- Seidel, B., Innis, C. A., Wilson, D. N., Gartmann, M., Armache, J. P., Villa, E., et al. (2009). Structural insight into nascent polypeptide chain-mediated translational stalling. *Science (80-)* 326, 1412–1415. doi: 10.1126/science.1177662
- Shi, Z., Fujii, K., Kovary, K. M., Genuth, N. R., Röst, H. L., Teruel, M. N., et al. (2017). Heterogeneous Ribosomes Preferentially Translate Distinct Subpools of mRNAs Genome-wide. *Mol. Cell* 67, 71–83.e7. doi: 10.1016/j.molcel.2017.05.021
- Simm, S., Fragkostefanakis, S., Paul, P., Keller, M., Einloft, J., Scharf, K. D., et al. (2015). Identification and expression analysis of ribosome biogenesis factor co-orthologs in solanum lycopersicum. *Bioinform. Biol. Insights* 9, 1–17. doi: 10.4137/BBi.s20751
- Simon, L., Rabanal, F. A., Dubos, T., Oliver, C., Lauber, D., Poulet, A., et al. (2018). Genetic and epigenetic variation in 5S ribosomal RNA genes reveals genome dynamics in Arabidopsis thaliana. *Nucleic Acids Res.* 46, 3019–3033. doi: 10.1093/nar/gky163
- Simsek, D., and Barna, M. (2017). An emerging role for the ribosome as a nexus for post-translational modifications. *Curr. Opin. Cell Biol.* 45, 92–101. doi: 10.1016/j.ccb.2017.02.010

- Simsek, D., Tiu, G. C., Flynn, R. A., Byeon, G. W., Leppek, K., Xu, A. F., et al. (2017). The Mammalian Ribo-interactome Reveals Ribosome Functional Diversity and Heterogeneity. *Cell* 169, 1051–1065.e18. doi: 10.1016/j.cell.2017.05.022
- Slavov, N., Semrau, S., Airoldi, E., Budnik, B., and van Oudenaarden, A. (2015). Differential Stoichiometry among Core Ribosomal Proteins. *Cell Rep.* 13, 865–873. doi: 10.1016/j.celrep.2015.09.056
- Song, J., Wei, X., Shao, G., Sheng, Z., Chen, D., Liu, C., et al. (2014). The rice nuclear gene WLP1 encoding a chloroplast ribosome L13 protein is needed for chloroplast development in rice grown under low temperature conditions. *Plant Mol. Biol.* 84, 301–314. doi: 10.1007/s11103-013-0134-0
- Song, W., Joo, M., Yeom, J. H., Shin, E., Lee, M., Choi, H. K., et al. (2019). Divergent rRNAs as regulators of gene expression at the ribosome level. *Nat. Microbiol.* 4, 515–526. doi: 10.1038/s41564-018-0341-1
- Sormani, R., Delannoy, E., Lageix, S., Bitton, F., Lanet, E., Saez-Vasquez, J., et al. (2011a). Sublethal cadmium intoxication in Arabidopsis thaliana impacts translation at multiple levels. *Plant Cell Physiol.* 52, 436–447. doi: 10.1093/pcp/pcr001
- Sormani, R., Masclaux-Daubresse, C., Daniele-Vedele, F., and Chardon, F. (2011b). Transcriptional regulation of ribosome components are determined by stress according to cellular compartments in Arabidopsis thaliana. *PLoS One* 6. doi: 10.1371/journal.pone.0028070
- Steffen, K. K., McCormick, M. A., Pham, K. M., Mackay, V. L., Delaney, J. R., Murakami, C. J., et al. (2012). Ribosome deficiency protects against ER stress in *Saccharomyces cerevisiae*. *Genetics* 191, 107–118. doi: 10.1534/genetics.111.136549
- Stirnberg, P., Liu, J. P., Ward, S., Kendall, S. L., and Leyser, O. (2012). Mutation of the cytosolic ribosomal protein-encoding RPS10B gene affects shoot meristematic function in Arabidopsis. *BMC Plant Biol.* 12, 160. doi: 10.1186/1471-2229-12-160
- Sulima, S. O., and Dinman, J. D. (2019). The Expanding Riboverse. *Cells* 8, 1205. doi: 10.3390/cells8101205
- Sun, Y., and Zerges, W. (2015). Translational regulation in chloroplasts for development and homeostasis. *Biochim. Biophys. Acta Bioenerg.* 1847, 809–820. doi: 10.1016/j.bbabi.2015.05.008
- Sun, L., Yu, Y., Hu, W., Min, Q., Kang, H., Li, Y., et al. (2016). Ribosomal protein S6 kinase1 coordinates with TOR-Raptor2 to regulate thylakoid membrane biosynthesis in rice. *Biochim. Biophys. Acta Mol. Cell Biol. Lipids* 1861, 639–649. doi: 10.1016/j.bbalip.2016.04.009
- Szakonyi, D., and Byrne, M. E. (2011). Ribosomal protein L27a is required for growth and patterning in Arabidopsis thaliana. *Plant J.* 65, 269–281. doi: 10.1111/j.1365-313X.2010.04422.x
- Szick, K., Springer, M., and Bailey-Serres, J. (1998). Evolutionary analyses of the 12-kDa acidic ribosomal P-proteins reveal a distinct protein of higher plant ribosomes. *Proc. Natl. Acad. Sci. U. S. A.* 95, 2378–2383. doi: 10.1073/pnas.95.5.2378
- Szick-Miranda, K., Zaniak, A. S., Zaniak, A. S., Abidayo, S., and Slater, K. L. C. (2010). Analysis of RPS15aE, an isoform of a plant-specific evolutionarily distinct ribosomal protein in Arabidopsis thaliana, reveals its potential role as a growth regulator. *Plant Mol. Biol. Rep.* 28, 239–252. doi: 10.1007/s11105-009-0148-6
- Talkish, J., Zhang, J., Jakovljevic, J., Horsey, E. W., and Woolford, J. L. (2012). Hierarchical recruitment into nascent ribosomes of assembly factors required for 27SB pre-rRNA processing in *Saccharomyces cerevisiae*. *Nucleic Acids Res.* 40, 8646–8661. doi: 10.1093/nar/gks609
- Thompson, M. K., Rojas-Duran, M. F., Gangaramani, P., and Gilbert, W. V. (2016). The ribosomal protein Asc1/RACK1 is required for efficient translation of short mRNAs. *Elife* 5. doi: 10.7554/eLife.11154
- Tiller, N., Weingartner, M., Thiele, W., Maximova, E., Schöttler, M. A., and Bock, R. (2012). The plastid-specific ribosomal proteins of Arabidopsis thaliana can be divided into non-essential proteins and genuine ribosomal proteins. *Plant J.* 69, 302–316. doi: 10.1111/j.1365-313X.2011.04791.x
- Tiruneh, B. S., Kim, B. H., Gallie, D. R., Roy, B., and Von Arnim, A. G. (2013). The global translation profile in a ribosomal protein mutant resembles that of an eIF3 mutant. *BMC Biol.* 11, 123. doi: 10.1186/1741-7007-11-123
- Turkina, M. V., Årstrand, H., and Vener, A. V. (2011). Differential phosphorylation of ribosomal proteins in Arabidopsis thaliana plants during day and night. *PLoS One* 6. doi: 10.1371/journal.pone.0029307
- Tzafir, I., Pena-Muralla, R., Dickerman, A., Berg, M., Rogers, R., Hutchens, S., et al. (2004). Identification of genes required for embryo development in Arabidopsis. *Plant Physiol.* 135, 1206–1220. doi: 10.1104/pp.104.045179
- Ueda, K., Matsuura, H., Yamaguchi, M., Demura, T., and Kato, K. (2012). Genome-wide analyses of changes in translation state caused by elevated temperature in *Oryza sativa*. *Plant Cell Physiol.* 53, 1481–1491. doi: 10.1093/pcp/pcs092
- Urquidí Camacho, R. A., Lokdarshi, A., and Arnim, A. G. (2020). Translational gene regulation in plants: A green new deal. *Wiley Interdiscip. Rev. RNA*, e1597. doi: 10.1002/wrna.1597
- Vaillant, I., Schubert, I., Tourmente, S., and Mathieu, O. (2006). MOM1 mediates DNA-methylation-independent silencing of repetitive sequences in Arabidopsis. *EMBO Rep.* 7, 1273–1278. doi: 10.1038/sj.embor.7400791
- Vaillant, I., Tutois, S., Cuvillier, C., Schubert, I., and Tourmente, S. (2007). Regulation of Arabidopsis thaliana 5S rRNA genes. *Plant Cell Physiol.* 48, 745–752. doi: 10.1093/pcp/pcm043
- Van Der Horst, S., Filipovska, T., Hanson, J., and Smeekens, S. (2020). Metabolite control of translation by conserved peptide uORFs: The ribosome as a metabolite multisensor. *Plant Physiol.* 182, 110–122. doi: 10.1104/pp.19.00940
- Van Lijsebettens, M., Vanderhaeghe, R., De Block, M., Bauw, G., Villarroel, R., and Van Montagu, M. (1994). An S18 ribosomal protein gene copy at the Arabidopsis PFL locus affects plant development by its specific expression in meristems. *EMBO J.* 13, 3378–3388. doi: 10.1002/j.1460-2075.1994.tb06640.x
- Van Minnebruggen, A., Neyt, P., Groeve, S., De Coussens, G., Ponce, M. R., Micol, J. L., et al. (2010). The ang3 mutation identified the ribosomal protein gene RPL5B with a role in cell expansion during organ growth. *Physiol. Plant* 138, 91–101. doi: 10.1111/j.1399-3054.2009.01301.x
- Vogel, C., and Marcotte, E. M. (2012). Insights into the regulation of protein abundance from proteomic and transcriptomic analyses. *Nat. Rev. Genet.* 13, 227–232. doi: 10.1038/nrg3185
- Von Arnim, A. G., Jia, Q., and Vaughn, J. N. (2014). Regulation of plant translation by upstream open reading frames. *Plant Sci.* 214, 1–12. doi: 10.1016/j.plantsci.2013.09.006
- Waltz, F., Nguyen, T. T., Arrivé, M., Bochler, A., Chicher, J., Hammann, P., et al. (2019). Small is big in Arabidopsis mitochondrial ribosome. *Nat. Plants* 5, 106–117. doi: 10.1038/s41477-018-0339-y
- Wang, Z., and Sachs, M. S. (1997). Ribosome stalling is responsible for arginine-specific translational attenuation in *Neurospora crassa*. *Mol. Cell Biol.* 17, 4904–4913. doi: 10.1128/MCB.17.9.4904
- Wang, J., Lan, P., Gao, H., Zheng, L., Li, W., and Schmidt, W. (2013). Expression changes of ribosomal proteins in phosphate- and iron-deficient Arabidopsis roots predict stress-specific alterations in ribosome composition. *BMC Genomics* 14, 783. doi: 10.1186/1471-2164-14-783
- Wang, W., Nag, S., Zhang, X., Wang, M. H., Wang, H., Zhou, J., et al. (2015). Ribosomal proteins and human diseases: Pathogenesis, molecular mechanisms, and therapeutic implications. *Med. Res. Rev.* 35, 225–285. doi: 10.1002/med.21327
- Wang, R., Zhao, J., Jia, M., Xu, N., Liang, S., Shao, J., et al. (2018). Balance between cytosolic and chloroplast translation affects leaf variegation. *Plant Physiol.* 176, 804–818. doi: 10.1104/pp.17.00673
- Wawiorka, L., Molestak, E., Szajwaj, M., Michalec-Wawiorka, B., Mołoń, M., Borkiewicz, L., et al. (2017). Multiplication of Ribosomal P-Stalk Proteins Contributes to the Fidelity of Translation. *Mol. Cell Biol.* 37, 17. doi: 10.1128/mcb.00060-17
- Weijers, D., Franke-van Dijk, M., Vencken, R.-J. J., Quint, A., Hooykaas, P., and Offringa, R. (2001). An Arabidopsis Minute-like phenotype caused by a semi-dominant mutation in a RIBOSOMAL PROTEIN S5 gene. *Development* 128, 4289–4299.
- Weis, B. L., Kovacevic, J., Missbach, S., and Schleiff, E. (2015a). Plant-Specific Features of Ribosome Biogenesis. *Trends Plant Sci.* 20, 729–740. doi: 10.1016/j.tplants.2015.07.003
- Weis, B. L., Palm, D., Missbach, S., Bohnsack, M. T., and Schleiff, E. (2015b). atBRX1-1 and atBRX1-2 are involved in an alternative rRNA processing pathway in Arabidopsis thaliana. *Rna* 21, 415–425. doi: 10.1261/rna.047563.114
- Whittle, C. A., and Krochko, J. E. (2009). Transcript profiling provides evidence of functional divergence and expression networks among ribosomal protein gene paralogs in *Brassica napus*. *Plant Cell* 21, 2203–2219. doi: 10.1105/tpc.109.068411

- Wickham, H. (2007). Reshaping data with the reshape package. *J. Stat. Software* 21, 1–20. doi: 10.18637/jss.v021.i12
- Williams, M. E., and Sussex, I. M. (1995). Developmental regulation of ribosomal protein L16 genes in *Arabidopsis thaliana*. *Plant J.* 8, 65–76. doi: 10.1046/j.1365-3113.1995.08010065.x
- Wilson, D. N., and Cate, J. H. D. (2012). The structure and function of the eukaryotic ribosome. *Cold Spring Harb. Perspect. Biol.* 4, 5. doi: 10.1101/cshperspect.a011536
- Wool, I. G., Chan, Y. L., and Glück, A. (1995). Structure and evolution of mammalian ribosomal proteins. *Biochem. Cell Biol.* 73, 933–947. doi: 10.1139/o95-101
- Woolford, J. L., and Baserga, S. J. (2013). Ribosome biogenesis in the yeast *Saccharomyces cerevisiae*. *Genetics* 195, 643–681. doi: 10.1534/genetics.113.153197
- Wu, S. H., Liu, M. J., Wu, S. H., and Chen, H. M. (2012). Widespread translational control contributes to the regulation of *Arabidopsis* photomorphogenesis. *Mol. Syst. Biol.* 8. doi: 10.1038/msb.2011.97
- Xiong, Y., and Sheen, J. (2014). The role of target of rapamycin signaling networks in plant growth and metabolism. *Plant Physiol.* 164, 499–512. doi: 10.1104/pp.113.229948
- Xu, T., Lei, L., Shi, J., Wang, X., Chen, J., Xue, M., et al. (2019). Characterization of maize translational responses to sugarcane mosaic virus infection. *Virus Res.* 259, 97–107. doi: 10.1016/j.virusres.2018.10.013
- Xue, S., and Barna, M. (2012). Specialized ribosomes: A new frontier in gene regulation and organismal biology. *Nat. Rev. Mol. Cell Biol.* 13, 355–369. doi: 10.1038/nrm3359
- Yamashita, Y., Takamatsu, S., Glasbrenner, M., Becker, T., Naito, S., and Beckmann, R. (2017). Sucrose sensing through nascent peptide-mediated ribosome stalling at the stop codon of *Arabidopsis* bZIP11 uORF2. *FEBS Lett.* 591, 1266–1277. doi: 10.1002/1873-3468.12634
- Yan, H., Chen, D., Wang, Y., Sun, Y., Zhao, J., Sun, M., et al. (2016). Ribosomal protein L18aB is required for both male gametophyte function and embryo development in *Arabidopsis*. *Sci. Rep.* 6. doi: 10.1038/srep31195
- Yao, Y., Ling, Q., Wang, H., and Huang, H. (2008). Ribosomal proteins promote leaf adaxial identity. *Development* 135, 1325–1334. doi: 10.1242/dev.017913
- Yu, P., Wang, S., Ma, C., Luo, X., Xing, Z., Wu, X., et al. (2019). Affirmation of Distinctive Ribosomal Protein Paralog-Specific Ribosomes. *SSRN Electron. J.* doi: 10.2139/ssrn.3334430
- Yu, H., Kong, X., Huang, H., Wu, W., Park, J., Yun, D. J., et al. (2020). STCH4/REIL2 Confers Cold Stress Tolerance in *Arabidopsis* by Promoting rRNA Processing and CBF Protein Translation. *Cell Rep.* 30, 229–242.e5. doi: 10.1016/j.celrep.2019.12.012
- Zakrzewska-Placzek, M., Souret, F. F., Sobczyk, G. J., Green, P. J., and Kufel, J. (2010). *Arabidopsis thaliana* XRN2 is required for primary cleavage in the pre-ribosomal RNA. *Nucleic Acids Res.* 38, 4487–4502. doi: 10.1093/nar/gkq172
- Zhang, X., Rosen, B. D., Tang, H., Krishnakumar, V., and Town, C. D. (2015). Polyribosomal RNA-seq reveals the decreased complexity and diversity of the *Arabidopsis* translome. *PLoS One* 10. doi: 10.1371/journal.pone.0117699
- Zhang, J., Yuan, H., Yang, Y., Fish, T., Lyi, S. M., Thannhauser, T. W., et al. (2016). Plastid ribosomal protein S5 is involved in photosynthesis, plant development, and cold stress tolerance in *Arabidopsis*. *J. Exp. Bot.* 67, 2731–2744. doi: 10.1093/jxb/erw106
- Zhang, S., Hu, H., Zhou, J., He, X., Jiang, T., and Zeng, J. (2017). Analysis of Ribosome Stalling and Translation Elongation Dynamics by Deep Learning. *Cell Syst.* 5, 212–220.e6. doi: 10.1016/j.cels.2017.08.004
- Zhang, C., Li, H., Yuan, C., Liu, S., Li, M., Zhu, J., et al. (2020). CKB1 regulates expression of ribosomal protein L10 family gene and plays a role in UV-B response. *Plant Biol.* 22, 143–152. doi: 10.1111/plb.12954
- Zhao, D. S., Zhang, C. Q., Li, Q. F., Yang, Q. Q., Gu, M. H., and Liu, Q. Q. (2016). A residue substitution in the plastid ribosomal protein L12/AL1 produces defective plastid ribosome and causes early seedling lethality in rice. *Plant Mol. Biol.* 91, 161–177. doi: 10.1007/s11103-016-0453-z
- Zheng, M., Wang, Y., Liu, X., Sun, J., Wang, Y., Xu, Y., et al. (2016). The RICE MINUTE-LIKE1 (RML1) gene, encoding a ribosomal large subunit protein L3B, regulates leaf morphology and plant architecture in rice. *J. Exp. Bot.* 67, 3457–3469. doi: 10.1093/jxb/erw167
- Zhou, F., Roy, B., and von Arnim, A. G. (2010). Translation reinitiation and development are compromised in similar ways by mutations in translation initiation factor eIF3h and the ribosomal protein RPL24. *BMC Plant Biol.* 10, 193. doi: 10.1186/1471-2229-10-193
- Zhou, Y., Musalgaonkar, S., Johnson, A. W., and Taylor, D. W. (2019). Tightly-orchestrated rearrangements govern catalytic center assembly of the ribosome. *Nat. Commun.* 10, 1–11. doi: 10.1038/s41467-019-08880-0
- Zsögön, A., Szakonyi, D., Shi, X., and Byrne, M. E. (2014). Ribosomal protein RPL27a promotes female gametophyte development in a dose-dependent manner. *Plant Physiol.* 165, 1133–1143. doi: 10.1104/pp.114.241778

Conflict of Interest: The authors declare that the research was conducted in the absence of any commercial or financial relationships that could be construed as a potential conflict of interest.

Copyright © 2020 Martinez-Seidel, Beine-Golovchuk, Hsieh and Kopka. This is an open-access article distributed under the terms of the Creative Commons Attribution License (CC BY). The use, distribution or reproduction in other forums is permitted, provided the original author(s) and the copyright owner(s) are credited and that the original publication in this journal is cited, in accordance with accepted academic practice. No use, distribution or reproduction is permitted which does not comply with these terms.

Chapter 3

Materials and Methods

Each of the original manuscripts that have been incorporated into this work contains its specific methods, which have sometimes been adapted or optimized and developed to solve specific problems. Nevertheless, the framework and origin of all the methods and variations of methods that I have used in the various publications can be traced back to the compendium of methods described in this section, which is part of the published material for which I am either the principal author or co-author (see the "Preface" section at the beginning of the thesis for details on authorship).

This section is divided into two broad methodological categories. Wet lab, covering all methods beyond computational biology experiments, and dry lab, covering only computational biology approaches. This division was made because the dissertation includes a number of advances in plant ribosome physiology that were only possible through a careful combination of *in silico* with wet-lab experiments.

A final aspect is that many of the methods presented here are described in detail in the appendices, as are other methods not described elsewhere. The appendices contain detailed step-by-step protocols that are intended as methodological guidelines for those who wish to use these methods in the future.

3.1 Wet Laboratory

3.1.1 Experimental Design

Two model plant organisms were studied. A monocotyledonous model cereal plant, *Hordeum vulgare* cultivar Keel, also known as barley, and a dicotyledonous molecular plant physiology model, *Arabidopsis thaliana* ecotype Col-0, also known as Arabidopsis. The experimental design used to study the low suboptimal temperature in these two plant models is shown in Figure 3.1.

The Australian barley cultivar Keel is considered moderately hardy and is generally more resistant to low temperatures as a cereal crop. Therefore, barley in this study was acclimated to a low suboptimal temperature of 4°C. Arabidopsis, on the other hand, germinates in spring at an optimal growth temperature of 20°C and is acclimated to suboptimal temperature at 10°C. The cold-acclimated phenotype of both species was carefully studied during a one-week acclimation period. Arabidopsis seedlings were mainly used to study plant molecular ribosome physiology at the end of an acclimation period of seven days, which is the time required for a wild-type plant to grow again after successful acclimation. On the other hand, barley acclimation was assessed on the fifth day of acclimation, which still reflects the transient state in which the plant's molecular physiology is rewired to develop an appropriate response to acclimation on the seventh day. Both species were labeled with stable isotopes to track the molecular processes that led to acclimation. In particular, the labeling strategy used ^{15}N to calculate protein biosynthesis during acclimation, which represents the biochemical function of ribosomes. Details of the quantities, media composition, rearing conditions, and other relevant experimental setup particulars can be found in the individual publications presented as chapters of the thesis.

3.1.2 Plant Growth Systems

For most of the studies conducted on the Arabidopsis plant model, a hydroponic system was developed to grow the plants while facilitating experimental design (Figure 3.2). The hydroponic growing system allowed cold acclimation experiments to be conducted in root systems by minimizing the normal temperature gradient that occurs in

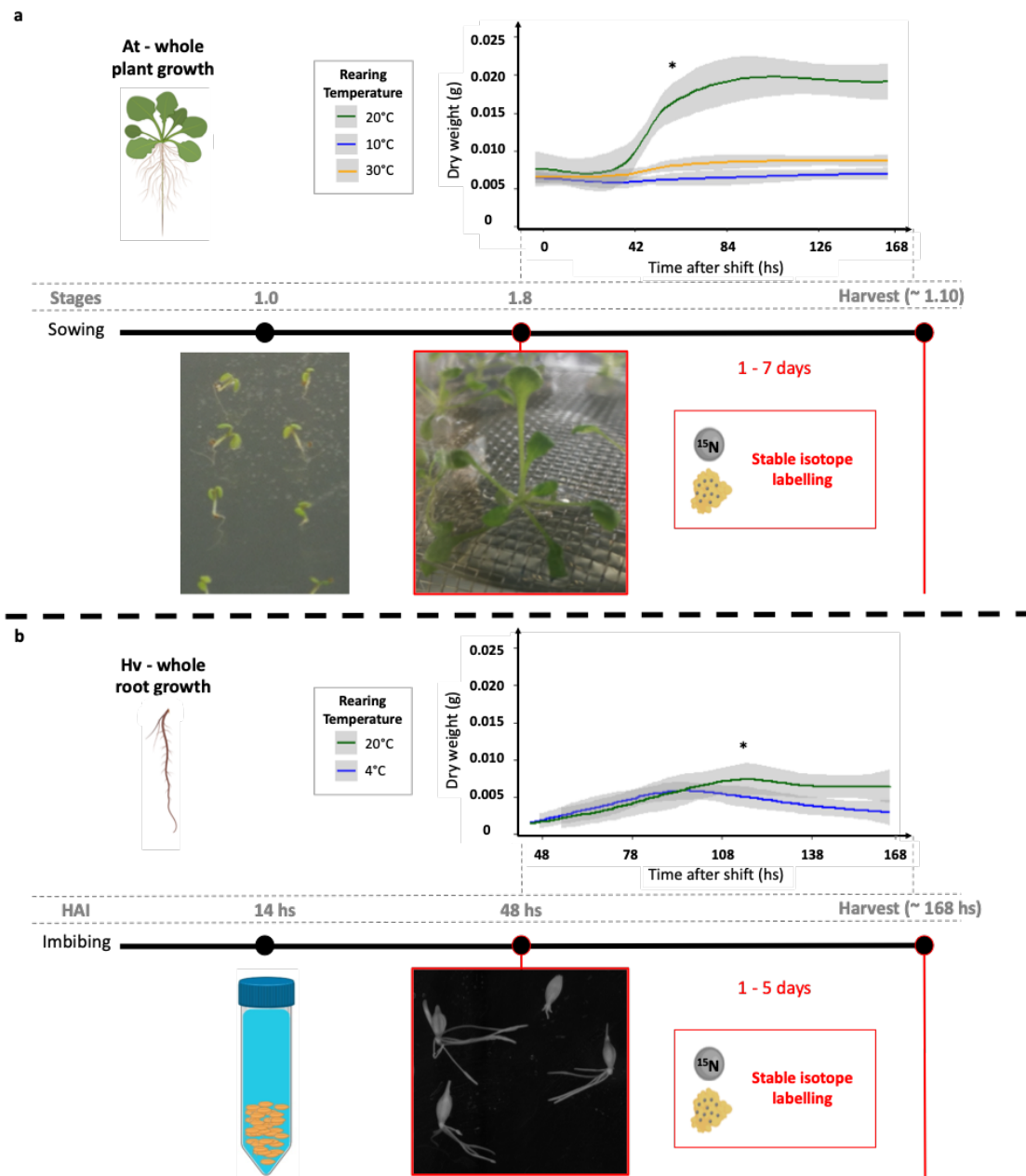


FIGURE 3.1: Simplified schematic of the experimental design used in this work to study acclimation to low suboptimal temperatures in (a) the cultivar Keel of *Hordeum vulgare* and (b) the ecotype Col-0 of *Arabidopsis thaliana*. Plants were always germinated under optimal conditions and placed in the cold while in a steady biological state with respect to developmental transitions in order to minimize biological variance between replicates. Both plant models were labelled with ^{15}N while exposed to low temperatures, and a detailed phenotypic analysis was performed to fully elucidate the physiological transition of the plants to an acclimated state. Note that in both plant models, the increase in dry weight at low temperatures was significantly reduced compared to plants raised at optimal temperature. Parts of this figure were created with [BioRender](#) and exported under a paid subscription.

nature when the soil buffers changes in ambient temperature fluctuations. In addition, the system allowed rapid exchange of liquid media to provide ^{15}N -stable isotope-labeled compounds to plants. This system was described in detail in a book chapter [6], and the Figure 3.2 is an adaptation of Figure 1 from that book chapter.

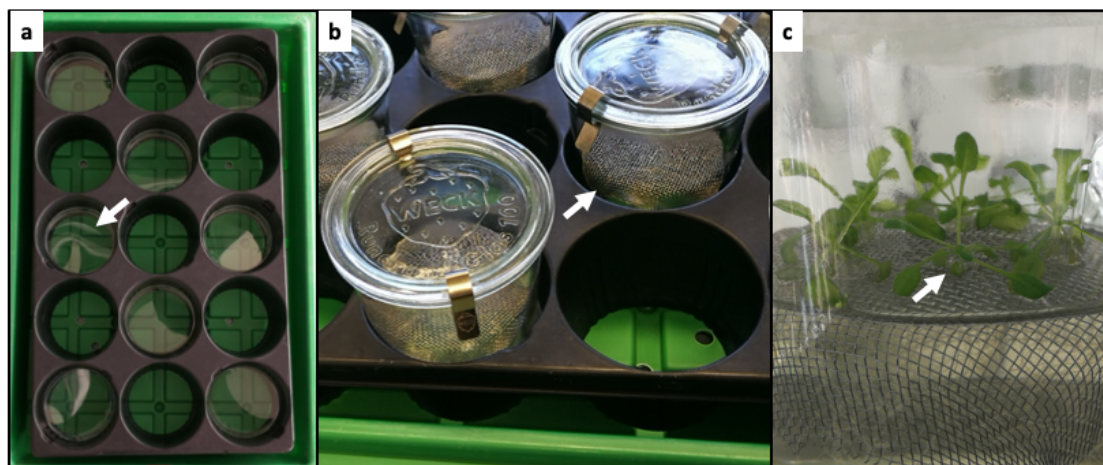


FIGURE 3.2: **Hydroponic plant cultivation.** (a) *Arabidopsis thaliana* plants (Col-0) at developmental stage 1.10. Plantlets were transferred with agar blocks (white arrow), precultivated hydroponically at 20 °C:18 °C (day–night) with 16 h:8 h light–darkness in liquid MS medium with 2% sucrose. The medium was substituted at stage 1.10 by medium containing ^{15}N -ammonium nitrate or other compounds containing the stable isotope. (b) Sterilized glass cultivation jars with stainless steel metal mesh inserts (white arrow) arrayed within the starter tray setup. (c) 15-position seedling starter tray with petri dish height adaptors (white arrow) in half of the wells. The black open-bottom insert tray is positioned in a green non-partitioned closed bottom seedling starter tray.

In contrast, the barley cereal model studies described in this thesis used a simpler germination system in which germination time was optimized to mimic the natural dark germination processes of barley seedlings without causing etiolation. From germination to harvest, plants were left in complete darkness, and experimental treatments were introduced, i.e., low temperatures for half of the plants and ^{15}N -labeled stable isotope compounds for half of the plants per temperature regime. For details of the system, the reader is referred to Chapters 4 and 7.

3.1.3 Profiling of the Plant Cytosolic Ribosomal Proteome

3.1.3.1 Purification of Ribosomes

In all cases, plant root material was harvested at the end of the experiment, immediately frozen in liquid nitrogen, and ground into powder for subsequent biochemical analyses.

Most importantly, our group developed a method for harvesting and purifying the plant cytosolic ribosomal proteome [7]. Figure 3.3 is an adaptation of Figure 1, which was originally published in the Methods publication mentioned above.

The optimized strategy enabled purification of non-translational free ribosomal complexes and low-oligomeric polysomes. In addition, we routinely measure complete profiles of translational complexes in our group; the details of the method can be found in Chapter 8. Another variant that allows biochemical profiling of all macromolecular complexes in the cell can be found in Chapter 7. Finally, in this thesis, the ribosome extraction buffer (REB) composition was modified to make ribosome extracts fully compatible with top-down, bottom-up, and native ribosomal proteome profiling. The proposed composition is shown in Table 3.1 and refers to a variant of REB called mass spectrometry friendly cytosolic ribosome extraction buffer (MS-friendly-^cREB).

TABLE 3.1: Composition, preparation and storage of mass spectrometry friendly cytosolic ribosome extraction buffer.

Product	Stock concentration (M)	Final concentration (M)	Volume of stocks for aliquots (ml)	Aliquot volume	Preparation Order
PRE-MS-friendly-^cREB	Prepare and store aliquots at -20°C for 6 months			40	
RNase-free H ₂ O			23.76		1
TRIS hydrochloride, pH 9.0: Tris(hydroxymethyl)aminomethane hydrochloride	1	0.2	8		-
KCl, Potassium chloride, Kaliumchlorid	2	0.2	4		-
EGTA, pH 8.0: Ethylene glycol-bis(2-aminoethylether) -N,N,N',N'-tetraacetic acid	0.5	25	2		-
MgCl ₂ *6H ₂ O, Magnesium chloride	1	35	1.4		-
Octyl beta-D-glucopyranoside, 98% (GC), Ribosome Top-down proteomics, Sigma Aldrich, O8001 1G (critical micelle concentration of 0.025 M)	100%	1% (W/V)	0.4	g	2 (solubilize)
	-	34	-		
Additions	Add fresh previous to usage while on ice				
Cyclohexamide	0.18	18	0.04	1 μL / mL	Last
DTT, Dithiothreitol	1	5	0.2	5 μL / mL	Last
PMSF, Phenylmethylsulfonyl fluoride	0.2	1	0.2	5 μL / mL	Last
PI, Protease inhibitor cocktail (Sigma cat. No. P9599)	100X	1X (1μL per 100μL)	0.4	10 μL /mL	Last

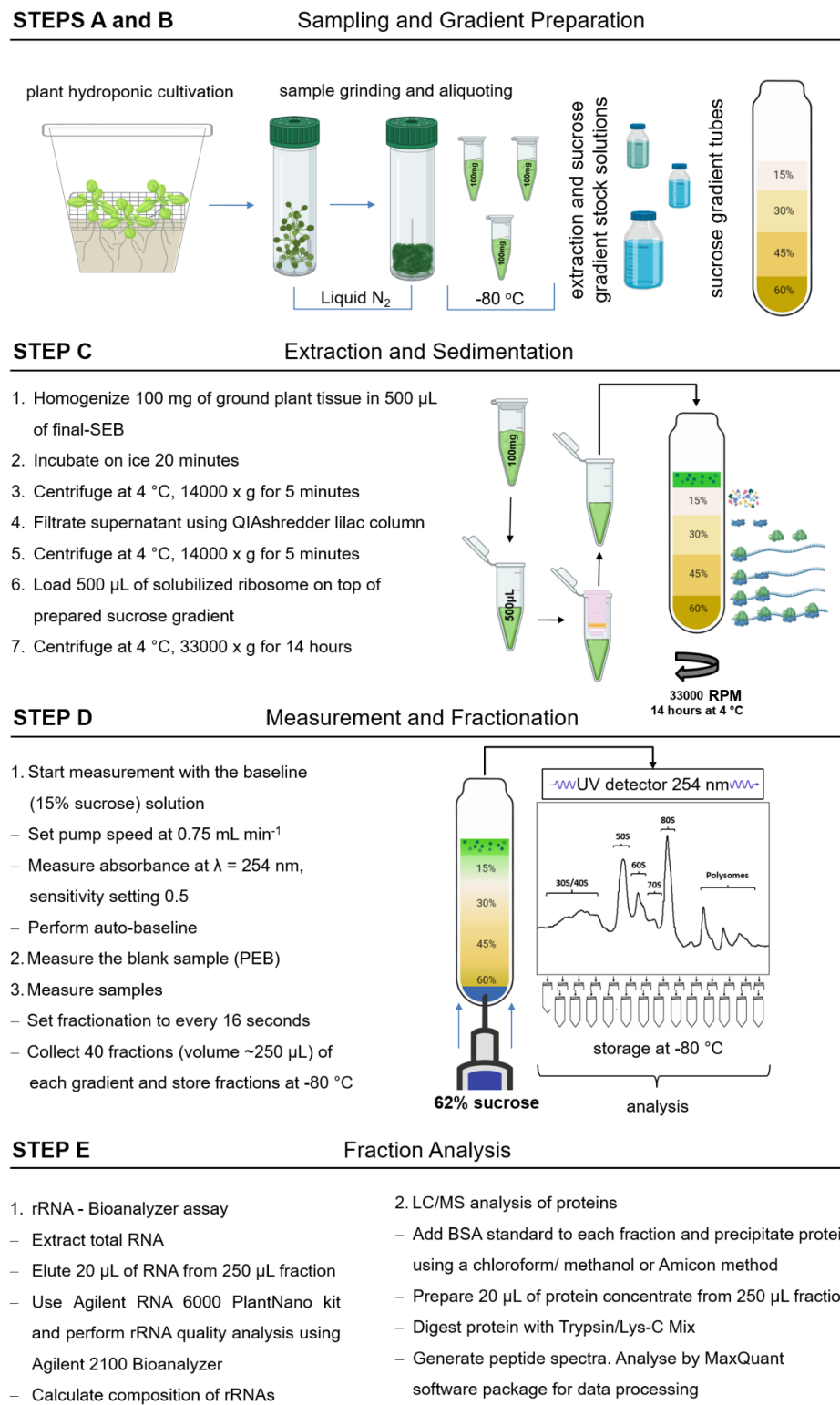


FIGURE 3.3: Schematic workflow of paired proteome profiling of non-translating and translating plant ribosome complexes. Steps include plant growth and sample processing (A), solution and sucrose gradient preparation (B), density gradient separation of macromolecular complexes (C), fractionation (D) and multiplexed analyses of resulting fractions (E). Details are reported in the Materials and Methods section of the original publication. Parts of this figure were created with [BioRender](#) and exported under a paid subscription.

Additionally, the solution used to form sucrose cushions that allow purification of macromolecular complexes is shown in Table 3.2.

TABLE 3.2: Composition, preparation and storage of sucrose cushion solution.

Product	Stock concentration (M)	Final concentration (M)	Volume of stocks for aliquots (ml)	Aliquot volume	Preparation Order
PRE-SC	Prepare and store aliquots at -20°C for 3 months			40	
RNase-free H ₂ O		volume max	17.92		1 (added half water first to wait for sucrose volume rise)
TRIS hydrochloride, pH 9.0: Tris(hydroxymethyl)aminomethane hydrochloride	1	0.4	16		3 (solubilize at 60°C - filter thorough 0.22µM)
KCl, Potassium chloride, Kaliumchlorid	2	0.2	4		-
EGTA, pH 8.0: Ethylene glycol-bis(2-aminoethylether) -N,N,N',N'-tetraacetic acid	0.5	5	0,4		-
MgCl₂*6H₂O, Magnesium chloride	1	35	1.4		-
Sucrose, ultracentrifuge grade, Fisher	100%	30% - 60% (W/V)	12 - 24	g	2
	-	876	-		
Additions	Add fresh previous to usage while on ice				
Chloramphenicol	0.15	15	0.04	1 µL / mL	Last
Cyclohexamide	0.18	18	0.04	1 µL / mL	Last
DTT, Dithiothreitol	1	5	0.2	5 µL / mL	Last

Notes on the Ribosome Extraction Buffer: EGTA, pH 8.0: Ethylene glycol-bis(2-aminoethylether) -N,N,N',N'-tetraacetic acid is a selective calcium chelator. It is useful in buffer solutions that resemble the environment in living cells, where calcium ions are usually at least a thousand times less concentrated than magnesium; when calcium is chelated, EGTA can increase endogenous DNA nuclease activity. The stock solutions dissolve only after the pH is adjusted. Cyclohexamide is a cytosolic translation inhibitor that blocks the translocation step. DTT, dithiothreitol prevents oxidation of cysteine residues that would cause protein aggregation. PMSF, phenylmethylsulfonyl fluoride is a serine protease inhibitor and has a short half-life in aqueous solutions.

3.1.3.2 Translation-related Omics Biochemical Assays

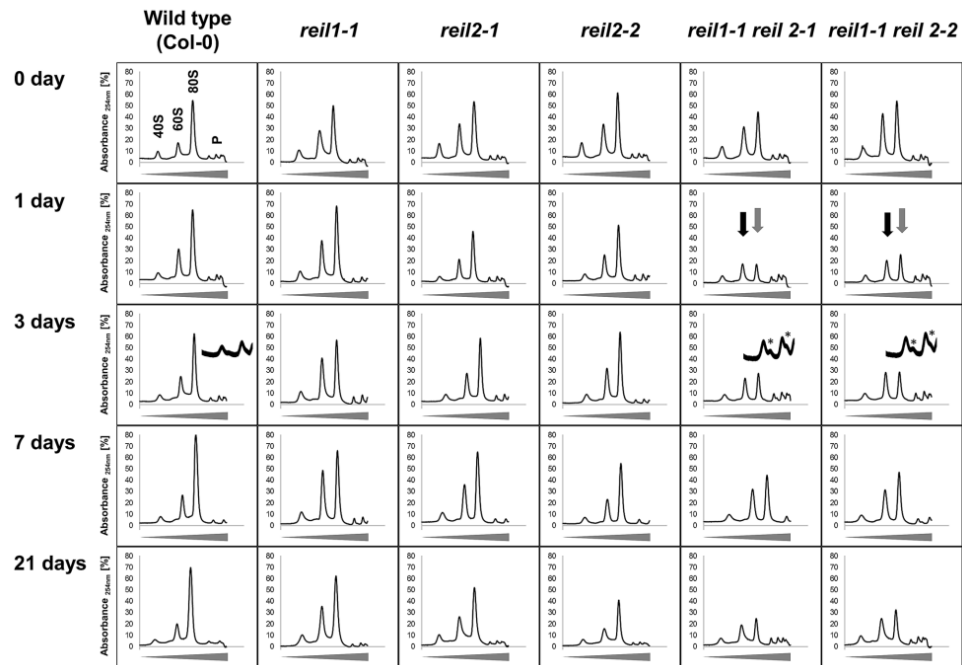
In this work, numerous omics technologies were used to fully characterize plant cytosolic ribosome complexes and investigate how they respond to low suboptimal temperature acclimation. For example, transcriptomics has been used to observe changes in the transcript levels of rProtein-coding genes and the overall machinery involved in assembling cytosolic ribosomes in the nucleolus. Similarly, purified ribosomes were used to examine shifts in the amount of non-translational and translational ribosomal complexes, as well as the overall composition of the rProteome, and how these change when the plant perceives a cold stimulus. The methodological framework and perhaps the starting point for developing such analyses has been published previously [3] and includes results obtained by reverse genetics on an already well-established and characterized mutant line of a protein ribosome biogenesis factor called REIL, which is critical for ribosome biogenesis during low suboptimal temperature acclimation. Example analyses are shown in Figure 3.4 to illustrate the methodologically basal analytical framework followed in this work and facilitated by the ribosome purification method explained. Figure 3.4 is adapted from Figure 1 and Figure 7C from the publication [3] mentioned above.

3.1.4 Molecular Biology

All methods, plant material, primers, vectors, and other resources used in this work to gain functional insights into the origin and role of ribosome heterogeneity in plants have been deposited in appendices.

3.1.5 Cloning Approaches

All methods and other resources directly related to cloning used in this work to gain functional insights into the origin and role of ribosome heterogeneity in plants have been deposited in Appendix A. The appendix provides a detailed step-by-step protocol of the methods compiled from the manufacturers' kits and relevant publications to begin planning and performing the functional characterization of the uL30 ribosomal protein paralogs, which is described in detail in Chapter 8 of this thesis.



RP Name	RP Class	Gene Symbol	Log ₂ -FC (<i>reil1-1 reil2-1</i> /Col-0)			Log ₂ -FC (<i>reil1-1 reil2-2</i> /Col-0)			ANOVA		
			0 d	1 d	1 w	0 d	1 d	1 w	P (genotype)	P (time)	P (interaction)
60S LSU											
<i>RPL3A</i>	uL3	AT1G43170.1	-0.302	0.097	0.167	-0.020	-0.140	0.189	9E-01	8E-06	8E-03
<i>RPL3B</i>	uL3	AT1G61580.1	-1.622	-1.328	-0.743	-0.727	-0.942	-0.788	1E-07	2E-04	6E-02
<i>RPL4A</i>	uL4	AT3G09630.1	-0.224	0.316	0.247	0.073	-0.029	0.332	3E-01	9E-06	3E-02
<i>RPL4D</i>	uL4	AT5G02870.1	-0.315	0.248	0.394	-0.084	0.091	0.497	5E-02	6E-05	1E-03
<i>RPP2A</i>	P1/P2	AT2G27720.1	-0.196	0.009	-0.001	0.040	0.050	0.121	4E-01	2E-04	9E-01
<i>RPP2B</i>	P1/P2	AT2G27710.3	-0.372	0.143	0.284	-0.032	0.017	0.376	4E-01	1E-03	4E-02
<i>RPP2C</i>	P1/P2	AT3G28500.1	0.745	2.104	2.720	0.269	0.899	2.590	1E-03	6E-01	2E-01
<i>RPP2D</i>	P1/P2	AT3G44590.1	-0.289	0.064	0.268	0.205	0.169	0.323	1E-01	1E-01	4E-01
<i>RPP2E</i>	P1/P2	AT5G40040.1	-2.382	0.315	2.035	-0.603	0.200	2.420	5E-02	2E-02	1E-04
<i>RPP3A</i>	P1/P2	AT4G25890.1	-0.320	0.147	0.510	-0.232	0.381	0.590	2E-01	6E-03	1E-01
<i>RPP3B</i>	P1/P2	AT5G57290.1	0.109	0.430	0.479	0.252	0.466	0.480	4E-04	2E-03	5E-01
40S LSU											
<i>RPS23A</i>	uS12	AT3G09680.1	-0.077	0.975	1.819	1.217	1.274	1.875	4E-06	4E-04	2E-02
<i>RPS23B</i>	uS12	AT5G02960.1	-0.293	0.149	0.180	0.030	0.131	0.205	2E-01	6E-03	8E-02
<i>RPS27A</i>	eS27	AT2G45710.1	-0.208	0.510	0.268	0.072	0.675	0.459	8E-04	5E-06	3E-02
<i>RPS27B</i>	eS27	AT3G61110.1	-0.083	0.067	0.320	-0.050	-0.127	0.104	3E-01	8E-05	3E-01
<i>RPS27C</i>	eS27	AT3G61111.1	0.001	4.179	2.839	0.257	4.034	1.859	4E-09	8E-10	2E-06
<i>RPS27D</i>	eS27	AT5G47930.1	-0.375	0.123	0.023	-0.208	0.055	0.210	5E-01	1E-03	2E-01

FIGURE 3.4: Sucrose density gradient analyses of ribosome complexes in the upper panel and Log₂-fold changes relative to Col-0 at several cold acclimation time points of selected cytosolic RP families in the lower panel. (Upper panel) Analyses of ribosome complexes from equal amounts (fresh weight) of hydroponically grown total root material before (0 day) and at 1, 3, 7, or 21 days after shift from 20 °C (day)/18 °C (night) to 10 °C (day) and 8 °C (night). The *Arabidopsis thaliana* wild type (Col-0) was compared to the single-paralog mutants, *reil1-1*, *reil2-1*, *reil2-2*, and to the double mutants, *reil1-1 reil2-1* and *reil1-1 reil2-2*. Absorbance at wavelength 254 nm was recorded continuously during fractionation and background corrected by a non-sample control. (Lower panel) Log₂-fold changes relative to Col-0 at each time point of selected cytosolic RP families. Two-factorial analysis of variance (ANOVA) indicates differential effects of the genotype, cold exposure (time) or the interaction of both on the expression of paralogous RPs from the 60S and the 40S subunits in the mutants. The three-color scale of the log₂ FC heat map ranges from -3 (blue) to 0 (yellow) to larger or equal to + 3 (red). The two-color significance scale ranges from P less than 1 x 10⁻¹⁰ (1⁻¹⁰, dark green) to P larger than 0.05 (5⁻², light green), P larger or equal to 0.05 (white).

3.1.6 T-DNA Lines

All methods, plant material, primers, and other resources used in this work to characterize T-DNA insertion lines of uL30 protein paralogs have been deposited in Appendix [B](#).

3.2 Dry Laboratory

The *in silico* methods developed as part of this work to assess plant cytosolic ribosomes, their composition, remodeling potential, structure, and specialized functions have been deposited individually in the chapters containing the original publications. This section addresses statistical methods that have been both developed and compiled to perform a comprehensive analysis of the various omics datasets generated as part of this work.

The full scope of the statistical tools developed and compiled is summarized in the book chapter [6] entitled "Multiplexed Profiling and Data Processing Methods to Identify Temperature-Regulated Primary Metabolites Using Gas Chromatography Coupled to Mass Spectrometry", Section 3.14 "Nontargeted Data Mining of Relevant Mass Features", which was originally intended for metabolomics data matrices, but can and has been extrapolated to many other omics data sets. The section reads (the following text is a paraphrase of the book chapter; the original references are numbered as in the chapter but are not reproduced in the bibliography of this thesis; the reader is referred to the original manuscript for access to them):

" Nontargeted data mining is a prerequisite for nonbiased discovery of relevant mass features from metabolite profiling experiments. Many options exist, as for example reviewed by Wolfender and coauthors [26]. The following approach and workflow includes previous suggestions but is specialized and can be used to find mass features that differentially accumulate (e.g., stable isotope incorporation). The focus lies on statistical relevance and explanation of datasets. This workflow equally weighs large and small changes of relative metabolite pool sizes, reducing bias of large variances. This implementation becomes necessary, if we consider that small changes in the abundance of signaling molecules can be amplified, triggering larger signaling cascades [27]. Untargeted data mining can be divided into four steps:

Preprocessing entails the mathematical transformation of data matrices that result from chromatogram data processing steps (see Subheading 3.11) to meet the prerequisites and enable multivariate testing.

Class comparison by supervised statistical tests and procedures is meant to find mass features that significantly change according to a predefined set of experimentally tested treatments. Typical examples of class comparison procedures are applications of generalized linear models (GLMs), false discovery rate (FDR) correction, analysis of variance (ANOVA), Bonferroni correction for multiple testing, or the Tukey honest significant difference test.

Class discovery methods are aiming to uncover hidden and unexpected patterns in data matrices. Class discovery algorithms are unsupervised and entail analyses of the general variance and trends. Examples are bootstrapped HCA, K-means clustering, PCA and mutual information or correlation matrices for network inference.

Class prediction finds potential metabolic markers that represent predefined sample classes. Such classes can be expected according to the choice of experimental design or unexpected and result in class discovery. Examples cover machine learning technologies such as Random Forests, Support Vector Machines (SVM), or discriminant analyses (DA) such as orthogonal partial least squares-DA.

3.2.1 Preprocessing

1. Process data by Log-transformation. This step partially solves typically right-skewed distribution of metabolite abundances into an approximately normally distributed scale of increases and decreases retaining the variance structure [28].
2. Scale data to null mean and unit standard deviation (Autoscaling): Several scaling and transformations procedures exist [29]; autoscaling performs better to infer the biological context, namely weighing small and large changes equally. By default, unsupervised class discovery methods will grant greater explanatory value to mass features with larger variance in an unscaled matrix (groups based on covariance). Alternatively, in a scaled matrix the grouping will be done according to correlation of mass features (e.g., PCA based on covariance or correlation matrices [30]). The latter represents better molecular systems in which a subtle change in a metabolite can be amplified by a

signaling cascade [27]. Metabolite levels are monitored by protein sensors [31] that ultimately trigger responses at the onset of changed metabolite pools (e.g., metabolite level homeostasis) [32]. The cascade of responses and the magnitude of changed metabolite pools are not uniform over biological samples treated differently (e.g., “all-or-nothing” switches) [33]. Therefore, the standard deviation of mean abundances differs between treated and control samples. These molecular mechanisms define the heteroscedastic nature of metabolite variance structures (i.e., each experimental treatment has a different variance).

3. Impute missing values depending on the scope of the experiment. Use k nearest neighbor method (KNN) [34, 35] to replace missing values by the average abundance of k nearest neighbors that do not have a missing value at that specific X_{ij} cell. Nearest neighbors are defined by Euclidean distance (after scaling, Euclidean distance and correlation are equivalent and hence using one or the other will not alter the results). Similar methods include Bayesian principal component analysis (bPCA), a multiple correspondence analysis (MCA) model, a multiple factor analysis (MFA), and random forests [36]. Imputation of missing data in metabolite matrices has been shown to be biologically more accurate when using KNN [37] than the other mentioned models. Use small values imputing only when the aim is to find metabolic markers of the type presence/absence. Any other imputation of small values has been shown to be detrimental in the analysis of datasets [38]. Depending on the subsequently applied algorithm one may as well skip missing value imputing.

4. Deisotope (i.e., remove all isotopologs except the a_0) the data set. This step becomes necessary to avoid groups forming in the following analyses only based on isotopolog correlation. It is best to also remove alternative fragments representing the same analyte manually, guided by statistics (e.g., correlation analysis) (see Subheading 3.11.4).

3.2.2 Class Comparison

1. Analyze the distribution of your data before selecting an appropriate statistical test. A Cullen and Frey graph plots skewness in the x-axis and kurtosis in the y-axis. Skewness measures the asymmetry of the probability distribution around the mean, similarly kurtosis defines the shape of the probability distribution at the tails of it. Moreover, known distributions should be test-plotted before using the data at hand

in order to have a better estimate to what distribution your data may fit. The R-package “fitdistrplus” contains these and more features [39]. Due to the preprocessing, the abundances of mass features tend to follow a log-normal distribution. Evaluation of normality can be further done with the Kolmogorov–Smirnov test [40].

2. Test the equality of variance assumptions (i.e., homoscedastic vs. heteroscedastic variance structures) using the Levene test [41].
3. Select an appropriate statistical test. If the data is normally distributed and the means have equal variances, ANOVA may be applied. If the data is not normally distributed and the means have equal variances, the nonparametric versions of ANOVA may be applied (e.g., Kruskal–Wallis or Wilcoxon rank) [42]. If the data is normally distributed and the means do not have equal variances, a linear model will suffice to cope with the heteroscedastic nature of mass features. If the data is not normally distributed and the means do not have equal variances, a robust solution is a generalized linear mixed model (GLMM) [43], which parametrizes the mean and the variance using a link function for statistical comparison instead of the actual mean values [28].
4. Correct for multiple statistical testing. P-values must be adjusted to avoid Type I and II errors. The FDR correction avoids the loss of potentially significant mass features [44]

3.2.3 Class Discovery

1. Find relevant groups of behavior by clustering the scaled data matrix (in both X and Y axes). Bootstrap [45] the clusters in order to avoid isolated clustering conditions from a single solution and thereby confirm that these groups of mass features confer identity to the clustered biological samples. The resulting groups are visually accessible through a clustered heatmap of scaled abundances (e.g., Clustering algorithm: HCA or Kmeans) that has the mass features on the y-axis and the conditions in the x-axis. The unsupervised grouping map discovers which mass features determine that certain biological samples cluster together, suggesting that these features give identity to each set of clustered biological replicates.
2. After bootstrapping, confirm the separation between experimental conditions relative to the within-replicate variance using PCA. Furthermore, using the conditions as

eigenvectors and the masses as projections into the plane, the previously found clusters of mass features can be traced in the biplot to rank their importance.

3. Create a distance matrix on selected masses that belong to significant clusters and subsequent networks in which each node is a metabolite with properties that define its influence in the data set. Consequently, the network approach makes it possible to determine highly influential metabolites acting within the significantly misrepresented clusters [46].

3.2.4 Class Prediction

1. Apply several algorithms that differ in their mathematical procedures to interpret the overlapping metabolic markers found.

2. Methods that provide inherent means of validation are preferred, such as Random Forest and SVM. Random Forest [47, 48] iterates the classification procedure of the samples across a n-number of repetitions in order to robustly select mass features that are good metabolic markers, namely highly ranked in the classification procedure. By removing one mass feature at a time and reclassifying the dataset, the algorithm is able to assign a value of “importance for classification” to each mass feature. Finally, a fraction of the biological samples can be taken as training or evaluation sets in order to have a degree of external validation for the predictors. In SVMs [49], the training set is mapped into a hyperplane (projection), in which known categories of biological samples become separated by the greatest possible gap or margin between them. The samples that reside in the margin become the support vectors for the boundary between categories. SVMs accomplish high classification rates with a relatively small training set.

3. Other methods do not provide inherent means of validation; for example, orthogonal partial least squares-DA (OPLS-DA) allows for bifactorial class prediction only, while partial least squares-DA (PLS-DA) allows for multifactorial prediction [50]. The use of projection methods based on partial least squares is suitable as a control to confirm the best biological markers after acknowledging the risk of overfitting. Overfitting may be caused by the lack of internal validation procedures such as the splitting of datasets into training and evaluation sets. ”

This compendium of methods and algorithms was developed, compiled, and used to answer various biological questions in the context of scientific collaborations with different socio-economical contexts. To name a few examples: we found metabolic markers in products containing superfoods such as chia or sesame using machine learning and validated them for authenticity assessment of commercial products. We elucidated the metabolomics/transcriptomic basis of somatic embryogenesis in coffee, providing tools to propagate plants efficiently. We developed tools to explore the metabolic basis of cold acclimation, providing a framework for crop protection under climate change. We uncovered the metabolic basis for the beneficial interaction of roots-bacteria in the cereal model *Brachypodium* under nutrient deficiency to enhance nutrient uptake and avoid reliance on chemical fertilizers. We identified suitable mating partners for commercial breeding of cherry tomatoes to improve endogenous plant protection and minimize the use of pesticides. The compendium of developed methods was deposited in the R package [RandoDiStats](#), which is publicly available and can be installed via `devtools::install_github("MSeidelFed/RandodiStats_package")` in any R statistical programming environment. In the following section, I use example results from common publications to illustrate the scope of the tools developed. The figures to which I contributed were taken from the original publications, and the legends were paraphrased.

The first and most fundamental advance in statistics provided by the R package [RandoDiStats](#) relates to class comparison. First, we validated that variables typically measured by metabolomics and other omics technologies are rarely homoscedastic and normally distributed [9], as shown in Figure 3.5 for metabolomics data and all original publication chapters in this work for proteomics, transcriptomics, and translomics data.

Based on this finding, we have developed a method to approximate the distribution of measured variables to the best-fitting regression family supported by a generalized linear model, to provide a fitted link function for selecting an appropriate regression family, and to satisfy the assumptions of a univariate statistical test. This effort is currently embedded in the master's thesis of Bernhard Bodenberger with the goal of publishing our package.

Next, we implemented tools for class prediction. We used machine learning to find metabolic markers in products containing superfoods such as chia or sesame (see Figure

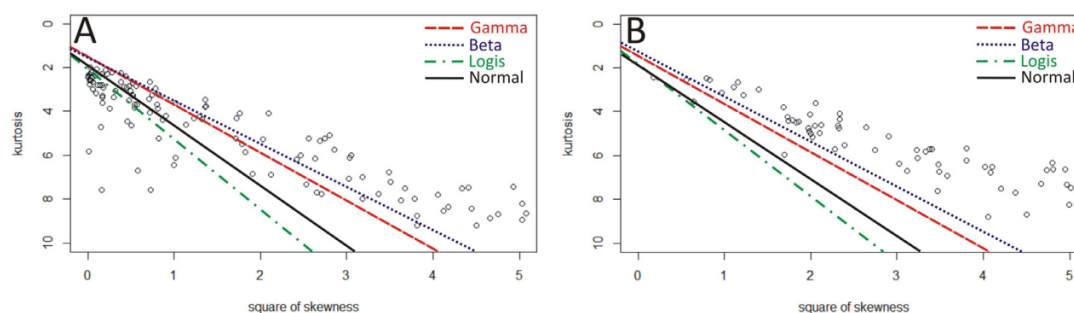


FIGURE 3.5: **Random response variables with specific distribution shapes, as determined by kurtosis and square of skewness parameters, were used to determine the regression family model for a GLM evaluating both N dose response (A, $n = 7617$) and comparative Amazonian soils (B, $n = 3393$) datasets.** Kurtosis was plotted in the ordinates and square of skewness in the abscissa and the random vectors with specific distributions (i.e., normal, logis, beta and gamma) were simplified by average-linearization and plotted in the curves. The R function used to build the distributions is reported in the RandoDiStats GitHub repository [RandoDiStats](#).

[5]) and validated them for authenticity assessment of commercial products (see Figure [2]).

This collaboration enabled the compilation of the numerous Random Forest-based classification methods used in the R packages "randomForest" and "varSelRF". The code was compiled in such a way that it can be used intuitively by any external user without R experience. In addition, R functions that depend on these packages are currently being developed to further automate the process.

Finally, all subsequent collaborations enabled the development of the class discovery section of the package. First, we elucidated the metabolomics [1] and transcriptomics basis (manuscript to be submitted, so figures are not used) of developmental transitions during somatic embryogenesis in coffee, as shown in Figure 3.7, providing tools for efficient plant propagation.

This collaboration enabled the development of two functions deposited in the R package [RandoDiStats](#) called "ClustPlus.R" and "KmeansPlus.R". They contain class discovery algorithms that allow the identification of key features that categorize the main sources of variance in a dataset, as described in the introduction of this subsection.

Second, we have developed tools to explore the metabolic basis of cold acclimation, providing a framework for plant protection under climate change at both the primary metabolome [6] and lipidome [4] levels; the latter is detailed in Figure 3.8.

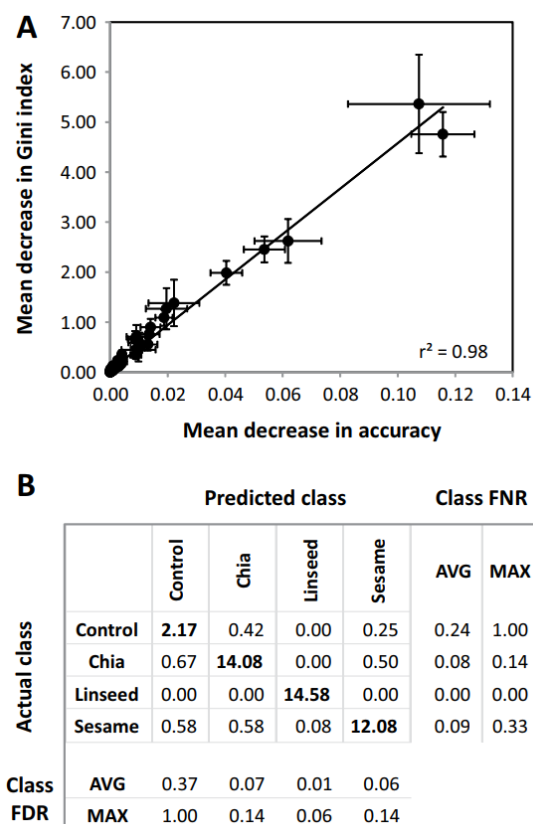


FIGURE 3.6: RF based selection of seed identity markers from mass features of non-targeted metabolite profiles of experimental bakery products that were prepared with or without additions of chia, linseed, or sesame seeds. (A) Analysis of variable importance by mean decrease of Gini index and mean decrease of accuracy measures (means±standard deviations) of 12 random forest analyses using 84 pre-selected processing-dependent mass features and eight manually added mass features containing previously identified markers of non-processed seeds. These mass features were selected from 19761 mass features of a non-targeted metabolite profiling analysis of polar extracts from experimental cookies that were prepared with 5, 10, 15, or 20% (w/w) defatted seed flour or 10 or 20% (w/w) whole seeds (Supplemental Table S4). The classification models predicted four classes, cookies without added seeds and cookies with chia, linseeds or sesame seeds irrespective of amount of added seed material or seed pre-processing. The importance of top mass features was ranked according to mean decreases in accuracy (Supplemental Table S4). (B) Characterization of the trained classification models by a confusion matrix, class false negative rates (FNR) and class false discovery rates (FDR). Averages (AVG) and maxima (MAX) of class FNR and FDR were calculated from the individual confusion matrices of 12 classification models that were trained from 46 random samplings of a total set of 93 profiles of cookies without added seeds (n=5) and cookies with chia (n=28), linseeds (n=30) or sesame seeds (n=30). The overall classification error was $6.70 \pm 3.27\%$ (mean±standard deviation).

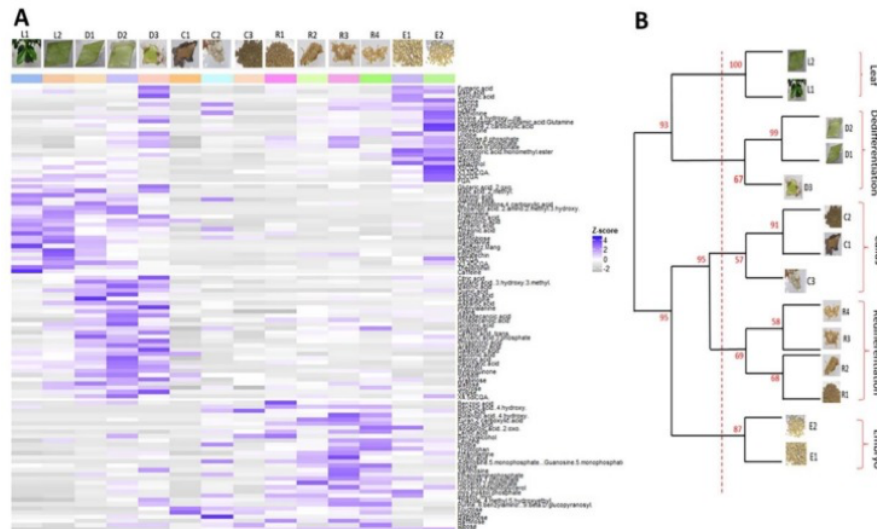


FIGURE 3.7: **Profiling primary and secondary metabolites during 14 key sampled stages of the Arabica somatic embryogenesis process.** (A) Heatmap generated from the Z-score values of a total of 92 primary metabolites and 12 secondary metabolites detected. Rows correspond to metabolites and columns to the sampled stages. Positive Z-score values are shown in blue and negative values in grey. (B) Hierarchical clustering of the 14 sampled stages according to the similarities in their metabolic profiles. The clustering was performed using Pearson's correlation coefficient. Cluster probabilities were calculated via a multiscale bootstrap with a total of 1000 iterations. Clustering yielded 5 major nodes: Leaf, Dedifferentiation, Callus, Redifferentiation and Embryo.

This collaboration allowed me to further develop the two aforementioned R functions, "ClustPlus.R" and "KmeansPlus.R", to customize them to provide intuitive and easy-to-interpret results.

Third, we uncovered the metabolic basis for the beneficial interaction between roots and bacteria in the cereal model *Brachypodium* under nutrient deficiency [10] to enhance nutrient uptake and avoid dependence on chemical fertilizers. Figure 3.9 shows the mean response of similarly responding metabolites as an example.

This collaboration allowed me to develop a feature of the "KmeansPlus.R" function that creates average charts of the variables within each cluster and outputs these charts with their standard deviations or standard errors as shading around a moving average in solid color. The charts are now output to a PDF file by default when the user enters a data matrix to be analyzed into the function.

Finally, we identified suitable mating partners for commercial breeding of cherry tomato [8] to improve endogenous plant protection and minimize pesticide use. The main metabolic criteria for mate selection are summarized in Figure 3.10.

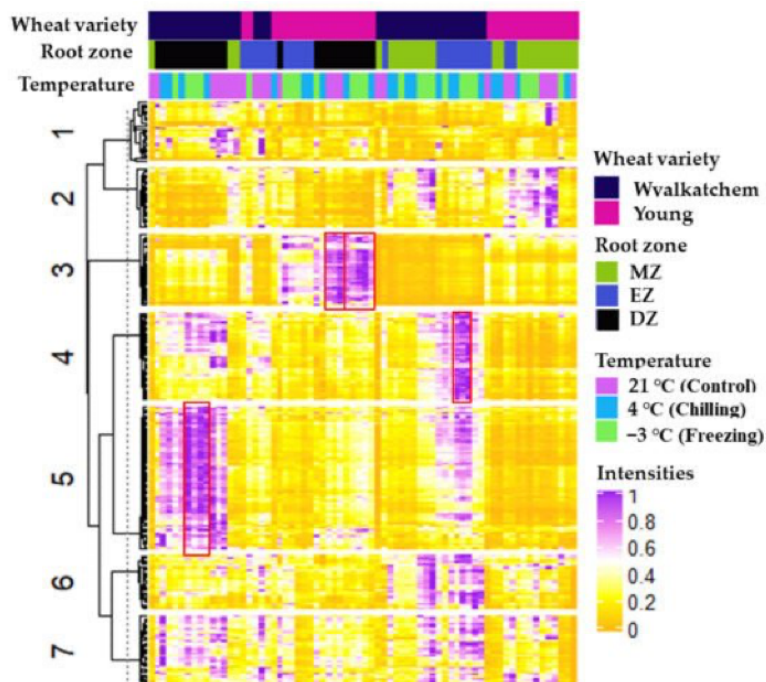


FIGURE 3.8: **Bootstrapped hierarchical clustering analysis (HCA) of lipid autoscaled intensities from all the root samples (control and subjected to cold stress for three developmental root zones) of cold-sensitive Wwalkatchem and cold-tolerant Young varieties.** Rows were clustered using K-means with K equal to 7, and with n clustering reiterations ($n = 1000$). R packages "ComplexHeatmap" and "pvclust" were used to do and extract the heatmap image.

This collaboration enabled the development of an R function called "PlusPCA.R" that now integrates the results of multiple clustering algorithms into a PCA representation to assess how the dispersion of similar or dissimilar variables is related to the main sources of variance. The function is still under development, but can be used via the R package [RandoDiStats](#). Current manuscript collaborations ready for submission include novel applications of this specific function to elucidate the volatilome of ripening fruit.

3.2.5 GitHub Repositories

All the GitHub repositories, an introduction to the code, its usage and the written functions have been compiled in several repositories that are linked to published or unpublished work of this thesis. The repositories are:

Publicly available repositories:

[RandoDiStats](#): Random distributions and their statistics.

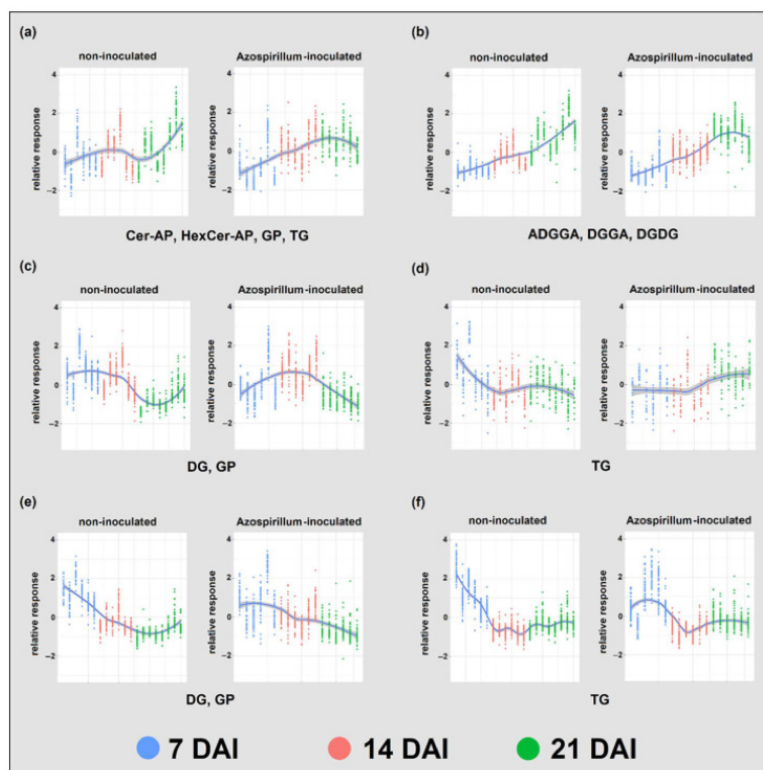


FIGURE 3.9: **Profile of lipid species identified in Azospirillum-inoculated and non-inoculated samples harvested at 7, 14, and 21 DAI using K-means clustering.** Clusters formed in the two treatments were paired based on their lipid species composition (a–f). At each time point, biological replicates are displayed as lines of dots, where each dot represents a lipid species. The main lipid classes of each cluster couple are also displayed. Shade of the fitting line represents the standard deviation within metabolite groups. ADGGA: acyl diacylglyceryl glucuronide, Cer-AP: ceramide alpha-hydroxy fatty acid-phytospingosine, DG: diacylglycerol, DGDG: digalactosyldiacylglycerol, DGGGA: diacylglyceryl glucuronide, GP: glycerophospholipids, HexCer-AP: hexosylceramide alpha-hydroxy fatty acid-phytospingosine, TG: triacylglycerol.

COSNET_i: Integration of omics relative changes into sampled interaction networks translated from cryogenic or crystallographic based atomic structures of multiprotein complexes.

Align two FASTA files: Align two FASTA files

Private repositories until publication: (The private repositories have been compiled as Supplemental Files of this thesis)

KineticMSI: functions to interpret stable isotope assisted mass spectrometry imaging experiments. Supplemental File 1.

KineticMSI adaptation to kLCMS data: Adaptation of kLCMS data for usage with the KineticMSI R package. Supplemental File 2.

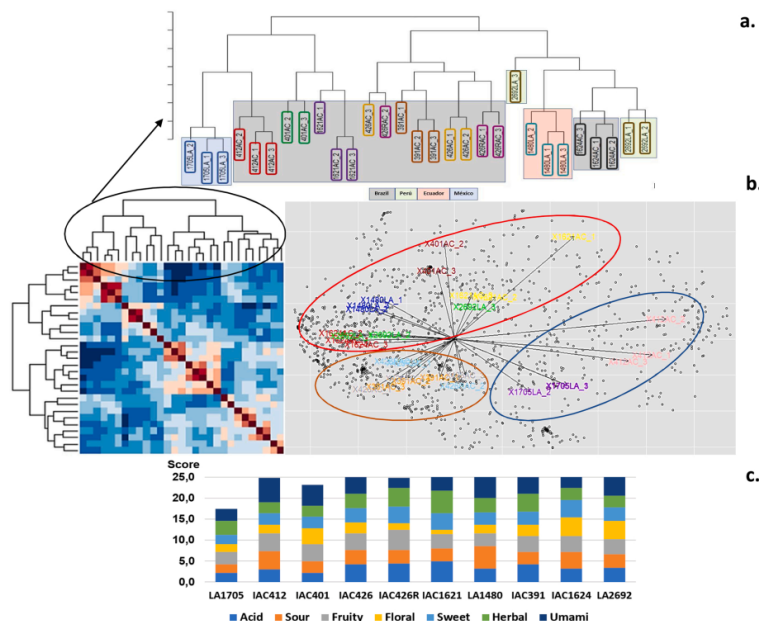


FIGURE 3.10: Differences among profiles of ten wild cherry tomato accessions obtained by HS-SPME/GC/MS and sensory analysis. a. Correlation dendrogram differentiated by country of origin. Colored delineated squares show each accession, blue: LA1705, red: IAC412, green: IAC401, purple: IAC1621, yellow: IAC426, fuchsia: IAC426R, orange: IAC391, brown: LA2692, light blue: LA1480, black: IAC1624. b. [Left] Heatmap and correlation dendrogram visualizing hierarchical clustering of the accessions according to VOCs mass feature expression profiles. Color scale ranges from light blue to red, smallest to largest values respectively. [Right] PCA carried out on auto scaled mass features that comprise the volatilome of evaluated accessions. Blue circle: LA1705 and IAC412. Red circle: IAC401, LA1480, IAC1421, IAC1624 and LA2692. Orange circle: IAC391, IAC426 and IAC426R. c. Sensory profile with seven descriptors, scores are the overall mean of each descriptor.

ProtSynthesis: R package to calculate fractional protein synthesis rates. Supplemental File 3.

ProteoMSI: Functions and methods for peptide fingerprinting from mass spec imaging data. Supplemental File 4.

3.3 Extended Methods

Since this thesis contains material that has not yet been published, all supplementary methods used to generate these data, as well as all other experimental procedures that have not yet been reported, have been included in the appendix C.

Bibliography

- [1] Rayan Awada, Claudine Campa, Estelle Gibault, Eveline Déchamp, Frédéric Georget, Maud Lepelley, Cécile Abdallah, Alexander Erban, Federico Martinez-Seidel, Joachim Kopka, Laurent Legendre, Sophie Léran, Geneviève Conéjéro, Jean Luc Verdeil, Dominique Crouzillat, David Breton, Benoît Bertrand, and Hervé Etienne. Unravelling the metabolic and hormonal machinery during key steps of somatic embryogenesis: A case study in coffee. *International Journal of Molecular Sciences*, 20(19):4665, 2019. ISSN 14220067. doi: 10.3390/ijms20194665.
- [2] Federico I. Brigante, Agustin Lucini Mas, Alexander Erban, Ines Fehrle, Federico Martinez-Seidel, Joachim Kopka, Daniel A. Wunderlin, and Maria V. Baroni. Authenticity assessment of commercial bakery products with chia, flax and sesame seeds: Application of targeted and untargeted metabolomics results from seeds and lab-scale cookies. *Food Control*, 140:109114, 2022. ISSN 09567135. doi: 10.1016/j.foodcont.2022.109114.
- [3] Bo Eng Cheong, Olga Beine-Golovchuk, Michal Gorka, William Wing Ho Ho, Federico Martinez-Seidel, Alexandre Augusto Pereira Firmino, Aleksandra Skiryecz, Ute Roessner, and Joachim Kopka. Arabidopsis REI-LIKE proteins activate ribosome biogenesis during cold acclimation. *Scientific Reports*, 11(1):1–25, 2021. ISSN 20452322. doi: 10.1038/s41598-021-81610-z.
- [4] Bo Eng Cheong, Dingyi Yu, Federico Martinez-Seidel, William Wing Ho Ho, Thusitha W. T. Rupasinghe, Rudy Dolferus, and Ute Roessner. The Effect of Cold Stress on the Root-Specific Lipidome of Two Wheat Varieties with Contrasting Cold Tolerance. *Plants*, 11(10):1364, 2022. ISSN 2223-7747. doi: 10.3390/plants11101364.
- [5] Alexander Erban, Ines Fehrle, Federico Martinez-Seidel, Federico Brigante, Agustín Lucini Más, Veronica Baroni, Daniel Wunderlin, and Joachim Kopka. Discovery of food identity markers by metabolomics and machine learning technology. *Scientific Reports*, 9(1):1–19, 2019. ISSN 20452322. doi: 10.1038/s41598-019-46113-y.
- [6] Alexander Erban, Federico Martinez-Seidel, Yogeswari Rajarathinam, Frederik Dethloff, Isabel Orf, Ines Fehrle, Jessica Alpers, Olga Beine-Golovchuk, and

- Joachim Kopka. Multiplexed Profiling and Data Processing Methods to Identify Temperature-Regulated Primary Metabolites Using Gas Chromatography Coupled to Mass Spectrometry. In Dirk K Hinch and Ellen Zuther, editors, *Methods in Molecular Biology*, volume 2156, pages 203–239. Springer US, New York, NY, 2020. ISBN 978-1-0716-0660-5. doi: 10.1007/978-1-0716-0660-5_15.
- [7] Alexandre Augusto Pereira Firmino, Michal Gorka, Alexander Graf, Aleksandra Skiryecz, Federico Martinez-Seidel, Kerstin Zander, Joachim Kopka, and Olga Beine-Golovchuk. Separation and paired proteome profiling of plant chloroplast and cytoplasmic ribosomes. *Plants*, 9(7):1–29, 2020. ISSN 22237747. doi: 10.3390/plants9070892.
- [8] L. M. Londoño-Giraldo, A. M. Baena-Pedroza, F. Martinez-Seidel, E. Corpas-Iguarán, and G. Taborda-Ocampo. Gone wild: Integration of antioxidative, physicochemical, volatilomic and sensorial profiles ratify rustic relatives of cherry tomato as ideal mating partners. *Scientia Horticulturae*, 277:109814, 2021. ISSN 03044238. doi: 10.1016/j.scienta.2020.109814.
- [9] Tamires Oliveira Melo, Luziane Franciscan, George Brown, Joachim Kopka, Luis Cunha, Federico Martinez-Seidel, Luiz Augusto dos Santos Madureira, and Fabricio Augusto Hansel. Univariate statistical analysis of gas chromatography – mass spectrometry fingerprints analyses. *Chemical Data Collections*, 33:100719, 2021. ISSN 24058300. doi: 10.1016/j.cdc.2021.100719.
- [10] Martino Schillaci, Cheka Kehelpannala, Federico Martinez-Seidel, Penelope M.C. Smith, Borjana Arsova, Michelle Watt, and Ute Roessner. The metabolic response of brachypodium roots to the interaction with beneficial bacteria is affected by the plant nutritional status. *Metabolites*, 11(6):358, 2021. ISSN 22181989. doi: 10.3390/metabo11060358.

Chapter 4

Membrane-Enriched Proteomics Link Ribosome Accumulation and Proteome Reprogramming With Cold Acclimation in Barley Root Meristems



Membrane-Enriched Proteomics Link Ribosome Accumulation and Proteome Reprogramming With Cold Acclimation in Barley Root Meristems

Federico Martinez-Seidel^{1,2*†}, Pipob Suwanhaikasem^{1†}, Shuai Nie³, Michael G. Leeming^{3,4}, Alexandre Augusto Pereira Firmino², Nicholas A. Williamson^{3,5}, Joachim Kopka², Ute Roessner¹ and Berin A. Boughton^{1,6}

¹ School of BioSciences, The University of Melbourne, Parkville, VIC, Australia, ² Willmitzer Department, Max-Planck-Institute of Molecular Plant Physiology, Potsdam-Golm, Germany, ³ Bio21 Institute of Molecular Science and Biotechnology, The University of Melbourne, Parkville, VIC, Australia, ⁴ School of Chemistry, The University of Melbourne, Parkville, VIC, Australia, ⁵ Department of Biochemistry and Molecular Biology, The University of Melbourne, Parkville, VIC, Australia, ⁶ Australian National Phenome Centre, Murdoch University, Murdoch, WA, Australia

OPEN ACCESS

Edited by:

Dominique Job,
UMR 5240 Microbiologie, Adaptation
et Pathogenie (MAP), France

Reviewed by:

Riffat John,
University of Kashmir, India
Klára Kosová,
Crop Research Institute (CRI),
Czechia

*Correspondence:

Federico Martinez-Seidel
mseidel@mpimp-golm.mpg.de

†These authors share first authorship

Specialty section:

This article was submitted to
Plant Proteomics and Protein
Structural Biology,
a section of the journal
Frontiers in Plant Science

Received: 21 January 2021

Accepted: 22 March 2021

Published: 30 April 2021

Citation:

Martinez-Seidel F,
Suwanhaikasem P, Nie S,
Leeming MG, Pereira Firmino AA,
Williamson NA, Kopka J, Roessner U
and Boughton BA (2021)
Membrane-Enriched Proteomics Link
Ribosome Accumulation
and Proteome Reprogramming With
Cold Acclimation in Barley Root
Meristems.
Front. Plant Sci. 12:656683.
doi: 10.3389/fpls.2021.656683

Due to their sessile nature, plants rely on root systems to mediate many biotic and abiotic cues. To overcome these challenges, the root proteome is shaped to specific responses. Proteome-wide reprogramming events are magnified in meristems due to their active protein production. Using meristems as a test system, here, we study the major rewiring that plants undergo during cold acclimation. We performed tandem mass tag-based bottom-up quantitative proteomics of two consecutive segments of barley seminal root apices subjected to suboptimal temperatures. After comparing changes in total and ribosomal protein (RP) fraction-enriched contents with shifts in individual protein abundances, we report ribosome accumulation accompanied by an intricate translational reprogramming in the distal apex zone. Reprogramming ranges from increases in ribosome biogenesis to protein folding factors and suggests roles for cold-specific RP paralogs. Ribosome biogenesis is the largest cellular investment; thus, the vast accumulation of ribosomes and specific translation-related proteins during cold acclimation could imply a divergent ribosomal population that would lead to a proteome shift across the root. Consequently, beyond the translational reprogramming, we report a proteome rewiring. First, triggered protein accumulation includes spliceosome activity in the root tip and a ubiquitous upregulation of glutathione production and S-glutathionylation (S-GSH) assemblage machineries in both root zones. Second, triggered protein depletion includes intrinsically enriched proteins in the tip-adjacent zone, which comprise the plant immune system. In summary, ribosome and translation-related protein accumulation happens concomitantly to a proteome reprogramming in barley root meristems during cold acclimation. The cold-accumulated proteome is functionally implicated in feedbacking transcript to protein translation at both ends and could guide cold acclimation.

Keywords: *Hordeum vulgare*, cv Keel, abiotic stress, translation, ribosomal protein paralog, fungal priming elicitors, chitin, chitosan

INTRODUCTION

Cereals face two kinds of low-temperature challenges. The first is vernalization (Chouard, 1960; Von Zitzewitz et al., 2005; Deng et al., 2015), which is bound to seasonal climate and acts as a cue to induce the transition from vegetative to reproductive development. The second is cold acclimation (Thomashow, 1999; Miura and Furumoto, 2013), which occurs in response to sudden cold stimuli and requires phenotypic plasticity to respond. Plants acclimate to low temperatures using a systemic response (Hinch and Zuther, 2020) that ranges from hormonal, auxin-dependent signaling (Shibasaki et al., 2009; Rahman, 2013), through primary metabolism (Kaplan et al., 2004; Zuther et al., 2019; Erban et al., 2020), and to membrane-lipidome compositional changes (Uemura et al., 1995; Cheong et al., 2019, 2020). Typical cold responses have been divided according to the response time after the initial stimulus (Seki et al., 2002) and involve proteins that function as the principal modulators. A well-known example of an immediate cold response is the C-repeat binding factor (CBF) regulatory pathway (Jaglo-Ottosen et al., 1998; Thomashow, 1999; Fowler and Thomashow, 2002) that operates a transcriptional regulon both in dicots (Park et al., 2015) and in monocots (Novák et al., 2017). On the other hand, long-term responses are less well understood and could partially rely on more permanent changes, for instance, by including altered protein translation or ribosomes as a main hub of the cold response or memory (Beine Golovchuk et al., 2018; Garcia-Molina et al., 2020; Cheong et al., 2021).

At the physiological level, changes occurring due to cold acclimation are coupled to molecular mechanisms in the roots from the model dicot *Arabidopsis thaliana* (Ashraf and Rahman, 2019). *Arabidopsis* roots respond to 4°C by reducing root growth, specifically mitotic division but not cell elongation, which significantly decreases the size of the meristem. A partial growth arrest occurs because of altered trafficking of auxin efflux carriers. The resulting imbalance in the intracellular auxin concentrations is caused by inhibition of the ARF guanine-nucleotide exchange factor GNOM (Ashraf and Rahman, 2019), which functions as an ADP ribosylation/GTP exchange factor (ARF-GEF; Steinmann et al., 1999). Reduced GNOM abundances delay papillae formation, which are localized cell-wall appositions implicated in plant innate immunity, e.g., against barley powdery mildew fungus (Nielsen et al., 2012). Consequently, the inhibition of GNOM during cold stress could render plants more susceptible to fungal pathogens. Contrary to expectations, cold stress seems to improve immunity against fungi in cereals (Płazek et al., 2003; Kuwabara and Imai, 2009), where linked mechanisms are even less clear, indicating some level of unknown cellular remodeling.

Monocots, which include cultivated cereal crops, and dicots share convergent evolution and common ancestors. Barley root systems (*Hordeum vulgare* L.), for instance, have unique

and conserved features (Kirschner et al., 2017) that outline root evolution. Thus, interchangeable insights from shared molecular mechanisms routinely provide design rationale for crop science improvement. Expanding upon our understandings of root molecular physiology will further detail unique and conserved mechanisms across plant lineages, where the current gaps extend to root spatial proteome composition, biological steady states, and plasticity. The landscape of root cells is intrinsically heterogeneous, with cells coexisting in multiple biological steady states (Dinneny and Benfey, 2008), while meristems establish the primary root and machinery to import and utilize nutrients (Nelson et al., 2014), and differentiated root tissue matures and engages in metabolism. These transient developmental states serve as a basal level to compare the proteome of plants challenged with biotic or abiotic stress cues. Moreover, by carefully studying specific developmental stages, a quasi-steady state rate of turnover for subsets of proteins might be assumed (Huffaker and Peterson, 1974), allowing clear distinctions between unperturbed and challenged plant proteomes. Spatially, compositional changes in the plant proteome can be magnified in root zones with high protein production rates such as meristem apices and cell division zones (Clowes, 1958; Verbelen et al., 2006).

Cold responses can be traced back to proteins and proteome shifts (Janmohammadi et al., 2015) affecting root molecular physiology. Studying the *in planta* responsiveness of the root proteome to cold presents its own difficulties. For instance, hydroponic systems imply adding exogenous sugar to the growth media and/or triggering roots with undesired light stimuli. Additionally, harvesting of whole root systems precludes distinguishing rapid proteome changes because newly synthesized and preexisting proteins are pooled together. The impact of these limitations can be minimized using prolonged stratification to study cold acclimation in root tips. Seed stratification, an early cold cue applied to imbibed seeds during germination, is comparable in magnitude with low temperature plant acclimation. Stratification enhances and synchronizes seed germination through the action of reactive oxygen species (ROS) oxidizing biomolecules and acting in concert with phytohormones (Su et al., 2016; Bailly, 2019). However, we argue that extended and maintained stratification triggers acclimation. First, the cold stimulus induces upregulation of the protein post-translational modification (PTM), specifically the S-glutathionylation machinery that could act proteome-wide as will be described in this study. Low temperature induction of both thiol-modifying and antioxidative machineries has been reported in plants (Koehler et al., 2012; Golemic and Gołębiowska-Pikania, 2015). Glutathione is added to newly formed proteins via cysteine residues where they act as ROS scavengers (Diaz-Vivancos et al., 2015). Second, typical cold acclimation triggers a transcriptome-wide reprogramming characterized by a rapid increase of transcript splicing variants (Calixto et al., 2018). Spliceosome activity co-occurs with a vast translational reprogramming in root apices (this study). Thus, the mentioned observations along with accumulation of cold markers in our datasets ratify stratified barley root tips as a legitimate study system for plant proteome cold acclimation. Additionally, these

Abbreviations: AU-P, approximately unbiased probability values; BSA, bovine serum albumin; FDR, false discovery rate; FW, fresh weight; GLMs, generalized linear models; LB, lysis buffer; PTM, post-translational modification; RAP, ribosome-associated protein; REB, ribosome extraction buffer; ROS, reactive oxygen species; RP, ribosomal protein; SC, sucrose cushion; S-GSH, S-glutathionylation; TMT, tandem mass tag.

observations warrant exploration as to whether they are linked. This hypothesis stands to reason and could involve cold-specialized ribosomes in plants (Martinez-Seidel et al., 2020) that may select alternatively spliced transcripts for translation while generating feedback on the PTM machinery.

Here, we uncover previously hidden aspects of cold proteome-wide responses that are concomitant to a highly committed ribosome accumulation. We provide an overview of the changes in the apical and adjoined more distal seminal root segments. The biological responses are clear and specific for each root zone but share commonalities. An observed translational reprogramming event near the root meristem, where the cold triggered ribosome accumulation happened, led us to analyze homology between both *Arabidopsis* ribosome-associated proteins (RAPs) and ribosomal protein (RP) families and barley homologs. This information was previously not available and allowed us to test for and compare cold-specific RAP and RP paralogs. Finally, we outline cold-triggered shifts of the proteome where specific molecular functions were enhanced or diminished. As an example, we discuss seedling priming for biotic stress, which could be interpreted as both enhanced and diminished by cold in our dataset. Thus, in order to understand how cold-acquired resistance arises, we treated the plants with conventional fungal priming elicitors, chitin and chitosan, as they would be treated in the field. This allowed us to understand that the priming elicitors do not trigger significant proteome shifts that are shared with cold derived responses and thus speculate on how cold-acquired resistance might stem from different cellular processes in barley roots as compared with elicitor-induced resistance.

MATERIALS AND METHODS

Growth Conditions

Hordeum vulgare cv Keel seeds were sourced from The University of Melbourne from previous studies (Gupta et al., 2019). Parental plants were grown under optimized conditions for seed production. Seeds were surfaced-sterilized in 70% (1 min) ethanol and 1% bleach (10 min) and washed. Imbibition lasted 12 h. Seeds were transferred to Petri dishes containing a filter paper and 3 cm³ Hoagland medium. For priming, 1% chitin or chitosan was mixed (Lowe et al., 2012; Cretoi et al., 2013). Dishes were left in the dark at 25°C/18°C (16 h/8 h), inside a phytotron growth chamber (Weiss Technik, Germany) for 48 h of germination. Then half of the dishes were shifted to 4°C. Seeds were germinated for a total of 7 days. The treatments were as follows: control (7 days at 25°C/18°C) with or without 1% chitin or chitosan priming compounds, and cold (2 days control germination and 5 days at 4°C). Roots were cut and instantly frozen; ~1.5-cm seminal root (Supplementary Figure 1) segment pools were ground in liquid nitrogen, separated in ~40-mg aliquots, and stored at -80°C.

Proteomics Profiling

Protein Extraction

Aliquots were solubilized in 200 mm³ of ribosome extraction buffer (REB), incubated on ice for 20 min, and centrifuged

at 17,900 × *g* for 10 min at 4°C. Supernatant was loaded into a QIAshredder (Qiagen) and centrifuged full-speed for 1 min; 400 mm³ of 6 M guanidine-HCl was added to the flow through, followed by 4 mm³ of neat trifluoroacetic acid (TFA). Centrifugation was repeated to precipitate out RNA. The final supernatant was reserved. The initial pellet was solubilized in 600 mm³ of lysis buffer (LB), vortexed, incubated at 95°C for 3 min, and sonicated for 5 min. Centrifugation was carried out as before, and supernatant was collected. Both supernatants were mixed with -20°C precooled 10% trichloroacetic acid (TCA) dissolved in acetone and freshly supplemented with 1× protease inhibitor cocktail (Sigma, P9599) for 16 h. The solution was centrifuged at 17,900 × *g* for 10 min. Finally, the protein pellet was washed twice with -20°C acetone and air-dried.

Ribosome extraction buffer was prepared as previously described (Firmino et al., 2020) without sodium deoxycholate (DOC).

Lysis buffer was 4% sodium dodecyl sulfate (SDS); 100 mM of Tris/HCl, pH 7.4; 1× protease inhibitor cocktail (Sigma, P9599).

Ribosomal Protein Content

Modified REB was used in order to extract ribosomes from a total of six biological replicates (*n* = 6). Briefly, the detergent mix was replaced by octyl beta-D-glucopyranoside (≥98% Sigma-Aldrich, O8001) concentrated 0.01 M above the critical micelle concentration of 0.025 M in order to hold micelles after cell lysis. Diluted extracts (3.5×) derived from 200 mg of fresh weight (FW) were centrifuged at 330,000 × *g* for 4.5 h on a 70.1Ti rotor (Type 70.1 Ti Rotor, Beckman Coulter, United States). Extracts were layered inside thick-walled polycarbonate tubes with three-piece caps (10.4 cm³, polycarbonate bottle with cap assembly, 16 mm × 76 mm—6Pk, 355603, Beckman Coulter, United States) on top of 2.5 cm³ of 30% sucrose cushion (SC) solution.

Sucrose cushion was 0.4 M of Tris, pH 9.0, 0.2 M of KCl, 0.005 M of EGTA, pH 8.0, 0.035 M of MgCl₂ × 6H₂O, and sucrose (Molecular Biology Grade, 573113, Sigma-Aldrich, Australia). Additions before extraction were 0.15 mM of chloramphenicol, 0.18 mM of cycloheximide, and 5 mM of DTT.

Pure *Escherichia coli* ribosomes (P0763S, NEB, Australia) were ultracentrifuged following the same procedure as a control of the ribosomal particles passing the cushion. After ultracentrifugation, pellets enriched in ribosomes were diluted in 6 M of GuHCl, acidified to 1% TFA, and centrifuged at max speed in a benchtop microcentrifuge. The supernatant was recovered, and protein content was evaluated using the bicinchoninic acid (BCA) kit (Thermo Scientific, United States) assay as detailed in the following section.

Protein Digestion

Protein pellets were resuspended using 8 M of urea in 50 mM of triethylammonium bicarbonate (TEAB), pH 8.5, sonicated for 20 min at 37°C, and centrifuged at 20,627 × *g* for 2 min. Protein contents were measured using the BCA assay (see section “Induced Changes of the Root Proteome”). Protein of 1 mg/cm³ was reduced with tris(2-carboxyethyl)phosphine (TCEP; 10 mM of final concentration) at 37°C for 45 min and alkylated with iodoacetamide (IAA; 55 mM of final concentration) at 37°C for

45 min in the dark. Solution was diluted with 25 mM of TEAB at pH 8.5 to 1 M of urea. Trypsin (Pierce Trypsin Protease, mass spectrometry grade, Thermo Fisher Scientific) in 25 mM of TEAB was added to the samples (1:40) and shaken overnight at 37°C. TFA was added to 1% final volume. Peptides were loaded in Oasis solid-phase extraction (SPE) cartridges (Waters Co., United States), washed with 0.1% TFA, and eluted out using 80% acetonitrile (ACN) with 0.1% TFA. Peptides were dried in a vacuum concentrator (Savant ISS110, Thermo Fisher Scientific) and a freeze-dryer (Alpha 3-4 LSCbasic, Christ).

Tandem Mass Tag Labeling

Tandem mass tag (TMT) labeling was done as previously reported (Zecha et al., 2019) with minor modifications. Ten micrograms of peptides was labeled with 4 mm³ of 6-plex TMT labeling reagent (0.8 mg of TMT in 41 mm³ of ACN). Labeling reaction was incubated for 1 h at 25°C and 400 rpm in a benchtop-shaking incubator. One cubic millimeter of 5% hydroxylamine was added and incubated for 15 min as before. Finally, 10 mm³ of labeled peptides from each sample was mixed and cleaned using the SPE cartridge procedure. Cleaned peptides were resuspended in MS loading buffer (2% ACN, 0.05% TFA) and loaded into a nano-electrospray ionization–liquid chromatography–tandem MS (nano-ESI-LC-MS/MS).

LC-MS/MS Analyses

The nano-LC system, Ultimate 3000 RSLC (Thermo Fisher Scientific), was equipped with an Acclaim PepMap nano-trap column (C18, 100 Å, 75 µm × 2 cm, Thermo Fisher Scientific) and an Acclaim PepMap RSLC analytical column (C18, 100 Å, 75 µm × 50 cm, Thermo Fisher Scientific) maintained at a temperature of 50°C. For each LC-MS/MS experiment, 1 µg of peptides was loaded onto the enrichment (trap) column at an isocratic flow of 5 mm³/min of 3% ACN containing 0.05% TFA for 6 min before the enrichment column was switched in-line with the analytical column. The eluents used for the LC were water with 0.1% v/v formic acid and 5% v/v dimethyl sulfoxide (DMSO) for solvent A, and ACN with 0.1% v/v formic acid and 5% DMSO for solvent B. The gradient used (300 nl/min) was from 3% B to 23% B for 144 min, 23% B to 45% B in 10 min, and 45% B to 80% B in 10 min and maintained at 80% B for the final 5 min before dropping to 3% B in 1 min and equilibration for 9 min at 3% B prior to the next analysis. The MS experiments were performed using a nano-ESI source at positive mode and Orbitrap Eclipse mass spectrometer (Thermo Fisher Scientific, San Jose, CA, United States). The spray voltages, capillary temperature, and S-lens RF level were set to 1.9 kV, 275°C, and 30%. The MS data were acquired with a 3-s cycle time for one full-scan MS spectra and as many data-dependent higher-energy collisional dissociation (HCD)-MS/MS spectra as possible. Full-scan MS spectra had a *m/z* of 375–1,500, a resolution of 120,000 at *m/z* 200, an automatic gain control (AGC) target value of 4e⁵, and a maximum ion trapping time of 50 ms. The data-dependent HCD-MS/MS of precursor ions (charge states from 2 to 7) was performed using an *m/z* isolation window of 1.6, a first mass at *m/z* of 100, an AGC target value of 5e⁴, a normalized collision energy (NCE) of 30%, a resolution of

15,000 at *m/z* 200, and a maximum ion trapping time of 22 ms. Dynamic exclusion was used for 30 s.

Data Acquisition and Interpretation Barley Proteome

The recovered proteome from different extraction methods was evaluated from a total of three biological replicates (*n* = 3, **Supplementary Figure 2**). *H. vulgare* gene IDs and FASTA sequences (**Supplementary Table 1**) were obtained by aligning Swiss-Prot entries (351 reviewed proteins downloaded on 21. March 2020, “uniprot-hordeum + vulgare-filtered-reviewed_yes + AND + organism__Hordeum + vulgar.fasta”) with high-confidence proteogenomics annotations.¹ The same annotations were then used to evaluate proteome shifts occurring due to experimental conditions from a total of five biological replicates (*n* = 5, **Supplementary Figure 3**). Gene ontology (GO) terms were obtained by intersecting *H. vulgare* GOs from the AmiGO database (Carbon et al., 2009; Mi et al., 2019) and the GOexpress (Rue-Albrecht et al., 2016) R package (**Supplementary Figure 4** and **Supplementary Table 1**). Ontology assignments were performed using GO enrichment (the GO resource) (Carbon et al., 2009; Mi et al., 2019). Outputs were hierarchically sorted and interpreted as a group. The false discovery rate (FDR)-corrected Fisher exact test was applied. Lists of GOs were inputted into REVIGO (Supek et al., 2011) to remove redundant GOs and build semantic similarity-based scatterplots **Supplementary Table 2**.

Homology Alignments

A function to align two FASTA files was written. The usage is detailed in a GitHub repository.² The alignment is a dependency of the pairwiseAlignment R function (Durbin et al., 1998; Haubold and Wiehe, 2006; Malde, 2008).³ pairwiseAlignment solves the global (Needleman and Wunsch, 1970), local (Smith and Waterman, 1981), or (ends-free) overlap pairwise sequence alignment problems. BLAST (Altschul et al., 1990), in comparison, is a development of the Smith–Waterman algorithm. Accuracy is significantly better in the Smith and Waterman as compared with BLAST (Pearson, 1995; Shpaer et al., 1996). However, the efficiency is lower in the Smith and Waterman global alignment. All alignments were performed with the default settings of the pairwiseAlignment function, i.e., global, which is equivalent to the online version of BLAST that has an interface for global (Needleman–Wunsch) alignment.⁴ Alignment scores were treated as a relative scale where the largest numbers represent the best alignments and comparisons can be then drawn for lower scores. Alignment scores > 10 were selected as acceptable for potential homology based on the examples provided in the package documentation.

¹<http://pgsb.helmholtz-muenchen.de/plant/barley/index.jsp>

²<https://github.com/MSeidelFed/Align2FASTAs>

³<https://www.rdocumentation.org/packages/Biostrings/versions/2.40.2/topics/pairwiseAlignment>

⁴https://blast.ncbi.nlm.nih.gov/Blast.cgi?PAGE_TYPE=BlastSearch&PROGRAM=blastn&BLAST_PROG_DEF=blastn&BLAST_SPEC=GlobalAln&LINK_LOC=BlastHomeLink

Protein Contents

Protein contents ($n = 5$) were fitted in a linear regression of bovine serum albumin (BSA) (**Supplementary Table 3**). Values were transformed into $\mu\text{g}/\text{mg}$ of FW by normalizing to initial weight. The Shapiro–Wilk test and the Brown–Forsythe Levene-type test (bootstrapped when $n > 10$) were done to test normality and homoscedasticity. Kurtosis and square of skewness defined the distribution shapes of variables (**Supplementary Figure 5**). Variable distributions were plotted in a scatterplot along with exemplary distributions as detailed in RandoDiStats.⁵ Based on the known distributions, generalized linear models (GLMs) with an appropriate link function were used to test mean differences.

Shotgun Proteomics

Pre-processing

Proteomics data have been deposited to the ProteomeXchange Consortium (Deutsch et al., 2020) via the PRIDE (Perez-Riverol et al., 2019) partner repository with the dataset identifier PXD021731. RAW chromatograms were processed with MaxQuant, version 1.6.10.43 (Cox and Mann, 2008). TMT data correction (Thompson et al., 2003) was performed using the relative enrichment percentages of the tags. Isotope purity-corrected reporter ion intensities were obtained for each isobaric labeling channel summed over all MS/MS spectra matching to each protein group from the MaxQuant search. Search parameters include the following: (1) fixed—carbamidomethyl (C) and variable—oxidation (M), acetyl (protein N-term) modifications. (2) Allowed missed cleavages = two. Everything else was set as default. The TMT-corrected intensity matrix was imported into Perseus (Tyanova et al., 2016). Intensities were \log_2 transformed and normalized to pooled samples (analyzed together with each 6-plex TMT sample), enabling relative quantitation between root zones. Reverse search rows were used to adjust the annotations using the FDR (1%), complemented by acceptance of razor + unique peptides (UP) with a collective value of two or more. A multitude of volcano plots, a.k.a. a Hawaii plot, was built using Perseus (Tyanova et al., 2016). The \log_2 ratio between samples and controls was plotted in the x -axis against $-\log_{10}(P \text{ adjusted values})$ in the y -axis (**Supplementary Figure 3**).

Statistics

Class discovery was applied on a non-scaled \log_2 -transformed matrix (**Supplementary Table 4**, columns B–AN); proteins were clustered by covariance, enabling to find correlated proteins with large absolute changes, i.e., highly abundant in roots. Values in cells are proportions relative to pooled samples. Hierarchical cluster analysis (HCA) was performed using Pearson correlation as distance and average clustering as building method. Clustering was bootstrapped 10,000 and 1,000 times for treatments and proteins, respectively. “Approximately unbiased” (AU) P values were calculated using the R package pvclust (Suzuki and Shimodaira, 2006). Heatmaps were built using the R package ComplexHeatmap (Gu et al., 2016) enhanced for data pre-processing with the packages circlize (Gu et al., 2014) and matrixStats⁶ (**Supplementary Table 4**).

⁵https://github.com/MSeidelFed/RandodiStats_package

⁶<http://CRAN.R-project.org/package=matrixStats>

Class comparison was applied to a normalized matrix; gamma parametrization of means through a link function is impaired by negative values. The distribution of proteins was analyzed (**Supplementary Figure 5**).⁵ Variables were tested for normality and homoscedasticity (**Supplementary Table 4**, column BG). Parametric data were fitted using the identity link function and a GLM. Non-parametric data were fitted with an appropriate link function after calculating the point distance, using the raster R package,⁷ between exemplary fitted distributions and each response variable in our matrix (**Supplementary Figure 5**). There were two factors, root zone (two levels; tip and tip-adjacent) and treatments (four levels; control, cold, chitin, and chitosan). All interactions between factors were included. The control was the root zone tip-adjacent and the treatment “control.” There were eight regressors, i.e., β_0 - Intercept, β_1 - Factor 1 tip, β_2 - Factor 2 chitin, β_3 - Factor 2 chitosan, β_4 - Factor 2 cold, $\beta_1 \times \beta_2$ - Factor 1 tip:Factor 2 chitin, $\beta_1 \times \beta_3$ - Factor 1 tip:Factor 2 chitosan, $\beta_1 \times \beta_4$ - Factor 1 tip:Factor 2 cold. Finally, P values were adjusted with the FDR proposed by Benjamini and Hochberg (1995) (FDR-BH95; **Supplementary Table 4**).

Class prediction was applied to the same matrix used for class comparison. A combination of prediction methods with internal validation procedures and discriminant analyses based on least squares projections (PLS-DA or OPLS-DA) was used. Random forest used default settings of the R package randomForest (Wiener and Liaw, 2003); the classification error was plotted to decide which classes had good predictors. Two parallel tests were conducted, i.e., (1) between root zones and (2) cold against the other treatments. The importance of proteins as classification variables was evaluated using the Gini mean decrease. Simultaneously, the R package ropls (Thévenot et al., 2015) was used to fit an OPLS-DA to the root zone factor and a PLS-DA to the treatment factor. The variable importance for prediction (VIP) scores judged variable importance. Given that the latter analyses are more prone to overfitting, VIP scores were used as an interpretation aid (**Supplementary Table 4**).

RESULTS

Our sterile germination system avoided any light perception, allowing us to mimic optimal conditions during imbibition and early germination. After germination, barley seedlings were subjected to cold or mimic-biotic stimuli with fungal elicitors for a period of 5 days. This period of treatment-germination mimicked the natural time of seedling emergence, i.e., the time required for seeds when planted at a 50-mm depth to reach the soil surface (Kirby, 1993), while avoiding unnatural etiolation. Lack of etiolation was confirmed, and high-resolution images of the plants were taken (**Supplementary Figure 1**). Subsequently, the seminal root tips were harvested in two consecutive segments of 1.5 cm (**Supplementary Figure 1**), named as tip and tip-adjacent, and processed for proteome profiling (**Figure 1**). The tip sample contained the root cap, the meristematic cell division zone, the elongation zone, and parts of the early maturation

⁷<http://CRAN.R-project.org/package=raster>

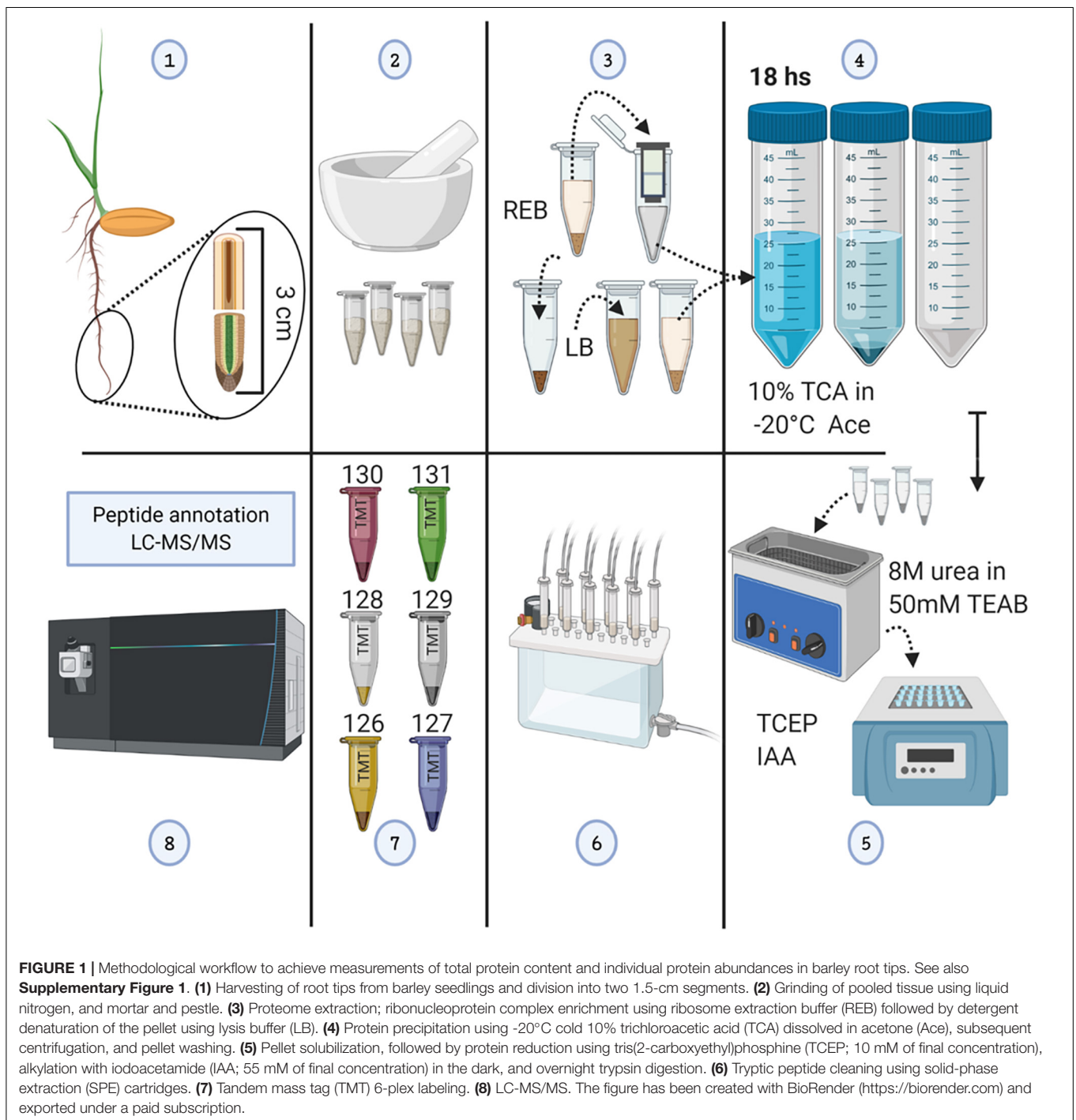


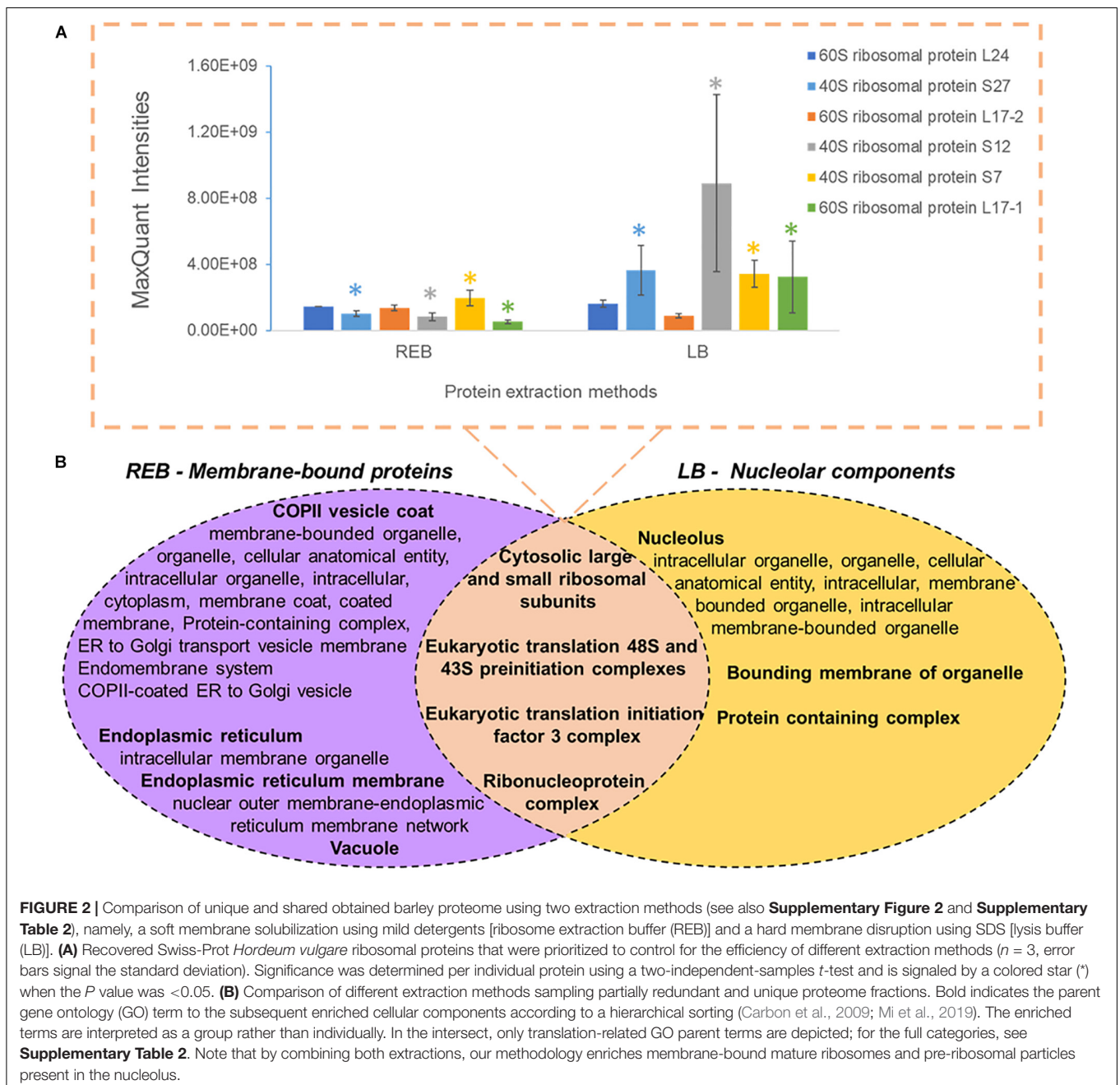
FIGURE 1 | Methodological workflow to achieve measurements of total protein content and individual protein abundances in barley root tips. See also **Supplementary Figure 1**. **(1)** Harvesting of root tips from barley seedlings and division into two 1.5-cm segments. **(2)** Grinding of pooled tissue using liquid nitrogen, and mortar and pestle. **(3)** Proteome extraction; ribonucleoprotein complex enrichment using ribosome extraction buffer (REB) followed by detergent denaturation of the pellet using lysis buffer (LB). **(4)** Protein precipitation using -20°C cold 10% trichloroacetic acid (TCA) dissolved in acetone (Ace), subsequent centrifugation, and pellet washing. **(5)** Pellet solubilization, followed by protein reduction using tris(2-carboxyethyl)phosphine (TCEP; 10 mM of final concentration), alkylation with iodoacetamide (IAA; 55 mM of final concentration) in the dark, and overnight trypsin digestion. **(6)** Tryptic peptide cleaning using solid-phase extraction (SPE) cartridges. **(7)** Tandem mass tag (TMT) 6-plex labeling. **(8)** LC-MS/MS. The figure has been created with BioRender (<https://biorender.com>) and exported under a paid subscription.

zone without root hairs. The tip-adjacent zone contained the remainder of the maturation zone without lateral roots.

Sampling the Barley Root Proteome

We used “housekeeping” RP abundances as a proxy of ribosome abundance and protein synthesis. We gave priority to six RPs that were part of the manually curated entries in UniProt (**Figure 2A**). See **Supplementary Table 1** for master annotation file. REB recovered significantly less protein of S7,

S27, S12, and L17-1 as than did LB (**Figure 2A**). Oppositely, statistically equivalent protein abundances of L17-2 and L24 were recovered with both methods (**Figure 2A**). In general, raw protein intensities derived from identical amounts of roots extracted by equal buffer volumes were higher when using LB as compared with REB (**Supplementary Figure 2**). Moreover, lysis methods using REB or strong LB for plant root cells solubilized different and overlapping fractions of the proteome (**Figure 2B**).



We performed GO enrichment of cellular components using the Protein ANalysis THrough Evolutionary Relationships (PANTHER) classification system, followed by summarized semantic similarity-based plots obtained in REduce + VIualize Gene Ontology (REVIGO) in order to understand the shared and specific proteomes between extraction methods (**Supplementary Table 2**). The strong extraction by LB, containing SDS, enhanced membrane disruption, allowing enrichment of nucleolar components. The milder detergent-mediated REB extraction solubilized membrane-bound complexes, cytoskeleton, or other insoluble proteins and protein complexes from transport vesicles, endoplasmic reticulum (ER), and Golgi components (**Figure 2B**).

Consequently, we combined the two extraction methods by performing first the native ribosome complex extraction via REB and then washing the pellet in denaturing LB buffer to recover the remaining proteome (**Figure 1**, step 3), thereby increasing proteome coverage while enriching for native ER-bound, nuclear and nucleolar associated ribosomes and RAPs.

Induced Changes of the Root Proteome Total Protein Contents

There was significantly more total protein in the root tip compared with tip-adjacent material (**Supplementary Table 3**). The tip was also significantly depleted in total protein more

during cold treatments than when using elicitor treatments (Figure 3A). Conversely, the tip-adjacent zone did not undergo drastic protein content changes upon either of the treatments. We observed similar changes of the bulk proteome using Hawaii plots of our treated samples normalized to protein content and measured through LC-MS/MS (Supplementary Figure 3).

There were 2.12 times more protein in the tip segment with a mean value of 9.57 $\mu\text{g}/\text{mg}$ FW. Cold treatment decreased the protein content significantly in the tip to 4.15 $\mu\text{g}/\text{mg}$ FW, and the proteome composition differed markedly from control, implying that a reprogramming with less bulk protein occurs

during the period of acclimation in root tips. Interestingly, proteome extracts enriched in ribosome complexes dramatically increased their content during cold acclimation (Figure 3B). The RP-enriched protein content increased from 2.6% (0.25 $\mu\text{g}/\text{mg}$ FW) of the total protein in the control to 18% (0.75 $\mu\text{g}/\text{mg}$ FW) of the total protein in the cold, suggesting a highly committed decision to either produce or not degrade ribosomes because the overall protein content drops significantly. By comparison, homeostasis of total protein content was retained in the tip-adjacent root zone during cold treatment with no significant change; however, many individual proteins were upregulated or

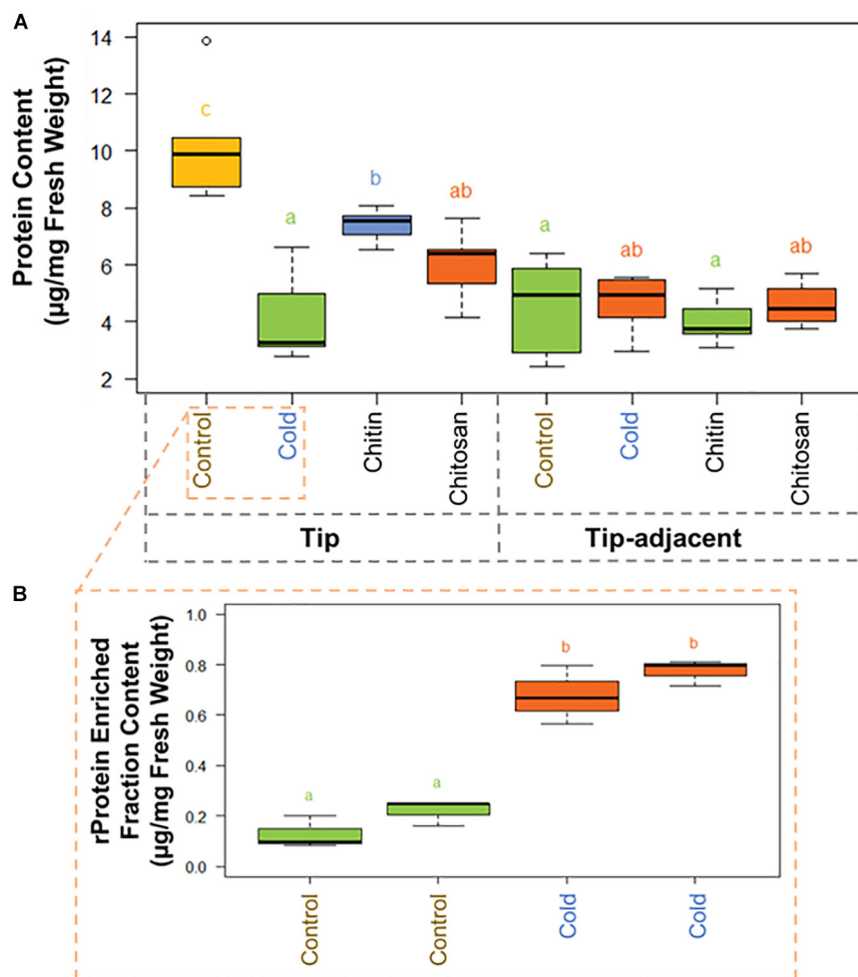


FIGURE 3 | Protein content boxplots from *Hordeum vulgare* roots treated during germination with cold temperature, or additions to the germination solution (chitin or chitosan). See also **Supplementary Figure 5** and **Supplementary Table 3**. **(A)** Total protein content was measured after protein extraction from $40 \text{ mg} \pm 5\%$ of starting root material and overnight precipitation ($n = 5$). **(B)** Ribosomal protein (rProtein) content was measured after ribosome enrichment from $200 \text{ mg} \pm 5\%$ of starting root material using a sucrose cushion and ribosomal protein dissociation using GuHCl as chaotrope ($n = 3 \times 2$ experimental blocks). Protein contents were measured using the bicinchoninic acid (BCA) assay with starting tissue amounts that yielded protein concentrations in the linear range of the assay. The protein content values were calculated from a linear regression of bovine serum albumin (BSA) standards after blank correction [i.e., to 3 M of urea in 50 mM of triethylammonium bicarbonate (TEAB)]. Subsequently, we tested the data normality and homoscedasticity assumptions to assess the applicability of univariate statistical tests; we used the Shapiro–Wilk and the Brown–Forsythe Leven-type test based on the absolute deviations from the median, bootstrapped when $n > 10$. The tip and upper root zone datasets are normally distributed and homoscedastic; the full dataset is gamma distributed and homoscedastic (**Supplementary Figure 5**). Generalized linear models (GLMs) of the Gaussian and gamma families were used to evaluate the difference between the means in the datasets and gave equivalent statistical differences as an ANOVA comparison followed by Tukey honestly significant difference (HSD) test between means. Therefore, small letters and color progressions derived from the Tukey HSD test are used to denote statistically different means.

downregulated. Mimicked-biotic stress treatments using chitin and chitosan elicitors significantly decreased the protein content to 7.39 and 6.00 $\mu\text{g}/\text{mg}$ FW, respectively, only in the root tips and not in the tip-adjacent segments.

Individual Protein Abundances

Statistical inference showed clear spatial and treatment-induced differences in proteome responses, validating previous observations and providing a proteomics fingerprint of the underlying biology (Figure 4 and Supplementary Table 4).

K-mean clustering of the ordinates found protein groups describing spatial root zones and treatments. Cluster 1 (Figure 4) featured proteins significantly increased in the tip-adjacent

zone and significantly depleted during cold at an FDR Benjamini–Hochberg 1995 (FDR-BH95') adjusted P values (aka Q values) < 0.05 . Cluster 3 (Figure 4) contained proteins significantly increased in the root tips and/or during cold. Most protein markers of root zones and/or cold treatment, according to variable selection by random forest methodology, were found in these two clusters. The remaining cold predictors were in cluster 2, which featured the strongest cold-induced increases that were consistent in both tip-adjacent and tip segments. Cluster 4 contained proteins significantly depleted during cold and low abundant in root tips, similar to cluster 1 but with smaller intensity amplitudes. Cluster 5 featured only few significantly changed proteins. In order to prevent a single clustering solution

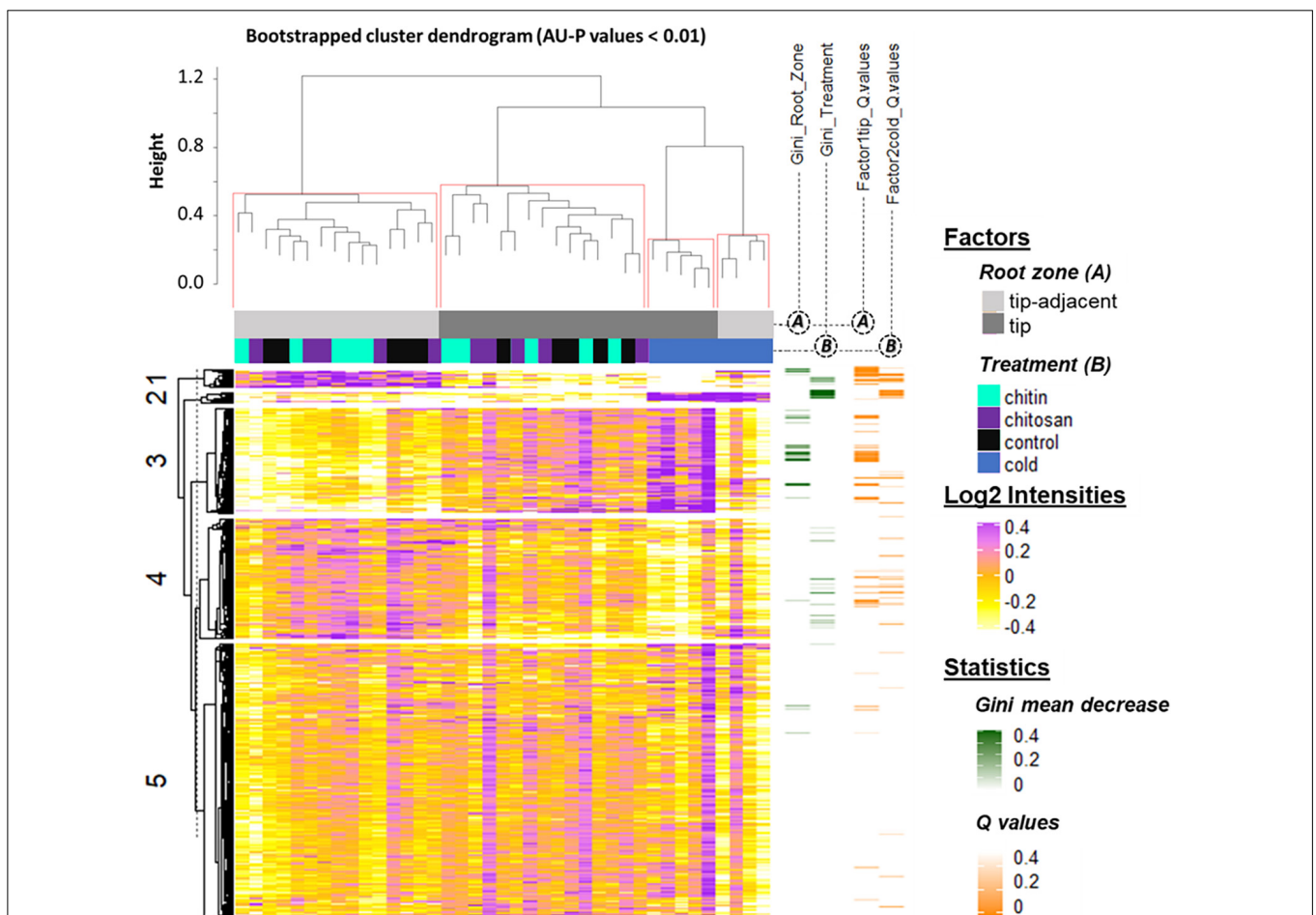


FIGURE 4 | Summary \log_2 -heatmap of statistical methods applied for class comparison, class discovery, and class prediction in LC-MS ($n = 5$). See also **Supplementary Figures 3, 5,** and **Supplementary Table 4**. Abscissa and ordinates were clustered using hierarchical cluster analysis (HCA) with Pearson correlation as distance measurement and average distance as clustering method. The clusters were bootstrapped, and approximately unbiased probability values (AU- P) values were calculated (red squares in the top cluster; see in **Supplementary Table 4** the clustered ordinates). Additionally, to aid interpretation, K-means clustering was performed in the ordinates and indicated by numbers from 1 to 5 to the left side of the clusters. Response variables were tested for homoscedasticity and normality. Non-parametric tandem mass tag (TMT)-corrected protein intensity distributions from *Hordeum vulgare* roots (detailed in **Supplementary Table 4**) were evaluated (**Supplementary Figure 5**) by functions of the GitHub repository RandoDiStats (https://github.com/MSeidelFed/RandodiStats_package). Subsequently, an appropriate link function was selected to fit a generalized linear model (GLM). P values were adjusted into Q values using the FDR-BH95'. Orange colored rows in the third heatmap to the right indicate Q values < 0.05 in treatments that constituted a differential proteome. Finally, a random forest (Wiener and Liaw, 2003) analysis with default parameter settings was used to find markers suitable to predict the main factors of variance in the dataset, i.e., the classification of the two root zones and all treatments compared with cold. The green heatmap to the right contains the mean decrease Gini coefficient; a larger (dark-green) decrease means greater contribution of respective protein to predict sample classifications.

to bias our statistical groups, we performed a bootstrapped HCA. The HCA was bootstrapped 10,000 times, and the results supported the same sample grouping. Briefly, approximately unbiased probability values (AU-*P* values) smaller than 1% from the bootstrapping analysis (Figure 4, red brackets) grouped separately the tip-adjacent root zone without the cold samples, the root tips without the cold samples, the cold-tip samples, and cold-tip-adjacent samples for a total of four significant groups. This means that the grouped samples would cluster together more than 99% of the times when clustering different sample proportions.

Biological Context of Induced Protein Changes

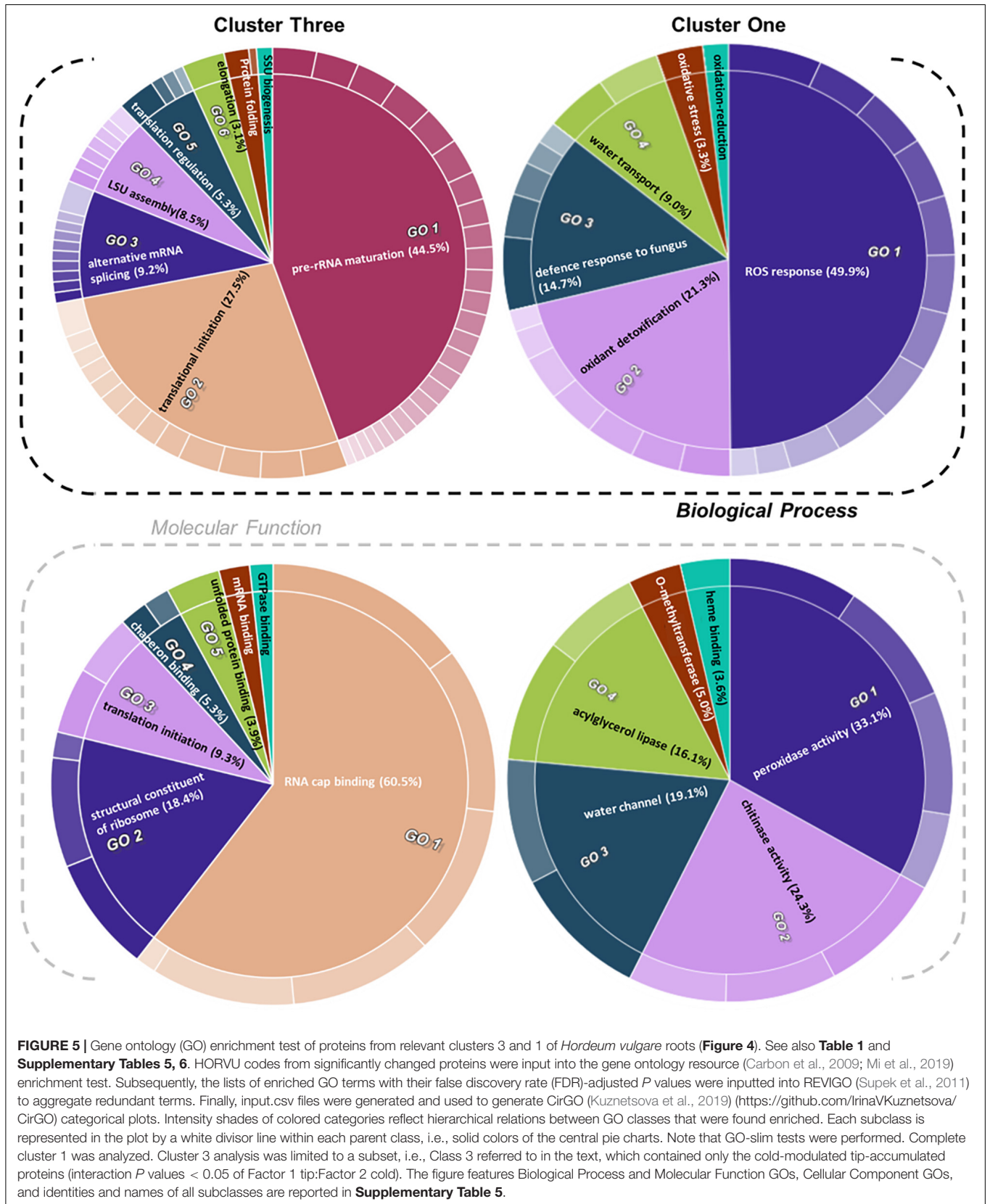
We selected significantly modulated proteins from the clusters that characterized the spatial sampling and cold treatment for a GO enrichment analysis (Figure 5, see column AO of Supplementary Table 4). In a second, more stringent approach, we selected protein clusters that were supported by AU-*P* values < 0.01 (see column AP of Supplementary Table 4) for alternative GO enrichment analyses (Supplementary Table 5). To define significant changes, we fitted a GLM tailored to the distribution shape of each vector of protein intensities across treatments. When not parametric nor homoscedastic, the variance and mean components were parametrized with an appropriate link function by comparing with the square of skewness and kurtosis of average GLM distributions. The details of the statistical test are deposited and publicly available in a GitHub repository.⁸ Additionally, *P* values were adjusted for multiple testing using BH95' to *Q* values (Figure 4, orange bars).

Cluster 1 contained proteins implicated in ROS production and plant defense (Figures 4, 5). In terms of biological processes, six categories were enriched: ROS response (49.9%), oxidant detoxification (21.3%), defense response to fungus (14.7%), water transport (9.0%), oxidative stress (3.3%), and oxidation-reduction (<1%). In terms of molecular function, peroxidase (33%) and chitinase (24%) activity hoarded more than 50% of the enrichments. The tip-adjacent region of barley root was well equipped in terms of defenses against environmental stresses compared with the younger root-tip tissue. Additionally, the lack of significant groupings of elicitor-treated plants (Figure 4) implies that priming the plants by exogenous chitin polymers did not induce a global-proteome reprogramming. A limited number of changes occurred. Proteins that play a role in fungal defense response were significantly decreased by chitin and chitosan treatments, for example, putatively annotated pathogenesis-related proteins (HORVU5Hr1G023720.1 and HORVU5Hr1G023740.2) and major pollen allergens with confident annotations (HORVU0Hr1G011720.5, HORVU4Hr1G054870.4, and HORVU7Hr1G034230.5), while chitinase-related proteins such as HORVU1Hr1G072250.1, HORVU7Hr1G113270.8, and HORVU7Hr1G121850.3 significantly increased following both priming conditions.

Cluster 2 contained cold-responsive proteins and the most relevant cold class predictors according to the Gini mean decrease of our random forest analysis. The cold response happened ubiquitously in both root zones, indicating a group of proteins that appears to be essential to the cold response in barley roots irrespective of spatial constraints. A GO enrichment test for biological processes revealed two categories: protein glutathionylation and glutathione metabolic process. Glutathione metabolism and *S*-glutathione conjugation upregulation included a hydroxyacylglutathione hydrolase-like protein, which produces glutathione [HORVU3Hr1G060920 (9 UP)]; a glyoxalase family protein, which produces glutathione [HORVU4Hr1G059270 (6 UP)]; and five different glutathione *S*-transferase family proteins [HORVU4Hr1G057890 (10 UP), HORVU1Hr1G049190 (11 UP), HORVU5Hr1G103430 (8 UP), HORVU4Hr1G057740 (16 UP), and HORVU6Hr1G026810 (13 UP)]. Additionally, this cluster contained 12 typical plant cold markers, COR/LEA proteins (Jaglo-Ottosen et al., 1998; Kume et al., 2005; Thalhammer and Hinch, 2013): HORVU6Hr1G064620 (13 UP), HORVU4Hr1G010750 (3 UP), HORVU3Hr1G066340 (7 UP), HORVU4Hr1G051780 (12 UP), HORVU2Hr1G099870 (11 UP), HORVU1Hr1G079280 (10 UP), HORVU1Hr1G056570 (7 UP), HORVU1Hr1G079290 (23 UP), HORVU4Hr1G074750 (31 UP), HORVU7Hr1G082040 (6 UP), HORVU5Hr1G092150 (2 UP), and HORVU6Hr1G083960 (19 UP); and finally, two abiotic stress markers, heat shock proteins, HORVU4Hr1G059260 (8 UP) and HORVU3Hr1G006530 (2 UP).

Proteins with significantly altered abundances from cluster 3 (Figure 4 and Supplementary Table 4) showed three types of responses: (Class 1) 60% of proteins (294/496) increased in the root tips, (Class 2) 11% of proteins (56/496) increased during cold, and importantly (Class 3) 29% of proteins (142/496) increased significantly in root tips after cold exposure. Class 3 contains 76 Class 1 and 19 Class 2 proteins and describes cold-modulated tip-accumulated proteins (interaction *P* values <0.05 of Factor 1 tip:Factor 2 cold). Considering that meristems are metabolic hotspots in active need of new proteins, we regarded Class 3 as potential holder of the newly synthesized proteome during cold. Hence, we focused on Class 3 for the following GO analysis. Class 3 revealed enrichment in translation-related processes and functions according to molecular function, biological process, and cellular component GOs (Figure 5 and Supplementary Table 5). Enriched terms from GO-slim analyses were hierarchically aggregated to reduce redundancy. In terms of biological processes, nine main categories were enriched, five related to translation or ribosome biogenesis: pre-rRNA maturation (44.5%), translational initiation (27.5%), ribosomal large subunit (LSU) assembly (8.5%), translation regulation, translation regulation (5.3%), elongation (3.1%), and ribosomal small subunit (SSU) biogenesis (<1%). Two additional categories were processes that feedback translation, namely, alternative mRNA splicing via spliceosome (9.2%) and chaperone-mediated protein folding (<1%). Molecular function analysis revealed seven enriched categories linked to the translational context: RNA cap binding (60.5%), structural constituent of ribosome (18.4%), translation initiation (9.3%), chaperone binding (5.3%),

⁸https://github.com/MSeidelFed/RandodiStats_package



unfolded protein binding (3.9%), mRNA binding (<1%), and GTPase binding (<1%). Finally, cellular component analysis (**Supplementary Table 5**) yielded two categories related to ribosomes: cytosolic LSU (95.4%) and cytosolic SSU (4.6%).

Cluster 4 mimicked cluster 1 in terms of the direction of protein changes. Functionally, it contained biotic stress response components and enzymes that belong to the central metabolism. GO analysis did not reveal clear trends of enrichment patterns.

The functional categories enriched within statistically relevant clusters from K-means analyses outline the biological processes that were triggered in our dataset in response to the applied treatments. Nevertheless, the pattern of change of those categories across treatments remained unclear. Thus, we grouped protein responses per functional group in order to understand how those categories were changing in relative protein abundance across treatments (**Table 1** and **Supplementary Table 6**). This

TABLE 1 | Median protein intensity (log₂ transformed, pooled-normalized) per ontology functional group sorted according to molecular function (clusters 1 and 3) or biological process (cluster 2).

GO term ID	Description	No. of proteins	Tip-adjacent control	Tip-adjacent cold	Tip-adjacent chitin	Tip-adjacent chitosan	Tip control	Tip cold	Tip chitin	Tip chitosan
(1) GO:0015250	Water channel activity	4								
GO:0005372	Water transmembrane Transporter activity									
(2) GO:0047372	Acylglycerol lipase activity	40								
GO:0003824	catalytic activity									
(3) GO:0004568	Chitinase activity	8								
GO:0004553	hydrolase activity, hydrolyzing O-glycosyl compounds									
GO:0016798	Hydrolase activity, acting on glycosyl bonds									
(4) GO:0008171	O-Methyltransferase activity	3								
(5) GO:0004601	Peroxidase activity	14								
GO:0016209	Antioxidant activity									
GO:0016491	Oxidoreductase activity									
GO:0016684	Oxidoreductase activity, acting on peroxide as acceptor									
(6) GO:0020037	Heme binding	7								
(7) GO:0006749	Glutathione metabolic process	6								
GO:0006790	Sulfur compound metabolic process									
GO:0006575	Cellular modified amino Acid metabolic process									
(8) GO:0010731	Protein glutathionylation	2								
(9) GO:0000339	RNA cap binding	66								
GO:0005488	binding									
GO:0097159	Organic cyclic compound binding									
GO:0003676	Nucleic acid binding									
GO:0003723	RNA binding									
GO:1901363	Heterocyclic compound binding									
(10) GO:0003743	Translation initiation factor activity	12								
GO:0045182	Translation regulator activity									
GO:0008135	Translation factor activity, RNA binding									
GO:0090079	Translation regulator activity, nucleic acid binding									
(11) GO:0051082	Unfolded protein binding	20								
GO:0005515	Protein binding									
(12) GO:0003746	Translation elongation factor activity	3								
(13) GO:0043022	Ribosome binding	4								
GO:0043021	Ribonucleoprotein complex binding									
(14) GO:0030695	GTPase regulator activity	4								
(15) GO:0003735	Structural constituent of ribosome	20								
GO:0005198	Structural molecule activity									
(16) GO:0003729	mRNA binding	9								

Scale goes from -1 (yellow), through 0 (white) to 1 (purple).

allowed us to dissect the finer response of the elicitor treatments as compared with the global proteome reprogramming triggered by cold acclimation.

Functional categories related to cluster 1 (groups 1–6 in **Table 1**) are enriched in the tip-adjacent root segment while also depleted in this segment preferentially during cold. Additionally, the protein functional categories related to biological processes like ROS response, oxidant detoxification, and response stress to fungus are enriched in the elicitor treatments. The enrichment becomes evident analyzing boxplots of the mean response across treatments (**Supplementary Table 6**) and was not statistically evident before because the relative change of these proteins as compared with other treatments is rather small. A similar accumulation of the proteins comprising these functional categories happened in the more distal root-tip zone, where relative to the other treatments within the tip group these proteins increased in abundance during the elicitor treatments (shift from yellow in control to pale yellow/white in elicitor treatments). Biological process categories related to cluster 2 (groups 7 and 8 in **Table 1**) are majorly induced by cold across root zones with an additional interesting observation; i.e., glutathione metabolism is enriched in root tips, while protein glutathionylation is enriched in tip-adjacent segments. Functional categories related to cluster 3 (Class 3) (groups 9–16 in **Table 1**) are root-tip molecular markers that outline the accumulated proteome due to the cold response and are biologically related to the process of mRNA to protein translation. Noteworthy is that proteins within functional groups share mean responses with few outliers (boxplots in **Supplementary Table 6**), which implies that the chosen dissimilarity metric between protein abundances legitimately clustered responses across treatments.

Finally, we replicated the bootstrapped HCA, but this time using single proteins as variables. The HCA was bootstrapped 10,000 times using correlation as dissimilarity measure between proteins and average linkage as clustering method. We found protein sub-clusters supported by AU-*P* values <0.01 that indicated the tightest protein correlations across treatments. These typically small clusters of 2–12 proteins resided within all K-mean groupings (**Supplementary Table 5**). In cluster 3, we located three of these smaller high-confidence sub-clusters. Sub-cluster X109 consisted of nine proteins and contained chaperons functioning in ATP and unfolded protein binding that belong to the biological process, protein folding. Sub-cluster X151 consisted of five proteins from the process of ribosome biogenesis. Sub-cluster X1632 with 10 proteins contained GOs of membrane fission during mitotic cytokinesis, beta-glucan biosynthesis, and cell-wall biogenesis. Cluster 2 had a small sub-cluster X733 consisting of five proteins. This sub-cluster represented the same biological process as complete parent cluster 2, that is, glutathione metabolism and protein glutathionylation. Cluster 1 contained one sub-cluster, cluster X614 of 12 proteins that are implicated in enzyme-mediated hydrolysis by chitinase activity. Cluster 4 contained two small clusters: sub-cluster X904 with five proteins with functions in ubiquitin conjugating enzyme activity and sub-cluster X1347 with seven proteins, which are largely part of the

proton-transporting V-type ATPase complex cellular component. Cluster 5 did not contain a high-confidence sub-cluster.

Adjusting the Ribosomal Proteome During Cold Acclimation

Proteogenomics predicted open reading frame (ORF) redundancies are reduced in the high-confidence annotations provided by the barley consortium (Mascher et al., 2017). We used these annotations to sequence LC-MS/MS peptides and aligned those peptides to *Arabidopsis* RP paralogs. We report 68/80 RP families. Our alignment focused on the cytosolic ribosome-associated proteome, which shares a great extent of sequence similarity due to a common ribosome universal core (Bernier et al., 2018; Bowman et al., 2020). Additionally, the two aligned species are closely related metazoans, thus increasing the potential sequence similarity. Therefore, we used an algorithm based on Needleman–Wunsch (Needleman and Wunsch, 1970) global sequence alignment problem (Durbin et al., 1998; Haubold and Wiehe, 2006; Malde, 2008). This allowed us to interpret matching scores in a relative scale. A score of 10 was selected to filter out ambiguous annotations that map to multiple genes (**Supplementary Table 7A**).

Molecular markers of acclimated tips (**Figure 4**) were functionally related to multiple aspects of translation (**Figure 5**). Yet another group of translational-related proteins was significantly over accumulated in the tip (i.e., *P* values <0.05 for Factor1tip, **Supplementary Table 4**), but their abundances remained unchanged during cold (**Supplementary Table 7B**), suggesting that specific components from the translational machinery were modulated differently after the temperature shift. This prompted us to explore how the ribosome structural components and interacting factors were affected in barley roots upon a cold shift. We considered proteins related to translation when they included one of the translation-related GO terms or contained in their FASTA identifier the terms “translation,” “ribosome,” or “ribosomal.” In total, we found 269 translation-related proteins, including structural RPs, translation factors, and ribosome biogenesis factors mostly linked to cytosolic translation; 74% (198 of 269) of these proteins had a matching score higher than 10 to *Arabidopsis* homologs, which were further considered and included RAP and RP paralogs; 78% of the matched proteins (155 of 198) belonged to cluster 3, 20% (40 of 198) to cluster 5, and 1.5% (3 of 198) to cluster 4 (**Supplementary Table 7**).

Due to our protein extraction method, the displayed changes were an average of all mature, immature, translationally competent, and translationally inactive “reserve” ribosomes in the cell. In plants, there are 80 cytosolic RP families, and *Arabidopsis* features two to seven paralog genes of each RP (Barakat et al., 2001). In our study, after aligning the protein sequences of the barley translational machinery with the *Arabidopsis* reviewed proteome (Swiss-Prot, UniProt), we found barley representatives from 74 cytosolic and two mitochondrial RP families. We found unique peptides and used them to define 85 certain RP paralog matches. After including matches from non-unique peptides, we defined 101 potential RP paralogs (**Supplementary Table 7C**).

Abundances of 22 paralogs significantly differed during cold in the root tips (**Figure 6** and **Supplementary Table 7**). We mapped the significant changes onto a 2D projection derived from a 3D Cryo-EM structural model of the wheat translating monosome (Armache et al., 2010) in order to understand the spatial distribution of the cold-induced changes. This allowed us to obtain an overview of total RP shifts relative to the complex structure that happened in barley root tips at the onset of cold acclimation (**Figure 6**).

Besides structural RPs, we assessed several RAPs that transiently bind and assist translation at different stages and were modulated in the root tips by cold in our dataset. Eleven translation initiation factors (TIFs), one maturation factor homolog (i.e., Tif6-homolog), one tRNA ligase (lysine), and two elongation factors (i.e., elongation factors 1 β 2 and δ 2) had significantly different abundances during cold in the root tips (**Supplementary Table 7** and **Figure 6**). All the *P* values that belong to cold enrichments outlined in **Figure 6** have been compiled and extended in **Table 2**. The extended version in **Table 2** includes *H. vulgare* identified protein peptides, *A. thaliana* homolog matches with their respective match score, and RP or RAP paralog identities.

Finally, we found additional clusters of RPs with high probability support (AU-*P* value < 0.01 in **Supplementary Table 7**). We considered those sub-clusters of four or more RPs as groups having strong co-dependence: sub-cluster X151 with SSU-RP eS7_RPS7B and LSU-RPs uL22_RPL17B, S1_RPS3aB, eL6_RPL6C, and uL18_RPL5A. These proteins were significantly more abundant during cold and good molecular markers of root tip characterized by a large Gini mean decrease: cluster X471 with SSU-RPs eS6_RPS6B, eS24_RPS24A, and uS17_RPS11C and LSU-RPs uL5_RPL11A, eL34_RPL34A, and eL13_RPL13B. Proteins within these two sub-clusters were significantly more abundant in the root tips. The top five molecular markers according to the mean decrease of Gini ranking among RPs of the root tip were eL8_RPL7aA, eS28_RPS28A or B, uS2_RPSaA, uS7_RPS5A, and eL14_RPL14A; as for roots acclimated to cold, the best and only RP marker was eS26_RPS26C.

DISCUSSION

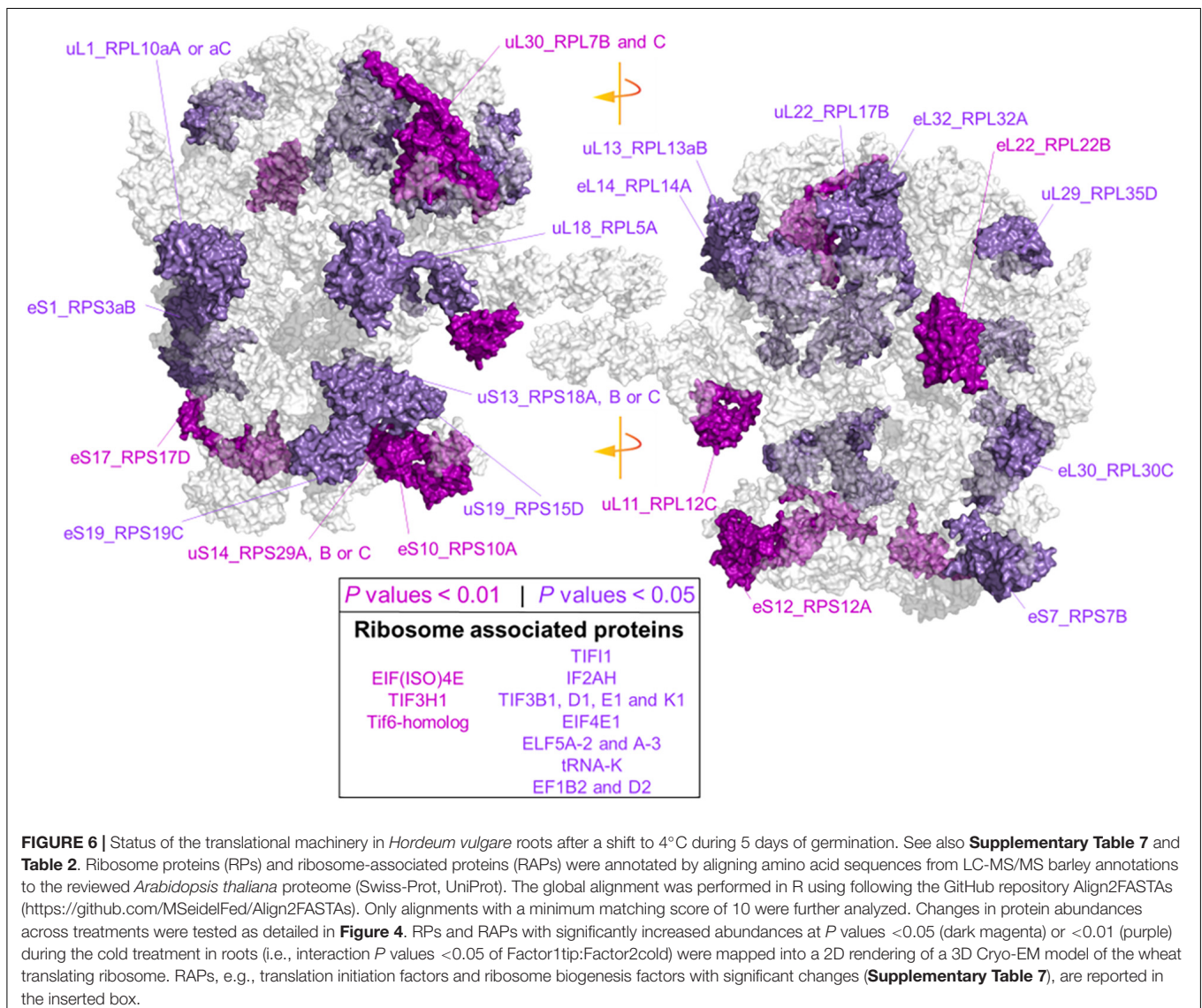
Translational Reprogramming

During cold acclimation, total protein contents relative to fresh root weight drop in root tips, while a fraction enriched in ribosome-bound protein increases its protein content dramatically. Thus, in spite of reducing significantly total protein, a highly committed decision to either produce *de novo* or retain old ribosomes is made by the plant. A second, MS, piece of evidence shows that specific proteins, in samples normalized to protein content, significantly increase their relative abundance in barley root tips during cold exposure. GO analysis revealed that those proteins were involved in protein synthesis. The results range from ribosome biogenesis, structure, to mRNA-splicing, recruiting, translation initiation, elongation, and protein folding, suggesting that specific components of the translation machinery need to be accumulated to cope with cold. This fits

into what is known for *Arabidopsis* protein translation apparatus, which is a central hub mediating responses to cold acclimation (Beine Golovchuk et al., 2018; Garcia-Molina et al., 2020). Interestingly, RAPs and RP paralogs differ in their amino acid sequence from barley to *Arabidopsis* homologs with varying degrees (**Supplementary Table 7**). Scores indicated that multiple barley RP paralogs match differently to the same *Arabidopsis* family (e.g., uL3_RPL3A and uL1_RPL10aA). The ranges in matches indicate sequence and potential functional divergence of paralogs. Moreover, cold-induced changes in specific paralogs suggest that the composition of barley cold-acclimated ribosomes differs from a canonical complex, and during cold, there might be a paralog-specialized ribosome (Gerst, 2018; Samir et al., 2018; Segev and Gerst, 2018; Ghulam et al., 2020). Additionally, the abundance of many RAPs, especially TIFs, increased. If there is a temperature-induced slowing-down of both translation initiation and elongation, and the former is being slowed down more than the latter, the expectation is an increase of 80S, 48S, and 43S complexes relative to a decreased amount of polysomes, which could contribute to the increased amount of TIFs during cold acclimation.

Interpretation of shifts in individual translational components must be contextualized to the cell lysis and protein extraction methods. Solubilization differences in control RPs argue that the nucleolus is recovered when using LB extraction (**Figure 2B**). Ribosome biogenesis in eukaryotes starts in the nucleolus (Woolford and Baserga, 2013; Baßler and Hurt, 2019; Sáez-Vásquez and Delseny, 2019; Martinez-Seidel et al., 2020); thus, many pre-ribosomal complexes at different stages coexist inside. Non-translational particles may change their RP stoichiometry as compared with translationally competent complexes upon temperature changes (Cheong et al., 2021), suggesting that a cold-specific ribosome biogenesis could give rise to specialized ribosomes in plants (Ohbayashi and Sugiyama, 2018; Martinez-Seidel et al., 2020). Thus, solubilizing the nucleolus implies that, first, our results indicate a total average status of translational protein components and, second, they might signal essential RP-mediated mechanisms of cold-specific ribosome biogenesis.

Shifts in the plant proteome occur during cold acclimation. Several possibilities could contribute to such shifts. For instance, through a cold-specialized ribosome population, the root-tip cells could direct translation toward a subset of alternatively spliced transcripts (Thompson et al., 2016). Alternative splicing is a major response to cold in *Arabidopsis* (Calixto et al., 2018), and now we have shown that protein components of the spliceosome need to be accumulated as a cold response in barley roots (**Figure 5** and **Supplementary Table 5**, Biological Process, cluster 3). The activation of the spliceosome happens in root tips only, suggesting a correlation to cold-accumulated ribosomes and specific ribosome components. Interestingly, the Partner of Y14 and Mago (PYM) protein factor was drastically accumulated during cold (Cluster 2, **Figure 4**). In yeast, PYM is anchored to the 48S preinitiation complex and is able to promote translation of spliced mRNAs (Diem et al., 2007) by interacting with the exon junction complex (EJM), which is a cellular shuttle for spliced transcripts from the nucleus to the cytosol (Boisramé et al., 2019). Recruiting of spliced



transcripts could be one of multiple layers complementing an altered ribosomal proteome to achieve selective translation and rapid proteome shifts during cold. Alternatively, cold acclimation has been shown to trigger transcriptional reprogramming events in cereals that lead to nucleosome and chromatin remodeling (Janská et al., 2011). These events could tailor the translated proteome by changing the transcriptional dynamics of cold-responsive genes and eventually altering the transcript substrate availability for ribosomes to translate. These strategies are not mutually exclusive and might act independently but converge on a proteome shift or act in concert to achieve selective transcript translation and rapid proteome shifts during cold acclimation.

Freezing tolerance and cold stress memory are triggered by the same stimuli but might be executed to completion by different cellular machinery. Freezing tolerance is partly achieved by induction of the CBF regulon and its subsequent modulation on the COR/LEA signal transduction pathway in

plants (Jaglo-Ottosen et al., 1998). Plant reports of this correlation include cereals such as wheat (Kume et al., 2005; Sasaki et al., 2014) or rice (Wang et al., 2016; Xiao et al., 2018). In wheat, there is an accumulation of COR/LEA proteins in the crowns during cold acclimation (Houde et al., 1995), and, as we now report, these proteins accumulate in actively dividing barley root meristems during cold acclimation. The same link between the CBF regulon and a posterior COR/LEA upregulation is established in *Arabidopsis* (Hundertmark and Hinch, 2008). Cold stress memory in *Arabidopsis* is maintained for 7 days and partly depends on induction of lipid, secondary metabolism, and stress or growth-related functions (Zuther et al., 2019), depending on how cold-tolerant the accession is. Typical cold-responsive genes such as the CBF regulon or COR/LEA protein coding genes are less implicated in cold stress memory (Zuther et al., 2019; Leuendorf et al., 2020). Thus, cold stress memory could make use of a primordial cellular machinery to conserve a recording of the stimulus. In this context, an altered ribosomal

TABLE 2 | Statistics of cold acclimated and homology alignments of significantly changed-*Arabidopsis thaliana* (AT) and *Hordeum vulgare* (HORVU) RP and RAP paralogs outlined in **Figure 6**.

Paralog	AT code	Match score	HORVU Code	P value*
eS10_RPS10A	AT4G25740	135.3	HORVU0Hr1G004700.1	0.003
uS14_RPS29A B, or C	AT3G43980,AT3G44010,AT4G33865	192.0	<u>HORVU5Hr1G098740.1;HORVU0Hr1G011940.3;HORVU4Hr1G037800.1</u>	0.003
uS14_RPS29A, B, or C	AT3G43980,AT3G44010,AT4G33865	181.3	<u>HORVU5Hr1G098740.1;HORVU0Hr1G011940.3;HORVU4Hr1G037800.1</u>	0.003
EIF(ISO)4E	AT5G35620	22.9	HORVU1Hr1G039260.2	0.003
eS17_RPS17D	AT5G04800	41.5	HORVU1Hr1G042220.1	0.003
uL30_RPL7B	AT2G01250	275.0	HORVU2Hr1G100970.4	0.003
AtTIF3H1	AT1G10840	563.2	HORVU2Hr1G068360.8	0.005
eS12_RPS12A	AT1G15930	93.0	HORVU2Hr1G053290.6	0.006
eL22_RPL22B	AT3G05560	210.1	HORVU2Hr1G019160.1	0.008
uL11_RPL12C	AT5G60670	414.9	HORVU6Hr1G067870.1	0.008
Tif6-homolog	AT3G55620	715.5	HORVU2Hr1G026220.5	0.009
IF5A2	AT1G26630	364.9	HORVU2Hr1G063210.2	0.010
eL30_RPL30C	AT3G18740	127.4	<u>HORVU0Hr1G023290.1;HORVU1Hr1G068640.1</u>	0.012
eL30_RPL30C	AT3G18740	74.2	<u>HORVU0Hr1G023290.1;HORVU1Hr1G068640.1</u>	0.012
IF2AH	AT2G40290	641.6	HORVU2Hr1G014580.1	0.013
IF5A3	AT1G69410	371.2	HORVU2Hr1G034400.4	0.014
EF1D2	AT2G18110	246.3	HORVU2Hr1G031450.6	0.015
EF1B2	AT5G19510	299.6	HORVU2Hr1G022090.4	0.015
eS7_RPS7B	AT3G02560	296.6	HORVU1Hr1G029870.1	0.017
uL13_RPL13aB	AT3G24830	103.2	HORVU2Hr1G063880.1	0.018
AtTIF11	AT2G46280	573.0	HORVU4Hr1G040280.4	0.019
tRNA-K	AT1G69410	663.9	HORVU5Hr1G106380.6	0.021
AtTIF3E1	AT3G57290	303.7	HORVU5Hr1G072560.1	0.024
AtTIF3K1	AT4G33250	238.0	HORVU4Hr1G077250.1	0.024
uL18_RPL5A	AT3G25520	284.8	HORVU2Hr1G073320.1	0.027
AtTIF3B1	AT5G27640	965.0	HORVU5Hr1G106440.1	0.028
uL29_RPL35D	AT5G02610	282.0	HORVU2Hr1G068120.2	0.029
uL22_RPL17B	AT1G67430	419.0	HORVU7Hr1G054010.1	0.031
IF4E1	AT4G18040	74.1	HORVU3Hr1G113940.1	0.031
eS1_RPS3aB	AT4G34670	548.5	HORVU4Hr1G070370.1	0.033
eL32_RPL32A	AT4G18100	264.9	HORVU5Hr1G075420.2;HORVU5Hr1G075500.3	0.034
eL32_RPL32A	AT4G18100	262.2	HORVU5Hr1G075420.2;HORVU5Hr1G075500.3	0.034
uS4_RPS9C	AT5G39850	553.3	HORVU5Hr1G038920.1	0.039
eS19_RPS19C	AT5G61170	146.3	HORVU5Hr1G052240.6	0.040
uS19_RPS15D	AT5G09510	63.4	HORVU2Hr1G057430.1	0.041
uS13_RPS18A, B, or C	AT1G22780,AT1G34030,AT4G09800	332.0	HORVU5Hr1G104720.1	0.043
uL1_RPL10aA	AT1G08360	624.7	<u>HORVU7Hr1G059090.5;HORVU4Hr1G001350.5</u>	0.045
uL1_RPL10aC	AT5G22440	246.8	<u>HORVU7Hr1G059090.5;HORVU4Hr1G001350.5</u>	0.045
eL14_RPL14A	AT2G20450	335.3	HORVU6Hr1G058560.1	0.046
uL30_RPL7C	AT2G44120	465.0	HORVU5Hr1G108990.2	0.047
AtTIF3D1	AT4G20980	400.8	HORVU1Hr1G088760.2	0.049

*P values of the interaction term of cold and root-tip factor, i.e., $\beta_1 \times \beta_4$. Underlined duplicated HORVU and their respective AT entries are explained in **Supplementary Table 7B**.

RP, ribosomal protein; RAP, ribosome-associated protein.

composition may act as molecular memory of the initial cold cue. This seems logical considering that ribosomes have a typical half-life of 3–4 days in plants (Salih et al., 2019), which might be stretched due to the slower cold molecular dynamics. Thus, to prevent the high costs of triggering an appropriate response from scratch upon new stress cues (Van Hulten et al., 2006), it is likely that an altered ribosome composition is stored as molecular memory.

Acquired Cold Tolerance

Priming, in the context of plant stress, is defined as a trigger cue that increases the future performance of plants responding to stress (Hilker et al., 2016). To achieve the primed state, plants must improve the overall stress management, strengthening self-defense systems to defy environmental cues (Hilker and Schmölling, 2019). Upon specific cues, plants change epigenetic patterns, accumulate transcriptional factors, and modify the

expression levels of genes and accumulation of proteins, including PTM status and metabolites (Hilker et al., 2016; Hilker and Schmölling, 2019). Our study evidenced the intrinsic enrichment in root tip-adjacent zones of ROS response, oxidative detoxification, and fungal defense proteins. Many of these possess pathogen-resisting enzymatic activities, e.g., peroxidase and chitinase. Nevertheless, many of these proteins do not dramatically respond to pathogen-associated molecular patterns (PAMPs) such as chitin and chitosan. Thus, general response patterns and molecular consequences from a pathogen attack in the root tips must stem from other components of the stress.

Acquired cold tolerance for later biotic stress in plants is attributed to the elements in common that both the stresses have (Ben Rejeb et al., 2014). First, a common group of transcription factors (TFs) such as the mentioned cold-specific CBF factors or the MYB, NAC, and DREB factors. These TFs enable a cross-talk between abiotic and biotic stresses by modulating pathogen resistance (PR) genes and their proteoforms (Snider et al., 2000; Tsutsui et al., 2009; Seo and Park, 2010; Seo et al., 2010). PR proteins function for disease resistance and are also implicated in protecting the plant during overwintering (Kuwabara and Imai, 2009). Second, during the plant cold response, the first shared elements with responses to biotic stress are ROS signaling and calcium influxes (Ben Rejeb et al., 2014). The oxidative component of both stresses produces an oxidized cellular status (Pastor et al., 2013). This state could be compensated for, especially at the proteome level, to avoid ROS-derived damages.

Our results offer testable hypotheses that could form a solid mechanistic link between cold acclimation and cold-induced plant defense against pathogens (Kuwabara and Imai, 2009; Szechyńska-Hebda et al., 2013; Szechyńska-Hebda et al., 2015; Sasaki et al., 2016). Defense-triggered cold processes can be divided into two in our dataset. First, proteins in the tip-adjacent root zone are functionally related to defense and are both depleted during cold and accumulated as a functional group during the elicitor treatments. This implies that elicitor-derived resistance relies on the upregulation of a defense-related cellular machinery to confer a primed state while cold-acquired resistance makes use of a different cellular machinery. Second, GO analyses revealed that the machinery involved in synthesis and assemblage of glutathione as a PTM is upregulated in both root zones. S-Glutathionylation shields against oxidative stress by acting as a ROS scavenger (Diaz-Vivancos et al., 2015). Thus, it seems likely that cold-acquired resistance does not rely on upregulating the plant immune system protein components. Rather, we argue that chilling temperature could prepare plants to withstand oxidative stress, thus providing the means to resist forthcoming cold-related diseases, presumably caused by winter or fungal pathogens. Due to its ubiquitous upregulation, all proteins are likely being shielded by S-glutathione during a cold cue. Hence, we argue that resistance for a later pathogenic fungal interaction may be gained because the accumulated ribosomes or any other proteins that are newly synthesized would be less affected by the oxidative component of biotic stress. Methodological steps employed for proteomics analysis using global reduction and

latter alkylation of reduced thiols precludes us to distinguish between reduced cysteine from S-S disulfide bonds, free thiols, or S-glutathionylation. Thus, it would not be possible to find in our current dataset S-glutathionylated peptides. These additional experiments with dedicated methods and method developments are now motivated by our findings. At which point, it will become evident what portion of the proteome is actually protected by the PTM.

Finally, after a thorough search of the fungal-elicitor-induced proteome changes, we did not find global proteome modulatory effects. Rather, the observable shifts happened when specific defense-related proteins were pooled into functional groups and analyzed as a combined mean response. Hence, we constrained the search to enzymes that are directly related to chitin polymers and could be measured. Our results indicate that chitin polymers modulate the plant defense system without triggering major proteome rearrangements in the host plants. Comprehensive effects of chitin naturally occurring polymers on barley seedlings along with a precise measurement of the proteins involved in the responses still need further investigation.

Summary

Our results indicate that cold acclimation triggers a drop in protein content in barley root tips, while specific proteins are accumulated. We found specific accumulation of cold markers such as COR/LEA proteins that also accumulate in mature tissues such as cereal crowns during cold. We couple these changes to a highly committed and drastic ribosome accumulation, which could imply the assembly of cold-rewired ribosomes characterized by substoichiometric RP compositions. Substoichiometry can arise from the significant changes in relative abundances of specific RP paralogs found in our study. Divergent ribosomes are further supported by the accumulation of spliceosome components in root tips, which could tailor an alternatively cold-spliced transcriptome that would rely on selective translation. These regulatory mechanisms, acting upon the proteome, can be amplified using root meristems as a model to study rapid proteome reprogramming. We exemplify the accumulation of proteins involved in S-glutathione biosynthesis and S-glutathione conjugation as indicators of S-glutathionylation PTM of proteins during cold acclimation and put it forward as a new hypothesis on which to build future studies of cold-acquired tolerance linked to defense and protein synthesis. Finally, in spite of the gained advantages of using only root tips instead of complete root systems to identify proteome shifts, finer spatial resolution will be needed to allow discriminating between all the biological steady states coexisting in apical root zones.

DATA AVAILABILITY STATEMENT

The datasets presented in this study can be found in online repositories. The names of the repository/repositories and accession number(s) can be found below: <http://proteomecentral.proteomexchange.org/cgi/GetDataset>, PXD021731.

AUTHOR CONTRIBUTIONS

FM-S and PS performed the experimental work. SN, ML, and NW contributed in LC-MS/MS. FM-S, PS, and AAPF contributed in the protein extraction. FM-S, PS, ML, and BB contributed in the conceptualization and production of *in silico* resources. UR, JK, and BB contributed in the conceptualization, experiment planning, and manuscript editing. FM-S, PS, and BB contributed in the manuscript writing and figure designing. All authors contributed to the article and approved the submitted version.

FUNDING

PS would like to thank the Melbourne Research Scholarship and Nutrifield Pty Ltd., for financially supporting his Ph.D. program. FM-S would like to acknowledge the Max-Planck Society (Max Planck Institute of Molecular Plant Physiology) and

The University of Melbourne for funding his research via the Melbourne-Potsdam Ph.D. Programme (MelPoPP).

ACKNOWLEDGMENTS

We thank the Mass Spectrometry and Proteomics Facility of The Bio21 Molecular Science and Biotechnology Institute at The University of Melbourne for the support of mass spectrometry analysis. We thank Dr. Sneha Gupta for providing the seed material used in this work.

SUPPLEMENTARY MATERIAL

The Supplementary Material for this article can be found online at: <https://www.frontiersin.org/articles/10.3389/fpls.2021.656683/full#supplementary-material>

REFERENCES

- Altschul, S. F., Gish, W., Miller, W., Myers, E. W., and Lipman, D. J. (1990). Basic local alignment search tool. *J. Mol. Biol.* 215, 403–410. doi: 10.1016/S0022-2836(05)80360-2
- Armache, J. P., Jarasch, A., Anger, A. M., Villa, E., Becker, T., Bhushan, S., et al. (2010). Localization of eukaryote-specific ribosomal proteins in a 5.5-Å cryo-EM map of the 80S eukaryotic ribosome. *Proc. Natl. Acad. Sci. U.S.A.* 107, 19754–19759. doi: 10.1073/pnas.1010010107
- Ashraf, M. A., and Rahman, A. (2019). Cold stress response in *Arabidopsis thaliana* is mediated by GNOM ARF-GEF. *Plant J.* 97, 500–516. doi: 10.1111/tpj.14137
- Bailly, C. (2019). The signalling role of ROS in the regulation of seed germination and dormancy. *Biochem. J.* 476, 3019–3032. doi: 10.1042/BCJ20190159
- Barakat, A., Szick-Miranda, K., Chang, I. F., Guyot, R., Blanc, G., Cooke, R., et al. (2001). The organization of cytoplasmic ribosomal protein genes in the *Arabidopsis* genome. *Plant Physiol.* 127, 398–415. doi: 10.1104/pp.010265.398
- Başler, J., and Hurt, E. (2019). Eukaryotic ribosome assembly. *Annu. Rev. Biochem.* 88, 281–306. doi: 10.1146/annurev-biochem-013118-110817
- Beine Golovchuk, O., Firmino, A. A. P., Dąbrowska, A., Schmidt, S., Erban, A., Walther, D., et al. (2018). Plant temperature acclimation and growth rely on cytosolic ribosome biogenesis factor homologs. *Plant Physiol.* 176, 2251–2276. doi: 10.1104/pp.17.01448
- Ben Rejeb, I., Pastor, V., and Mauch-Mani, B. (2014). Plant responses to simultaneous biotic and abiotic stress: molecular mechanisms. *Plants* 3, 458–475. doi: 10.3390/plants3040458
- Benjamini, Y., and Hochberg, Y. (1995). Controlling the false discovery rate: a practical and powerful approach to multiple testing. *J. R. Stat. Soc. Ser. B* 57, 289–300. doi: 10.1111/j.2517-6161.1995.tb02031.x
- Bernier, C. R., Petrov, A. S., Kovacs, N. A., Penev, P. I., and Williams, L. D. (2018). Translation: the universal structural core of life. *Mol. Biol. Evol.* 35, 2065–2076. doi: 10.1093/molbev/msy101
- Boisramé, A., Devillers, H., Onésime, D., Brunel, F., Pouch, J., Piot, M., et al. (2019). Exon junction complex components Y14 and Mago still play a role in budding yeast. *Sci. Rep.* 9:849. doi: 10.1038/s41598-018-36785-3
- Bowman, J. C., Petrov, A. S., Frenkel-Pinter, M., Penev, P. I., and Williams, L. D. (2020). Root of the tree: the significance, evolution, and origins of the ribosome. *Chem. Rev.* 120, 4848–4878. doi: 10.1021/acs.chemrev.9b00742
- Calixto, C. P. G., Guo, W., James, A. B., Tzioutziou, N. A., Entizne, J. C., Panter, P. E., et al. (2018). Rapid and dynamic alternative splicing impacts the arabidopsis cold response transcriptome. *Plant Cell* 30, 1424–1444. doi: 10.1105/tpc.18.00177
- Carbon, S., Ireland, A., Mungall, C. J., Shu, S., Marshall, B., Lewis, S., et al. (2009). AmiGO: Online access to ontology and annotation data. *Bioinformatics* 25, 288–289. doi: 10.1093/bioinformatics/btn615
- Cheong, B. E., Beine-Golovchuk, O., Gorka, M., Ho, W. W. H., Martinez-Seidel, F., Firmino, A. A. P., et al. (2021). *Arabidopsis* REI-LIKE proteins activate ribosome biogenesis during cold acclimation. *Sci. Rep.* 11:2410. doi: 10.1038/s41598-021-81610-z
- Cheong, B. E., Ho, W. W. H., Biddulph, B., Wallace, X., Rathjen, T., Rupasinghe, T. W. T., et al. (2019). Phenotyping reproductive stage chilling and frost tolerance in wheat using targeted metabolome and lipidome profiling. *Metabolomics* 15:144. doi: 10.1007/s11306-019-1606-2
- Cheong, B. E., Onyemaobi, O., Wing Ho Ho, W., Biddulph, T. B., Rupasinghe, T. W. T., Roessner, U., et al. (2020). Phenotyping the chilling and freezing responses of young microspore stage wheat spikes using targeted metabolome and lipidome profiling. *Cells* 9:1309. doi: 10.3390/cells9051309
- Chouard, P. (1960). Vernalization and its relations to dormancy. *Annu. Rev. Plant Physiol.* 11, 191–238. doi: 10.1146/annurev.pp.11.060160.001203
- Clowes, F. A. L. (1958). Protein synthesis in root meristems. *J. Exp. Bot.* 9, 229–238. doi: 10.1093/jxb/9.2.229
- Cox, J., and Mann, M. (2008). MaxQuant enables high peptide identification rates, individualized p.p.b.-range mass accuracies and proteome-wide protein quantification. *Nat. Biotechnol.* 26, 1367–1372. doi: 10.1038/nbt.1511
- Cretoi, M. S., Korthals, G. W., Visser, J. H. M., and Van Elsas, J. D. (2013). Chitin amendment increases soil suppressiveness toward plant pathogens and modulates the actinobacterial and oxalobacteraceal communities in an experimental agricultural field. *Appl. Environ. Microbiol.* 79, 5291–5301. doi: 10.1128/AEM.01361-13
- Deng, W., Casao, M. C., Wang, P., Sato, K., Hayes, P. M., Finnegan, E. J., et al. (2015). Direct links between the vernalization response and other key traits of cereal crops. *Nat. Commun.* 6:5882. doi: 10.1038/ncomms6882
- Deutsch, E. W., Bandeira, N., Sharma, V., Perez-Riverol, Y., Carver, J. J., Kundu, D. J., et al. (2020). The proteomexchange consortium in 2020: enabling “big data” approaches in proteomics. *Nucleic Acids Res.* 48, D1145–D1152. doi: 10.1093/nar/gkz984
- Diaz-Vivancos, P., De Simone, A., Kiddle, G., and Foyer, C. H. (2015). Glutathione – linking cell proliferation to oxidative stress. *Free Radic. Biol. Med.* 89, 1154–1164. doi: 10.1016/j.freeradbiomed.2015.09.023
- Diem, M. D., Chan, C. C., Younis, L., and Dreyfuss, G. (2007). PYM binds the cytoplasmic exon-junction complex and ribosomes to enhance translation of spliced mRNAs. *Nat. Struct. Mol. Biol.* 14, 1173–1179. doi: 10.1038/nsmb1321
- Dinneny, J. R., and Benfey, P. N. (2008). Plant stem cell niches: standing the test of time. *Cell* 132, 553–557. doi: 10.1016/j.cell.2008.02.001

- Durbin, R., Eddy, S. R., Krogh, A., and Mitchison, G. (1998). *Biological Sequence Analysis*. Cambridge: Cambridge University Press. doi: 10.1017/cbo9780511790492
- Erban, A., Martinez-Seidel, F., Rajarathinam, Y., Dethloff, F., Orf, I., Fehrle, I., et al. (2020). "Multiplexed profiling and data processing methods to identify temperature-regulated primary metabolites using gas chromatography coupled to mass spectrometry," in *Methods in Molecular Biology*, eds D. K. Hincha and E. Zuther (New York, NY: Springer US), 203–239. doi: 10.1007/978-1-0716-0660-5_15
- Firmino, A. A. P., Gorka, M., Graf, A., Skirycz, A., Martinez-Seidel, F., Zander, K., et al. (2020). Separation and paired proteome profiling of plant chloroplast and cytoplasmic ribosomes. *Plants* 9, 1–29. doi: 10.3390/plants9070892
- Fowler, S., and Thomashow, M. F. (2002). *Arabidopsis* transcriptome profiling indicates that multiple regulatory pathways are activated during cold acclimation in addition to the CBF cold response pathway. *Plant Cell* 14, 1675–1690. doi: 10.1105/tpc.003483
- Garcia-Molina, A., Kleine, T., Schneider, K., Mühlhaus, T., Lehmann, M., and Leister, D. (2020). Translational components contribute to acclimation responses to high light, heat, and cold in *Arabidopsis*. *iScience* 23:101331. doi: 10.1016/j.isci.2020.101331
- Gerst, J. E. (2018). Pimp my ribosome: ribosomal protein paralogs specify translational control. *Trends Genet.* 34, 832–845. doi: 10.1016/j.tig.2018.08.004
- Ghulam, M. M., Catala, M., and Abou Elela, S. (2020). Differential expression of duplicated ribosomal protein genes modifies ribosome composition in response to stress. *Nucleic Acids Res.* 48, 1954–1968. doi: 10.1093/nar/gkz1183
- Golemic, E., and Gołębiewska-Pikania, G. (2015). Cold-Enhanced gene expression of the foliar thiol-specific antioxidant protein in *Triticale* (*x Triticosecale* Wittm.) seedlings resistant to *Microdochium Nivale* (Samuels & I.C. Hallett) infection. *Acta Biol.* 22, 98–117. doi: 10.18276/ab.2015.22-08
- Gu, Z., Eils, R., and Schlesner, M. (2016). Complex heatmaps reveal patterns and correlations in multidimensional genomic data. *Bioinformatics* 32, 2847–2849. doi: 10.1093/bioinformatics/btw313
- Gu, Z., Gu, L., Eils, R., Schlesner, M., and Brors, B. (2014). Circlize implements and enhances circular visualization in R. *Bioinformatics* 30, 2811–2812. doi: 10.1093/bioinformatics/btu393
- Gupta, S., Rupasinghe, T., Callahan, D. L., Natera, S. H. A., Smith, P. M. C., Hill, C. B., et al. (2019). Spatio-temporal metabolite and elemental profiling of salt stressed barley seeds during initial stages of germination by MALDI-MSI and μ -XRF spectrometry. *Front. Plant Sci.* 10:1139. doi: 10.3389/fpls.2019.01139
- Haubold, B., and Wiehe, T. (2006). *Introduction to Computational Biology: An Evolutionary Approach*. Berlin: Springer. doi: 10.1007/3-7643-7387-3
- Hilker, M., and Schmölling, T. (2019). Stress priming, memory, and signalling in plants. *Plant Cell Environ.* 42, 753–761. doi: 10.1111/pce.13526
- Hilker, M., Schwachtje, J., Baier, M., Balazadeh, S., Bäurle, I., Geiselhardt, S., et al. (2016). Priming and memory of stress responses in organisms lacking a nervous system. *Biol. Rev.* 91, 1118–1133. doi: 10.1111/brv.12215
- Hincha, D. K., and Zuther, E. (2020). "Introduction: plant cold acclimation and winter survival," in *Methods in Molecular Biology*, eds D. K. Hincha and E. Zuther (New York, NY: Springer US), 1–7. doi: 10.1007/978-1-0716-0660-5_1
- Houde, M., Daniel, C., Lachapelle, M., Allard, F., Laliberté, S., and Sarhan, F. (1995). Immunolocalization of freezing-tolerance-associated proteins in the cytoplasm and nucleoplasm of wheat crown tissues. *Plant J.* 8, 583–593. doi: 10.1046/j.1365-313X.1995.8040583.x
- Huffaker, R. C., and Peterson, L. W. (1974). Protein turnover in plants and possible means of its regulation. *Annu. Rev. Plant Physiol.* 25, 363–392. doi: 10.1146/annurev.pp.25.060174.002051
- Hundertmark, M., and Hincha, D. K. (2008). LEA (Late Embryogenesis Abundant) proteins and their encoding genes in *Arabidopsis thaliana*. *BMC Genomics* 9:118. doi: 10.1186/1471-2164-9-118
- Jaglo-Ottosen, K. R., Gilmour, S. J., Zarka, D. G., Schabenberger, O., and Thomashow, M. F. (1998). *Arabidopsis* CBF1 overexpression induces COR genes and enhances freezing tolerance. *Science* 280, 104–106. doi: 10.1126/science.280.5360.104
- Janmohammadi, M., Zolla, L., and Rinalducci, S. (2015). Low temperature tolerance in plants: changes at the protein level. *Phytochemistry* 117, 76–89. doi: 10.1016/j.phytochem.2015.06.003
- Janská, A., Aprile, A., Zámečník, J., Cattivelli, L., and Ovesná, J. (2011). Transcriptional responses of winter barley to cold indicate nucleosome remodelling as a specific feature of crown tissues. *Funct. Integr. Genomics* 11, 307–325. doi: 10.1007/s10142-011-0213-8
- Kaplan, F., Kopka, J., Haskell, D. W., Zhao, W., Schiller, K. C., Gatzke, N., et al. (2004). Exploring the temperature-stress metabolome of *Arabidopsis*. *Plant Physiol.* 136, 4159–4168. doi: 10.1104/pp.104.052142
- Kirby, E. J. M. (1993). Effect of sowing depth on seedling emergence, growth and development in barley and wheat. *Field Crop Res.* 35, 101–111. doi: 10.1016/0378-4290(93)90143-B
- Kirschner, G. K., Stahl, Y., Von Korff, M., and Simon, R. (2017). Unique and conserved features of the barley root meristem. *Front. Plant Sci.* 8:1240. doi: 10.3389/fpls.2017.01240
- Koehler, G., Wilson, R. C., Goodpaster, J. V., Sønsteby, A., Lai, X., Witzmann, F. A., et al. (2012). Proteomic study of low-temperature responses in strawberry cultivars (*Fragaria × ananassa*) that differ in cold tolerance. *Plant Physiol.* 159, 1787–1805. doi: 10.1104/pp.112.198267
- Kume, S., Kobayashi, F., Ishibashi, M., Ohno, R., Nakamura, C., and Takumi, S. (2005). Differential and coordinated expression of Cbf and Cor/Lea genes during long-term cold acclimation in two wheat cultivars showing distinct levels of freezing tolerance. *Genes Genet. Syst.* 80, 185–197. doi: 10.1266/ggs.80.185
- Kuwabara, C., and Imai, R. (2009). Molecular basis of disease resistance acquired through cold acclimation in overwintering plants. *J. Plant Biol.* 52, 19–26. doi: 10.1007/s12374-008-9006-6
- Kuznetsova, I., Lugmayr, A., Siira, S. J., Rackham, O., and Filipovska, A. (2019). CirGO: an alternative circular way of visualising gene ontology terms. *BMC Bioinformatics* 20:84. doi: 10.1186/s12859-019-2671-2
- Leuendorf, J. E., Frank, M., and Schmölling, T. (2020). Acclimation, priming and memory in the response of *Arabidopsis thaliana* seedlings to cold stress. *Sci. Rep.* 10:689. doi: 10.1038/s41598-019-56797-x
- Lowe, A., Rafferty-McArdle, S. M., and Cassells, A. C. (2012). Effects of AMF and PGPR-root inoculation and a foliar chitosan spray in single and combined treatments on powdery mildew disease in strawberry. *Agric. Food Sci.* 21, 28–38. doi: 10.23986/afsci.4997
- Malde, K. (2008). The effect of sequence quality on sequence alignment. *Bioinformatics* 24, 897–900. doi: 10.1093/bioinformatics/btn052
- Martinez-Seidel, F., Beine-Golovchuk, O., Hsieh, Y. C., and Kopka, J. (2020). Systematic review of plant ribosome heterogeneity and specialization. *Front. Plant Sci.* 11:948. doi: 10.3389/fpls.2020.00948
- Mascher, M., Gundlach, H., Himmelbach, A., Beier, S., Twardziok, S. O., Wicker, T., et al. (2017). A chromosome conformation capture ordered sequence of the barley genome. *Nature* 544, 427–433. doi: 10.1038/nature22043
- Mi, H., Muruganujan, A., Ebert, D., Huang, X., and Thomas, P. D. (2019). PANTHER version 14: more genomes, a new PANTHER GO-slim and improvements in enrichment analysis tools. *Nucleic Acids Res.* 47, D419–D426. doi: 10.1093/nar/gky1038
- Miura, K., and Furumoto, T. (2013). Cold signaling and cold response in plants. *Int. J. Mol. Sci.* 14, 5312–5337. doi: 10.3390/ijms14035312
- Needleman, S. B., and Wunsch, C. D. (1970). A general method applicable to the search for similarities in the amino acid sequence of two proteins. *J. Mol. Biol.* 48, 443–453. doi: 10.1016/0022-2836(70)90057-4
- Nelson, C. J., Li, L., and Millar, A. H. (2014). Quantitative analysis of protein turnover in plants. *Proteomics* 14, 579–592. doi: 10.1002/pmic.201300240
- Nielsen, M. E., Feechan, A., Böhlenius, H., Ueda, T., and Thordal-Christensen, H. (2012). *Arabidopsis* ARF-GTP exchange factor, GNOM, mediates transport required for innate immunity and focal accumulation of syntaxin PEN1. *Proc. Natl. Acad. Sci. U.S.A.* 109, 11443–11448. doi: 10.1073/pnas.1117596109
- Novák, A., Boldizsár, A., Gierczik, K., Vágújfalvi, A., Ádám, E., Kozma-Bognár, L., et al. (2017). Light and temperature signalling at the level of CBF14 gene expression in wheat and barley. *Plant Mol. Biol. Rep.* 35, 399–408. doi: 10.1007/s11105-017-1035-1
- Ohbayashi, I., and Sugiyama, M. (2018). Plant nucleolar stress response, a new face in the NAC-dependent cellular stress responses. *Front. Plant Sci.* 8:2247. doi: 10.3389/fpls.2017.02247
- Park, S., Lee, C. M., Doherty, C. J., Gilmour, S. J., Kim, Y., and Thomashow, M. F. (2015). Regulation of the *Arabidopsis* CBF regulon by a complex low-temperature regulatory network. *Plant J.* 82, 193–207. doi: 10.1111/tjp.12796

- Pastor, V., Luna, E., Ton, J., Cerezo, M., García-Agustín, P., and Flors, V. (2013). Fine tuning of reactive oxygen species homeostasis regulates primed immune responses in *Arabidopsis*. *Mol. Plant Microbe Interact.* 26, 1334–1344. doi: 10.1094/MPMI-04-13-0117-R
- Pearson, W. R. (1995). Comparison of methods for searching protein sequence databases. *Protein Sci.* 4, 1145–1160. doi: 10.1002/pro.5560040613
- Perez-Riverol, Y., Csordas, A., Bai, J., Bernal-Llinares, M., Hewapathirana, S., Kundu, D. J., et al. (2019). The PRIDE database and related tools and resources in 2019: improving support for quantification data. *Nucleic Acids Res.* 47, D442–D450. doi: 10.1093/nar/gky1106
- Plazek, A., Hura, K., Zur, I., and Niemczyk, E. (2003). Relationship between frost tolerance and cold-induced resistance of spring barley, meadow fescue and winter oilseed rape to fungal pathogens. *J. Agron. Crop Sci.* 189, 333–340. doi: 10.1046/j.1439-037X.2003.00052.x
- Rahman, A. (2013). Auxin: a regulator of cold stress response. *Physiol. Plant.* 147, 28–35. doi: 10.1111/j.1399-3054.2012.01617.x
- Rue-Albrecht, K., McGettigan, P. A., Hernández, B., Nalpas, N. C., Magee, D. A., Parnell, A. C., et al. (2016). GOexpress: an R/Bioconductor package for the identification and visualisation of robust gene ontology signatures through supervised learning of gene expression data. *BMC Bioinformatics* 17:126. doi: 10.1186/s12859-016-0971-3
- Sáez-Vásquez, J., and Delseny, M. (2019). Ribosome biogenesis in plants: from functional 45S ribosomal DNA organization to ribosome assembly factors. *Plant Cell* 31, 1945–1967. doi: 10.1105/TPC.18.00874
- Salih, K. J., Duncan, O., Li, L., Troesch, J., and Millar, A. H. (2019). Refining the composition of the *Arabidopsis thaliana* 80S cytosolic ribosome. *bioRxiv* [Preprint]. doi: 10.1101/764316
- Samir, P., Browne, C. M., Rahul, Sun, M., Shen, B., Li, W., et al. (2018). Identification of changing ribosome protein compositions using mass spectrometry. *Proteomics* 18:1800217. doi: 10.1002/pmic.201800217
- Sasaki, K., Christov, N. K., Tsuda, S., and Imai, R. (2014). Identification of a novel LEA protein involved in freezing tolerance in wheat. *Plant Cell Physiol.* 55, 136–147. doi: 10.1093/pcp/ptt164
- Sasaki, K., Kuwabara, C., Umeki, N., Fujioka, M., Saburi, W., Matsui, H., et al. (2016). The cold-induced defensin TAD1 confers resistance against snow mold and *Fusarium* head blight in transgenic wheat. *J. Biotechnol.* 228, 3–7. doi: 10.1016/j.jbiotec.2016.04.015
- Segev, N., and Gerst, J. E. (2018). Specialized ribosomes and specific ribosomal protein paralogs control translation of mitochondrial proteins. *J. Cell Biol.* 217, 117–126. doi: 10.1083/jcb.201706059
- Seki, M., Narusaka, M., Ishida, J., Nanjo, T., Fujita, M., Oono, Y., et al. (2002). Monitoring the expression profiles of 7000 *Arabidopsis* genes under drought, cold and high-salinity stresses using a full-length cDNA microarray. *Plant J.* 31, 279–292. doi: 10.1046/j.1365-313X.2002.01359.x
- Seo, P. J., and Park, C. M. (2010). MYB96-mediated abscisic acid signals induce pathogen resistance response by promoting salicylic acid biosynthesis in *Arabidopsis*. *New Phytol.* 186, 471–483. doi: 10.1111/j.1469-8137.2010.03183.x
- Seo, P. J., Kim, M. J., Park, J. Y., Kim, S. Y., Jeon, J., Lee, Y. H., et al. (2010). Cold activation of a plasma membrane-tethered NAC transcription factor induces a pathogen resistance response in *Arabidopsis*. *Plant J.* 61, 661–671. doi: 10.1111/j.1365-313X.2009.04091.x
- Shibasaki, K., Uemura, M., Tsurumi, S., and Rahman, A. (2009). Auxin response in *Arabidopsis* under cold stress: underlying molecular mechanisms. *Plant Cell* 21, 3823–3838. doi: 10.1105/tpc.109.069906
- Shpaer, E. G., Robinson, M., Yee, D., Candlin, J. D., Mines, R., and Hunkapiller, T. (1996). Sensitivity and selectivity in protein similarity searches: a comparison of Smith-Waterman in hardware to BLAST and FASTA. *Genomics* 38, 179–191. doi: 10.1006/geno.1996.0614
- Smith, T. F., and Waterman, M. S. (1981). Identification of common molecular subsequences. *J. Mol. Biol.* 147, 195–197. doi: 10.1016/0022-2836(81)90087-5
- Snider, C. S., Hsiang, T., Zhao, G., and Griffith, M. (2000). Role of ice nucleation and antifreeze activities in pathogenesis and growth of snow molds. *Phytopathology* 90, 354–361. doi: 10.1094/PHYTO.2000.90.4.354
- Steinmann, T., Geldner, N., Grebe, M., Mangold, S., Jackson, C. L., Paris, S., et al. (1999). Coordinated polar localization of auxin efflux carrier PIN1 by GNOM ARF GEF. *Science* 286, 316–318. doi: 10.1126/science.286.5438.316
- Su, L., Lan, Q., Pritchard, H. W., Xue, H., and Wang, X. (2016). Reactive oxygen species induced by cold stratification promote germination of *Hedysarum scoparium* seeds. *Plant Physiol. Biochem.* 109, 406–415. doi: 10.1016/j.plaphy.2016.10.025
- Supek, F., Bošnjak, M., Škunca, N., and Šmuc, T. (2011). Revigo summarizes and visualizes long lists of gene ontology terms. *PLoS One* 6:e21800. doi: 10.1371/journal.pone.0021800
- Suzuki, R., and Shimodaira, H. (2006). Pvcust: an R package for assessing the uncertainty in hierarchical clustering. *Bioinformatics* 22, 1540–1542. doi: 10.1093/bioinformatics/btl117
- Szechyńska-Hebda, M., Hebda, M., Mierzwiński, D., Kuczyńska, P., Mirek, M., Wedzony, M., et al. (2013). Effect of cold-induced changes in physical and chemical leaf properties on the resistance of winter triticale (*×Triticosecale*) to the fungal pathogen *Microdochium nivale*. *Plant Pathol.* 62, 867–878. doi: 10.1111/ppa.12001
- Szechyńska-Hebda, M., Wasek, I., Golebiowska, G., Dubas, E., Zur, I., and Wedzony, M. (2015). Photosynthesis-dependent physiological and genetic crosstalk between cold acclimation and cold-induced resistance to fungal pathogens in triticale (*Triticosecale* Wittm.). *J. Plant Physiol.* 177, 30–43. doi: 10.1016/j.jplph.2014.12.017
- Thalhammer, A., and Hincha, D. K. (2013). “The function and evolution of closely related COR/LEA (Cold-regulated/late embryogenesis abundant) proteins in *Arabidopsis thaliana*,” in *Plant and Microbe Adaptations to Cold in a Changing World*, eds R. Imai, M. Yoshida, and N. Matsumoto (New York, NY: Springer), 89–105. doi: 10.1007/978-1-4614-8253-6_8
- Thévenot, E. A., Roux, A., Xu, Y., Ezan, E., and Junot, C. (2015). Analysis of the human adult urinary metabolome variations with age, body mass index, and gender by implementing a comprehensive workflow for univariate and OPLS statistical analyses. *J. Proteome Res.* 14, 3322–3335. doi: 10.1021/acs.jproteome.5b00354
- Thomashow, M. F. (1999). Plant cold acclimation: freezing tolerance genes and regulatory mechanisms. *Annu. Rev. Plant Biol.* 50, 571–599. doi: 10.1146/annurev.arplant.50.1.571
- Thompson, A., Schäfer, J., Kuhn, K., Kienle, S., Schwarz, J., Schmidt, G., et al. (2003). Tandem mass tags: a novel quantification strategy for comparative analysis of complex protein mixtures by MS/MS. *Anal. Chem.* 75, 1895–1904. doi: 10.1021/ac0262560
- Thompson, M. K., Rojas-Duran, M. F., Gangaramani, P., and Gilbert, W. V. (2016). The ribosomal protein Asc1/RACK1 is required for efficient translation of short mRNAs. *Elife* 5:e11154. doi: 10.7554/eLife.11154
- Tsutsui, T., Kato, W., Asada, Y., Sako, K., Sato, T., Sonoda, Y., et al. (2009). DEAR1, a transcriptional repressor of DREB protein that mediates plant defense and freezing stress responses in *Arabidopsis*. *J. Plant Res.* 122, 633–643. doi: 10.1007/s10265-009-0252-6
- Tyanova, S., Temu, T., Sinitcyn, P., Carlson, A., Hein, M. Y., Geiger, T., et al. (2016). The Perseus computational platform for comprehensive analysis of (prote)omics data. *Nat. Methods* 13, 731–740. doi: 10.1038/nmeth.3901
- Uemura, M., Joseph, R. A., and Steponkus, P. L. (1995). Cold acclimation of *Arabidopsis thaliana*: effect on plasma membrane lipid composition and freeze-induced lesions. *Plant Physiol.* 109, 15–30. doi: 10.1104/pp.109.1.15
- Van Hulten, M., Pelsler, M., Van Loon, L. C., Pieterse, C. M. J., and Ton, J. (2006). Costs and benefits of priming for defense in *Arabidopsis*. *Proc. Natl. Acad. Sci. U.S.A.* 103, 5602–5607. doi: 10.1073/pnas.0510213103
- Verbelen, J. P., De Cnodder, T., Le, J., Vissenberg, K., and Baluška, F. (2006). The root apex of *Arabidopsis thaliana* consists of four distinct zones of growth activities: meristematic zone, transition zone, fast elongation zone and growth terminating zone. *Plant Signal. Behav.* 1, 296–304. doi: 10.4161/psb.1.6.3511
- Von Zitzewitz, J., Szűcs, P., Dubcovsky, J., Yan, L., Francia, E., Pecchioni, N., et al. (2005). Molecular and structural characterization of barley vernalization genes. *Plant Mol. Biol.* 59, 449–467. doi: 10.1007/s11103-005-0351-2
- Wang, D., Liu, J., Li, C., Kang, H., Wang, Y., Tan, X., et al. (2016). Genome-wide association mapping of cold tolerance genes at the seedling stage in rice. *Rice* 9:61. doi: 10.1186/s12284-016-0133-2
- Wiener, M., and Liaw, A. (2003). Classification and regression by randomForest. *R News* 2/3, 18–22.

- Woolford, J. L., and Baserga, S. J. (2013). Ribosome biogenesis in the yeast *Saccharomyces cerevisiae*. *Genetics* 195, 643–681. doi: 10.1534/genetics.113.153197
- Xiao, N., Gao, Y., Qian, H., Gao, Q., Wu, Y., Zhang, D., et al. (2018). Identification of genes related to cold tolerance and a functional allele that confers cold tolerance. *Plant Physiol.* 177, 1108–1123. doi: 10.1104/pp.18.00209
- Zecha, J., Satpathy, S., Kanashova, T., Avanesian, S. C., Kane, M. H., Clauser, K. R., et al. (2019). TMT labeling for the masses: a robust and cost-efficient, in-solution labeling approach. *Mol. Cell. Proteomics* 18, 1468–1478. doi: 10.1074/mcp.TIR119.001385
- Zuther, E., Schaarschmidt, S., Fischer, A., Erban, A., Pagter, M., Mubeen, U., et al. (2019). Molecular signatures associated with increased freezing tolerance due to low temperature memory in *Arabidopsis*. *Plant Cell Environ.* 42, 854–873. doi: 10.1111/pce.13502
- Conflict of Interest:** The authors declare that the research was conducted in the absence of any commercial or financial relationships that could be construed as a potential conflict of interest.
- Copyright © 2021 Martinez-Seidel, Suwanthakasem, Nie, Leeming, Pereira Firmino, Williamson, Kopka, Roessner and Boughton. This is an open-access article distributed under the terms of the Creative Commons Attribution License (CC BY). The use, distribution or reproduction in other forums is permitted, provided the original author(s) and the copyright owner(s) are credited and that the original publication in this journal is cited, in accordance with accepted academic practice. No use, distribution or reproduction is permitted which does not comply with these terms.

Chapter 5

COSNet_i:

ComplexOme-Structural Network

Interpreter Used to Study Spatial

Enrichment in Metazoan

Ribosomes

SOFTWARE

Open Access



COSNet_i: ComplexOme-Structural Network Interpreter used to study spatial enrichment in metazoan ribosomes

Federico Martinez-Seidel^{1,2*†} , Yin-Chen Hsieh^{1,3†}, Dirk Walther¹, Joachim Kopka¹ and Alexandre Augusto Pereira Firmino¹

*Correspondence: mseidel@mpimp-golm.mpg.de

[†]Federico Martinez-Seidel and Yin-Chen Hsieh have contributed equally to this work.

¹Willmitzer Department, Max-Planck-Institute of Molecular Plant Physiology, 14476 Potsdam-Golm, Germany

Full list of author information is available at the end of the article

Abstract

Background: Upon environmental stimuli, ribosomes are surmised to undergo compositional rearrangements due to abundance changes among proteins assembled into the complex, leading to modulated structural and functional characteristics. Here, we present the ComplexOme-Structural Network Interpreter (COSNet_i), a computational method to allow testing whether ribosomal proteins (rProteins) that exhibit abundance changes under specific conditions are spatially confined to particular regions within the large ribosomal complex.

Results: COSNet_i translates experimentally determined structures into graphs, with nodes representing proteins and edges the spatial proximity between them. In its first implementation, COSNet_i considers rProteins and ignores rRNA and other objects. Spatial regions are defined using a random walk with restart methodology, followed by a procedure to obtain a minimum set of regions that cover all proteins in the complex. Structural coherence is achieved by applying weights to the edges reflecting the physical proximity between purportedly contacting proteins. The weighting probabilistically guides the random-walk path trajectory. Parameter tuning during region selection provides the option to tailor the method to specific biological questions by yielding regions of different sizes with minimum overlaps. In addition, other graph community detection algorithms may be used for the COSNet_i workflow, considering that they yield different sized, non-overlapping regions. All tested algorithms result in the same node kernels under equivalent regions. Based on the defined regions, available abundance change information of proteins is mapped onto the graph and subsequently tested for enrichment in any of the defined spatial regions. We applied COSNet_i to the cytosolic ribosome structures of *Saccharomyces cerevisiae*, *Oryctolagus cuniculus*, and *Triticum aestivum* using datasets with available quantitative protein abundance change information. We found that in yeast, substoichiometric rProteins depleted from translating polysomes are significantly constrained to a ribosomal region close to the tRNA entry and exit sites.

Conclusions: COSNet_i offers a computational method to partition multi-protein complexes into structural regions and a statistical approach to test for spatial enrichments of any given subsets of proteins. COSNet_i is applicable to any multi-protein complex



given appropriate structural and abundance-change data. COSNet_i is publicly available as a GitHub repository https://github.com/MSeidelFed/COSNet_i and can be installed using the python installer pip.

Keywords: Structural systems biology, Ribosome structure, Omics integration, Specialized ribosomes, Ribosomal protein substoichiometry

Background

The function of cytosolic ribosomes is optimized to produce more ribosomes [1] through the translation of mRNAs. Translation creates ribosomal proteins (rProteins) that are used to produce functional ribosomes according to cellular needs. Moreover, translation builds the cellular machinery that initiates rRNA transcription and ribosome biogenesis, enabling processing of pre-ribosomes into translationally competent complexes [2–4]. Conceivably, ribosomes exist in various alternative forms, which vary structurally, and are functionally divergent, specialized complexes that meet translational requirements according to developmental or environmental cues [5–8]. Evidence for ribosome heterogeneity and specialization is rapidly growing across a wide variety of organisms [7, 9, 10].

Cytosolic ribosomes have a universal core that remained largely unchanged across evolutionary scales [11]. Compared to archaeal and bacterial ribosomes, metazoan cytosolic ribosomes logarithmically accumulated RNA expansion segments (ES) since approximately two billion years [11, 12]. Metazoan rProteins increased in number, duplicated, diverged, and acquired novel properties [13–17] which, when added to the accumulation of ES, implies extra potential to neo- and subfunctionalize. The ribosome considered as an entity is subject to selection and can be functionally specialized via heterogeneity of ES, rRNA modifications, substoichiometry of rProteins, i.e., the deviation from a canonical ribosomal proteome composition, the use of diverse rProtein paralogs or post-translational modification of rProteins and rRNAs [18, 19]. An important source of heterogeneity is rProteins substoichiometry, which can affect groups of rProteins [3]. In yeast, mutants deficient in individual rProteins can be defective in specific rRNA processing steps and consequently affect the assembly of multiple rProteins. Such defects are spatially constrained within the ribosome according to the sequence of ribosome assembly and thus depend on the overall location of the defective rProteins. Similarly, we expect that triggered structural heterogeneity may influence the assembly of specific rProteins, paralogs or post-translationally modified rProteins. Thereby, variants of ribosome complexes may arise with spatially constrained structural heterogeneity that extends across multiple adjacent rProteins. We hypothesize that such concerted structural heterogeneity may be at the core of ribosome specialization and influence the mRNA preference of mature ribosome complexes.

Available ribosome structures make it possible to test for spatial rearrangement in ribosomal complexes as a mode of functional specialization in response to specific cues. Such a test offers the possibility of integrating atomic structures and omics measurements of constituent ribosomal components. Integration of cryogenic or crystallographic atomic structures and omics data on abundances of structural components are part of the research field of structural systems biology [20] and begin with constructing a coarse-grained simplified representation of the structure, often represented as a graph. Using graphs, one can assign and compare node and edge-properties in order to

answer biological questions at a single protein level [21]. Similarly, at the multi-protein level, structural models of protein complexes can preserve protein-protein interactions as edges connecting single protein components as nodes. Such networks enable topological analysis and comparison of node- and edge-properties. More detailed information on spatial relationships between proteins within a complex can be integrated by weighing the edges, where the edge weight describes specific properties of the interactions [22]. The edge weights can encode diverse properties, ranging from physical proximity to experimental evidence of said interaction. Using this approach, highly complex structures can be simplified to a network graph that represents essential structural information within orthologous protein complexes, such as the diverse variants of cytosolic ribosomes.

Cytosolic ribosomes readily lend themselves to a graph-based representation. These complexes are mixed ribonucleoprotein entities that consist of two subunits, namely the large 60S (LSU) and the small 40S (SSU) that combine to form a functionally mature 80S ribosome complex. Both subunits contain distinct ribosomal RNAs (rRNAs) as scaffolds for the binding of a multitude of rProteins [23]. If rRNAs, mRNA and tRNAs are excluded from the structural models, the outcome is an interconnected spatial array of rProteins that constitutes what we may call the structural ribosomal proteome (rProteome). A graph interpretation of the rProteome generates a specific topology that is the product of protein-protein interconnectivity and RNA mediated structural interactions generating community gaps within the network. Proteins within this network comprise sub-structures of physically adjacent entities. Thus, graph properties such as modularity [24], i.e., a measure of the division of a network into modules or communities, could be exploited to yield approximate rProtein communities. Likewise, coherent rProtein subsets can be sampled from these weighted rProteome networks. Random walks through weighted graphs are a well-documented procedure [25] capable of identifying communities within convoluted networks [26, 27] and correlations to hidden molecular functions. Community detection approaches enabled elucidating organizing principles of enzyme physical interaction networks and their relation to metabolic status [28]. Similarly, rProtein physical interaction networks provide the basis to define structurally coherent rProteome subsets that can be used to answer specific functional and biological questions. Going back to ribosome biogenesis, we may ask whether upon external cues, adjacent rProteins comprise significantly modulated sets of proteins.

Once coherent rProteome subsets are defined, these can be analyzed to identify localized changes based on systems biology data. Transcriptomic measurements of rProtein gene expression changes can be considered as a first level of information integration, supporting prediction and hypothesis generation. On the other hand, measurements of rProteome composition can verify assumptions of localized changes within the ribosome complex. The spatial enrichment analyses proposed in this manuscript contribute to the prediction and verification of ribosome heterogeneity, e.g., substoichiometry of ribosome complexes or changes in rProtein paralog composition, and more importantly, add the aspect of concerted ribosome heterogeneity affecting sets of co-localized rProteins. Concerted heterogeneity can be expected, as ribosome biogenesis is a highly regulated sequential process that is far from random. Alternatively, post-assembly changes are conceivable but restricted to surface accessible rProteins. Modulation of

spatially-linked groups of rProteins rather than heterogeneity of single rProteins may be the basis of ribosome specialization and confer ribosome complexes the ability to influence the translational status of transcripts, favoring those that require active translation upon environmental or developmental cues, a concept known as the “ribosomal code” [29].

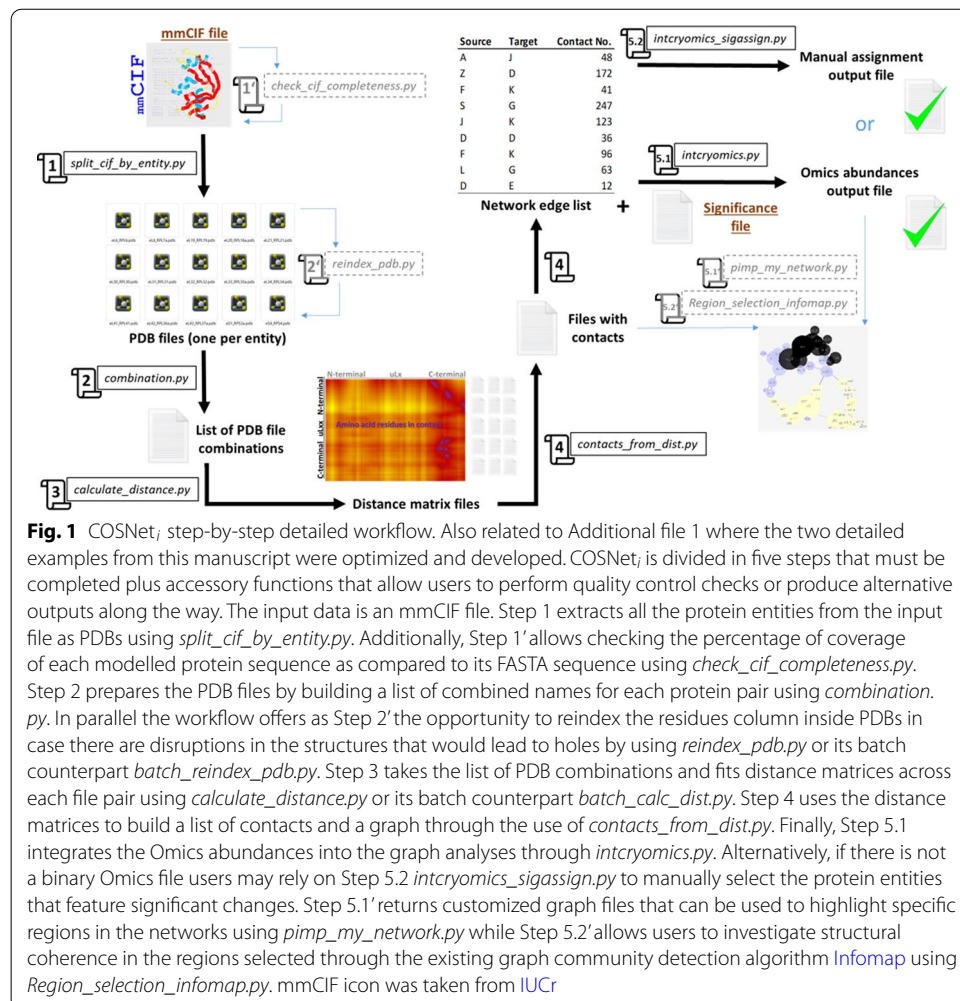
In the current study, we present a workflow enabled by the ComplexOme-Structural Network Interpreter (COSNet_i) python module that decomposes cryogenic or crystallographic atomic structures of multi-protein complexes into subsets of physically adjacent proteins and subsequently tests them for enrichment of concerted changes relative to other parts of the complex. Thereby we integrate structural information with readily available omics-measurements from systems analyses. To achieve this integration, we subset protein interaction networks of multi-protein complexes derived from elucidated structures using a random-walk sampling with restart. Structural coherence and region consensus is achieved by iterating the sampling procedure through a translated graph weighted by protein physical proximity as a proxy of traversal probability. We test the performance of COSNet_i by comparing regional coherence with several graph community detection algorithms. We highlight as a novelty that COSNet_i, unlike the tested algorithms, allows users to customize coherent regions for specific biological questions. Consequently, we describe a procedure to optimize parameters of our sampling and evaluation method using as case studies the cytosolic ribosome complexes of various metazoans. More specifically, we compare the relatively simple yeast ribosome to the more complex mammalian and plant counterparts and integrate available systems data of each species. To gather information on a previously unanswered biological question, we explore concerted localized rProtein heterogeneity that suggests ribosome specialization. We specifically ask whether changing physiological conditions affect rProtein heterogeneity in a way that is constrained to specific spatial regions of metazoan ribosomes.

Implementation

COSNet_i is a python module organized based on a collection of scripts that allow any user to select coherent spatial neighborhoods of protein entities from a multi-protein complex in order to test whether these communities characterize a region within the complex that becomes significantly enriched upon any experimental procedure. The complete workflow is detailed in a step-by-step manner in Fig. 1 and Additional file 1.

Structural data preprocessing

RCSB PDB entries 6SNT, 6GZ5, and 4V7E were retrieved as PDBx/mmCIF files and the following pre-processing steps were implemented to ensure their usability for this study. Nonstandard amino acids labeled as “hetero atoms” (HETATMs) and duplicate atoms were removed from all proteins. rRNA, ions, tRNA, and mRNA components of the original structure were ignored. The percentage of missing residues per ribosomal protein (rProtein) was noted (see Structure Quality Requirements section in the Discussion). Each rProtein sequence was verified as correctly labeled via BLAST [30] against the protein entry originally modelled into the Cryo-EM densities. Proteins were renamed according to the new rProtein naming scheme [31].



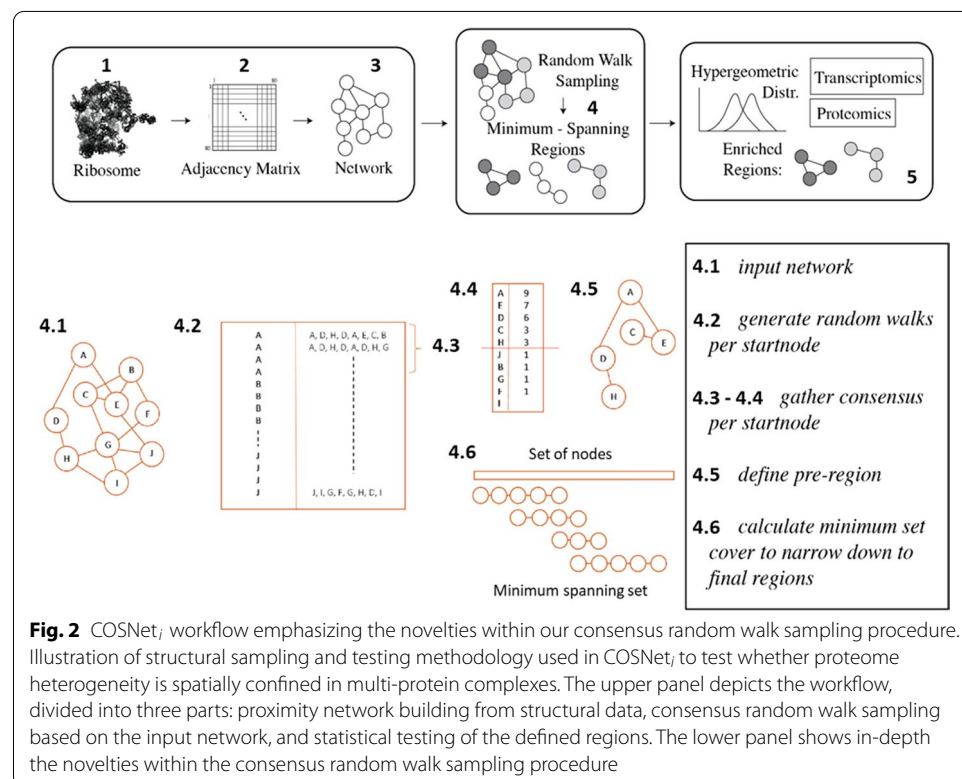
Proximity network building

Translating ribosome atomic structures to rProtein proximity networks allowed characterization of the overall topology and protein relative positions. The structural interactions of rRNA and rProteins were not considered because the rRNA structures were ignored when building the network. Thus, the concept of proximity in the current study does not imply direct physical interaction between rProteins, rather a high potential for interaction due to physical proximity. The resulting network is an undirected graph, with nodes representing proteins and weighted edges between two proteins sharing at least one spatial contact at a given proximity threshold. To calculate contacts between proteins, all amino acid residues belonging to both proteins were represented in the three-dimensional space of coordinates of the given model by their geometric center of mass (i.e., coarse-grained to a single point). The Euclidean distances between each pair of amino acids from paired rProteins were calculated. The choice to coarse-grain at amino acid residue level enabled detection of potential interactions of extended non-globular proteins that branch out far across the ribosome, such as universal large ribosomal protein 4 (uL4) or eukaryotic large ribosomal protein 19 (eL19). Edges were accepted at different distance thresholds (e.g., $d_t = 5, 8, 12, \text{ or } 20$ Ångströms [Å]). Thereby, we

generated several proximity networks varying around the common consensus of 8 Å for residues to be considered in contact, according to the 8th Critical Assessment of Protein Structure Prediction experiment (CASP8) [32]. Weighting of edges was performed according to the proportion of inter-amino acid residue contacts found between two proteins as compared to all the inter-amino acid residue contacts from the source node-protein. Networks were visualized with the R package *igraph* [33] and Cytoscape software [34].

Structural region definition

Splitting ribosomes into separate structurally coherent regions allowed for targeted statistical testing of protein features within regions (Fig. 2—upper panel) and ensured that any regions of interest could be further validated by known biological domains. The main priority was avoiding pre-knowledge biases while selecting node associations. To achieve this, randomness was introduced when sampling nodes. In detail, a consensus random walk sampling procedure with restart methodology was implemented. The procedure (Fig. 2—lower panel) involved: (4.1) a proximity network was taken as input, and a walk length and iteration number were defined. The walk does not reverse and is completely memoryless. The walk length represented the number of steps a random walk takes before terminating, and the iteration number was the number of random walk restarts from a particular starting node. Edges between protein nodes were weighted based on the number of amino acid residues in contact normalized by the number of amino acid residues of the source node and transformed into a transit probability. Given two protein nodes, x and y , the probability of walking from node x to y is computed as



$P_{x,y} = w_{x,y}/w_x$, where w_x is the sum of all weights of all outgoing edges of node x . Thus, the probability corresponds to how many contacts there are between node x and y , relative to all other nodes connected to x . The random walk is no longer purely 'random' in the strict sense, but has a higher probability to walk along an edge with a higher weight. (4.2) A collection of all walks for every start node for all nodes in the network was compiled. Exemplary sample walks for start nodes A and J were selected for illustration purposes (Fig. 2—lower panel step 4.2). (4.3) For all sets of walks that share the same start node, (4.4) a count-based summary of node visits was calculated, where every instance of a visit to a node, even those within the same walk, was tallied. In our example (Fig. 2—lower panel step 4.4), walks with start node A often visited nodes E and D, followed by visits to nodes C and H. (4.5) Pre-regions were defined for all start nodes, consisting of nodes that were visited with a frequency of at least half of the iteration number. Using a count-based consensus ensured that nodes, which were relatively far away from the start node and were visited by chance, were excluded from the pre-regions. As an example, the pre-region for start node A is A, E, D, C, H (Fig. 2—lower panel step 4.5). Steps (2-5) were carried out to ensure that the pre-regions were not biased towards a single walk from a certain start node and also that each node in the network served as start node. Thereby, all nodes were visited at least once. At this point, the number of pre-regions equaled the number of nodes in the network since each of the nodes served as starting point. The level of node overlap among the pre-regions varied, where two pre-regions with different start nodes could in one extreme case be fully distinct from one another or in the other extreme be identical. (4.6) Final regions were aggregated from the pre-regions by calculating the minimum set cover that spanned the entire universe of protein nodes. This procedure gave the minimum number of final regions that spanned the entire node space, and returned a small set of regions with minimized redundancy. Finding the minimum set cover gave preference to large and more complete regions that mapped to the entire node space, as opposed to a large number of small regions.

Testing of enriched relative changes within regions

The statistical testing procedure used the set of all known rProtein paralogs and aimed to discover whether there is an association between protein nodes being part of a structural region, and having changed in relative abundance (CRA) in response to experimental conditions. CRA was defined as differential stoichiometry between ribosomal complexes as determined by proteomics data. CRA was defined as a binary data-type, where a code of "1" indicates abundance changes and a code of "0" indicates otherwise. The testing scheme assumes a background hypergeometric distribution, and is thus equivalent to the Fisher's exact test, with baseline probability of enrichment equal to the total fraction of paralogs with CRA compared to all rProtein paralogs. The null hypothesis here states that there is no relationship between being part of a particular structural region and having the CRA property. In other words, the null hypothesis assumes that proteins exhibiting the CRA property are distributed randomly throughout the complex. For statistical testing, the SciPy implementation of the Fisher's exact test was used [35]. Due to multiple testing, computed p -values generated by the Fisher's exact test were adjusted via Bonferroni correction [36].

Test case datasets

Three ribosome structures were used in order to optimize the parameters of our methodology. All datasets corresponded to metazoans ribosomes with varying complexities. More specifically, the ribosome structures of *Saccharomyces cerevisiae*—2.80 Å (<https://www.rcsb.org/structure/6SNT>), *Oryctolagus cuniculus*—3.50 Å (<https://www.rcsb.org/structure/6GZ5>), and *Triticum aestivum*—5.50 Å (<https://www.rcsb.org/structure/4V7E>) were used. The datasets varied in structural resolution, which allowed us to determine whether a relatively low resolution would preclude the use of our method (see Structure Quality Requirements section in the Discussion). In agreement with these considerations only two exemplary structures were tested for spatial rearrangements of the riboproteome. The third (i.e., the only available plant cytosolic ribosome structure) one should be used carefully considering the parameters provided in COSNet_i. We selected proteomics datasets that indicated substoichiometry of rProteins in mammalian cell cultures and yeast. The following selected datasets evaluated rProtein substoichiometry between pools of free non-translational subunits or monosomes and translationally competent polysomes:

1. Mammalian [37] taken from Shi et al. (2017). **Species:** *Mus musculus*. **Cell line:** Low-passage E14 mouse embryonic stem cells (mESCs). **Riboproteome:** Additional file 2 from Shi et al. (2017). rProteins that were significantly substoichiometric, i.e., $P < 0.05$ were set to “1”, similarly proteins that did not have a statistical change with $P > 0.05$ were set to “0”. Ribosomal protein coding genes and paralogs have been compiled from Supplementary Table 1 from Perry (2005) [38] by translating the nomenclature into the common new rProtein family names [31]. If the sequence of significantly changed paralog rProteins within one family was identical, all paralogs were set to one.

2. Yeast [39] taken from Slavov et al., (2015). **Species:** *Saccharomyces cerevisiae*. **Cell line:** “prototrophic diploid strain (DBY12007) with an S288c background and wild-type HAP1 alleles (Slavov and Botstein, 2011)”. **Riboproteome:** Additional file 4, mmc5. Additional file 4 treated paralog ambiguities as a united rProtein family response. Thus, the top substoichiometric rProteins, including all paralogs per family, with a larger than 0.5 absolute \log_2 -fold change among translating polysomes loaded with different amounts of monosomes were set to “1”, the rest of the proteins were set to “0”. The complexes were isolated from glucose-fed yeast, growing at stationary rate, and recovered from ribosomal fractions corresponding to four loaded 80S-ribosomes per mRNA. rProtein coding genes and paralogs have been compiled from the *Saccharomyces* Genome Database (SGD) by translating the nomenclature into the common new rProtein family names [31].

In both cases, the entire set of rProteins was considered as all the paralogs from the proteins that were available in the structural files. Therefore, to prevent false significances, the annotated peptides were verified against the FASTA sequences of paralogs within rProtein families to make sure that they were not redundant. In case of redundancy, both paralogs were considered to have contributed to the sequenced peptide identified protein and thus were set to “1” if significant.

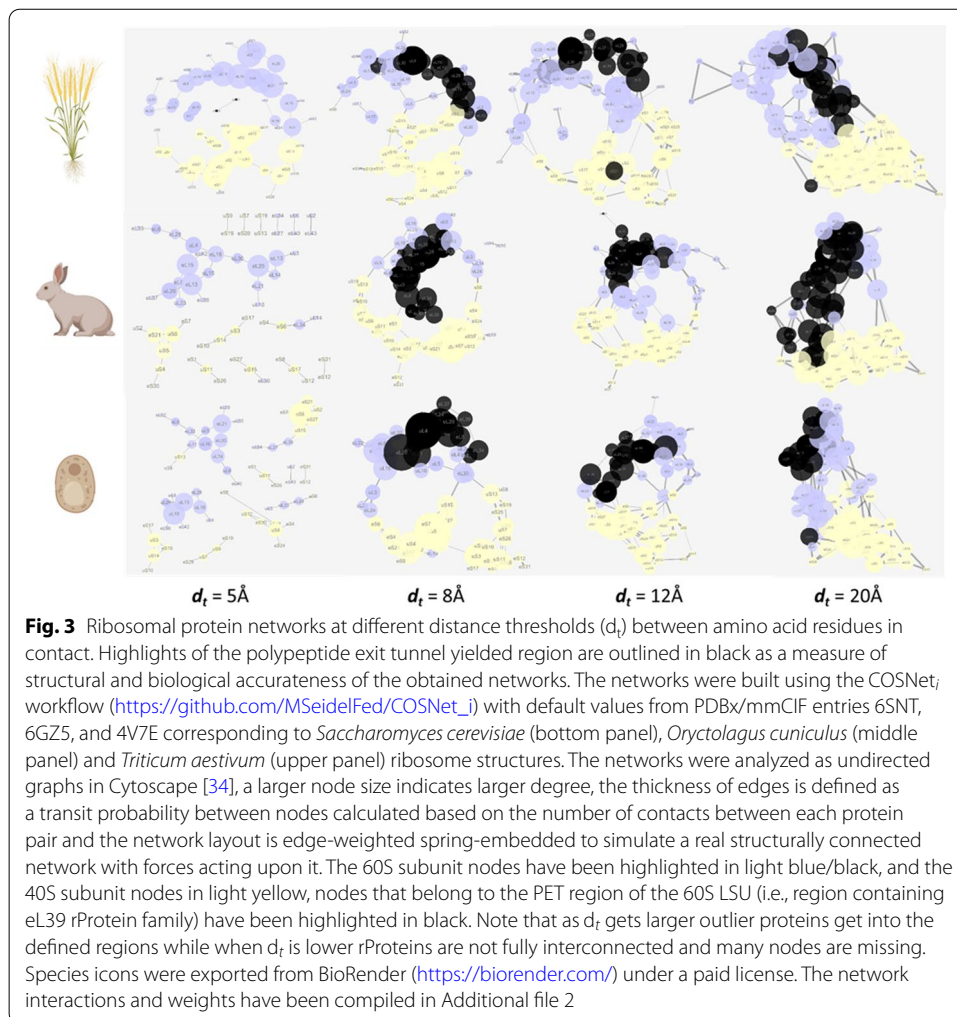
Results

The COSNet_{*t*} workflow, outlined in Figs. 1 and 2, can be generalized to accommodate any multi-protein complex as long as paired orthologous structures and differential omics abundances are available. Numerical parameters such as the structural proximity threshold (d_t) and module-sampling related walking length need to be tuned based on prior analyses of size and resolution-quality of the studied complex. In the following sections, we use the cytosolic ribosome as a test case to exemplify the fine-tuning of those parameters. As is explained in our introduction, we aimed the method towards analysis of the rProteome, i.e., the compendium of structural rProtein components. Consequently, parameter optimization coped with the intrinsic proteome diversity that our test cases, the metazoan ribosomes, have. We analyzed structures from less complex riboproteomes that contain only one to two paralogs per rProtein, i.e., the yeast and mammalian riboproteomes. As more complex cases, we selected the highly complex plant riboproteome, which potentially harbors combinations of two to seven paralogs per rProtein family in the dicot model plant *Arabidopsis* [40] or two to three per rProtein family in the monocot example, rice [41]. The canonical structures of ribosome complexes accommodate single copies of each rProtein. Therefore, we designed the procedure to perform regardless of the number of paralogs per rProtein family and organism. We chose to always test the whole set of annotated rProtein paralogs per genome, thereby using the near comprehensive information from omics studies.

Translating structures into graphs

The first critical parameter to obtain a weighted graph from an atomic structure is the definition of a distance threshold that determines the adjacency matrices between protein nodes, and ultimately influences the resulting network of nodes and edges. According to CASP8, the consensus distance for a residue-residue contact within a protein structure is 8 Å [32]. More specifically, residues in contact have their $C\beta$ atoms (β -carbon or $C\beta$, or $C\alpha$ for glycine) within a distance of 8 Å. Nevertheless, as many rProtein interactions are mediated by rRNA molecules, we tested whether the 8 Å threshold correctly reflects the structure of the ribosome in the obtained protein network. The aim of a network representation is to simplify the three-dimensional atomic models, while retaining structural and biological accuracy. Thus, the proximity network topology must reveal known ribosome structures as an internal means of validation. To investigate the biological accuracy of our networks, the clustering behavior within both ribosomal subunits, i.e. the LSU and SSU, was determined at different distance thresholds (Fig. 3). Our network layouts treated the edges between nodes as elastic springs. The springs organized themselves according to a force function influenced by the weight of each edge. The function minimized the sum of forces in the network, i.e. Edge-weighted Spring-Embedded algorithm in Cytoscape [34]. This layout algorithm treats a network as an interconnected structure of actual physical interactions. The rearranged network allowed us to describe topological features of the complexes that support biological knowledge (Fig. 3).

The topology of the proximity networks at varying distance thresholds ($d_t = 5, 8, 12$ and 20 Å see Additional file 2) outlined structural features of the ribosome. A consensus random sampling was done for one exemplary variable region, i.e., the polypeptide



exit tunnel (PET), characterized by at least the eL39 and eL37 protein families (PET in Fig. 3). It became evident that varying thresholds affected region coverage. Increasing the distance threshold resulted in increasing variability of defined regions. In other words, a higher threshold included “outlier” proteins, which were not physically close to the canonical rProtein cluster of the region. By contrast, if the threshold was too small, the network contained separate islands with some expected nodes omitted from the network. Hence, the outcome was a low connectivity among rProteins. An ideal distance threshold should produce a network, in which all the expected nodes or constituent proteins of the structure link by at least one edge. The possible optimized outcomes are a compromise between connectivity and coverage (Table 1).

Considering the PET region, at $d_t = 5\text{\AA}$, the PET rProteins eL37 and eL39 were only visible in the wheat structure due to a single mutual link, while eL39 was not at all included in the yeast and rabbit networks (Fig. 2). Similarly, more than 15% of the rProteins were omitted from the three networks at $d_t = 5\text{\AA}$ (Table 1). At the other extreme, with $d_t = 20\text{\AA}$, the entire network is highly inter-connected. An indication of over-represented connectivity is the transition to an exponential rate at which the number of edges increases relative to the nodes with increasing d_t (Table 1). Returning to our example

Table 1 Compromise between connectivity and coverage among networks fitted at varying distance (Å) thresholds

Species	Nodes	Edges	Threshold
<i>Triticum aestivum</i>	68	73	5 Å
	75	131	8 Å
	78	172	12 Å
	79	203	15 Å
	80	238	18 Å
	80	263	20 Å
<i>Oryctolagus cuniculus</i>	59	49	5 Å
	71	123	8 Å
	75	164	12 Å
	77	200	15 Å
	77	232	18 Å
	77	263	20 Å
<i>Saccharomyces cerevisiae</i>	60	57	5 Å
	67	115	8 Å
	68	146	12 Å
	71	180	15 Å
	71	207	18 Å
	71	227	20 Å

Italic style represents the node number and **bold** the edge number

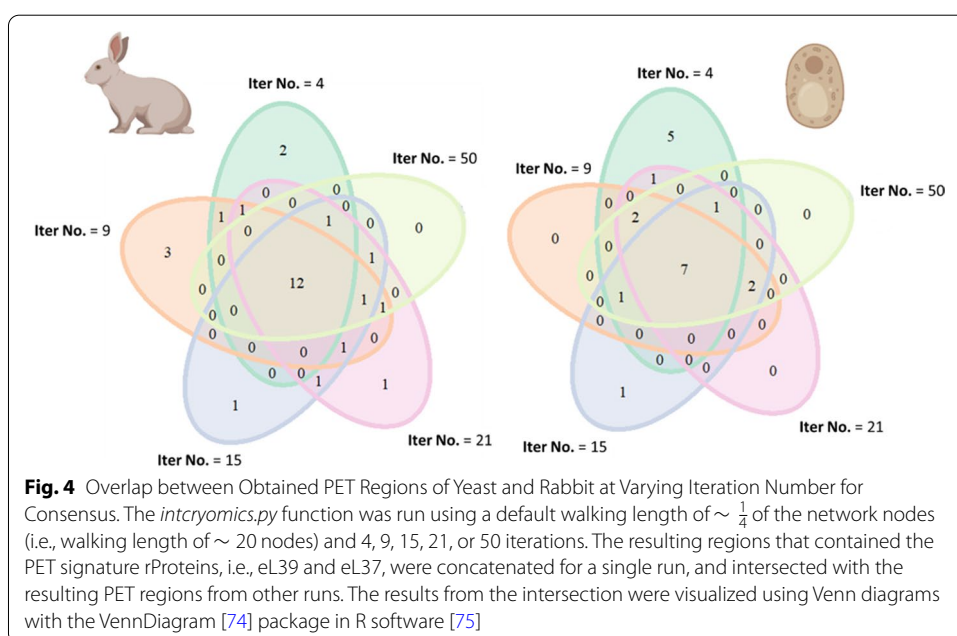
(Fig. 3), the PET is a densely packed region that increased in size with increasing d_t beyond the canonical PET definition and contained a large proportion of LSU proteins in the rabbit and wheat networks. Problems became apparent, too, with across structure interactions. For instance, rProteins found at opposite parts of the ribosome were included into the same region in wheat already at $d_t = 12\text{Å}$, while this happened in the yeast case only at $d_t = 20\text{Å}$. Inversely at $d_t = 8\text{Å}$, the plant P-stalk proteins became disconnected from the network. Disconnection creates a bias in as much as at every sampling step the P-Stalk will be an isolated region. Upon inspection of the wheat structure, we realized that this problem arises due to partially incomplete rProtein sequence coverage (see Structure Quality Requirements section in the Discussion). For this structural quality reason, we omitted the plant structure from the following analyses. The rabbit and yeast networks were 95% connected at $d_t = 12\text{Å}$, without isolated sub-regions, while “outlier” proteins were still absent. We therefore identified $d_t = 12\text{Å}$ as the ideal distance based on which to define regions in the yeast and rabbit structures. Using the same concepts, in the wheat structure a $d_t = 8\text{Å}$ would be the preferred threshold, were we to proceed with this analysis as concurrently done [42]. The chosen distance thresholds covered at least 95% of the nodes in all three cases.

Defining spatial regions

Once a network is compiled, walking across the network requires a predefined number of random steps and definition of a starting node. The direction of each step of the walk is influenced by the edges weights and the node interconnectivity. The clustering coefficient of the starting node is a determinant of the defined regions. The clustering coefficient is a measure of connectivity among neighbors of the starting node. A

high clustering coefficient of the starting node means that a random walk will stay in the vicinity or may even return to the starting node. By contrast, if the starting node has a low clustering coefficient and high betweenness centrality, the walk will likely lead to one of the parts of the network that the starting node connects. The measure of betweenness centrality refers to node importance in a network. A node that often acts as a bridge within shortest paths across the network has high betweenness centrality and connects largely separate modules within a network. In this sense, our methodology defines densely packed regions or modules of nodes in the weighted graph. Hubs that connect modules are attached to the closest group of highly interconnected neighbors. In order to avoid bias of a single walk trajectory, we iterate the random walk following a restart methodology from each node by a predefined number of times. The iteration number has high impact in the reproducibility of obtained regions and increasing it achieves region consensus, e.g., our exemplary analysis of PET variability (Fig. 4). After each walk, we gather a consensus of the most visited nodes from each start node and form pre-regions. Initially, the number of pre-regions equals the number of nodes. The following steps reduce the number of regions to a minimum set that covers the whole network with minimum overlap between regions.

In general, a core PET region occurred in every consensus, with seven nodes in the yeast and twelve nodes in rabbit network. When the iteration number was small, outlier proteins that did not belong to the canonical regions tended to be part of them after the network sampling procedure. For example, five specific nodes for yeast and rabbit are only part of the consensus walk when the iteration number is smaller than 10 in Fig. 4. This exemplifies the necessity of iterating the consensus walk to increase the reproducibility in region picking. As the iteration number increased, fewer outlier proteins, product of biased consensus walks, were found. Proteins from a consensus replaced outlier proteins from low iterated walks at higher iteration numbers. For instance, there were



three and two proteins shared by Iteration No. 21 and Iteration No. 50 in the rabbit and yeast PET region, respectively (Fig. 4).

In addition to the iteration number, the walking length parameter (i.e., number of steps in a walk) influenced the size and number of regions identified as the minimum spanning set covering all nodes. Here, we exemplify how the resulting ribosomal regions varied due to taking different proportions of the total node set as walking length (Table 2 and Additional file 3). Going beyond or below the proposed proportions may suit different computational needs and biological questions. In our case, we aimed at testing the relative proportion of significantly changed nodes in the resulting regions as compared to the whole ribosome. Therefore, regions with varying degrees of overlaps are acceptable. If partially overlapping regions have a different significance p -value, it means that not all structurally related proteins from a given region are changed, rather a specific combination of rProteins needs to be changed in order to call a region significantly enriched.

Region size needs can vary with different biological questions. To cover variable regions sizes we introduced the walking length parameter, which, when increasing, progressively yields larger regions (Table 2 and Additional file 3). The defined regions could then be tested for enrichment based on abundance changes of their constituting proteins. In the ribosomal example, we optimized the region size to match the significant proportion of nodes. In other words, regions had to be large enough for a single node to be proportionally equivalent to the percentage of significant nodes in the network. For instance, if 20% of the nodes in the network were significantly changed, i.e., showed evidence of changed abundance, then the region must be at least five nodes in length in order to have one significant node meeting the background proportion. Smaller regions imply that a changed node may be interpreted as a local enrichment of changed abundance in the multi-protein complex. This becomes especially relevant when the percentage of significant nodes in the network is low. The proportion of significant nodes in our ribosome test cases varied (Additional file 4). Therefore, we tuned the average region

Table 2 Tuning the walking length enables yielding region sizes needed for specific biological questions

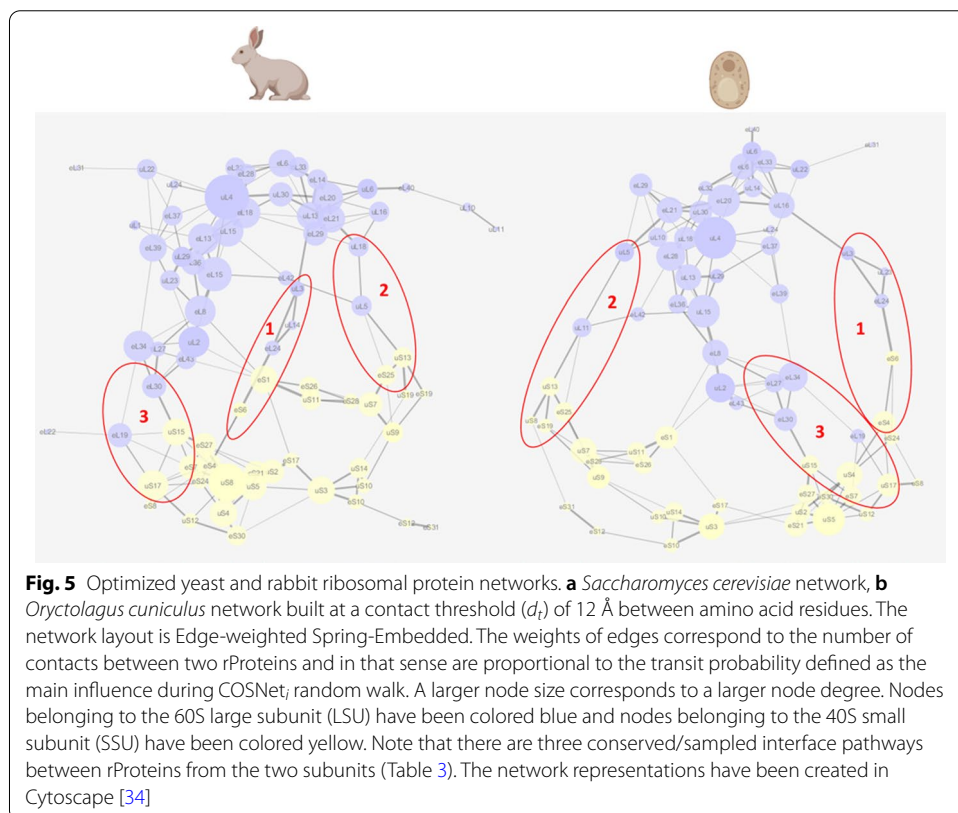
Species	Node proportion/ set	0.5	0.33	0.25	0.2	0.17	0.14	0.13	0.11	0.1
<i>Oryctolagus cuniculus</i>	77	39	26	19	15	13	11	10	9	8
Region number		8	11	12	14	15	19	17	21	21
Average region length		15	12	10	8	7	7	6	5	5
1st quartile		10	10	8	7	6	6	5	4	4
Median		17	12	9	8	7	7	7	5	5
3rd quartile		19	14	12	9	8	7	7	6	6
<i>Saccharomyces cerevisiae</i>	71	36	24	18	14	12	10	9	8	7
Region number		13	12	13	15	16	18	19	20	22
Average region length		17	13	11	9	8	7	6	6	5
1st quartile		15	11	10	8	6	6	5	4	5
Median		17	14	11	9	8	7	7	7	5
3rd quartile		18	15	13	10	8	8	7	7	6

sizes to contain at least the number of rProteins that would make a single unit equivalent to the baseline proportion of significances. This enabled us to test whether rProtein dependent ribosome specialization is locally enriched in ribosomal regions.

Building a ribosomal protein network

The consensus networks for our ribosomal test case were built with a threshold of 12 Å that allowed a coverage > 95% of the nodes corresponding to 75 and 68 nodes (proteins) in the rabbit and yeast networks, respectively. Secondly, we made sure that the region selection did not contain outlier proteins by iterating the region consensus 50 times. Finally, a random walk length equal to 0.13 times the node set was selected. This proportion achieved regions sizes that enabled us to match the baseline probability of significances for the prioritized test cases (see Testing the Spatial Constraints of Ribosome Specialization and Additional file 4) in both networks, yeast and rabbit. Subsequently, we compared the resulting optimized ribosomal networks (Fig. 5). We uncovered interconnected paths, highly or poorly interconnected rProtein neighborhoods, dense module and inter-module connective hubs, bridges between important structural features and biological details that were either conserved or different between the investigated organisms (Fig. 5).

Both networks separated into 60S LSU and 40S SSU. Subunits were connected via nodes with a high betweenness centrality and a low clustering coefficient. There were four interface paths connecting both subunits. Path number one conserved rProtein families uL3, eL24 and eS6 as the main transit nodes. In yeast, there was an additional



edge connection between eL24 and uL3 via uL23, which was replaced in the rabbit network by uL14. Path number two conserved rProtein families uL5 and uS13. The connection in yeast was bridged via uL11. Path number three conserved two connective edges, eL30-uS15 and eL19-uS17. Finally, path number four conserved the connection between uS1, and nodes eL2 and eL8. The latter had lower weights between the interconnected edges. Each subunit had highly interconnected neighborhoods that formed around hubs, i.e., nodes with high degree and high interconnectivity among neighbors (high clustering coefficient). The conserved center of the LSU and node with largest degree was uL4. The PET stemmed right from uL4 and elongated to interface path number three. Next to uL4, nodes uL30 and eL20 acted as hubs to connect other highly interconnected neighbors from the LSU. Node eL20 connected the P-Stalk structure and its surrounding area, while uL30 connected both eL20 and uL4. The conserved centers of the SSU were uS3 and uS5. Both centers connected rProtein-condensed regions. Additionally, in the rabbit network, uS8 was the SSU node with the highest degree. Node uS3 positioned in the edge path stemming towards interface path number two while uS5 toward interface path number one and three. Overall, regions in the SSU were more compact and separated from each other as compared to regions in the LSU, which were evenly interconnected impairing visual separation.

As a verification step, we assessed the extent of defined regions and their match to biologically known ribosomal features outlined in the network topologies (Table 3), which gave us a clear understanding of the constraints and potential of our method during coherent regional definitions.

The defined regions (Fig. 5) reflected the overall structural organization of ribosomes. First, there were inter-subunit connective paths, which comprised interface regions defined on three highly weighted paths in yeast and rabbit (Table 3). There was a fourth path, characterized by eS1, which had a lower relative weight of the edges that connect subunits. Thus, the eS1 inter-subunit path was not defined as a region by our method. Within the subunit mainland, LSU in both test cases contained more regions than SSU, reflecting a higher edge number between nodes. Consequently, LSU regions contained more overlaps and less unique nodes. The SSU, on the other hand, formed communities, subsetting the SSU node-set into a less overlapped set of regions. In brief, defined LSU regions were structurally related to the PET, a central region, interface-adjacent regions and a subunit top-region. The latter positioned itself besides the P-Stalk. SSU regions divided into a central hub (i.e., uS3-containing region), a bottom tail that stemmed from the central hub, a central region that contained uS5 and interface adjacent regions. The center was defined as a separate region in the rabbit network but in the yeast network was attached to the interface regions.

Subsetting structures from multi-protein complexes into regions as performed by COSNet_i is equivalent to detecting communities inside of a network. Therefore, we compared the performance of COSNet_i to pick coherent regions or communities to that of publically available algorithms. Three types of algorithms were tested. One based also on random walks, i.e., [walktrap](#), a second one based on the map equation, i.e., [Infomap](#), and, in addition, a third one based on eigenvectors, i.e., [eigenvector based models](#). The three tested algorithms (see tests details in Additional file 5 for walktrap and eigenvector models, and in *Region_selection_infomap.py* for Infomap) have a crucial conceptual difference with

Table 3 Matching of coherent regions with biologically known network topologies

Regions	rProteins	Region identifiers
Rabbit—60S rProteins		IntCryoOmics_6gz5_d_t12_IN50_WL10
Region 1	eL32 uL4 eL14 eL20 eL6 uL13 eL28 eL33	LSU-TopRegion
Region 2	eL13 eL15 eL36 uL15 uL29 uL23 eL8 uL2	LSU-Center.2
Region 10	eL13 eL31 uL22 eL39 eL37 uL29 uL4	LSU-PET.1
Region 11	uL11 eL40 uL10 uL6	LSU-P-Stalk
Region 12	eL18 uL4 eL39 uL24 eL28 uL30	LSU-PET.2
Region 17	eL20 eL21 eL29 uL30 uL18	LSU-Interface2Adjacent.1
Region 16	eL13 eL15 eL36 uL15 uL1 uL29 eL8	LSU-Center.1
Region 19	eL14 eL20 eL21 uL16 uL18	LSU-Interface2Adjacent.2
Subunit interface rProteins		
Region 5	eL13 eL15 uL5 eL42 eL21 uS13 uL18	Interface2
Region 6	uS12 eS8 eL19 uS15 uS17 uS8	Interface3.2
Region 8	eL27 eL30 eL43 uL2 eL34 uS15	Interface3.1
Region 9	uL3 eL24 eS6 uL14	Interface1
Region 18	uS12 eS8 eL19 eL22 uS17	Interface3.2
40S rProteins		
Region 3	eS24 eS4 eS30 uS2 eS21 uS4 uS5 uS8	SSU-Interface3Adjacent
Region 4	eS25 uS7 eS28 eS1 uS9 eS26 uS11	SSU-Interface1Adjacent
Region 7	uS10 eS10 uS14 uS3 eS17 uS2	SSU-CentralHub
Region 13	eS7 uS15 eS21 eS27 uS5 uS8	SSU-Center
Region 14	eS12 uS3 eS31 eS10	SSU-BottomTail
Region 15	uS7 uS19 eS19 uS13 uS9	SSU-Interface2Adjacent
Yeast—60S rProteins		IntCryoOmics_6snt_d_t12_IN50_WL9
Region 2	eL8 uL2 eL28 eL36 uL13 uL15 eL43	LSU-Interface3Adjacent.1
Region 3	eL31 uL22 eL6 eL20 eL33 uL14 uL16	LSU-TopRegion.1
Region 6	eL39 eL37 uL29 uL4 eL28 uL13 uL18	LSU-PET
Region 11	eL20 eL21 uL10 uL30 uL5	LSU-Interface2Adjacent.1
Region 12	eL6 eL20 eL40 uL14 uL16 uL6	LSU-TopRegion.1
Region 15	eL34 eL27 eL30 uL2 eL43	LSU-Interface3Adjacent.2
Region 16	eL20 eL21 uL30 eL29 uL5	LSU-Interface2Adjacent.2
Region 17	eL6 eL33 uL14 uL16 eL32	LSU-TopRegion.3
Region 18	uL24 uL30 uL4 eL28 uL13 uL18	LSU-Center
Subunit interface rProteins		
Region 1	eL19 uS12 eS7 uS17 eS8 uS5 uS15	Interface3.2
Region 4	eL21 uL11 uL5 uS13 uS7 eL42 eS25	Interface2
Region 5	eL24 eS6 uS2 uS4 eS24 eS4 eS30	Interface1
Region 8	eS7 eS21 eL27 eL30 eS27 uS5 uS15	Interface3.1
Region 13	eS6 uL23 uL3 eL24	Interface1
40S rProteins		
Region 7	uS10 eS10 uS14 uS3 eS17	SSU-CentralHub
Region 9	eS1 uS7 eS26 uS11 eS28	SSU-Interface3Adjacent
Region 10	uS8 eS19 uS13 uS7 uS9 eS25	SSU-Interface2Adjacent
Region 14	eS10 eS12 uS3 eS31	SSU-BottomTail

COSNet_i, which is that nodes may not be redundant within communities, with the consequence that community size varies considerably (Additional file 6). This feature may be more or less desirable depending upon the experimental or biological question. Walktrap finds 11 communities both in the rabbit and yeast networks, varying in size from two to

17 nodes. The eigenvector method finds eight communities both in the rabbit and yeast networks, varying in size from one to 24 nodes, and Infomap finds 11 and nine communities in the rabbit and yeast networks, respectively, varying in size from three to 17 nodes. In terms of network topology, the regions or communities match to those reported in Table 3 by conserving the same node kernels or region core, with the main difference being the number of nodes per region. As an example, the PET region (highlighted green in Additional file 6), characterized at least by nodes eL39 and eL37, varies considerably in size and composition with each algorithm even though it conserves the same node core. For rabbit, the PET regions are always consistent with COSNet_i PET 1 and 2 but also reach beyond to borrow nodes from the adjacent central LSU regions. For yeast, the PET regions are pronouncedly variable in size and reach all over the LSU adjacent regions.

Testing the spatial constraints of ribosome specialization

Multi-protein complexes such as ribosomes can undergo changes in their associated structural rProteome. Variability from a canonical rProteome composition is known as substoichiometry. Deviations that qualify as substoichiometry can relate to subtractional heterogeneity, i.e., lost rProteins [43], also to exchanged rProtein paralogs [7, 18], to differential composition of immature and mature complexes [44], among others. In our test cases, rProtein substoichiometry has been linked to specialized ribosomal roles. Thus, we used the reported significantly substoichiometric rProteins as positive (“1”) binary input in our method while the rest of the ribosomal proteome was set to negative (“0”) or not changed. The percentage of total significantly changed rProteins was 22% and 15% for the mammalian and yeast systems, respectively (Additional file 4). In mammalian ribosomes, three subcategories could be created that comprise 8% (total substoichiometric rProteins), 4% (substoichiometric rProteins in non-translational ribosomal complexes) and 3% (substoichiometric rProteins in translational ribosomal complexes). With an 8% background significance, 13 rProteins per region are needed to test significances, implying a large number of steps in the walking length. This is already at the boundary of node proportion for test sampling. Going below 8% required a random walk of more than 50% of the nodes and thus neglected the capability of our method by picking up the entire subunits as coherent regions. In the yeast test case, two subcategories could be created that comprised 7% each of background significance ([1] significantly enriched and [2] depleted). Seven percent of background significance needs defined regions of 14 rProteins in average and thus the node proportion is still acceptable. Thus, the prioritized tests (see Code Chunk 1), two for mammalian and three for yeast, avoided those that had a low background significance in the mammalian system. The test specifics: region average size (RAS), background significance (BS), walking lengths (WL) and threshold (d_t) are compiled in Code Chunk 1. The binary columns used to run the *intcryomics.py* function are reported in Additional file 4. Statistically relevant results from testing the binary files on the optimized rabbit and yeast networks (see Building a Ribosomal Protein Network) are outlined in Fig. 6.

Code chunk 1

```

## total significantly changed rProteins mammalian (WL = 13%, dt = 12, BS =
  22%, RAS = 4)
python3 Python_Modules/intcryomics.py edges_with_weights_6gz5_t12.txt Data/
  significance_file_6gz5 10 50 > IntCryOmics_6gz5_t12_WL10_BP22.txt

## total substoichiometric rProteins mammalian (WL = 33%, dt = 12, BS = 8%,
  RAS = 13)
python3 Python_Modules/intcryomics.py edges_with_weights_6gz5_t12.txt Data/
  significance_file_6gz5_SbSt 26 50 > IntCryOmics_6gz5_t12_WL26_BP8.txt

## total significantly changed rProteins yeast (WL = 13%, dt = 12, BS = 15%,
  RAS = 7)
python3 Python_Modules/intcryomics.py edges_with_weights_6snt_t12.txt Data/
  significance_file_6snt 9 50 > IntCryOmics_6snt_t12_WL9_BP15.txt

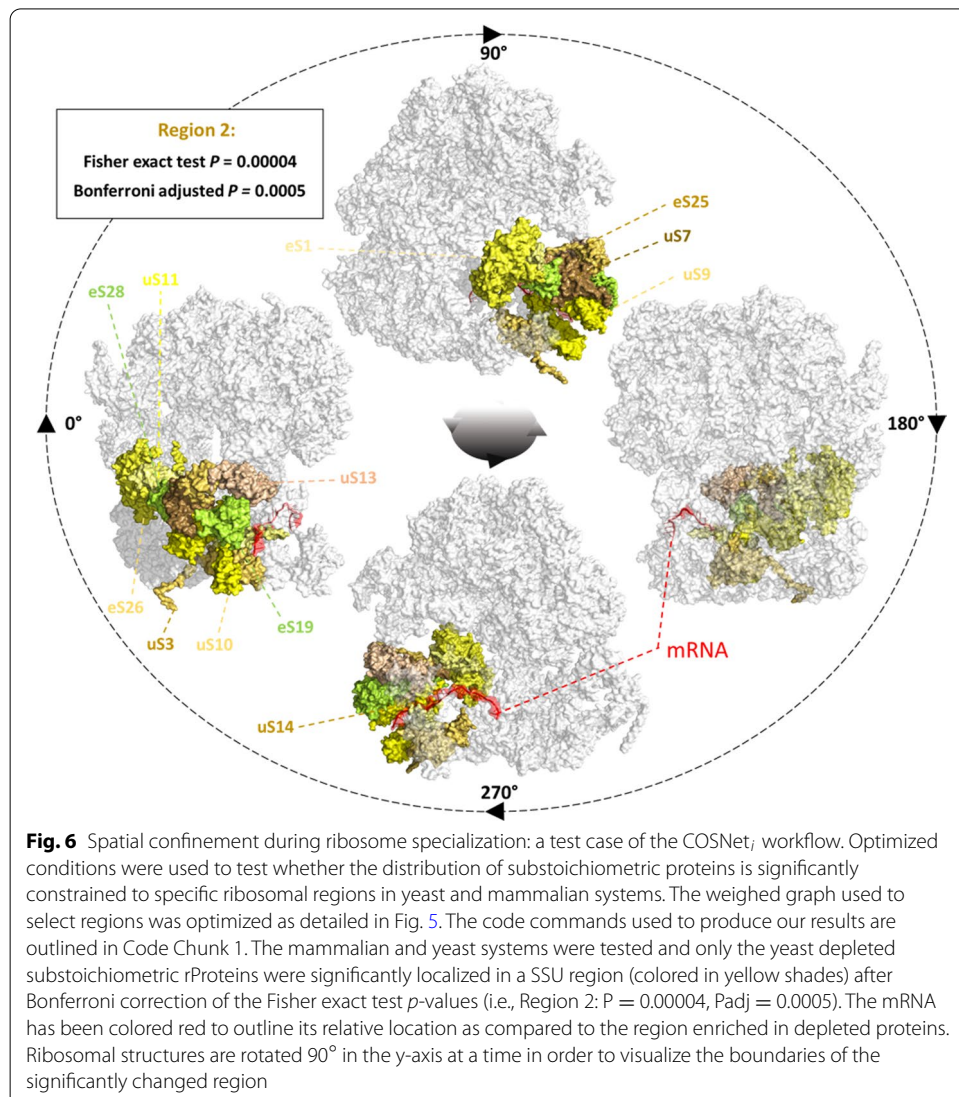
## enriched rProteins yeast (WL = 33%, dt = 12, BS = 7%, RAS = 14)
python3 Python_Modules/intcryomics.py edges_with_weights_6snt_t12.txt Data/
  significance_file_6snt_enriched 24 50 >
  IntCryOmics_6snt_t12_WL24_BP7_enr.txt

## depleted rProteins yeast (WL = 33%, dt = 12, BS = 7%, RAS = 14)
python3 Python_Modules/intcryomics.py edges_with_weights_6snt_t12.txt Data/
  significance_file_6snt_depleted 24 50 >
  IntCryOmics_6snt_t12_WL24_BP7_dep.txt

```

We found spatially constrained rProtein substoichiometry in the yeast network. More specifically, in the subcategory of depleted substoichiometric rProteins. Our results support the notion that depleted rProteins from actively translating polysomes as compared to monosomes, in glucose fed yeast growing at stationary rate, are significantly constrained to the 40S SSU region adjacent to the mRNA and tRNA entry points. The structural coherence of the resulting region is evident when multiple graph community detection algorithms are used in the yeast rProtein network (highlighted in yellow in Additional file 6). Infomap-, walktrap-, and eigenvector-based models all yielded the same 40S SSU region, namely consisting of nodes uS3, uS14, eS10, eS17, and uS10. The difference with the COSNet_i-derived regions is the lack of some significantly changed nodes, such as eS1, in the alternative algorithms, which further emphasizes the importance of COSNet_i's flexibility during region definition.

Two more regions exhibited significant *p*-values, but were no longer significant after the stringent Bonferroni correction. The regions both belonged to the yeast test case, one at the total substoichiometric category, and the other at the enriched substoichiometric category. The regions were overlapping heavily, the total constituent rProteins were: ['eL31', 'uL22', 'eL6', 'eL20', 'eL33', 'uL14', 'uL16', 'uL6', 'eL32', 'eL40'], The *p*-values went from 0.025 and 0.016 to 0.477 and 0.177 after Bonferroni correction. In the mammalian system, no significant *p*-values were obtained.



Discussion

COSNet_i contributes to the field of structural systems biology [20], where structural and system biology approaches converge to contextualize shifts in omics abundances from molecular species that belong to a multi-protein complex. COSNet_i translates multi-protein complex atomic structures into weighted graphs. Typically, these type of network analyses have been used to capture inter-residue interactions and provide structure to function insights in individual protein structures [21] [45–47]. Here, we extend the approach to study interactions between proteins that belong to multi-protein complexes. In order to avoid prior-knowledge biases during region selection, the defined interactions are a proximity probability and not inferred based on domain knowledge of the proteins that comprise the studied complex. A random walk with restart methodology is used to define structurally coherent regions as opposed to regions of biological interest defined based on known domains and accessory proteins (Example of the latter in Woolford et al. [3]). Regarding the integration to systems biology omics data, we propose a

structural contextualization that goes beyond estimating significances of protein abundance changes. An initial mapping of protein changes onto structures of complexes can already indicate whether the changed components are spatially adjacent or may have any obvious functional implications. Our goal was to devise a methodology that enables asking whether relevant protein changes are significantly confined to specific parts of a complex. The proposed approach is built under the null hypothesis that the proportion of changes between the whole complex and randomly selected regions are not different. In other words, that the significantly changed molecular species are randomly scattered across the structure. To test deviations from the background proportion of significances, COSNet_i uses the Fisher exact test [48, 49]. This test allows for the significance value of mean deviations to be calculated exactly.

Structure quality requirements

COSNet_i starts its procedure from an experimentally elucidated complex structure. The structure needs to fulfill quality parameters, especially those regarding accurate placement of the protein features. Accurate representation of the protein positions within a multi-protein complex is influenced by the cryogenic or crystallographic resolution. Atomic models can be effectively built at resolutions below to 4 Å [50–53]. Additionally, at low resolutions the models tend to overfit the data. This is a recognized problem that has been addressed in multiple ways [54]. The implication for mmCIF/PDBx files is that, when overfitted, there might not be sufficient sequence coverage for some of the proteins that are actually modelled onto the structure. In order to evaluate this, we provide users the quality assessing script *check_cif_completeness.py*. The script compares the coverage of the modeled sequences relative to the original FASTA sequence of the protein. As a working example of the ribosomal test case, the *Triticum aestivum* 80S structure can be taken, which is relatively poorly resolved as compared to the yeast and rabbit counterparts. A threshold of 12 Å does not achieve connectivity of the P-Stalk feature, while outlier proteins already appear in the defined regions (Fig. 3). Thus, a good consensus between connectivity and lack of outlier proteins or island regions seems unlikely for the wheat ribosome structure. Additionally, when the model was interrogated by *check_cif_completeness.py*, it became clear that many rProteins have a low sequence coverage in this structure (Additional file 7A and Fig. 7).

We recommend users inputting into the method the best available resolved structure for the investigated complex. Accurate protein densities will translate into a reliable weighted graph that allows structure-directed region selection. Additionally, we recommend that users make use of the *check_cif_completeness.py* in order to assess the general quality of the protein features modelled onto the initial structure densities. The preferred outcome would be modeled protein sequences that fully overlap with the FASTA sequences that are reported for those proteins, just as what we report here for the yeast and rabbit modelled rProteins (Additional file 7B and C).

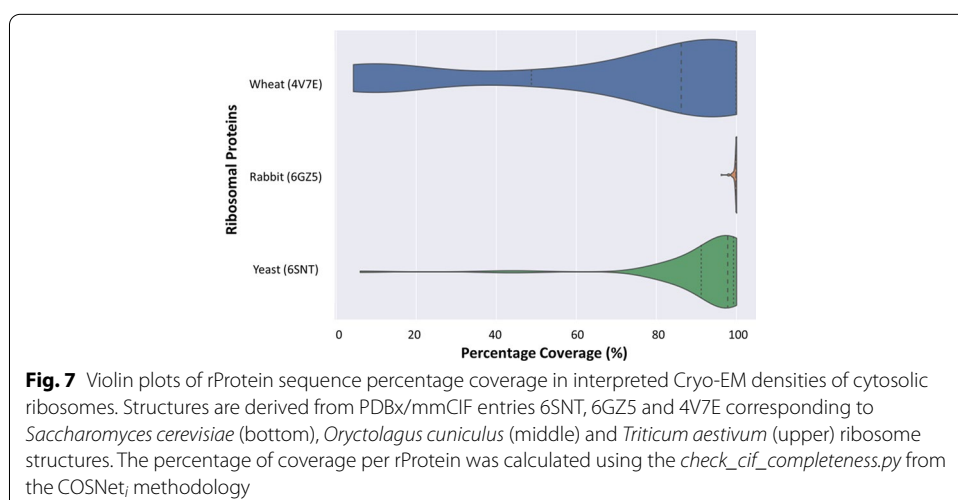
Optimization of region definition

The random walk procedure used by COSNet_i belongs to the most standard types of stochastic walks, i.e., moving through a network with a probability that equals the edge

weights [55]. COSNet_i subsets the original graph and tests properties of the subset-nodes as compared to the node set as a whole. Thus, the region selection procedure must not violate the independence assumption implicit to the proportion test [56]. The assumption is not violated because networks are based on spatial distances and not similarities or dissimilarities between empirically measured omics data. The latter produces indirect protein interaction networks that outline relationships of shared functionality and interdependence [57]. Thus, COSNet_i samples node clusters independently without any bias from shared functionality.

Defined regions are based on an adjacency matrix of protein-protein interactions calculated at a distance threshold of predefined Ångströms (Å). The distance threshold can be selected based on the quality of the resulting regions, e.g., connectivity, biological accuracy, lack of outlier node-components. Thus, a quality metric to assess the quality of defined regions is their resemblance to characterized features of the investigated complex. Additionally, users can rely on the established consensus distance of 8Å between amino acid residues within a protein structure [32] or, equally legitimate, on elucidated contacts from empirical evidence. The structure-translated graph features edges that are weighted by the percentage of contact coverage among nodes indicating a transit probability, which probabilistically guides the random-walk path trajectory. Edge weights are the single most influencing attribute in the outcome of a random walk through a weighted graph [58] and as such are the attribute that enables structural coherence in our method. This property of the edges bounds the region-definition process to the network topology [59], which ultimately depends in the original structure.

Other parameters influencing the region definition process are the walking length and the iteration number. Generally, increasing the iteration number achieves region consensus in the defined regions (Fig. 4). Regarding the walk length, in our test case we propose optimizing it according to the omics data to be tested. More specifically, since the walking length affects the region size, we aimed at an average region size that allowed for a single feature within a selected region to equal in proportion the baseline proportion of significances. In this way, we avoided overweighting a single



significance beyond its actual importance. In practice, going beyond the test case provided will allow users to vary the walk length for different inquiries. For instance, increasing the walking length implies uncovering structural features of the network [55, 60] that identify central nodes, edges or other community substructures [61] in the original network. Thus, our algorithm can be used without any omics tests in order to investigate the very nature of node communities at different scales within the entire graph.

Graph community detection algorithms [62, 63], as those used here to compare to COSNet_i, are suited for the detection of non-overlapping coherent regions. These regions or communities can be used to validate observations made with COSNet_i about the network topology. This validation in turn reveals robust topological aspects of the biological networks under study. At the same time, due to the intrinsic nature of the alternative algorithms, the selected communities tend to be largely of different sizes, so that a quasi-standardized number of nodes is unlikely to be obtained. This feature precludes their further use with COSNet_i if the background significances require a specific region size. Nevertheless, there are many experimental scenarios that are not limited by background significance. In these cases, the non-overlapping set of regions can even be used to follow up the COSNet_i algorithm. The synergy of the innovations implemented by COSNet_i and the capabilities of the existing graph community detection algorithms creates a comprehensive set of tools for studying decomposed networks from multi-protein complexes.

In our test case, it is necessary to consider the biology of ribosome specialization, in which different sub-populations of rProtein-enriched ribosomes can selectively translate transcripts [7, 10]. In this context, approximately equally-sized ribosomal regions with the right combinations of rProteins might be more relevant than analysis of strictly non-overlapping regions of highly diverse size to study the phenomenon of specialization. Therefore, continuing the COSNet_i workflow with a minimal set of overlapping regions as defined in our method would be the first choice. Additional information on ribosomal protein networks and their internal community topology may then be inferred from the comparison to regions obtained by existing graph community detection algorithms.

Ribosomal networks

RNA physically mediates many contacts in the interaction network of ribosomes [23]. Thus, the 8 Å consensus, a catch-all type of threshold under which Van der Waals, hydrogen bonding, electrostatic interactions can occur, can be increased to include those rRNA-mediated contacts as edges. A threshold of 12 Å achieves more than 95% of interconnected nodes in the yeast and rabbit networks while avoiding outlier proteins. Regarding the random walk parameters: (1) an iteration number of 50 consensus samplings avoided bias towards outlier rProteins. (2) A customized walking length to the conducted tests allowed increasing the step number until covering 33% of the node set in a single walk. The ribosomal networks represented as weighted graphs resemble the topology and relative distribution of rProteins in the actual 3D structure. This becomes clearer when the layout is deterministically defined by minimizing the weight (edge)

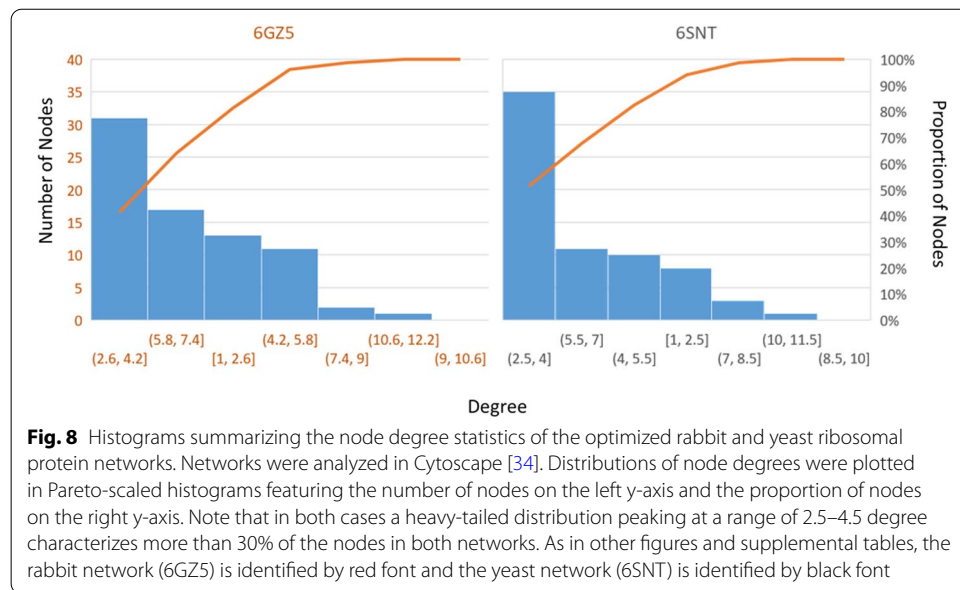
total force on the networks (Fig. 5) according to the Kamada-Kawai Algorithm [64] as applied in Cytoscape [65]. Thus, the selected thresholds become further validated.

In the two tested ribosomal networks, degree distributions are heavy-tailed and almost identical (Fig. 8). “Heavy-tailed” means that density histograms from degree distributions will reach zero later than expected by an exponential function [66]. This implies that several nodes with high degrees dominate the tail of the distribution histograms. Upon inspection, these nodes are hubs in densely packed graph subsets, and as such, could influence their surroundings rather than be affected individually by any regulatory mechanism. Hub removal could cause major disruptions to the structural stability of ribosomes, which can be aggravated by the propensity of rProteins to aggregate [67]. Promiscuous binding into aggregates occurs due to the rProtein own basic nature that enhances rRNA binding [68, 69].

The tested ribosomal networks also share interconnected paths through similar edges, i.e., influential hubs that connect modules or communities. Thus, the topology seems to be well conserved between yeast and rabbit cytosolic rProtein networks. From an evolutionary perspective, both networks should be conserved since the main rProteome acquisitions are shared [12]. An exception is that higher metazoans (except plants) share an increase of basic LSU rProtein components as compared to lower eukaryotes [14]. Importantly, in such a conserved system, COSNet_i finds equivalent regions when the parameters are tuned equally. The resulting regions contain shared rProteins, especially in the highly interconnected neighborhoods. Overlaps imply that significantly changed regions after Bonferroni correction of the initial Fisher test *p*-values do not represent a fixed, isolated region. Rather, significance might be tied to the right combination of interconnected rProteins, which could be targeted by non-random complex remodeling or de novo synthesis of components.

Spatially enriched ribosomal protein substoichiometry

Using the COSNet_i workflow, we tested previous claims of rProtein-dependent ribosome specialization in mammalian [37] and yeast [39] systems. We aimed at uncovering if the specialized complexes feature spatially enriched regions in substoichiometric proteins. We found that significantly depleted substoichiometric rProteins in yeast polysomes are spatially constrained. The interrogated polysomes correspond to four monosomes loaded into an mRNA. Thus, the substoichiometric complexes were translationally competent, and as such, an altered ribosomal region in those complexes might signal functional features that feedback on translation. Interestingly, substoichiometric rProteins were constrained to a region in the 40S SSU that lies at the tRNA exit and entry sites and is adjacent to the mRNA entry channel. This observation increases the possibility of the regulation found being a targeted response to modify translational preferences toward certain transcripts. Moreover, the same region seems to be depleted in rProteins, according to quantitative structural analyses, in yeast shifted from glucose to glycerol medium [70]. Ribosomes with depleted proteins were already visible in glucose-fed yeast, but increased when shifted to glycerol. The previous observation was made in enriched ribosomal pellets



with contributions from polysomes and monosomes. Conversely, the exemplary yeast dataset presented here accounts for substoichiometry of heavily loaded polysomes as compared to monosomes. Thus, the most likely linking explanation is that a balance between rProtein-depleted translationally competent complexes and monosomes that are not depleted from the mentioned rProteins, is necessary upon shifting yeast from glucose to glycerol as a carbon source. In order to evaluate whether the findings outlined in Sun et al. [70] are significantly constrained to the same region outlined in Fig. 6, we deliver a variation of the *intcryomics.py* function named *intcryomics_sigasign.py*, the function only needs as input an edge list, a walking length and an iteration number. The output are defined regions, which the user can then select and input which proteins are significantly changed. Finally, the Fisher test is performed, *p*-values are adjusted and the function returns as output a logical string accompanied by Bonferroni *p*-adjusted values indicating whether the input proteins are significantly constrained to the selected region. The test determined that rProteins uL16(RPL10), eS1(RPS1), uS11(RPS14A/B)) and eS26(RPS26A/B), lacking in 80S ribosomes as detailed in Sun et al. [70], are significantly constrained to the same region outlined in Fig. 6 with a Bonferroni *p*-adjusted value always below 0.005.

Different possibilities could explain significantly depleted rProteins as a functional mechanism to modulate translation: (1) rProteins that cannot be associated with actively translating ribosomes because they imply translational restrictions for some transcripts. Functional depletion of rProteins has been described as subtractional heterogeneity [43]. (2) Alternatively, rProteins could be tightly bound to other ribosome associated factors that assist mRNA recruiting (e.g., [71]). Tight interactions could cause force on rProtein links during ribosome purification, and rProteins could then be systemically lost from polysomes. (3) Another alternative is that rProteins have extra-ribosomal functions

directly or indirectly involved in mRNA recruiting (e.g., [72, 73]), for which they could be depleted from polysomes while involved in the formation of initiation complexes.

Conclusion

COSNet_i achieves a structure-directed partitioning into regions within any multi-protein complex for which a sufficiently resolved structure exists. A plant cytosolic ribosome structure is needed to increase the quality of the current rProtein network without compromising isolated regions. By contrast, the yeast and rabbit ribosomal networks could be successfully used to optimize the COSNet_i parameters. Optimization of distance threshold to call proteins to be in contact, walking length to define regions and consensus sampling iterations largely depend on the type of multi-protein complex investigated and the structure resolution. The optimization makes use of prior knowledge of the investigated complexes and is influenced by the observed number of significant abundance changes. Finally, using the COSNet_i fully optimized method, we scrutinized previous claims of specialized ribosomes. More specifically, we tested whether the rProtein-dependent claims could be traced to a specific ribosomal region being modulated. For this purpose, we used the minimal set of overlapping regions covering most rProtein nodes, as inferred by COSNet_i, instead of using non-overlapping different sized regions, as determined by existing graph community detection algorithms. The latter set of regions or communities allowed us to validate the topology of the ribosomal protein networks. We found that indeed subtractional heterogeneity is confined to the tRNA exit and entry sites in actively translating yeast polysomes. Furthermore, based on validation by three independent graph community detection algorithms, we conclude that the regulated region is structurally coherent. Thus, the constraint might signal functional features of translation, i.e., depleted spatially related structural rProteins influencing the translational status of transcripts in yeast fed with different carbon sources. Our method has been made publicly available as a GitHub repository (https://github.com/MSeidelFed/COSNet_i) and can be installed using the python package installer pip.

Availability and requirements

Project name: COSNet_i—ComplexOme-Structural Network Interpreter

Project home page: https://github.com/MSeidelFed/COSNet_i

Operating system(s): Platform independent

Programming language: Python

Other requirements: Python-3.6.5 or higher, numpy 1.18.1 or higher, biopython 1.78 or higher, os-sys 2.1.4 or higher, scipy 1.5.2 or higher, networkx 2.5 or higher, matplotlib 3.3.1 or higher.

License: BSD 2-Clause “Simplified” License.

Any restrictions to use by non-academics: None.

Abbreviations

COSNet; ComplexOme-Structural Network Interpreter; rProteome: Ribosomal Structural Proteome; rProtein: Ribosomal Protein; ES: Expansion Segments; RAS: Region Average Size; PET: Polypeptide Exit Tunnel; BS: Background Significance; WL: Walking Lengths; d; Distance Threshold; Å: Ångströms; SSU: Small Subunit; LSU: Large Subunit; CRA: Changed in Relative Abundance.

Supplementary Information

The online version contains supplementary material available at <https://doi.org/10.1186/s12859-021-04510-z>.

Additional file 1. COSNet; python module USAGE.md file for the integration of relative changes obtained by omics-technologies into Cryo-EM or crystallography based randomly sampled interaction networks of multi-protein complex structures. The module is composed of independent components, written as python scripts (found in the Modules folder), which can be run in batch with bash or python scripts (bash scripts are found in the Batch files' folder).

Additional file 2. Nodes and edges structure of ribosomal networks from mmCIF entries 6SNT, 6GZ5 and 4V7E corresponding to *Saccharomyces cerevisiae* (Column N-S), *Oryctolagus cuniculus* (Column H-M) and *Triticum aestivum* (Column B-G). Each cell corresponds to one string representing a single contact that can be separated by the space character. The first element of the string is the source node, the second element the target node, the third element the number of contacts between them (edge weights), the fourth and fifth columns are color identifiers for the nodes in the networks as outlined in Figure 3.

Additional file 3. Defined ribosomal regions at different walking lengths (WL). Optimized parameters were used, the °Angström threshold was 12, and the iteration number of the consensus sampling was 50 iterations. Tab A contains regions derived from the 6SNT yeast ribosome structure. Tab B contains regions derived from the 6GZ5 rabbit ribosome structure. Both tabs contain the selected regions at varying walking lengths, from which Table 2 was built.

Additional file 4. Baseline proportions for statistical testing of spatial enrichment in ribosome multiprotein complexes test case. (Columns F-H) Mammalian binary input necessary for `intcryomics.py` featuring changed rProtein paralogs with 1 and non-changed with 0. (Columns K-N) Yeast binary input necessary for `intcryomics.py` featuring changed rProtein paralogs with 1 and non-changed with 0. Non-tested cases are signaled with grey font. Prioritized and tested case are signaled with black font.

Additional file 5. Community Detection within Graphs. R implementation of walktrap and eigenvector based models algorithms.

Additional file 6. Modules or communities found in optimized ribosomal networks from mmCIF entries 6SNT and 6GZ5 corresponding to *Saccharomyces cerevisiae* (Column H-M) and *Oryctolagus cuniculus* (Column B-G). Three different contrasting algorithms were used to find communities across optimized ribosomal protein graphs. Namely, Infomap, walktrap and eigenvector based models. The resulting regions were then used to compare to those obtained from the COSNet; procedure as outlined in Table 3. Green highlights the exemplary PET region as was picked out by each algorithm.

Additional file 7. Percentage of sequence coverage modelled into the exemplary mmCIF/PDBx structures used to optimize the COSNet; workflow. (A) The yeast (*Saccharomyces cerevisiae* PDB ID: 6snt), (B) rabbit (*Oryctolagus cuniculus* PDB ID: 6GZ5) and (C) plant (*Triticum aestivum* PDB ID: 4v7e) ribosomal complexes. The assessment can be replicated in any structure using the python function `check_cif_completeness.py` as documented in (https://github.com/MSeidelFed/COSNet_i).

Acknowledgements

We acknowledge the long-standing support by Prof. Dr. L. Willmitzer, Prof. Dr. M. Stitt, and Prof. Dr. R. Bock (Max-Planck Institute of Molecular Plant Physiology, Potsdam, Germany). FMS would like to acknowledge the Max-Planck Society (Max Planck Institute of Molecular Plant Physiology) and The University of Melbourne for funding his research via the Melbourne-Potsdam PhD Programme (MelPoPP). YH would like to acknowledge and thank Prof. Dr. Aalt-Jan van Dijk (Wageningen University and Research) for his supervision and support in this work.

Authors' contributions

FM-S and YH contributed in literature research, Python-scripting for development of ribosomal structural analyses, statistics, implementation of the method and structural analysis. conceptualization, manuscript writing and shaping and interpretation of results. DW and JK contributed to the development of ribosomal structural analyses and related statistics, conceptualization, manuscript writing and shaping and interpretation of results. AAPF contributed in interpretation of results, figures shaping, manuscript formatting, and manuscript writing. All authors have read and approved the manuscript.

Funding

Open Access funding enabled and organized by Projekt DEAL. FMS would like to acknowledge the Max-Planck Society (Max Planck Institute of Molecular Plant Physiology) and the University of Melbourne for funding his research via the Melbourne-Potsdam PhD Programme (MelPoPP). YH would like to acknowledge the Max-Planck Society (MPIMP) and UiT The Arctic University of Norway for funding her work. All authors would like to acknowledge the Max-Planck Society (Max Planck Institute of Molecular Plant Physiology). The funders played no role in the collection, analysis, interpretation of data or in the writing of the manuscript.

Availability of data and materials

The datasets generated and/or analysed during the current study are available in the **COSNet_i** repository, https://github.com/MSeidelFed/COSNet_i/tree/master/Data. Additionally, the datasets supporting the conclusions of this article are included within the article (and its additional files).

Declarations

Competing interests

The authors declare that they have no competing interests.

Author details

¹Willmitzer Department, Max-Planck-Institute of Molecular Plant Physiology, 14476 Potsdam-Golm, Germany. ²School of BioSciences, University of Melbourne, Parkville, VC 3010, Australia. ³Institute for Arctic and Marine Biology, UiT Arctic University of Norway, 9037 Tromsø, Norway.

Received: 1 May 2021 Accepted: 1 December 2021

Published online: 20 December 2021

References

1. Reuveni S, Ehrenberg M, Paulsson J. Ribosomes are optimized for autocatalytic production. *Nature*. 2017;547:293–7.
2. Baßler J, Hurt E. Eukaryotic ribosome assembly. *Annu Rev Biochem*. 2019;88:281–306.
3. Woolford JL, Baserga SJ. Ribosome biogenesis in the yeast *Saccharomyces cerevisiae*. *Genetics*. 2013;195:643–81.
4. Sáez-Vásquez J, Delseny M. Ribosome biogenesis in plants: from functional 45S ribosomal DNA organization to ribosome assembly factors. *Plant Cell*. 2019;31:1945–67.
5. Emmott E, Jovanovic M, Slavov N. Ribosome stoichiometry: from form to function. *Trends Biochem Sci*. 2019;44:95–109.
6. Simsek D, Tiu GC, Flynn RA, Byeon GW, Leppek K, Xu AF. The Mammalian Ribo-interactome reveals ribosome functional diversity and heterogeneity. *Cell*. 2017;169:1051–65.
7. Martinez-Seidel F, Beine-Golovchuk O, Hsieh YC, Kopka J. Systematic review of plant ribosome heterogeneity and specialization. *Front Plant Sci*. 2020;11:948.
8. Martinez-Seidel F, Suwanchaikasem P, Nie S, Leeming MG, Pereira Firmino AA, Williamson NA, et al. Membrane-Enriched Proteomics Link Ribosome Accumulation and Proteome Reprogramming With Cold Acclimation in Barley Root Meristems. *Front Plant Sci*. 2021;12:656683.
9. Norris K, Hopes T, Aspden JL. Ribosome heterogeneity and specialization in development. *Wiley Interdiscip Rev RNA*. 2021;12:e1644.
10. Genuth NR, Barna M. The discovery of ribosome heterogeneity and its implications for gene regulation and organismal life. *Mol Cell*. 2018;71:364–74.
11. Bernier CR, Petrov AS, Kovacs NA, Penev PI, Williams LD. The universal structural core of life. *Mol Biol Evol*. 2018;35:2065–76.
12. Bowman JC, Petrov AS, Frenkel-Pinter M, Penev PI, Williams LD. Root of the tree: the significance, evolution, and origins of the ribosome. *Chem Rev*. 2020;120:4848–78.
13. Parker MS, Sah R, Balasubramaniam A, Sallee FR, Park EA, Parker SL. On the expansion of ribosomal proteins and RNAs in eukaryotes. *Amino Acids*. 2014;46:1589–604.
14. Parker MS, Balasubramaniam A, Parker SL. On the segregation of protein ionic residues by charge type. *Amino Acids*. 2012;43:2231–47.
15. Melnikov S, Manakongtreecheep K, Söll D. Revising the structural diversity of ribosomal proteins across the three domains of life. *Mol Biol Evol*. 2018;35:1588–98.
16. Evangelisti AM, Conant GC. Nonrandom survival of gene conversions among yeast ribosomal proteins duplicated through genome doubling. *Genome Biol Evol*. 2010;2:826–34.
17. Petibon C, Parenteau J, Catala M, Elela SA. Introns regulate the production of ribosomal proteins by modulating splicing of duplicated ribosomal protein genes. *Nucleic Acids Res*. 2016;44:3878–91.
18. Gerst JE. Pimp my ribosome: ribosomal protein paralogs specify translational control. *Trends Genet*. 2018;34:832–45.
19. Segev N, Gerst JE. Specialized ribosomes and specific ribosomal protein paralogs control translation of mitochondrial proteins. *J Cell Biol*. 2018;217:117–26.
20. Chasapis CT. Building bridges between structural and network-based systems biology. *Mol Biotechnol*. 2019;61:221–9.
21. Chakrabarty B, NAPS PN. Network analysis of protein structures. *Nucleic Acids Res*. 2016;44:W375–82.
22. Brandes U. Network analysis: methodological foundations. New York: Springer; 2005.
23. Ben-Shem A, De Loubresse NG, Melnikov S, Jenner L, Yusupova G, Yusupov M. The structure of the eukaryotic ribosome at 3.0 Å resolution. *Science*. 2011;334(1524–9):80.
24. Brandes U, Dellling D, Gaertler M, Görke R, Hoefler M, Nikoloski Z. On modularity clustering. *IEEE Trans Knowl Data Eng*. 2008;20:172–88.
25. Coppersmith D, Doyle P, Raghavan P, Snir M. Random walks on weighted graphs and applications to on-line algorithms. *J ACM*. 1993;40:421–53.
26. Rosvall M, Bergstrom CT. Maps of random walks on complex networks reveal community structure. *Proc Natl Acad Sci USA*. 2008;105:1118–23.
27. Pons P, Latapy M. Computing communities in large networks using random walks. *J Graph Algorithms Appl*. 2006;10:191–218.

28. Durek P, Walther D. The integrated analysis of metabolic and protein interaction networks reveals novel molecular organizing principles. *BMC Syst Biol.* 2008;2:1–20.
29. Komili S, Farny NG, Roth FP, Silver PA. Functional specificity among ribosomal proteins regulates gene expression. *Cell.* 2007;131:557–71.
30. Altschul SF, Gish W, Miller W, Myers EW, Lipman DJ. Basic local alignment search tool. *J Mol Biol.* 1990;215:403–10.
31. Ban N, Beckmann R, Cate JHD, Dinman JD, Dragon F, Ellis S. A new system for naming ribosomal proteins. *Curr Opin Struct Biol.* 2014;24:165–9.
32. Ezkurdia L, Grana O, Izarzugaza JMG, Tress ML. Assessment of domain boundary predictions and the prediction of intramolecular contacts in CASP8. *Proteins Struct Funct Bioinform.* 2009;9:196–209.
33. Csardi G, Nepusz T. The igraph software package for complex network research. *Int J Complex Syst.* 2006;25:1–9.
34. Shannon P, Markiel A, Ozier O, Baliga NS, Wang JT, Ramage D. Cytoscape: a software environment for integrated models of biomolecular interaction networks. *Genome Res.* 2003;13:2498–504.
35. Jones E, Oliphant T, Peterson P. SciPy org O. SciPy: Open source scientific tools for Python2; 2001. <https://www.scipy.org>.
36. Bland JM, Altman DG. Multiple significance tests: the Bonferroni method. *BMJ.* 1995;310:170.
37. Shi Z, Fujii K, Kovary KM, Genuth NR, Röst HL, Teruel MN. Heterogeneous ribosomes preferentially translate distinct subpools of mRNAs genome-wide. *Mol Cell.* 2017;67:71–83.
38. Perry RP. The architecture of mammalian ribosomal protein promoters. *BMC Evol Biol.* 2005;5:1–16.
39. Slavov N, Semrau S, Airolidi E, Budnik B, Oudenaarden A. Differential stoichiometry among core ribosomal proteins. *Cell Rep.* 2015;13:865–73.
40. Barakat A, Szick-Miranda K, Chang IF, Guyot R, Blanc G, Cooke R. The organization of cytoplasmic ribosomal protein genes in the Arabidopsis genome. *Plant Physiol.* 2001;127:398–415.
41. Moin M, Bakshi A, Saha A, Dutta M, Madhav SM, Kirti PB. Rice ribosomal protein large subunit genes and their spatio-temporal and stress regulation. *Front Plant Sci.* 2016;7:1284.
42. Martinez-Seidel F, Beine-Golovchuk O, Hsieh YC, Eshraky KE, Gorka M, Cheong BE, et al. Spatially enriched paralog rearrangements argue functionally diverse ribosomes arise during cold acclimation in Arabidopsis. *Int J Mol Sci.* 2021;22:6160.
43. Briggs JW, Dinman JD. Subtractional heterogeneity: a crucial step toward defining specialized ribosomes. *Mol Cell.* 2017;67:3–4.
44. Cheong BE, Beine-Golovchuk O, Gorka M, Ho WWH, Martinez-Seidel F, Firmino AAP. Arabidopsis REI-LIKE proteins activate ribosome biogenesis during cold acclimation. *Sci Rep.* 2021;11:1–25.
45. Di Paola L, De Ruvo M, Paci P, Santoni D, Giuliani A. Protein contact networks: an emerging paradigm in chemistry. *Chem Rev.* 2013;113:1598–613.
46. Grewal R, Roy S. Modeling proteins as residue interaction networks. *Protein Pept Lett.* 2015;22:923–33.
47. Greene LH. Protein structure networks. *Brief Funct Genom.* 2012;11:469–78.
48. Lury DA, Fisher RA. Statistical methods for research workers. Edinburgh: Oliver and Boyd; 1972.
49. Yates F, Fisher R. Statistical methods for research workers. Edinburgh: Oliver and Boyd; 1971.
50. Zhang X, Settembre E, Xu C, Dormitzer PR, Bellamy R, Harrison SC. Near-atomic resolution using electron cryomicroscopy and single-particle reconstruction. *Proc Natl Acad Sci USA.* 2008;105:25.
51. Yu X, Jin L, Zhou ZH. 3.88 Å structure of cytoplasmic polyhedrosis virus by cryo-electron microscopy. *Nature.* 2008;453:415–9.
52. Jiang W, Baker ML, Jakana J, Weigele PR, King J, Chiu W. Backbone structure of the infectious 15 virus capsid revealed by electron cryomicroscopy. *Nature.* 2008;451:1130–4.
53. Jiang W, Tang L. Atomic cryo-EM structures of viruses. *Curr Opin Struct Biol.* 2017;46:122–9.
54. Scheres SHW, Chen S. Prevention of overfitting in cryo-EM structure determination. *Nat Methods.* 2012;9:853–4.
55. Masuda N, Porter MA, Lambiotte R. Random walks and diffusion on networks. *Phys Rep.* 2017;717:1–58.
56. Fisher RA. On the interpretation of X² from contingency tables, and the calculation of P. *J R Stat Soc.* 1922;85:87.
57. Szklarczyk D, Franceschini A, Wyder S, Forslund K, Heller D, Huerta-Cepas J. STRING v10: protein-protein interaction networks, integrated over the tree of life. *Nucleic Acids Res.* 2015;43:D447–52.
58. Zhang Z, Shan T, Chen G. Random walks on weighted networks. *Phys Rev E Stat Nonlinear Soft Matter Phys.* 2013;87:012112.
59. Noh JD, Rieger H. Random walks on complex networks. *Phys Rev Lett.* 2004;92:118701.
60. Newman M. *Networks: An Introduction.* Oxford University Press; 2010.
61. Jeub LGS, Balachandran P, Porter MA, Mucha PJ, Mahoney MW. Think locally, act locally: Detection of small, medium-sized, and large communities in large networks. *Phys Rev E Stat Nonlinear Soft Matter Phys.* 2015;91:012821.
62. Csardi G, Nepusz T. The igraph software package for complex network research. *Int J Complex Syst.* 2006;25:1695.
63. Farage C, Edler D, Eklof A, Rosvall M, Pilosof S. Identifying flow modules in ecological networks using Infomap. *Methods Ecol Evol.* 2021;12:854.
64. Kamada T, Kawai S. An algorithm for drawing general undirected graphs. *Inf Process Lett.* 1989;31:7–15.
65. Baryshnikova A. Exploratory analysis of biological networks through visualization, clustering, and functional annotation in Cytoscape. *Cold Spring Harb Protoc.* 2016;2016:541–8.
66. Bryson MC. Heavy-tailed distributions: properties and tests. *Technometrics.* 1974;16:61–8.
67. Koplin A, Preissler S, Llina Y, Koch M, Scior A, Erhardt M. A dual function for chaperones SSB-RAC and the NAC nascent polypeptide-associated complex on ribosomes. *J Cell Biol.* 2010;189:57–68.
68. Jakel S. Importins fulfil a dual function as nuclear import receptors and cytoplasmic chaperones for exposed basic domains. *EMBO J.* 2002;21:377–86.
69. Christie M, Chang CW, Róna G, Smith KM, Stewart AG, Takeda AAS. Structural biology and regulation of protein import into the nucleus. *J Mol Biol.* 2016;428:2060–90.
70. Sun M, Shen B, Li W, Samir P, Browne CM, Link AJ. A time-resolved Cryo-EM study of *Saccharomyces cerevisiae* 80S ribosome protein composition in response to a change in carbon source. *Proteomics.* 2021;21:2000125.

71. Philipp D, Andrea B, DT SN. RGG-proteins are translational regulators during stress response and cell proliferation. In: 11th tri-national Arabidopsis meeting; 2019. p. 64.
72. Jha S, Rollins MG, Fuchs G, Procter DJ, Hall EA, Cozzolino K. Trans-kingdom mimicry underlies ribosome customization by a poxvirus kinase. *Nature*. 2017;546:651–5.
73. Inglis AJ, Masson GR, Shao S, Perisic O, McLaughlin SH, Hegde RS. Activation of GCN2 by the ribosomal P-stalk. *Proc Natl Acad Sci USA*. 2019;116:25.
74. Chen H, Boutros PC. VennDiagram: a package for the generation of highly-customizable Venn and Euler diagrams in R. *BMC Bioinform*. 2011;12:1–7.
75. R Development Core Team 3.0.1. A Language and Environment for Statistical Computing. R Found Stat Comput. 2013;2. <http://www.r-project.org>.

Publisher's Note

Springer Nature remains neutral with regard to jurisdictional claims in published maps and institutional affiliations.

Ready to submit your research? Choose BMC and benefit from:

- fast, convenient online submission
- thorough peer review by experienced researchers in your field
- rapid publication on acceptance
- support for research data, including large and complex data types
- gold Open Access which fosters wider collaboration and increased citations
- maximum visibility for your research: over 100M website views per year

At BMC, research is always in progress.

Learn more biomedcentral.com/submissions



Chapter 6

Spatially Enriched Paralog

Rearrangements Argue

Functionally Diverse Ribosomes

Arise during Cold Acclimation in

Arabidopsis



Article

Spatially Enriched Paralog Rearrangements Argue Functionally Diverse Ribosomes Arise during Cold Acclimation in Arabidopsis

Federico Martinez-Seidel ^{1,2,*}, Olga Beine-Golovchuk ^{1,3}, Yin-Chen Hsieh ^{1,4}, Kheloud El Eshraky ¹, Michal Gorka ¹, Bo-Eng Cheong ^{1,2,5}, Erika V. Jimenez-Posada ^{6,7}, Dirk Walther ¹, Aleksandra Skirycz ¹, Ute Roessner ², Joachim Kopka ¹ and Alexandre Augusto Pereira Firmino ¹

- ¹ Willmitzer Department, Max-Planck-Institute of Molecular Plant Physiology, 14476 Potsdam-Golm, Germany; olga.beine@bzh.uni-heidelberg.de (O.B.-G.); hsieh.y.chen@uit.no (Y.-C.H.); eshraky@mpimp-golm.mpg.de (K.E.E.); michal.gorka@celonpharma.com (M.G.); becheong@ums.edu.my (B.-E.C.); walther@mpimp-golm.mpg.de (D.W.); skirycz@mpimp-golm.mpg.de (A.S.); kopka@mpimp-golm.mpg.de (J.K.); firmino@mpimp-golm.mpg.de (A.A.P.F.)
- ² School of BioSciences, University of Melbourne, Parkville, VIC 3010, Australia; u.roessner@unimelb.edu.au
- ³ Heidelberg University, Biochemie-Zentrum, Nuclear Pore Complex and Ribosome Assembly, 69120 Heidelberg, Germany
- ⁴ Institute for Arctic and Marine Biology, UiT Arctic University of Norway, 9037 Tromsø, Norway
- ⁵ Biotechnology Research Institute, Universiti Malaysia Sabah, Jalan UMS, 88400 Kota Kinabalu, Malaysia
- ⁶ Grupo de Biotecnología-Productos Naturales, Universidad Tecnológica de Pereira, Pereira 660003, Colombia; evjimenez@utp.edu.co
- ⁷ Emerging Infectious Diseases and Tropical Medicine Research Group—Sci-Help, Pereira 660009, Colombia
- * Correspondence: mseidel@mpimp-golm.mpg.de; Tel.: +49-331-567-8210
- † These authors contributed equally to this work.



Citation: Martinez-Seidel, F.; Beine-Golovchuk, O.; Hsieh, Y.-C.; Eshraky, K.E.; Gorka, M.; Cheong, B.-E.; Jimenez-Posada, E.V.; Walther, D.; Skirycz, A.; Roessner, U.; et al. Spatially Enriched Paralog Rearrangements Argue Functionally Diverse Ribosomes Arise during Cold Acclimation in Arabidopsis. *Int. J. Mol. Sci.* **2021**, *22*, 6160. <https://doi.org/10.3390/ijms22116160>

Academic Editor: Lasse Lindahl

Received: 30 April 2021

Accepted: 1 June 2021

Published: 7 June 2021

Publisher's Note: MDPI stays neutral with regard to jurisdictional claims in published maps and institutional affiliations.



Copyright: © 2021 by the authors. Licensee MDPI, Basel, Switzerland. This article is an open access article distributed under the terms and conditions of the Creative Commons Attribution (CC BY) license (<https://creativecommons.org/licenses/by/4.0/>).

Abstract: Ribosome biogenesis is essential for plants to successfully acclimate to low temperature. Without dedicated steps supervising the 60S large subunits (LSUs) maturation in the cytosol, e.g., Rei-like (REIL) factors, plants fail to accumulate dry weight and fail to grow at suboptimal low temperatures. Around REIL, the final 60S cytosolic maturation steps include proofreading and assembly of functional ribosomal centers such as the polypeptide exit tunnel and the P-Stalk, respectively. In consequence, these ribosomal substructures and their assembly, especially during low temperatures, might be changed and provoke the need for dedicated quality controls. To test this, we blocked ribosome maturation during cold acclimation using two independent *reil* double mutant genotypes and tested changes in their ribosomal proteomes. Additionally, we normalized our mutant datasets using as a blank the cold responsiveness of a wild-type Arabidopsis genotype. This allowed us to neglect any *reil*-specific effects that may happen due to the presence or absence of the factor during LSU cytosolic maturation, thus allowing us to test for cold-induced changes that happen in the early nucleolar biogenesis. As a result, we report that cold acclimation triggers a reprogramming in the structural ribosomal proteome. The reprogramming alters the abundance of specific RP families and/or paralogs in non-translational LSU and translational polysome fractions, a phenomenon known as substoichiometry. Next, we tested whether the cold-substoichiometry was spatially confined to specific regions of the complex. In terms of RP proteoforms, we report that remodeling of ribosomes after a cold stimulus is significantly constrained to the polypeptide exit tunnel (PET), i.e., REIL factor binding and functional site. In terms of RP transcripts, cold acclimation induces changes in RP families or paralogs that are significantly constrained to the P-Stalk and the ribosomal head. The three modulated substructures represent possible targets of mechanisms that may constrain translation by controlled ribosome heterogeneity. We propose that non-random ribosome heterogeneity controlled by specialized biogenesis mechanisms may contribute to a preferential or ultimately even rigorous selection of transcripts needed for rapid proteome shifts and successful acclimation.

Keywords: functional heterogeneity; paralog subfunctionalization; remodeling; ribosomal code; ribosome-associated proteins; ribosome biogenesis; stress-specialized ribosomes; substoichiometry

1. Introduction

Due to the sequential nature of ribosome biogenesis, groups of ribosome-associated proteins (RAPs), including structural ribosomal proteins (RPs), are transiently or permanently mounted into the pre-ribosomal complexes [1–3]. Transiently binding RAPs include ribosome biogenesis factors (RBFs), which monitor and assist assembly, processing, and maturation of ribosomes. Permanently binding proteins include RPs, which are part of mature translationally competent ribosomes. RPs are encoded by several paralogs in plants [4], thus compared to other eukaryotes, the ribosomal proteome of plants is highly diverse [5]. The high number of RP paralogs creates a combinatorial explosion of theoretically possible heterogeneous ribosomes. What may be seen as random and likely redundant paralog heterogeneity might have been directed towards functional divergence in the course of plant evolution, by paralog sub- and/or neofunctionalization [6,7]. Differential use of RPs or paralogs to build specialized ribosomes requires the complexes to be newly synthesized or remodeled after an environmental stimulus. *De novo* synthesized ribosomes with altered paralog compositions first appear in non-translational complexes, i.e., free 40S (SSU) and 60S (LSU) subunit fractions, before these are assembled into translating monosomes and polysomes. Subunits are assembled during the early nucleolar biogenesis steps where different factors catalyze defined steps in a highly ordered assembly line. Groups of RPs are mounted in concert following systematic directives. Thus, stress cues that compromise specific biogenesis steps may trigger regional rearrangements in spatially adjacent RP groups. Additionally, even though the assembly of RPs or individual paralogs into ribosome complexes may depend purely on the relative abundance of available, not yet assembled proteins at the assembly sites, structural constraints may exist that prefer concerted mounting of combinations of RPs or individual paralogs that are structurally or functionally adjusted to each other. These two possibilities imply that upon external stimuli groups of RPs may be jointly modulated and constitute an altered spatial region of the ribosome with a defined function. Thus, stress-remodeled ribosomal fractions are likely to be substoichiometric [8] compared to canonical RP compositions. A substoichiometric stress-specific ribosome population may carry structural features that influence the translational status of transcripts to achieve selective translation and rapid proteome shifts, a concept termed the ribosomal code [9–11].

Already in simpler eukaryotic ribosomal proteomes, as compared to that of plants, selective translation can be achieved by differential use of RPs or RP paralogs [12,13]. In fact, however, eukaryotes select transcripts for translation through several distinct mechanisms [14,15]. These mechanisms usually rely on either transcript features, altered ribosome structures, and/or RAPs. In plants, for example, there are global translational responses to abiotic and biotic stresses that imply differential association of transcripts with ribosomes [16–18]. A prominent example is heat stress, which causes extensive repression of mRNA translation in both *Oryza sativa* and *Arabidopsis thaliana* [19,20]. Besides global regulatory mechanisms, there are targeted translation constraints triggered by exogenous stimuli. A first class of targeted mechanisms relies on transcript features. For instance, plants undergoing oxygen deprivation favor translation of mRNAs that have low GC content in their 5' UTR [21–23]. Conversely, transcripts with GC rich 5' UTRs are translationally repressed during dark and hypoxia conditions [24]. Transcripts with a cis-element, TAGGGTTT, in their 5' UTR feature longer half-lives and shorter cDNAs, which correlate with increased translation rates in *Arabidopsis* [25]. A second class of targeted mechanism relies on altered ribosome structures to impose translational controls. For example, altered RP compositions endow ribosomes with selectivity towards sub-pools of mRNAs in mammalian cells [12]. The selectivity is partly achieved by recognition of transcript IRES- elements (i.e., internal ribosome entry sites) that influence translation initiation in a cap-independent manner. In *Caenorhabditis elegans*, methylation of an 18S rRNA adenosine enhances selective binding and translation of mRNA subsets [26]. In humans, poxviruses are able to remodel the host ribosome by phosphorylation of a plant-like charged RACK1 loop, mimicking a plant-like state that favors translation of viral RNA [27]. Finally, a third

class of targeted mechanisms actually relies on transient ribosome-associated factors to achieve selective translation. For instance, the yeast homolog of RACK1, ASC1, promotes efficient translation of short mRNAs [28]. mRNAs that are translationally favored by RACK1 preferentially associate with the initiation complex composed of eIF4E, eIF4G, and Pab1 [28]. Similarly, in plants, the phosphorylation event of eukaryotic initiation factor 2 α by GCN2 mediates cadmium stress and confers selection capabilities for translated transcripts [29]. Non-canonical RAPs such as kinases can even connect translation to diverse cellular processes [30]. RAP-mediated selective translation generally involves the modification of RPs, which, when linked to specialized TIFs [31], serves the purpose of shaping the translated proteome. Evidently, heterogeneity of the ribosome structure alone does not suffice to enable a ribosomal code. Rather, interactions between transcript recruiting mechanisms, specialized ribosomal populations, and associated ribosomal factors must be considered.

The struggle of plants to cope with cold acclimation is especially critical due to their sessile habit and has emerged as an exemplary case where many of the mentioned translational mechanisms appear to act independently or synergistically to achieve successful acclimation [32,33]. At the onset of cold acclimation, plants halt growth for a quiescent period of ~7 days, during which a global reprogramming of the transcriptome occurs [34]. The reprogramming is concomitant to transcript splicing [35], ribosome and spliceosome component accumulation, and proteome shifts [36]. At the transcriptome level, genes that have been termed as “early” and “late cold responsive” peak in altered expression levels at 2 and 12 h after the initial stimulus [37]. These responsive categories include protein coding genes from the cytosolic ribosomal proteome, which appear to retain their altered expression patterns beyond the initial 24 h of acclimation [34,38]. In our current study, we used the same cold stress treatments previously characterized to trigger a classical plant cold response [34,39] in order to delve into the more specific aspect of translational reprogramming. Consequently, we report that structural RP coding genes peak in altered expression at the end of the quiescent period (~7 d), whereas biogenesis and other ribosome-associated factors peak in altered expression patterns within the first day of acclimation. Thus, triggering an early ribosome biogenesis cold response may be extremely important and induce a later transcriptional response in RPs. In agreement with the indispensability of cold-induced ribosome assembly, RBFs such as REIL proteins are essential to activate biogenesis only during cold in both yeast and in Arabidopsis [34,38–43]. These temperature-specialized proteins mediate the final LSU subunit maturation events in the cytoplasm, which happen concomitantly with the polypeptide exit tunnel (PET) quality control and the P-Stalk assembly [44,45]. PET assembly occurs much earlier in the nucleolus when pre-ribosomal particles are slowly processed and crafted [46]. Thus, disrupting PET assembly in the early biogenesis steps might cause a debilitated tunnel structure [47] and cause the need for a dedicated proof reading step catalyzed by REIL later on in the cytoplasm. After testing this example, we propose that plant ribosome heterogeneity is non-random and is likely controlled by specialized mechanisms during biogenesis that preferentially assemble groups of RPs or RP paralogs in a concerted process. This creates structurally diversified ribosome subpopulations. Specialized functions of these ribosome subpopulations may be executed and assisted by respective specialized RAPs that target all ribosome functions from translation initiation and elongation to termination.

In our current study, we investigate whether suboptimal low temperatures induce protein-heterogeneity in ribosomal complexes, and test whether the induced changes are confined to specific regions of the ribosome structure. To do that, we conjugated three independent genotypes to produce a proteomic dataset that statistically excluded any induced changes that happen to LSU ribosomal particles after the cytosolic maturation steps. We achieved that by using two independent double knock out mutants of the REIL alleles in conjunction with the Arabidopsis wild type Col-0. Then in order to identify cold-specific effects on the ribosomal proteome, we analyzed altered transcript levels and RP abundances after sucrose density sedimentation. Our analyses center on free

LSU fractions since REIL genotypes allowed us to block their maturation during cold. We then explored co-localization of temperature-responsive RPs and paralogs within the ribosome body and found changed ribosomal regions of spatially related RPs. These RPs constitute significantly modulated regions whose entities feature transcripts or proteoforms that are differentially accumulated during cold. We discuss potential functions of the altered ribosome substructures at the onset of cold acclimation taking into account concomitant cold changes. In summary, our work provides evidence of stress-inducible and spatially constrained heterogeneity arising in plant ribosomes that is likely non-random and therefore functional.

2. Results

Plant roots contain three types of ribosomes: mitochondrial, plastid, and cytoplasmic. Chloroplasts are largely absent from roots, but non-green plastids are present. These plastids are required for root function [48] but generally do not perform photosynthesis and are present in lower amounts than leaf chloroplasts. Thus, ribosome preparations of root tissue allowed us to obtain larger relative amounts of cytosolic ribosomes than preparations from similar amounts of shoots. Hydroponic cultures, as those described in Firmino et al., 2020 [49] and Erban et al., 2020 [50], allowed rapid harvesting of root tissue with minimal perturbations. Hydroponic glass pots for *Arabidopsis* are small, making them optimal for highly replicated use within growth chambers set to varied environmental conditions, such as different temperature regimes.

Conventional plant cold stress experiments are performed at 4 °C, e.g., Ashraf and Rahman, 2019 [51]. The first and direct target of cold stress is the shoot, with root cold stress being more complex in terms of variables. The soil buffers temperature changes and causes a top-to-deeper soil temperature gradient, which typically increases with soil depth [52]. Hence, the soil delays corresponding temperature changes of the root system. By choosing a hydroponic growth system, we minimized temperature gradients and the delay of temperature changes between root and shoots. Thus, the typical 4 °C cold stress, which would affect shoots and then be buffered to the roots by soil layers, was translated into a 10 °C stimulus applied directly to the roots. Consequently, we ratified 10 °C as a legitimate meteorological condition within the temperature ranges that *Arabidopsis* roots face during natural autumnal or spring low temperature acclimation.

2.1. Early Temperature Acclimation Effects on Plant Growth

Physiological effects of plant cold acclimation include slower growth rates and increased water contents [53,54]. We estimated that during the first seven days of cold acclimation following a shift in the middle of the light cycle from 20 °C to 10 °C, *Arabidopsis thaliana* at vegetative stage 1.10 [55] halts growth and development in terms of leaf number, rosette area [34], and, according to our current study, dry weight accumulation (Figure 1). Plants reared and maintained at 20 °C confirm that without a temperature shift, plants significantly accumulate dry weight (Figure 1). Growth arrest after a temperature shift is not a specific cold response. Plants shifted to 30 °C halted dry weight accumulation as well (Figure 1). Plants exposed to 10 °C or 30 °C for longer periods than 7 days typically resume growth and develop inflorescences, which is why these ranges are regarded as suboptimal temperatures for plants. These observations imply that halted or reduced dry weight accumulation is a shared early and transitory response of *Arabidopsis* to suboptimal temperature shifts.

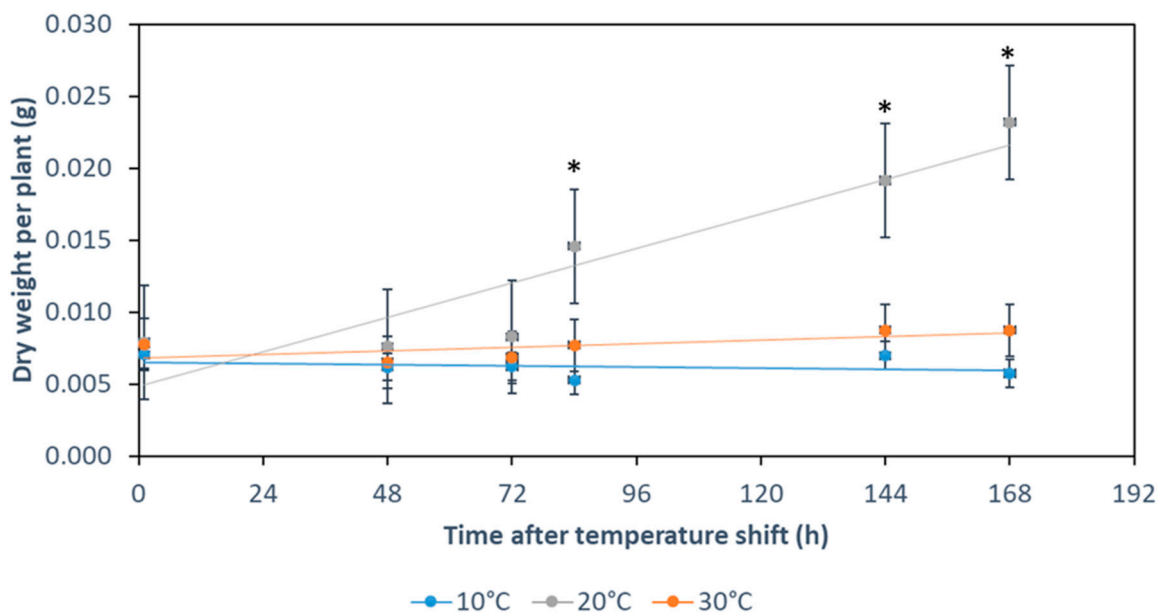


Figure 1. Arabidopsis Col-0 arrests biomass accumulation after shift to suboptimal temperatures. Plants were temperature shifted in the middle of the light phase at developmental stage 1.10, i.e., a rosette with 10 leaves with at least 1 mm in length, as defined by Boyes et al. [55]. Shift at 0 h from 20 °C to 30 °C (orange), to 10 °C (blue), or continuous 20 °C (grey). Note that control plants at 20 °C continued to accumulate dry weight during the first 7 days. Plants submitted to suboptimal temperature, either 10 °C or 30 °C, did not accumulate dry weight in the same period. The dry weight differences at and following 84 h of temperature acclimation were significant (asterisks, *t*-test significance $p < 0.05$). Means were calculated based on three biological replicates at each time point. The error bars correspond to the maximum standard deviation encountered across time points (Table S1). Biological replicates were composed of three independent plants grown in hydroponic cultivation systems (Figure S1).

Plants have a tissue- and developmental stage-specific expression of RPs and RP paralogs [56–58]. Similarly, there may not be an invariant standard ribosome population across all environmental conditions. We argue that ribosomal-related plant physiology during temperature acclimation periods of induced growth arrest (Figure 1) is not dormant [36]. Instead, Arabidopsis could accumulate, for instance, specialized ribosomes in order to cope with prolonged temperature changes. In this study, we focused our transcriptomic and shotgun proteomic analyses on the rewiring of the translational apparatus and attempt to reveal RP or RP paralog changes triggered by temperature acclimation during early biogenesis. Our analyses stay within the vegetative growth phase and precede the *de novo* synthesis of ribosome piles that is inevitably associated with resumed growth of new tissue at suboptimal temperature. Instead, we analyze bulk root tissue that pre-formed at optimized temperature and subsequently acclimated to reduced temperature.

2.2. Cytosolic Ribosomal Transcriptome Reprogramming

We tested changes of transcript abundances in whole root systems immediately before the 10 °C cold shift and at 1 day or 7 days into cold acclimation (Table S2 and Figure S2). We initially included probe hybridization data of all potential RPs and RAPs that were reported earlier (Table S2 of Beine-Golovchuk and co-authors, 2018). Of these probes, 329 and 82 indicated changed expression of RAPs only after 1 day and 7 days of cold, respectively, at a false discovery rate (FDR) < 0.05. On the other hand, 153 differentially hybridizing probes were shared among the time points (Figure S3A and Table S2B). General expression trends over time were evident among the differentially hybridizing RP and RAP probes. Four clusters emerged that indicated a major cold-induced reprogramming of the ribosomal and associated translation-related transcriptome (Figure S3B).

Subsequently, we focused our analyses on the cytosolic RP genes in an attempt to reveal cold-induced reprogramming of the cytosolic ribosomal proteome (RP) transcrip-

tome (based on Table S1 from Martinez-Seidel et al., 2020). A considerable part of the 242 structural cytosolic RP genes that were represented by partially redundant 310 gene probes changed expression upon cold shift and contributed to the overall transcriptional reprogramming of translation-related genes. Of the RP probes indicated, 35 (11.3%) and 75 (24.2%) indicated changed gene expression after 1 day and 7 days of cold, respectively, at $p < 0.05$. A total of 15 (4.8%) differentially hybridizing probes were shared among the time points (Figure S3C and Table S2A). Four expression trends of cytosolic RP genes were apparent among the significantly cold responsive transcripts of both the 40S SSU and the 60S LSU (Figure 2A,B and Table S2C). Additionally, a fifth group of non-cold-responsive probes indicated that 66 of 100 SSU transcripts and 86 of 142 of LSU transcripts remained unchanged (Table S2). Among the four groups of responsive genes (Figure S3B), part of the transcripts increased early after cold shift and continued to increase (Cluster 4). A second group decreased inversely (Cluster 3). A third cluster of RP transcripts increased late at 7 days after cold shift (Cluster 2). Finally, a fourth cluster of RP transcripts increased transiently at 1 day after cold shift and returned to initial expression levels (Cluster 1). A 40S group of responsive genes showed an opposite behavior, decreasing transiently at 1 day after cold shift and increasing again after 7 days. In summary, the transcriptional response of RAs peaked at 1 day after cold shift (Figure S3A), while only less than 1/3 of the responsive RAs belonged to this second group of early cold responsive genes [37]. The majority of structural RP transcripts are responsive at 7 days of cold acclimation (Figure S3C).

Subdividing our expression data by RP family indicated that some paralogs within single gene families exhibited similar responses whereas other paralogs responded differentially, e.g., by early maintained increases and inverse early maintained decreases (Figure 2C). To simplify subsequent analyses, we subdivided the transcript data according to time after cold shift. Considering the two time points separately, we encountered three types of differential expression patterns among paralogs of the cytosolic ribosome gene families and mapped these trends onto a 3D rendering of the 80S wheat translating monosome [59] (Figure 3). The differential expression patterns were: (1) only significant increase of one or multiple paralogs within one family (Figure 2D top and Figure 3, purple color-code). (2) Only significant decrease of one or multiple paralogs of a gene family (Figure 2D bottom and Figure 3, yellow color-code), and (3) at least two significantly inverse temperature regulated paralogs within a RP family (Figures 2D and 3—black color code). Cases where only specific paralogs of a cytosolic RP family have a differential expression, but other members of the same family do not share or even express the inverse of this response, may be interpreted as an indication of a paralog exchange during temperature acclimation.

Inverse transcriptional responses of RP paralogs are more abundant among the class of late responding transcripts (Figure 3—black color-code) at day 7. Upon visual inspection, we found that inversely changed paralogs appear spatially localized and are apparently not randomly scattered throughout the ribosome. Inversely temperature regulated paralog transcripts within an RP family may be seen as a strong indication of subfunctionalized paralogs, which are exchanged in ribosome pools according to changes of ambient temperature. A first example from our data set is the P-stalk that experiences an initial paralog-specific increase of gene expression at day 1, followed by an inverse regulatory pattern at day 7 after cold shift. A similar observation is apparent among protein-coding genes that constitute or are in proximity to the polypeptide exit tunnel (PET). Such spatial constraints may further indicate functional relevance of temperature-induced paralog exchanges in ribosome populations. Only a subset of RP transcripts were differentially regulated during cold. The identity of those transcripts as well as the outcome of a statistical test tailored to evaluate their spatial relationship in the ribosome structure are found in the results Section 2.6, “Spatially Constrained Cold Triggered Ribosome Heterogeneity”.

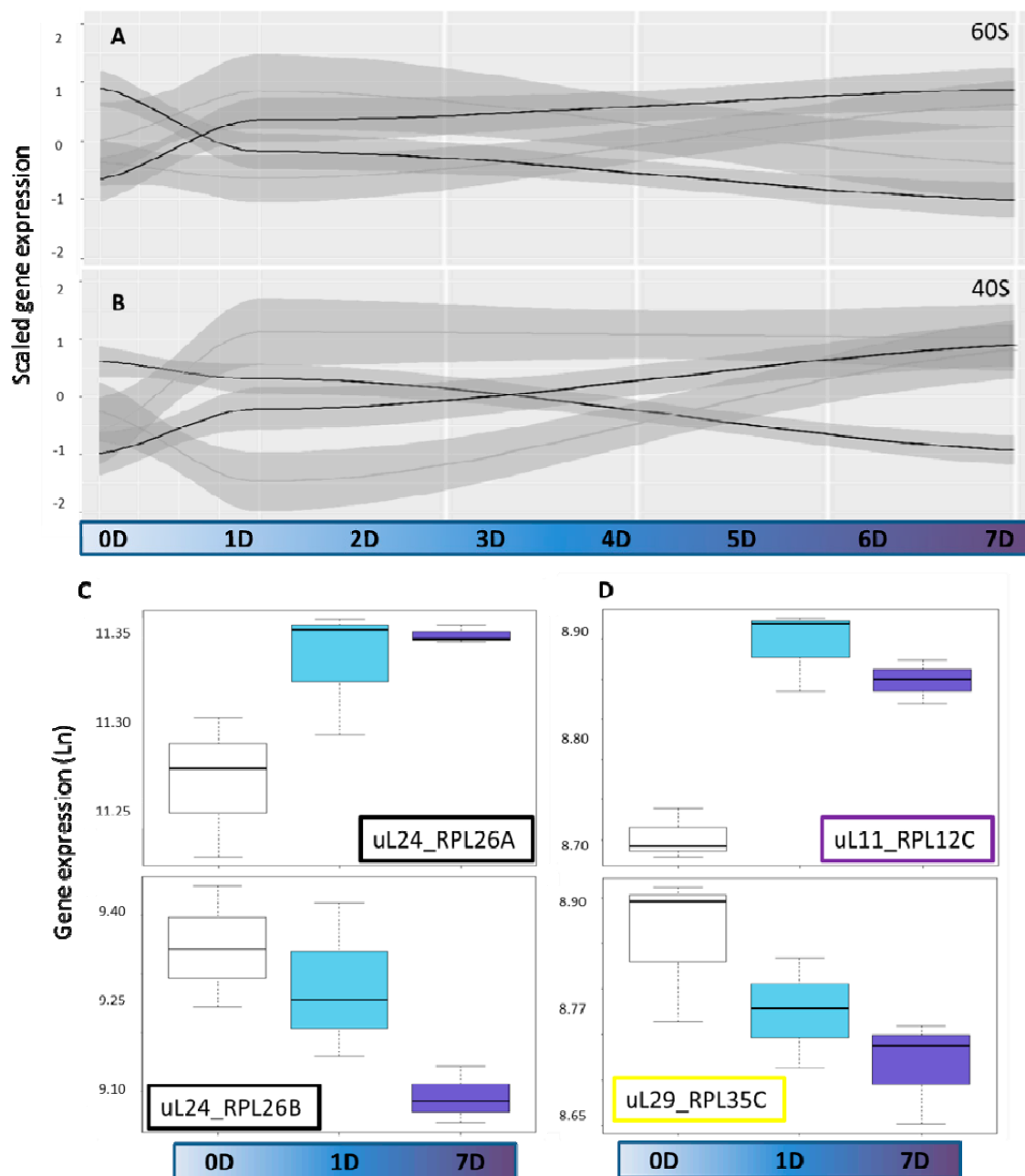


Figure 2. Changes of gene expression of cytosolic structural ribosome proteins in roots of *Arabidopsis thaliana* acclimating to suboptimal temperature. *Arabidopsis* wild type Col-0 plants grew at 20 °C to vegetative developmental stage 1.10 [55]. The transcriptome of whole root systems was profiled prior to a 10 °C cold shift (0D) and at 1 or 7 days after (1D or 7D) the shift. Replicates $n =$ three independent biological replicates at each time point. Probe hybridization intensities are natural logarithm-transformed, quantile-normalized, and statistically tested applying a generalized linear model with details reported in the methods section using R functions compiled in the GitHub repository RandoDiStats (<https://github.com/MSeidelFed/RandodiStats>, accessed on 30 April 2021). Scaled differential intensities cluster into four expression trends (K-means clustering) and identify response groups of cytosolic RP genes (Table S2C). Cluster means, indicated by solid grays and standard error intervals, light gray underlay, reveal four expression trends in (A) 60S LSU and (B) 40S SSU. (C) Example of inversely regulated paralog transcripts from the RPL26 (uL24) ribosomal protein family. (D) Examples of up and downregulated transcripts of the uL11 and uL29 ribosomal protein families respectively. The remaining paralogs within these two exemplary families did not show significant changes in their abundances and thus are not shown in the figure. Note that (C,D) represent non-scaled natural logarithm-transformed probe hybridization values. Colored boxes of ribosomal protein names indicate the temperature dependent type of upregulation or downregulation in paralog expression patterns (see Figure 3).

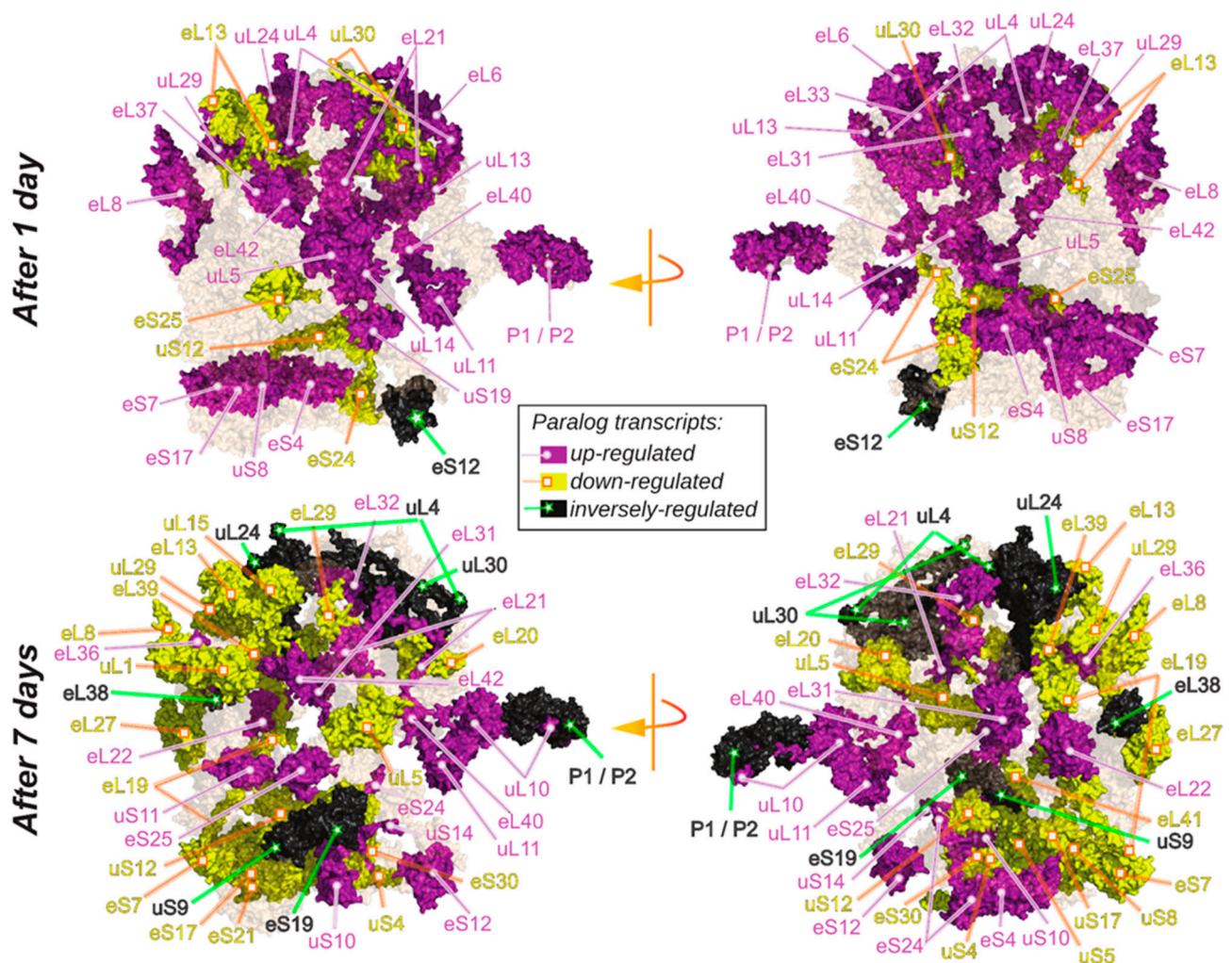


Figure 3. Differentially expressed ribosomal paralog genes from RP families of *Arabidopsis thaliana* root. Visualized data refers to significant differential hybridization of one or multiple probes per gene after 1 day (**top**) or 7 days (**bottom**) of cold exposure (Table S2). Differential paralog expression is mapped onto a 3D rendering derived from a Cryo-EM model of the wheat 80S ribosome [59]. Statistical analyses are identical to those in Figure 2. Purple-colored proteins have increased transcript abundances, yellow decreased abundances, and black inversely regulated transcript abundances of a single or multiple paralogs of the same gene family. Note left and right parts of the figure rotate the model by 180°. The model does not contain the rRNA scaffold.

2.3. Cytosolic Ribosomal Proteome Reprogramming

Protein abundances are not predictable from respective transcript abundances due to regulatory mechanisms that remain elusive [60]. For instance, features of mRNA affect initiation, elongation, and termination of translation and thereby protein abundance. Inversely, mRNA degradation or sequestration [61,62] and protein degradation rates influence protein levels in a predictable manner [63]. Thus, in order to account for the limitations of predicting RP abundance based on transcript analyses, we performed shotgun proteomics after trypsin digest of ribosome complexes (Figure S4) enriched from whole root tissue extracts. We chose the same vegetative developmental stage and hydroponic cultivation conditions as in our transcriptome study. According to our transcriptomic results, ribosomes would more probably carry triggered RP structural changes 7 days after cold acclimation, thus we focused our proteomic analyses at this time point. We compared all ribosomal populations among them, taking samples harvested prior to the cold shift as control. Considering that stress-responsive RP paralogs with functional roles should differentially accumulate in translating and non-translating ribosome complexes, we in-

investigated differential accumulation in polysomic compared to non-translating fractions and then focused only on the translating fractions. We omitted the 80S fraction because it can be a mixture of translating and non-translating mRNA-free complex species [38]. Moreover, we used three independent genotypes, wild type Col-0 and two independent knock out mutants of the Arabidopsis REIL proteins (*reil-dko*), i.e., cytosolic RBFs involved in late 60S maturation [34,39]. This allowed us to shed light on cold-triggered RP changes that are likely to occur in the early nucleolar biogenesis, since in the absence of REIL, 60S subunits are unable to mature during cold [38]. Thus, by including the *reil-dko* mutants we obtained cold response changes happening independent of REIL function that might trigger the well documented REIL-factors necessity during cold.

2.4. Substoichiometry in Non-Translating Versus Translating Ribosome Complexes

We tested whether RPs ubiquitously present in all samples (i.e., 66 RPs outlined in Table S4C) were significantly substoichiometric during cold. We found that upon acclimation some RPs significantly change their relative abundances in non-translational LSUs compared to polysomes (Figure 4). The changes are presented as the natural logarithm of 60S to polysome ratios, which means that a positive (Figure 4—purple) value represents a protein that is more abundant in the 60S fraction. Conversely, a negative (Figure 4—yellow) value means that a protein is more abundant in polysomes. There are several groups of responses in the context of RP stoichiometry. For example, specific paralogs from the RP families uL16, uL15, eL32, eL14, eL36, and eL18 are more abundant in the 60S fraction at 20 °C in Col-0 accession (i.e., the putative control or canonical RP composition for the WT genotype alone). The mentioned RPs are depleted from polysomes in relation to the non-translating 60S at 20 °C in the WT genotype. In other words, these RPs would be considered canonically more abundant in the non-translating fraction of Col-0 accession. After a shift to 10 °C, if these proteins were no longer more abundant in the 60S subunit and the ratios would be nearer to zero; these RPs would be considered substoichiometric in comparison to the previous canonical composition, which would entail that during cold these RPs are more abundant in the polysomes compared to their previous state.

The canonical stoichiometry shared by the three Arabidopsis genotypes at optimized temperature features uL15 paralogs aB and aC as intrinsically more abundant in the 60S subunit as compared to the polysomes. Similarly, paralog C from family eL18 is more abundant in the 60S subunit as compared to the polysomes. These increased abundances imply that fewer protein units from the mentioned RPs are associated with actively translating polysomes at optimized physiological conditions. Oppositely, the canonical stoichiometry between 60S and polysomes is lost during cold acclimation. At 10 °C, plants exhibit relatively decreased abundances in polysomes as compared to 60S of paralogs A, C, and D from families uL3, eL28, and eL13, respectively. Interestingly, the canonical stoichiometry at 20 °C relates to a surplus of proteins in the 60S, which is then lost during cold acclimation, where the stoichiometry is subtractional, i.e., there is a deficit of proteins in the free 60S subunit pools. A list of the paralogs of RP families with altered stoichiometry, including trends that are genotype-specific, can be seen in Table 1.

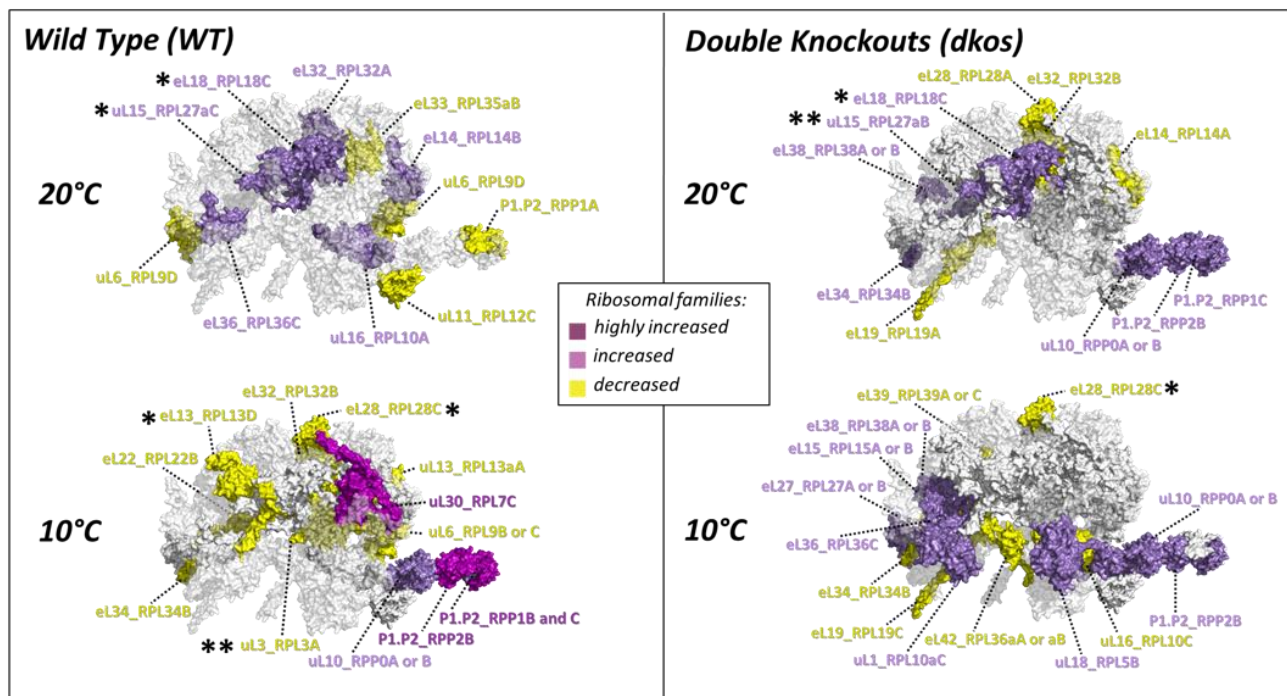


Figure 4. Substoichiometry of 60S proteome LSU-RPs 7 days after shifting from 20 °C to 10 °C in *Arabidopsis thaliana* Col-0 roots (**left panel**) and at the same time point in two double knockouts (*dkos*) genotypes of REIL proteins (**right panel**). Normalized protein abundances (Table S3) were used to calculate Ln-transformed ratios between the 60S and the polysome fraction. Only RPs that appeared in all replicates across the ratio components were considered. Ratios were genotype and temperature-specific (Table S4). The resulting RP paralog ratios were divided into four groups: dark-purple, high increase or higher abundance of one or more RP paralogs in polysomes ($\text{Ln-ratios} < 2.0$ and > 1.0); purple, increase or more abundance ($\text{Ln-ratios} > 0.0$ and ≤ 1.0); yellow, decrease or less abundance ($\text{Ln-ratios} \geq -1.0$ and < 0.0); off-white, no change. The 60S-RP ratios that belonged to the highest and lowest ten magnitudes were colored into a 3D rendering of the 60S subunit. * Black asterisks indicate RP families with significant substoichiometric paralogs (GLM— p Values $> 0.01 \wedge < 0.05 = **$; $> 0.05 \wedge < 0.1 = *$) in polysomic compared to the 60S fractions with a single regressor, namely temperature as the sole experimental factor ($n = 4$; *dko1*, *dko2*, WT-DS1, WT-DS2). Only one significant change does not coincide with the largest fold changes and hence is not visualized (i.e., eL8_RPL7aB—see Table S3).

Table 1. Paralogs of RP families that showed altered stoichiometry in 60S and polysome fractions.

Temperature	Genotypes	More Abundant in 60S	More Abundant in Polysomes
20 °C	Genotype-independent *	uL15_RPL27aB, uL15_RPL27aC, eL18_RPL18C	
10 °C			uL3_RPL3A, eL28_RPL28C, eL13_RPL13D
20 °C	WT	eL36_RPL36C, eL18_RPL18C, eL32_RPL32A, uL15_RPL27aC, eL14_RPL14B, uL16_RPL10A	P1.P2_RPP1A, uL11_RPL12C, uL6_RPL9D, eL27_RPL27A or B, eL33_RPL35aB
	<i>dkos</i>	eL34_RPL34B, eL38_RPL38A or B, uL10_RPP0A or B, P1.P2_RPP1C, P1.P2_RPP2B	eL19_RPL19A, eL14_RPL14A, eL28_RPL28A, eL32_RPL32B
10 °C	WT	P1.P2_RPP2B, uL10_RPP0A or B, uL30_RPL7C, P1.P2_RPP1C, P1.P2_RPP1B, P1.P2_RPP2A	eL22_RPL22B, eL32_RPL32B, uL13_RPL13aA, uL6_RPL9B or C
	<i>dkos</i>	eL15_RPL15A or B, P1.P2_RPP2A, uL18_RPL5B, eL36_RPL36C, eL38_RPL38A or B, uL10_RPP0A or B, uL1_RPL10aC, eL27_RPL27A or B	uL16_RPL10C, eL42_RPL36aA or aB, eL39_RPL39A or C, eL19_RPL19C

* Signals the significant changes, i.e., shared among genotypes, which are likely to arise during early biogenesis.

Genotype-specific trends: We found indications of potential paralog exchanges or opposite 60S to polysome fold changes. For instance, during cold, the B or C paralogs potentially replace uL6_RPL9D. Similarly, P1.P2_RPP1A, canonically less abundant in 60S, is potentially replaced by B and C paralogs that became more abundant in the 60S fraction

during cold. eL32_RPL32A is canonically more abundant in the 60S and less abundant during cold acclimation, while the B paralog is less abundant at 10 °C and already at 20 °C in the *dkos*. P1.P2_RPP2B, uL10_RPP0A or B and P1.P2_RPP1C are more abundant in the 60S LSU during cold acclimation in the WT, while already more abundant at 20 °C in the *dkos*.

2.5. Cold-Induced Changes in Active Translating Polysomes

In order to identify candidates that most likely represent functional remodeling in an acclimation context, we delimited our search focusing in changed low-oligomeric polysomal complexes (Figure 5). Polysomes are mRNAs loaded with several 80S translating monosomes and can be taken as a proxy of the translational fraction of ribosomes in the cell. Furthermore, grabbing entire roots or shoots for proteomics entails diluting *de novo* synthesized potentially specialized ribosomes with the pre-existing species. Therefore, candidate proteins that are present/absent during cold may be highly significant in a biological context. We weighed equally candidate proteins that are present or absent in a specific temperature-genotype combination (i.e., proteins standing in the red dashed lines in Figure S5) and those amenable to mean comparison between conditions. Relative quantitation and visualization of the changes through a bi-plot enabled us to encounter shared and significant responses among genotypes (Figure 5).

Shared significant cold responses common to *dko1*, *dko2*, and WT in Arabidopsis roots are clear in polysomal complexes. RPs uL30_RPL7C, eS24_RPS24A, and eL20_RPL18C are significantly less abundant in polysomes after seven days of shift to 10 °C, whereas eL14_RPL14B, eL34_RPL34A, eL42_RPL36aB or aA, and eL39_RPL39A or C are significantly more abundant in polysomes upon cold acclimation. Furthermore, genotype-specific trends can be inferred by analyzing each genotype and dataset individually (Figure S5). The trends coincide with the highest increases and lowest decreases in RPs according to fold change depicted in Figure 5. We picked robust changes based on their repeatability between datasets. Some changes appeared further robust taking into account that several RPs with unique peptide identifications from the same family follow the trends, e.g., uL30 paralogs in Figure S5 are depleted during cold from all the genotypes.

WT-specific responses: Reprogramming of ribosomes in WT Col-0 entails decreased abundances of at least P1.P2_RPP1C and possibly P1.P2_RPP1A and 2A. These are components of the P-stalk. Abundances uL16_AtRPL10 increase during cold. The cold responsiveness of P-Stalk elements is not visible in two independent *reil-dko* mutants.

dko-specific responses: The *dko2* appears to be more responsive in terms of the number of log fold-changed RPs in the polysomes. eL34_RPL34B is enriched during cold and P1.P2_RPP0A or B are depleted during cold. Both changes are consistent with their relative abundance in the 60S fraction (Figure 4).

Candidates derived from presence/absence calls: Most of the candidates that appear to be present or absent during cold appear to be spatially related to the PET or P-stalk region, i.e., eL39_AtRPL39, uL10_AtRPP0, eL22_AtRPL22. eL22_AtRPL22B was amenable to relative quantitation in the first dataset and it is enriched during cold in both genotypes, in the second dataset this RP is also cold responsive in the WT and is only present at 20 °C in the *dko2*.

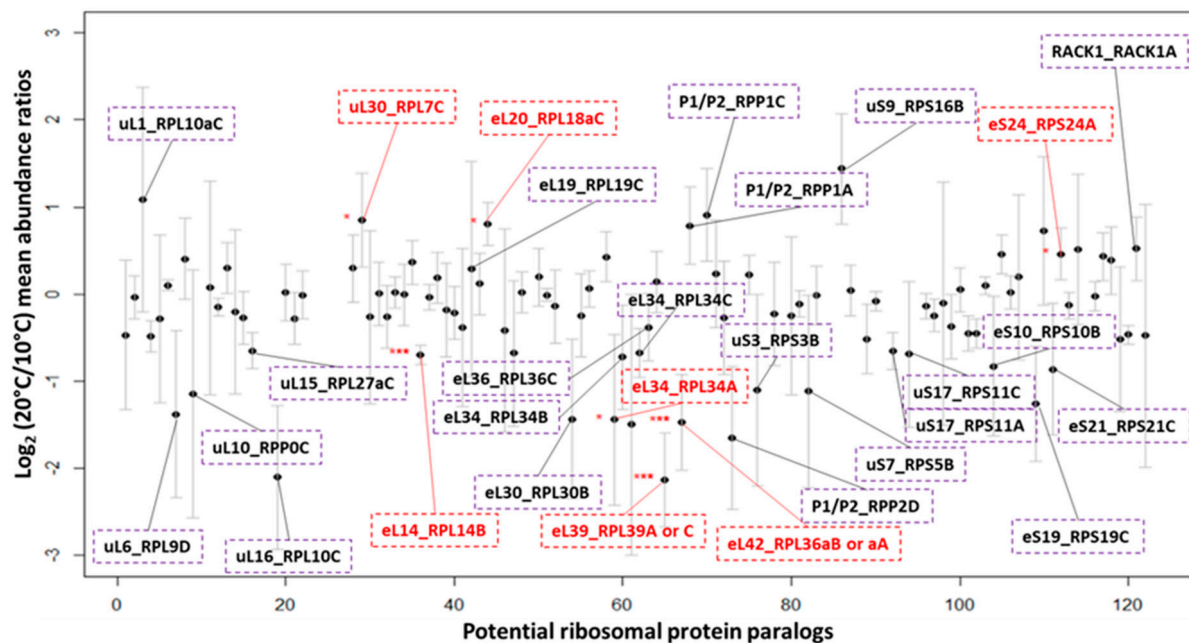


Figure 5. RP candidates of temperature-induced rearrangements in active translating ribosomes. Mean Log_2 ratios of $20^\circ\text{C}/10^\circ\text{C}$ ribosomal protein abundances during cold acclimation in *Arabidopsis thaliana* roots across independent genotypes in polysomes ($n = 4$; *dko1*, *dko2*, WT-DS1, WT-DS2 outlined in Table S5). The abundances were LFQ-normalized and corrected to the total amount of protein per ribosomal subunit in order to avoid relative subunit abundance to influence the results (Table S3). The x-axis contains 123 ribosomal proteins in common between two independent shotgun proteomics runs. The y-axis contains the mean Log_2 ratios of normalized abundances and the error bars represent the standard error. Only RPs with a Log_2 ratio >0.5 or <-0.5 have been named in the plot. In order to account for RPs that were cold-specific in at least one replicate causing an $-\text{inf}$ as a result of the ratio, $-\text{inf}$ was replaced by -2 only for graphical purposes. This means that those values did not affect the statistical testing. Statistical testing (p Values $< 0.01 = ***$; $> 0.01 \wedge < 0.05 = **$; $> 0.05 \wedge < 0.1 = *$) was done by fitting a GLM of the Gaussian family after testing the distribution of protein abundances using R functions compiled in the GitHub repository RandoDiStats (<https://github.com/MSeidelFed/RandodiStats>, accessed on 30 April 2021) and realizing that after normalization proteins in our datasets approximate a normal distribution (Figure S2).

2.6. Spatially Constrained Cold-Triggered Ribosome Heterogeneity

After mapping significant RP transcript or protein changes into a 3D rendering of the plant cytosolic ribosome, we observed the recurrent spatial closeness in cold responses. Thus, we used the methodology detailed in the GitHub repository COSNet_i (https://github.com/MSeidelFed/COSNet_i, accessed on 30 April 2021) to formulate a statistical testing scheme that enabled us to probe for spatial enrichment in the ribosome complex, using both an available Cryo-EM structure and our own omics data. The test selects, through a random walk, coherent ribosomal regions based on protein–protein interactions at a given distance threshold (i.e., we assume structural proximity in interpreted Cryo-EM densities as a proxy for biochemical interaction) and test whether the proportion of significantly changed RPs in these regions differs to that of the entire ribosome. The null hypothesis is that significant changes are randomly scattered throughout the ribosome structure. Thus, the method uses the Fisher exact test to detect significant differences in the proportion of up, down, or inversely regulated paralogs (Table S6). Using this method, we tested our transcriptome and proteome datasets to verify if specific regions are modulated during early ribosome biogenesis in plants undergoing cold acclimation (Figure 6).

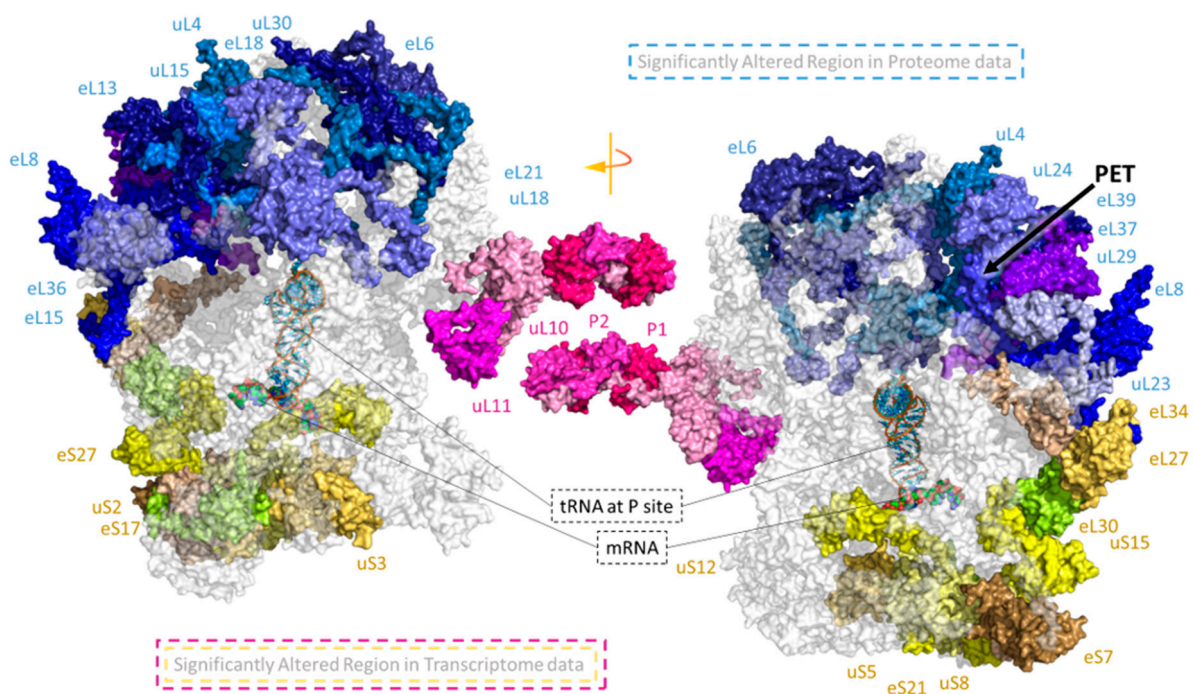


Figure 6. Significantly altered ribosomal regions during cold acclimation in *Arabidopsis thaliana* roots measured in three independent genotypes and four biological replicates in total. The figure is a visualization of the random walk sampling results and tested regions of interest detailed in the GitHub repository COSNet_i (https://github.com/MSeidelFed/COSNet_i, accessed on 30 April 2021). Sampled regions with a significantly increased proportion of RP changes as compared to the entire ribosome are depicted based on testing of the transcriptomic (shades of magenta and yellow) and proteomic (shades of blue) datasets. The binary input for the tests has been compiled in Table S6. Additionally, several regions had significant results at a threshold p value < 0.05 before the multiple testing correction and are reported in Figure S6. Note that at the transcript level one of the significantly altered regions co-localizes with the P site where tRNA binds as well as where the decoding of mRNA occurs. At the proteome level, the significances co-localized with the polypeptide exit tunnel (PET) depicted with a solid arrow. Both ribosomal images represent a 180° rotated mirror image of each other.

We tested three different levels in both the transcriptome (xT) and proteome (xP) data (Table S6): (1T) inversely regulated, (2T) inverse and upregulated, (3T) inverse, down, and upregulated as detailed in Figure 3. (1P) 60S to polysome ratios, (2P) polysome or (3P) both instances as detailed in Figures 4 and 5. At a significance level of Q value < 0.05 (i.e., Bonferroni adjusted p value), the spatial regions identified as significantly changed upon cold acclimation are depicted in Figure 6. At the transcript level, the molecular species from the 60S—P-Stalk and the 40S—60S transition of the ribosomal head were significantly enriched in relevant cold-induced changes. At the proteome level, abundances of RPs that belong to the polypeptide exit tunnel (PET) region were significantly changed during cold; this region includes RPs inserted into the tunnel. Moreover, since the Bonferroni correction can be statistically stringent, we report several regions that resulted significant with p values < 0.05 (Table 2 and Figure S6).

Even though not all significant changes remained below 0.05 after the multiple test correction, the same regions emerge across datasets and testing schemes. For example, the P-Stalk is a major reprogramming event at the transcriptome level as well as the PET at the proteome level. Both are supported by multiple cases of significance across our results. Similarly, the region containing the ribosomal head at the 60S—40S transition zone is significantly changed at the transcriptome level. Finally, several regions are outstanding due to their recurrence, namely the uL30—uL3 containing regions, which exhibit p values < 0.05 both at the transcriptome and proteome level.

Table 2. Paralog abundance changes that imply significantly modulated regions during cold acclimation in plants. Different sources of omics data were interpreted in their structural context using the procedures detailed in the GitHub repository COSNet; (https://github.com/MSeidelFed/COSNet_i, accessed on 30 April 2021). The data tested were transcriptome (1T) inversely regulated, (2T) inverse and upregulated, (3T) inverse, down, and upregulated as detailed in Figure 3. Proteome (1P) 60S to polysome ratios, (2P) polysome or (3P) both instances as detailed in Figures 4 and 5. Multiple entries per test indicate that several regions tested significant according to a Fisher exact test comparing the proportion of RP significances within selected regions to the total amount of significances among RPs.

Regions	Ribosomal Protein Families	Region Identifiers	p Values (Fisher)	Q Values (Bonferroni)
	Transcriptomics	4v7e_d ₈ _IN20_WL10		
1T—A	eL39 eL37 uL24 uL23 uL4 uL29 eL8 uL30 eL27 eL30 eL34	LSU-PET	0.07	0.80
1T—A	uL11 P1 P2 uL10	LSU-P-Stalk	0.05	0.51
2T—B	uS15 uS12 uS8 uS3 eS17 uS2 eS7 eS21 eS27 uS5 eL27 eL30 eL34	SSU-LSU-RibosomalHead.1	0.00	0.02
2T—B	uS15 uS12 eS17 eL19 eS7 uS2 uS17 eS21 eS27 uS5 uS8	SSU-LSU-RibosomalHead.2	0.00	0.00
2T—B	uL11 P1 P2 uL10	LSU-P-Stalk	0.00	0.05
3T—C	uL13 eL24 eS8 uL14 uL3	SSU-LSU-uL3 region	0.01	0.18
3T—C	uL11 P1 P2 uL10	LSU-P-Stalk	0.02	0.36
	Proteomics	4v7e_d ₈ _IN20_WL10		
1P—D	eL13 eL15 uS7 uL15 eL18 uL29 eS25 uL23 uL5 eL36 eL42 eL8 uL30 uS13 eL21 uS11	SSU-LSU-uL30 region	0.03	0.42
1P—D	uL15 uL13 eL24 eS8 uL14 uL3	SSU-LSU-uL3 region	0.03	0.39
3P—E	eL13 eL15 eL18 uL15 eL39 eL37 uL4 uL24 eL6 uL23 uL29 eL36 eL8 uL30 eL21 uL18	LSU-PET	0.00	0.04
3P—E	eL32 eL13 eL18 uL15 eL33 uL4 eL14 eL20 eL6 uL13 uL30 eL21 uL3 eL28	LSU-uL30-uL3 region	0.00	0.05

IN: iteration number, WL: Walking length, d_i: distance threshold in Å, **bold**: significant regions after Bonferroni correction.

2.7. Paralog Specific Cold Responses—uL30 Family

The four uL30 paralogs were consistently changed during cold acclimation both at the transcript and protein level. The C and D paralogs were inversely regulated 7 days after cold acclimation at the transcript level (Figure 3). At the protein level, The C paralog became more abundant in the 60S subunits as compared to polysomes (Figure 4) while being significantly less abundant in the polysomal fraction (Figure 5). Paralogs B, C, and D exhibited a two-fold decrease during acclimation in WT and *reil-dko* mutants polysomes (Figure S5) while the A paralog was only detected in polysomes in the shoots during cold (Figure S7). Regions containing uL30 RP were frequently enriched for cold-relevant changes (Figure S6) and remained significant at the proteome level after Bonferroni correction (Figure 6). Thus, we investigated the length to which uL30 functions are known in model eukaryotes, aiming to determine if there is a relation between uL30s, conserved cold responses, and the spatial constraints encountered. We interpreted reported functional aspects of this gene family in other eukaryotes using a phylogenetic tree alignment of the protein coding regions of *Arabidopsis thaliana*, *Saccharomyces cerevisiae*, and *Homo sapiens* (Figure 7).

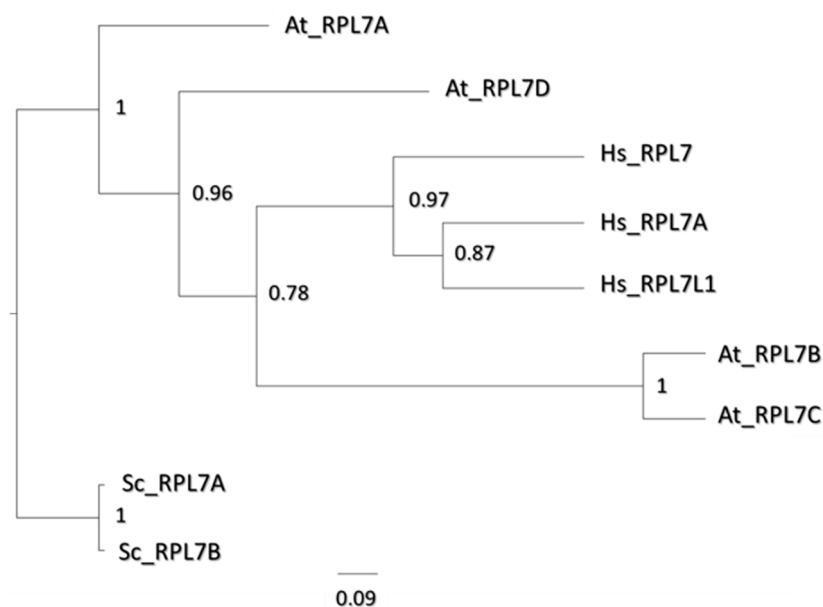


Figure 7. Phylogenetic tree resulting from the Bayesian analysis of the uL30 ribosomal protein gene family found in *Arabidopsis thaliana*, *Homo sapiens*, and *Saccharomyces cerevisiae*. Node values represent posterior probabilities calculated through Bayesian confidence methods (Table S7). Branch lengths represent substitutions for each branch, where the bottom scale represents the length of a 9% nucleotide substitution rate per site (i.e., number of changes per 100 nucleotides) according to a hypothetical common ancestor.

Yeast—*Saccharomyces cerevisiae* (Sc)—has two paralog genes (i.e., ScRPL7A and ScRPL7B) coding the uL30 homologs. According to a phylogenetic tree alignment of the protein coding regions (Figure 7), yeast homologs are the nearest to a “common” eukaryotic ancestor as compared to plants and mammals. Two paralogs (i.e., HsRPL7 and HsRPL7A) and one alike-protein (i.e., HsRPL7L1) code the *Homo sapiens* (Hs) homologs, which differ in their degree of divergence as compared to a common hypothetical ancestor. Still, the three proteins cluster together, suggesting low diversification between them. In *Arabidopsis*, AtRPL7A and D are the least diversified in comparison to the common ancestor. AtRPL7A is adjacent to Sc homologs in terms of nucleotide substitutions, whereas AtRPL7B and C appear to have diversified substantially and are closer to Hs homologs. Notably, At paralogs do not cluster together as do Hs and Sc, suggesting that these might have diverged the most.

3. Discussion

3.1. Different Types of RAP Transcripts Mediate the Initial and Long-Term Responses to Temperature Acclimation

The transcriptomic fingerprints of cold acclimation in *Arabidopsis thaliana* are compiled in Genevestigator [64], where experiments across mutant and wild-type genotypes [65–73] make clear that a major transcriptome reprogramming occurs [74]. During cold, changes in gene expression remodel machinery and metabolic pathways to enable acclimation. There are two main groups of transcriptional responses [37]: immediate responding genes (responding after 1 h) that modulate the direct response, and late responsive genes (responding after 1 day) that keep changes more permanently, thus enabling acclimation. Between these two classes of early responsive genes, translation-related genes are a main hub mediating cold acclimation [32]. The transcriptome of ribosome-associated protein (RAP) transcripts responds at 1–7 days of cold acclimation [34] and there are paralog-specific abundance shifts (Figures 2 and 3 in this manuscript and Figures 3 and 4 from Martinez-Seidel et al., 2020) indicating potential paralog functional divergence [7] adjusted to different temperatures.

In order to extend previous insights, in this manuscript we interrogated the cold response dynamics of transiently binding RAPs and structural RPs. A larger amount of transiently binding RAPs (including RBFs and TIFs) become differentially regulated after one day of temperature acclimation ($FDR < 0.05 = 482$, Figure S3A) as compared to 7 days ($FDR < 0.05 = 236$, Figure S3A). In consequence, most transiently binding RAPs can be classified in the second group of late responsive genes proposed by Seki et al. (2002). Next, we inquired about ribosome biogenesis factors (RBFs) as effectors of the transcriptional response. Genes coding for RBFs and putative nucleic acid binding proteins are specially regulated 1 day after shifting to cold. Apart from one transmembrane chaperone, all the other genes from 24 significantly changed RBFs are related to nucleic acid binding and rRNA transcription and processing (Table S8) [2,75–77]. At the later time-point, i.e., day 7, only three RBFs were differentially regulated, two of them featuring nucleic acid binding domains and rRNA processing functions. On the other hand, continuously regulated RBF genes in both 1 and 7 days are mostly related to rRNA processing pathways. Cold-triggered modulation of rRNA processing and decrease of pre-rRNA species has been reported in rice, maize, and *Arabidopsis* [43,78,79]. Rather than just rRNA synthesis arrest, we argue that in essence, cold exposure seems to reprogram the synthesis of new ribosomes by modifying rRNA via transcription and processing, in order to rearrange the concomitant and serial assembly of new cold-related protein paralogs. Accordingly, co- and post-transcriptional modifications on the rRNA topography may lead to different possibilities of protein interactions and stoichiometry [80].

Assembly of RPs during biogenesis relies on an orchestrated serial “entry and exit” of sets of RAPs. For instance, early in the nucleolus, the 60S GTPase-Associated Center (GAC), Polypeptide Exit Tunnel (PET), and Peptidyl Transferase Center (PTC) start to be formed and mounted with some of their RPs. In our datasets, structural RPs show the opposite trend as compared to total RAPs, with a larger number of RPs being differentially regulated after 7 days of acclimation (Figure 3 and Figure S3 and Table S2). Thus, structural RPs might constitute a third group of cold responsive genes regulated in response to altered ribosome biogenesis in order to store a molecular memory of low temperatures as structural changes in the ribosome.

3.2. Cold-Triggered Reprogramming Indicates That Spatial Constraints Adjust the Ribosomal Proteome

The initial transcriptome regulation of RBFs and other RAPs at day 1 of acclimation is followed by the differential regulation of the transcriptome coding for structural RPs at day 7. Thus, seven days after the initial cold cue is the essential time-point to understand what the initial transcriptome regulation implies for the ribosome structure. Previously we have shown that plants alter their RP stoichiometry upon a transition to cold [36,38].

Here, we outline that paralog-specific cold changes deviate from a canonical stoichiometry. The cold RP substoichiometry is related to molecular species from the PET region, whereas transcriptome RP substoichiometry is related to molecular species from the P- Stalk and the ribosomal head. Within the significantly enriched regions, paralog-specific exchanges indicate that functional divergence among RP paralogs occurred. Redundant paralogs are likely to sub and/or neofunctionalize [6]. In our case, we present changes that include simultaneous down and up-regulation of RP paralogs within the same family, or up-down- regulation of a single paralog within a RP family, suggesting paralog adjustment to temperature. Moreover, spatially adjacent changes suggest that evolutionary forces driving paralog divergence could be structurally constrained, either by co-evolution of binding sites for RPs or RP paralogs [81], or fundamentally influenced by the concerted mounting of RPs that happens during ribosome biogenesis [82]. Plant ribosome biogenesis, for example, features several specific factors that mediate processing steps of the 60S LSU [1,2]. The RBFs assisting and mounting RPs are not exclusive but rather assist with the mounting of several RPs at a specific stage. Therefore, a single RBF could affect a group of similarly located RPs. Consequently, the regional adjustments in the ribosomal proteome can be expected and may be used to further modulate cold acclimation by enabling ribosomes to select transcripts for translation.

Selecting ribosomal regions and studying the interactions between all ribosomal components was initially enhanced by the first high-resolution structure of an eukaryotic ribosome that helped to decipher in detail all the interactions [83]. This type of information allowed us to define coherent ribosomal regions, which is the most influential step towards finding spatial enrichments. Several considerations and criteria needed to be met. For instance, ribosomal regions of biological interest could be defined based on rRNA domains and accessory proteins [84]. However, pre-knowledge biases must be avoided while selecting coherent independent regions in order to fulfill the statistical test assumptions. We achieved this by weighting protein–protein interaction networks with the percentage of contact coverage between proteins. This allowed us to draw spatial constraints by defining a transit probability during the subsetting procedure. We selected an 8 Ångströms threshold based on the quality of the resulting regions (e.g., connectivity and biological accuracy) and literature consensus on distances between amino acid residues within a protein structure [85]. Later on, we used the coherent regions to test if the proportion of significances in each RP subset compared to the RP universe changes. The statistical test selected was the Fisher exact test [86,87], followed by the strict Bonferroni correction [88].

Spatial adjustments of the ribosomal proteome may be at the core of ribosome specialization. The functional centers of ribosomes actively communicate to perform ribosomal functions. The communication among functional centers is optimized by the coevolution of a non-random RP network [89]. These RP graphs harbor specific neuron-like properties that led to the realization of RPs being instrumental in the process of information transfer across ribosomal complexes [90,91]. For example, mutating specific amino acid residues from uL5 in yeast leads to impaired inter-subunit communication, which in turn causes structural alterations in 40S and 60S rRNA [92], highlighting the large scale of information flow within the network. Similarly, uL3 in yeast plays a role in the coordination of the elongation cycle by communicating the tRNA site status to the elongation factor binding region and the peptidyltransferase center [93]. Thus, small changes in RPs can lead to vast rearrangements in the RP network and adjustment of ribosomal function. We used the plant RP network to define coherent ribosomal regions and used those regions to interpret our omics data in their structural context. We found that altered stoichiometry in specific RP and RP paralogs is correlated to modulated ribosomal substructures during cold acclimation in plants, suggesting for example that uL30 acts as a communication hub that restructures the ribosome during cold. Moreover, we argue that after stopping ribosome biogenesis during cold, the modulation of these substructures is likely to occur in the early nucleolar biogenesis as a response to maintain protein synthesis during acclimation.

3.3. Cold Ribosomal Protein Changes during Early Biogenesis

The ribosome physiology of cold acclimation indicates that Arabidopsis wild type plants start accumulating 60S free subunits rapidly after a cold cue and steadily during the first 7 days of acclimation [38]. By comparison, *reil-dko* genotypes present an accumulation of 60S subunits before the shift to cold, which are rapidly depleted upon a cold cue and are only slowly replenished across the acclimation period until a wild type-like abundance level [38]. Nevertheless in spite of the accumulation of 60S subunits in the mutants, these complexes appear not to be competent since *reil* mutants fail to restart growth after 7 days of acclimation [34]. Thus, the 60S subunits that are accumulated are most likely defective. Here we show that such defects are probably stemming from nucleolar biogenesis, since beyond wild type-specific or *reil-dko*-specific RP changes, there is a spatially constrained cold substoichiometry supported by several RP changes shared among genotypes.

Deviations from the canonical RP composition comprise at the proteome level the PET region. Specific RP changes entail at least increased abundances of uL15_RPL27aB, uL15_RPL27aC, eL18_RPL18C in the LSU as compared to polysomes at 20 °C and increased abundances of uL3_RPL3A, eL28_RPL28C, eL13_RPL13D in polysomes as compared to LSUs at 10 °C. Importantly, the intrinsic increased abundances across several RPs in the 60S population before the temperature shift indicates a surplus of proteins bound to the non-translational 60S subunits. RPs can exhibit promiscuous binding in archaeal ribosomes with some proteins being present at more than one location per 50S ribosome [94]. Moreover, metazoan cytosolic ribosomes acquired novel expansion segments (ES) logarithmically over the past two billion years as compared to archaeal and bacterial ribosomes [95,96]. Metazoan RPs have also diversified, increased in number, and in parts diverged [97–101]. Thus, it is likely that the availability of novel rRNA expansion segments and the diversification of RPs enhances promiscuous binding of multiple RP or RP paralog copies per ribosomal particle in metazoans and specially also in plant ribosomes. Moreover, storing these “RP abundant” complexes in a non-translational fraction might be a on the run strategy to rapidly tune the ribosomal network and meet translational needs. Consequently, the surplus of RPs in 60S subunits supports one of our previous notions, i.e., “that Arabidopsis may buffer fluctuating translation by pre-existing non-translating ribosomes before *de novo* synthesis meets temperature-induced demands” [38]. Once a shift to cold occurs, the stoichiometry of 60S subunits is intrinsically subtractional [102], indicating that the surplus population that was stored to meet translational demands likely got depleted. On the other hand, in active translating polysomes, the RP stoichiometry changes bilaterally, that is, abundances of bound uL30_RPL7C, eS24_RPS24A, and eL20_RPL18C significantly decrease during cold acclimation, while the abundances of bound eL14_RPL14B, eL34_RPL34A, eL42_RPL36aB or aA, and eL39_RPL39A or C significantly increase. This indicates that active ribosomes need a finer adjustment of their structural proteome to meet translational demands during cold.

3.4. Cold Dynamics of Ribosomal Protein Assembly

Assembly and specific interactions of different RP or RP paralogs may be a product of the effect of lower temperatures on protein stability and folding states. Agozzino and Dill [103] described a model for the sequence adaptation of proteins according to temperature changes and argued that the least stable proteins are the ones that adapt faster to temperature changes and help the organism adapt faster. In this process, chaperones and their properties are essential as capacitors of cellular evolution. One process that can alter folding states of globular proteins is cold denaturation [104–107]. Besides heat, cold can denature proteins due to the disturbance of the forms of noncovalent bonding that are responsible for the folding state at physiological conditions. Thus, cold denaturation is essentially dependent of the protein structure and the hydrophobic effect [106]. Due to different amino acid composition and structural features, the temperature in which cold triggers denaturation can vary for different proteins.

At 10 °C in our experiments, cold denaturation could account for the spatially changed PET region in both transcript and proteome data (Figure 6 and Table 2) and the choice of assembling different RP or RP paralogs. Many RNA-binding proteins have linkers as intrinsically disordered regions (IDRs) in their natural native state, which confer flexibility and plasticity to the RNA-binding domains [108]. In RPs, IDRs are disordered extensions that can stretch to different parts of the subunits. Extensions can penetrate the core of subunits and transition to a more ordered structure and assist rRNA folding, and different categories of extensions may have distinct functions in assembly stages [109–111]. Moreover, many eukaryotic RPs' disordered extensions interact with the rRNA expansion segments (ES) around the peptide exit tunnel (PET) [83], and from the P-stalk to the L1 side. ES are present in the surface of both subunits, but in the 60S they are more abundant and form a nearly continuous ring around the PET. It may be that cold structurally modulated RP paralog extensions can lead to different interactions with rRNA helices and ES due to different folding states, leading to heterogeneous subpopulations of subunits and ultimately ribosomal complexes.

3.5. Cold-Induced Ribosomal Protein Substoichiometry Co-Localizes With *Rei1* Binding Site

In yeast, *Rei1* inserts its C-Terminus inside the PET in order to probe the integrity of the tunnel [41]. *Rei1* binds in the vicinity of the PET exit [112]. The binding site was initially thought to be eL24, but the deletion of eL24 did not prevent the factor to bind to the LSU [113]. Cryo-EM structures [41] show *Rei1* to be bound to eL22 in its tunnel inserted state (see Figure S8). Residues 355–385 might enhance the opening of the PET to achieve C-Terminus insertion [41]. In plants, *Rei1*-like (REIL) proteins mediate low temperature perception and the molecular implications of REIL loss compared to yeast homologous mutants are similar [34]. Thus, altered RP stoichiometry near or inside the tunnel can be very relevant for REIL proteins since it would co-localize with their functional and binding site.

The ribosomal proteome surrounding the PET is significantly remodeled during cold. These rearrangements may be the cause of REIL necessity because they occur indistinctly in wild type and two independent *rei1-dko* genotypes. Thus, rearrangements directly associated or happening after the 60S-REIL interaction are omitted. The encountered remodeling implies altered paralog dynamics around REIL's binding and operating site. Hence, among possibilities, the tunnel structure could be weaker or binding sites for canonical maturation factors may be lost, and then, the appearance of a specialized protein to prove the integrity of the rebuilt tunnel, such as REIL, would be ideal. As an example of paralog-specific changes, within RP family eL22 (blue in Figure S8), paralog eL22-RPL22B is decreased in the WT-60S as compared to the polysomes during cold, potentially signaling a cold-specific binding event for REIL. The eL22 paralogs have effectively subfunctionalized in *Drosophila* [114]. Additionally, in yeast, paralog-specific phenotypes of eL22 are related to translational control of the serine and methionine metabolic pathways [115]. Thus, variations in eL22 paralogs can effectively produce functional divergence and may be used by plants to enhance the REIL-60S interaction.

3.6. Cold Dynamics of uL30 Paralogs Could Orchestrate Spatially Constrained Rearrangements in Ribosomes

Paralog rearrangements can characterize ribosome specialization in eukaryotes [13,116,117]. Similarly, as we have shown, several paralog-specific changes characterize cold-acclimated ribosomes in *Arabidopsis*. We interrogated the uL30 gene family as an exemplary case of induced changes that may occur as a response to cold early on during nucleolar biogenesis. This RP family is also responsive to cold in other higher eukaryotes, for example, in wood frog *Rana sylvatica* RsRPL7 is upregulated during cold acclimation, conferring resistance to freeze tolerance [118]. Functionally, uL30 mediates the pre-rRNA cleavage at site C2 in ITS2, separating precursors of rRNA into 5.8S and 25S in yeast [119]. In *Arabidopsis*, uL30 is encoded by four paralog genes, two of them, *rpl7a* and *b*, have a leaf phenotype [120], but the molecular implications of the loss have not been evaluated. An important observation

that explains a potential paralog-exchange was reported for the *Homo Sapiens* RPL7 (i.e., close homolog of AtRPL7B and C as detailed in Figure 7), which inhibits translation of specific mRNAs including its own [121,122]. Our work shows that the transcript of AtRPL7C becomes upregulated during cold acclimation, while its proteoform becomes depleted in the translational fraction during cold. This implies a translational regulatory mechanism that relies on the increased transcript abundance of the C paralog. Interestingly, the C and D and not the A and B paralogs have been reported to contain upstream open reading frame (uORF) sequences that most likely regulate translation [123], providing a hypothetical testable mechanism. In shoots, AtRPL7A (i.e., the closest homolog to ScRPL7A and B) is cold-specific according to presence/absence calls (see Figure S6).

Evidence from model eukaryotes suggest that paralog exchanges in the uL30-AtRPL7 family may trigger regionally constrained ribosome heterogeneity. More specifically, knocking out yeast uL30 homologs triggers defects in the pre-RNA assembly step 27SA3 to 27SB, causing in the end reduction in four RPs that surround the polypeptide exit tunnel [124], similar to what we report. Therefore, decreased uL30s from translationally competent complexes could orchestrate structural rearrangements of the PET. From a ribosome perspective, remodeling the PET would be one of the most efficient mechanisms to constrain translation of specific mRNAs by stalling nascent peptides. The PET is one of the major determinants of ribosome velocity through a transcript [125] mainly due to the amount of negative charges across the tunnel slowing down positively charged amino acids; hence, the PET architecture would be highly susceptible to slight modifications that would make it improbable for specific positively charged peptides to be translated without stalling. Thus, remodeling the tunnel might enable ribosomes to rapidly shape the cold proteome by translating specific transcripts.

3.7. REIL Concomitant Ribosome Reprogramming Argues Potential Specialization

REIL proteins in plants have acquired functional changes including putative novel roles in processes such as cold acclimation [34]. Within the possibilities of acquired functions, and aligned with evidence, REIL factors either directly or indirectly enhance regional restructuring around the P-stalk during cold acclimation (Figure 5). In yeast, Rei1 interaction is followed by changes in the assembly of the last ribosomal component, namely the P-Stalk [45]. The P-Stalk recruits proteins from the large GTPase family directly assisting translation initiation [126], because this family contains the translation initiation factors (TIFs) [127]. Thus, remodeling the P-Stalk is a tremendous opportunity to achieve selective translation by directing TIFs towards specific mRNAs. At the transcriptome level, the P-Stalk and the ribosomal head are enriched in cold significant changes. At the protein level, the observed changes in several members of the P-stalk in polysomes are consistently wild-type specific (Figure S5), arguing that the lack of REIL may impair the P-Stalk remodeling that is necessary for successful acclimation. Functionally, both regions are involved in mRNA translation, the P-Stalk recruiting TIFs and the head laying right next to the mRNA passage sites on the ribosome. Therefore, a transcript-mediated mechanism used by the ribosome to constrain total or specific translation events could be initiated by these ribosomal components. Similarly, at the proteome level, the PET is significantly enriched in RP cold-induced changes. The PET is the transit point for every single polypeptide that is synthesized. Also described as the “birth canal of biology” [95], it is as such also a hotspot to constrain total or specific translation for ribosomes according to external stimuli. These reprogramming events could represent fast strategies used by the ribosome to constrain translation upon cold acclimation, mediated partly by REIL newly acquired functions.

4. Materials and Methods

4.1. Plant Material

The Arabidopsis double homozygous *reil1-1 reil2-1*, and *reil1-1 reil2-2* mutant lines (*dko1* and *dko2*) were created by crossing the T-DNA insertion mutant SALK_090487 (*reil1-1*) with GK_166C10 (*reil2-1*), i.e., double knock-out mutant 1 (*dko1*) or SALK_040068

(*reil2-2*) [39], i.e., double knock-out mutant 2 (*dko2*). The Nottingham Arabidopsis Stock Centre made the Salk lines available (<http://signal.salk.edu/>, accessed on 30 April 2021). The GK line was obtained through the GABI-Kat program [128]. Homozygous lines were verified by PCR amplification of genomic DNA [39]. The genetic background of the initial mutants is accession Col-0. Hence, all experiments were in comparison to this wild type and *Arabidopsis thaliana* Col-0 was used as positive control throughout this study.

4.2. Growth Conditions

Plants were grown in a hydroponic system. Autoclaved assembled glassware with metallic meshes were used to place Arabidopsis seedlings at vegetative developmental stage 1.0 [55] for sterile culture on top of liquid medium (Figure S1). Arabidopsis seedlings were germinated and transferred onto the mesh using small blocks of solid agar. Transferred plants were grown within the translucent glass pots with non-airtight glass lids until stage 1.10 inside growth chambers with a 16 h/8 h day/night cycle. Plant age at stage 1.10 was approximately 21 days after sowing. The hydroponic solution was Murashige and Skoog medium [129] supplemented with 2% (*w/v*) of sucrose. The growth chamber environment was kept as reproducible and controlled as possible. The chambers were set to a light intensity of 40 μE . The effective light intensity within the glassware was $\sim 30 \mu\text{E}$. The temperature inside the glassware was externally controlled but temperature inside the glass pots increased during illumination. External 10 °C of the growth chamber generated ~ 12 °C inside the glassware, external 20 °C and 30 °C, ~ 23 °C and ~ 31 °C during the light phase, respectively. Plants were temperature-shifted in the middle of the light phase. Minor fluctuations of light intensity and temperature were encountered according to the position within the growth chamber. These fluctuations were accounted for by rotating the position of glassware daily. Block and tray effects were minimized by pooling material across jars and different trays when collecting biological replicates.

4.3. Dry Weight Measurements

A BP210S balance (Sartorius AG, Göttingen, Germany) was used for weighing. To improve balance precision at different locations, the balance was temperature-equilibrated to locations at least a day prior to measurements (Table S1). Accuracy of weight determination after re-location of the balance was controlled by small metal calibration weights (Table S1C). Empty bags were folded to fit the balance and to speed up weight equilibration. The dry matter content of hydroponic plant material was determined using the weight loss after drying. Whole plants were taken from hydroponic cultivation and placed inside wax-layered and pre-weighed bags after 48, 72, 84, 144, and 168 h after shifting to either 10 or 30 °C, or continuous growth at 20 °C. To eliminate excess liquid from root material, roots were rapidly pre-dried with filter paper three times within a total period of 2–6 s. Adherent solid agar pieces were removed thoroughly without compromising the speed of weighing. The initial weights of empty and full bags were registered to calculate sample fresh weight. Full bags were dried at 70 °C for three days. Subsequently, the bags were temperature-equilibrated 1 h inside a desiccator and the dry weight of the full bag and emptied dried bag determined to calculate sample dry weight. Weight loss of bags was corrected by measurement of initial and dried weights of 155 empty bags (Table S1B).

4.4. Microarray-Based Transcriptome Analysis

Total RNA from hydroponic Arabidopsis root samples with fresh weights of 25.1–26.8 mg were harvested at time points 0 h, i.e., at 20 °C before shift to cold, and 1 or 7 days after shift to 10 °C. RNA was isolated using the RNeasy Plant Mini Kit (QIAGEN, Hilden, Germany) according to the manufacturer's instructions [130] with minor modifications. Briefly, 110 μL of RTL lysis buffer was used to extract RNA. 30 μL of RNase-free water was added to elute the RNA. Three replicates were prepared per time point ($n = 3$). The RNA integrity number (RIN) was determined by an Agilent 2100 Bioanalyzer and 2100 Expert software (Agilent Technologies, Santa Clara, CA, USA). RNA samples with

RIN of more than eight were used for 4x44K Agilent expression profiling (ATLAS Biolabs, Berlin, Germany). The expression data sets were uploaded to the Gene Expression Omnibus (<https://www.ncbi.nlm.nih.gov/geo/>, accessed on 30 April 2021) and are available through accession number GSE144916.

4.5. Transcriptome Data Analyses

A matrix of one-color-processed green signal values (gProcessedSignals) was obtained from ATLAS Biolabs (Berlin, Germany). Company signal processing comprised multiplicatively de-trended background subtraction, correction for spatial effects, and removal of outlier pixels. A subset of the complete transcriptome matrix was created that contained only probes encoding open reading frames of cytosolic RPs (based on Table S1 from Martinez-Seidel et al., 2020) [131] or total RAPs [34]. The resulting matrix contained in part redundant probes of gene models. The respective signals of redundant probes were analyzed separately to internally control for the quality of differential hybridization and to recognize potentially differential hybridization of included splice variants. The resulting Ln subset matrix was quantile normalized using the `normalize.quantile` function of the `preprocessCore` package (<https://github.com/bmbolstad/preprocessCore>, accessed on 30 April 2021) version 1.46.0. for R statistical computing and graphical visualization language (<https://www.r-project.org>, accessed on 30 April 2021). Batch effects that result from between chip variation of microarray experiments were accounted for using `comBAT` [132], an empirical Bayes normalization algorithm. The distribution of the resulting normalized probe hybridization abundances was tested using a dependency of the R-package `fitdistrplus` [133] through R functions located in the GitHub repository `RandodiStats` (<https://github.com/MSeidelFed/RandodiStats>, accessed on 30 April 2021). The distribution shapes were visualized by Cullen and Frey graphs featuring the kurtosis against the square of skewness (Figure S2) and indicated an approximately Gaussian distribution. Thus enabling statistical testing by fitting of linear models using the R-package `limma` [134]. A generalized linear model (GLM) procedure without parametrization of the mean and variance gave equivalent significance (p values) (Table S2). The resulting p values were corrected for multiple testing using the false discovery rate proposed by Benjamini and Hochberg (BH-95) [135]. K-means clustering [136] was applied to the autoscaled matrix of differentially expressed genes of cytosolic ribosome proteins and expression trends of cold acclimation were identified. Based on these trends, the RP families were tested for paralog-specific differential gene expression. We considered three possible paralog-scenarios. (1) The entire gene family or at least one paralog within has increased gene expression, (2) the entire family or at least one paralog has decreased gene expression, or (3) at least two paralogs of a gene family are inversely regulated during cold acclimation.

4.6. Cytosolic Ribosomal Proteome Preparation

We obtained non-translating and translating ribosomal complexes using previously reported methods [49]. Due to the complexity of ribosome preparation and respective ribo-proteome analysis, we performed two experiments resulting in dataset 1 (DS1) and dataset 2 (DS2) respectively. Each dataset contained a pooled Arabidopsis Col-0 sample and either a pooled double mutant sample of *reil1-1 reil2-2* (*ds1*) or *reil1-1 reil2-1* (*ds2*) for a total of 4 biological replicates used for the pooled genotype statistical analyses. Samples prior to shift were compared to samples prepared at 7 days after 10 °C cold shift. Polysome extraction buffer [137,138] was used to lyse membranes and isolate ribosome complexes from frozen and ground plant tissue. The extracted ribosome complexes were loaded onto sterile ultracentrifuge tubes, thinwall polyallomer tubes of 14 mL volume and 14 × 89 mm dimensions (Beckman Coulter, Brea, CA, USA). Sucrose gradients were prepared from 15%, 30%, 45%, and 60% (w/v) stock solutions. Ultracentrifugation was 14.5 h at 33,000 rpm using an Optima LM-80 XP ultracentrifuge and SW 41 Ti rotor (Beckman Coulter, Brea, CA, USA). The ribosome complexes separated according to their sedimentation coefficient [139] into 40S, 60S, 80S and low oligomeric polysomal complexes that were sampled into separate

fractions monitoring rRNA absorbance at 254 nm wavelength. A programmable density gradient fractionation system was used (Teledyne Isco Inc., Lincoln, NE, USA). Resulting ribosome fractions were loaded onto regenerated cellulose membranes, Amicon Ultra-0.5 centrifugal filter units, with a 3-kDa molecular size cutoff (Merck, Kenilworth, NJ, USA). The filter units were washed iteratively with 500 μ L of 0.04 M Tris-HCL buffer (pH 8.4) with 0.2 M KCl and 0.1 M MgCl₂. Washing was repeated until the residual volume decreased to below 100 μ L within 10 min of centrifugation at the recommended 5000–7000 rpm and 4 °C. Volume reduction by centrifugation was timed to terminate washing because each of the fractions contained different percentages of sucrose and hence required varying numbers of cleaning steps. Cleaned fractions were digested with trypsin by filter-aided sample preparation (FASP) according to previously reported methods [140,141].

4.7. Proteome Analysis by Liquid Chromatography—Tandem Mass Spectrometry (LC-MS/MS)

Tryptic peptides were loaded onto an ACQUITY UPLC M-Class system (Waters Corporation, Milford, MA, USA) hyphenated with a Q-Exactive HF high-resolution mass spectrometer (Thermo Fisher Scientific, Waltham, MA, USA). For dataset 1 (DS1), samples were separated by reverse-phase nano-liquid chromatography using a 125 min gradient ramped from 3% to 85% acetonitrile (ACN). Mass spectrometry was performed by a data dependent top-N tandem mass spectrometry method (dd-MS2) that fragmented the top 10 most intense ions per full scan. Full scans were acquired at a resolution of 120,000 with automatic gain control (AGC) target set to 3×10^6 , maximum injection time 100 ms, scan range 300 to 1600 m/z in profile mode. Each dd-MS2 scan was recorded in profile mode at a resolution of 15,000 with AGC target set to 1×10^5 , maximum injection time 150 ms, isolation window of 1.2 m/z , normalized collision energy 27 eV and dynamic exclusion of 30 s. Settings of dataset 2 (DS2) were slightly modified. We used a 132 min gradient ramped from 3% to 85% ACN. The dd-MS2 method fragmented the top 15 most intense ions per full scan. Full scans were acquired at a resolution of 60,000 with AGC target set to 1×10^6 , maximum injection time 75 ms, and a scan range of 300 to 1600 m/z in profile mode. The dd-MS2 scans were recorded in profile mode at a resolution of 30,000 with AGC target set to 1×10^5 , maximum injection time 150 ms, isolation window of 1.4 m/z , normalized collision energy 27 eV and dynamic exclusion of 30 s. The mass spectrometry proteomics data have been deposited to the ProteomeXchange Consortium via the PRIDE partner repository [142] with the dataset identifier PXD016292.

4.8. Proteome Data Analyses

The initial tandem LC-MS/MS chromatogram files of raw data format were processed with the MaxQuant software (Version 1.6.0.16). We analyzed label-free quantitative peptide abundances [143] (LFQ) across all samples. Peptides were annotated with *Arabidopsis thaliana* FASTA files obtained from the UniProt database [144] that contained 15,893 proteins reviewed in the Swiss-Prot subsection. All peptides, including unique and redundant peptides of structural cytosolic ribosome proteins were used for the subsequent analyses. Independent LFQ matrices were created for each of the two experiments, DS1 and DS2. Each matrix contained all ribosome fractions of an *Arabidopsis Col-0* wild type to *reil1 reil2* double mutant comparison. Within the single fractions, the LFQ abundance of each small 40S subunit RP was normalized to the sum of abundances of all 40S SSU proteins. The LFQ abundance of each 60S subunit RP was normalized to the sum of abundances of all 60S LSU proteins per fraction, respectively. This normalization accounted for the varying amount of 40S SSU and 60S LSU subunits within each of the sucrose density fractions. After this normalization step, each cell in the resulting matrix (Table S3) represented the fraction of each individual RP within its total subunit, either 40S or 60S defined by the following equation:

$$NX_{ij} = X_{ij} / \sum [RPs]_i$$

where $\sum [RPs]_i$ represents the sum of abundances of structural RPs belonging to the 40S or 60S subunit per sample. Finally, matrices belonging to independent experiments were

merged yielding 149 potential structural RP paralogs or 123 RPs in total that were detectable in both experiments, DS1 and DS2. This matrix included non-unique peptides of paralog sets. As was observed with the transcript abundances of RPs, the distributions of protein abundances on average approximated normal distribution (Figure S2). Hence, GLM fitting with the Gaussian family of regression sufficed for statistical testing. We analyzed the fold changes between non-translational and polysomic fractions (Table S4) or within the acclimated versus non-acclimated polysomic fraction (Table S5) of each individual RP at day 7 after cold shift. The significance of substoichiometric RPs was tested using the three genotypes as joined validation for our statistics, namely, *dko1*, *dko2*, and Col-0. This decision provided robustness to our candidate selection and ensured that the significantly substoichiometric RPs are largely independent of REIL proteins.

4.9. Structural Analysis of Changes in Ribosome Protein or Transcript Abundance

Since there is currently no complete, highly resolved *Arabidopsis thaliana* ribosomal structure that is publicly available, the reference structure used for this project was that of the translating *Triticum aestivum* (common wheat) cytosolic ribosome, published in 2010 [145]. PDB entry in the RCSB databank [146] is 4V7E. This structure was generated through modeling of known RP structures from bacterial and archaeal templates onto a *Triticum aestivum* Cryo-EM ribosome map. This model is canonically complete and contains 47 RPs within the 60S LSU and 33 RPs of the 40S SSU subunit. Four rRNA structures, one t-RNA bounded to the P-site, and an mRNA transcript are included. It is important to note that the 5.5 Å resolution holds true for the best-resolved regions of the reference ribosome structure but resolution may locally vary. The in part low resolution of the Cryo-EM map was manually confirmed by visualization of selected regions at the Electron Microscopy Data Bank (EMDB), e.g., accession EMD-1780.

The methodology is divided into four steps: (1) initial structural data preprocessing, (2) proximity network building, (3) structural region sampling and definition, and (4) statistical testing of enriched relative changes within structural regions, and has been compiled in the GitHub repository COSNet; (https://github.com/MSeidelFed/COSNet_i, accessed on 30 April 2021). Code from this repository is written modularly, to reflect the steps of the methodology above, and is currently under development and testing to form a complete pipeline to encompass the entire workflow. To further explain the methodology: as preprocessing steps “Hetero atoms” (HETATMs) and duplicate atoms were removed from all proteins. Subsequently, the RP sequences were Blasted [147] to verify the correct annotation and renamed according to the last naming scheme [148]. Next, a proximity network was constructed of protein–protein interactions (based on structural proximity) omitting the rRNA, and based on a distance threshold of 8 Å [85] between individual amino acids coarse-grained to their center of gravity. Weights of this network’s edges were calculated as the proportion of inter-amino acid residue contacts between two proteins. A higher weight indicated a larger contact surface between two proteins. Networks were visualized using the R package *igraph* [149]. We sampled random regions from the proximity network defining a walk length and an iteration number. The weight of edges was used as transit probability (i.e., walking from x to y is written $P_{\{x,y\}} = w_{\{x,y\}} / \mathbf{w}_{\{x\}}$, where $\mathbf{w}_{\{x\}}$ represents the sum of all weights from the outgoing edges of node x). A consensus walk from the iteration was calculated and pre-regions defined for every start node. Finally, we calculated the minimum set cover that spans the whole edge universe while minimizing the number of overlapping regions. The Fisher exact test allowed us to test if the selected regions were significantly enriched as compared to the entire ribosome. The transcriptome or proteome significant changes were transformed into binary input (Table S6) where one equals significantly changed and zero not changed. The SciPy implementation of the Fisher’s exact test was used [150]. To counter the effects of multiple testing, the p values generated from Fisher’s exact test were adjusted via a strict, Bonferroni correction [88], and subsequently re-evaluated for significance.

4.10. Sequence Alignments

The coding sequence region of the nuclear encoded uL30_RPL7 gene RP family for the three taxa *Arabidopsis thaliana*, *Homo sapiens*, and *Saccharomyces cerevisiae* were aligned using the online Guidance2 Server [151–153]. The Bayesian inference analysis was performed in BEAST—v2.6.1 [154] and the parameters were assembled in Beauti, which is a part of the BEAST software package. The alignment was analyzed using a lognormal relaxed clock [155], a GTR + i model (as determined by the corrected AIC criteria in jModelTest 2.1.10 [156,157]—see Table S7), and a uniformly distributed Yule process speciation tree [158]. Markov chain Monte Carlo (MCMC) was set to 10,000,000 generations [159]; sampling was performed every 1000 generations and the burn-in set to 10%. The MCMC trace files generated were visualized in Tracer v1.7.1 [160], which presented statistical ESS summaries over 300 (Table S7). The TreeAnnotator tool from BEAST was used to combine all the log trees with a discarded burn-in of 10% into a single, maximum clade credibility tree, using common ancestor heights and a posterior probability of 0.5 [154]. FigTree [160] was used to visualize the final phylogenetic tree, the node labels were set to show the posterior probability values and the tree was re-rooted; *Saccharomyces cerevisiae* was set as the outgroup.

4.11. Software

Structural work was done using python scripts (Python programming language, RRID:SCR_008394) in a linux terminal through the enabler SmarTTY.

Fisher exact tests were executed in python 3: Jones, E., Oliphant, T., Peterson, P. & Others. SciPy.org. *SciPy: Open source scientific tools for Python2* (2001).

Structural visualization was enabled via PyMol [161]. (PyMOL, RRID:SCR_000305). PyMOL: The PyMOL Molecular Graphics System, Version 2.0 Schroedinger, LLC.

Transcriptome and proteome interactive data analyses were carried out in R [162,163]: R foundation for statistical computing, <https://www.R-project.org/>, accessed on 30 April 2021.

The following R packages were used (we report either a citation in the references or a link to the package website in this section):

- Ben Bolstad (2019). preprocessCore: A collection of pre-processing functions. R package version 1.46.0. Available online: <https://github.com/bmbolstad/preprocessCore> accessed on 30 April 2021.
- Ref. [164]. tidyverse: Easily Install and Load the ‘Tidyverse’. R package version 1.2.1.
- Ref. [165]. Reshaping Data with the reshape Package.
- Ref. [166]. stringr: Simple, Consistent Wrappers for Common String Operations. R package version 1.4.0.
- Ref. [133]. fitdistrplus: An R Package for Fitting Distributions.
- Ref. [167] ggplot2: Elegant Graphics for Data Analysis.
- Ref. [168] R package stringi: Character string processing facilities.
- Diethelm Wuertz, Tobias Setz and Yohan Chalabi (2017). timeSeries: Rmetrics—Financial Time Series Objects. R package version 3042.102. Available online: <https://CRAN.R-project.org/package=timeSeries> accessed on 30 April 2021.
- Ref. [169]. Complex heatmaps reveal patterns and correlations in multidimensional genomic data. Bioinformatics.
- Ref. [170]. Circlize implements and enhances circular visualization in R. Bioinformatics.
- Ref. [149] The igraph software package for complex network research.
- Ref. [171]. VennDiagram: Generate High-Resolution Venn and Euler Plots. R package version 1.6.20.
- Jan Graffelman (2013). calibrate: Calibration of Scatterplot and Biplot Axes. R package version 1.7.2. Available online: <https://CRAN.R-project.org/package=calibrate> accessed on 30 April 2021.
- Diethelm Wuertz, Tobias Setz and Yohan Chalabi (2017). fBasics: Rmetrics—Markets and Basic Statistics. R package version 3042.89. Available online: <https://CRAN.R-project.org/package=fBasics> accessed on 30 April 2021.

5. Conclusions

A ribosome biogenesis transcriptional response is triggered 1 day after plants experience cold suboptimal temperature. The response is followed by differential accumulation of RP transcripts and proteoforms 7 days after the initial cue. The outcome is altered RP stoichiometry in non-translational and low-oligomeric translational ribosomal fractions. The divergent ribosomal populations arising during cold present altered stoichiometry around the PET, both in *Arabidopsis* wild type and two independent *reil* double knock out genotypes. Thus, altered stoichiometry of the PET might be a typical cold response triggered during early biogenesis and could explain why REIL proteins are absolutely necessary only during cold to mature competent 60S subunits. In alignment with the former statement, uL30s are depleted from active translating polysomes in *Arabidopsis* during cold. In yeast, uL30 depletion causes PET-altered stoichiometry. Thus, supported by the functional roles and sequence alignments of uL30, we suggest that these two events are linked in the context of cold acclimation. After REIL action, the P-Stalk is assembled and altered stoichiometry is observed in the P-Stalk at the transcriptome level during early biogenesis. Further experiments are needed to verify the P-Stalk remodeling at the proteome level. We propose that REIL proteins could enable maturation of PET-remodeled LSUs that lead toward ribosome specialization supported in subsequent direct or indirect REIL actions upon the P-Stalk and ribosomal head substructures.

Supplementary Materials: The following are available online at <https://www.mdpi.com/article/10.3390/ijms22116160/s1>.

Author Contributions: Literature research, F.M.-S., J.K., A.A.P.F.; cytosolic ribosomal proteome optimization, F.M.-S., O.B.-G.; optimization of growth method F.M.-S., O.B.-G., E.V.J.-P., K.E.E.; dry weight measurements, F.M.-S., E.V.J.-P.; R-scripting for proteome and transcriptome data analyses, F.M.-S., E.V.J.-P.; figures shaping F.M.-S., O.B.-G., Y.-C.H., J.K., A.A.P.F.; statistics, F.M.-S., Y.-C.H., D.W., J.K.; phylogenetic tree construction and interpretation, F.M.-S., K.E.E.; development of ribosomal structural analyses, F.M.-S., Y.-C.H., D.W., J.K.; structural analysis, F.M.-S., Y.-C.H.; formatting, F.M.-S., O.B.-G., U.R., J.K., A.A.P.F.; manuscript writing and shaping F.M.-S., U.R., J.K., A.A.P.F., A.S.; proteomics data interpretation, F.M.-S., A.S., M.G., O.B.-G.; Shotgun proteomics, proteome annotation and data pre-processing, M.G.; microarray transcriptome experiment, O.B.-G., B.-E.C., U.R. All authors have read and agreed to the published version of the manuscript.

Funding: All authors would like to acknowledge the Max-Planck Society (Max Planck Institute of Molecular Plant Physiology). F.M.-S. would like also to acknowledge the University of Melbourne for funding his research via the Melbourne-Potsdam PhD Programme (MelPoPP). Y.H. would like also to acknowledge UiT The Arctic University of Norway for funding her work.

Data Availability Statement: The expression data sets are available from the Gene Expression Omnibus (<https://www.ncbi.nlm.nih.gov/geo/>, accessed on 30 April 2021) through accession GSE144916. The mass spectrometry proteomics data have been previously deposited to the ProteomeXchange Consortium via the PRIDE partner repository [142] with the dataset identifier PXD016292.

Acknowledgments: We acknowledge the long-standing support by L. Willmitzer, M. Stitt, and R. Bock (Max-Planck Institute of Molecular Plant Physiology, Potsdam, Germany). F.M.-S. acknowledges the Max-Planck Society (Max Planck Institute of Molecular Plant Physiology) and The University of Melbourne for funding his research via the Melbourne-Potsdam PhD Programme (MelPoPP). Y.H. would like to acknowledge and thank Aalt-Jan van Dijk (Wageningen University & Research) for his supervision and support in this work.

Conflicts of Interest: The authors declare no conflict of interest. The funders had no role in the design of the study; in the collection, analyses, or interpretation of data; in the writing of the manuscript, or in the decision to publish the results.

References

1. Weis, B.L.; Kovacevic, J.; Missbach, S.; Schleiff, E. Plant-Specific Features of Ribosome Biogenesis. *Trends Plant Sci.* **2015**, *20*, 729–740. [[CrossRef](#)]
2. Palm, D.; Streit, D.; Shanmugam, T.; Weis, B.L.; Ruprecht, M.; Simm, S.; Schleiff, E. Plant-specific ribosome biogenesis factors in *Arabidopsis thaliana* with essential function in rRNA processing. *Nucleic Acids Res.* **2019**, *47*, 1880–1895. [[CrossRef](#)]
3. Sáez-Vásquez, J.; Delseny, M. Ribosome biogenesis in plants: From functional 45S ribosomal DNA organization to ribosome assembly factors. *Plant Cell* **2019**, *31*, 1945–1967. [[CrossRef](#)]
4. Barakat, A.; Szick-Miranda, K.; Chang, I.F.; Guyot, R.; Blanc, G.; Cooke, R.; Delseny, M.; Bailey-Serres, J. The organization of cytoplasmic ribosomal protein genes in the *Arabidopsis* genome. *Plant Physiol.* **2001**, *127*, 398–415. [[CrossRef](#)]
5. Delaunay, J.; Creusot, F.; Schapira, G. Evolution of ribosomal proteins. *Eur. J. Biochem.* **1973**, *39*, 305–312. [[CrossRef](#)]
6. Wang, Y.; Wang, X.; Paterson, A.H. Genome and gene duplications and gene expression divergence: A view from plants. *Ann. N. Y. Acad. Sci.* **2012**, *1256*, 1–14. [[CrossRef](#)]
7. Braasch, I.; Bobe, J.; Guiguen, Y.; Postlethwait, J.H. Reply to: ‘Subfunctionalization versus neofunctionalization after whole-genome duplication’. *Nat. Genet.* **2018**, *50*, 910–911. [[CrossRef](#)]
8. Gerst, J.E. Pimp My Ribosome: Ribosomal Protein Paralogs Specify Translational Control. *Trends Genet.* **2018**, *34*, 832–845. [[CrossRef](#)]
9. Komili, S.; Farny, N.G.; Roth, F.P.; Silver, P.A. Functional Specificity among Ribosomal Proteins Regulates Gene Expression. *Cell* **2007**, *131*, 557–571. [[CrossRef](#)]
10. Genuth, N.R.; Barna, M. Heterogeneity and specialized functions of translation machinery: From genes to organisms. *Nat. Rev. Genet.* **2018**, *19*, 431–452. [[CrossRef](#)]
11. Bates, C.; Hubbard, S.J.; Ashe, M.P. Ribosomal flavours: An acquired taste for specific mRNAs? *Biochem. Soc. Trans.* **2018**, *46*, 1529–1539. [[CrossRef](#)]
12. Shi, Z.; Fujii, K.; Kovary, K.M.; Genuth, N.R.; Röst, H.L.; Teruel, M.N.; Barna, M. Heterogeneous Ribosomes Preferentially Translate Distinct Subpools of mRNAs Genome-wide. *Mol. Cell* **2017**, *67*, 71–83.e7. [[CrossRef](#)]
13. Hopes, T.; Agapiou, M.; Norris, K.; McCarthy, C.G.P.; O’Connell, M.J.; Fontana, J.; Aspden, J.L. Specialisation of ribosomes in gonads through paralog-switching. *bioRxiv* **2020**. [[CrossRef](#)]
14. Bailey-Serres, J. Selective translation of cytoplasmic mRNAs in plants. *Trends Plant Sci.* **1999**, *4*, 142–148. [[CrossRef](#)]
15. Browning, K.S.; Bailey-Serres, J. Mechanism of Cytoplasmic mRNA Translation. *Arab. Book* **2015**, *13*, e0176. [[CrossRef](#)]
16. Kawaguchi, R.; Girke, T.; Bray, E.A.; Bailey-Serres, J. Differential mRNA translation contributes to gene regulation under non-stress and dehydration stress conditions in *Arabidopsis thaliana*. *Plant J.* **2004**, *38*, 823–839. [[CrossRef](#)]
17. Nicolai, M.; Roncato, M.A.; Canoy, A.S.; Rouquié, D.; Sarda, X.; Freyssinet, G.; Robaglia, C. Large-scale analysis of mRNA translation states during sucrose starvation in *Arabidopsis* cells identifies cell proliferation and chromatin structure as targets of translational control. *Plant Physiol.* **2006**, *141*, 663–673. [[CrossRef](#)] [[PubMed](#)]
18. Moeller, J.R.; Moscou, M.J.; Bancroft, T.; Skadsen, R.W.; Wise, R.P.; Whitham, S.A. Differential accumulation of host mRNAs on polyribosomes during obligate pathogen-plant interactions. *Mol. Biosyst.* **2012**, *8*, 2153–2165. [[CrossRef](#)]
19. Ueda, K.; Matsuura, H.; Yamaguchi, M.; Demura, T.; Kato, K. Genome-wide analyses of changes in translation state caused by elevated temperature in *Oryza sativa*. *Plant Cell Physiol.* **2012**, *53*, 1481–1491. [[CrossRef](#)]
20. Matsuura, H.; Ishibashi, Y.; Shinmyo, A.; Kanaya, S.; Kato, K. Genome-wide analyses of early translational responses to elevated temperature and high salinity in *Arabidopsis thaliana*. *Plant Cell Physiol.* **2010**, *51*, 448–462. [[CrossRef](#)]
21. Branco-Price, C.; Kaiser, K.A.; Jang, C.J.H.; Larive, C.K.; Bailey-Serres, J. Selective mRNA translation coordinates energetic and metabolic adjustments to cellular oxygen deprivation and reoxygenation in *Arabidopsis thaliana*. *Plant J.* **2008**, *56*, 743–755. [[CrossRef](#)]
22. Branco-Price, C.; Kawaguchi, R.; Ferreira, R.B.; Bailey-Serres, J. Genome-wide analysis of transcript abundance and translation in *Arabidopsis* seedlings subjected to oxygen deprivation. *Ann. Bot.* **2005**, *96*, 647–660. [[CrossRef](#)] [[PubMed](#)]
23. Mastroph, A.; Zanetti, M.E.; Jang, C.J.H.; Holtan, H.E.; Repetti, P.P.; Galbraith, D.W.; Girke, T.; Bailey-Serres, J. Profiling translationalomes of discrete cell populations resolves altered cellular priorities during hypoxia in *Arabidopsis*. *Proc. Natl. Acad. Sci. USA* **2009**, *106*, 18843–18848. [[CrossRef](#)] [[PubMed](#)]
24. Juntawong, P.; Bailey-Serres, J. Dynamic light regulation of translation status in *Arabidopsis thaliana*. *Front. Plant Sci.* **2012**, *3*, 66. [[CrossRef](#)] [[PubMed](#)]
25. Wu, S.H.; Liu, M.J.; Wu, S.H.; Chen, H.M. Widespread translational control contributes to the regulation of *Arabidopsis* photomorphogenesis. *Mol. Syst. Biol.* **2012**, *8*, 566. [[CrossRef](#)]
26. Liberman, N.; O’Brown, Z.K.; Earl, A.S.; Boulias, K.; Gerashchenko, M.V.; Wang, S.Y.; Fritsche, C.; Fady, P.E.; Dong, A.; Gladyshev, V.N.; et al. N6-adenosine methylation of ribosomal RNA affects lipid oxidation and stress resistance. *Sci. Adv.* **2020**, *6*, eaaz4370. [[CrossRef](#)]
27. Jha, S.; Rollins, M.G.; Fuchs, G.; Procter, D.J.; Hall, E.A.; Cozzolino, K.; Sarnow, P.; Savas, J.N.; Walsh, D. Trans-kingdom mimicry underlies ribosome customization by a poxvirus kinase. *Nature* **2017**, *546*, 651–655. [[CrossRef](#)]
28. Thompson, M.K.; Rojas-Duran, M.F.; Gangaramani, P.; Gilbert, W.V. The ribosomal protein Asc1/RACK1 is required for efficient translation of short mRNAs. *eLife* **2016**, *5*, e11154. [[CrossRef](#)]

29. Sormani, R.; Delannoy, E.; Lageix, S.; Bitton, F.; Lanet, E.; Saez-Vasquez, J.; Deragon, J.M.; Renou, J.P.; Robaglia, C. Sublethal cadmium intoxication in *Arabidopsis thaliana* impacts translation at multiple levels. *Plant Cell Physiol.* **2011**, *52*, 436–447. [[CrossRef](#)]
30. Simsek, D.; Tiu, G.C.; Flynn, R.A.; Byeon, G.W.; Leppek, K.; Xu, A.F.; Chang, H.Y.; Barna, M. The Mammalian Ribo-interactome Reveals Ribosome Functional Diversity and Heterogeneity. *Cell* **2017**, *169*, 1051–1065.e18. [[CrossRef](#)]
31. Boex-Fontvieille, E.; Daventure, M.; Jossier, M.; Zivy, M.; Hodges, M.; Tcherkez, G. Photosynthetic Control of Arabidopsis Leaf Cytoplasmic Translation Initiation by Protein Phosphorylation. *PLoS ONE* **2013**, *8*, e70692. [[CrossRef](#)]
32. Garcia-Molina, A.; Kleine, T.; Schneider, K.; Mühlhaus, T.; Lehmann, M.; Leister, D. Translational Components Contribute to Acclimation Responses to High Light, Heat, and Cold in Arabidopsis. *iScience* **2020**, *23*, 101331. [[CrossRef](#)]
33. Martinez-Seidel, F.; Beine-Golovchuk, O.; Hsieh, Y.C.; Kopka, J. Systematic review of plant ribosome heterogeneity and specialization. *Front. Plant Sci.* **2020**, *11*, 948. [[CrossRef](#)]
34. Beine Golovchuk, O.; Firmino, A.A.P.; Dąbrowska, A.; Schmidt, S.; Erban, A.; Walther, D.; Zuther, E.; Hinch, D.K.; Kopka, J. Plant temperature acclimation and growth rely on cytosolic ribosome biogenesis factor homologs. *Plant Physiol.* **2018**, *176*, 2251–2276. [[CrossRef](#)]
35. Calixto, C.P.G.; Guo, W.; James, A.B.; Tzioutziou, N.A.; Entizne, J.C.; Panter, P.E.; Knight, H.; Nimmo, H.G.; Zhang, R.; Brown, J.W.S. Rapid and dynamic alternative splicing impacts the Arabidopsis cold response transcriptome. *Plant Cell* **2018**, *30*, 1424–1444. [[CrossRef](#)]
36. Martinez-Seidel, F.; Suwanchaikasem, P.; Nie, S.; Leeming, M.G.; Firmino, A.A.P.; Williamson, N.A.; Kopka, J.; Roessner, U.; Boughton, B.A. Membrane-Enriched Proteomics Link Ribosome Accumulation and Proteome Reprogramming With Cold Acclimation in Barley Root Meristems. *Front. Plant Sci.* **2021**, *12*. [[CrossRef](#)]
37. Seki, M.; Narusaka, M.; Ishida, J.; Nanjo, T.; Fujita, M.; Oono, Y.; Kamiya, A.; Nakajima, M.; Enju, A.; Sakurai, T.; et al. Monitoring the expression profiles of 7000 Arabidopsis genes under drought, cold and high-salinity stresses using a full-length cDNA microarray. *Plant J.* **2002**, *31*, 279–292. [[CrossRef](#)]
38. Cheong, B.E.; Beine-Golovchuk, O.; Gorka, M.; Ho, W.W.H.; Martinez-Seidel, F.; Firmino, A.A.P.; Skirycz, A.; Roessner, U.; Kopka, J. Arabidopsis REI-LIKE proteins activate ribosome biogenesis during cold acclimation. *Sci. Rep.* **2021**, *11*, 1–25. [[CrossRef](#)]
39. Schmidt, S.; Dethloff, F.; Beine-Golovchuk, O.; Kopka, J. The REIL1 and REIL2 proteins of Arabidopsis thaliana are required for leaf growth in the cold. *Plant Physiol.* **2013**, *163*, 1623–1639. [[CrossRef](#)]
40. Beine-Golovchuk, O. Characterization and Functional Complementation of the Arabidopsis Ribosomal Reil1-1Reil2-1 Double Mutant. Ph.D. Thesis, University of Potsdam, Potsdam, Germany, 2016.
41. Greber, B.J.; Gerhardy, S.; Leitner, A.; Leibundgut, M.; Salem, M.; Böhringer, D.; Leulliot, N.; Aebersold, R.; Panse, V.G.; Ban, N. Insertion of the Biogenesis Factor Rei1 Probes the Ribosomal Tunnel during 60S Maturation. *Cell* **2016**, *164*, 91–102. [[CrossRef](#)]
42. Meyer, A.E.; Hoover, L.A.; Craig, E.A. The cytosolic J-protein, Jj1, and Rei1 function in the removal of the Pre-60 S subunit factor Arx1. *J. Biol. Chem.* **2010**, *285*, 961–968. [[CrossRef](#)]
43. Yu, H.; Kong, X.; Huang, H.; Wu, W.; Park, J.; Yun, D.J.; Lee, B.H.; Shi, H.; Zhu, J.K. STCH4/REIL2 Confers Cold Stress Tolerance in Arabidopsis by Promoting rRNA Processing and CBF Protein Translation. *Cell Rep.* **2020**, *30*, 229–242.e5. [[CrossRef](#)]
44. Klingauf-Nerurkar, P.; Gillet, L.C.; Portugal-Calisto, D.; Oborská-Oplová, M.; Jäger, M.; Schubert, O.T.; Pisano, A.; Peña, C.; Rao, S.; Altvater, M.; et al. The gtpase nog1 co-ordinates the assembly, maturation and quality control of distant ribosomal functional centers. *eLife* **2020**, *9*, e52474. [[CrossRef](#)]
45. Zhou, Y.; Musalgaonkar, S.; Johnson, A.W.; Taylor, D.W. Tightly-orchestrated rearrangements govern catalytic center assembly of the ribosome. *Nat. Commun.* **2019**, *10*, 1–11. [[CrossRef](#)] [[PubMed](#)]
46. Gamalinda, M.; Jakovljevic, J.; Babiano, R.; Talkish, J.; De La Cruz, J.; Woolford, J.L., Jr. Yeast polypeptide exit tunnel ribosomal proteins L17, L35 and L37 are necessary to recruit late-assembling factors required for 27SB pre-rRNA processing. *Nucleic Acids Res.* **2013**, *41*, 1965–1983. [[CrossRef](#)]
47. Wilson, D.M.; Li, Y.; LaPeruta, A.; Gamalinda, M.; Gao, N.; Woolford, J.L. Structural insights into assembly of the ribosomal nascent polypeptide exit tunnel. *Nat. Commun.* **2020**, *11*, 1–15. [[CrossRef](#)]
48. Nakata, M.T.; Sato, M.; Wakazaki, M.; Sato, N.; Kojima, K.; Sekine, A.; Nakamura, S.; Shikanai, T.; Toyooka, K.; Tsukaya, H.; et al. Plastid translation is essential for lateral root stem cell patterning in Arabidopsis thaliana. *Biol. Open* **2018**, *7*. [[CrossRef](#)]
49. Firmino, A.A.P.; Gorka, M.; Graf, A.; Skirycz, A.; Martinez-Seidel, F.; Zander, K.; Kopka, J.; Beine-Golovchuk, O. Separation and paired proteome profiling of plant chloroplast and cytoplasmic ribosomes. *Plants* **2020**, *9*, 892. [[CrossRef](#)]
50. Erban, A.; Martinez-Seidel, F.; Rajarathinam, Y.; Dethloff, F.; Orf, I.; Fehrl, I.; Alpers, J.; Beine-Golovchuk, O.; Kopka, J. Multiplexed Profiling and Data Processing Methods to Identify Temperature-Regulated Primary Metabolites Using Gas Chromatography Coupled to Mass Spectrometry. In *Methods in Molecular Biology*; Hinch, D.K., Zuther, E., Eds.; Springer: New York, NY, USA, 2020; Volume 2156, pp. 203–239. ISBN 978-1-0716-0660-5.
51. Ashraf, M.A.; Rahman, A. Cold stress response in Arabidopsis thaliana is mediated by GNOM ARF-GEF. *Plant J.* **2019**, *97*, 500–516. [[CrossRef](#)]
52. Kaspar, T.C.; Bland, W.L. Soil temperature and root growth. *Soil Sci.* **1992**, *154*, 290–299. [[CrossRef](#)]
53. Levitt, J. *Responses of Plants to Environmental Stresses: Chilling, Freezing, and High Temperature Stresses*; Academic Press: New York, NY, USA; London, UK, 1980; Volume 1.

54. Hinch, D.K.; Zuther, E. Introduction: Plant Cold Acclimation and Winter Survival. In *Methods in Molecular Biology*; Hinch, D.K., Zuther, E., Eds.; Springer: New York, NY, USA, 2020; Volume 2156, pp. 1–7. ISBN 978-1-0716-0660-5.
55. Boyes, D.C.; Zayed, A.M.; Ascenzi, R.; McCaskill, A.J.; Hoffman, N.E.; Davis, K.R.; Görlach, J. Growth Stage-Based Phenotypic Analysis of Arabidopsis: A Model for High Throughput Functional Genomics in Plants. *Plant Cell* **2001**, *13*, 1499–1510. [[CrossRef](#)]
56. Williams, M.E.; Sussex, I.M. Developmental regulation of ribosomal protein L16 genes in Arabidopsis thaliana. *Plant J.* **1995**, *8*, 65–76. [[CrossRef](#)]
57. Horiguchi, G.; Van Lijsebettens, M.; Candela, H.; Micoli, J.L.; Tsukaya, H. Ribosomes and translation in plant developmental control. *Plant Sci.* **2012**, *191–192*, 24–34. [[CrossRef](#)]
58. Hernández-Hermenegildo, R.A.; Bernal, L.; Jiménez-Pérez, L.V.; Bernal-Lugo, I.; de Jiménez, E.S. Ribosomal Heterogeneity of Maize Tissues: Insights of Biological Relevance. *Plant Mol. Biol. Rep.* **2018**, *36*, 491–499. [[CrossRef](#)]
59. Armache, J.P.; Jarasch, A.; Anger, A.M.; Villa, E.; Becker, T.; Bhushan, S.; Jossinet, F.; Habeck, M.; Dindar, G.; Franckenberg, S.; et al. Localization of eukaryote-specific ribosomal proteins in a 5.5-Å cryo-EM map of the 80S eukaryotic ribosome. *Proc. Natl. Acad. Sci. USA* **2010**, *107*, 19754–19759. [[CrossRef](#)] [[PubMed](#)]
60. Piques, M.; Schulze, W.X.; Höhne, M.; Usadel, B.; Gibon, Y.; Rohwer, J.; Stitt, M. Ribosome and transcript copy numbers, polysome occupancy and enzyme dynamics in Arabidopsis. *Mol. Syst. Biol.* **2009**, *5*, 314. [[CrossRef](#)] [[PubMed](#)]
61. Maldonado-Bonilla, L.D. Composition and function of P bodies in Arabidopsis thaliana. *Front. Plant Sci.* **2014**, *5*, 201. [[CrossRef](#)]
62. Jang, G.J.; Yang, J.Y.; Hsieh, H.L.; Wu, S.H. Processing bodies control the selective translation for optimal development of Arabidopsis young seedlings. *Proc. Natl. Acad. Sci. USA* **2019**, *116*, 6451–6456. [[CrossRef](#)]
63. Eraslan, B.; Wang, D.; Gusic, M.; Prokisch, H.; Hallström, B.M.; Uhlén, M.; Asplund, A.; Pontén, F.; Wieland, T.; Hopf, T.; et al. Quantification and discovery of sequence determinants of protein-per-mRNA amount in 29 human tissues. *Mol. Syst. Biol.* **2019**, *15*, e8513. [[CrossRef](#)]
64. Zimmermann, P.; Hirsch-Hoffmann, M.; Hennig, L.; Gruissem, W. GENEVESTIGATOR. Arabidopsis microarray database and analysis toolbox. *Plant Physiol.* **2004**, *136*, 2621–2632. [[CrossRef](#)]
65. McKown, R.; Kuroki, G.; Warren, G. Cold responses of Arabidopsis mutants impaired in freezing tolerance. *J. Exp. Bot.* **1996**, *47*, 1919–1925. [[CrossRef](#)]
66. Lee, B.H.; Henderson, D.A.; Zhu, J.K. The Arabidopsis cold-responsive transcriptome and its regulation by ICE1. *Plant Cell* **2005**, *17*, 3155–3175. [[CrossRef](#)]
67. Hannah, M.A.; Wiese, D.; Freund, S.; Fiehn, O.; Heyer, A.G.; Hinch, D.K. Natural genetic variation of freezing tolerance in Arabidopsis. *Plant Physiol.* **2006**, *142*, 98–112. [[CrossRef](#)]
68. Chiba, Y.; Mineta, K.; Hirai, M.Y.; Suzuki, Y.; Kanaya, S.; Takahashi, H.; Onouchi, H.; Yamaguchi, J.; Naito, S. Changes in mRNA stability associated with cold stress in Arabidopsis cells. *Plant Cell Physiol.* **2013**, *54*, 180–194. [[CrossRef](#)]
69. Maeda, H.; DellaPenna, D. Tocopherol functions in photosynthetic organisms. *Curr. Opin. Plant Biol.* **2007**, *10*, 260–265. [[CrossRef](#)] [[PubMed](#)]
70. Hannah, M.A.; Heyer, A.G.; Hinch, D.K. A global survey of gene regulation during cold acclimation in Arabidopsis thaliana. *PLoS Genet.* **2005**, *1*, e26. [[CrossRef](#)]
71. Kilian, J.; Whitehead, D.; Horak, J.; Wanke, D.; Weinl, S.; Batistic, O.; D’Angelo, C.; Bornberg-Bauer, E.; Kudla, J.; Harter, K. The AtGenExpress global stress expression data set: Protocols, evaluation and model data analysis of UV-B light, drought and cold stress responses. *Plant J.* **2007**, *50*, 347–363. [[CrossRef](#)] [[PubMed](#)]
72. Vogel, J.T.; Zarka, D.G.; Van Buskirk, H.A.; Fowler, S.G.; Thomashow, M.F. Roles of the CBF2 and ZAT12 transcription factors in configuring the low temperature transcriptome of Arabidopsis. *Plant J.* **2005**, *41*, 195–211. [[CrossRef](#)]
73. Juntawong, P.; Sorenson, R.; Bailey-Serres, J. Cold shock protein 1 chaperones mRNAs during translation in Arabidopsis thaliana. *Plant J.* **2013**, *74*, 1016–1028. [[CrossRef](#)]
74. Rihan, H.Z.; Al-Issawi, M.; Fuller, M.P. Advances in physiological and molecular aspects of plant cold tolerance. *J. Plant Interact.* **2017**, *12*, 143–157. [[CrossRef](#)]
75. Missbach, S.; Weis, B.L.; Martin, R.; Simm, S.; Bohnsack, M.T.; Schleiff, E. 40S Ribosome Biogenesis Co-Factors Are Essential for Gametophyte and Embryo Development. *PLoS ONE* **2013**, *8*, e54084. [[CrossRef](#)] [[PubMed](#)]
76. Palm, D.; Simm, S.; Darm, K.; Weis, B.L.; Ruprecht, M.; Schleiff, E.; Scharf, C. Proteome distribution between nucleoplasm and nucleolus and its relation to ribosome biogenesis in Arabidopsis thaliana. *RNA Biol.* **2016**, *13*, 441–454. [[CrossRef](#)] [[PubMed](#)]
77. Gasse, L.; Flemming, D.; Hurt, E. Coordinated Ribosomal ITS2 RNA Processing by the Las1 Complex Integrating Endonuclease, Polynucleotide Kinase, and Exonuclease Activities. *Mol. Cell* **2015**, *60*, 808–815. [[CrossRef](#)] [[PubMed](#)]
78. Hang, R.; Wang, Z.; Deng, X.; Liu, C.; Yan, B.; Yang, C.; Song, X.; Mo, B.; Cao, X. Ribosomal RNA Biogenesis and Its Response to Chilling Stress in *Oryza sativa*. *Plant Physiol.* **2018**, *177*, 381–397. [[CrossRef](#)] [[PubMed](#)]
79. Liu, G.; Yan, P.; Du, Q.; Wang, Y.; Guo, Y.; Fu, Z.; Wang, H.; Tang, J. Pre-rRNA processing and its response to temperature stress in maize. *J. Exp. Bot.* **2020**, *71*, 1363–1374. [[CrossRef](#)]
80. Jiang, J.; Seo, H.; Chow, C.S. Post-transcriptional Modifications Modulate rRNA Structure and Ligand Interactions. *Acc. Chem. Res.* **2016**, *49*, 893–901. [[CrossRef](#)]
81. Yin, C.; Yau, S.S.T. A coevolution analysis for identifying protein-protein interactions by Fourier transform. *PLoS ONE* **2017**, *12*, e0174862. [[CrossRef](#)]
82. Maekawa, S.; Yanagisawa, S. Nucleolar stress and sugar response in plants. *Plant Signal. Behav.* **2018**, *13*, e1442975. [[CrossRef](#)]

83. Ben-Shem, A.; De Loubresse, N.G.; Melnikov, S.; Jenner, L.; Yusupova, G.; Yusupov, M. The structure of the eukaryotic ribosome at 3.0 Å resolution. *Science* **2011**, *334*, 1524–1529. [[CrossRef](#)]
84. Woolford, J.L.; Baserga, S.J. Ribosome biogenesis in the yeast *Saccharomyces cerevisiae*. *Genetics* **2013**, *195*, 643–681. [[CrossRef](#)] [[PubMed](#)]
85. Ezkurdia, I.; Graña, O.; Izarzugaza, J.M.G.; Tress, M.L. Assessment of domain boundary predictions and the prediction of intramolecular contacts in CASP8. *Proteins Struct. Funct. Bioinform.* **2009**, *77*, 196–209. [[CrossRef](#)]
86. Lury, D.A. Statistical Methods for Research Workers. *J. R. Stat. Soc. Ser. D Stat.* **1972**, *21*, 229. [[CrossRef](#)]
87. Fisher, R.A. Statistical Methods for Research Workers. *Biometrics* **1971**, *27*, 1106. [[CrossRef](#)]
88. Bland, J.M.; Altman, D.G. Multiple significance tests: The Bonferroni method. *BMJ* **1995**, *310*, 170. [[CrossRef](#)] [[PubMed](#)]
89. Timsit, Y.; Sergeant-Perthuis, G.; Bennequin, D. Evolution of ribosomal protein network architectures. *Sci. Rep.* **2021**, *11*, 1–13. [[CrossRef](#)]
90. Timsit, Y.; Bennequin, D. Nervous-like circuits in the ribosome facts, hypotheses and perspectives. *Int. J. Mol. Sci.* **2019**, *20*, 2911. [[CrossRef](#)]
91. Poirot, O.; Timsit, Y. Neuron-Like Networks between Ribosomal Proteins Within the Ribosome. *Sci. Rep.* **2016**, *6*, 26485. [[CrossRef](#)]
92. Rhodin, M.H.J.; Dinman, J.D. An extensive network of information flow through the B1b/c intersubunit bridge of the yeast ribosome. *PLoS ONE* **2011**, *6*, e20048. [[CrossRef](#)]
93. Meskauskas, A.; Dinman, J.D. A molecular clamp ensures allosteric coordination of peptidyltransfer and ligand binding to the ribosomal A-site. *Nucleic Acids Res.* **2010**, *38*, 7800–7813. [[CrossRef](#)]
94. Armache, J.P.; Anger, A.M.; Márquez, V.; Franckenberg, S.; Fröhlich, T.; Villa, E.; Berninghausen, O.; Thomm, M.; Arnold, G.J.; Beckmann, R.; et al. Promiscuous behaviour of archaeal ribosomal proteins: Implications for eukaryotic ribosome evolution. *Nucleic Acids Res.* **2013**, *41*, 1284–1293. [[CrossRef](#)]
95. Bowman, J.C.; Petrov, A.S.; Frenkel-Pinter, M.; Penev, P.I.; Williams, L.D. Root of the Tree: The Significance, Evolution, and Origins of the Ribosome. *Chem. Rev.* **2020**, *120*, 4848–4878. [[CrossRef](#)] [[PubMed](#)]
96. Bernier, C.R.; Petrov, A.S.; Kovacs, N.A.; Penev, P.I.; Williams, L.D. Translation: The universal structural core of life. *Mol. Biol. Evol.* **2018**, *35*, 2065–2076. [[CrossRef](#)] [[PubMed](#)]
97. Parker, M.S.; Sah, R.; Balasubramaniam, A.; Sallee, F.R.; Park, E.A.; Parker, S.L. On the expansion of ribosomal proteins and RNAs in eukaryotes. *Amino Acids* **2014**, *46*, 1589–1604. [[CrossRef](#)]
98. Parker, M.S.; Balasubramaniam, A.; Parker, S.L. On the segregation of protein ionic residues by charge type. *Amino Acids* **2012**, *43*, 2231–2247. [[CrossRef](#)]
99. Melnikov, S.; Manakongtreecheep, K.; Söll, D. Revising the structural diversity of ribosomal proteins across the three domains of life. *Mol. Biol. Evol.* **2018**, *35*, 1588–1598. [[CrossRef](#)]
100. Evangelisti, A.M.; Conant, G.C. Nonrandom survival of gene conversions among yeast ribosomal proteins duplicated through genome doubling. *Genome Biol. Evol.* **2010**, *2*, 826–834. [[CrossRef](#)]
101. Petibon, C.; Parenteau, J.; Catala, M.; Elela, S.A. Introns regulate the production of ribosomal proteins by modulating splicing of duplicated ribosomal protein genes. *Nucleic Acids Res.* **2016**, *44*, 3878–3891. [[CrossRef](#)]
102. Briggs, J.W.; Dinman, J.D. Subtractional Heterogeneity: A Crucial Step toward Defining Specialized Ribosomes. *Mol. Cell* **2017**, *67*, 3–4. [[CrossRef](#)]
103. Agozzino, L.; Dill, K.A. Protein evolution speed depends on its stability and abundance and on chaperone concentrations. *Proc. Natl. Acad. Sci. USA* **2018**, *115*, 9092–9097. [[CrossRef](#)]
104. Privalov, P.L. Cold denaturation of protein. *Crit. Rev. Biochem. Mol. Biol.* **1990**, *25*, 281–306. [[CrossRef](#)] [[PubMed](#)]
105. Graziano, G. On the mechanism of cold denaturation. *Phys. Chem. Chem. Phys.* **2014**, *16*, 21755–21767. [[CrossRef](#)]
106. Dias, C.L.; Ala-Nissila, T.; Wong-ekkabut, J.; Vattulainen, I.; Grant, M.; Karttunen, M. The hydrophobic effect and its role in cold denaturation. *Cryobiology* **2010**, *60*, 91–99. [[CrossRef](#)]
107. Sanfelice, D.; Temussi, P.A. Cold denaturation as a tool to measure protein stability. *Biophys. Chem.* **2016**, *208*, 4–8. [[CrossRef](#)] [[PubMed](#)]
108. Balcerak, A.; Trebinska-Stryjewska, A.; Konopinski, R.; Wakula, M.; Grzybowska, E.A. RNA-protein interactions: Disorder, moonlighting and junk contribute to eukaryotic complexity. *Open Biol.* **2019**, *9*, 190096. [[CrossRef](#)] [[PubMed](#)]
109. Timsit, Y.; Acosta, Z.; Allemand, F.; Chiaruttini, C.; Springer, M. The role of disordered ribosomal protein extensions in the early steps of eubacterial 50 S ribosomal subunit assembly. *Int. J. Mol. Sci.* **2009**, *10*, 817–834. [[CrossRef](#)]
110. Tutuncuoglu, B.; Jakovljevic, J.; Wu, S.; Gao, N.; Woolford, J.L. The N-terminal extension of yeast ribosomal protein L8 is involved in two major remodeling events during late nuclear stages of 60S ribosomal subunit assembly. *RNA* **2016**, *22*, 1386–1399. [[CrossRef](#)]
111. Zengel, J.M.; Jerauld, A.; Walker, A.; Wahl, M.C.; Lindahl, L. The extended loops of ribosomal proteins L4 and L22 are not required for ribosome assembly or L4-mediated autogenous control. *RNA* **2003**, *9*, 1188–1197. [[CrossRef](#)]
112. Greber, B.J.; Boehringer, D.; Montellese, C.; Ban, N. Cryo-EM structures of Arx1 and maturation factors Rei1 and Jjj1 bound to the 60S ribosomal subunit. *Nat. Struct. Mol. Biol.* **2012**, *19*, 1228–1233. [[CrossRef](#)] [[PubMed](#)]
113. Lo, K.Y.; Li, Z.; Bussièrè, C.; Bresson, S.; Marcotte, E.M.; Johnson, A.W. Defining the pathway of cytoplasmic maturation of the 60S ribosomal subunit. *Mol. Cell* **2010**, *39*, 196–208. [[CrossRef](#)]

114. Mageehey, C.M.; Ware, V.C. Specialized eRpL22 paralogue-specific ribosomes regulate specific mRNA translation in spermatogenesis in *Drosophila melanogaster*. *Mol. Biol. Cell* **2019**, *30*, 2240–2253. [[CrossRef](#)]
115. Maitra, N.; He, C.; Blank, H.M.; Tsuchiya, M.; Schilling, B.; Kaeberlein, M.; Aramayo, R.; Kennedy, B.K.; Polymenis, M. Translational control of methionine and serine metabolic pathways underpin the paralogue-specific phenotypes of Rpl22 ribosomal protein mutants in cell division and replicative longevity. *bioRxiv* **2020**. [[CrossRef](#)]
116. Yu, P.; Wang, S.; Ma, C.; Luo, X.; Xing, Z.; Wu, X.; Clyne, R.K.; Hwang, G.-J. Affirmation of Distinctive Ribosomal Protein Paralogue-Specific Ribosomes. *SSRN Electron. J.* **2019**, 3334430. [[CrossRef](#)]
117. Ghulam, M.M.; Catala, M.; Elela, S.A. Differential expression of duplicated ribosomal protein genes modifies ribosome composition in response to stress. *Nucleic Acids Res.* **2020**, *48*, 1954–1968. [[CrossRef](#)]
118. Wu, S.; De Croos, J.N.A.; Storey, K.B. Cold acclimation-induced up-regulation of the ribosomal protein L7 gene in the freeze tolerant wood frog, *Rana sylvatica*. *Gene* **2008**, *424*, 48–55. [[CrossRef](#)]
119. Gadal, O.; Strauss, D.; Petfalski, E.; Gleizes, P.E.; Gas, N.; Tollervy, D.; Hurt, E. Rlp7p is associated with 60S preribosomes, restricted to the granular component of the nucleolus, and required for pre-rRNA processing. *J. Cell Biol.* **2002**, *157*, 941–952. [[CrossRef](#)] [[PubMed](#)]
120. Wang, R.; Zhao, J.; Jia, M.; Xu, N.; Liang, S.; Shao, J.; Qi, Y.; Liu, X.; An, L.; Yu, F. Balance between cytosolic and chloroplast translation affects leaf variegation. *Plant Physiol.* **2018**, *176*, 804–818. [[CrossRef](#)]
121. De Las Heras-Rubio, A.; Peruchó, L.; Paciucci, R.; Vilardell, J.; Lleonart, M.E. Ribosomal proteins as novel players in tumorigenesis. *Cancer Metastasis Rev.* **2014**, *33*, 115–141. [[CrossRef](#)]
122. Neumann, F.; Krawinkel, U. Constitutive expression of human ribosomal protein L7 arrests the cell cycle in G1 and induces apoptosis in Jurkat T-lymphoma cells. *Exp. Cell Res.* **1997**, *230*, 252–261. [[CrossRef](#)]
123. Von Arnim, A.G.; Jia, Q.; Vaughn, J.N. Regulation of plant translation by upstream open reading frames. *Plant Sci.* **2014**, *214*, 1–12. [[CrossRef](#)] [[PubMed](#)]
124. Jakovljevic, J.; Ohmayer, U.; Gamalinda, M.; Talkish, J.; Alexander, L.; Linnemann, J.; Milkereit, P.; Woolford, J.L. Ribosomal proteins L7 and L8 function in concert with six A3 assembly factors to propagate assembly of domains I and II of 25S rRNA in yeast 60S ribosomal subunits. *RNA* **2012**, *18*, 1805–1822. [[CrossRef](#)] [[PubMed](#)]
125. Charneski, C.A.; Hurst, L.D. Positively Charged Residues Are the Major Determinants of Ribosomal Velocity. *PLoS Biol.* **2013**, *11*, e1001508. [[CrossRef](#)]
126. Diaconu, M.; Kothe, U.; Schlünzen, F.; Fischer, N.; Harms, J.M.; Tonevitsky, A.G.; Stark, H.; Rodnina, M.V.; Wahl, M.C. Structural basis for the function of the ribosomal L7/12 stalk in factor binding and GTPase activation. *Cell* **2005**, *121*, 991–1004. [[CrossRef](#)]
127. Bourne, H.R.; Sanders, D.A.; McCormick, F. The GTPase superfamily: Conserved structure and molecular mechanism. *Nature* **1991**, *349*, 117–127. [[CrossRef](#)] [[PubMed](#)]
128. Rosso, M.G.; Li, Y.; Strizhov, N.; Reiss, B.; Dekker, K.; Weisshaar, B. An Arabidopsis thaliana T-DNA mutagenized population (GABI-Kat) for flanking sequence tag-based reverse genetics. *Plant Mol. Biol.* **2003**, *53*, 247–259. [[CrossRef](#)]
129. Murashige, T.; Skoog, F. A Revised Medium for Rapid Growth and Bio Assays with Tobacco Tissue Cultures. *Physiol. Plant.* **1962**, *15*, 473–497. [[CrossRef](#)]
130. QIAGEN. RNeasy Mini Handbook. HB-0435-005 10/2019. Available online: <http://www.qiagen.com> (accessed on 30 April 2021).
131. Hummel, M.; Dobrenel, T.; Cordewener, J.J.H.G.; Davanture, M.; Meyer, C.; Smeekens, S.J.C.M.; Bailey-Serres, J.; America, T.A.H.P.; Hanson, J. Proteomic LC-MS analysis of Arabidopsis cytosolic ribosomes: Identification of ribosomal protein paralogs and re-annotation of the ribosomal protein genes. *J. Proteom.* **2015**, *128*, 436–449. [[CrossRef](#)]
132. Johnson, W.E.; Li, C.; Rabinovic, A. Adjusting batch effects in microarray expression data using empirical Bayes methods. *Biostatistics* **2007**, *8*, 118–127. [[CrossRef](#)]
133. Delignette-Muller, M.L.; Dutang, C. fitdistrplus: An R package for fitting distributions. *J. Stat. Softw.* **2015**, *64*, 1–34. [[CrossRef](#)]
134. Smyth, G.K. Limma: Linear Models for Microarray Data. In *Bioinformatics and Computational Biology Solutions Using R Bioconductor*; Springer: New York, NY, USA, 2005; pp. 397–420. [[CrossRef](#)]
135. Benjamini, Y.; Hochberg, Y. Controlling the False Discovery Rate: A Practical and Powerful Approach to Multiple Testing. *J. R. Stat. Soc. Ser. B* **1995**, *57*, 289–300. [[CrossRef](#)]
136. Hartigan, J.A.; Wong, M.A. Algorithm AS 136: A K-Means Clustering Algorithm. *J. R. Stat. Soc. Ser. C Appl. Stat.* **1979**, *28*, 100. [[CrossRef](#)]
137. Kawaguchi, R.; Williams, A.J.; Bray, E.A.; Bailey-Serres, J. Water-deficit-induced translational control in *Nicotiana tabacum*. *Plant, Cell Environ.* **2003**, *26*, 221–229. [[CrossRef](#)]
138. Reynoso, M.A.; Juntawong, P.; Lancia, M.; Blanco, F.A.; Bailey-Serres, J.; Zanetti, M.E. Translating ribosome affinity purification (TRAP) followed by RNA sequencing technology (TRAP-SEQ) for quantitative assessment of plant translomes. In *Plant Functional Genomics: Methods in Molecular Biology*; Humana Press: New York, NY, USA, 2015; pp. 185–207. ISBN 9781493924448.
139. Lebowitz, J.; Lewis, M.S.; Schuck, P. Modern analytical ultracentrifugation in protein science: A tutorial review. *Protein Sci.* **2009**, *11*, 2067–2079. [[CrossRef](#)] [[PubMed](#)]
140. Erde, J.; Loo, R.R.O.; Loo, J.A. Enhanced FASP (eFASP) to increase proteome coverage and sample recovery for quantitative proteomic experiments. *J. Proteome Res.* **2014**, *13*, 1885–1895. [[CrossRef](#)]
141. Swart, C.; Martínez-Jaime, S.; Gorka, M.; Zander, K.; Graf, A. Hit-Gel: Streamlining in-gel protein digestion for high-throughput proteomics experiments. *Sci. Rep.* **2018**, *8*, 8582. [[CrossRef](#)] [[PubMed](#)]

142. Perez-Riverol, Y.; Csordas, A.; Bai, J.; Bernal-Llinares, M.; Hewapathirana, S.; Kundu, D.J.; Inuganti, A.; Griss, J.; Mayer, G.; Eisenacher, M.; et al. The PRIDE database and related tools and resources in 2019: Improving support for quantification data. *Nucleic Acids Res.* **2019**, *47*, D442–D450. [CrossRef] [PubMed]
143. Zhang, W.; Zhang, J.; Xu, C.; Li, N.; Liu, H.; Ma, J.; Zhu, Y.; Xie, H. LFQuant: A label-free fast quantitative analysis tool for high-resolution LC-MS/MS proteomics data. *Proteomics* **2012**, *12*, 3475–3484. [CrossRef]
144. The UniProt Consortium. UniProt: The universal protein knowledgebase. *Nucleic Acids Res.* **2017**, *45*, D158–D169. [CrossRef]
145. Armache, J.P.; Jarasch, A.; Anger, A.M.; Villa, E.; Becker, T.; Bhushan, S.; Jossinet, F.; Habeck, M.; Dindar, G.; Franckenberg, S.; et al. Cryo-EM structure and rRNA model of a translating eukaryotic 80S ribosome at 5.5-Å resolution. *Proc. Natl. Acad. Sci. USA* **2010**, *107*, 19748–19753. [CrossRef]
146. Rose, P.W.; Bi, C.; Bluhm, W.F.; Christie, C.H.; Dimitropoulos, D.; Dutta, S.; Green, R.K.; Goodsell, D.S.; Prlić, A.; Quesada, M.; et al. The RCSB Protein Data Bank: New resources for research and education. *Nucleic Acids Res.* **2013**, *41*, D475–D482. [CrossRef]
147. Altschul, S.F.; Gish, W.; Miller, W.; Myers, E.W.; Lipman, D.J. Basic local alignment search tool. *J. Mol. Biol.* **1990**, *215*, 403–410. [CrossRef]
148. Ban, N.; Beckmann, R.; Cate, J.H.D.; Dinman, J.D.; Dragon, F.; Ellis, S.R.; Lafontaine, D.L.J.; Lindahl, L.; Liljas, A.; Lipton, J.M.; et al. A new system for naming ribosomal proteins. *Curr. Opin. Struct. Biol.* **2014**, *24*, 165–169. [CrossRef] [PubMed]
149. Csardi, G.; Nepusz, T. The igraph software package for complex network research. *Interf. Complex Syst.* **2006**, *1695*, 1–9.
150. Virtanen, P.; Gommers, R.; Oliphant, T.E.; Haberland, M.; Reddy, T.; Cournapeau, D.; Burovski, E.; Peterson, P.; Weckesser, W.; Bright, J.; et al. SciPy 1.0: Fundamental algorithms for scientific computing in Python. *Nat. Methods* **2020**, *17*, 261–272. [CrossRef]
151. Sela, I.; Ashkenazy, H.; Katoh, K.; Pupko, T. GUIDANCE2: Accurate detection of unreliable alignment regions accounting for the uncertainty of multiple parameters. *Nucleic Acids Res.* **2015**, *43*, W7–W14. [CrossRef] [PubMed]
152. Landan, G.; Graur, D. Local reliability measures from sets of co-optimal multiple sequence alignments. In Proceedings of the Pacific Symposium on Biocomputing 2008, PSB 2008, Kohala Coast, HI, USA, 4–8 January 2008; pp. 15–24.
153. Penn, O.; Privman, E.; Ashkenazy, H.; Landan, G.; Graur, D.; Pupko, T. GUIDANCE: A web server for assessing alignment confidence scores. *Nucleic Acids Res.* **2010**, *38*, W23–W28. [CrossRef]
154. Bouckaert, R.; Heled, J.; Kühnert, D.; Vaughan, T.; Wu, C.H.; Xie, D.; Suchard, M.A.; Rambaut, A.; Drummond, A.J. BEAST 2: A Software Platform for Bayesian Evolutionary Analysis. *PLoS Comput. Biol.* **2014**, *10*, e1003537. [CrossRef]
155. Drummond, A.J.; Suchard, M.A.; Xie, D.; Rambaut, A. Bayesian phylogenetics with BEAUti and the BEAST 1.7. *Mol. Biol. Evol.* **2012**, *29*, 1969–1973. [CrossRef]
156. Darriba, D.; Taboada, G.L.; Doallo, R.; Posada, D. JModelTest 2: More models, new heuristics and parallel computing. *Nat. Methods* **2012**, *9*, 772. [CrossRef]
157. Guindon, S.; Gascuel, O. A Simple, Fast, and Accurate Algorithm to Estimate Large Phylogenies by Maximum Likelihood. *Syst. Biol.* **2003**, *52*, 696–704. [CrossRef]
158. Steel, M.; McKenzie, A. Properties of phylogenetic trees generated by yule-type speciation models. *Math. Biosci.* **2001**, *170*, 91–112. [CrossRef]
159. Drummond, A.J.; Nicholls, G.K.; Rodrigo, A.G.; Solomon, W. Estimating mutation parameters, population history and genealogy simultaneously from temporally spaced sequence data. *Genetics* **2002**, *161*, 1307–1320. [CrossRef] [PubMed]
160. Rambaut, A.; Drummond, A.J.; Xie, D.; Baele, G.; Suchard, M.A. Posterior summarization in Bayesian phylogenetics using Tracer 1.7. *Syst. Biol.* **2018**, *67*, 901–904. [CrossRef] [PubMed]
161. DeLano, W.L. *The PyMOL Molecular Graphics System, Version 1.8*; Schrödinger LLC: New York, NY, USA, 2014. Available online: <http://www.pymol.org> (accessed on 30 April 2021).
162. Ihaka, R.; Gentleman, R. R: A Language for Data Analysis and Graphics. *J. Comput. Graph. Stat.* **1996**, *5*, 299–314. [CrossRef]
163. R Development Core Team 3.0.1. *A Language and Environment for Statistical Computing*; R Foundation for Statistical Computing: Vienna, Austria, 2013; Volume 2.
164. Wickham, H.; Averick, M.; Bryan, J.; Chang, W.; McGowan, L.; François, R.; Grolemund, G.; Hayes, A.; Henry, L.; Hester, J.; et al. Welcome to the Tidyverse. *J. Open Source Softw.* **2019**, *4*, 1686. [CrossRef]
165. Wickham, H. Reshaping data with the reshape package. *J. Stat. Softw.* **2007**, *21*, 1–20. [CrossRef]
166. Hadley Wickham Stringr: Simple, Consistent Wrappers for Common String Operations. R Package Version 1.3.1. *R Packag. version* **2018**. Available online: <http://stringr.tidyverse.org> and <https://github.com/tidyverse/stringr> (accessed on 30 April 2021).
167. Ginestet, C. ggplot2: Elegant Graphics for Data Analysis. *J. R. Stat. Soc. Ser. A Stat. Soc.* **2011**, *174*, 245–246. [CrossRef]
168. Gagolewski, M. Package “stringi”: Character String Processing Facilities. *Cran* **2016**. Available online: <http://www.gagolewski.com/software/stringi/> (accessed on 30 April 2021).
169. Gu, Z.; Eils, R.; Schlesner, M. Complex heatmaps reveal patterns and correlations in multidimensional genomic data. *Bioinformatics* **2016**, *32*, 2847–2849. [CrossRef]
170. Gu, Z.; Gu, L.; Eils, R.; Schlesner, M.; Brors, B. Circlize implements and enhances circular visualization in R. *Bioinformatics* **2014**, *30*, 2811–2812. [CrossRef]
171. Chen, H.; Boutros, P.C. VennDiagram: A package for the generation of highly-customizable Venn and Euler diagrams in R. *BMC Bioinform.* **2011**, *12*, 35. [CrossRef] [PubMed]

Chapter 7

Remodelled Ribosomes

Synthesise a Specific Proteome in Proliferating Plant Tissue during Cold

Remodelled Ribosomes Synthesise a Specific Proteome in Proliferating Plant Tissue during Cold

Federico Martinez-Seidel^{1*,2¶}, Pipob Suwanchaikasem², Dione Gentry-Torfer^{1,2}, Yogeswari Rajarathinam¹, Alina Ebert^{1, 2}, Alexander Erban¹, Alexandre Augusto Pereira Firmino¹, Shuai Nie³, Michael G. Leeming^{3,4}, Nicholas A. Williamson^{3,5}, Ute Roessner², Joachim Kopka¹, Berin A. Boughton^{2,6}

*For correspondence:

mseidel@mpimp-golm.mpg.de
(FM-S)

Present address: [¶]Willmitzer Department, Max-Planck-Institute of Molecular Plant Physiology, Potsdam-Golm, Germany

¹ Molecular Physiology Department, Max-Planck-Institute of Molecular Plant Physiology, Potsdam-Golm, Germany; ² School of BioSciences, The University of Melbourne, Parkville, VIC, Australia; ³ Bio21 Institute of Molecular Science and Biotechnology, The University of Melbourne, Parkville, VIC, Australia; ⁴ School of Chemistry, The University of Melbourne, Parkville, VIC, Australia; ⁵ Department of Biochemistry and Molecular Biology, The University of Melbourne, Parkville, VIC, Australia; ⁶ Australian National Phenome Centre, Murdoch University, Murdoch, WA, Australia

Abstract

Plant acclimation to low temperatures occurs through system-wide mechanisms that include proteome shifts, some of which occur at the level of protein synthesis. All proteins are synthesised by ribosomes. Rather than being monolithic, transcript-to-protein translation machines, ribosomes can be selective and cause effective proteome shifts required for successful temperature acclimation. Here, we use apical root meristems of germinating seedlings of the monocotyledonous plant barley as a model to study changes in protein abundance and synthesis rates during cold acclimation. We measure metabolic and physiological parameters that allow us to compare protein synthesis rates in different physiological states, e.g., in cold acclimation compared to the optimal temperature state. We show that ribosomal proteins are independently synthesised and assembled into ribosomal complexes in root proliferative tissue, and assess how the ribo-proteome shifts during cold may be associated with changes in synthesis and accumulation of macromolecular complexes. We demonstrate that translation initiation is the limiting step during cold acclimation and based on our data propose a model of a ribosomal code that depends on a reconfigured ribosome population, where as a mode of cold acclimation, specific ribosomal protein compositions may confer selective association capabilities between 60S subunits and 48S initiation complexes. Whether selective translation in barley proliferative tissue depends directly or indirectly on altered ribosomal proteome compositions remains an open question.

Introduction

Cold acclimation is a physiological challenge for sessile plant organisms (*Hincha and Zuther, 2020; Middleton et al., 2014; Thomashow, 1999*). Next to extensively studied transcriptional responses (*Seki et al., 2002; Jaglo-Ottosen et al., 1998; Thomashow, 1999; Fowler and Thomashow, 2002; Hincha et al., 2012*), cold-triggered translational reprogramming moves into the focus as a hub

41 for temperature acclimation (*Garcia-Molina et al., 2020; Beine Golovchuk et al., 2018; Schmidt*
42 *et al., 2013*). Translation provides a second regulatory layer that integrates signals from cellular
43 processes and generates a cold acclimated proteome based on the primary layer of a remodeled
44 transcriptome (*Yu et al., 2020; Martinez-Seidel et al., 2021a,c; Cheong et al., 2021*).

45
46 The functional importance of translation is evident in germinating barley seedlings when they
47 stop growing during the first days of acclimation to a cold shift (*Martinez-Seidel et al., 2021c*)
48 and yet continue to accumulate translation-related complexes in the root tip well above the
49 level of plants grown at optimized temperature (*Martinez-Seidel et al., 2021c*). In the absence
50 of growth, synthesis of new ribosomes appears activated or alternatively, the existing ones are
51 less degraded. Regardless of the mechanism, the accumulation of translation-related complexes
52 correlates with evidence of a cold-induced total proteome shift in root proliferative tissue. This
53 shift comprises not only evidence of the accumulation of structural ribosomal proteins (rProteins)
54 but also of elements of ribosome assembly and translation initiation (*Martinez-Seidel et al., 2021c*).

55
56 In *Arabidopsis*, the ribosome population that accumulates after a cold-shift in roots has altered
57 ribosomal protein (rProtein) composition compared to temperature-optimised control conditions
58 (*Cheong et al., 2021; Martinez-Seidel et al., 2021a*), suggesting that temperature-shifts trigger
59 ribosome heterogeneity. Ribosome heterogeneity can contribute to proteome shifts by selective
60 translation of the transcriptome. Targeted translation of mRNAs based on altered ribosomal
61 structures is referred to as ribosome specialization (*Genuth and Barna, 2018; Martinez-Seidel*
62 *et al., 2020; Slavov et al., 2015*). Functional specialization of ribosomes entails translational events
63 that drive a response to an external (*Lambers, 2022; Berková et al., 2020; Moin et al., 2021; Appels*
64 *et al., 2021*) or a developmental (*Norris et al., 2021; Shrestha et al., 2022; Xiong et al., 2021*) cue,
65 for example, the preferred translation of specific groups of proteins that facilitate acclimation
66 to low temperatures. These concepts suggest that the previously observed abundance changes
67 of the translational machinery in cold-acclimating root tips of barley seedlings (*Martinez-Seidel*
68 *et al., 2021c*) may indicate the production of ribosomes tuned to cold-specialized translation.
69 Protein biosynthesis, including ribosome biogenesis, is the largest energy expenditure in the cell
70 (*Ingolia et al., 2019; Russell and Cook, 1995; Verduyn et al., 1991*) and consequently building a
71 specialized ribosome population *de novo* would consume much time and resources. In plants,
72 cytosolic ribosomes have an rProtein-based half-life of 3-4 days (*Salih et al., 2020*), and thus
73 ribosome biogenesis alone may fail to satisfy the demand for customized ribosomal complexes
74 during cold. Thus, there may be a ribosome remodeling mechanism that relies on increased
75 biogenesis and/or *in-situ* ribosome remodelling to alter steady proteome dynamics by causing a
76 cold-induced proteome shift.

77
78 The cellular proteome is highly dynamic in sessile plants. The transition between different
79 proteome states is a constant feature in the plant life cycle and varies between organs and
80 tissues (*Nelson and Millar, 2015*). Plant roots contain cells at multiple different developmental
81 and ontological stages that coexist along longitudinal and radial axes (*Dinneny and Benfey, 2008*).
82 The proteome of the root tip is highly dynamic and demonstrably differed from the longitudinal
83 adjacent older tissue, specifically considering the cold triggered abundance changes of translation-
84 and ribosome-associated proteins (*Martinez-Seidel et al., 2021c*). Root apical meristems are
85 "hotspots" of growth and require a high amount of newly synthesised ribosomes to support
86 cell proliferation compared to the adjacent elongation and differentiation zones (*Clowes, 1958;*
87 *Verbelen et al., 2006*). The relatively large size of barley roots makes them an ideal system to
88 compare proteome dynamics in response to environmental cues. Barley roots allow for feasible
89 sampling of a sufficiently large tip enriched for meristematic cells. Such sampling circumvents
90 one of the major limitations in analysing complex root landscapes as it avoids pooling of highly
91 diverse root zones and the masking of phenomena linked to rapidly proliferating cells by the more

92 abundant static root zones.

93

94 The proteome dynamics are related to protein turnover, which is the balance between protein
95 synthesis and degradation. These two processes lead in different contexts to shifts in the relative
96 abundances of active protein pools. Translation is related mainly to protein biosynthesis and
97 approaches to study translational dynamics typically involve the use of stable isotope mass
98 spectrometry as an empirical measure of protein synthesis (K_s) and degradation (K_d) (*Nelson*
99 *et al., 2014b,a*). The calculation of plant protein K_s using a stable isotope pulse depends on several
100 parameters that must be considered (*Ishihara et al., 2015, 2021; Li et al., 2017*). The amount of pro-
101 tein fraction that has taken up the externally supplied stable isotope tracer can be determined by
102 isotopolog analysis of proteinogenic amino acids from isolated and hydrolyzed protein fractions or
103 individual purified proteins. Alternatively, proteomics technology allows multiparallel isotopolog
104 distribution analysis of peptides obtained by digestion of complex protein preparations. The time
105 of stable isotope pulse to sample collection allows conversion of observed isotope enrichment
106 and protein concentration values into rates. To prevent physiological differences in plant tissue
107 and environmental factors from confounding these calculations, several variables are required
108 to correct and normalize protein K_s rates. The first two variables are protein content and relative
109 growth rate (RGR), which are required to adjust K_s rates between plant systems that differ in these
110 characteristics. A third set of variables describes the dynamics of tracer incorporation into soluble
111 amino acid pools, and label incorporation into these pools may differ between the physiological
112 conditions being compared and between individual proteinogenic amino acids (*Ishihara et al.,*
113 *2021*). All of these variables are necessary to correct the isotopic envelopes of proteins or digested
114 peptides based on knowledge of their individual amino acid sequences. These corrections are
115 particularly important when the compared plant systems are transitioning between physiological
116 quasi-stable states, as is the case in most studies of development, physiology, and environment x
117 genome interactions, and especially during the well-described sequences of cold acclimation. The
118 non-acclimated and acclimated states of plants drastically alter protein accumulation (*Martinez-*
119 *Seidel et al., 2021c*), growth dynamics (*Beine Golovchuk et al., 2018; Martinez-Seidel et al.,*
120 *2021a,c*), and pools of soluble amino acids (*Kaplan et al., 2004; Guy et al., 2008*). Such changes
121 could strongly bias the observed protein K_s rates without correction.

122

123 In this study, we explore the proteome dynamics in barley root tips by stable isotope trac-
124 ing and proteomic mass spectrometry of a protein fraction enriched for assembled translation-
125 related complexes. We aim to provide new insight into non-steady-state translation dynamics of
126 this rapidly developing plant tissue. We calculate K_s rates of individual peptides from samples of
127 barley seedlings germinated in the dark prior to emergence of photosynthetic activity and compare
128 acclimation to sub-optimal temperature (4°C) with optimal temperature (20°C). Our experiments
129 correct for differential growth and protein accumulation and validate the calculation of K_s rates
130 by morphometric and metabolic phenotype analyses. We monitor protein abundances, RGR, and
131 label incorporation into soluble amino acid pools and thereby correct for expected differential iso-
132 tope tracer dilution of the peptide building blocks. Using the corrected K_s rates, we investigate
133 whether the ribosome population that accumulates during cold acclimation consists of *de novo*
134 synthesised rProteins or alternatively, whether rProteins remain non-labelled and are re-used. We
135 report changes of rProteins in cold-acclimated ribosomal populations and compare these findings
136 to various other co-purified cellular protein complexes that are preferentially synthesised during
137 cold and are either functionally related to the protein biosynthesis machinery or have different
138 cellular functions.

139 **Results**

140 **Experimental design**

141 To ensure legitimate, physiological rearing conditions for barley seedlings, we followed previously
142 published procedures (*Martinez-Seidel et al., 2021c*) with few modifications (Figure 1). Seeds were
143 imbibed for 14 hours under sterile conditions, then transferred to liquid medium and germinated
144 on plates for another 48 hours. At this time, we applied different temperature regimes to mimic an
145 agronomically relevant temperature drop after sowing barley in the field. Germination occurred
146 in the dark for an additional 60 hours, which corresponds to an optimal seeding depth equivalent
147 to the typical period of about 5 days before barley seedlings emerge from the soil in the field
148 (*Kirby, 1993*).

149

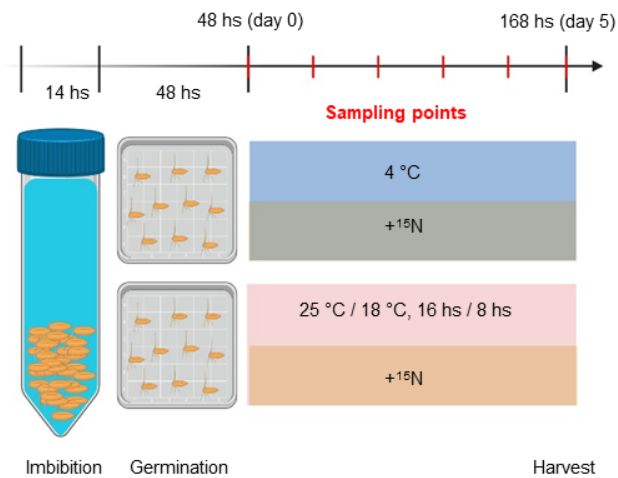


Figure 1-Figure supplement 1. Root phenotype during germination assay in optimal control and suboptimal cold temperatures.

Figure 1-Figure supplement 2. Summary of the methodological workflow to achieve measurements of protein synthesis and abundance in barley root tips.

Figure 1. Experimental setup. *Hordeum vulgare* seeds were soaked in sterile H_2O for 14 h imbibition. Seeds were transferred to plates for germination for 48 h. At 48 h treatments were applied and it was considered as experimental day 0. Half of remaining seedlings were treated with media supplemented with ^{15}N compounds and the other half continued on media supplemented with ^{14}N compounds as a control. Half of the seeds in treatment and in control plates were shifted to 4 °C to induce cold acclimation. The other half remained in the control growth chamber with a temperature fluctuation of 25 °C for 16 h and 18 °C for 8 h. Six seedlings were harvested daily per treatment after day 0 for phenotypic analyses. After harvest, each seedling was scanned for phenotyping, roots were weighed for fresh weight and dried for 70 h at 70 °C and weighed again for dry weight. For primary metabolome analysis, root tips were collected in 1.5-cm segments on the fifth day of acclimation. Created with BioRender.com

150 Control seedlings continued to germinate at an optimal temperature of 25°C/ 18°C in a 16-hour
151 day/8-hour night regime (Figure 1 - Figure S1) with an average temperature of 22°C over 24 hours.
152 Barley seedlings treated with low temperatures were cultured at a suboptimal, but not lethal, tem-
153 perature of a constant 4°C. Differential growth, one of the necessary variables for calculating in-
154 dividual protein synthesis rates, was monitored by high-resolution imaging of independently ger-
155 minated seedlings at 12-hour intervals (Figure S1). Throughout the approximately 5-day period,
156 etiolation, premature greening, seed nutrient starvation, and other processes resulting from un-
157 naturally long darkness were avoided (*Kirby, 1993*). Seedlings at 4°C developed more slowly but
158 showed no other macroscopic phenotypic changes (Figure S1). We began labeling seedlings with
159 ^{15}N coincident with the temperature shift 48 hours after germination (t_0) and throughout the dif-

160 ferential temperature treatment to ensure that the dynamics of tracer incorporation reflected the
161 physiological change associated with cold acclimation and delayed growth. After 108 hours of ger-
162 mination, i.e. at the last experimental time point (t_f) of the labeling experiments, the root tips of
163 the seedlings were harvested to analyze the isotope incorporation and pool sizes of soluble amino
164 acids and to measure the relative abundances and ^{15}N enrichment of individual proteins (Figure 1
165 - Figure S2).

166 **Root growth dynamics**

167 Root systems of germinating barley seedlings were carefully phenotyped using non-destructive
168 and paired destructive measurements to characterize differential growth and biomass dynamics
169 induced by different temperature regimes. We expected a strong effect on growth based on
170 previous observations of cold-acclimated *Arabidopsis thaliana* rosette plants delaying growth for
171 a period of 7 days after switching to suboptimal temperatures (Beine Golovchuk et al., 2018;
172 Martinez-Seidel et al., 2021a). Such a growth difference can be a confounding variable when
173 comparing protein synthesis rates of acclimated and non-acclimated plants. For example, a
174 non-acclimated plant may produce more protein X (Px) in absolute terms than a cold-acclimated
175 plant, but growth will also differ and is likely to be lower in a cold-acclimated plant. Whether a
176 non-acclimated or a cold-acclimated plant preferentially synthesises Px can only be determined
177 by normalizing biomass accumulation.

178
179 We selected an optimized growth measure from several variables that described morphologi-
180 cal phenotypes of roots from germinating barley seedlings (Figure 2, Figure 2 - Figure S1 to S2 &
181 Table S1). To this end, we monitored root growth at 12h intervals between t_0 and t_f across the
182 germination period.

183
184 The roots of the control seedlings accumulated significantly more fresh weight (FW) compared
185 to the roots of the cold-acclimated seedlings within the monitored period between 48h (t_0) and
186 108h (t_f) after germination (Figure 2A above). FW accumulation ceased after 60 hours and
187 subsequently remained significantly reduced in the cold-shifted group compared to the control
188 group. In contrast, dry weight (DW) increased equally in the cold-shifted group and the control
189 group, increasing significantly at 72 hours compared with 48 hours (Figure 2B above). After 72
190 hours, DW was constant. The cold-shifted group appeared to reduce DW, but this observation
191 did not remain significant during the observation period. Analysis of the FW/DW ratio (Figure 2C)
192 showed a significant difference between the cold-acclimated and control roots after 72 hours and
193 an overall reduced ratio in the cold-acclimated roots.

194
195 Based on these observations of complex dynamic changes, we determined the RGRs by FW
196 (Figure 2A below) and DW (Figure 2B below) at five intervals (N_i) relative to the average final root
197 mass at t_f of the cold-shifted and control groups. We used equation 1.

$$198 \quad RGR = \frac{1}{W} \cdot \frac{dW}{dt} \quad (1)$$

199
200
201 where W is the weight or weight proxy at time (t_f), dW is the weight change at time dt , which is
202 the time after germination in hours. Consequently, RGR_{FW} and RGR_{DW} have units $\text{mg} \cdot \text{mg}(t_f)^{-1}$
203 $\cdot \text{h}^{-1}$, or in short h^{-1} . For the RGR calculation at 48h (t_0), i.e., the start of germination before the
204 temperature shift, we set the root mass at 0h to zero. RGR_{FW} and RGR_{DW} of the control group
205 were constant during the observation period of 48-108h with small, non-significant fluctuations.
206 While the control group grew steadily, RGR_{FW} and RGR_{DW} of the cold-transferred group peaked

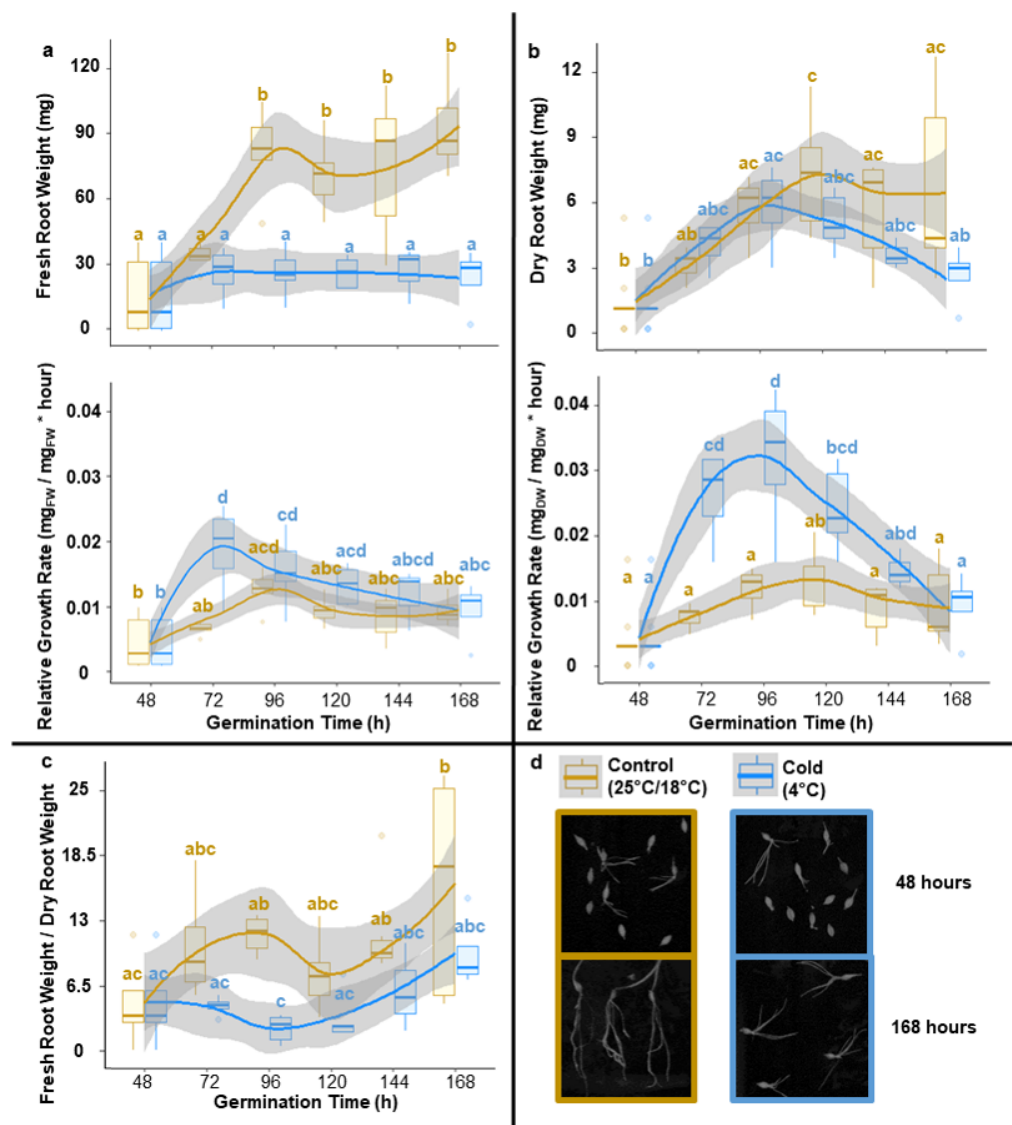


Figure 2-Figure supplement 1. Summary of 95% confidence level Tukey-HSD statistical differences in mean levels of growth related variables across treated and control barley seedlings.

Figure 2-Figure supplement 2. Statistical differences in mean levels (95% confidence level Tukey-HSD) of growth related variables derived from scanning treated (blue) and control (gold) barley seedlings at each time-point.

Figure 2-Figure supplement 3. Linear regression after natural logarithm transformation of growth related variables.

Figure 2. Root growth dynamics of barley seedlings reared at optimal and cold suboptimal temperatures. Barley seeds were imbibed and germinated for 48 hours at optimal rearing conditions and then were transferred to different temperature regimes for five days. Panels A, B, & C contain measurements of specific growth related variables measured in roots, outlined as plots where means are solid coloured lines (blue for cold and gold for control) and standard deviations are shades around the mean. All mean values were compared using an ANOVA followed by the posthoc Tukey HSD test. The boxplots are labelled according to significant differences in the Tukey HSD test, where shared letters indicate lack of significance. Starting at 48 hours after imbibition, seedlings were scanned every 24 hours to measure root growth with a subsequent destructive harvesting to measure root fresh weight (A - upper panel). Subsequently root systems were dried for 3 days at 70°C and weighed again to measure root dry weight (B - upper panel). The recorded weights were used to assess the statistical changes in the fresh to dry weight ratio during the experimental period (C). Finally, both weights were used to calculate RGRs (A & B - lower panels) based on root weight at the imbibition stage (i.e., 0 hours) being zero grams. RGR would subsequently serve the purpose of normalizing protein synthesis rates to basal root growth, preventing biomass accumulation biases.

207 at 60 and 72h, respectively. In this case, we expected transient growth, particularly a decrease in
 208 RGRs, due to the transition between optimized and suboptimal temperature regimes. Instead, we
 209 found a transient increase in the roots of the cold-acclimated seedlings, which can be explained
 210 by the initial DW accumulation after the temperature shift and the partial compensation by the
 211 fluctuating water content (Figure 2).

212

213 In previous studies on Arabidopsis seedlings, RGR was derived as the slope from log-linear
 214 regressions of growth-related variables over time (*Ishihara et al., 2015*). These systems satisfied
 215 the assumption of linearity with correlation coefficients (r^2) approaching 1. For roots of germi-
 216 nating barley seedlings, we had to reject the linearity assumption with r^2 less than 0.5 for all
 217 observed variables, including root length, diameter, volume, length * volume⁻¹, number of tips, or
 218 branching, as well as FW and DW (Figure 2 - Figure S3). To account for the obviously different RGRs
 219 of control and cold-acclimated roots, we chose the average of RGR_{DW} over the experimental ¹⁵N
 220 labeling period, 48h (t₀) - 108h (t_f), for the required normalization (Table 1). Since protein synthesis
 221 directly contributes to DW accumulation, RGR_{DW} is the most relevant option for correcting protein
 222 synthesis rates of two experimental systems that differ in their growth rates. However, DW
 223 determination (as well as FW determination) is destructive and requires a significant sample
 224 mass. For these reasons, ¹⁵N-label incorporation analyses cannot be directly paired and require
 225 additional replicated experiments. We investigated the potential of non-destructive methods for
 226 RGR determination but were unable to find a suitable replacement for RGR_{DW} (Table 1). Averaged
 227 RGRs by root length and length * volume⁻¹ reflected accelerated RGR_{DW} in the cold acclimation
 228 condition, however, they did not accurately represent the excessive transient increase in RGR_{DW},
 229 but rather corresponded to what is observed in RGR_{FW} (Table 1).

230

Table 1. Relative growth rates calculated from multiple root growth proxies from germinating barley seedlings

Relative Growth Rates (RGR)	Control	Cold
Fresh Weight (mg/mg.FW*hs)	0.008	0.011
Dry Weight (mg/mg.DW*hs)	0.008	0.017
Length Per Volume (cm*m ³ /cm*m ³ *hs)	0.008	0.01
Length (cm/cm*hs)	0.008	0.01
Volume (cm ³ /cm ³ *hs)	0.008	0.008
Average Diameter (mm/mm*hs)	0.014	0.014
Number of Forks (#/#*hr)	0.012	0.007
Number of Tips (#/#*hr)	0.007	0.007

231 **Reprogramming of the Primary Metabolome**

232 Primary metabolism is fundamentally reprogrammed during temperature acclimation (*Kaplan*
 233 *et al., 2004; Guy et al., 2008*). The cold-induced reprogramming involves central metabolism,
 234 the source of amino acid building blocks for translation. Therefore, we characterized the
 235 primary metabolome of root tips of germinating barley seedlings in the cold-acclimated and non-
 236 acclimated condition at t_f (Figure 3). Cold acclimation contributed most to the overall variance of
 237 the resulting multidimensional metabolic data set (Table S2). Principal component analysis (PCA)
 238 assigned 65% and 75% of the explained variance to PC1 of the autoscaled or non-scaled data,
 239 respectively (Figure 3C-D). The combined technical and biological variance between replicates
 240 evident in PC2 was minimal (Figure 3A). In addition to fructans and organic acids, amino acids
 241 contributed most to the variance caused by cold acclimation, as inferred from the measure of
 242 variable importance in PCA (Figure 3B). Additionally, the externally supplied ¹⁵N tracer dilutes
 243 and distributes differentially among the proteinogenic amino acids, which accumulate in the

244 cold with \log_2 -fold changes of approximately 2-50 (Table S2). These observations highlight the
 245 need to monitor and correct for ^{15}N enrichment in each of the soluble proteinogenic amino acid
 246 pools, ideally in split and paired samples of the protein or peptide ^{15}N enrichment assays. The
 247 amino acids that contributed most to the PCA separation of the primary metabolome from cold
 248 and control samples were pyroglutamic acid (derived from glutamine converted via our extrac-
 249 tion/derivatization procedures), cysteine, serine, homocysteine, glutamine, glycine, and glutamic
 250 acid, all of which were among the top 20 \log_2 -fold changed metabolites between conditions.
 251

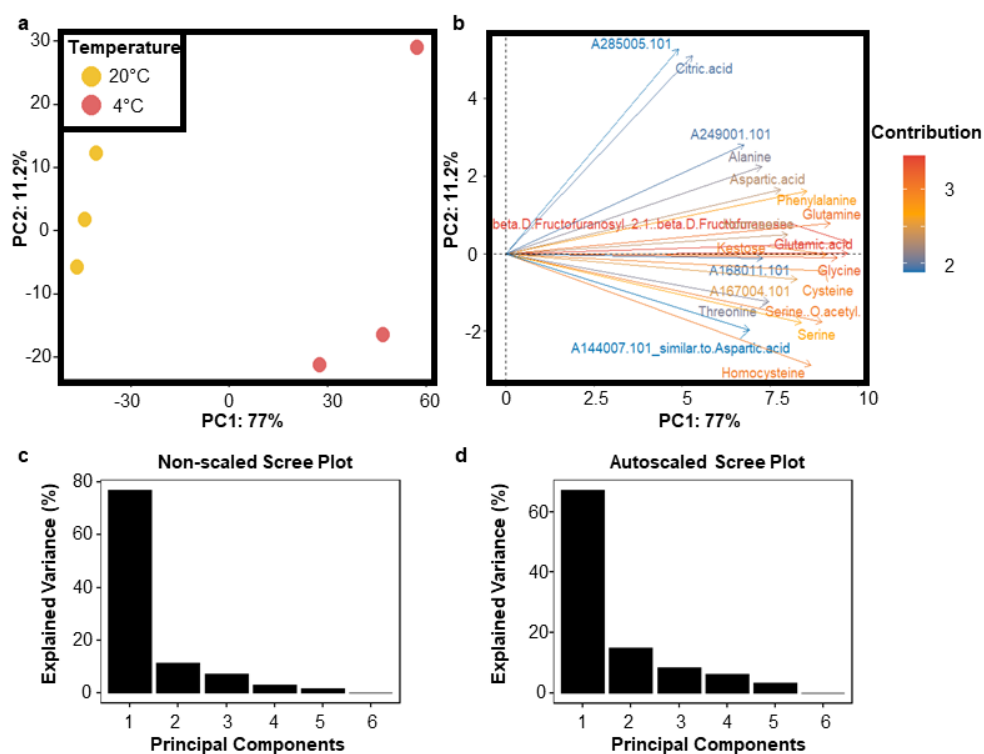


Figure 3. Primary metabolome dynamics of barley seedlings reared at optimal and cold suboptimal temperatures. Also relates to Table S2. The soluble primary metabolome was obtained from frozen and ground plant tissue by methanol / chlorophorm extraction, and the metabolite extracts were chemically derivatized using trimethylsilyl groups to enhance volatility across the gas chromatographic column. Subsequently, the metabolome was measured in a multiplexed array by GC-EI-ToF-MS and GC-APCI-qToF-MS (Erban et al., 2020) in technical triplicates. Metabolites were manually annotated in TagFinder and representative tags for each metabolite chosen. Primary metabolome data were analyzed with functions of the RandoDiStats R package. Panel A contains the principal component analyses (PCA) plot where experimental samples are variables and metabolites eigenvectors determining the separation of the samples. Panel B highlights the best 20 metabolite features contributing to the separation outlined in the samples by a contribution PCA plot. Panel C & D contain the scree plot of variance explained in each principal component (PC) in the non-scaled and autoscaled dataset respectively.

252 Tracer Dynamics in Soluble Amino Acid Pools

253 In this study, we used free proteinogenic amino acids as a proxy for estimating the labelling of
 254 aminoacyl-tRNAs and monitored the ^{15}N -tracer dynamics of the soluble amino acid pools in root
 255 tips at t_r (Figure 4). We supplied a mixture of 99% ^{15}N -labelled glycine and serine to obtain a
 256 rectangular stable isotope pulse. We chose not to use inorganic ^{15}N tracers, which slowly label
 257 soluble amino acid pools (Nelson et al., 2014b). Inorganic ^{15}N labelling arguably leads to low ^{15}N
 258 incorporation, especially under reserve mobilization conditions of a germinating barley seedling

259 (cf. Discussion). Consistent with our labelling strategy, soluble serine and glycine retained most
 260 of the ^{15}N tracer within root tips at 15% ^{15}N enrichment of the two amino acids in the cold-shifted
 261 group and at 2.5 - 5.0% in the control group (Figure 4, Table S3, File S1). The ^{15}N enrichment values
 262 represent the experimental ^{15}N incorporation after correction for the natural isotopic abundances
 263 of the elements (NIA). The large difference between conditions clearly indicates that additional
 264 correction between experimental conditions is required to allow comparison.
 265

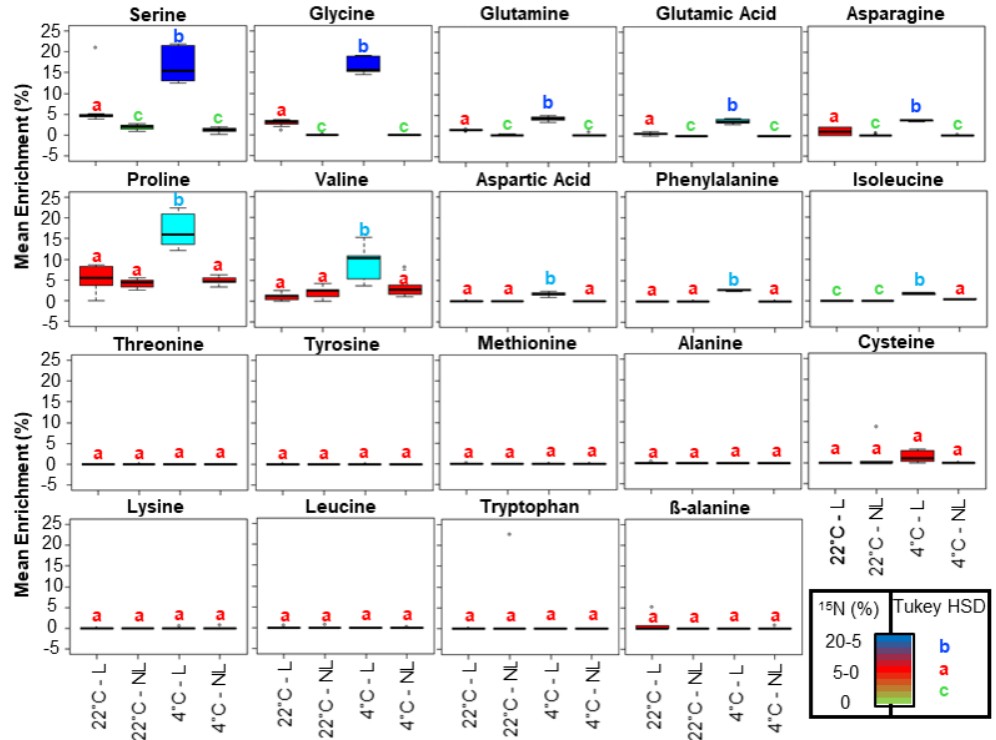


Figure 4. Mean isotopic enrichment of amino acid soluble pools in barley root tips from seedlings germinated at suboptimal (4°C) and optimal (20°C) temperatures. Also relates to Table S3 and File S1. The soluble primary metabolome was obtained exactly as described in Figure 3. Subsequently, at least three independent mass fragments per amino acid analyte along with their isotopolog peak intensities were extracted from total ion chromatograms. The selected fragments for ^{15}N enrichment percentage calculations were those that appeared in spectra containing less co-eluting ions as well as those with evidently increased mass accuracy (e.g., from the APCI platform) summing up to less noisy spectra. The fragments were corrected for natural isotopic abundance, enabling calculation of enrichment percentages using the R package IsoCorrector (Heinrich et al., 2018). Finally, mean enrichments were statistically compared across treatments using an ANOVA, followed by a posthoc Tukey HSD test. Boxplots are coloured according to mean significant differences, further emphasised by the letters above each box.

266 Further correction is required because the ^{15}N tracer was incorporated to different extents
 267 among the different proteinogenic amino acid pools under the experimental conditions. We moni-
 268 tored 18 proteinogenic amino acids (Figure 4). Histidine and arginine were below the detection
 269 limit in our current study. Under control conditions, glutamine, estimated by GC-MS profiling
 270 proxy, pyroglutamic acid, glutamate, and asparagine were significantly labelled at 2.5 to 5.0% ^{15}N
 271 enrichment. The cold-shifted root tips picked up to 2.5-15.0% ^{15}N labelling in glutamine, gluta-
 272 mate, asparagine, and additionally in proline, valine, aspartate, phenylalanine, and isoleucine (Fig-
 273 ure 4, Table S3). The remaining monitored proteinogenic amino acids and beta-alanine, a non-
 274 proteinogenic amino acid control, did not absorb ^{15}N . Our analysis provided accurate ^{15}N enrich-
 275 ment of most proteinogenic amino acids that could be paired with protein and peptide enrichment

276 measurements. Because even minor contributions from multiply labelled amino acids add up to
 277 substantial ^{15}N incorporation into peptides, failure to account for these contributions may intro-
 278 duce bias into estimated protein synthesis rates. This confirms the need to study the dynamics of
 279 the internalized tracer.

280 **Protein Synthesis during Transition from a Physiological Steady State**

281 Throughout their lifespan, plants constantly transition through physiological and proteomic
 282 states that adapt to developmental and environmental factors (*Nelson and Millar, 2015*). Finding
 283 conditions that approach a steady state and allow assessment of protein turnover using stable
 284 isotope mass spectrometry to track both synthesis rates (K_s) and degradation rates (K_d) of specific
 285 proteins is no easy task. Like many other plant systems that respond to stressors, the root of
 286 the barley seedling acclimated to cold is constantly changing (Figure 2) and did not reach an
 287 equilibrium state within our observation period. Therefore, we determined K_s over the observed
 288 time interval rather than turnover.

289 We based our calculations on two published strategies used to determine K_s from turnover
 290 calculations of plant proteins (*Ishihara et al., 2015; Li et al., 2017*). Both of these studies normalize
 291 K_s of individual proteins using growth and protein accumulation rates, as described in the Methods
 292 section by equations 3a & 3b (*Ishihara et al., 2015*) and 4a, 4b, 4c & 4d (*Li et al., 2017*). Specifically,
 293 we determine the ^{15}N enrichment of peptides, consider ^{15}N enrichment in soluble proteinogenic
 294 amino acid pools, and correct K_s by relative growth transformed into relative protein accumulation
 295 rates. Equation 2a calculates K_s as the product of labelled peptide fraction (LPF) times a modified
 296 version of RGR (\overline{RGR}_{pf} in equation 2b) times a factor of 100, which ensures that K_s units are
 297 expressed as a percentage (%) of the normalized labelled peptide fraction accumulated per unit
 298 of protein weight per hour. (equation 5a).

300

$$K_s = LPF \cdot \overline{RGR}_{pf} \cdot 100 \quad (2a)$$

301 Since our study is not at a biological steady state, we introduced the modified \overline{RGR}_{pf} calcula-
 302 tion. First, we calculate the average RGR_{DW} over the labelling period (\overline{RGR}_{DW}), i.e., the observed
 303 sum of the measured RGR_{DW} of the analyzed time intervals between t_0 and t_f divided by the
 304 number of time intervals (N_t), replacing dW (weight accumulation at time t) with P_f (equation 2b).

305

$$\overline{RGR}_{pf} = \frac{\sum_{t=0}^f \left(\frac{1}{W_{tf}} \cdot \frac{P_f}{dt} \right)}{N_t} \quad (2b)$$

306 The factor P_f is used to convert the RGR_{DW} into a relative accumulation rate of total protein
 307 with respect to DW (RGR_{pf}). To this end, we determined P_f , which is the ratio of the final total
 308 protein mass (mg [P_{pf}]) to the dry mass at time t (mg [dW_t]), equation 2c. For both empirical
 309 measurements in milligrams, this process cancels the units and converts them to a fraction of the
 310 total final protein relative to the cumulative weight.

311

$$P_f = \frac{mg_{prot}[P_{pf}]}{mg_{DW}[dW_t]} \quad (2c)$$

312 To calculate the labelled peptide fraction (LPF, equation 2d), we extracted the distributions
 313 of the mass isotopologs from the parent ion masses of LC-MS/MS data sets. We calculated the
 314 expected parent ion monoisotopic masses of the peptides based on their molecular formula
 315 derived from the known amino acid composition. We determined the isotopolog abundances at
 316 mass intervals corresponding to the mass-to-charge ratio of the peptide. These initial isotopolog

317 distributions were corrected for the natural isotopic abundances (NIA) of the elements according
 318 to their molecular formula. The resulting NIA-corrected isotopolog distributions exclusively re-
 319 flected the experimental ^{15}N labelling and allowed the calculation of the fractional ^{15}N enrichment
 320 of peptides, i.e., the ratio of ^{15}N atoms in a peptide to the sum of all N atoms. Finally, the fractional
 321 enrichment or non-corrected LPF is corrected by a constant that differs for each peptide as a
 322 quotient, equation 2d.

323

$$LPF = \frac{\frac{NIA_{corr}(^{15}N_{pep})}{NIA_{corr}(^{14}N_{pep})+NIA_{corr}(^{15}N_{pep})}}{^{15}N_{Aver.AA}} \quad (2d)$$

324 The $^{15}N_{Aver.AA}$ needs to be the quotient dividing non-corrected LPF in order to increase the
 325 fractional enrichment in individual peptides, which assumes a fully labelled source, by what
 326 is actually the achieved labelling, which is always only fractional given the partial labelling in
 327 soluble amino acid pools. Thus, the varying condition-dependent ^{15}N incorporation into soluble
 328 proteinogenic amino acids and the amino acid composition of peptides determine the maximum
 329 fractional enrichment that peptides can achieve. To account for these factors, we correct the
 330 fractional ^{15}N enrichment of peptides by dividing by a peptide- and condition-specific correction
 331 factor ($^{15}N_{Aver.AA}$ in equation 2e) to obtain a corrected version of the LPF. $^{15}N_{Aver.AA}$ is the average
 332 NIA-corrected fractional ^{15}N enrichment over all amino acids in a peptide assuming that the
 333 fractional ^{15}N enrichment of each amino acid incorporated into protein is equal to its observed
 334 fractional ^{15}N enrichment in the soluble amino acid pools, Equation 2e. In other words, $^{15}N_{Aver.AA}$
 335 corresponds to the maximum fractional ^{15}N enrichment that each peptide can achieve under
 336 specific labelling conditions. $^{15}N_{Aver.AA}$ only considers the labelled amino acid residues because
 337 these are entered as potentially labelled N atoms to define the combinatorial matrix used to
 338 correct for NIA. Thus, unlabelled soluble amino acids have no effect on our calculations.

339

$$^{15}N_{Aver.AA} = \frac{\sum_{i=0}^n AA_s}{N_{aa}} \quad (2e)$$

340 Consistent with an expected immediate rectangular ^{15}N label incorporation into soluble amino
 341 acid pools, we used the NIA-corrected ^{15}N incorporation into amino acids as determined at t_f
 342 (*Ishihara et al., 2015*). We tested an alternative scenario for delayed incorporation by modelling
 343 incorporation as a linear function between t_0 and t_f (Table S4F and File S2.1 & S2.2). This leads to a
 344 more conservative trend of enrichment incorporation. Otherwise, the assumption of rectangular
 345 incorporation would mean that the average labelling in soluble amino acid pools over the experi-
 346 mental period is overestimated. Nevertheless, because of the large increase in peptides exceeding
 347 the maximum possible LPF (> 1.0), we rejected the alternative assumption of substantially delayed
 348 incorporation of label into soluble amino acid pools. Similarly, we used the maximum possible
 349 LPF as a reference to accept or reject low-enriched soluble amino acids as part of the correction
 350 factor and thus be able to decide on the correct amino acid combination. In both cases, it was
 351 clear that the optimal solution in the barley system was a nearly rectangular uptake of the tracer
 352 into the plant roots and a late dilution of labelled glycine and serine into other amino acid pools
 353 that did not affect peptide enrichment. The complete workflow for data mining and computation
 354 of our results (Figure 5) is provided by the [ProtSynthesis R package](#), which contains detailed code
 355 annotations and descriptions of the computational procedures used in this and previous studies
 356 (*Ishihara et al., 2015; Li et al., 2017*). The complete workflow (Figure 5) and its usage details are
 357 deposited in two GitHub repositories. Namely, the repository [ProtSynthesis](#), from which the R
 358 package can be installed directly in any R environment, and the repository [isotopeEnrichment](#),
 359 which contains the usage instructions and the Python function that allows direct mining of peptide
 360 isotopolog abundances.

361

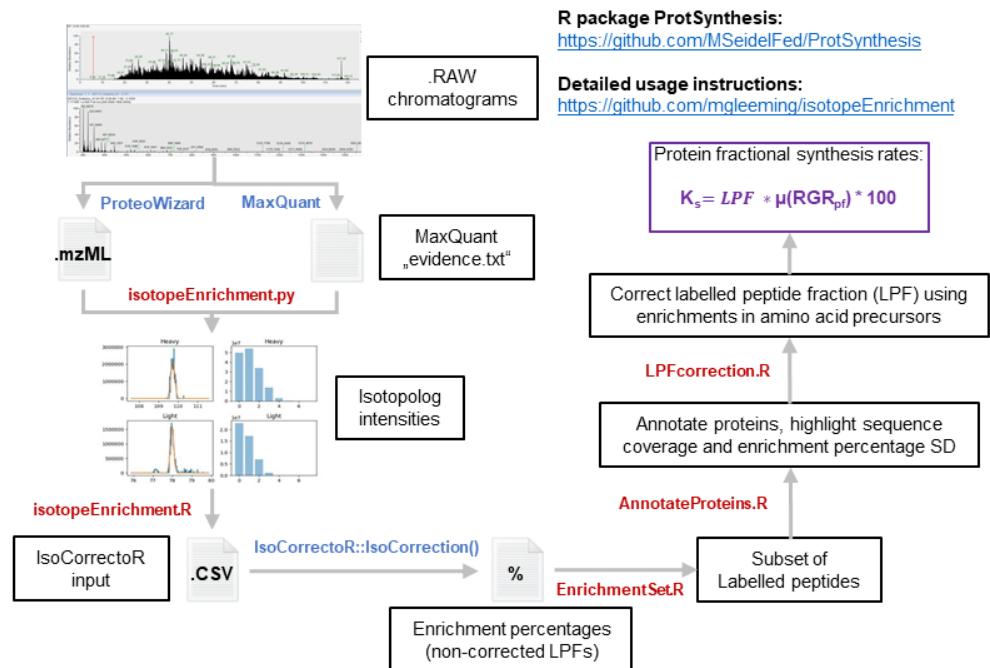


Figure 5–Figure supplement 1. Summary of 95% confidence level Tukey-HSD statistical differences in mean levels of protein content from proteome fractions enriched in ribosomes across treated and control barley seedlings.

Figure 5–Figure supplement 2. Subset of peptides considered as having optimal quality for interpretation of their relative fractional synthesis rates during the physiological transition of roots from germinating barley seedlings from optimal to suboptimal temperature.

Figure 5. Bioinformatics pipeline written as a python function and an R package that jointly enable to calculate stable isotope tracer incorporation into peptides from LC-MS/MS data and derive fractional protein synthesis rates in the organismal physiological context. Also relates to Table S4. The whole pipeline has been made publicly available in two repositories. The [isotopeEnrichment](#) GitHub repository, which contains detailed usage instruction of both python and R functions and the [ProtSynthesis R package](#), which can be installed into any R environment via devtools. All the self-written steps in the pipeline are signalled by red font, while existing algorithms that are external dependencies are depicted in blue font. The pipeline entails using the MaxQuant software to locate proteins and peptides in the chromatograms and then trace back their position and recover their full isotopolog intensities from .mzML files using "isotopeEnrichment.py". Subsequently, an optimal number of isotopolog peaks are derived for individual peptides based on the molecular formula and the enrichment percentages in soluble amino acids using "isotopeEnrichment.R". The data delivered is organised as is required by the IsoCorrectoR R package, which is then used to correct for the natural isotopic abundance and calculate the enrichment percentage of individual peptides (LPF). Subsequently, statistical filters are used to identify and annotate significantly labelled proteins as well as to derive relevant statistics that detail the quality of the protein hit using "EnrichmentSet.R" and "AnnotateProteins.R" respectively. Finally, "LPFcorrection.R" is used to correct the calculated LPFs using the enrichment in soluble amino acid pools, with these corrected values fractional protein synthesis rates are calculated by multiplying them by relative growth rates times 100.

362 Synthesis and Accumulation of Macromolecular Complexes during Cold

363 To validate our method, we obtained a ribosome-enriched fraction of the barley root tip proteome
 364 by filtering a cell lysate through a 60% sucrose cushion, recovering the pelleted fraction. This
 365 ensured that only assembled macromolecular complexes were monitored. The comparative
 366 fractions obtained were from treated and control seedlings. Using the same extraction procedure,
 367 the total protein content of cell complexes was significantly higher in the roots of treated plants
 368 than in the roots of control plants (Figure 5 - Figure S1 and Table S5). Using the LFQ-normalized
 369 protein abundances (Zhang et al., 2012) of peptides extracted from the recovered fraction, we then
 370 report what fraction of the monitored complexes accumulate in barley root tips at sub-optimal
 371 low compared with optimized rearing temperatures (Table 2). At the same time, we monitored the
 372 incorporation of ¹⁵N into the individual protein components of these complexes and found 1379
 373 good quality peptides after applying our method (Figure 5 - Figure S2 and Table S4G), from which
 374 we can confidently report fractional synthesis rates. From this information, we can estimate what
 375 part of the complexome proteome accumulation is due to protein synthesis and what part is due
 376 to the lack of protein degradation (Table 2).
 377

Table 2. Accumulation and origin of protein components from detected multi-protein complexes in barley root tips classified in four groups of responses during the experimental period: (Group 1) accumulated and newly synthesised, (Group 2) accumulated and not degraded, (Group 3) not accumulated but newly synthesised, (Group 4) and not accumulated and not synthesised.

Parent Categories	Detected Complexes	Cold (4°C)	Control (22°C)
Cytosolic ribosome	cytosolic large ribosomal subunit (GO:0022625)	Group 3	Group 1
	cytosolic small ribosomal subunit (GO:0022627)	Group 4	Group 1
Mitochondrial ribosome	mitochondrial large ribosomal subunit (GO:0005762)	Group 4	Group 2
	mitochondrial small ribosomal subunit (GO:0005763)	Group 4	Group 2
Ribosome biogenesis complex	preribosome, small subunit precursor (GO:0030688)	Group 2 (GO:0030692)	Group 4
	preribosome, large subunit precursor (GO:0030687)	Group 2	Group 4
	small-subunit processome (GO:0032040)	Group 1	Group 4
	Pwp2p-containing subcomplex of 90S preribosome (GO:0034388)	Group 2	Group 4
Translation initiation complex	eukaryotic 48S preinitiation complex (GO:0033290)	Group 1	Group 4
	eukaryotic 43S preinitiation complex (GO:0016282)	Group 1	Group 4
	eukaryotic translation initiation factor 3 complex (GO:0005852)	Group 1	Group 4
	eukaryotic translation initiation factor 2B complex (GO:0005851)	Group 3	Group 4
	eukaryotic translation initiation factor 2 complex (GO:0005850)	Group 3	Group 4
Protein folding	chaperonin-containing T-complex (GO:0005832)	Group 1	Group 4
ER-Golgi complex	clathrin adaptor complex (GO:0030131)	Group 3	Group 4
	clathrin vesicle coat (GO:0030125)	Group 3	Group 4
	EMC complex (GO:0072546)	Group 1 (GO:0005789)	Group 4

	endoplasmic reticulum exit site (GO:0070971)	Group 1	Group 4
	COPII vesicle coat (GO:0030127)	Group 2	Group 4
	trans-Golgi network (GO:0005802)	Group 3	Group 4
	Golgi membrane (GO:0000139)	Group 1	Group 4
	Golgi transport complex (GO:0017119)	Group 3	Group 4
	COP1 vesicle coat (GO:0030126)	Group 3	Group 4
	exocyst (GO:0000145)	Group 4	Group 4
	endoplasmic reticulum-Golgi intermediate compartment (GO:0005793)	Group 2 (GO:0098791)	Group 4
Stress related complexes	cytoplasmic stress granule (GO:0010494)	Group 4	Group 4
	P-body (GO:0000932)	Group 4	Group 4
Proteasome	proteasome core complex, alpha-subunit complex (GO:0019773)	Group 3	Group 4
	proteasome regulatory particle, lid subcomplex (GO:0008541)	Group 4	Group 4
	proteasome regulatory particle, base subcomplex (GO:0008540)	Group 3	Group 4
Oxidative complex	peroxisome (GO:0005777)	Group 4	Group 4
protein degradation complex	COP9 signalosome (GO:0008180)	Group 4	Group 4
Transcriptional regulation complex	THO complex part of transcription export complex (GO:0000445)	Group 2 (GO:0000347)	Group 4
	catalytic step 2 spliceosome (GO:0071013)	Group 2 (GO:0097525)	Group 4
Nuclear complex	DNA topoisomerase type II (double strand cut, ATP-hydrolyzing) complex (GO:0009330)	Group 2 (GO:0030870)	Group 4
	perinuclear region of cytoplasm (GO:0048471)	Group 1	Group 4
	nuclear periphery (GO:0034399)	Group 2 (GO:0070603)	Group 4
	nuclear pore (GO:0005643)	Group 2 (GO:0031080)	Group 4
Cell cycle related complexes	condensin complex (GO:0000796)	Group 1	Group 4
	MCM complex (GO:0042555)	Group 2	Group 4
	alpha DNA polymerase;primase complex (GO:0005658)	Group 2	Group 4
	DNA replication factor C complex (GO:0005663)	Group 2	Group 4
Cell wall and membrane complex	oligosaccharyltransferase complex (GO:0008250)	Group 4	Group 4
	endosome membrane (GO:0010008)	Group 3	Group 4
	cellulose synthase complex (GO:0010330)	Group 4	Group 4
	endocytic vesicle (GO:0030139)	Group 4	Group 4
	cell wall (GO:0005618)	Group 4	Group 4
	plasma membrane protein complex (GO:0098797)	Group 4	Group 4

Vacuolar complex	plant-type vacuole (GO:0000325)	Group 4	Group 4
	vacuolar proton-transporting V-type ATPase complex (GO:0016471)	Group 3	Group 4
	proton-transporting V-type ATPase, V1 domain (GO:0033180)	Group 3	Group 4
Metabolon	oxoglutarate dehydrogenase complex (GO:0045252)	Group 3	Group 2 (GO:0045254)
Motor related complex	myosin complex (GO:0016459)	Group 2	Group 4
Transmembrane complex	transmembrane transporter complex (GO:1902495)	Group 4	Group 4
Cytoskeleton complex	microtubule (GO:0005874)	Group 1	Group 4
Mitochondrial complex	mitochondrial outer membrane (GO:0005741)	Group 1	Group 4
	mitochondrial inner membrane (GO:0005743)	Group 4	Group 4
Chloroplast complex	chloroplast membrane (GO:0031969)	Group 4	Group 4

378 • **Note:** the table integrates the information from A1 and G1 tabs in Table S4 (both tabs contain their own legends for
379 clarity of the information being presented). GO terms have been defined in parenthesis at first appearance. When
380 cellular complex subsets and not the whole monitored complex belongs to one of the response groups, the GO terms
381 are indicated in parenthesis.

382 There are four groups of responses for protein-complexes and their components in Table 2.
383 Group one contains proteins that accumulate and are preferentially synthesised at a specific tem-
384 perature. Group two contains proteins that accumulate due to lack of protein degradation because
385 they do not incorporate the nitrogen isotope. Group three contains proteins that do not accu-
386 mulate and nevertheless are preferentially synthesised at a specific temperature, implying high
387 turnover. Group four contains proteins that are detected but do not accumulate nor are preferen-
388 tially synthesised. The three significant groups (1-3) can be found at sub-optimal low temperature
389 whereas only group one and two are found at optimal temperature.

390 Altered Ribozyme-Mediated Proteome Remodelling

391 The global ontology term of cytosolic translation in Table 2, which includes ribosome biogenesis,
392 has proteins that belong to the three significant groups of responses (1-3) at both temperature
393 regimes.

394
395 The accumulation dynamics of ribosome biogenesis complexes, which give rise to mature and
396 translationally competent ribosomes, provides insight into the origin of assembled ribosomes.
397 For example, the 90S pre-ribosome in the nucleolus leads to pre-60S and pre-40S complexes.
398 Following their maturation, pre-40S complexes are shaped by the small-subunit processome.
399 Protein components from all these four types of biogenesis complexes significantly accumulate
400 at sub-optimal low temperature. Interestingly, the small-subunit processome features proteins
401 from group one, i.e., accumulating due to *de novo* synthesis. Whereas the other three complexes
402 accumulate due to lack of degradation (group two). This implies that the only remodelled complex
403 from the biogenesis subset is the small-subunit processome, while the others keep functioning in
404 the same state as that from plants growing at optimised temperature.

405
406 In terms of assembled cytosolic ribosomes, their structural protein components, as well as
407 those from mitochondrial ribosomes, are accumulated preferentially at optimised temperature.

408 The cytosolic ribosome components are preferentially synthesised, which categorises them in
409 group one. In contrast, the mitochondrial ribosome components are not preferentially synthe-
410 sised and thus accumulate due to lack of degradation (group two). On the other hand, the protein
411 structural components of the cytosolic large ribosomal subunit are preferentially synthesised but
412 not accumulated during cold, which categorises them in group three and indicates a remodelling
413 aspect that is coupled to high turnover of these complexes at sub-optimal temperature.

414

415 Translation initiation complexes preferentially accumulate only at sub-optimal low temper-
416 ature and, all of them belong to group one, where their proteins accumulate due to *de novo*
417 synthesis.

418

419 Beyond the translation ontology term, many of the detected protein complexes that preferen-
420 tially accumulated at low sub-optimal temperature belonged to group one, where their protein
421 components are also newly synthesised. Two major ontological groups stand out as being newly
422 synthesised by ribosomes and accumulated during cold. In brief, cellular machinery to cope with
423 protein misfolding and aggregation is newly synthesised and accumulated (CCT complex protein
424 components and heat shock proteins) as well as cellular complexes that mediate remodelling of
425 the cell walls and cellular membranes. Thus, this prompted us to analyse in more depth the extent
426 of triggered ribosome heterogeneity and its potential structural link to the observed proteome
427 shift that happens due to protein synthesis by ribosomes.

428 **Recycled and Remodelled Ribosomes Accumulate during Cold Acclimation**

429 To characterise cold-induced rProtein heterogeneity and decipher its origin, we adjusted the
430 protease digestion to the requirements of a highly basic ribosomal proteome (Figure 6 - Figure
431 S1 and Table S6), and used the optimized method to profile ribosome-enriched barley proteome
432 extracts. To validate that our method enabled recovery of native ribosomes, we subjected
433 *Escherichia coli* 70S ribosomes to the same purification method and assessed the completeness
434 of the recovered ribo-proteome. We found 21/21 30S small subunit rProteins and 33/33 50S large
435 subunit rProteins, which featured reproducible abundances in triplicated measurements (Figure
436 6 - Figure S2 and Table S7). We then calculated protein abundances, relative stoichiometry, and
437 fractional synthesis rates for ribosome structural protein components of the barley extracts at
438 the onset of the physiological transition from optimized germination conditions to sub-optimal
439 low temperatures (Figure 6 and Table S4H).

440

441 Previously, we observed that rProteins, when averaging ribosome-bound and ribosome-free
442 forms, increase in abundance in barley root tips of germinating seedlings subjected to cold
443 acclimation (*Martinez-Seidel et al., 2021c*). Here, we found reliable LFQ intensities for 17 rProtein
444 families from the small 40S subunit (SSU) and 38 rProtein families from the large 60S subunit
445 (Table S4C), all of which were bound to ribosomal complexes. Among these 55/80 high confidence
446 rProtein families, a total of 95 paralog genes were identified.

447

448 **Ribosomal Protein Substoichiometry**

449 The sum of SSU-rProtein abundances correlated linearly over an r^2 of 0.98 with the sum of
450 LSU-rProtein abundances across all samples, maintaining a constant ratio of 3x LSU to 1X SSU
451 (Figure 6 - Figure S3 and Table S4C). Nevertheless, the LFQ abundances of all identified paralogs
452 decreased in their ribosome-bound form during cold acclimation, either significantly (Table S4B)
453 or not. Thus, the control seedlings had in average more 40S and 60S assembled subunits in their
454 root tips. Consequently, we used the sum of 40S proteins to normalize the individual rProtein
455 abundances of SSU and the sum of 60S proteins to normalize the individual rProtein abundances
456 of LSU in order to correct for the relative amount of complexes across samples, as was previously

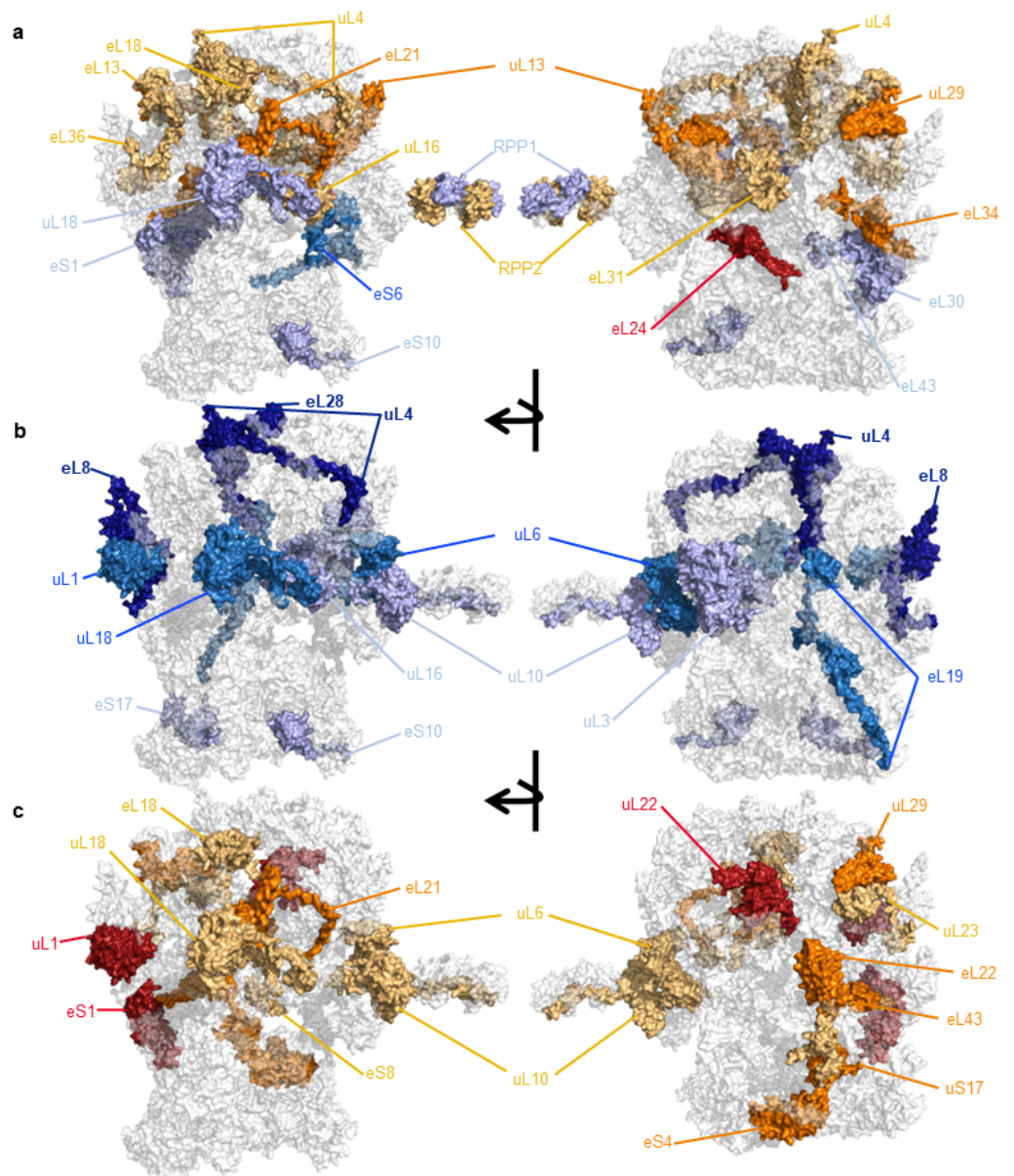


Figure 6–Figure supplement 1. Volcano plot outlining the differences in mean peptide length produced with Lys-C or Trypsin, during an *in silico* protease digestion test, as proteases to digest the Arabidopsis signature plant ribosomal proteome.

Figure 6–Figure supplement 2. Positive control and complete coverage of *escherichia coli* 70S ribosomal proteome from a commercially available preparation used to verify the ribosomal proteomics pipeline.

Figure 6–Figure supplement 3. Ratio between 40S SSU and 60S LSU abundances across experimental samples

Figure 6. Characterization of cold heterogeneous barley ribosomes, their ribosomal protein (rProtein) composition, fractional synthesis rates and induced substoichiometry. Barley ribosomes from plant ^{15}N labelled proliferative tissue were purified and used to profile the rProteome. Abundances and isotopolog envelopes were recovered from the Mass Spectrometry data and used to calculate average ribosome relative stoichiometry of rProteins and their fractional synthesis rates. (a) rProtein substoichiometry; orange and reds are rProteins accumulated at optimal temperature and blues rProteins accumulated during cold in the ribosomal population. (b) Preferential synthesis of assembled rProteins during cold acclimation. (c) Preferential synthesis of assembled rProteins during control temperature. Preferential synthesis refers to peptides with significant changes (P_{adj} values < 0.05, $n = 3$, tested using a customized generalized linear model) in their fractional synthesis rates.

457 reported (*Martinez-Seidel et al., 2021a*). The normalization allowed us to determine whether
458 these complexes exhibit induced substoichiometry in their rProtein compositions (Figure 6A).

459

460 The population of 40S subunits was enriched in four rProtein paralogs during cold, namely
461 eS10 (HORVU3Hr1G111760), eS1 (HORVU1Hr1G032060 and HORVU4Hr1G070370), and eS6
462 (HORVU2Hr1G010870). Thus, the population of 40S subunits in barley root tips is not canonically
463 complete and sometimes these paralogs are absent compared with the cold population. The
464 population of 60S subunits contains paralogs that are relatively depleted or accumulated in
465 cold conditions. The rProtein families P2 (HORVU1Hr1G073640), uL16 (HORVU1Hr1G024710),
466 eL13 (HORVU7Hr1G067060), eL18 (HORVU2Hr1G018820), eL31 (HORVU7Hr1G050170),
467 eL36 (HORVU5Hr1G009600), uL4 (HORVU4Hr1G075710), eL34 (HORVU7Hr1G071240),
468 uL29 (HORVU2Hr1G068120), eL21 (HORVU1Hr1G038890), uL13 (HORVU5Hr1G096060 and
469 HORVU2Hr1G063900), eL24 (HORVU3Hr1G080130 and HORVU5Hr1G111510) are depleted during
470 cold. The rProtein families P1/P2/P3 (HORVU7Hr1G075360), eL30 (HORVU0Hr1G023290), eL43
471 (HORVU1Hr1G085170), uL18 (HORVU2Hr1G073320) are accumulated during cold.

472

473 Altered Ribosomal Protein Synthesis and Ribosome Remodelling

474 We next examined rProtein synthesis rates to understand what constituted the newly synthe-
475 sised rProtein substoichiometry (Figure B-C). In general, the cold-induced changes in rProtein
476 synthesis did not coincide with substoichiometry, suggesting independence between rProtein
477 synthesis and ribosome assembly/remodeling. The population of 40S subunits was assem-
478 bled or remodeled using four rProtein paralogs that were significantly more synthesised at
479 optimized temperature, namely eS8 (HORVU6Hr1G056610), uS17 (HORVU2Hr1G067370), eS4
480 (HORVU1Hr1G021720), eS1 (HORVU1Hr1G032060). Similarly, two rProtein paralogs were signifi-
481 cantly more synthesised during cold: eS10 (HORVU3Hr1G111760), eS17 (HORVU6Hr1G056610).
482 The population of 60S subunits was assembled or remodeled using several rProtein paralogs,
483 which were significantly more synthesised at optimized temperature or during cold. Par-
484 alogos uL10 (HORVU7Hr1G073720), eL18 (HORVU2Hr1G018820), uL23 (HORVU2Hr1G086360),
485 uL18 (HORVU2Hr1G073320), eL6 (HORVU7Hr1G00206), eL21 (HORVU1Hr1G038890), eL22
486 (HORVU2Hr1G019160), uL29 (HORVU2Hr1G068120), eL43 (HORVU1Hr1G085170), uL22
487 (HORVU5Hr1G052280), uL1 (HORVU7Hr1G059090) were preferentially synthesised and assem-
488 bled at optimized temperature. Paralogs uL16 (HORVU1Hr1G024710), uL3 (HORVU4Hr1G019980),
489 eL19 (HORVU2Hr1G018700), uL1 (HORVU3Hr1G084310 and HORVU1Hr1G085730),
490 uL18 (HORVU5Hr1G092630 and HORVU2Hr1G073320), eL6 (HORVU7Hr1G00206), eL28
491 (HORVU1Hr1G079370), uL4 (HORVU4Hr1G075710), eL8 (HORVU7Hr1G054670) were prefer-
492 entially synthesised and assembled in the cold.

493

494 From our results, five types of paralog-specific and rProtein family ribosome association and
495 synthesis dynamics can be deduced:

496 1. Paralog switches:

- 497 • based on protein synthesis, the uL1 paralogs HORVU3Hr1G084310 and
498 HORVU1Hr1G085730 (cold) and HORVU7Hr1G059090 (control).
- 499 • based on substoichiometry, P1/P2/P3 paralogs HORVU7Hr1G075360 (cold) and
500 HORVU1Hr1G073640 (control).

501 2. Families with paralogs sharing ribosome-bound accumulation or synthesis dynamics:

- 502 • based on protein synthesis, uL18 HORVU5Hr1G092630 and HORVU2Hr1G073320 (cold-
503 specific); uL1 HORVU3Hr1G084310 and HORVU1Hr1G085730 (cold-specific).
- 504 • based on substoichiometry, eL24 HORVU3Hr1G080130 and HORVU5Hr1G111510

505 (control-specific); uL13 HORVU5Hr1G096060 and HORVU2Hr1G063900 (control-
506 specific); eS1 HORVU1Hr1G032060 and HORVU4Hr1G070370 (cold-specific).

507 **3. Paralog splice variants (peptides from the same protein with different synthesis dy-**
508 **namics under cold and control conditions):**

509 • uL10 HORVU7Hr1G073720 (one peptide from exon 5 is cold-synthesized and one from
510 exon 4 control-synthesized).

511 **4. Paralogs that share ribosome-bound accumulation and synthesis dynamics:**

512 • eS10 HORVU3Hr1G111760; eL18 HORVU2Hr1G018820; eL21 HORVU1Hr1G038890;
513 uL29 HORVU2Hr1G068120; uL18 HORVU2Hr1G073320

514 **5. Paralogs with inverse ribosome-bound accumulation and synthesis dynamics:**

515 • accumulated in control ribosomes but preferentially synthesised in cold; uL16
516 HORVU1Hr1G024710; uL4 HORVU4Hr1G075710

517 • accumulated in cold ribosomes but preferentially synthesised during control; eS1
518 HORVU1Hr1G032060; eL43 HORVU1Hr1G085170

519 **Discussion**

520 **Morphological Phenotype of Barley Roots during Low Temperature Germination**

521 At the physiological level, plants exhibit a growth arrest during the first week of cold acclimation
522 (*Beine Golovchuk et al., 2018; Martinez-Seidel et al., 2021a,c*). *Arabidopsis thaliana* roots reduce
523 mitotic division but not cell elongation at a sub-optimal temperature of 4°C, which significantly re-
524 duces meristem size (*Ashraf and Rahman, 2019*). Similarly, barley roots from acclimated seedlings
525 reduce their protein content (*Martinez-Seidel et al., 2021c*), which is mainly related to dry weight ac-
526 cumulation and thus by proxy to mitotic division, suggesting that the cold phenotype of barley and
527 *Arabidopsis* may share this aspect. In our system, the root length and volume of non-acclimated
528 seedlings increased significantly and steadily compared to the acclimated counterparts, which was
529 enhanced by water accumulation as shown by differences in fresh weight. Conversely, root dry
530 weight did not differ between acclimated and non-acclimated seedlings. The ratio of fresh weight
531 to dry weight remained constant at the end of the acclimation period, and yet there was a transient
532 relative increase in dry weight accumulation from the second to the third day causing a significant
533 imbalance in the dry to fresh weight ratio of acclimated seedlings. In consequence, the dynamics
534 of dry weight accumulation during germination of acclimated barley seedlings are not comparable
535 to their non-acclimated pairs and, therefore, global analyses of protein turnover need to account
536 for this difference.

537 **Cold Metabolic Phenotype and Testable Links to Translational Responses**

538 In spite of not growing, roots from acclimated barley seedlings show a transition to cold-induced
539 metabolic states. After two days of cold treatment (4 °C) in the dark, glucose increases in barley
540 seedlings, while proline, sucrose, and total lipids decrease (*Zúñiga et al., 1990*). Thus, there is a
541 transient decrease in the abundance of these compounds during the early stages of acclimation,
542 coinciding with the peak of dry weight accumulation reported in our study. The transient decrease
543 in metabolites could subsequently attenuate and then increase again at later stages of acclimation.
544 Transcriptional studies in barley leaves on the third day of cold acclimation (3°C during the day,
545 2°C at night) predict the accumulation of sugars and polyols such as maltose, glucose, trehalose,
546 and galactinol (*Janská et al., 2011*), and we show that glucose and sucrose were accumulated on
547 the fifth day of acclimation (maltose was not accumulated, and galactinol and trehalose were not
548 detectable). In contrast, the amino acid biosynthetic pathway is not predicted to be upregulated at
549 the transcriptional level, and yet we observed that 25 of the 29 amino acids we detected (including
550 the well-known osmoprotectant proline) were accumulated under cold conditions compared with
551 the optimal temperature. Thus, a cold-metabolic state in our system is consistent with evidence for

552 potential translational control that influences the acclimation response by differentially impacting
553 the amino acid biosynthesis pathway. Amino acid pools can increase from mobilised nitrogen
554 resources or from enzymatic synthesis, the latter of which requires the accumulation of specific
555 proteins through direct or indirect translational control, because amino acid biosynthesis is not
556 predicted to be upregulated based on barley cold-transcriptional dynamics (*Janská et al., 2011*).
557 Our report demonstrates that some of the accumulated amino acids also incorporated ¹⁵N during
558 cold, suggesting that they may be in part newly synthesized and not just degradation products
559 of storage proteins, as will be discussed in the following paragraph. The role of all accumulated
560 soluble sugars, amino acids, and polyols in the context of cold acclimation is thought to be that of
561 an osmoprotector, i.e., compounds that stabilise proteins and membranes and thus contribute to
562 freezing tolerance (*Rontein et al., 2002*).

563 **Amino Acid Metabolism and ¹⁵N Isotopic Flux**

564 How nitrogen uptake and supply occurs in germinating barley seedlings determines the best strat-
565 egy for isotope flux studies in this system. Most of the nitrogen resources used by germinating
566 barley embryos come from degraded storage proteins located in the endosperm during germi-
567 nation (*Ma et al., 2017; Rosental et al., 2014; Nonogaki, 2008; Lea and Joy, 1983*). Thus, nitrogen
568 transport into the embryo in the form of amino acids and peptides is critical for controlling and
569 setting efficient germination. For example, nitrogen transport and reassimilation is fundamental
570 for the development of gene expression programs in barley caryopses (*Mangelsen et al., 2010*).
571 Consequently, germinating barley embryos activate genes involved in biosynthesis, metabolism,
572 and transport of amino acids at an early stage of 2 to 3 days after germination (*Sreenivasulu et al.,*
573 *2008*), with peptide transporters considered particularly critical for normal germination processes
574 (*Waterworth et al., 2000*). At the proteome level, nitrogen mobilization systems that supply
575 nutrients to the growing embryo are induced and activated (*Osama et al., 2021*). For example,
576 proteases, including carboxypeptidases and aminopeptidases, provide peptide or amino acid
577 substrates that are released, transported, and used during germination (*Sreenivasulu et al., 2008;*
578 *Shutov and Vaintraub, 1987; Hammerton and Ho, 1986; Dal Degan et al., 1994*). Similarly, just prior
579 to radicle sprouting, genes encoding proteins involved in amino acid biosynthesis and transport
580 are upregulated, whereas genes involved in amino acid degradation are largely unresponsive (*Ma*
581 *et al., 2017*). This suggests that nitrate reductase activity is not required to reassimilate nitrogen
582 from amino acid catabolism. Our results suggest that after feeding enriched amino acids, the
583 spread of the tracer across all proteinogenic soluble amino acid pools is rather limited and only
584 increases at low sub-optimal temperature. Thus, it appears that amino acid degradation and
585 reassimilation are suppressed processes during barley germination at optimized temperature.
586 Instead, barley seeds may be genetically tuned to rely on amino acid mobilization during the early
587 stages of embryo development. Therefore, using labelled amino acids to introduce the tracer into
588 germinating barley seedlings may be the best and only strategy to follow *in vivo* isotopic fluxes
589 into protein.

590
591 Germinating barley seedlings have at least four systems for successful amino acid uptake
592 (*Salmenkallio and Sopanen, 1989*), all of which depend on storage proteins or their hydrolysis prod-
593 ucts being taken up into the scutellum for further hydrolysis and utilization (*Higgins and Payne,*
594 *1981*). Thus, the supply of ¹⁵N-labeled amino acid compounds in the germination media ensures
595 that these nitrogen atoms are introduced into and utilized by the plants. However, because of the
596 generous availability of endogenous amino acid resources, the incorporated ¹⁵N-labeled amino
597 acids are diluted in the roots of germinating seedlings. Moreover, at low temperatures, all en-
598 zymatic activities and cellular dynamics slow down. Therefore, mobilization of amino acids and
599 peptides for nitrogen supply during germination is also likely to be affected by lower tempera-
600 tures. Our results suggest that barley seedlings subjected to acclimation take up more labelled
601 amino acids through their roots and use / spread their nitrogen supply across soluble amino acid

602 pools. Thus, it is possible that nitrogen deficiency resulting from slowed nutrient mobilization is
603 compensated for by increased uptake of nutrients through the roots, and since amino acid and pep-
604 tide transporters are already available from the germination process, these compounds would be
605 adsorbed. The bottom line is that the physiological transition triggered by acclimation to low tem-
606 peratures causes differential incorporation of amino acids carrying the tracer, differential spread
607 of the tracer across amino acid pools and different accumulation of soluble amino acids, and all of
608 these differences must be accounted for if biological insights are to be derived from tracking the
609 tracer incorporation into polypeptides.

610 **Ribozyme-mediated ¹⁵N Incorporation Into Protein**

611 In all living organisms, the proteome is synthesised by ribosomes, whose ribozyme activities
612 catalyse the formation of peptide bonds between the existing peptidyl-tRNA and the subsequent
613 aminoacyl-tRNA (*Rodnina, 2013*). Thus, the natural pathway of ¹⁵N-labeled amino acids is to
614 conjugate with tRNAs and be transported to ribosomes, where they enter the elongation cycle
615 and end up as a monomer in a synthesised polypeptide. Amino acids exist as soluble pools in the
616 cytoplasm and are loaded onto aminoacyl-tRNAs, which are present in much lower proportions
617 as compared to amino acid pools and are much more labile, i.e., their turnover is extremely rapid
618 (*Gomez and Ibba, 2020*), suggesting that the enrichment in soluble amino acid pools is a valid
619 proxy for isotope enrichment in aminoacyl-tRNA conjugates.

620
621 The main activity of ribosomes is autocatalysis (*Reuveni et al., 2017*), and as such the tracer
622 is expected to be incorporated first into the machinery within one degree of ribosomes (*Bowman*
623 *et al., 2020*), which include rProteins, aminoacyl-tRNA synthetases, tRNAs, initiation, elongation
624 and release factors. The cellular proteome within one degree of ribosomes is part of macromolec-
625 ular complexes. Thus, by purifying a complexome proteome, one can recover translation-related
626 multiprotein complexes in a near-native state while co-purifying other complexes. In this way, it
627 is possible to test the link between ribosome structural divergence and altered rates of protein syn-
628 thesis at sub-optimal low temperature. Altered protein synthesis can be caused by direct or indirect
629 translational control determining which transcripts are translated under the limited growth of cold
630 acclimation. Direct translational control implies an altered and selective ribozyme-functionality
631 shaping the proteome. In our system, translation during cold is carried out by a ribosomal popula-
632 tion that is heterogeneous and substoichiometric in its rProtein composition. Altered rProteome
633 compositions confer metazoan ribosomes the ability to selectively recruit transcripts for transla-
634 tion, i.e., to specialize (*Shi et al., 2017; Genuth and Barna, 2018*). Additionally, Plants have an in-
635 creased number of rProtein paralogs compared to all higher metazoans (*Barakat et al., 2001*), and
636 the fate of duplicated genes usually leads to novel and divergent functions (*Kosová et al., 2021*).
637 Thus, it is probable that specialized rProtein proteoforms may equip heterogenous ribosomes to
638 perform direct translational control, efficiently adapting them to cold temperatures.

639 **Translational Dynamics of Heterogeneous Ribosomes**

640 In Arabidopsis, cold heterogeneous translating ribosomes exhibit rProtein substoichiometry
641 around the polypeptide exit tunnel (PET), with many of the rProteins being relatively removed
642 during cold (*Martinez-Seidel et al., 2021a*). Here, we report that barley ribosomes also exhibit, on
643 average, subtractive heterogeneity (*Briggs and Dinman, 2017*) in the cold-ribosomal population
644 around protein uL4 and uL29, the former being essential for PET assembly during ribosome
645 biogenesis (*Lawrence et al., 2016; Gamalinda and Woolford, 2014; Stelter et al., 2015; Pillet et al.,*
646 *2015*), as its internal loops form the constriction sites of the nascent PET (*Micic et al., 2022*) along
647 uL29. The PET and its assembly are likely to be particularly critical during cold acclimation because
648 both yeast (*Hung and Johnson, 2006*) and plants (*Schmidt et al., 2013*) have a 60S maturation
649 factor that when knocked out, leads to cold sensitivity, namely Rei-1 in yeast and its homolog
650 REIL in plants. The functional role of Rei-1 in yeast is to insert its C-terminus into the PET to check

651 the integrity of the tunnel as a quality control step before making 60S subunits translationally
652 competent (*Greber et al., 2016*). Thus, subtractive rProtein heterogeneity near the tunnel could
653 indicate higher rRNA disorder, defective tunnel assembly, and/or defective structure, causing the
654 observed need for PET quality control during cold.

655
656 On the other hand, the 60S rProteins accumulated in the cold population of ribosomes, uL18
657 and eL30, are located near important intersubunit bridges (*Martinez-Seidel et al., 2021b; Tamm
658 et al., 2019*). Similarly, the population of 40S subunits, which shows accumulation of specific
659 rProteins only during cold, has two rProteins, eS6 and eS1, that also form important intersub-
660 unit bridges in the form of connections between the 40S and 60S and their constituent rProteins
661 (*Martinez-Seidel et al., 2021b; Tamm et al., 2019*). The third rProtein more abundant in 40S sub-
662 units, eS10, links the large uS3 hub (containing the ribosomal region adjacent to the tRNA-mRNA
663 entry sites) to the uS13-uL11 subunit bridge (*Martinez-Seidel et al., 2021b*). Bridges between sub-
664 units in bacteria have been shown to directly affect initiation factor-dependent translation (*Kipper
665 et al., 2009*). Thus, these observations suggest that the rProteins accumulated during cold in ribo-
666 somal populations are related to subunit connectivity and may influence their association during
667 initiation, elongation or termination.

668 **Translation Initiation: Newly Synthesised Complexes**

669 Complexes related to translation initiation were accumulated during cold acclimation in our
670 system due to synthesis of their protein components, implying tight control over what type of
671 translation initiation complexes form and participate in 40S transcript association. Translation ini-
672 tiation is a sequential and complex process that is highly conserved (*Jackson et al., 2010; Hashem
673 and Frank, 2018*) and nonetheless exhibits peculiarities in its regulation in plants (*Castellano
674 and Merchante, 2021*). Translation initiation begins with the binding of multiple factors to the
675 40S subunit to form a 43S pre-initiation complex (PIC) (*Aylett et al., 2015; Hashem et al., 2013;
676 Majumdar et al., 2003*), which then binds the mRNA to be translated, supported by multiple
677 factors, to form the 48S initiation complex (IC) (*Brito Querido et al., 2020; Pisareva and Pisarev,
678 2014*). Finally, the IC is supported by several factors to allow the 60S subunits to connect, making
679 the elongation process competent in the newly formed 80S monosome (*Fringer et al., 2007; Shin
680 et al., 2002*). In our study, we found that several protein components of the initiation machinery
681 are both significantly accumulated and synthesised during cold:

- 682
683 1. First, the eukaryotic translation initiation factor 3 subunits A, B, C, and E (eIF3A-C,E). The eIF3
684 complex consists of 13 subunits (A-M) and is the most complex initiation factor in eukaryotes
685 and also the largest (*Des Georges et al., 2015; Zhou et al., 2008*). Moreover, eIF3 has been
686 associated with various pathological conditions in higher metazoans (*Gomes-Duarte et al.,
687 2018*). Subunits A and C bind eIF3 to 40S subunits via the platform on the solvent side (*Aylett
688 et al., 2015*) and can also interact with eIF1 and eIF4G via subunit E (*LeFebvre et al., 2006*).
689 Thus, 3/4 of the preferentially accumulated and synthesised eIF3 subunits serve as anchors
690 between ribosomes and mRNA recruitment factors. Subunit B is part of the eIF3b-i-g module
691 and presumably interacts with the 40S subunit directly at the mRNA entry channel by
692 occupying it (*Chiu et al., 2010*). Accumulation of these specific subunits of the eIF3 complex
693 is associated with cancer in humans via increased (*Scoles et al., 2006; Xu et al., 2012; Wang
694 et al., 2013*) and selective (*Dong et al., 2004; Parasuraman et al., 2017*) translational output.
- 695
696 2. Second, eukaryotic translation initiation factor 2 subunit 1 (eIF2 α). This eIF catalyses the
697 first step of 40S - initiator-tRNA (Met-tRNA) association (*Hinnebusch, 2017*). This factor is
698 the central element of the integrated stress response in eukaryotes (*Pakos-Zebrucka et al.,
699 2016*), as it leads to a global decrease in protein synthesis through a phosphorylation event

700 mediated by eIF2 α kinases, while promoting the selective translation of specific transcripts
701 whose protein products are required for survival (*Lu et al., 2004*). In this case plants may
702 be using this robust and well-characterized stress response for successful acclimation to
703 sub-optimal low temperatures.
704

705 Importantly, the significant accumulation of a protein fraction enriched in rProteins during cold,
706 which we reported previously (*Martinez-Seidel et al., 2021c*) and demonstrated again in this study
707 (Figure 5 - Figure S1), originated from complexes related to ribosome biogenesis and translation ini-
708 tiation, highlighting the functional importance of translation initiation during cold acclimation and
709 assigning a potential regulatory and functional role to the group of cold heterogeneous rProteins.
710 The accumulation of machinery at both sides of competent ribosomes, i.e. pre-ribosomes and
711 translation initiation complexes, along with the maintained ratio of 40S to 60S subunits suggests
712 that the limiting step during cold acclimation is successful initiation. Thus, the set of competent
713 60S subunits assembled during cold might select which transcript to translate based on an excess
714 of PICs and ICs.

715 **Ribosome Biogenesis: Assembled and Remodelled Ribosomes**

716 The increasing complexity uncovered in the process of ribosome biogenesis suggests that the
717 highly energy demanding process of assembling ribosomes is connected to major environmen-
718 tal and developmental cellular responses (*Lindahl, 2022*). In our study, ribosome biogenesis
719 complexes accumulated during cold acclimation due to the lack of degradation, as their protein
720 components did not take up the ¹⁵N tracer and yet were significantly more abundant during cold
721 compared with control conditions. The only pre-ribosomal complex that accumulated newly syn-
722 thesised protein components was the small subunit processome. The small subunit processome
723 is the earliest pre-40S complex found to date in eukaryotes, and it uses many accessory factors to
724 process and mature 40S subunits (*Barandun et al., 2017*). Therefore, the protein components that
725 are newly synthesised during cold might indicate alternative processing of pre-40S subunits, which
726 could be related to the reported cold-specific accumulation of 40S rProteins in assembled SSU
727 complexes. At the structural rProtein level, there were fewer competent ribosomes during cold,
728 and only 60S subunit components were generally and preferentially synthesised during cold, to
729 such an extent that GO enrichment of the 60S structural component category was detected when
730 the cold-synthesised proteome was examined. Thus, our results suggest that there is restructur-
731 ing due to altered LSU rProtein synthesis in cold-acclimated 60S large subunits and variability in
732 processing of pre-40S small subunits of cytosolic ribosomes due to differential protein synthesis
733 of components from the small subunit processome. Both aspects are complemented by increased
734 abundances of ribosome biogenesis complexes, suggesting that ribosome heterogeneity arises in
735 part from the ribosome assembly line at low sub-optimal temperatures.
736

737 At the individual protein level, it is clear that ribosomes are assembled or remodelled using
738 new and old rProteins. Only a subset of rProteins significantly incorporated the tracer ¹⁵N, confirm-
739 ing the previously observed fact that in plants cytosolic rProteins exhibit the greatest variability in
740 degradation rates among protein components of large cellular complexes (*Li et al., 2017*). This vari-
741 ability makes economic sense, as ribosome assembly and protein biosynthesis impose the greatest
742 cellular costs (*Shore and Albert, 2022*) and continued synthesis of each component within the trans-
743 lational apparatus would be detrimental. In addition, rProteins in plants have a half-life of about 4
744 days (*Salih et al., 2020*), and given the slower cell dynamics at cold temperatures, relying solely on
745 ribosome biogenesis to control translational dynamics would be too slow. Therefore, remodelling
746 old ribosomes to adapt them for the work at hand could be an efficient way to alter their function.
747 For example, in higher metazoans, ribosomes in neuropil (far from the nucleolus) are remodelled
748 *in situ* rather than undergoing a new cycle of ribosome biogenesis and subsequent transport to

749 dendrites and axons, and this is a means of regulating local protein synthesis depending on the
750 cellular context (*Fusco et al., 2021*). Whether this is the case in plants remains to be tested, because
751 we do not report rRNA synthesis rates required to determine whether a complete biogenesis cycle
752 generated the heterogeneous ribosomes using new and old rProteins or whether, on the contrary,
753 these ribosomes were remodelled in the cytoplasm.

754 **Translational Outcome of Heterogeneous Ribosomes: A Proteome Shift**

755 The assembled and remodelled heterogeneous ribosomes are able to cause a significant part of
756 the proteome shift observed during cold (the rest of the shift is due to the lack of degradation
757 of specific proteins). In addition to complexes related to translation, cold-remodelled ribosomes
758 significantly affect the synthesis and accumulation of protein folding machinery, complexes from
759 the endoplasmic reticulum (ER) and Golgi, nuclear complexes and complexes related to the cell
760 cycle, cell wall and microtubule complexes, and protein complexes from the outer mitochondrial
761 membrane. All of these complexes and their individual proteins could be of great importance for
762 acclimation, as the plant accumulates them beyond the level reached in plants grown at optimal
763 temperature, despite its limited resources and slow growth dynamics.

764
765 We found that 6/8 subunits of the cytosolic chaperonin T-complex-protein 1 ring complex
766 or chaperonin-containing TCP-1 (CCT) are preferentially synthesised during cold, leading to
767 accumulation of the complex, which may be directly related to the altered functionality of cold
768 heterogeneous ribosomes. The CCT binds and promotes protein folding of newly synthesised
769 polypeptides (*Lopez et al., 2015; Yébenes et al., 2011*) or promotes their aggregation and thus
770 protein degradation to maintain proteostasis (*Lopez et al., 2015; Hartl et al., 2011; Spiess et al.,*
771 *2004*). We have shown that during cold in plants, ribosome remodeling, i.e., subtractive hetero-
772 geneity, occurs in the proteome surrounding the PET, and the signature of a defective tunnel
773 is protein misfolding (*Micic et al., 2022; Peterson et al., 2010; Wruck et al., 2021*). Thus, it is
774 conceivable that an altered tunnel structure leads to increased protein misfolding and this forces
775 the plant cell to produce more CCT complexes to properly fold or aggregate misfolded proteins in
776 order to fix or degrade them, respectively. Moreover, we found that several heat shock proteins
777 are preferentially synthesised and accumulated at cold temperatures, underscoring that protein
778 misfolding is an urgent problem that plants need to address during acclimation to sub-optimal
779 low temperatures.

780
781 We also found that nuclear and cell cycle complexes were preferentially synthesised and
782 accumulated. Among them was condensin, which in addition to its role in the cell cycle promoting
783 chromosome assembly, is also known to directly regulate gene expression (*Iwasaki et al., 2019; Li*
784 *et al., 2015*). Plants stop their mitotic activity in response to cold (*Ashraf and Rahman, 2019*), and
785 thus condensin is less likely to accumulate to promote further cell cycle progression, but rather
786 may accumulate to promote mechanisms of transcriptional control in response to cold.

787
788 All other preferentially synthesised and accumulated complexes can be classified into the
789 machinery that transports and targets the cell membrane and wall. Among this type of complexes
790 we found ER and Golgi components as well as cell wall and microtubule proteins. They were
791 all directly related to protein transporters, glycosyltransferases, membrane transport compo-
792 nents, and cell wall structure. The integrity of cell membranes and walls is threatened in plants
793 during cold as membrane fluidity decreases and dehydration increases (*Takahashi et al., 2020*).
794 Therefore, physical changes such as remodelling of the lipidome of membranes (*Barrero-Sicilia*
795 *et al., 2017*) are essential to survive cold (*Johnson, 2018*). For example, abundance changes of
796 specific lipid species in other cereal models confer cold resistance (*Cheong et al., 2022*). Such
797 membrane remodelling mechanisms in plants can rely on enzymatic activity to deliver new
798 components needed to enhance cold acclimation (*Fourrier et al., 2008*). Many of the proteins

799 that are transported to the cell periphery are initially synthesised near the ER - Golgi organelles,
800 where the shuttles that transport them are ready to deliver them to their site of function. We have
801 provided evidence that the transport machinery is active during cold, accumulating and being
802 newly synthesised. This may be part of the plant's attempt to mitigate the loss of membrane
803 integrity by transporting necessary membrane and wall components or the enzymes to produce
804 them. Most importantly, translation of this sub-proteome demonstrates that cold-heterogeneous
805 ribosomes are able to directly or indirectly control their translational output to efficiently acclimate.

806
807 Cold-heterogenous ribosomes also synthesise components of other macromolecular com-
808 plexes without accumulating them. This type of synthesis implies potential remodelling of com-
809 plexes that continue to be present in equal amounts due to ongoing protein turnover. Complexes
810 that fall into this category include the 60S ribosomal subunit, translation initiation, ER-Golgi, protea-
811 some, vacuolar proton-transporting ATPase, and the oxoglutarate metabolon.

812 **Conclusions**

813 With careful consideration of the ^{15}N isotope flux and plant phenotype, we were able to monitor
814 tracer incorporation into digested peptides of proteins at the complexome proteome level and
815 compare between experimental conditions. Our strategy can be applied to any system that transi-
816 tions between different biological steady states to study the dynamics of protein synthesis, as long
817 as the right variables can be measured. We have made available our equations and complete bioin-
818 formatics method as a public R package, i.e., the [ProtSynthesis R package](#). We applied this strategy
819 to understand the transition of proliferative root tissue from germinating barley seedlings to a cold
820 acclimated state. The proliferating root tissue of germinating barley seedlings undergoing cold ac-
821 climation, like Arabidopsis, requires ribosome biogenesis to overcome the initial stimulus. In ad-
822 dition, plants build remodelled and heterogeneous ribosomes that cause a shift in the proteome.
823 To characterize the heterogeneity, we mapped the relative stoichiometry of ribosome-assembled
824 rProteins and their synthesis rates using proteome-wide ^{15}N labelling to determine which part of
825 the rProteome shift is due to synthesis and which part is due to reuse of pre-existing rProteins. We
826 can currently conclude that plants significantly modulate the relative synthesis rates of ribosome-
827 bound rProteins differentially when confronted with environmental factors, such as a shift to sub-
828 optimal temperature, and that such modulation appears to be independent of *de novo* ribosome
829 assembly. Moreover, ribosomes remodelled in the cold exhibit subtractive heterogeneity around
830 the polypeptide exit tunnel (PET) and an accumulation of specific rProteins, in both 40S and 60S sub-
831 units, that are structurally linked to key intersubunit bridges. In addition, we examined general pro-
832 teome shifts and found that 43S and 48S translation initiation complexes are preferentially synthe-
833 sised and accumulate during cold, leading to a higher requirement for 60S subunits, which are at
834 a constant ratio with 40S subunits but appear to be insufficient to form elongation-competent 80S
835 monosomes and solve the over-accumulation of initiation complexes. We therefore hypothesize
836 that 60S subunits are not able to bind all of the translation initiation complexes, and consequently
837 they selectively associate with specific transcript-associated 48S complexes. This hypothesis is sup-
838 ported by the cold-induced heterogeneity, which mainly relates to the association of 40S and 60S
839 subunits and as such could be a way to identify translational needs inherent to the cold context.
840 The other major shift in the newly synthesised proteome is a response to protein aggregation and
841 misfolding, which we propose is linked to missing rProteins around the PET in cold-remodelled
842 ribosomes. This mechanism may be a second layer of translational control that allows ribosomes
843 to misfold and target for degradation the part of the proteome that is currently not needed. From
844 this study, we can currently conclude that there are major responses in the plant translational ap-
845 paratus during cold that cause ribosomes to build a proteome to respond to the consequences
846 of their own structural adaptations. Concomitantly the cold-heterogeneous ribosomes are able to
847 directly or indirectly cause proteome shifts to remodel the cellular membrane and cell wall as part
848 of the agenda to transition to an acclimated state and eventually resume growth.

849 **Methods and Materials**

850 **Plant rearing**

851 **Surface Seed Sterilisation and Imbibition**

852 *Hordeum vulgare* cultivar Keel seeds were obtained from The University of Melbourne from previ-
853 ous studies (Gupta *et al.*, 2019). Seeds were placed inside sterile 50 mL falcon tubes (max 2 g per
854 falcon tube approx. 40 seeds) amounting to a total of approx. 600 seeds (i.e., 15 falcon tubes). The
855 non-biological materials were surface sterilised with 70 % ethanol and placed inside a clean bench,
856 followed by UV-sterilisation. The seeds were soaked in 70 % ethanol and shaken gently for 1 min,
857 ethanol was then discarded. A 1 % bleach solution (0.042 % sodium hypochlorite) was then added
858 to the falcon tube and gently shaken for 10 min, after which the bleach solution was discarded.
859 The seeds were rinsed five times with sterile MilliQ H₂O and gently shaken for 5 min each time
860 to completely remove the hypochlorite. The water was discarded. After straining the water, the
861 seeds were soaked in sterile MilliQ H₂O and the falcon tubes were wrapped in aluminium foil to
862 prevent any light exposure for 14 to 18 hours, half of which was at 25 °C and the other half at 18
863 °C, to mimic the daily temperature fluctuations and initiate imbibition of the seeds.

864 **Seedling Germination and Treatment**

865 Seeds were germinated and treated in complete perceived darkness by using a green light filter
866 to cover the light entering the clean bench when the seeds were transferred to plates. For ger-
867 mination, seeds were transferred to 72 Petri dishes that were filled with 10 ml non-labelled, non-
868 supplemented Scheible medium (Scheible *et al.*, 2004) for 48 hours, 8 to 16 seeds were transferred
869 into each petri dish. The dishes were sealed with micropore tape, wrapped in aluminium foil and
870 placed in a phytotron growth chamber (Weiss Technik, Germany) with temperature settings of 25
871 °C for 16 h and 18 °C for 8 h until the completion of 48 h to allow germination. When 48 hours had
872 passed, six germinated plants from a petri dish were harvested and processed to calculate RGR
873 at time point zero (to be explained below). Then, working on the clean bench and under a green
874 light filter, the medium in the dishes was disposed and exchanged for labelled and non-labelled
875 supplemented media. 42 dishes with 10 mL non-labelled Scheible medium supplemented with 0.5
876 mM ¹⁴N Serine and Glycine and 30 dishes with 10 mL labelled Scheible medium supplemented with
877 0.5 mM ¹⁵N Serine (609005, Lot: MBBB0411V, Sigma Aldrich) and Glycine (299294, Lot: MBBC7772,
878 CAS: 7299-33-4, Sigma Aldrich). Half of the labelled and non-labelled dishes were shifted to 4 °C to
879 induce cold acclimation for 5 days. The other half remained in the control growth chamber with
880 temperature fluctuation of 25 °C for 16 h and 18 °C for 8 h.

881 **Plant Harvest and Phenotyping**

882 For phenotyping, each individual plant was considered a biological replicate. In total 12 dishes were
883 used, one per treatment, per time-point. Six cold-germinated and six control-germinated plants
884 were harvested each day from day 0 until day 5. Immediately, the seedlings were scanned in order
885 to determine the length, width, volume and area of the roots. Then, the roots of each plant were
886 harvested separately and the excess media was completely removed with a paper towel. Sam-
887 ples were wrapped in a folded piece of Pergamin paper and immediately weighed for the fresh
888 weight (FW), and then dried for 70 h at approx. 70 °C and weighed again for dry weight (DW). For
889 all subsequent analysis, root tips were collected in 1.5 cm segments on the fifth day of acclima-
890 tion. Labelled and non-labelled plants reared at cold and control temperatures were collected for
891 primary metabolome and complexome / ribo-proteomic assays. Root segments of plants from
892 the remaining 60 dishes were harvested by pooling root segments from 5 dishes per biological
893 replicate (for a total of 3 biological replicates per labelling - temperature treatment combination).
894 Briefly, 1.5 cm segments of the root tip were collected using a sharp blade and flash frozen with
895 liquid nitrogen. Handling the plant material in frozen conditions, root pools were grinded in a pre-
896 frozen mortar and pestle, followed by preparation of 200 mg and 60 mg aliquots for complexome /

897 ribo-proteomic and primary metabolome analyses respectively. Ground plant material was stored
898 at -80°C until further use.

899 **Morphometric Image Processing**

900 Images of the complete roots were acquired with an image analysis system and scanner (Perfec-
901 tion V800 Photo, Epson). Subsequently the software winRHIZO (Regent Instruments Inc., version
902 released as 2019a) was used to delineate the root tissue and quantify the relevant morphological
903 variables, root length, root average diameter, root volume, number of forks or bifurcations, num-
904 ber of tips, root length per volume. The software parameters were: ImgType - Grey, CalibMeth
905 - Intr, TPU Units - cm, PxSizeH - 0.006353, PxSizeV - 0.006347 [CalFile] - Scanner.Cal, PxClassif -
906 GreyThdAutom-57, Filters - Smooth Off Area Off LWRatio Off, Fractal PxMin PxMax - Off.

907 **Primary Metabolome Analysis**

908 To extract metabolites, 360 µL of pre-cooled extraction mix containing Methanol:Chloroform:Water
909 (2.5:1:1(v/v)) and 30 µL of U-¹³C sorbitol (0.2 mg/mL), as internal standard, was added to 60 mg
910 flash-frozen, grounded root tip tissue, vortexed vigorously and incubated at 70 °C for 15 min.
911 Once the samples were cooled down to room temperature, 200 µL of CHCl₃ was added and
912 incubated at 37 °C for 5 min with shaking. Phase separation was induced by adding 400 µL H₂O,
913 vortexed and centrifuged at 20,800 rcf for 10 min. 160 µL aliquot from the upper polar phase was
914 transferred to fresh 2 mL microvials and dried by vacuum centrifugation for 18 hours at room
915 temperature. The dried samples were stored at -20°C until further use.

916
917 Primary metabolites were analysed by gas chromatography-mass spectrometry (GC-MS) of
918 methoxyaminated and trimethylsilylated metabolite preparations (*Erban et al., 2020*). Metabolite
919 extraction, chemical derivatization were as previously described. C₁₀, C₁₂, C₁₅, C₁₈, C₁₉, C₂₂, C₂₈,
920 C₃₂, C₃₆ n-alkane mixture was added to each sample for retention index calculation. Samples
921 were processed using a Factor Four Capillary Column VF-5ms of dimensions 30 m length, 0.25
922 mm internal diameter and 0.25 mm film thickness (Variant Agilent) mounted to an Agilent 6890N
923 gas chromatograph with split/splitless injector and electronic pressure control up to 150 psi
924 (Agilent, Böblingen, Germany). Mass spectrometric data were acquired through a Pegasus III
925 time-of-flight mass spectrometer (LECO Instrumente GmbH, Mönchengladbach, Germany), and in
926 parallel using the same samples at high mass resolution using a microTOF-Q II hybrid quadrupole
927 time-of-flight mass spectrometer (Bruker Daltonics, Bremen, Germany) with a multipurpose APCI
928 source. Detailed GC-electron spray ionization TOF-MS settings were as reported previously (*Erban*
929 *et al., 2020*).

930
931 Metabolites were annotated and identified by mass spectral and retention index matching to
932 data of authenticated reference compounds from the [Golm Metabolome Database](#) (*Kopka et al.,*
933 *2005*).

934 **Ribosome Enriched Proteomics**

935 **Protease Considerations**

936 Lys-C over Trypsin: Amino acids enriched in RNA protein-binding domains are histidine, arginine
937 and lysine, which are all basic amino acids and. The rProteome is enriched in basic amino acids in
938 order to be able to bind rRNA. Trypsin cleaves peptide sequences at the C-terminal of lysine and
939 arginine residues, thus it would digest rProteins into smaller pieces as compare to Lys-C, which
940 cleaves peptide sequences only at the C-terminal side of lysine residues. Thus Lys-C cuts sets of
941 basic proteins such as the rProteins into significantly longer pieces as compared to trypsin (Figure
942 6 - Figure S1).

943 Ribosomal Protein Purification and Processing

944 Cell lysis was induced in grounded plant tissue using reported methods (*Firmino et al., 2020;*
945 *Martinez-Seidel et al., 2021c*) with minor modifications. Briefly, aliquots were placed in liquid
946 nitrogen-cooled mortars and mass spectrometry friendly ribosome extraction buffer (MS_r-REB)
947 was added at a buffer (V) to tissue (FW) ratio of two. The extract was then homogenised for
948 20 minutes while the mortars stayed on ice to prevent temperature from rising. Big particles
949 were filtered through a pre-made, autoclaved and tip-amputated 5 mL pipette tip containing a
950 ©Mira cloth clog inside, and the filtrate was aliquoted in 2 mL microcentrifuge tubes. Samples
951 were centrifuged at 14,000 x g for 20 min (4°C) to pellet insoluble cell debris and supernatants
952 were transferred to violet QIAshredder mini spin columns (Qiagen, Australia) and centrifuged
953 again for one minute. Sample volume was adjusted to 4.5 ml in order to fill the ultracentrifuge
954 tubes until 50 %. Subsequently, extracts were loaded carefully into thick-walled polycarbonate
955 tubes with three-piece caps (10.4 mL, Polycarbonate Bottle with Cap Assembly, 16 x 76 mm - 6Pk,
956 355603, Beckman Coulter, USA) pre-filled with 2.5 mL sucrose cushion (SC) solution.

957
958 MS_r-REB: 0.2 M of Tris, pH 9.0, 0.2 M of KCl, 0.025 M of EGTA, pH 8.0, 0.035 M of MgCl₂, 1 %
959 (W/V) octyl beta-D-glucopyranoside (98 %, O8001, Sigma Aldrich, Australia), 0.18 mM cyclohex-
960 amide (Sigma Aldrich, Australia), 5 mM Dithiothreitol (R0861, Thermo Fisher, Australia), 1 mM
961 Phenylmethylsulfonyl fluoride (36978, Thermo Fisher, Australia), 1X protease inhibitor cocktail
962 (cat. No. P9599, Sigma Adrich, Australia).

963
964 SC: 0.4 M of Tris, pH 9.0, 0.2 M of KCl, 0.005 M of EGTA, pH 8.0, 0.035 M of MgCl₂ × 6H₂O, and
965 60 % sucrose (Molecular Biology Grade, 573113, Sigma Aldrich, Australia), 0.18 mM cyclohexamide
966 (Sigma Aldrich, Australia), 5 mM Dithiothreitol (R0861, Thermo Fisher, Australia), 1 mM Phenyl-
967 methylsulfonyl fluoride (36978, Thermo Fisher, Australia), 1X protease inhibitor cocktail (cat. No.
968 P9599, Sigma Adrich, Australia).

969
970 Loaded samples were centrifuged at 4°C, 330,000 x g / 60,000 RPM for 4.5 hours using a TY
971 70.1Ti rotor (Type 70.1 Ti Rotor, Beckman Coulter, USA) loaded into an Optima XE-100 Ultracent-
972 rifuuge (Beckman Coulter, USA). After centrifugation, the supernatant was removed including the
973 sucrose cushion taking care that the only solution in contact with the pellet was the SC. Tubes were
974 completely dried by placing them upside down for a couple of minutes and dried pellets stored at
975 -80°C until further usage. Ribosomal pellets were resuspended in 60 µL, freshly prepared, GuHCl
976 to dissociate rProteins and TFA was added to 1 % final volume to induce precipitation of nucleic
977 acids. The solution was then centrifuged in a microcentrifuge at 20,800 x g for 20 minutes and the
978 supernatant recovered. Protein content was determined in samples using the bicinchoninic acid
979 (BCA) kit (Thermo Scientific, United States) assay. As a control *Escherichia coli* ribosomes (P0763S,
980 NEB, Australia) were used in 4 µL aliquots (approx. 2000 A260 units that are equivalent to 102 µg
981 of ribosomes and 23 µg of rProtein) to undergo the full protocol (Figure 6 - Figure S2), confirming
982 the integrity of ribosomal complexes when passing through the SCs solution and subsequent
983 rProtein dissociation.

984
985 Protein amounts were standardised to the minimum concentration, i.e., 13.7 µg in 50 µL 6M
986 GuHCl, 1 % TFA. Proteins were reduced and alkylated by adding tris(2-carboxyethyl)phosphine
987 (TCEP) (77720, Thermo Scientific, United States) and iodoacetamide (IAA) (A3221, Sigma Aldrich,
988 Australia) to 10 mM and 55 mM respectively, and shaking for 45 minutes at 37°C. The alkylation
989 step was shaken in the dark. Acetonitrile was then added to 70 % and a 10:1 ratio of mag-
990 netic beads (Hydrophilic- Part no: 45152105050250, GE Healthcare plus Hydrophobic- Part no:
991 65152105050250, GE Healthcare, Australia) were added and mixed with the solution. Beads were
992 prepared according to the manufacturers instructions to a concentration of 20 µg/µL stock. So-

1093 lution sat for 20 minutes with two pipette mixes, one every 10 minutes. Tubes were placed on
1094 a magnetic rack (DynaMag-2, 12321D, Life Technologies) and allowed to separate for 30 seconds.
1095 Washes were performed while the tubes remained in the rack. 1 ml of neat acetonitrile was added
1096 for 10 seconds and removed followed by 1 ml of 70 % ethanol for 10 seconds and removed. Tubes
1097 were removed from the rack and 1:10 protein (μg) to digestion buffer (μL) was immediately added.
1098 The digestion buffer (25mM triethylammonium bicarbonate (TEAB)) contained the Lys-C protease
1099 (P8109S, NEB, Australia) at a 1:20 protease to protein ratio. Samples were incubated for 18 hours
1000 at 37°C at 1000 RPM in a thermomixer (Eppendorf, Australia). TFA was added to 1 % to quench the
1001 reaction and then the tubes were put on the magnetic rack and the supernatant transferred to new
1002 tubes, twice. Finally a centrifugation step at 14,000 x g was performed to get rid of any residual
1003 beads and only 90 % of the supernatant was recovered. The recovered fraction was frozen for an
1004 hour at -80°C and then freeze-dried. Peptides were resuspended in MS-loading buffer (2 % Acn +
1005 0.05 % TFA) and loaded into a LC-MS/MS platform.

1006 LC-MS/MS Analysis

1007 All samples were analysed in the Nano-ESI-LC-MS/MS. The Nano-LC system, Ultimate 3000 RSLC
1008 (ThermoFisher Scientific, San Jose, CA, USA) was set up with an Acclaim Pepmap RSLC analytical
1009 column (C18, 100 Å, 75 μm x 50 cm, Thermo Fisher Scientific, San Jose, CA, USA) and Acclaim
1010 Pepmap nano-trap column (75 μm x 2 cm, C18, 100 Å) and controlled at 50 °C. Solvent A was 0.1 %
1011 v/v formic acid and 5 % v/v dimethyl sulfoxide (DMSO) in water and solvent B was 0.1 % v/v formic
1012 acid and 5 % DMSO in ACN. The trap column was loaded with digested peptides at an isocratic
1013 flow 3 % ACN containing 0.05 % trifluoroacetic acid (TFA) at 6 $\mu\text{l}/\text{min}$ for 6 min, followed by the
1014 switch of the trap column as parallel to the analytical column.

1015
1016 To measure peptides from barley experimental rProteome samples, the gradient settings for
1017 the LC runs, at a flow rate 300 nl/min, were as follows: solvent B 3 % to 23 % in 89 min, 23 % to
1018 40 % in 10 min, 40 % to 80 % in 5 min, maintained at 80 % for 5 min before dropping to 3 % in 0.1
1019 min and equilibration at 3 % solvent B for 9.9 min. An Exploris 480 Orbitrap mass spectrometer
1020 (Thermo Fisher Scientific, San Jose, CA, USA) with nano electrospray ionization (ESI) source at
1021 positive mode was employed to execute the MS experiments using settings of spray voltages,
1022 ion funnel RF, and capillary temperature level at 1.9 kV, 40 %, 275 °C, respectively. The mass
1023 spectrometry data was acquired with a 3-s cycle time for one full scan MS spectrum and as many
1024 data dependent higher-energy C-trap dissociation (HCD)-MS/MS spectra as possible. Full scan MS
1025 spectra feature ions at m/z of 300-1600, a maximum ion trapping time of 25 msec, an auto gain
1026 control target value of $3e^6$, and a resolution of 120,000 at m/z 200. An m/z isolation window of
1027 1.2, an auto gain control target value of $7.5e^4$, a 30 % normalized collision energy, a first mass at
1028 m/z of 120, an automatic maximum ion trapping time, and a resolution of 15,000 at m/z 200 were
1029 used to perform data dependent HCD-MS/MS of precursor ions (charge states from 2 to 6).

1030
1031 To measure peptides from commercially available *Escherichia coli* ribosomes processed into
1032 rProteome samples gradient settings for the LC runs, at a flow rate 300 nl/min, were as follows:
1033 solvent B 3 % to 23 % in 59 min, 23 % to 40 % in 10 min, 40 % to 80 % in 5 min, maintained at
1034 80 % for 5 min before dropping to 3 % in 0.1 min and equilibration at 3 % solvent B for 9.9 min.
1035 An Eclipse Orbitrap mass spectrometer (Thermo Fisher Scientific, San Jose, CA, USA) with nano
1036 electrospray ionization (ESI) source at positive mode was employed to execute the MS experiments
1037 using settings of spray voltages, ion funnel RF, and capillary temperature level at 1.9 kV, 30 %, 275
1038 °C, respectively. The mass spectrometry data was acquired with a 3-s cycle time for one full scan
1039 MS spectra and as many data dependent higher-energy C-trap dissociation (HCD)-MS/MS spectra
1040 as possible. Full scan MS spectra features ions at m/z of 375-1500, a maximum ion trapping time
1041 of 50 msec, an auto gain control target value of $4e^5$, and a resolution of 120,000 at m/z 200. An
1042 m/z isolation window of 1.6, an auto gain control target value of $5e^4$, a 30 % normalized collision

1043 energy, a maximum ion trapping time of 22 msec, and a resolution of 15,000 at m/z 200 were
1044 used to perform data dependent HCD-MS/MS of precursor ions (charge states from 2 to 6).

1045

1046 Complete dataset proteomics submissions have been deposited to the ProteomeXchange Con-
1047 sortium (*Deutsch et al., 2020*) via the PRIDE (*Perez-Riverol et al., 2019*) partner repository with the
1048 dataset identifiers PXD032923 for *H. vulgare* experimental samples (DOI: 10.6019/PXD032923) and
1049 PXD032938 for *E.coli* control samples (DOI: 10.6019/PXD032938).

1050 Data Analyses

1051 Phenotyping

1052 Relative growth rates using fresh, dry weight and varied phenotype measurements were calculated
1053 using R programming language with equation 1. The output units were $\text{mg} \cdot (\text{mg}^{-1} \cdot \text{h}^{-1})$. W is total
1054 weight accumulation at t_f and it is used in equation 1 to transform the growth rates into fractional
1055 of the final weight. ΔW or dW is the change in fresh or dry weight accumulation in milligrams
1056 from time 0 or non-germinated until Δt or dt , which represents hours after germination. Thus
1057 assuming an initial root weight of 0 leads to dW_t being represented by the weight measurement at
1058 time-point t . The Tukey-HSD test was performed after an ANOVA with a confidence level of 95 %.

1059 Primary Metabolome

1060 Amino acid abundances were analytically derived from GC-EI-ToF-MS acquired data using the
1061 software TagFinder (*Luedemann et al., 2008*) and the Golm Metabolome Database (*Kopka et al.,*
1062 *2005*). Extraction, standardisation, derivatization and GC-MS analytics were performed according
1063 to Erban et al., 2020 (*Erban et al., 2020*). Three biological replicates were measured in technical
1064 triplicates. For high abundant metabolites reaching the detection limit measurements of all sam-
1065 ples were repeated with a 1:30 dilution (split) of extracts. Compounds were manually annotated
1066 in TagFinder and representative Tags for each metabolite chosen. Metabolome data were normal-
1067 ized to the levels of an internal $^{13}\text{C}_6$ sorbitol standard (CAS 121067-66-1), the background levels of
1068 the blanks were subtracted and data were normalized to the fresh weight of plant material in each
1069 sample. For Table S2, primary metabolome data were analysed with the "OmicsUnivariateStats.R"
1070 function of the [RandoDiStats](#) R package. Here, missing values were replaced by a small normally
1071 distributed numeric vector. Additionally, the fold change of metabolite abundances under cold
1072 conditions as well as the logical induction of metabolites (absence-presence-scenarios) were
1073 calculated.

1074

1075 ^{15}N enrichment percentages of labelled metabolite pools was analytically derived from a mul-
1076 tiplexed GC-EI-ToF-MS and GC-APCI-qToF-MS platform. In the first case, the workflow entailed
1077 baseline correction of the raw chromatogram files using the vendor software and transformation
1078 into CDF files. Pre-processing of the chromatograms for increasing data matrices quality (internal
1079 standard normalization and chromatogram alignment, mass scan width synchronisation) using
1080 TagFinder. Similarly, in the latter case, the vendor software was used to find the amino acid peaks
1081 in the chromatograms. peaks were manually mined and integrated in order to derive relative abun-
1082 dances. Every step of the targeted manual annotation of N containing mass tags is deposited in
1083 Table S3. Since ^{15}N feeding can cause differential abundances in monoisotopic fragments from the
1084 same amino acid analyte depending on the lack or presence of a N atom, multiple fragments per
1085 analyte and multiple isotopologs per fragment were considered. Thus, in order to account for the
1086 stable isotope variation, the correlation between fragment abundances was modified from a clas-
1087 sical correlation among monoisotopic abundances to a correlation of the sum from all measured
1088 isotopologs for each fragment pair. Finally, for each amino acid analyte, three or more fragments
1089 were considered to provide a well-rounded annotation. From the final list of fragments, the most
1090 abundant ones (i.e., in the linear range of MS detection) were selected in order to calculate the
1091 percentage of ^{15}N enrichment. Only fragments with null enrichment in the control were let to pass

1092 to the next stage. When all fragments presented residual "enrichment" in non-labelled samples
 1093 this way considered a technical bias, and as such the mean "enrichment" in non-labelled samples
 1094 was subtracted from the labelled samples and those fragments in which the final variance in control
 1095 "enrichment" was minimal were further used. Finally, when multiple fragments satisfied the
 1096 criteria to be useful as a proxy for amino acid synthesis, the most accurate were defined to be
 1097 those fragments with the lowest relative standard deviation across technical triplicates and biological
 1098 replicates (File S1). Subsequently, using the molecular formula information per fragment, NIA
 1099 corrections and % of enrichment calculations (*Heinrich et al., 2018*) were performed, followed by
 1100 a statistical comparison using the [RandoDiStats](#) R package (Tukey-HSD test was performed after
 1101 an ANOVA with a confidence level of 95 %).

1102 Plant Protein Synthesis Rates (K_s)

1103 Two main approaches were used to derive our own calculations of protein synthesis rates,
 1104 which are both detailed below. In Ishihara et al., protein synthesis rates are calculated using
 1105 the amino acid alanine and its enrichment percentage in proteinogenic (ALA_p) and soluble
 1106 (ALA_s) pools as a proxy for label incorporation into protein (K_s , equation 3a). The experimental
 1107 time from the beginning of the experiment (t_0) until the end (t_f) is used to transform the nominal
 1108 values into rates, which are expressed in percentage (%) per hour after a multiplication by 100.
 1109

$$1110 \quad K_s = \frac{(ALA_p[t_f]) - (ALA_p[t_0])}{ALA_s(t_f - t_0)} * \frac{100}{(t_f - t_0)} \quad (3a)$$

1111 Protein degradation rates are then derived from K_s minus the product between plant relative
 1112 growth rates (RGR) times the fractional change in protein content (P_p), accounting for differential
 1113 growth (K_d , equation 3b).
 1114

$$1115 \quad K_d = (K_s - RGR * P_p) * 100 \quad (3b)$$

1116 In Li et al., protein degradation rates are defined as the product of fold change in protein (FCP,
 1117 equation 4c), natural logarithm normalized, by the non-labelled peptide fraction (1 - LPF) (K_d ,
 1118 equation 4a). LPF corresponds to the integer of the area under the curve observed in isotopolog
 1119 envelope shifts caused by tracer incorporation for specific peptides. The calculations are per-
 1120 formed using an in-house script written in Mathematica and the percentages differ from the
 1121 peptide enrichment values.
 1122

$$1123 \quad K_d = \frac{\ln FCP * (1 - LPF)}{T} \quad (4a)$$

1124 Protein synthesis rates are then derived as a product of FCP, weighed by the K_d and experimental
 1125 time (T, 4d), times the K_d rate (K_s , equation 4b).
 1126

$$1127 \quad \frac{K_s}{A} = \frac{FCP - e^{-K_d * T}}{1 - e^{-K_d * T}} * K_d \quad (4b)$$

1128 FCP is calculated as the ratio between the products of fresh weight (FW) times total final (P_{pf}), in
 1129 the numerator, and total initial (P_{p0}) protein content in the denominator (FCP, equation 4c).
 1130

$$FCP = \frac{FW * P_{pf}}{FW * P_{p0}} \quad (4c)$$

1131

1132 Time (T, equation 4d) equals to the difference between the initial experimental time (t_0) and the
1133 final experimental time (t_f).

1134

$$T = t_f - t_0 \quad (4d)$$

1135

1136

1137 Measurement Units of Protein Synthesis Rates (K_s)

1138 Our K_s units imply percentage (%) of normalised labelled peptide fraction accumulated per unit of
1139 weight per hour (equation 5a).

1140

$$K_s(\text{units}) = \frac{\%NormLPF_{pf}}{mg_{DW} * h} \quad (5a)$$

1141

1142

1143 The product of the protein fraction (P_f) times the labelled peptide fraction equals a normalised
1144 version of the labelled peptide fraction (NormLPF_{pf}, equation 5b) that is turned into percentage
1145 fraction when multiplied by 100.

1146

$$\%NormLPF_{pf} = P_f * LPF * \% \quad (5b)$$

1147

1148

1149 This operation intends to normalise the enrichment in single peptides by the fraction of
1150 accumulated total protein, preventing biases derived from differential protein accumulation.
1151 Ultimately, the NormLPF_{pf} units conserve the rate terms from the RGR formula, i.e., NormLPF_{pf}
1152 accumulated per unit of weight per hour (equations 5a & 5c).

1153

$$K_s(\text{units}) = LPF * \frac{P_f}{mg_{DW} * h} * \% \quad (5c)$$

1154

1155

1156 Ribosome Enriched Proteome

1157 RAW chromatograms, including labelled and non-labelled samples, were processed
1158 with MaxQuant, version 1.6.10.43 (Cox and Mann, 2008). Search parameters included
1159 fixed—carbamidomethyl (C) and variable—oxidation (M), acetyl (protein N-term) modifica-
1160 tions. Everything else was set as default. Subsequently all .RAW files were converted into .mzML
1161 using the MSConverterGUI from the ProteoWizard toolbox. The threshold peak filter was set to
1162 “absolute intensity”, ensuring the retention of all the peaks with an intensity greater than 100.
1163 This step allowed retaining in the files all the low abundant isotopes to conserve the isotopic
1164 envelopes of single peptides. Subsequently, using a python script, "isotopeEnrichment.py",
1165 developed in-house (isotopeEnrichment), the abundances of individual isotopolog peaks for
1166 peptide signals were mined out of the .mzML files (Table S4 - D tab). Briefly, the sequence,
1167 mass, charge and retention times for peptides derived from proteins were taken from MaxQuant
1168 search results (i.e., the “evidence” MaxQuant output file). For each peptide localised at a single

1169 point in the chromatograms, theoretical exact masses were then used to create an extracted ion
1170 chromatogram (EIC) that is a summation of the intensities of each of the target isotopolog peaks.
1171 A Gaussian curve was then fitted to the EIC and the target isotopolog intensities were taken as
1172 the average of the observed intensities in a given number of mass spectra at either side of the
1173 Gaussian peak maxima. The procedure avoids skewing subsequent calculations to single scan
1174 isotopic ratios and thus ensures that the measured isotopolog abundances and relative ratios
1175 across the peptide peak are conserved with high fidelity. The script is written for python 3.7 and
1176 uses PymzML (*Bald et al., 2012*) and Pyteomics (*Levitsky et al., 2019*) to read mass spectrometry
1177 data files and calculate peptide masses respectively. The exemplary code used to produce our
1178 results was:

```
1179  
1180  
1181 //Python-3.6.5  
1182  
1183 ## loading the correct module and specification of the correct python version (when working  
1184     with a modular server system):  
1185  
1186 module add devel/Python-3.6.5  
1187  
1188 ## Returning peptides with potentially labelled amino acid resiudes during cold:  
1189  
1190 python3 isotopeEnrichment.py --evidenceFile evidence.txt --mzmlFileDir . --specialResidue S  
1191     --specialResidue G --addSpecialResidues --outDir results_cold  
1192  
1193 ## Returning peptides with potentially labelled amino acid resiudes at optimized temperature:  
1194  
1195 python3 isotopeEnrichment.py --evidenceFile evidence.txt --mzmlFileDir . --specialResidue S  
1196     --specialResidue G --addSpecialResidues --outDir results_control  
1197
```

1198 The mined isotopolog peaks for individual peptide species were then used to construct the
1199 necessary files for enrichment calculation (Table S4 - E tabs). Natural isotopic abundance (NIA)
1200 was calculated and abundances corrected using the R package IsoCorrector (*Heinrich et al., 2018*).
1201 The package requires first a "molecule" file that features the molecular formulas of the masses
1202 to be corrected. Secondly, an "intensities" file, containing the measured mass features and their
1203 isotopologs. Finally, an "elemental" file, containing the chemical elements with their NIA. Input files
1204 have been compiled in Table S4 - E tabs. An R function, "isotopeEnrichment.R", was built to take
1205 up the abundances mined by "isotopeEnrichment.py" and turn them into the necessary format
1206 of IsoCorrector. Subsequently, the .csv files containing the enrichment percentages were used
1207 as input for the R function "EnrichmentSet.R", which generates subsets of significantly labelled
1208 peptides using dependencies to the [RandoDiStats](#) R package. Additionally the function outputs
1209 the subset of unlabelled peptides as a control to monitor in the annotated proteins. The next
1210 function is named "AnnotateProteins.R", which takes the outputs from "EnrichmentSet.R" in order
1211 to build protein enrichment percentages that are calculated based on the average enrichment of
1212 their monitored peptides. The function outputs protein sequences with the highlighted monitored
1213 peptides, the mean non-corrected protein enrichment percentage (non-corrected LPF, Table S4 -
1214 E4 tab) and standard deviations as a measure of reliability from the obtained averages. Finally,
1215 "LPFcorrect.R" corrects the outputs using the enrichment percentage in soluble amino acids and
1216 protein enrichments are transformed into fractional synthesis rates using equation 2a, all these
1217 calculations have been implemented into R functions and can be used from the [ProtSynthesis](#)
1218 [R package](#). The workflow can be used averaging peptides from the same protein into a single
1219 entry or conserving peptides individually. We chose the latter option in this manuscript because
1220 the proteogenomic resources from barley contain many truncated rProtein-like coding sequences
1221 that increase the chance of missinterpretation if peptides are assigned to the matching protein
1222 sequences, and thus may harbor protein isoforms that are independently regulated, and second,

1223 because cold can trigger transcriptome-wide alternative splicing events that may result in peptides
1224 from the same protein sequence being differentially regulated. Therefore, users are advised to
1225 manually evaluate discrepancies in peptide synthesis from the same protein to avoid bias due to
1226 the biological nature of the system. Protein acceptance thresholds for final interpretation of the
1227 data were set by the search in non-labelled samples and acceptance of razor + unique peptides
1228 (UP) with a collective value of two or more. Our FASTA files contain mitochondrial and chloroplast
1229 encoded and translated protein coding sequences. Nevertheless, we cannot properly estimate the
1230 synthesis rates for these proteins because the amino acid pools of organelles are different from
1231 those of the cytosol and thus the enrichments are likely to be different. In addition, the preparation
1232 process of intact organelles alters the amino acid composition as metabolism proceeds relatively
1233 rapidly and metabolites escape. Therefore, we are not able to empirically verify the endogenous
1234 amino acid pools within organelles.

1235 **Acknowledgments**

1236 We thank the Mass Spectrometry and Proteomics Facility of The Bio21 Molecular Science and
1237 Biotechnology Institute at The University of Melbourne for the support of mass spectrometry anal-
1238 ysis. We thank Dr. Sneha Gupta for providing the seed material used in this work.

1239 **References**

- 1240 **Appels R**, Wang P, Islam S. Integrating wheat nucleolus structure and function: variation in the wheat ribosomal
1241 RNA and protein genes. *Frontiers in plant science*. 2021; 12:686586. doi: [10.3389/fpls.2021.686586](https://doi.org/10.3389/fpls.2021.686586).
- 1242 **Ashraf MA**, Rahman A. Cold stress response in *Arabidopsis thaliana* is mediated by GNOM ARF-GEF. *Plant*
1243 *Journal*. 2019; 97(3):500–516. doi: [10.1111/tbj.14137](https://doi.org/10.1111/tbj.14137).
- 1244 **Aylett CH**, Boehringer D, Erzberger JP, Schaefer T, Ban N. Structure of a Yeast 40S-eIF1-eIF1A-eIF3-eIF3j ini-
1245 tiation complex. *Nature structural & molecular biology*. 2015; 22(3):269–271. doi: [10.1038/nsmb.2963](https://doi.org/10.1038/nsmb.2963).
- 1246 **Bald T**, Barth J, Niehues A, Specht M, Hippler M, Fufezan C. PymzML-Python module for high-throughput bioin-
1247 formatics on mass spectrometry data. *Bioinformatics*. 2012; 28(7). doi: [10.1093/bioinformatics/bts066](https://doi.org/10.1093/bioinformatics/bts066).
- 1248 **Barakat A**, Szick-Miranda K, Chang IF, Guyot R, Blanc G, Cooke R, Delseny M, Bailey-Serres J. The organization
1249 of cytoplasmic ribosomal protein genes in the *Arabidopsis* genome. *Plant physiology*. 2001; 127(2):398–415.
1250 doi: [10.1104/pp.010265](https://doi.org/10.1104/pp.010265).
- 1251 **Barandun J**, Chaker-Margot M, Hunziker M, Molloy KR, Chait BT, Klinge S. The complete structure of the small-
1252 subunit processome. *Nature structural & molecular biology*. 2017; 24(11):944–953. doi: [10.1038/nsmb.3472](https://doi.org/10.1038/nsmb.3472).
- 1253 **Barrero-Sicilia C**, Silvestre S, Haslam RP, Michaelson LV. Lipid remodelling: Unravelling the response to cold
1254 stress in *Arabidopsis* and its extremophile relative *Eutrema salsugineum*. *Plant Science*. 2017; 263:194–200.
1255 doi: [10.1016/j.plantsci.2017.07.017](https://doi.org/10.1016/j.plantsci.2017.07.017).
- 1256 **Beine Golovchuk O**, Firmino AAP, Dąbrowska A, Schmidt S, Erban A, Walther D, Zuther E, Hinch DK, Kopka
1257 J. Plant temperature acclimation and growth rely on cytosolic ribosome biogenesis factor homologs. *Plant*
1258 *Physiology*. 2018; 176(3):2251–2276. doi: [10.1104/pp.17.01448](https://doi.org/10.1104/pp.17.01448).
- 1259 **Berková V**, Kameniarová M, Ondrisková V, Berka M, Menšíková S, Kopecká R, Luklová M, Novák J, Spíchal L,
1260 Rashotte AM, et al. *Arabidopsis* response to inhibitor of cytokinin degradation INCYDE: Modulations of cy-
1261 tokinin signaling and plant proteome. *Plants*. 2020; 9(11):1563. doi: [10.3390/plants9111563](https://doi.org/10.3390/plants9111563).
- 1262 **Bowman JC**, Petrov AS, Frenkel-Pinter M, Penev PI, Williams LD. Root of the tree: the significance, evolution, and
1263 origins of the ribosome. *Chemical reviews*. 2020; 120(11):4848–4878. doi: [10.1021/acs.chemrev.9b00742](https://doi.org/10.1021/acs.chemrev.9b00742).
- 1264 **Briggs JW**, Dinman JD. Subtractional heterogeneity: a crucial step toward defining specialized ribosomes.
1265 *Molecular cell*. 2017; 67(1):3–4. doi: [10.1016/j.molcel.2017.06.022](https://doi.org/10.1016/j.molcel.2017.06.022).
- 1266 **Brito Querido J**, Sokabe M, Kraatz S, Gordiyenko Y, Skehel JM, Fraser CS, Ramakrishnan V. Structure of a human
1267 48 S translational initiation complex. *Science*. 2020; 369(6508):1220–1227. doi: [10.1126/science.aba4904](https://doi.org/10.1126/science.aba4904).
- 1268 **Castellano MM**, Merchante C. Peculiarities of the regulation of translation initiation in plants. *Current Opinion*
1269 *in Plant Biology*. 2021; 63:102073. doi: [10.1016/j.pbi.2021.102073](https://doi.org/10.1016/j.pbi.2021.102073).

- 1270 **Cheong BE**, Beine-Golovchuk O, Gorka M, Ho WWH, Martinez-Seidel F, Firmino AAP, Skirycz A, Roessner U,
1271 Kopka J. Arabidopsis REI-LIKE proteins activate ribosome biogenesis during cold acclimation. *Scientific Re-*
1272 *ports*. 2021; 11(1):1–25. doi: 10.1038/s41598-021-81610-z.
- 1273 **Cheong BE**, Yu D, Martinez-Seidel F, Ho WWH, Rupasinghe TW, Dolferus R, Roessner U. The Effect of Cold
1274 Stress on the Root-Specific Lipidome of Two Wheat Varieties with Contrasting Cold Tolerance. *Plants*. 2022;
1275 11(10):1364. doi: 10.3390/plants11101364.
- 1276 **Chiu WL**, Wagner S, Herrmannova A, Burela L, Zhang F, Saini AK, Valasek L, Hinnebusch AG. The C-terminal
1277 region of eukaryotic translation initiation factor 3a (eIF3a) promotes mRNA recruitment, scanning, and, to-
1278 gether with eIF3j and the eIF3b RNA recognition motif, selection of AUG start codons. *Molecular and cellular*
1279 *biology*. 2010; 30(18):4415–4434. doi: 10.1128/MCB.00280-10.
- 1280 **Clowes FAL**. Protein synthesis in root meristems. *Journal of Experimental Botany*. 1958; 9(2):229–238. doi:
1281 10.1093/jxb/9.2.229.
- 1282 **Cox J**, Mann M. MaxQuant enables high peptide identification rates, individualized p.p.b.-range mass ac-
1283 curacies and proteome-wide protein quantification. *Nature Biotechnology*. 2008; 26(12):1367–1372. doi:
1284 10.1038/nbt.1511.
- 1285 **Dal Degan F**, Rocher A, Cameron-Mills V, Von Wettstein D. The expression of serine carboxypeptidases during
1286 maturation and germination of the barley grain. *Proceedings of the National Academy of Sciences of the*
1287 *United States of America*. 1994; 91(17):8209–8213. doi: 10.1073/pnas.91.17.8209.
- 1288 **Des Georges A**, Dhote V, Kuhn L, Hellen CU, Pestova TV, Frank J, Hashem Y. Structure of mammalian eIF3 in
1289 the context of the 43S preinitiation complex. *Nature*. 2015; 525(7570):491–495. doi: 10.1038/nature14891.
- 1290 **Deutsch EW**, Bandeira N, Sharma V, Perez-Riverol Y, Carver JJ, Kundu DJ, García-Seisdedos D, Jarnuczak AF,
1291 Hewapathirana S, Pullman BS, Wertz J, Sun Z, Kawano S, Okuda S, Watanabe Y, Hermjakob H, Maclean B,
1292 Maccoss MJ, Zhu Y, Ishihama Y, et al. The ProteomeXchange consortium in 2020: Enabling 'big data' ap-
1293 proaches in proteomics. *Nucleic Acids Research*. 2020; 48(D1):D1145–D1152. doi: 10.1093/nar/gkz984.
- 1294 **Dinneny JR**, Benfey PN. Plant Stem Cell Niches: Standing the Test of Time. *Cell*. 2008; 132(4):553–557. doi:
1295 10.1016/j.cell.2008.02.001.
- 1296 **Dong Z**, Liu LH, Han B, Pincheira R, Zhang JT. Role of eIF3 p170 in controlling synthesis of ribonucleotide
1297 reductase M2 and cell growth. *Oncogene*. 2004; 23(21):3790–3801. doi: 10.1038/sj.onc.1207465.
- 1298 **Erban A**, Martinez-Seidel F, Rajarathinam Y, Dethloff F, Orf I, Fehrle I, Alpers J, Beine-Golovchuk O, Kopka J. Multi-
1299 plexed Profiling and Data Processing Methods to Identify Temperature-Regulated Primary Metabolites Using
1300 Gas Chromatography Coupled to Mass Spectrometry. In: Hinch DK, Zuther E, editors. *Methods in Molecular*
1301 *Biology*, vol. 2156 New York, NY: Springer US; 2020.p. 203–239. https://doi.org/10.1007/978-1-0716-0660-5_15,
1302 doi: 10.1007/978-1-0716-0660-5_15.
- 1303 **Firmino AAP**, Gorka M, Graf A, Skirycz A, Martinez-Seidel F, Zander K, Kopka J, Beine-Golovchuk O. Separation
1304 and paired proteome profiling of plant chloroplast and cytoplasmic ribosomes. *Plants*. 2020; 9(7):1–29. doi:
1305 10.3390/plants9070892.
- 1306 **Fourrier N**, Bédard J, Lopez-Juez E, Barbrook A, Bowyer J, Jarvis P, Warren G, Thorlby G. A role for sensitive to
1307 freezing2 in protecting chloroplasts against freeze-induced damage in Arabidopsis. *The Plant Journal*. 2008;
1308 55(5):734–745. doi: 10.1111/j.1365-313X.2008.03549.x.
- 1309 **Fowler S**, Thomashow MF. Arabidopsis transcriptome profiling indicates that multiple regulatory pathways
1310 are activated during cold acclimation in addition to the CBF cold response pathway. *The Plant Cell*. 2002;
1311 14(8):1675–1690. doi: 10.1105/tpc.003483.
- 1312 **Fringer JM**, Acker MG, Fekete CA, Lorsch JR, Dever TE. Coupled release of eukaryotic translation initiation factors
1313 5B and 1A from 80S ribosomes following subunit joining. *Molecular and cellular biology*. 2007; 27(6):2384–
1314 2397. doi: 10.1128/MCB.02254-06.
- 1315 **Fusco CM**, Desch K, Dörrbaum AR, Wang M, Staab A, Chan IC, Vail E, Villeri V, Langer JD, Schuman EM. Neuronal
1316 ribosomes exhibit dynamic and context-dependent exchange of ribosomal proteins. *Nature communica-*
1317 *tions*. 2021; 12(1):1–14. doi: 10.1038/s41467-021-26365-x.
- 1318 **Gamalinda M**, Woolford JL. Deletion of L4 domains reveals insights into the importance of ribosomal protein
1319 extensions in eukaryotic ribosome assembly. *Rna*. 2014; 20(11):1725–1731. doi: 10.1261/rna.046649.114.

- 1320 **Garcia-Molina A**, Kleine T, Schneider K, Mühlhaus T, Lehmann M, Leister D. Translational Components Con-
1321 tribute to Acclimation Responses to High Light, Heat, and Cold in Arabidopsis. *iScience*. 2020; 23(7):101331.
1322 doi: [10.1016/j.isci.2020.101331](https://doi.org/10.1016/j.isci.2020.101331).
- 1323 **Genuth NR**, Barna M. Heterogeneity and specialized functions of translation machinery: From genes to organ-
1324 isms. *Nature Reviews Genetics*. 2018; 19(7):431–452. doi: [10.1038/s41576-018-0008-z](https://doi.org/10.1038/s41576-018-0008-z).
- 1325 **Gomes-Duarte A**, Lacerda R, Menezes J, Romão L. eIF3: a factor for human health and disease. *RNA biology*.
1326 2018; 15(1):26–34. doi: [10.1080/15476286.2017.1391437](https://doi.org/10.1080/15476286.2017.1391437).
- 1327 **Gomez MAR**, Ibba M. Aminoacyl-tRNA synthetases. *Rna*. 2020; 26(8):910–936. doi: [10.1261/rna.071720.119](https://doi.org/10.1261/rna.071720.119).
- 1328 **Greber BJ**, Gerhardy S, Leitner A, Leibundgut M, Salem M, Boehringer D, Leulliot N, Aebersold R, Panse VG, Ban
1329 N. Insertion of the biogenesis factor Rei1 probes the ribosomal tunnel during 60S maturation. *Cell*. 2016;
1330 164(1-2):91–102. doi: [10.1016/j.cell.2015.11.027](https://doi.org/10.1016/j.cell.2015.11.027).
- 1331 **Gupta S**, Rupasinghe T, Callahan DL, Natera SHA, Smith PMC, Hill CB, Roessner U, Boughton BA. Spatio-
1332 Temporal Metabolite and Elemental Profiling of Salt Stressed Barley Seeds During Initial Stages of Germin-
1333 ation by MALDI-MSI and μ -XRF Spectrometry. *Frontiers in Plant Science*. 2019; 10:1139. doi: [10.3389/f-](https://doi.org/10.3389/fpls.2019.01139)
1334 [pls.2019.01139](https://doi.org/10.3389/fpls.2019.01139).
- 1335 **Guy C**, Kaplan F, Kopka J, Selbig J, Hinch DK. Metabolomics of temperature stress. *Physiologia plantarum*.
1336 2008; 132(2):220–235. doi: [10.1111/j.1399-3054.2007.00999.x](https://doi.org/10.1111/j.1399-3054.2007.00999.x).
- 1337 **Hammerton RW**, Ho THD. Hormonal Regulation of the Development of Protease and Carboxypeptidase Activ-
1338 ities in Barley Aleurone Layers. *Plant Physiology*. 1986; 80(3):692–697. doi: [10.1104/pp.80.3.692](https://doi.org/10.1104/pp.80.3.692).
- 1339 **Hartl FU**, Bracher A, Hayer-Hartl M. Molecular chaperones in protein folding and proteostasis. *Nature*. 2011;
1340 475(7356):324–332. doi: [10.1038/nature10317](https://doi.org/10.1038/nature10317).
- 1341 **Hashem Y**, Frank J. The jigsaw puzzle of mRNA translation initiation in eukaryotes: a decade of structures
1342 unraveling the mechanics of the process. *Annual review of biophysics*. 2018; 47:125. doi: [10.1146/annurev-](https://doi.org/10.1146/annurev-biophys-070816-034034)
1343 [biophys-070816-034034](https://doi.org/10.1146/annurev-biophys-070816-034034).
- 1344 **Hashem Y**, des Georges A, Dhote V, Langlois R, Liao HY, Grassucci RA, Hellen CU, Pestova TV, Frank J. Structure
1345 of the mammalian ribosomal 43S preinitiation complex bound to the scanning factor DHX29. *Cell*. 2013;
1346 153(5):1108–1119. doi: [10.1016/j.cell.2013.04.036](https://doi.org/10.1016/j.cell.2013.04.036).
- 1347 **Heinrich P**, Kohler C, Ellmann L, Kuerner P, Spang R, Oefner PJ, Dettmer K. Correcting for natural isotope
1348 abundance and tracer impurity in MS-, MS/MS- and high-resolution-multiple-tracer-data from stable isotope
1349 labeling experiments with IsoCorrectoR. *Scientific Reports*. 2018; 8(1):1–10. doi: [10.1038/s41598-018-36293-](https://doi.org/10.1038/s41598-018-36293-4)
1350 [4](https://doi.org/10.1038/s41598-018-36293-4).
- 1351 **Higgins CF**, Payne JW. The Peptide Pools of Germinating Barley Grains: Relation to Hydrolysis and Transport
1352 of Storage Proteins. *Plant Physiology*. 1981; 67(4):785–792. doi: [10.1104/pp.67.4.785](https://doi.org/10.1104/pp.67.4.785).
- 1353 **Hincha DK**, Espinoza C, Zuther E. Transcriptomic and metabolomic approaches to the analysis of plant freezing
1354 tolerance and cold acclimation. In: *Improving crop resistance to abiotic stress* Wiley Online Library; 2012.p.
1355 255–287.
- 1356 **Hincha DK**, Zuther E. Plant Cold Acclimation Methods and Protocols Methods in Molecular Biology. In: *Methods*
1357 *in Molecular Biology*; 2020.
- 1358 **Hinnebusch AG**. Structural insights into the mechanism of scanning and start codon recognition in eukaryotic
1359 translation initiation. *Trends in biochemical sciences*. 2017; 42(8):589–611. doi: [10.1016/j.tibs.2017.03.004](https://doi.org/10.1016/j.tibs.2017.03.004).
- 1360 **Hung NJ**, Johnson AW. Nuclear recycling of the pre-60S ribosomal subunit-associated factor Arx1 depends
1361 on Rei1 in *Saccharomyces cerevisiae*. *Molecular and cellular biology*. 2006; 26(10):3718–3727. doi:
1362 [10.1128/MCB.26.10.3718-3727.2006](https://doi.org/10.1128/MCB.26.10.3718-3727.2006).
- 1363 **Ingolia NT**, Hussmann JA, Weissman JS. Ribosome profiling: Global views of translation. *Cold Spring Harbor*
1364 *Perspectives in Biology*. 2019; 11(5):1–20. doi: [10.1101/cshperspect.a032698](https://doi.org/10.1101/cshperspect.a032698).
- 1365 **Ishihara H**, Moraes TA, Arrivault S, Stitt M. Assessing Protein Synthesis and Degradation Rates in Arabidopsis
1366 thaliana Using Amino Acid Analysis. *Current Protocols*. 2021; 1(5):e114. doi: [10.1002/cpz1.114](https://doi.org/10.1002/cpz1.114).

- 1367 **Ishihara H**, Obata T, Sulpice R, Fernie AR, Stitt M. Quantifying protein synthesis and degradation in arabidopsis
1368 by dynamic ¹³CO₂ labeling and analysis of enrichment in individual amino acids in their free pools and in
1369 protein. *Plant Physiology*. 2015; 168(1):74–93. doi: [10.1104/pp.15.00209](https://doi.org/10.1104/pp.15.00209).
- 1370 **Iwasaki O**, Tanizawa H, Kim KD, Kossenkov A, Nacarelli T, Tashiro S, Majumdar S, Showe LC, Zhang R, Noma
1371 Ki. Involvement of condensin in cellular senescence through gene regulation and compartmental reorgani-
1372 zation. *Nature communications*. 2019; 10(1):1–20. doi: [10.1038/s41467-019-13604-5](https://doi.org/10.1038/s41467-019-13604-5).
- 1373 **Jackson RJ**, Hellen CU, Pestova TV. The mechanism of eukaryotic translation initiation and principles of its
1374 regulation. *Nature reviews Molecular cell biology*. 2010; 11(2):113–127. doi: [10.1038/nrm2838](https://doi.org/10.1038/nrm2838).
- 1375 **Jaglo-Ottosen KR**, Gilmour SJ, Zarka DG, Schabenberger O, Thomashow MF. Arabidopsis CBF1 overex-
1376 pression induces COR genes and enhances freezing tolerance. *Science*. 1998; 280(5360):104–106. doi:
1377 [10.1126/science.280.5360.104](https://doi.org/10.1126/science.280.5360.104).
- 1378 **Janská A**, Aprile A, Zámečník J, Cattivelli L, Ovesná J. Transcriptional responses of winter barley to cold indicate
1379 nucleosome remodelling as a specific feature of crown tissues. *Functional and Integrative Genomics*. 2011;
1380 11(2):307–325. doi: [10.1007/s10142-011-0213-8](https://doi.org/10.1007/s10142-011-0213-8).
- 1381 **Johnson KL**. Baby, It's Cold Inside: Maintaining Membrane Integrity during Freezing. *Plant Physiology*. 2018;
1382 177(4):1350–1351. doi: [10.1104/pp.18.00809](https://doi.org/10.1104/pp.18.00809).
- 1383 **Kaplan F**, Kopka J, Haskell DW, Zhao W, Schiller KC, Gatzke N, Sung DY, Guy CL. Exploring the temperature-stress
1384 metabolome of Arabidopsis. *Plant physiology*. 2004; 136(4):4159–4168. doi: [10.1104/pp.104.052142](https://doi.org/10.1104/pp.104.052142).
- 1385 **Kipper K**, Hetényi C, Sild S, Remme J, Liiv A. Ribosomal intersubunit bridge B2a is involved in factor-dependent
1386 translation initiation and translational processivity. *Journal of molecular biology*. 2009; 385(2):405–422. doi:
1387 [10.1016/j.jmb.2008.10.065](https://doi.org/10.1016/j.jmb.2008.10.065).
- 1388 **Kirby EJM**. Effect of sowing depth on seedling emergence, growth and development in barley and wheat. *Field
1389 Crops Research*. 1993; 35(2):101–111. doi: [10.1016/0378-4290\(93\)90143-B](https://doi.org/10.1016/0378-4290(93)90143-B).
- 1390 **Kopka J**, Schauer N, Krueger S, Birkemeyer C, Usadel B, Bergmüller E, Dörmann P, Weckwerth W, Gibon Y, Stitt
1391 M, et al. GMD@ CSB. DB: the Golm metabolome database. *Bioinformatics*. 2005; 21(8):1635–1638. doi:
1392 [10.1093/bioinformatics/bti236](https://doi.org/10.1093/bioinformatics/bti236).
- 1393 **Kosová K**, Vítámvás P, Prášil IT, Klíma M, Renaut J. Plant Proteoforms Under Environmental Stress: Func-
1394 tional Proteins Arising From a Single Gene. *Frontiers in Plant Science*. 2021; 12:793113. doi: [10.3389/f-
pls.2021.793113](https://doi.org/10.3389/f-
1395 pls.2021.793113).
- 1396 **Lambers H**. Phosphorus acquisition and utilization in plants. *Annual Review of Plant Biology*. 2022; 73:11–126.
1397 doi: [10.1146/annurev-arplant-102720-125738](https://doi.org/10.1146/annurev-arplant-102720-125738).
- 1398 **Lawrence MG**, Shamsuzzaman M, Kondopaka M, Pascual C, Zengel JM, Lindahl L. The extended loops of ribo-
1399 somal proteins uL4 and uL22 of Escherichia coli contribute to ribosome assembly and protein translation.
1400 *Nucleic acids research*. 2016; 44(12):5798–5810. doi: [10.1093/nar/gkw493](https://doi.org/10.1093/nar/gkw493).
- 1401 **Lea PJ**, Joy KW. Amino Acid Interconversion in Germinating Seeds. In: *Mobilization of Reserves in Germination*;
1402 1983.p. 77–109. doi: [10.1007/978-1-4684-1167-6_5](https://doi.org/10.1007/978-1-4684-1167-6_5).
- 1403 **LeFebvre AK**, Korneeva NL, Trutschl M, Cvek U, Duzan RD, Bradley CA, Hershey JW, Rhoads RE. Translation
1404 initiation factor eIF4G-1 binds to eIF3 through the eIF3e subunit. *Journal of Biological Chemistry*. 2006;
1405 281(32):22917–22932. doi: [10.1074/jbc.M605418200](https://doi.org/10.1074/jbc.M605418200).
- 1406 **Levitsky LI**, Klein JA, Ivanov MV, Gorshkov MV. Pyteomics 4.0: Five Years of Development of
1407 a Python Proteomics Framework. *Journal of Proteome Research*. 2019; 18(2):709–714. doi:
1408 [10.1021/acs.jproteome.8b00717](https://doi.org/10.1021/acs.jproteome.8b00717).
- 1409 **Li L**, Nelson CJ, Trösch J, Castleden I, Huang S, Millar AH. Protein degradation rate in Arabidopsis thaliana leaf
1410 growth and development. *Plant Cell*. 2017; 29(2):207–228. doi: [10.1105/tpc.16.00768](https://doi.org/10.1105/tpc.16.00768).
- 1411 **Li W**, Hu Y, Oh S, Ma Q, Merkurjev D, Song X, Zhou X, Liu Z, Tanasa B, He X, et al. Condensin I and II complexes
1412 license full estrogen receptor α -dependent enhancer activation. *Molecular cell*. 2015; 59(2):188–202. doi:
1413 [10.1016/j.molcel.2015.06.002](https://doi.org/10.1016/j.molcel.2015.06.002).
- 1414 **Lindahl L**. Increasing Complexity of Ribosomes and Their Biogenesis. *International Journal of Molecular Sci-
1415 ences*. 2022; 23(15):8264. doi: [10.3390/ijms23158264](https://doi.org/10.3390/ijms23158264).

- 1416 **Lopez T**, Dalton K, Frydman J. The mechanism and function of group II chaperonins. *Journal of molecular*
1417 *biology*. 2015; 427(18):2919–2930. doi: [10.1016/j.jmb.2015.04.013](https://doi.org/10.1016/j.jmb.2015.04.013).
- 1418 **Lu PD**, Harding HP, Ron D. Translation reinitiation at alternative open reading frames regulates gene expression
1419 in an integrated stress response. *The Journal of cell biology*. 2004; 167(1):27–33. doi: [10.1083/jcb.200408003](https://doi.org/10.1083/jcb.200408003).
- 1420 **Luedemann A**, Strassburg K, Erban A, Kopka J. TagFinder for the quantitative analysis of gas chromatogra-
1421 phy—mass spectrometry (GC-MS)-based metabolite profiling experiments. *Bioinformatics*. 2008; 24(5):732–
1422 737. doi: [10.1093/bioinformatics/btn023](https://doi.org/10.1093/bioinformatics/btn023).
- 1423 **Ma Z**, Bykova NV, Igamberdiev AU. Cell signaling mechanisms and metabolic regulation of germination and
1424 dormancy in barley seeds. *Crop Journal*. 2017; 5(6):459–477. doi: [10.1016/j.cj.2017.08.007](https://doi.org/10.1016/j.cj.2017.08.007).
- 1425 **Majumdar R**, Bandyopadhyay A, Maitra U. Mammalian translation initiation factor eIF1 functions with eIF1A
1426 and eIF3 in the formation of a stable 40 S preinitiation complex. *Journal of Biological Chemistry*. 2003;
1427 278(8):6580–6587. doi: [10.1074/jbc.M210357200](https://doi.org/10.1074/jbc.M210357200).
- 1428 **Mangelsen E**, Wanke D, Kilian J, Sundberg E, Harter K, Jansson C. Significance of light, sugar, and amino acid
1429 supply for diurnal gene regulation in developing barley caryopses. *Plant Physiology*. 2010; 153(1):14–33. doi:
1430 [10.1104/pp.110.154856](https://doi.org/10.1104/pp.110.154856).
- 1431 **Martinez-Seidel F**, Beine-Golovchuk O, Hsieh YC, Kopka J. Systematic review of plant ribosome heterogeneity
1432 and specialization. *Frontiers in Plant Science*. 2020; 11:948. doi: [10.3389/fpls.2020.00948](https://doi.org/10.3389/fpls.2020.00948).
- 1433 **Martinez-Seidel F**, Beine-golovchuk O, Hsieh YC, El Eshraky K, Gorka M, Cheong BE, Jimenez-posada EV, Walther
1434 D, Skiryicz A, Roessner U, Kopka J, Firmino AAP. Spatially enriched paralog rearrangements argue functionally
1435 diverse ribosomes arise during cold acclimation in arabidopsis. *International Journal of Molecular Sciences*.
1436 2021; 22(11):6160. doi: [10.3390/ijms22116160](https://doi.org/10.3390/ijms22116160).
- 1437 **Martinez-Seidel F**, Hsieh YC, Walther D, Kopka J, Pereira Firmino AA. COSNet.; ComplexOme-Structural Net-
1438 work Interpreter used to study spatial enrichment in metazoan ribosomes. *BMC bioinformatics*. 2021;
1439 22(1):1–29. doi: [10.1186/s12859-021-04510-z](https://doi.org/10.1186/s12859-021-04510-z).
- 1440 **Martinez-Seidel F**, Suwanthakasem P, Nie S, Leeming MG, Pereira Firmino AA, Williamson NA, Kopka J, Roess-
1441 ner U, Boughton BA. Membrane-Enriched Proteomics Link Ribosome Accumulation and Proteome Repro-
1442 gramming With Cold Acclimation in Barley Root Meristems. *Frontiers in Plant Science*. 2021; 12:656683. doi:
1443 [10.3389/fpls.2021.656683](https://doi.org/10.3389/fpls.2021.656683).
- 1444 **Micic J**, Rodríguez-Galán O, Babiano R, Fitzgerald F, Fernández-Fernández J, Zhang Y, Gao N, Woolford JL,
1445 de la Cruz J. Ribosomal protein eL39 is important for maturation of the nascent polypeptide exit tun-
1446 nel and proper protein folding during translation. *Nucleic Acids Research*. 2022; 50(11):6453–6473. doi:
1447 [10.1093/nar/gkac366](https://doi.org/10.1093/nar/gkac366).
- 1448 **Middleton AJ**, Vanderbeld B, Bredow M, Tomalty H, Davies PL, Walker VK. *Plant Cold Acclimation*. . 2014;
1449 1166:255–277. doi: [10.1007/978-1-4939-0844-8](https://doi.org/10.1007/978-1-4939-0844-8).
- 1450 **Moin M**, Saha A, Bakshi A, Madhav M, Kirti P. Constitutive expression of ribosomal protein L6 modulates salt
1451 tolerance in rice transgenic plants. *Gene*. 2021; 789:145670. doi: [10.1016/j.gene.2021.145670](https://doi.org/10.1016/j.gene.2021.145670).
- 1452 **Nelson CJ**, Alexova R, Jacoby RP, Harvey Millar A. Proteins with high turnover rate in barley leaves estimated
1453 by proteome analysis combined with in planta isotope labeling. *Plant Physiology*. 2014; 166(1):91–108. doi:
1454 [10.1104/pp.114.243014](https://doi.org/10.1104/pp.114.243014).
- 1455 **Nelson CJ**, Li L, Millar AH. Quantitative analysis of protein turnover in plants. *Proteomics*. 2014; 14(4-5):579–592.
1456 doi: [10.1002/pmic.201300240](https://doi.org/10.1002/pmic.201300240).
- 1457 **Nelson CJ**, Millar AH. Protein turnover in plant biology. *Nature Plants*. 2015; 1:1–7. doi: [10.1038/n-](https://doi.org/10.1038/n-)
1458 [plants.2015.17](https://doi.org/10.1038/nplants.2015.17).
- 1459 **Nonogaki H**. Seed Germination and Reserve Mobilization. In: *eLS* Wiley Online Library; 2008. doi:
1460 [10.1002/9780470015902.a0002047.pub2](https://doi.org/10.1002/9780470015902.a0002047.pub2).
- 1461 **Norris K**, Hopes T, Aspden JL. Ribosome heterogeneity and specialization in development. *Wiley interdis-
1462 ciplinary reviews: RNA*. 2021; 12(4):e1644. doi: [10.1002/wrna.1644](https://doi.org/10.1002/wrna.1644).

- 1463 **Osama SK**, Kerr ED, Yousif AM, Phung TK, Kelly AM, Fox GP, Schulz BL. Proteomics reveals commitment to germination in barley seeds is marked by loss of stress response proteins and mobilisation of nutrient reservoirs. *Journal of Proteomics*. 2021; 242:104221. doi: [10.1016/j.jprot.2021.104221](https://doi.org/10.1016/j.jprot.2021.104221).
- 1466 **Pakos-Zebrucka K**, Koryga I, Mnich K, Ljujic M, Samali A, Gorman AM. The integrated stress response. *EMBO reports*. 2016; 17(10):1374–1395. doi: [10.15252/embr.201642195](https://doi.org/10.15252/embr.201642195).
- 1468 **Parasuraman P**, Mulligan P, Walker JA, Li B, Boukhali M, Haas W, Bernards A. Interaction of p190A RhoGAP with eIF3A and other translation preinitiation factors suggests a role in protein biosynthesis. *Journal of Biological Chemistry*. 2017; 292(7):2679–2689. doi: [10.1074/jbc.M116.769216](https://doi.org/10.1074/jbc.M116.769216).
- 1471 **Perez-Riverol Y**, Csordas A, Bai J, Bernal-Llinares M, Hewapathirana S, Kundu DJ, Inuganti A, Griss J, Mayer G, Eisenacher M, Perez E, Uszkoreit J, Pfeuffer J, Sachsenberg T, Yilmaz S, Tiwary S, Cox J, Audain E, Walzer M, Jarnuczak AF, et al. The PRIDE database and related tools and resources in 2019: Improving support for quantification data. *Nucleic Acids Research*. 2019; 47(D1):D442–D450. doi: [10.1093/nar/gky1106](https://doi.org/10.1093/nar/gky1106).
- 1475 **Peterson JH**, Woolhead CA, Bernstein HD. The conformation of a nascent polypeptide inside the ribosome tunnel affects protein targeting and protein folding. *Molecular microbiology*. 2010; 78(1):203–217. doi: [10.1111/j.1365-2958.2010.07325.x](https://doi.org/10.1111/j.1365-2958.2010.07325.x).
- 1478 **Pillet B**, Garcia-Gomez JJ, Pausch P, Falquet L, Bange G, de la Cruz J, Kressler D. The dedicated chaperone Acl4 escorts ribosomal protein Rpl4 to its nuclear pre-60S assembly site. *PLoS genetics*. 2015; 11(10):e1005565. doi: [10.1371/journal.pgen.1005565](https://doi.org/10.1371/journal.pgen.1005565).
- 1481 **Pisareva VP**, Pisarev AV. eIF5 and eIF5B together stimulate 48S initiation complex formation during ribosomal scanning. *Nucleic acids research*. 2014; 42(19):12052–12069. doi: [10.1093/nar/gkab068](https://doi.org/10.1093/nar/gkab068).
- 1483 **Reuveni S**, Ehrenberg M, Paulsson J. Ribosomes are optimized for autocatalytic production. *Nature*. 2017; 547(7663):293–297. doi: [10.1038/nature22998](https://doi.org/10.1038/nature22998).
- 1485 **Rodnina MV**. The ribosome as a versatile catalyst: reactions at the peptidyl transferase center. *Current Opinion in Structural Biology*. 2013; 23(4):595–602. doi: [10.1016/j.sbi.2013.04.012](https://doi.org/10.1016/j.sbi.2013.04.012).
- 1487 **Rontein D**, Basset G, Hanson AD. Metabolic engineering of osmoprotectant accumulation in plants. *Metabolic Engineering*. 2002; 4(1):49–56. doi: [10.1006/mben.2001.0208](https://doi.org/10.1006/mben.2001.0208).
- 1489 **Rosental L**, Nonogaki H, Fait A. Activation and regulation of primary metabolism during seed germination. *Seed Science Research*. 2014; 24(1):1–15. doi: [10.1017/S0960258513000391](https://doi.org/10.1017/S0960258513000391).
- 1491 **Russell JB**, Cook GM. Energetics of bacterial growth: Balance of anabolic and catabolic reactions. *Microbiological Reviews*. 1995; 59(1):48–62. doi: [10.1128/mmbr.59.1.48-62.1995](https://doi.org/10.1128/mmbr.59.1.48-62.1995).
- 1493 **Salih KJ**, Duncan O, Li L, Trösch J, Millar AH. The composition and turnover of the Arabidopsis thaliana 80S cytosolic ribosome. *Biochemical Journal*. 2020; 477(16):3019–3032. doi: [10.1042/BCJ20200385](https://doi.org/10.1042/BCJ20200385).
- 1495 **Salmenkallio M**, Sopanen T. Amino Acid and Peptide Uptake in the Scutella of Germinating Grains of Barley, Wheat, Rice, and Maize. *Plant Physiology*. 1989; 89(4):1285–1291. doi: [10.1104/pp.89.4.1285](https://doi.org/10.1104/pp.89.4.1285).
- 1497 **Scheible WR**, Morcuende R, Czechowski T, Fritz C, Osuna D, Palacios-Rojas N, Schindelasch D, Thimm O, Udvardi MK, Stitt M. Genome-wide reprogramming of primary and secondary metabolism, protein synthesis, cellular growth processes, and the regulatory infrastructure of Arabidopsis in response to nitrogen. *Plant Physiology*. 2004; 136(1):2483–2499. doi: [10.1104/pp.104.047019](https://doi.org/10.1104/pp.104.047019).
- 1501 **Schmidt S**, Dethloff F, Beine-Golovchuk O, Kopka J. The REIL1 and REIL2 proteins of Arabidopsis thaliana are required for leaf growth in the cold. *Plant physiology*. 2013; 163(4):1623–1639. doi: [10.1104/pp.113.223925](https://doi.org/10.1104/pp.113.223925).
- 1503 **Scoles DR**, Yong WH, Qin Y, Wawrowsky K, Pulst SM. Schwannomin inhibits tumorigenesis through direct interaction with the eukaryotic initiation factor subunit c (eIF3c). *Human molecular genetics*. 2006; 15(7):1059–1070. doi: [10.1093/hmg/ddl021](https://doi.org/10.1093/hmg/ddl021).
- 1506 **Seki M**, Narusaka M, Ishida J, Nanjo T, Fujita M, Oono Y, Kamiya A, Nakajima M, Enju A, Sakurai T, et al. Monitoring the expression profiles of 7000 Arabidopsis genes under drought, cold and high-salinity stresses using a full-length cDNA microarray. *The Plant Journal*. 2002; 31(3):279–292. doi: [10.1046/j.1365-313X.2002.01359.x](https://doi.org/10.1046/j.1365-313X.2002.01359.x).
- 1509 **Shi Z**, Fujii K, Kovary KM, Genuth NR, Röst HL, Teruel MN, Barna M. Heterogeneous ribosomes preferentially translate distinct subpools of mRNAs genome-wide. *Molecular cell*. 2017; 67(1):71–83. doi: [10.1016/j.molcel.2017.05.021](https://doi.org/10.1016/j.molcel.2017.05.021).

- 1512 **Shin BS**, Maag D, Roll-Mecak A, Arefin MS, Burley SK, Lorsch JR, Dever TE. Uncoupling of initiation factor eIF5B/IF2 GTPase and translational activities by mutations that lower ribosome affinity. *Cell*. 2002; 1513 111(7):1015–1025. doi: 10.1016/S0092-8674(02)01171-6.
1514
- 1515 **Shore D**, Albert B. Ribosome biogenesis and the cellular energy economy. *Current Biology*. 2022; 32(12):R611–
1516 R617. doi: 10.1016/j.cub.2022.04.083.
- 1517 **Shrestha V**, Yobi A, Slaten ML, Chan YO, Holden S, Gyawali A, Flint-Garcia S, Lipka AE, Angelovici R. Multiomics
1518 approach reveals a role of translational machinery in shaping maize kernel amino acid composition. *Plant*
1519 *physiology*. 2022; 188(1):111–133. doi: 10.1093/plphys/kiab390.
- 1520 **Shutov AD**, Vaintraub IA. Degradation of storage proteins in germinating seeds. *Phytochemistry*. 1987;
1521 26(6):1557–1566. doi: 10.1016/S0031-9422(00)82245-1.
- 1522 **Slavov N**, Semrau S, Airoidi E, Budnik B, van Oudenaarden A. Differential Stoichiometry among Core Ribosomal
1523 Proteins. *Cell Reports*. 2015; 13(5):865–873. doi: 10.1016/j.celrep.2015.09.056.
- 1524 **Spieß C**, Meyer AS, Reissmann S, Frydman J. Mechanism of the eukaryotic chaperonin: protein folding in the
1525 chamber of secrets. *Trends in cell biology*. 2004; 14(11):598–604. doi: 10.1016/j.tcb.2004.09.015.
- 1526 **Sreenivasulu N**, Usadel B, Winter A, Radchuk V, Scholz U, Stein N, Weschke W, Strickert M, Close TJ, Stitt M,
1527 Graner A, Wobus U. Barley grain maturation and germination: Metabolic pathway and regulatory network
1528 commonalities and differences highlighted by new MapMan/PageMan profiling tools. *Plant Physiology*. 2008;
1529 146(4):1738–1758. doi: 10.1104/pp.107.111781.
- 1530 **Stelter P**, Huber FM, Kunze R, Flemming D, Hoelz A, Hurt E. Coordinated ribosomal L4 protein assembly into
1531 the pre-ribosome is regulated by its eukaryote-specific extension. *Molecular cell*. 2015; 58(5):854–862. doi:
1532 10.1016/j.molcel.2015.03.029.
- 1533 **Takahashi D**, Zuther E, Hinch DK. Analysis of Changes in Plant Cell Wall Composition and Structure During
1534 Cold Acclimation. In: *Plant cold acclimation* Springer; 2020.p. 255–268. doi: 10.1007/978-1-0716-0660-5_17.
- 1535 **Tamm T**, Kisly I, Remme J. Functional interactions of ribosomal intersubunit bridges in *Saccharomyces cere-*
1536 *visiae*. *Genetics*. 2019; 213(4):1329–1339. doi: 10.1534/genetics.119.302777.
- 1537 **Thomashow MF**. Plant cold acclimation: Freezing tolerance genes and regulatory mechanisms. *Annual Review*
1538 *of Plant Biology*. 1999; 50:571–599. doi: 10.1146/annurev.arplant.50.1.571.
- 1539 **Verbelen JP**, De Cnodder T, Le J, Vissenberg K, Baluška F. The root apex of *Arabidopsis thaliana* consists of
1540 four distinct zones of growth activities: Meristematic zone, transition zone, fast elongation zone and growth
1541 terminating zone. *Plant Signaling and Behavior*. 2006; 1(6):296–304. doi: 10.4161/psb.1.6.3511.
- 1542 **Verduyn C**, Stouthamer AH, Scheffers WA, van Dijken JP. A theoretical evaluation of growth yields of yeasts.
1543 *Antonie van Leeuwenhoek*. 1991; 59(1):49–63. doi: 10.1007/BF00582119.
- 1544 **Wang H**, Ru Y, Sanchez-Carbayo M, Wang X, Kieft JS, Theodorescu D. Translation Initiation Factor eIF3b Ex-
1545 pression in Human Cancer and Its Role in Tumor Growth and Lung Colonization eIF3b in Patient Outcome
1546 and Experimental Tumor Growth and Metastasis. *Clinical cancer research*. 2013; 19(11):2850–2860. doi:
1547 10.1158/1078-0432.CCR-12-3084.
- 1548 **Waterworth WM**, West CE, Bray CM. The barley scutellar peptide transporter: Biochemical characterization
1549 and localization to the plasma membrane. *Journal of Experimental Botany*. 2000; 51(348):1201–1209. doi:
1550 10.1093/jxb/51.348.1201.
- 1551 **Wruck F**, Tian P, Kudva R, Best RB, von Heijne G, Tans SJ, Katranidis A. The ribosome modulates folding inside
1552 the ribosomal exit tunnel. *Communications biology*. 2021; 4(1):1–8. doi: 10.1038/s42003-021-02055-8.
- 1553 **Xiong W**, Zhang J, Lan T, Kong W, Wang X, Liu L, Chen X, Mo B. High resolution RNA-seq profiling of genes en-
1554 coding ribosomal proteins across different organs and developmental stages in *Arabidopsis thaliana*. *Plant*
1555 *direct*. 2021; 5(5):e00320. doi: 10.1002/pld3.320.
- 1556 **Xu TR**, Lu RF, Romano D, Pitt A, Houslay MD, Milligan G, Kolch W. Eukaryotic translation initiation factor 3,
1557 subunit a, regulates the extracellular signal-regulated kinase pathway. *Molecular and cellular biology*. 2012;
1558 32(1):88–95. doi: 10.1128/MCB.05770-11.
- 1559 **Yébenes H**, Mesa P, Muñoz IG, Montoya G, Valpuesta JM. Chaperonins: two rings for folding. *Trends in bio-*
1560 *chemical sciences*. 2011; 36(8):424–432. doi: 10.1016/j.tibs.2011.05.003.

- 1561 **Yu H**, Kong X, Huang H, Wu W, Park J, Yun DJ, Lee Bh, Shi H, Zhu JK. STCH4/REIL2 confers cold stress tolerance in
1562 Arabidopsis by promoting rRNA processing and CBF protein translation. *Cell Reports*. 2020; 30(1):229–242.
1563 doi: [10.1016/j.celrep.2019.12.012](https://doi.org/10.1016/j.celrep.2019.12.012).
- 1564 **Zhang W**, Zhang J, Xu C, Li N, Liu H, Ma J, Zhu Y, Xie H. LFQ uant: a label-free fast quantitative analysis tool
1565 for high-resolution LC-MS/MS proteomics data. *Proteomics*. 2012; 12(23-24):3475–3484. doi: [10.1002/pmic.201200017](https://doi.org/10.1002/pmic.201200017).
1566
- 1567 **Zhou M**, Sandercock AM, Fraser CS, Ridlova G, Stephens E, Schenauer MR, Yokoi-Fong T, Barsky D, Leary JA,
1568 Hershey JW, et al. Mass spectrometry reveals modularity and a complete subunit interaction map of the
1569 eukaryotic translation factor eIF3. *Proceedings of the National Academy of Sciences*. 2008; 105(47):18139–
1570 18144. doi: [10.1073/pnas.0801313105](https://doi.org/10.1073/pnas.0801313105).
- 1571 **Zúñiga GE**, Fernandez J, Cristi R, Alberdi M, Corcuera LJ. Lipid changes in barley seedlings subjected to water
1572 and cold stress. *Phytochemistry*. 1990; 29(10):3087–3090. doi: [10.1016/0031-9422\(90\)80162-A](https://doi.org/10.1016/0031-9422(90)80162-A).

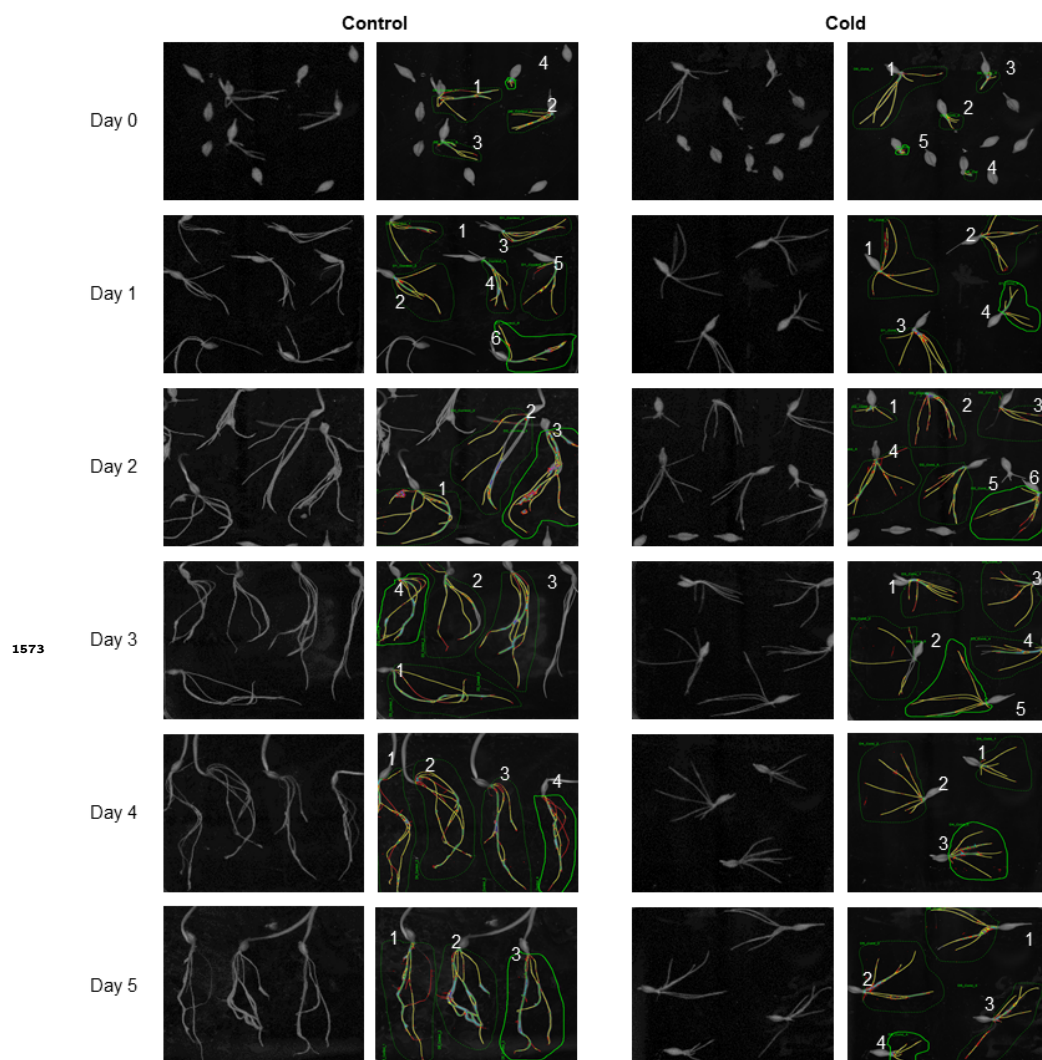


Figure 1-Figure supplement 1. Root phenotype during germination assay in optimal control and suboptimal cold temperatures. Root systems were scanned at each time-point, beginning from day 0 until day 5. The columns on the left represent roots reared at optimal temperature and 3-6 selected representative root systems for phenotypic analyses. The columns on the right represent the germination assay of roots acclimated to cold temperature during each time-point and 3-6 representative seedlings were phenotypically analyzed. winRHIZO software was used.

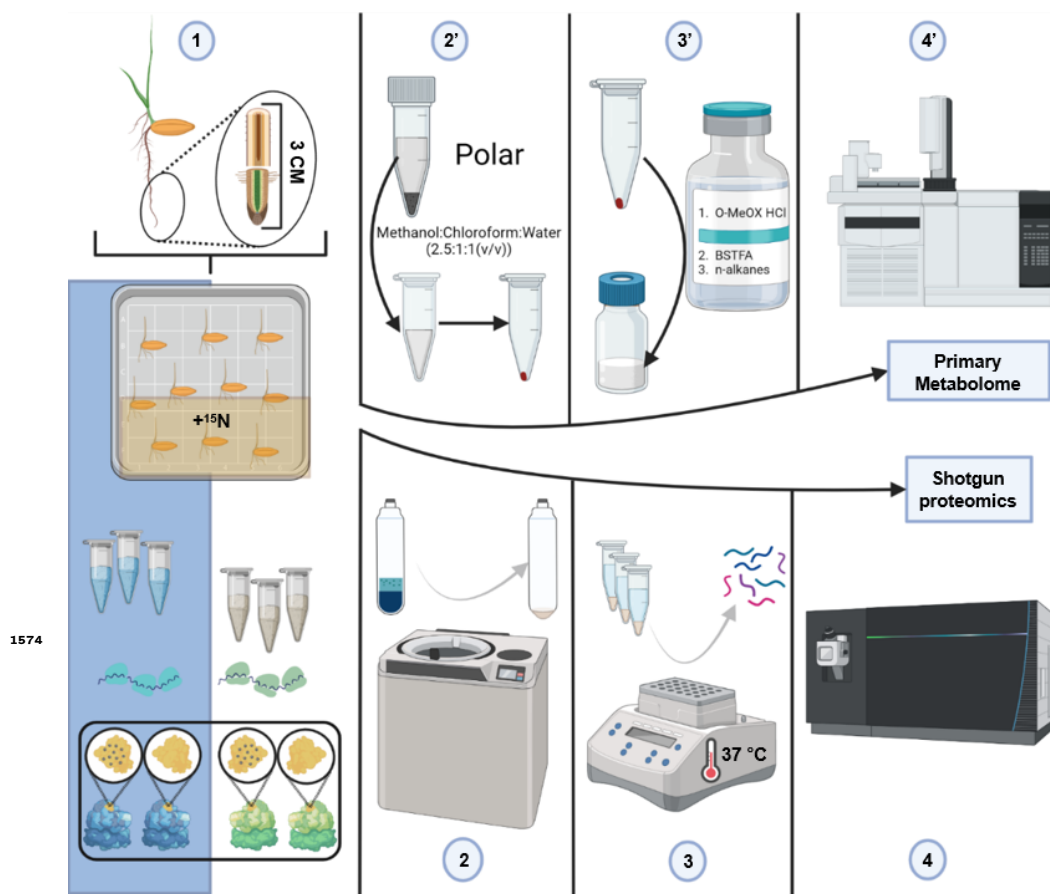


Figure 1–Figure supplement 2. Summary of the methodological workflow to achieve measurements of protein synthesis and abundance in barley root tips. (1) harvesting of root tips from barley seedlings and division into two 1.5cm segments. Barley seedlings were germinated in two temperature regimes with one quarter of the plants having additional labelled nitrogen source and another quarter the same non-labelled nitrogen sources. (2) grinding of pooled tissue using liquid nitrogen, mortar and pestle followed by ribosome enrichment by ultracentrifuge-mediated large cellular complex subproteome extraction and pelleting. (3) Reduction, alkylation, trypsin digestion and peptide cleaning. (4) LC-MS/MS. (2') Extraction of the polar primary metabolome using a methanol, chloroform, water ratio of 2.5:1:1 (V/V). (3') Methoximation and silylation of primary metabolites. (4') GC-ToF-MS multiplexed GC-APCI-MS.

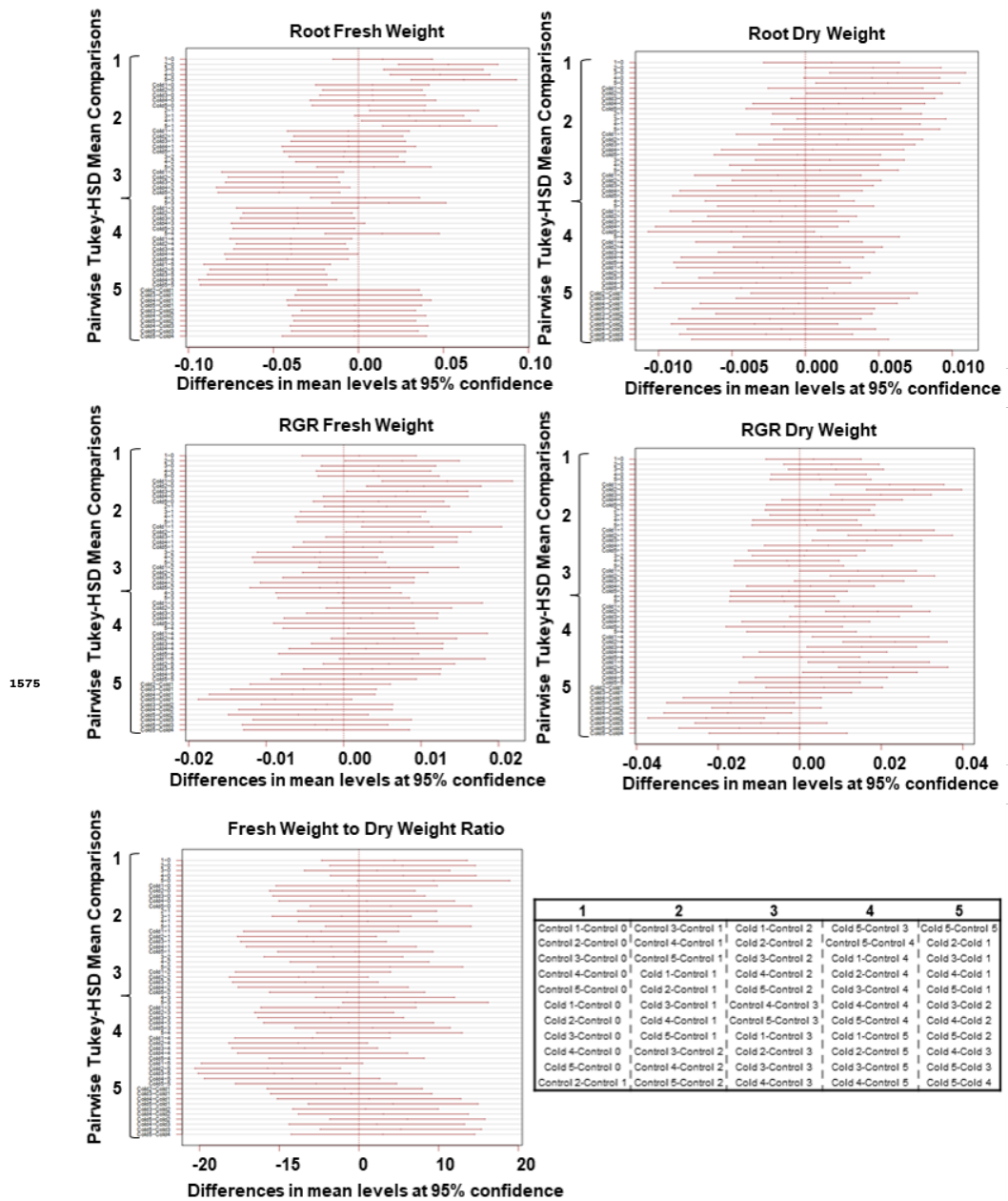


Figure 2–Figure supplement 1. Summary of 95% confidence level Tukey-HSD statistical differences in mean levels of growth related variables across treated and control barley seedlings. Each panel reflects the pairwise comparison across all treatments of specific variables reflecting plant growth. The table on the lower right panel contains the sequential order of the mean comparisons in the plots in five groups. The groupings are signalled in the y-axes of the plots for reference.

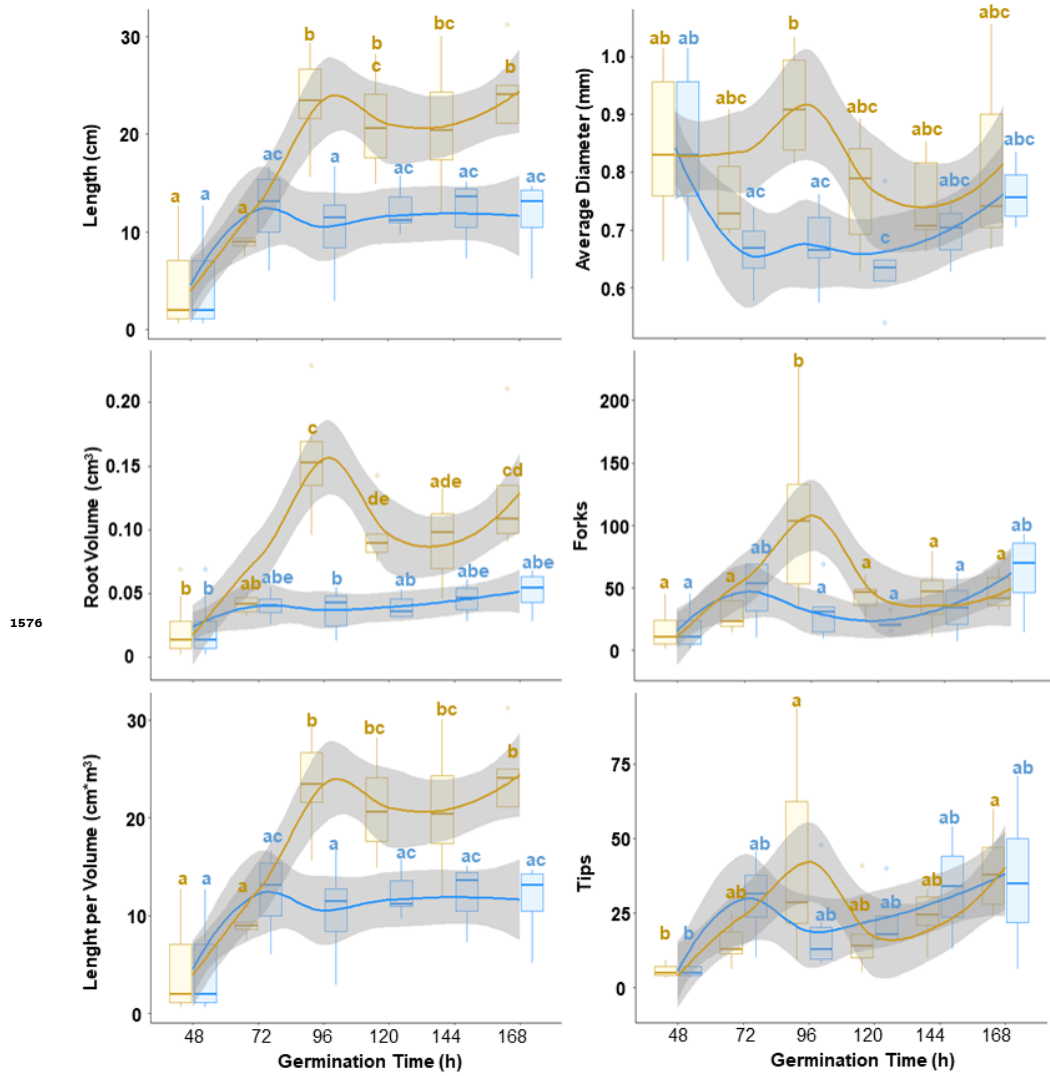


Figure 2–Figure supplement 2. Statistical differences in mean levels (95% confidence level Tukey-HSD) of growth related variables derived from scanning treated and control barley seedlings at each time-point. Each panel reflects plant growth dynamics at control and sub-optimal low temperature. All variables were measured using scanned images and the winRHIZO software.

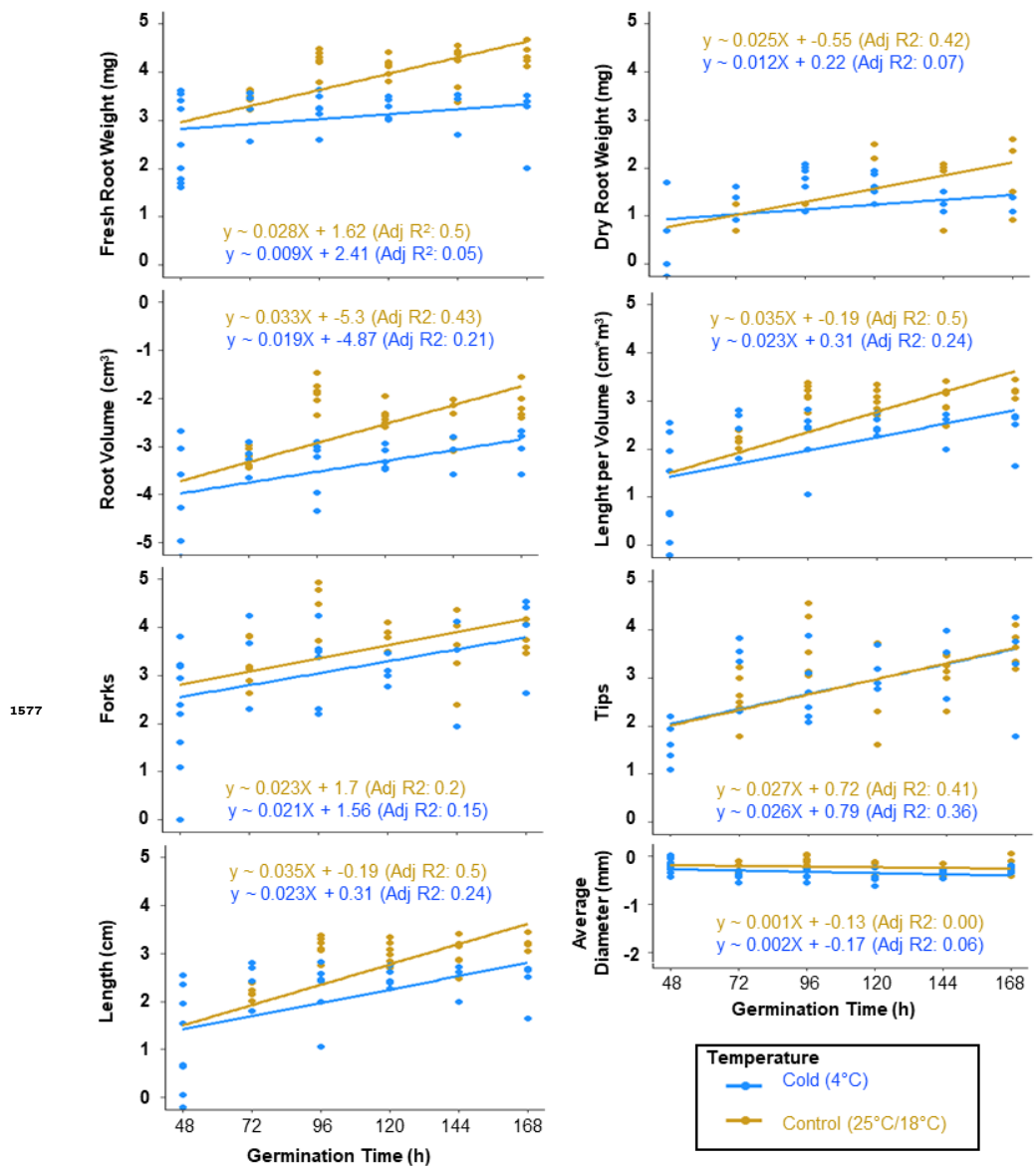


Figure 2-Figure supplement 3. Linear regression after natural logarithm transformation of growth related variables. Growth variables were transformed using the natural logarithm (Ln) and a subsequent linear regression was made on the transformed vector. The fitting was evaluated using the adjusted r^2 , and the respective equation was derived from the linear fitting following the equation of a straight line (i.e., $f(x) = mX + b$, where m represents the slope and b the intercept). The slope represents mean growth rate for each variable and its biological accuracy depends on the adjusted r^2 being close to 1.

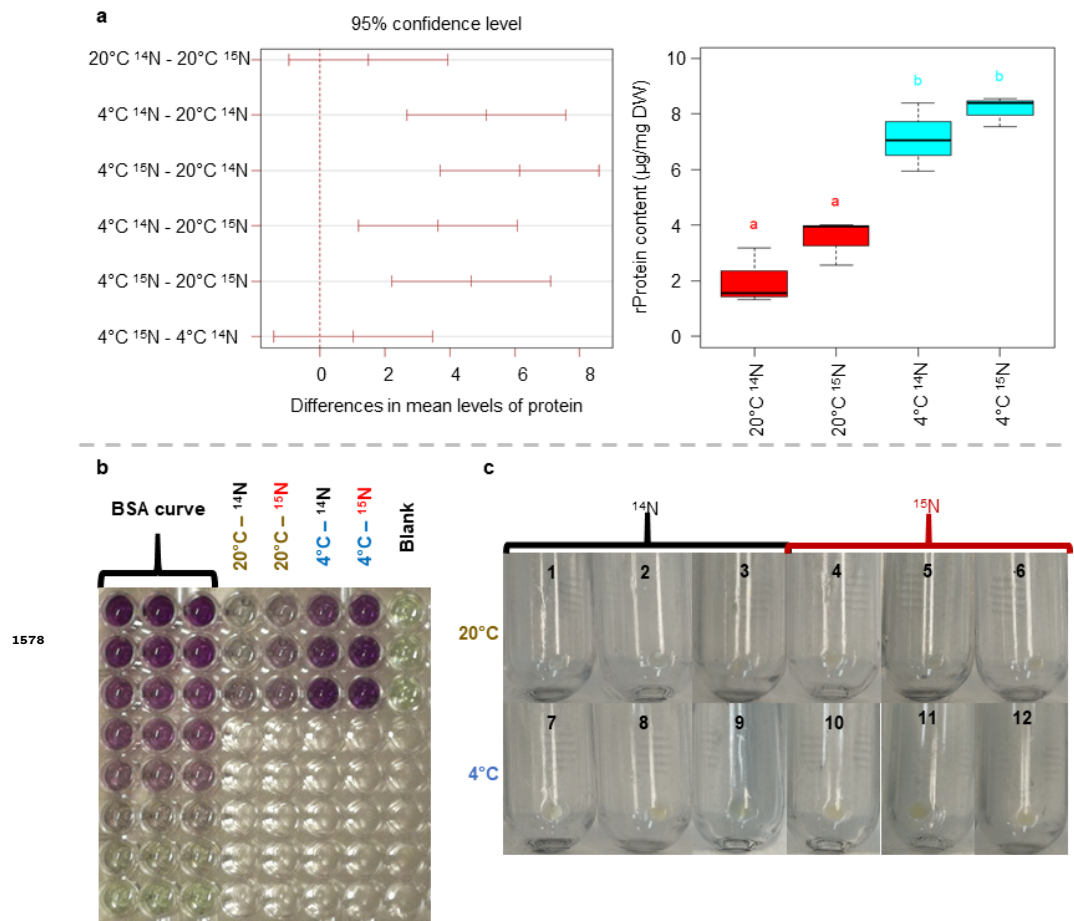


Figure 5-Figure supplement 1. Summary of 95% confidence level Tukey-HSD statistical differences in mean levels of protein content from proteome fractions enriched in ribosomes across treated and control barley seedlings. Also relates to Table S5. (a left-panel) Pairwise comparisons across all treatments of a proteome fraction enriched in ribosomal protein content. The paired mean differences are signalled in the y-axis of the plot for reference. (a right-panel) Boxplot representation of the ribosomal protein content mean differences across temperature regimes, significance is signalled by colour transitions and different letters above the boxes. (b) Features the original photograph of the plate used for the bicinchoninic acid assay from which the results portrayed in panel "a" were derived. (c) Features the original photographs of the ribosome-enriched pellets from all experimental samples after passing through the 60 % sucrose cushion.

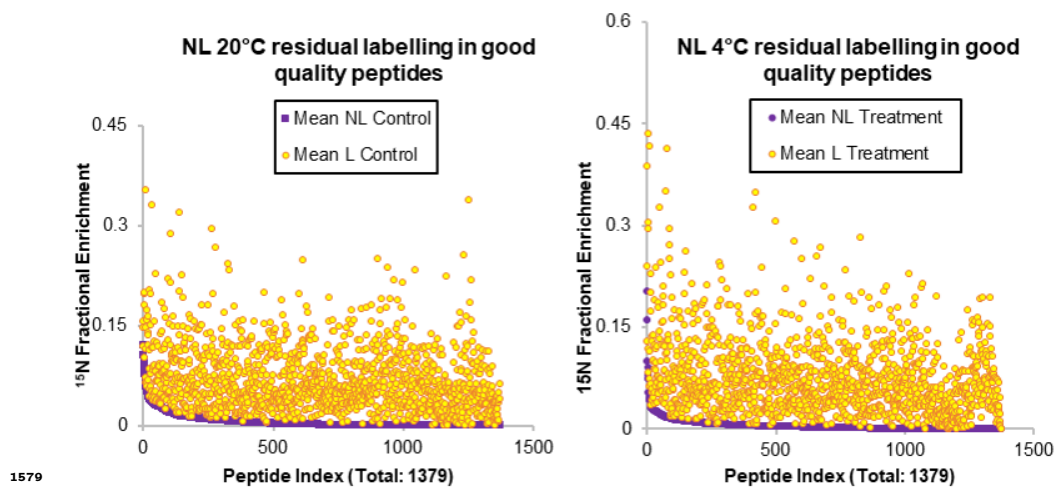


Figure 5–Figure supplement 2. Subset of peptides considered as having optimal quality for interpretation of their relative fractional synthesis rates during the physiological transition of roots from germinating barley seedlings from optimal to sub-optimal temperature. The peptides in the list have all the necessary isotopolog abundances to calculate enrichment percentages in both temperature treatments. Many of the peptides in the list still conserve "noise" in the sense of false enrichment in the non-labelled samples (purple dots in both graphs). Nevertheless this noise is mostly below 1 % enrichment and always below the labelled samples. In both graphs the enrichment fraction is portrayed in the y-axis while the x-axis contains the peptide indexes, which have been sorted from highest to lowest noise in the non-labelled samples. Thus both graphs present a different peptide order. The left graph contains the information of peptides as monitored in samples derived from roots of germinating seedlings growing at an average of 22°C. The right graph contains the information of peptides as monitored in samples derived from roots of germinating seedlings growing at an average of 4°C.

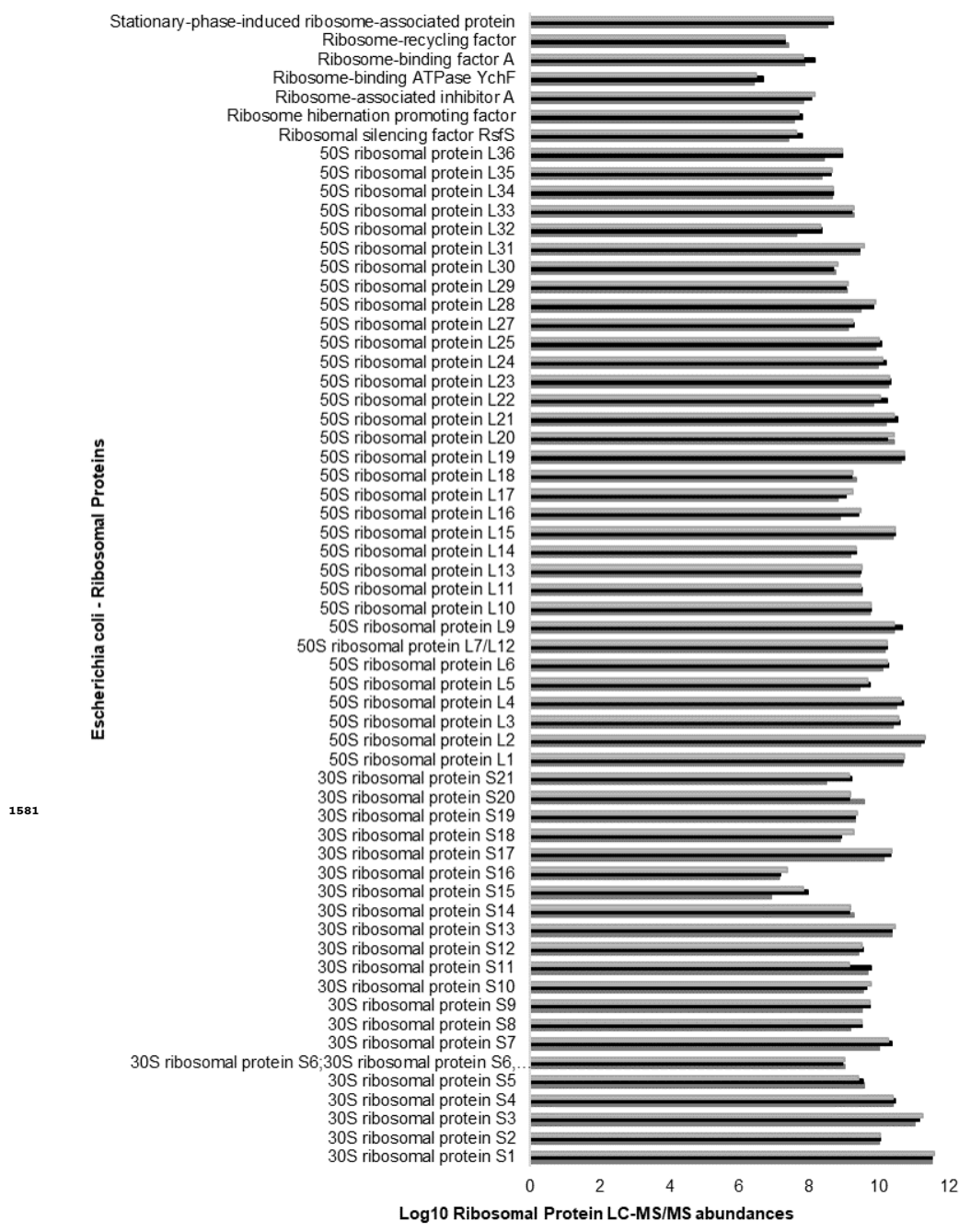


Figure 6-Figure supplement 2. Positive control and complete coverage of *escherichia coli* 70S ribosomal proteome from a commercially available preparation used to verify the ribosomal proteomics pipeline. Also related to Table S7. The ribosomal proteomics pipeline was verified with three independent replicates from the same commercial preparation of *escherichia coli* 70S ribosomes (P0763S, NEB, Australia). The pipeline tested included ribosome extraction, subsequent purification through a sucrose cushion, resuspension of the pelleted complexes with a chaotrope to promote ribosomal protein dissociation and rRNA removal before SP3 beads binding of the ribosomal proteins for protease digestion. The coverage of the 70S ribosomes was full, with 21 proteins from the 30S small subunit and 33 from the 50S large subunit, plus a small set of ribosome associated factors. The height of the triplicate bars in the plot (i.e., x-axis unit) represents the \log_{10} ribosomal protein abundances as measured by LC-MS/MS from the control ribosomal complexes. The y-axis contains the common name of the identified ribosomal proteins.

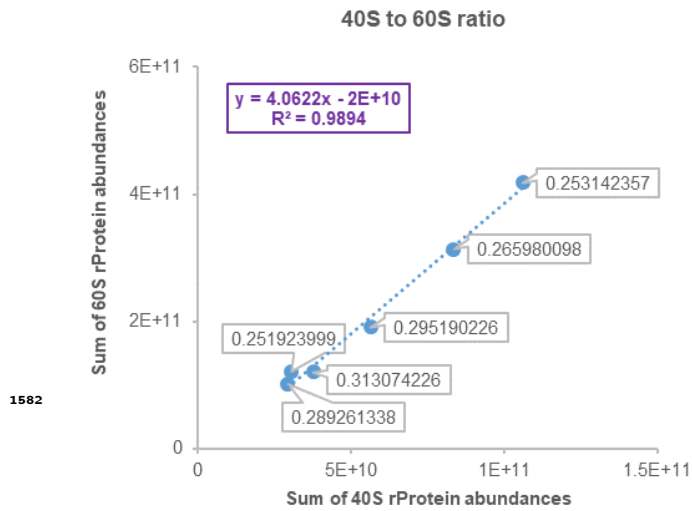


Figure 6–Figure supplement 3. Ratio between 40S SSU and 60S LSU abundances across experimental samples. Also related to Table S4 - Tab C3. The y-axis features the sum of all detected and reliable 60S rProtein abundances. Likewise the x-axis features the sum of all detected and reliable 40S rProtein abundances. The labels at each point are the 40S to 60S ratio as calculated for each sample, note that the ratios all lie between 0.25 and 0.31, which means that 60S proteins are always at a relationship of 3 to 1 with 40S proteins and this aligns with the number of protein paralogs per subunit. Finally, since the ratios are constant, note that the dispersion of the dots is well adjusted to a linear regression model with an r^2 above 0.98.

Chapter 8

Functional Translational Regulation during Cold Acclimation in Plants

This chapter is intended to be a compendium of all those sources of evidence that have not yet been published or submitted, but form an essential part of my contributions to the field of ribosome heterogeneity and specialization during temperature acclimation in plants. Each set of experiments comprises a section of this chapter, and the sections are organized according to concise biological stories. The first section presents evidence for functional divergence of uL30 paralogs based on sequence alignments and cold-specific protein accumulation dynamics and attempts to link this evidence to the main cold effect we have uncovered in heterogeneous ribosomes during cold, i.e. an altered polypeptide exit tunnel. The second section provides evidence for translational bias during cold as measured by Ribo-Seq of wild-type and *reil-dkos* translating polysomes. The third section addresses how the functional proteome shift demonstrated in the second section and in Chapter 7 is linked to the unambiguous accumulation of heterogeneous actively translating polysomes during cold. Finally, the fourth section aims to develop and demonstrate tools that can be used to study the spatial dynamics of the newly synthesized proteome in barley root tips. Work in all sections is ongoing. Supplemental material for all sections of this chapter is provided in File S6.

8.1 uL30 Ribosomal Protein Family

In yeast, there are two uL30 paralogs contributing to the assembly of pre-60 ribosomal particles [20]. Both yeast paralogs associate with pre-60S at different stages during ribosome biogenesis and have distinct ribosome-related roles [1]. As expected, both paralogs show differential localization, with one found in the nucleolus and cytosol and the other exclusively in the cytosol [21]. This suggests that only one of the paralogs mediates biogenesis, while both associate with translating ribosomes. During biogenesis, uL30 mediates the assembly step at which PET formation begins [13, 30]. The ribosomal proteome, which is structurally close to the PET (shown in Figure 8.1A) shows a link between the PET and uL30 that is established via uL4. Importantly, when both yeast uL30 paralogs are knocked out, a restructuring of the PET proteome occurs [20], suggesting that uL30 is crucial for the canonical assembly of the PET. Our own observations in Chapters 5 and 6 indicate that the uL30 paralogs accumulate in their soluble, not-yet assembled form on the fifth day of cold acclimation in barley, and that in Arabidopsis on the seventh day of acclimation, uL30 paralogs B, C, and D are depleted from the low-oligomeric polysomal population. Both lines of evidence suggest that uL30 paralogs are less associated with ribosomes during cold. Remarkably, the REIL phenotype is manifested only during cold, in the absence of uL30 paralogs bound to competent ribosomes and when the rProteome surrounding the tunnel is depleted. The REIL homolog in yeast, *Rei-1*, inserts its C-terminus into the PET to control its integrity, and this quality control is one of the final checks before the 60S subunits become translationally competent. Thus, our results suggest that the cold-induced altered protein accumulation dynamics of uL30 paralogs may explain the requirement for REIL in plants during cold. Further functional studies are needed to conclusively demonstrate this mechanism. These experiments were started by me and conducted in collaboration with Dione Gentry-Torfer, a PhD student who is continuing the project. The methods used for the functional study of uL30 proteins are summarized in the Appendix A.

The uL30 paralogs of Arabidopsis show exemplary sequence divergence compared with yeast and humans (Figure 8.1B). Paralog A in Arabidopsis differs the most from the other three, but remains closer to the hypothetical phylogenetic ancestor it shares with yeast. In addition, we never found this paralog bound to ribosomes in the cytosol (Chapter 6). This suggests that paralog A may be subfunctionalized and exclusively

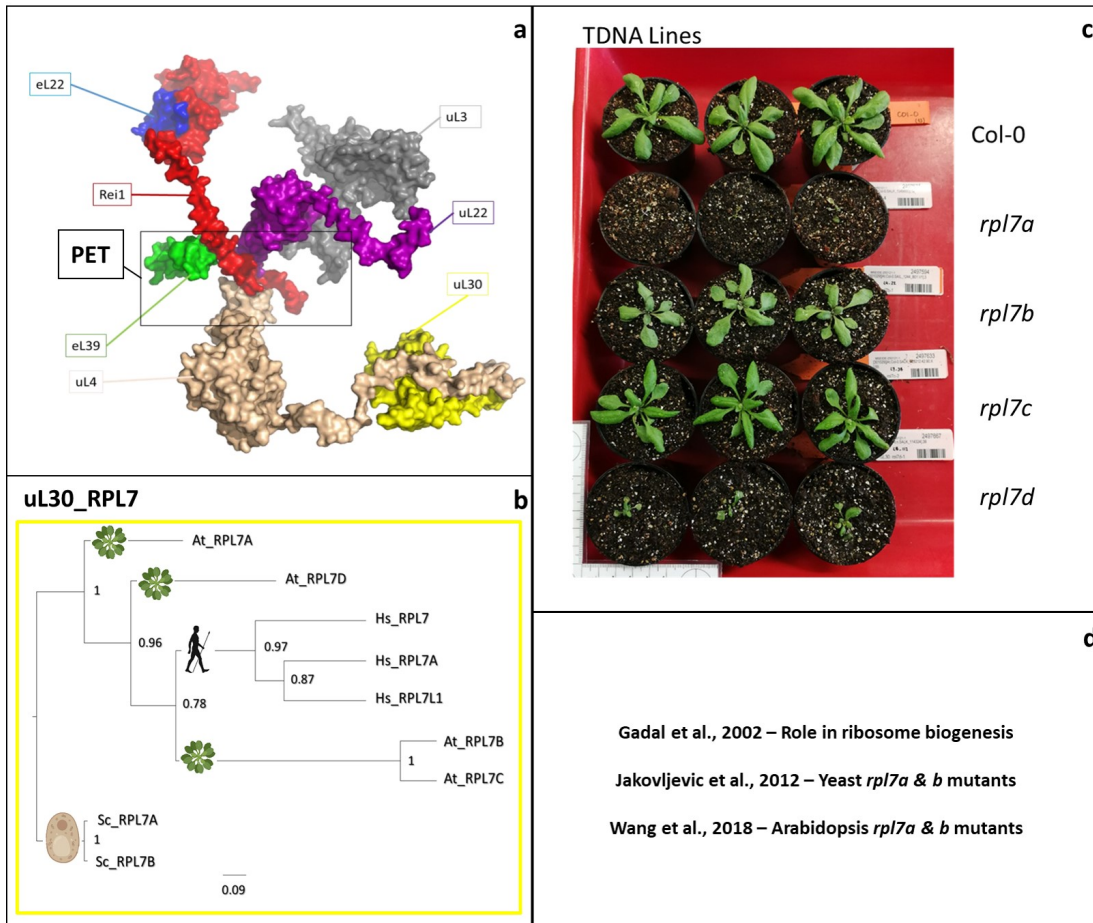


FIGURE 8.1: Compendium of evidence arguing that uL30 ribosomal protein paralogs are functionally divergent in plants and contribute to cold induced ribosomal protein heterogeneity. (a) Cryo-EM density model of the yeast cytosolic ribosome polypeptide exit tunnel showing the ribosomal proteins that surround the tunnel presumably to stabilize its assembly and function. (b) Phylogenetic alignment of Arabidopsis uL30 paralog coding sequences to those from human and yeast showing the sequence divergence of the Arabidopsis paralogs. (c) Homozygous T-DNA insertion lines of the four paralogs that code for uL30 ribosomal protein family in *Arabidopsis thaliana* outlining the phenotypic differences among paralogs when plants are germinated in antibiotic selective media and transferred to soil after two weeks of seedling emergence. (d) Main publications from yeast and Arabidopsis that contribute, along the observations made in this thesis, to the proposed hypothetical divergence of uL30 paralogs and their potential contributions to functional ribosomal protein heterogeneity during cold acclimation.

performing biogenesis functions known from the yeast B homolog. On the other hand, paralogs B and C have diverged the most compared to yeast, but are most abundant in their ribosome-bound form (Chapter 6). This suggests that they serve similar functions as paralog A in yeast, which is associated with ribosomes in the cytosol. Whether these paralogs exhibit exclusive localization in the cytosol remains to be tested. Paralog D shows an intermediate degree of divergence and is not as common in its ribosome-bound form (Chapter 6). We characterized T-DNA insertion lines of the uL30 Arabidopsis paralogs (Figure 8.1C) to provide an additional layer of evidence to support our mass spectrometry and phylogenetic studies. The methods used to characterize the mutant lines are compiled in the Appendix B. We found that when we germinated these lines in selective plates and placed them in soil, the mutant lines of paralogs A and D exhibited a dramatic reduction in growth compared with the wild type and mutant lines B and C. This suggests that the role of these two paralogs may be essential for plant germination and development, and thus agrees well with the results of the phylogenetic tree, which indicate that these two paralogs are structurally the least divergent. On the other hand, the mutant lines of paralogs B and C show a slight reduction in growth with a dramatic change in colour toward pale green in line B. Thus, these two paralogs could contribute differently and differentially toward regulating the translational output of competent ribosomes. Further functional studies with these lines are needed to clearly distinguish between possible ribosome specialization mechanisms, ribosome insufficiency in the mutant lines, or phenotypes resulting from acquired extra ribosomal functions.

8.2 Transcript Translational Control During Cold Acclimation

To link all the translational reprogramming events we uncovered in this thesis to the final acclimation that plants reach after seven days at cold temperatures, we performed a Ribo-Seq experiment that captures multiple time points during the acclimation period (Figure 8.2). Our goal was to uncover functional direct or indirect ribosome-mediated transcript selection mechanisms, which we see as the next step in uncovering ribosome specialization during cold. This section involved collaboration, from experimental design to data analysis, with Dr. Alexandre Augusto Pereira Firmino as well as collaboration with the Laboratory for Translational Regulation in Plants led by Dr. Reimo Zoschke.

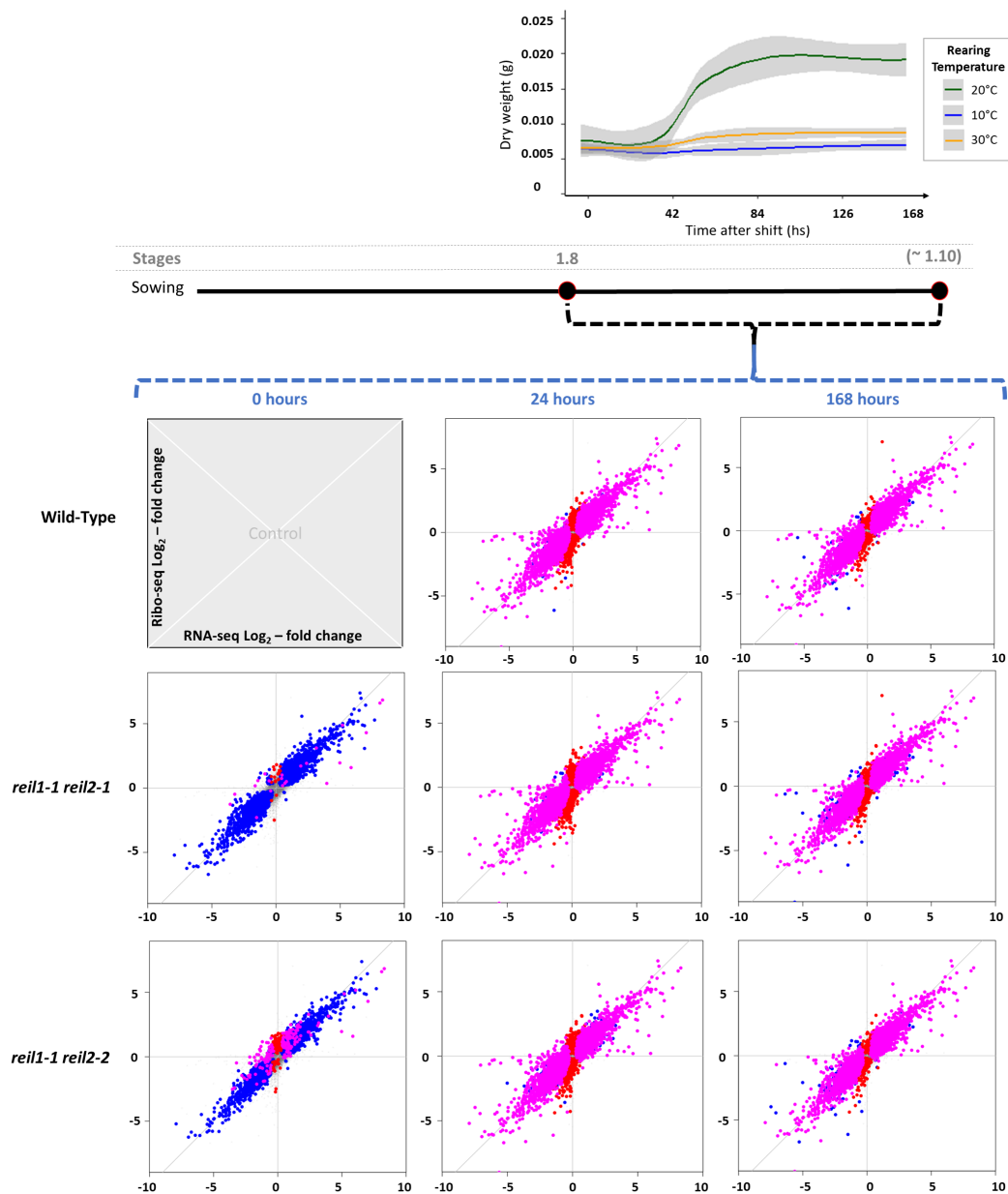


FIGURE 8.2: **General results of a Ribo-Seq experiment performed on cold acclimated *Arabidopsis* seedlings using Col-0 as wild-type and *reil-dkos* as a negative control to stop ribosome biogenesis during cold.** *Arabidopsis* seedlings were grown in soil to morphophysiological stage 1.8 [3] and transferred to cold for seven days. Samples of the three genotypes were harvested before, one day after, and seven days after the cold shift. The harvested samples were used to purify polysomes, digest their bound mRNA with nucleases, and recover the ribosome-protected fragments for sequencing, yielding a typical Ribo-Seq dataset [17]. The relative changes in total transcript abundances and ribosome-bound transcript abundances were compared using Log₂ fold changes in a single Cartesian system to obtain the translation efficiency for each transcript [6]. All conditions were compared with wild type at day 0 to identify significant changes in translation efficiency (DeltaTE), denoted by pink dots. Blue dots indicate control of abundance at the transcriptional level only, gray dots indicate no changes.

Both *reil-dkos* exhibit strong regulation compared to the wild-type genotype. Prior to acclimation, both mutants are regulated at the transcriptional level (Figure 8.2 - plots at 0 hr), implying that the absence of REIL proteins triggers reprogramming of plant molecular physiology at the transcriptome level even prior to acclimation, similar to what our group has previously reported [5, 14, 25]. Strikingly, although REIL proteins are 60S maturation factors, there is no translational difference between the output of *reil-dkos* and wild-type ribosomes in the non-acclimated state. Once acclimation begins, all three genotypes exhibit ribosomal populations that can either directly or indirectly control translational output.

The typical Ribo-Seq experiment involves purifying polysomes, using a nuclease to digest the mRNA that binds them, and then purifying the fragments that remained protected, called footprints, which are sequenced and compared to paired RNA-Seq data so that values for translation efficiency (TE) per transcript can be derived. The TE can then tell us whether ribosomes preferentially translate or filter out certain mRNAs based on their own abundances. We performed our experiment at two time points in the acclimation phase, day 1 and day 7, with day 0 as control. In addition, we included both REIL mutants to investigate the dependencies of ribosome biogenesis on translational control. The specifics of a Ribo-Seq experiment also imply that one of the determinants of the TEs will be the amount of translating polysomes. Thus, before addressing the differences in translational control among the three genotypes, we examined their polysomal profiles in control and cold conditions in order to understand the accumulation dynamics of functional and translating ribosomes (Figure 8.3). At day zero, the three genotypes have statistically the same polysome abundances. At day one, the WT begins to significantly accumulate high-oligomeric polysomes, while low-oligomeric polysomes remain at the level of both mutants, with the three genotypes accumulating low-oligomeric polysomes compared with day zero. At day seven, the same scenario as at day one progresses even further, that is, the WT continues accumulating significantly high oligomeric polysomes and the amount of low oligomeric polysomes remains at the level of that of the mutants, which are significantly accumulating low-oligomeric polysomes.

The unambiguous accumulation of low- and high-oligomeric polysomes in the wild-type genotype and only of low-oligomeric polysomes in the *reil-dkos* prompted us to analyze the differences in translational control between *reil-dkos* and wild-type ribosomes after 24 and 168 hr of acclimation (Figure 8.4). By combining the results from an RNA-Seq

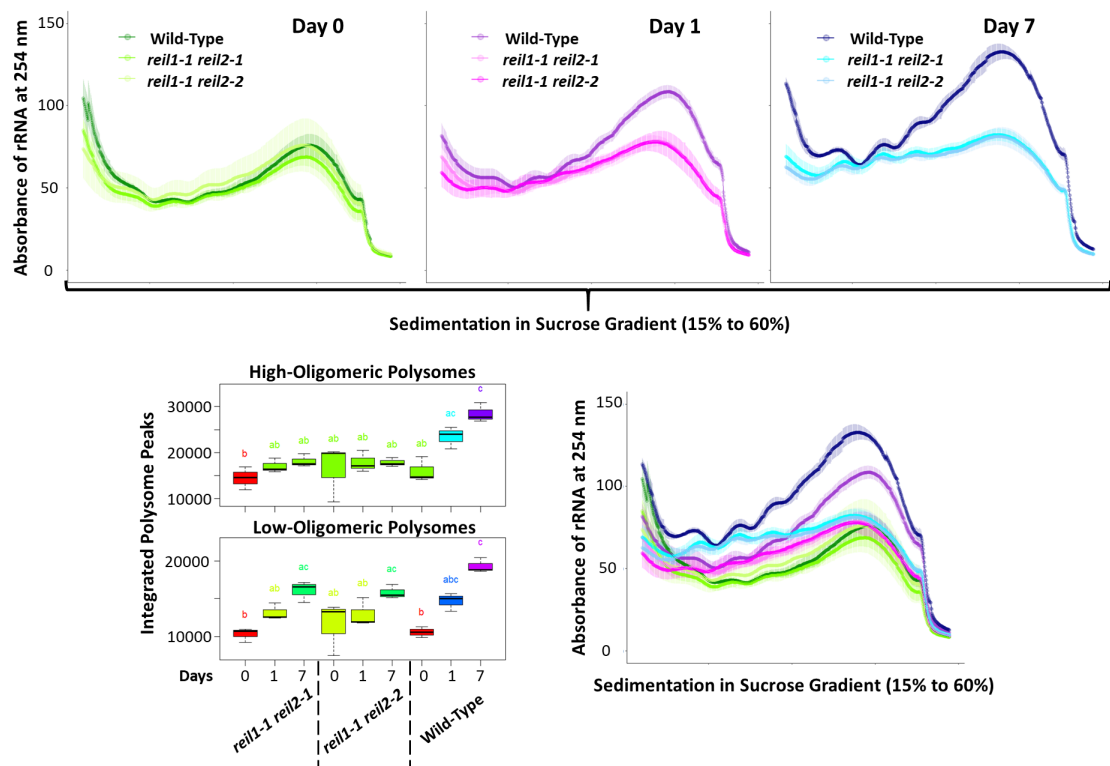


FIGURE 8.3: **Polysome accumulation dynamics during cold acclimation in Arabidopsis wild-type and *reil*-dkos.** The top panel contains the separate polysome profiles per time point, with the profile of each genotype shown with solid color for the mean and shading for the standard error. Polysome abundance is considered as the absorbance of the polysome peak at 254 nm after sedimentation of the complexes in a sucrose gradient from 15 % to 60 %. The bottom panel contains polysome profiles on the right with all time points for comparison of abundance levels and boxplots on the left summarizing statistical comparisons (P values were derived from an ANOVA plus Tukey-HSD combination) between integrated peak areas of low- and high-oligomeric polysomes.

and a paired Ribo-Seq experiment, we were able to distinguish between translational control and transcriptional responses (Figure 8.2). Translational control may be a direct effect of changes in ribosome structure that affects the preferential translation of certain transcripts, i.e., what we call ribosome specialization. Alternatively, translational control may be exclusively transcript-mediated and rely on transcript recruitment to provide the ribosome with the correct substrate for its catalytic activity. Consequently, it is not possible to distinguish between direct and indirect translational control in a Ribo-Seq experiment. Nevertheless, knowledge of which transcripts are preferentially translated or filtered out is essential to uncover mechanisms of direct translational control (ribosome specialization). Here, we show that ribosomes from Arabidopsis wild type and *reil*-dkos have different translational output (Figure 8.4), which may provide explanatory and testable hypothesis for the cold-sensitive REIL knockout phenotypes.

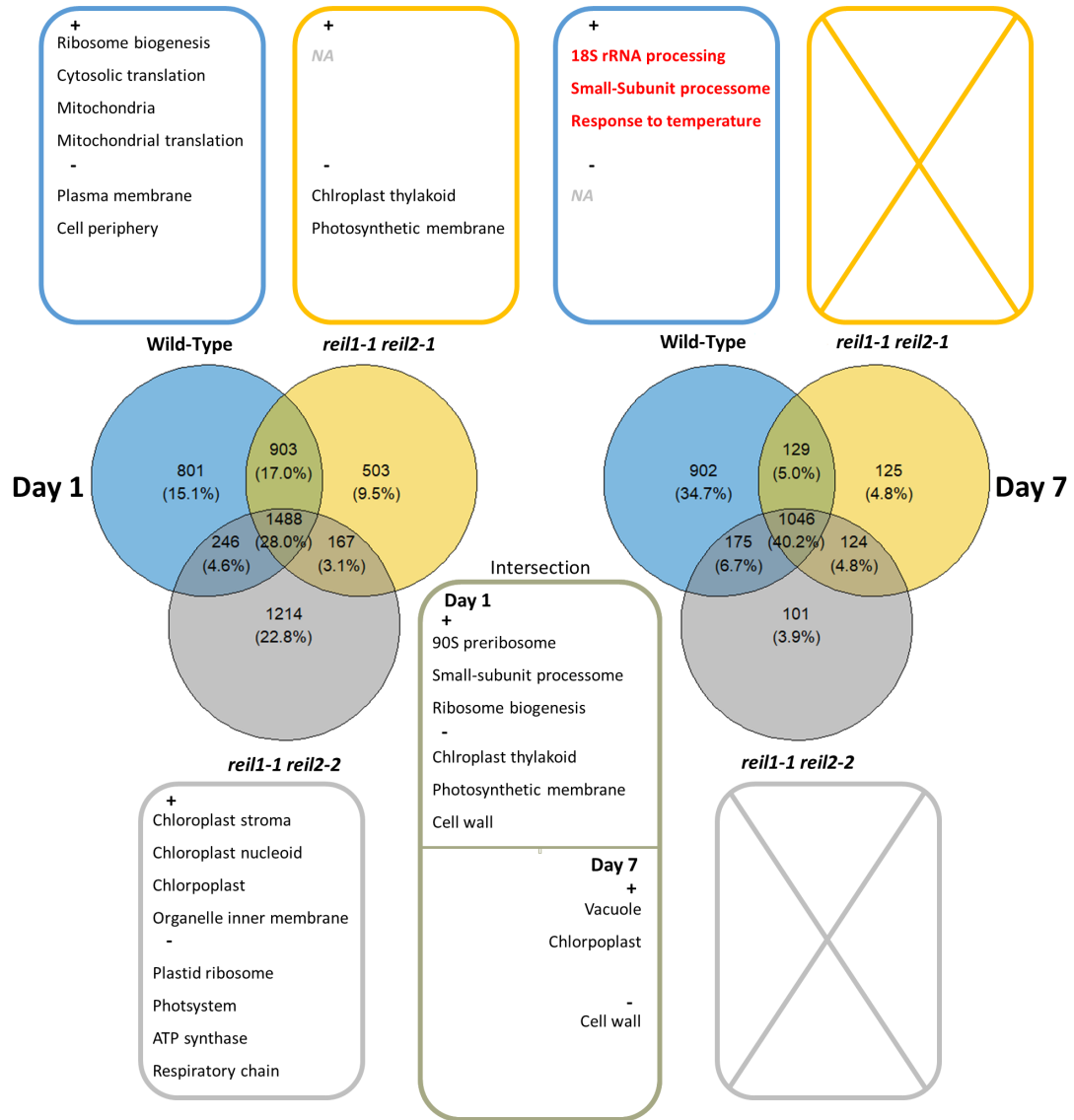


FIGURE 8.4: GO ontology categories that are enriched due to transcript translational control potentially leading to shifts in the translated cellular machinery during cold acclimation in *Arabidopsis* wild-type and *reil-dkos*. Positive or negative translational control was defined as the significant change in translational efficiency (TE) of specific transcripts between a control and a treated sample. TE was calculated as the number of normalized counts from a RIBO-Seq experiment for transcript x divided by the number of normalized counts from a RNA-Seq experiment for transcript x. Subsequently the change in TE (DeltaTE) was calculated as the interaction coefficient between RNA-Seq and Ribo-Seq sequence types in a Generalized linear model (GLM) that tested mean differences in transcript x between two conditions [6]. Mathematically DeltaTE is equivalent to $\text{Log}(TE_{\text{treatment}}) - \text{Log}(TE_{\text{control}})$. A significantly different DeltaTE for any transcript was defined with a Log_2 fold-change threshold larger than 2 or smaller than -2 and a P_{adj} (GLM-derived) value smaller than 0.05 for every sample pair. The transcripts beyond the selected threshold were used to derive enriched GO categories due to translational control.

The full ontology terms and individual ATG codes of transcripts preferentially translated or filtered out by Arabidopsis wild type and *reil-dko* ribosomes are listed in File S6 - Table S1. In the wild-type, Arabidopsis ribosomes enable cold acclimation by preferentially translating proteins of the cytosolic protein biosynthesis machinery. This includes the machinery that assembles ribosomes (the latter is preferentially translated at both day 1 and day 7), as well as mitochondrial translation and organellar machinery at day 1 of cold acclimation. Conversely, components from the plasma membrane and cell periphery are filtered out and not translated. Ribosomes from *reil1-1 reil2-1* do not perform preferential translation during cold, but are able to filter out protein components from chloroplasts, thylakoids, and photosynthetic membranes on day 1 of cold acclimation. The ribosomes from *reil1-1 reil2-2* also filter out protein components from chloroplasts, i.e., proteins from chloroplastidic ribosomes and photosystem-associated factors. In addition, these ribosomes also filter out proteins associated with ATP synthase and respiratory chain activities, potentially affecting the energy production system of the cell. The *reil1-1 reil2-2* ribosomes are capable of preferential translation and they engage in the assembly of proteins from the chloroplast nucleoid, stroma, and organellar inner membrane, perhaps to compensate for a low energy status that the filtered transcripts may have conferred to the plant. Regarding the common translational output among the three genotypes, on the first day of acclimation all the genotypes preferentially translated proteins related to ribosome biogenesis while filtering out proteins related to the chloroplast and photosynthesis. On day seven, all genotypes preferentially translated vacuole- and chloroplast-related proteins and filtered out cell wall proteins. Thus, two aspects can be highlighted. First, at the onset of acclimation, the *reil-dkos* do not preferentially translate mitochondria-related proteins and only partially translate ribosome biogenesis- and protein biosynthesis-related machinery; instead, the mutants appear to avoid translation of proteins leading to energy-producing complexes compared with wild type. *reil1-1 reil2-2* appears to compensate for this. Second, on the seventh day of acclimation, the ribosomes of the mutants share approx. 50 % of the translational control with the wild-type and do not accumulate low-oligomeric polysomes. Furthermore the mutants do have a few transcripts that undergo translational control but this control seems to be untargeted to any cellular machinery since no GO categories were enriched with the ATG codes of significantly changed transcripts. Therefore, it seems reasonable to conclude that the *reil-dkos* are only able to perform untargeted translational

control by virtue of their accumulated low-oligomeric 'sloppy' ribosomes, essentially because they lack the ability to form cold-ribosomes required for successful acclimation, which in the wild-type enhance their own catalysis through translation of the ribosome biogenesis machinery across the entire acclimation period.

A final consideration is that the three genotypes respond to stress when only the most significantly altered transcripts in DeltaTE are analyzed for their GO biological process, and by the seventh day of cold acclimation, all the genotypes are enriched with the GO term "response to cold" (File S6 - Table S1 - Tab C), implying that there is some robustness in the cold-responsive machinery that ensures preferential translation of some of the proteins that mediate cold responses. Standard quality controls such as three-nucleotide read periodicity plots centering on the transcription start and stop sites and the lack of reads in the UTRs are depicted in Figure 8.5, as well as ribosome occupancy levels for REIL paralog transcripts across experimental times in order to ratify the knock-out nature of the mutants used in this study.

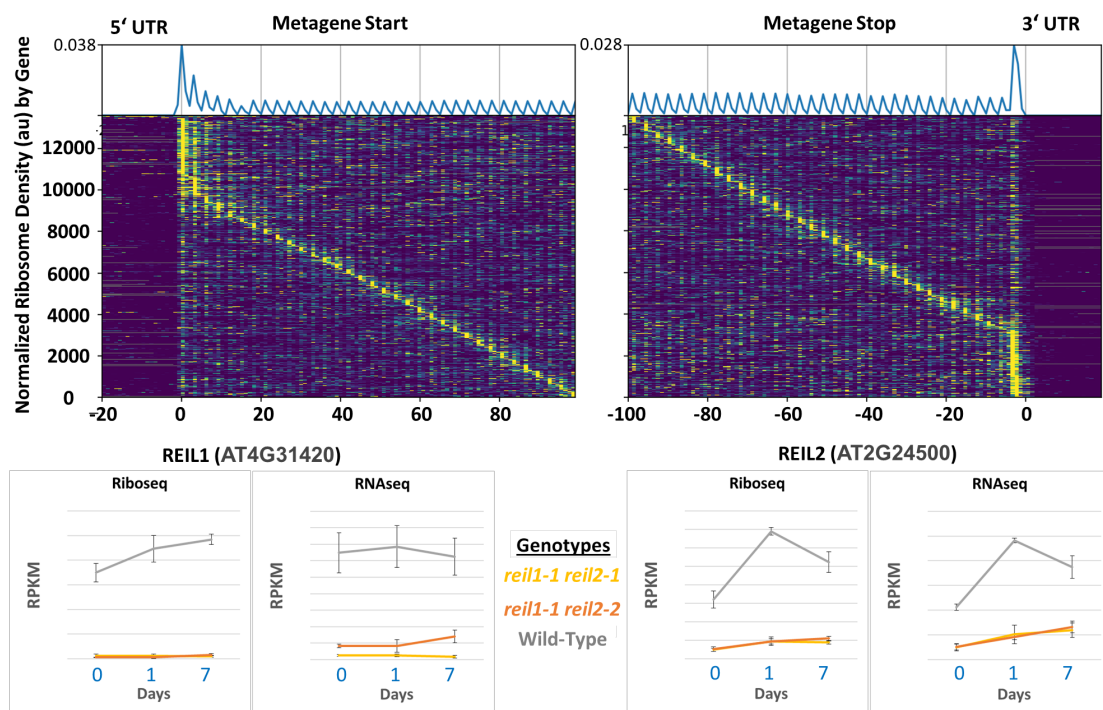


FIGURE 8.5: **Standard quality controls for the Ribo-Seq experiment.** The top panel shows three-nucleotide read periodicity plots focusing on transcription start and stop sites, representing the average of all transcripts and samples. The bottom panel shows the average ribosome occupancy in REIL transcripts under different experimental conditions and genotypes, demonstrating that the double knockout mutants do not have translation of the REIL CDS as compared to the WT.

8.3 ¹⁵Nitrogen Enrichment Characterizes Functionally Divergent Active Ribosomes during Cold Acclimation in Arabidopsis

8.3.1 Summary

During the first seven days of cold acclimation, plants adjust protein biosynthesis, including all molecular entities involved in this process, which coincides with the resumption of growth that had initially stalled after the cold stimulus. Among the main changes when comparing control and cold-treated plants, are changes in the relative growth rates, protein accumulation dynamics, and the size of proteinogenic amino acid pools, which determine a transition between biological steady states at the onset of acclimation. Calculations of protein turnover using stable isotopes typically elucidate the origin and temporal dynamics of proteome shifts. Nevertheless, these calculations (e.g., metabolic and isotopic fluxes) must inherently assume a biological steady state in order to legitimately compare experimental conditions. In this work, we comprehensively consider shifts in plant molecular physiology at the onset of cold acclimation to enable comparison of fractional protein synthesis rates with those of plants grown under optimal conditions. To this end, we introduce the isotope tracer and carefully consider its dynamics in the plant. We use differential labelling of soluble amino acid pools as tracer purity based on individual peptide sequences. Similarly, we correct for differential growth and protein accumulation. We provide extensive and detailed bioinformatics resources to contextualize and compare proteomics data acquired in both dependent and independent modes using stable isotopes in their physiological context. Experimentally, we modify the classical inorganic ¹⁵N-based labelling strategy to cause predictable peptide isotopolog shifts. With our modifications, we elucidate the origin, composition, and divergent ribozyme function of accumulated polysomes during cold acclimation. In summary, by controlled ¹⁵N labelling of the complicated metabolic network of soluble amino acid pools, we have developed a method for relative quantification of *de novo* protein synthesis during biological steady state transitions. Our optimized strategy allowed us to unambiguously dissect the role of functional and divergent ribosomes that are generated and accumulate during cold acclimation in *Arabidopsis thaliana*.

8.3.2 Results

Proteomics using stable isotopes represents a major advance over conventional shotgun proteomics approaches. In plants, the method has been steadily developed [19, 22, 23, 27, 28] and allows the study of plant protein turnover [26]. In our study, we aimed to further develop this method in order to enhance the study *in planta* of the harsh perturbations and physiological transitions that plant organisms experience when facing low temperatures. The methodological adjustments that improved the scalability of the method to our specific problem are: First, a ready-to-use, free bioinformatics pipeline that allows proteomic datasets from dependent or independent acquisition modes to be evaluated while incorporating relevant assumptions. Second, essential quality controls that account for shifts in biological steady states common to typical plant experimental systems. For example, during acclimation to low temperatures, there is a complete switch in metabolism that can affect the relative pool sizes of protein building blocks, i.e., amino acids. Third, improved experimental scalability for every transition to different steady states.

In our experimental design (Figure 3.1A - lower panel), we grow plants in agar plates at optimal temperature until they reach morphophysiological stage 1.0 [3]. We then transfer agar blocks with the roots embedded in them to an optimized Arabidopsis hydroponic system [7] at stage 1.8, at which time an equal number of plants are grown at different temperatures while simultaneously labelled with different ^{15}N sources in the liquid media until stage 1.10. Finally, at 1.10, the plants are harvested for further analysis. In addition, numerous precise phenotypic analyses are performed during the days of transition between temperature regimes. During acclimation to 10°C and 30°C, defined here as suboptimal low and high temperatures, respectively, Arabidopsis plants cease growth in terms of dry weight accumulation for at least 7 days (Figure 3.1A - upper right panel). This interruption of dry weight accumulation represents a stable transition from the optimized rearing temperature (i.e. 20 °C) to an acclimated state. The largest cellular investment in biomass is protein production [18]. Thus, arguably by stopping dry weight accumulation in plants, suboptimal temperatures will also trigger a proteome transition. Consequently, this biological shift presents an optimal system for evaluating and optimizing stable isotope-assisted proteomic studies that lie outside of a biological steady state.

8.3.3 Reaching a Steady State Rate of ^{15}N Incorporation

The uptake of nitrogen happens through the root system and, as an essential macronutrient, nitrogen is necessary for plant growth and development. Different cultivation strategies, as those typically used in experimental plant systems, imply different tuning of plant nutrition, metabolism, growth, and development [31]. In our study, we use a hydroponic system [7] that promotes mixotrophic nutrition of plants, with essential and non-essential elements in the form of macro- and micronutrients available to plants in the liquid medium containing fully submerged root systems. We fed the plants with different ^{15}N sources as part of the liquid medium so that the tracer was slowly taken up into soluble metabolite pools in the cytosol and then reached the rest of the nitrogen-containing components of the plant cells. Our goal was to accurately calculate protein synthesis rates based on the percent ^{15}N enrichment of each protein. Consequently, it was important to consider the dynamics of tracer incorporation in our hydroponic test culture system to understand what is the limited amount of ^{15}N that can be incorporated into active protein pools. For example, if the soluble pool of amino acid x was enriched to 50% on average during the labelling period, then the maximum amount of x residues enriched in a given peptide would be 50%. Thus, in the study of protein synthesis, these limits can be interpreted as the purity of the nitrogen source, i.e., ^{15}N as part of the amino acid precursors. We illustrate the dynamics of nitrogen uptake in the hydroponic test system by measuring the internal distribution of $^{15}\text{NH}_4^{15}\text{NO}_3$ in the pools of soluble amino acids from root and shoot systems (Figure 8.6, Table 8.1 and File S6 - Table S2).

All soluble amino acid pools are significantly more labelled in the root systems than in the shoots (Table 8.1) and exceed the values by at least 10% of the incorporated ^{15}N , which is expected given the need to transport the ^{15}N to the shoots after its uptake. Moreover, the percent enrichment of ^{15}N and the metabolite pools of individual amino acids did not differ statistically at the two rearing temperatures (i.e. 10°C and 20°C), implying that our mixotrophic-based hydroponic system provides a stable basis for studying protein synthesis rates at different rearing temperatures in plants. Consequently, we were able to determine when the steady-state rate of tracer incorporation began based on the enrichment percentages in each pool of soluble amino acids. In the context of stable isotope tracer dynamics, we refer to the steady-state rate as the period

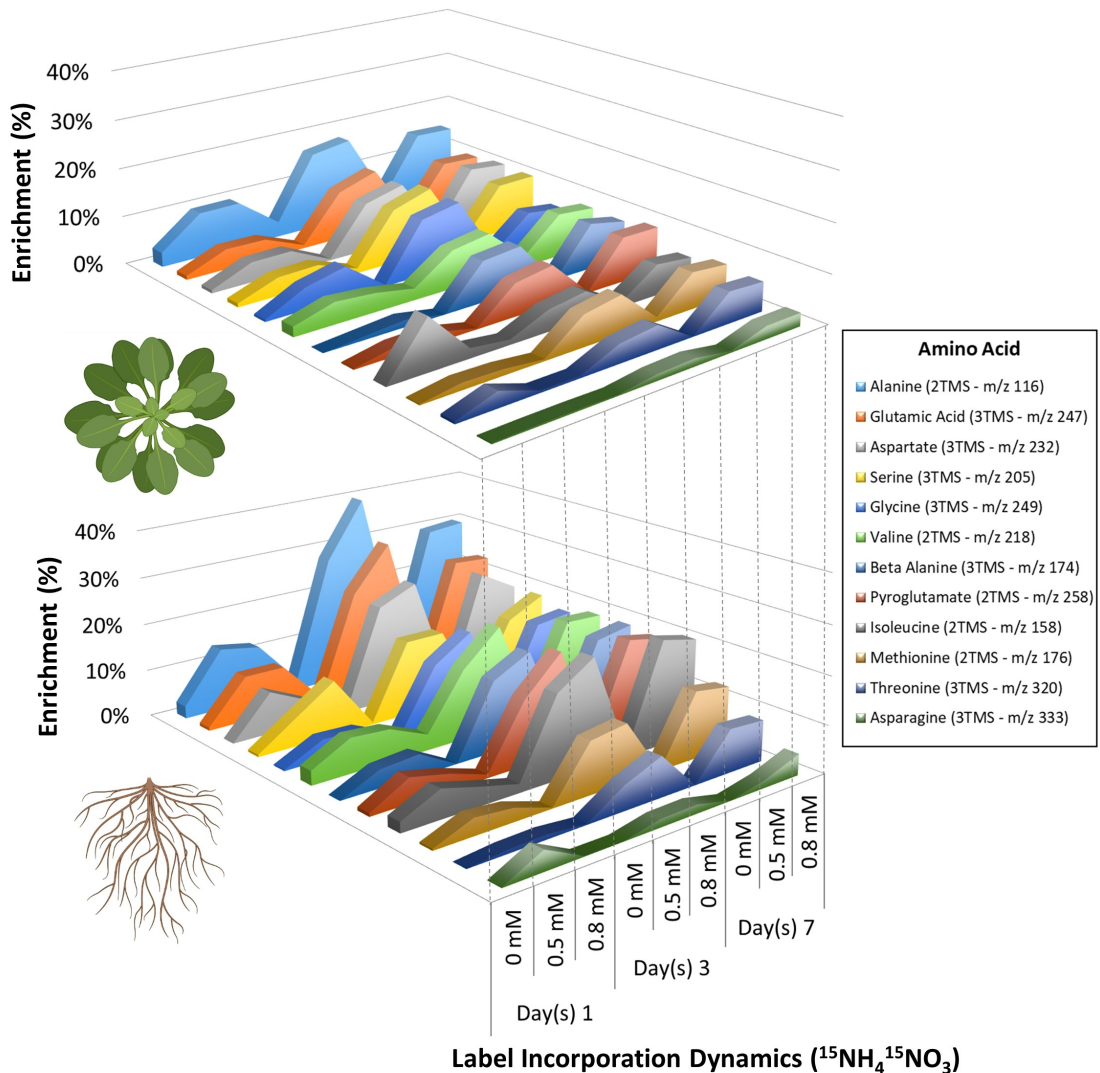


FIGURE 8.6: ^{15}N tracer incorporation dynamics into amino acid soluble pools from *Arabidopsis* plants reared in a hydroponic system. Also related to Table 8.1. Plants were labelled with three different concentrations of $^{15}\text{NH}_4^{15}\text{NO}_3$ (0, 0.5 and 0.8 mM) from 1.8 until 1.10 physiological stage [3] as detailed in Figure 3.1. The top and bottom panels detail the tracer incorporation dynamics into shoots and root systems respectively. In each panel, amino acids are represented by coloured bars. Amino acids abundances were measured with a GC-ToF-MS, chromatograms processed with TagFinder [24], where the isotopolog abundances were obtained. NIA correction and label incorporation were equivalent when calculated using the first four isotopes of each analyte with the software CORRECTOR [16] or IsoCorrector [15]. Note that there is a steady state rate of ^{15}N incorporation into amino acid soluble pools between day 3 and 7 days of labelling. This is defined by the absence of significant changes in amino acid enrichment between day 3 and day 7 (see Table 8.1), while both time points are significantly different from day 1 in terms of amino acid enrichment (for most amino acids). Parts of the figure were created with BioRender and exported under a paid subscription.

during which the percent enrichment in the pools of target metabolites is statistically stable. In our system, this is the case at both tracer concentrations, 0.5 mM or 0.8 mM, as early as day 3 and is maintained until day 7. Between these time points and across the two ammonium nitrate concentrations studied, there are no statistical changes in the enrichment percentages of the individual soluble amino acid pools. A consistent incorporation rate from day 3 to day 7 implies that this is the optimal time period to examine biological shifts that occur during experimental setups while maximizing the information content that the ^{15}N tracer could provide.

TABLE 8.1: ^{15}N enrichment percentage of soluble amino acid pools of Arabidopsis root and shoot.

	0.5 mM			Day 3		
	Day 1 (b)	Day 3 (a)	Day 7 (a)	0 mM (b)	0.5 mM (a)	0.8 mM (a)
Shoot (b)						
Alanine	9%	16%	15%	3%	16%	17%
Glycine	5%	12%	7%	0%	12%	13%
Serine	4%	11%	10%	1%	11%	14%
Glutamic Acid	4%	10%	11%	1%	10%	13%
Aspartate	4%	10%	12%	0%	10%	12%
Valine	4%	8%	9%	2%	8%	9%
Beta-Alanine	1%	8%	9%	0%	8%	9%
Pyroglutamate	2%	7%	9%	0%	7%	8%
Methionine (-)	1%	6%	8%	0%	6%	8%
Isoleucine (-)	11%	4%	6%	1%	4%	6%
Threonine (-)	3%	4%	6%	0%	4%	5%
Asparagine (-)	0%	1%	3%	0%	1%	2%
Root (a)						
Alanine	13%	28%	29%	2%	28%	39%
Glutamic Acid	10%	22%	24%	1%	22%	31%
Aspartate	9%	21%	23%	0%	21%	25%
Isoleucine	6%	18%	22%	2%	18%	23%
Serine	6%	16%	15%	0%	16%	16%
Valine	7%	15%	19%	0%	15%	19%
Beta-Alanine	4%	15%	18%	3%	15%	22%
Pyroglutamate	5%	14%	20%	1%	14%	22%
Glycine	4%	13%	16%	0%	13%	19%
Methionine (-)	4%	11%	14%	0%	11%	12%
Threonine (-)	1%	5%	9%	0%	5%	8%
Asparagine (-)	4%	2%	2%	0%	2%	2%

Notes: Letters a (increased) and b (decreased) denote mean differences as estimated through an ANOVA followed by a Tukey-HSD test for all amino acid enrichments except those with an (-), which lack significant changes. **Bold font** signals selected treatments for subsequent experiments, which have a significant enrichment (as measured by a GLM) as compared to the control.

Arabidopsis shoots had the highest enrichments in ALA, GLY, SER, GLU, and ASP. On the other hand, in the roots, the highest enrichments of GLY were replaced by ISO. Most amino acid compounds were significantly enriched. Clear exceptions were methionine, threonine, and asparagine, and although these compounds were enriched, the statistical limit for claiming significant enrichment was exceeded by the intrinsic variability of the enrichment percentages of these compounds. This illustrates the rather conservative statistical approach given the existing background of zero enrichment percentages, i.e., 0 mM. After NIA correction, the residual enrichment varied between 0 and 3%. This indicates that our statistical model must be robust to avoid false positives at the risk of increasing false negatives.

8.3.4 Tailoring a Customized ^{15}N Labelling Strategy

After carefully elucidating the dynamics of the tracer in our hydroponic system, we tested multiple ^{15}N labelling strategies aiming at finding conditions in which the label could be limited to specific soluble amino acid pools. This optimal strategy would then allow us to incorporate ^{15}N atoms into newly synthesized proteins in a controlled and predictable way. Furthermore, peptide detection in the Mass Spectrometer would then be a simpler task as compared to the scenario where all soluble amino acid pools are differentially labelled across experimental conditions. We tested three different labelling strategies detailed in Figure 8.7.

The ^{15}N labelling strategies differed markedly in terms of the distribution of the tracer across the primary metabolome. Feeding ammonium nitrate caused a huge dispersion of label, with many mass features from varied metabolites picking up the tracer. The amino acid mixture also caused a wide dispersion of labelling, but to a lesser extent across the primary metabolome. While using the amino acid mixture, the most highly labelled amino acids were serine and glycine, which led us to use these two amino acids as carriers of the labelled N in the plant. As expected, the tracer was limited to the serine and glycine pools when we used this strategy to label the plants. Therefore, this last strategy was chosen for subsequent experiments. With the chosen strategy, we were able to enrich the soluble amino acid pools of serine and glycine up to approximately 85 % in shoots and 78 %, 58 % in roots (Figure 8.8). Moreover, this strategy resulted in enrichment percentages that remained statistically unchanged between experimental conditions, i.e.,

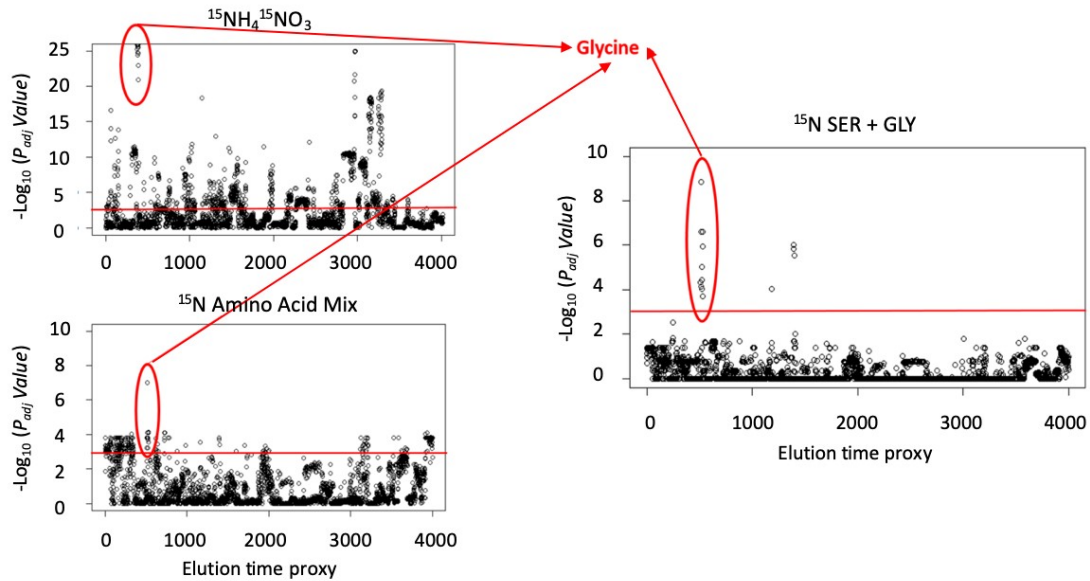


FIGURE 8.7: **Differential label incorporation into Arabidopsis roots among diverse labelling strategies.** Each plot represents a different labelling strategy, namely ammonium nitrate (top-left), amino acid mixture (bottom-left) and serine plus glycine (right), all delivered in the rearing media at a concentration of 0.5 mM. The x-axis represents sorted mass features according to their elution time and comprises all the good quality mass features detected in the chromatograms. The y-axis represents the $-\text{Log}_{10} P$ value that resulted of the comparison between labelled samples and non-labelled controls and thus significant differences among treatments reflect incorporation. The P values were adjusted with BH-95'. The red lines are the significance boundary. Finally the red circles outline the mass features detected for the amino acid glycine as an example of the outcome of the multiple labelling strategies.

between the "control" and "low suboptimal temperature" regimes (Figure 8.8), and thus allowed us to further minimize technical experimental variance.

In root systems, both serine and glycine were labelled to an approximately equal degree in their soluble pools, suggesting that the endogenous soluble pools of both amino acids may be tightly and jointly regulated. On the other hand, the same amino acid pools in shoots show different enrichment of about 20 %, suggesting that the mobile amino acid may be glycine and consequently it takes time until it is converted to serine in shoots. Both amino acid pools were highly enriched, suggesting that mass spectrometry measurements of peptides containing one or both amino acid residues would have noticeable and predictable shifts in Dalton that correlate linearly with the number of SER and GLY residues in each peptide (in the roots) with a lag of about 20 %. Furthermore, since there are no significant differences between the percent labelling in soluble amino acid pools at low suboptimal temperature and control temperature, this factor could be neglected as it would be considered an additional source of technical variation.

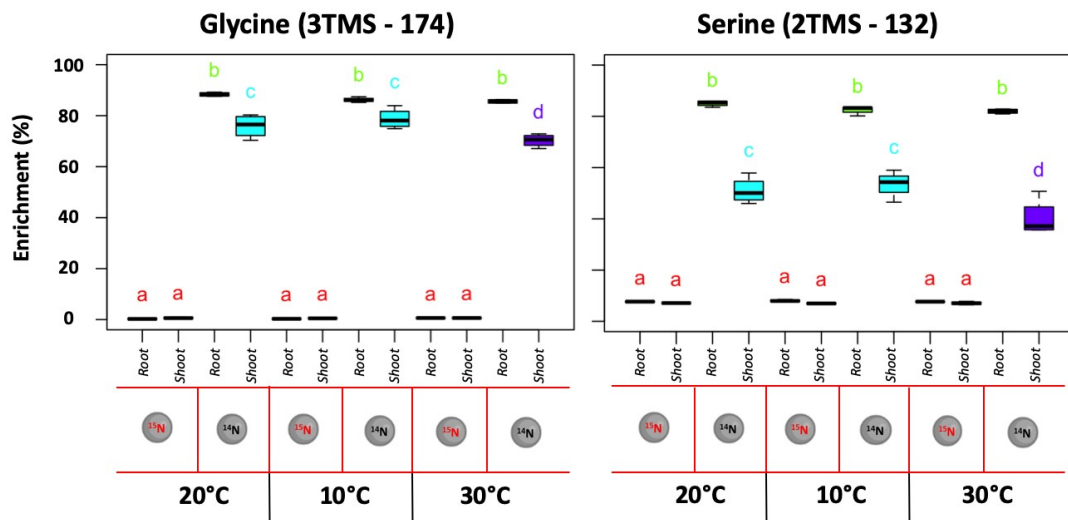


FIGURE 8.8: ^{15}N enrichment percentages selectively incorporated into the soluble pools of serine and glycine in the optimized enrichment strategy that allowed minimal technical variation during the study of plant acclimation to suboptimal low temperature. Whole plants were labelled with 99 % ^{15}N -labelled serine and glycine in liquid MS media. This strategy was selected as optimal for subsequent studies for two main reasons. First, the tracer did not spread to soluble amino acid pools other than SER and GLY (Figure 8.7), which facilitated processing and interpretation of the mass spectrometry metabolomics and proteomics data. Second, the enrichment percentages for both compounds did not differ statistically between the control temperature and the low suboptimal temperature, ensuring a predictable isotopolog envelope shift in the proteins containing the labelled residues. Mean differences in enrichment shown in the graphs are from an ANOVA + Tukey HSD posthoc test; letter and color changes denote statistical differences.

8.3.5 Incorporation of ^{15}N Labelled Serine and Glycine into Ribosomal Proteins

Next, we sought to elucidate changes in protein synthesis dynamics to understand what might constitute ribosome remodelling and associated ribosome-autocatalytic translational control in our plant system during cold. The first and necessary control step was to confirm that the tracer was indeed incorporated into the proteome (Figure 8.9). We chose ribosomal proteins as the test control for several reasons. First, the process of purifying ribosomes through high-density sucrose layers filters out all soluble material that may contain stable isotope impurities that have not yet been assembled into proteins. Thus, by using purified ribosomes, we prevent enrichment from being affected by technical artefacts. Second, we used plant shoots for our test case because the root systems were still embedded in labelled media at harvest and we needed to unambiguously demonstrate that the tracer was imported into the plant, metabolized via soluble amino

acid pools, and incorporated into proteins. With these two controls, we were able to confirm that our method worked as expected.

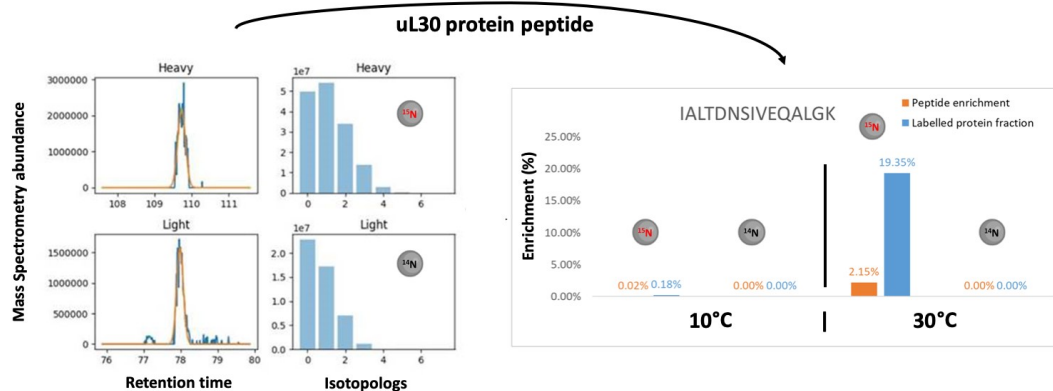


FIGURE 8.9: **Exemplary isotopolog shift, peptide and protein enrichment percentages in a ribosomal protein from 60S large subunits purified from plant shoot systems reared at suboptimal low or high temperature.** Plants were reared at optimized temperature and shifted to different temperature regimes. Cytosolic ribosomes were purified from plant roots and shoots, ribosomal proteins were purified and processed and peptides analysed through LC/MS-MS. In the left panel, the isotopolog envelope of a uL30 peptide is portrayed as detected in labelled (heavy - upper panel) and non-labelled shoot samples (light - lower panel). In the right panel, the peptide enrichment is converted into protein enrichment after accounting for differential labelling in soluble amino acid pools that comprise the peptide sequence.

The bioinformatics implementation for calculating protein synthesis rates is described in Chapter 7 and includes a physiological contextualization of the enrichment values in order to transform them into fractional synthesis rates. The physiological context is important because plants growing at different temperatures will have different protein accumulation and growth dynamics, and failure to account for these phenotypic characteristics will result in unrealistic protein turnover dynamics. In addition, the obtained peptide enrichment values are normalized by the average labelling in soluble amino acid pools of those residues that make up each peptide. This calculation can be traced from Figure 8.9, where the example peptide has one GLY and one SER residue and each of these pools is enriched to approximately 80 %. The peptide has a total of 18 N atoms and thus, of all the N in the peptide, only approximately 10 % can actually be labelled. Normalizing the peptide enrichment values by 0.1 essentially increases the protein enrichment by 10-fold, as shown in the conversion of the two values in Figure 8.9. Since the pools of SER and GLY are equally enriched at suboptimal high and suboptimal low temperature conditions, the correction factor is also approximately the same.

8.3.6 Accumulation of Actively Translating Polysomes during Cold Acclimation

After optimizing our method, we purified actively translating polysomes from plants that were cold acclimated for seven days to find out how these ribosomes are assembled in terms of the origin of their protein components, i.e., using newly synthesized or reused proteins. We separated the translational complexes in a sucrose gradient and monitored their abundance. The dynamics of polysome accumulation at optimal temperature compared with low and high suboptimal temperatures are summarized in Figure 8.10 and File S6 - Slides S1. In addition, we checked the position of polysome complexes in our profiles by examining the ratio between plant 25S and 18S rRNA, which indicate the relative abundance of 60S and 40S subunits, respectively. Finally, we verified that polysomes remained intact during our extraction and purification procedure.

The resulting chromatograms were aligned to allow comparison between biological replicates. Batch correction was then performed to normalize for technical differences between ^{14}N and ^{15}N samples. Because of the highly dynamic rRNA ratios, we ultimately considered only the polysomal peak to be sufficiently resolved to draw statistical conclusions. Therefore, we integrated the peak areas and compared the resulting abundances of polysomes in the different treatments using a generalized linear model (all analyses were performed in R using in-house developed scripts, which are deposited in file S6.1). We found that polysomes accumulated significantly in plants subjected to cold acclimation at day 7 after the initial stimulus. The shape and position of polysome peaks were not altered, suggesting that the accumulation was not due to slower translational dynamics, but merely to a greater absolute abundance of actively translating ribosomes. We found a non-significant trend toward accumulation of non-translational complexes at optimized temperature and yet the non-translational peaks were not increased further at high suboptimal temperature, ruling out the possible role of increased kinetic dynamics of translational complexes with increased temperature.

In the next step, we purified and digested the rProteome associated with the accumulated polysomes to elucidate the triggered rProtein substoichiometry in actively translating ribosomes and the fractional synthesis rates of their individual proteins using the resources described in Chapter 7. Data collection is ongoing.

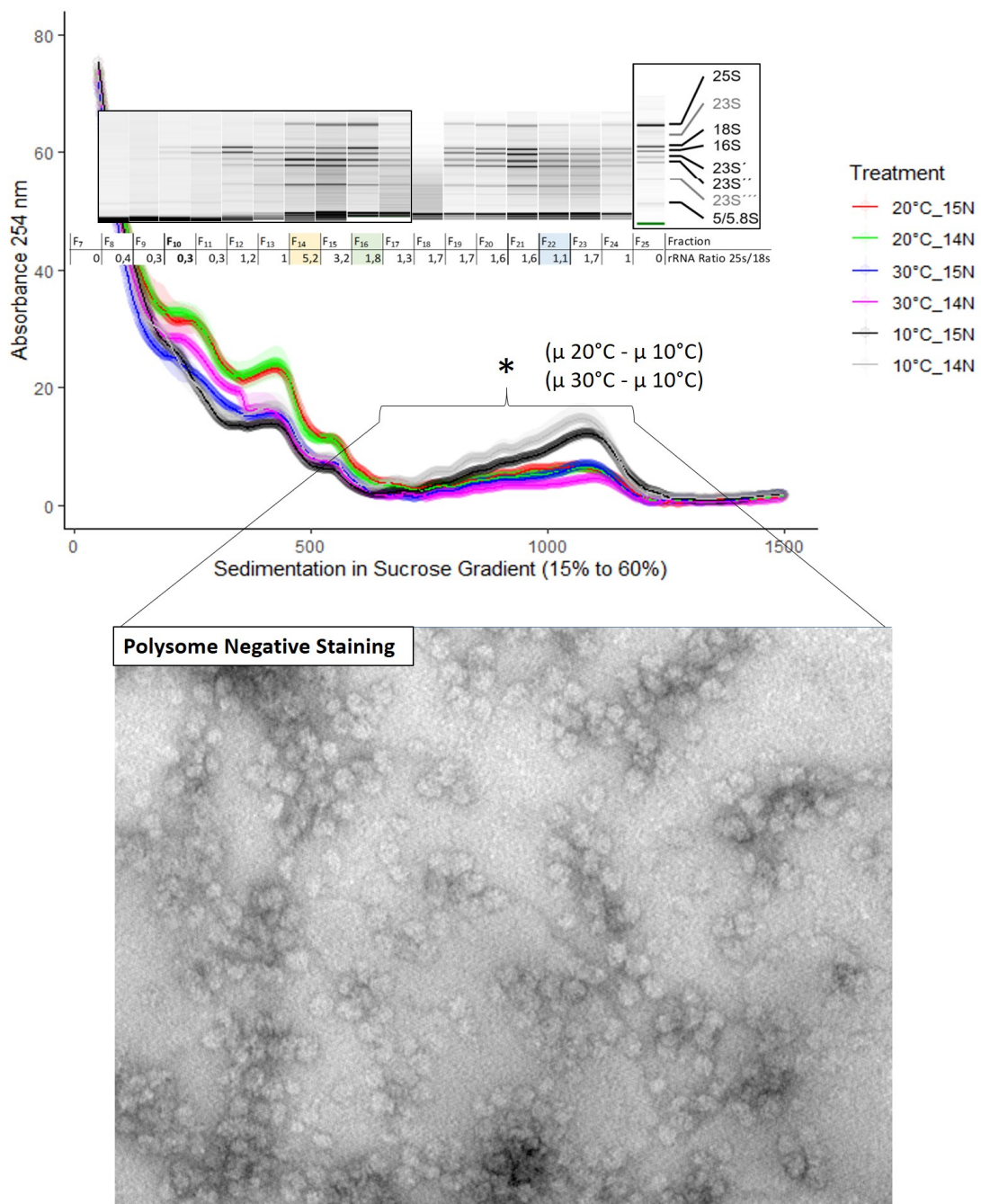


FIGURE 8.10: Relative abundance of free and actively translating ribosomal complexes purified from roots of *Arabidopsis* seedlings reared at different temperatures. Ribosomal complexes were purified and separated by a sucrose gradient. Relative abundances were derived from rRNA abundance measured at a wavelength of 254 nm, and fractions were collected every 16 s. Each of the 25 resulting fractions was monitored using the Bioanalyzer pico RNA assay to derive the ratio of 25S to 18S rRNA. The largest complexes sedimented further down and correspond to polysome peaks with an rRNA 25S to 18S ratio close to 1.6. The integrity of the polysome complexes was further verified by negative staining following a standard published protocol [4]. Briefly, the sample was loaded into the grid (hydrophilic carbon surface), washed with buffer and stained with the negative staining, heavy metal, solution for one minute. After air-drying the grids were imaged in a transmission electron microscope.

8.3.7 Future steps: Towards Physiological Validation of the Glycine-Serine Labelling Strategy

We attempted to monitor any potential negative effects of the feeding strategy, but could not find any evidence of growth or development being affected by amino acid feeding. To complement the experiments already shown, we fed different mixtures of amino acids (during optimization of the labelling method) and evaluated the changes in the pools of soluble amino acids, for which we did not find significant changes in abundance (supplemental Table 3). We also used these data sets to look for general effects on metabolism compared with inorganic N nutrition and found none. In addition, as described in previous sections, we examined the distribution of the tracer across the primary metabolome when labelled with serine and glycine only and found that it was restricted to the glycine and serine pools, suggesting that these two pools may not be accumulating above certain abundance thresholds in this plant system. Second, we selected our two candidate amino acids based on Forsum et al. 2008 [12]. Here, the authors show that serine and glycine are the amino acids that do not affect *Arabidopsis* growth when fed without inorganic nitrate (as the only N source). The authors also showed that glycine in combination with nitrate has no significant effect on growth in terms of accumulated biomass. These experiments confirm that these two amino acids are less intrusive for *Arabidopsis* as compared to the others.

Finally, this *Arabidopsis* system is photosynthetic and as such our labelling strategy could be quite sensitive to conditions when photorespiration is involved. For example, glycine added to the growth medium can supplement mutants deficient in serine biosynthesis (personal communication with [Sara Rosa-Téllez](#)). Thus future strategies should aim to buffer this potential negative effects, and considering that our own experiments with barley have clearly shown that a low percentage of tracer in soluble amino acid pools is sufficient to successfully characterize protein biosynthesis (Chapter 7), future labelling strategies should aim to grow *Arabidopsis* under more natural N nutritional regimes. It is known that plants in nature use N from inorganic and organic sources, which include amino acids and peptides, resulting in a nutritional scheme in which the plant obtains N via inorganic salts such as ammonium and potassium nitrate, but also via organic sources such as soluble amino acids in the media. This combination added to our current labelling scheme would lead to lower labelling percentages in the serine and

glycine pools, which we now know is desirable to avoid complexity in the mass spectra of the peptides. Therefore, the approximately 80% labelling that we have achieved in *Arabidopsis* may not actually be necessary, although it represents an upper limit that is physiologically relevant.

8.4 Using kinetic Mass Spectrometry Imaging to Unravel Spatial Translational Dynamics in Roots

One of the major limitations in circumventing the spatial variability of complex root landscapes is root harvesting procedures, as conventional macroscopic tissue-sampling groups root zones together. Consequently, any biological phenomena that would otherwise be noticeable in specific root zones or tissue are diluted. To overcome this limitation, mass spectrometry imaging (MSI) provides insight into the localization of biomolecules, e.g., [2], offering the opportunity to trace the locations where biological processes occur. In plants, MSI approaches have been developed and applied to many small molecules [8, 11, 29], while their application to larger, complex molecular species such as proteins has not yet been reported. This is likely due to the lack of instructive and comprehensive procedures for sample preparation, protein digestion, and bioinformatics for MSI proteomic analysis that will be reported in this work.

We used MSI and stable isotope assisted mass spectrometry (kMSI) to investigate the spatio-temporal dynamics of protein turnover in barley root meristems. We aimed to validate the spatial distribution of cold proteome shifts by using kinetic MSI to superimpose *de novo* synthesized peptides and reconstructed root tip. Major limitations needed to be surpassed in order to be able to acquire and interpret this data. First, the experimental design used to obtain paired root samples to investigate the spatial proteome is summarized in Figure 8.11. Second, we optimized the protocol for sample preparation and data collection (Appendix C). Third, we developed bioinformatics resources that were missing for the generated datasets. The GitHub repository ProteoMSI contains R functions for annotating peptide peaks in acquired kMSI data (File S4). We then developed functions to interpret kMSI experiments. To this end, we developed the KineticMSI R package [9, 10] (Figure 8.12 & File S1) and two sister GitHub repositories called KineticMSI.2_kLCMS (File S2) & [KineticMSI_HelpThreads](#) to enable the use

of KineticMSI functions for LCMS data and general help threads, respectively. These three repositories include the necessary bioinformatics tools to perform user-assisted interpretation of kinetic mass spectrometry imaging proteomics datasets.

KineticMSI is a collection of scripts that aid in the accurate data preparation and analysis of stable isotope (kinetic) mass spectrometry imaging experiments to derive functional biological interpretations. KineticMSI is divided into several steps (Figure 8.12):

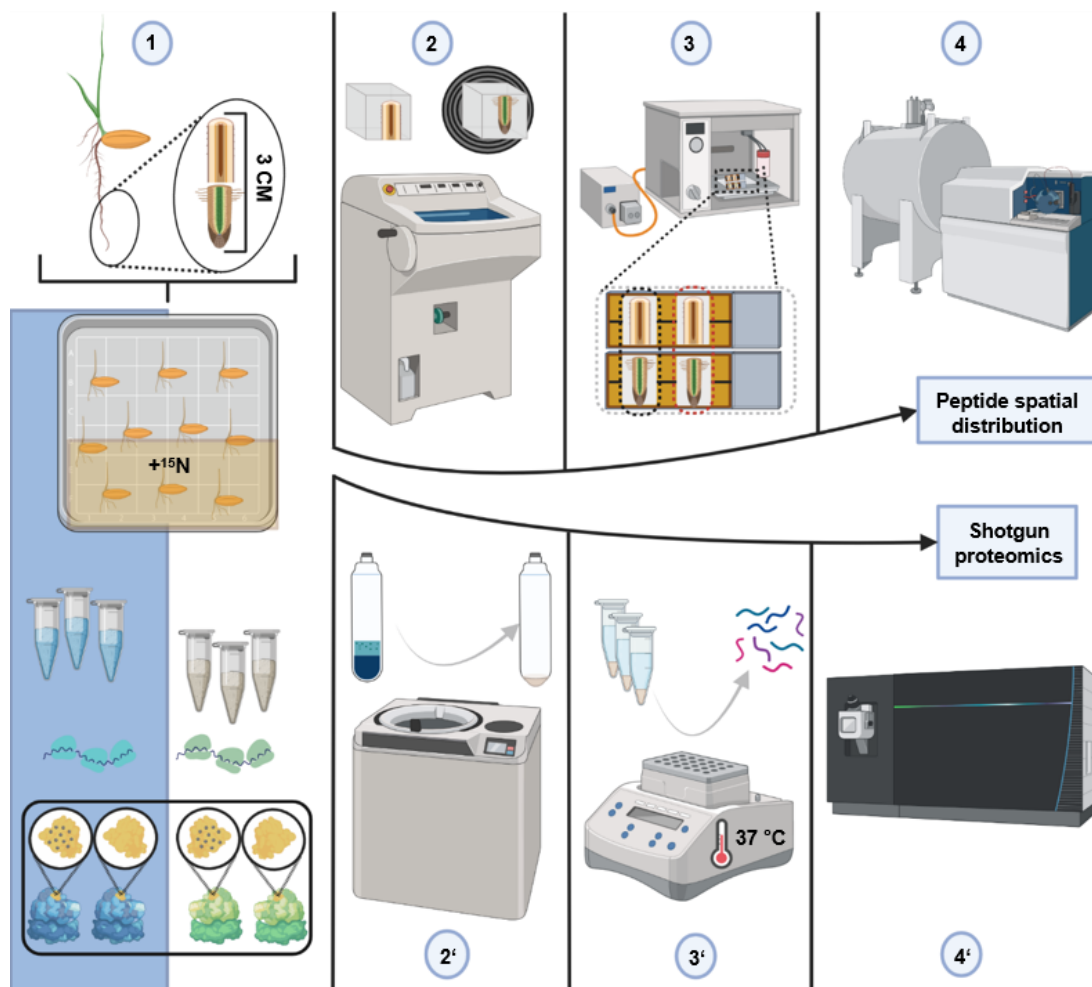


FIGURE 8.11: Summary of the methodological workflow to achieve measurements of protein synthesis, abundance and distribution across barley root tips. (1) harvesting of root tips from barley seedlings and division into two 1.5 cm segments. Barley seedlings were germinated in two temperature regimes with one quarter of the plants having additional labelled nitrogen source and another quarter the same non-labelled nitrogen sources (2) Embedding and freezing of root tissue in cryo-embedding medium cooled down with liquid nitrogen-cold isopropanol followed by slicing of the resulting block using a cryotome. (3) Fixing of the root tissue in copper tape covered slides followed by processing of the slides including on-slide protease digestion. (4) MALDI-FTICR-MS. (2') grinding of pooled tissue using liquid nitrogen, mortar and pestle followed by ribosome enrichment by ultracentrifuge-mediated large cellular complex subproteome extraction and pelleting. (3') Reduction, alkylation, protease digestion and peptide cleaning. (4') LC-MS/MS.

- Input data: Data matrices with normalized or comparison-ready abundances across MSI pixels are required. The input data must include the intensities of the isotopologs.
- Preprocessing of the data: The procedure is used to remove potentially spurious pixels that could be misinterpreted as enriched if they remain in the data sets when correcting for natural isotope abundance.
- Natural Isotope Abundance (NIA) Correction: Enrichment percentages can be easily derived from the corrected isotopolog pools.
- Compilation of isotope flux proxies for tracer dynamics analysis.
- Visualization and determination of the best isotope flux proxies. The chosen proxies may vary depending on the experimental strategy, i.e. tracer used, metabolic targets, isotopologs detected, enrichment percentages, isotopic envelope shifts.
- Visualization of the isotope flux proxies and analysis of the spatial dynamics of the tracer. This step is used to reconstruct kMSI images based on the derived proxies of isotope enrichment.
- Quality assessment of consolidated data matrices.
- Class comparison using pixel populations.
- Subsetting of the consolidated data matrices into equivalent coherent pixel subsets. In this step, the coordinates of individual molecular species are subclassed based on the selected enrichment proxies to avoid dilution of biology by averaging an entire region. The procedure allows comparison with anatomical regions of interest obtained by unsupervised statistical methods (e.g., from Cardinal SSC or SCiLS K-means clustering).
- Class comparison using pixel subsets: involves relative quantification and comparison of the enrichment dynamics of the labelled metabolic targets. The procedure uses the classes determined in the previous step.
- Class comparison using enriched pixel proportions.
- KineticMSI summary results.

Data collection and analyses from barley root tips labelled with ^{15}N is ongoing.

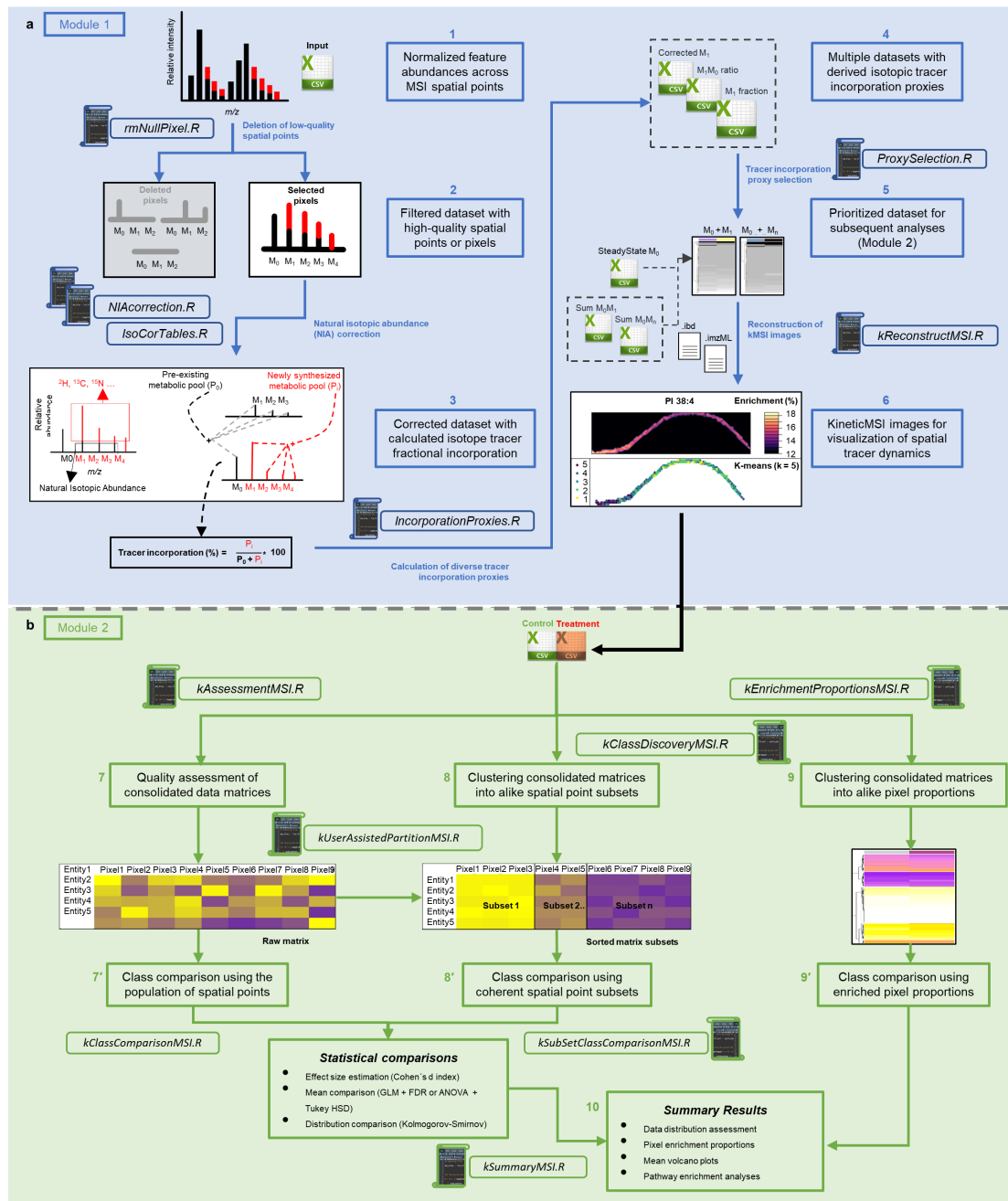


FIGURE 8.12: Simplified schematic diagram of the KineticMSI workflow for pre-processing and analysis of kMSI datasets. (a) Module 1 includes functions for data pre-processing as well as accurate graphical representation of kMSI images. 1, input matrix preparation; 2, low quality MSI pixels deletion; 3, natural isotope abundance (NIA) correction; 4, inference and 5, definition of the most appropriate isotope tracer proxies; and 6, kMSI image reconstruction. (b) Module 2 contains three different approaches. First, 7, data quality control and 7', class comparison using pixel population averages; second, 8, spatial segmentation into coherent pixel subsets and 8', class comparison using pixel subset averages; and third, 9, evaluation of pixel fractions falling within an incorporation range and 9', class comparison using the enriched pixel fractions. 10, summary of the results obtained with the above approaches.

Bibliography

- [1] Reyes Babiano, Gwenael Badis, Cosmin Saveanu, Abdelkader Namane, Antonia Doyen, Antonio Díaz-Quintana, Alain Jacquier, Micheline Fromont-Racine, and Jesus de la Cruz. Yeast ribosomal protein 17 and its homologue rlp7 are simultaneously present at distinct sites on pre-60s ribosomal particles. *Nucleic acids research*, 41(20):9461–9470, 2013. doi: 10.1093/nar/gkt726.
- [2] Berin A Boughton, Dinaiz Thinagaran, Daniel Sarabia, Antony Bacic, and Ute Roessner. Mass spectrometry imaging for plant biology: a review. *Phytochemistry Reviews*, 15(3):445–488, 2016. doi: 10.1007/s11101-015-9440-2.
- [3] Douglas C Boyes, Adel M Zayed, Robert Ascenzi, Amy J McCaskill, Neil E Hoffman, Keith R Davis, and Jorn Gorlach. Growth stage-based phenotypic analysis of arabidopsis: a model for high throughput functional genomics in plants. *The Plant Cell*, 13(7):1499–1510, 2001. doi: 10.1105/TPC.010011.
- [4] Lou Brillault and Michael J Landsberg. Preparation of proteins and macromolecular assemblies for cryo-electron microscopy. In *Protein Nanotechnology*, pages 221–246. Springer, 2020. doi: 10.1007/978-1-4939-9869-2_13.
- [5] Bo Eng Cheong, Olga Beine-Golovchuk, Michal Gorka, William Wing Ho Ho, Federico Martinez-Seidel, Alexandre Augusto Pereira Firmino, Aleksandra Skiryecz, Ute Roessner, and Joachim Kopka. Arabidopsis rei-like proteins activate ribosome biogenesis during cold acclimation. *Scientific Reports*, 11:1–25, 2021. ISSN 20452322. doi: 10.1038/s41598-021-81610-z.
- [6] Sonia Chothani, Eleonora Adami, John F Ouyang, Sivakumar Viswanathan, Norbert Hubner, Stuart A Cook, Sebastian Schafer, and Owen JL Rackham. deltate: Detection of translationally regulated genes by integrative analysis of ribo-seq and rna-seq data. *Current protocols in molecular biology*, 129(1):e108, 2019. doi: 10.1002/cpmb.108.
- [7] Alexander Erban, Federico Martinez-Seidel, Yogeswari Rajarathinam, Frederik Dethloff, Isabel Orf, Ines Fehrle, Jessica Alpers, Olga Beine-Golovchuk, and Joachim Kopka. Multiplexed Profiling and Data Processing Methods to Identify Temperature-Regulated Primary Metabolites Using Gas Chromatography Coupled to Mass Spectrometry. In Dirk K Hinch and Ellen Zuther, editors, *Methods in*

- Molecular Biology*, volume 2156, pages 203–239. Springer US, New York, NY, 2020. ISBN 978-1-0716-0660-5. doi: 10.1007/978-1-0716-0660-5_15.
- [8] Desalegn W Etalo, Ric CH De Vos, Matthieu HAJ Joosten, and Robert D Hall. Spatially resolved plant metabolomics: some potentials and limitations of laser-ablation electrospray ionization mass spectrometry metabolite imaging. *Plant physiology*, 169(3):1424–1435, 2015. doi: 10.1104/pp.15.01176.
- [9] Farheen Farzana, Federico Martinez-Seidel, Anthony Hannan, Danny Hatters, and Berin Boughton. Kineticmsi, an r-based framework for relative quantification of spatial isotopic incorporation in mass spectrometry imaging experiments. *bioRxiv*, 2022. doi: 10.1101/2022.08.31.505954.
- [10] Farheen Farzana, Malcolm McConville, Thibault Renoir, Shanshan Li, Shuai Nie, Harvey Tran, Anthony J Hannan, Danny M Hatters, and Berin A Boughton. Longitudinal spatial mapping of lipid metabolites reveals pre-symptomatic changes in the hippocampi of huntington’s disease transgenic mice. *Neurobiology of Disease*, page 105933, 2022. doi: 10.1016/j.nbd.2022.105933.
- [11] Adam D Feenstra, Liza E Alexander, Zhihong Song, Andrew R Korte, Marna D Yandea-Nelson, Basil J Nikolau, and Young Jin Lee. Spatial mapping and profiling of metabolite distributions during germination. *Plant physiology*, 174(4):2532–2548, 2017. doi: 10.1104/pp.17.00652.
- [12] Oskar Forsum, Henrik Svennerstam, Ulrika Ganeteg, and Torgny Näsholm. Capacities and constraints of amino acid utilization in arabidopsis. *New Phytologist*, 179(4):1058–1069, 2008. doi: 10.1111/j.1469-8137.2008.02546.x.
- [13] Olivier Gadal, Daniela Strauss, Elisabeth Petfalski, Pierre-Emmanuel Gleizes, Nicole Gas, David Tollervey, and Ed Hurt. Rlp7p is associated with 60s pre-ribosomes, restricted to the granular component of the nucleolus, and required for pre-rRNA processing. *The Journal of cell biology*, 157(6):941–952, 2002. doi: 10.1083/jcb.200111039.
- [14] Olga Beine Golovchuk, Alexandre Augusto Pereira Firmino, Adrianna Dabrowska, Stefanie Schmidt, Alexander Erban, Dirk Walther, Ellen Zuther, Dirk K. Hinch, and Joachim Kopka. Plant temperature acclimation and growth rely on cytosolic

- ribosome biogenesis factor homologs. *Plant Physiology*, 176:2251–2276, 2018. ISSN 15322548. doi: 10.1104/pp.17.01448.
- [15] Paul Heinrich, Christian Kohler, Lisa Ellmann, Paul Kuerner, Rainer Spang, Peter J Oefner, and Katja Dettmer. Correcting for natural isotope abundance and tracer impurity in ms-, ms/ms-and high-resolution-multiple-tracer-data from stable isotope labeling experiments with isocorrector. *Scientific reports*, 8(1):1–10, 2018. doi: 10.1038/s41598-018-36293-4.
- [16] Jan Huege, Jan Goetze, Frederik Dethloff, Bjoern Junker, and Joachim Kopka. Quantification of stable isotope label in metabolites via mass spectrometry. In *Plant Chemical Genomics*, pages 213–223. Springer, 2014.
- [17] Nicholas T Ingolia, Gloria A Brar, Silvia Rouskin, Anna M McGeachy, and Jonathan S Weissman. The ribosome profiling strategy for monitoring translation in vivo by deep sequencing of ribosome-protected mrna fragments. *Nature protocols*, 7(8):1534–1550, 2012. doi: 10.1038/nprot.2012.086.
- [18] Nicholas T Ingolia, Jeffrey A Hussmann, and Jonathan S Weissman. Ribosome profiling: global views of translation. *Cold Spring Harbor perspectives in biology*, 11(5):a032698, 2019. doi: 10.1101/cshperspect.a032698.
- [19] Hirofumi Ishihara, Toshihiro Obata, Ronan Sulpice, Alisdair R Fernie, and Mark Stitt. Quantifying protein synthesis and degradation in arabidopsis by dynamic ¹³co₂ labeling and analysis of enrichment in individual amino acids in their free pools and in protein. *Plant Physiology*, 168(1):74–93, 2015. doi: 10.1104/pp.15.00209.
- [20] Jelena Jakovljevic, Uli Ohmayer, Michael Gamalinda, Jason Talkish, Lisa Alexander, Jan Linnemann, Philipp Milkereit, and John L Woolford. Ribosomal proteins 17 and 18 function in concert with six a3 assembly factors to propagate assembly of domains i and ii of 25s rrna in yeast 60s ribosomal subunits. *Rna*, 18(10):1805–1822, 2012. doi: 10.1261/rna.032540.112.
- [21] Tae-Youl Kim, Cheol Woong Ha, and Won-Ki Huh. Differential subcellular localization of ribosomal protein 17 paralogs in saccharomyces cerevisiae. *Molecules and cells*, 27(5):539–546, 2009. doi: 10.1007/s10059-009-0077-0.

- [22] Lei Li, Clark J Nelson, Cory Solheim, James Whelan, and A Harvey Millar. Determining degradation and synthesis rates of arabidopsis proteins using the kinetics of progressive 15n labeling of two-dimensional gel-separated protein spots. *Molecular & Cellular Proteomics*, 11(6), 2012. doi: 10.1074/mcp.M111.010025.
- [23] Lei Li, Clark J Nelson, Josua Trösch, Ian Castleden, Shaobai Huang, and A Harvey Millar. Protein degradation rate in arabidopsis thaliana leaf growth and development. *The plant cell*, 29(2):207–228, 2017. doi: 10.1105/tpc.16.00768.
- [24] Alexander Luedemann, Katrin Strassburg, Alexander Erban, and Joachim Kopka. Tagfinder for the quantitative analysis of gas chromatography—mass spectrometry (gc-ms)-based metabolite profiling experiments. *Bioinformatics*, 24(5):732–737, 2008. doi: 10.1093/bioinformatics/btn023.
- [25] Federico Martinez-Seidel, Olga Beine-golovchuk, Yin Chen Hsieh, Kheloud El Eshraky, Michal Gorka, Bo Eng Cheong, Erika V. Jimenez-posada, Dirk Walther, Aleksandra Skiryecz, Ute Roessner, Joachim Kopka, and Alexandre Augusto Pereira Firmino. Spatially enriched paralog rearrangements argue functionally diverse ribosomes arise during cold acclimation in arabidopsis. *International Journal of Molecular Sciences*, 22:6160, 2021. ISSN 14220067. doi: 10.3390/ijms22116160.
- [26] Clark J Nelson and A Harvey Millar. Protein turnover in plant biology. *Nature plants*, 1(3):1–7, 2015. doi: 10.1038/nplants.2015.17.
- [27] Clark J Nelson, Ralitzia Alexova, Richard P Jacoby, and A Harvey Millar. Proteins with high turnover rate in barley leaves estimated by proteome analysis combined with in planta isotope labeling. *Plant physiology*, 166(1):91–108, 2014. doi: 10.1104/pp.114.243014.
- [28] Clark J Nelson, Lei Li, and A Harvey Millar. Quantitative analysis of protein turnover in plants. *Proteomics*, 14(4-5):579–592, 2014. doi: 10.1002/pmic.201300240.
- [29] Lenin D Sarabia, Berin A Boughton, Thusitha Rupasinghe, Damien L Callahan, Camilla B Hill, and Ute Roessner. Comparative spatial lipidomics analysis reveals cellular lipid remodelling in different developmental zones of barley roots in response to salinity. *Plant, cell & environment*, 43(2):327–343, 2020. doi: 10.1111/pce.13653.

-
- [30] Daniel M Wilson, Yu Li, Amber LaPeruta, Michael Gamalinda, Ning Gao, and John L Woolford. Structural insights into assembly of the ribosomal nascent polypeptide exit tunnel. *Nature communications*, 11(1):1–15, 2020. doi: 10.1038/s41467-020-18878-8.
- [31] Guohua Xu, Xiaorong Fan, and Anthony J Miller. Plant nitrogen assimilation and use efficiency. *Annual review of plant biology*, 63:153–182, 2012. doi: 10.1146/annurev-arplant-042811-105532.

Chapter 9

Discussion

Each of the original manuscripts that have been incorporated into this thesis contains its own discussion section. To avoid repetition, the focus of this section is on how the knowledge gained contributes to the general model of the mechanistic events that occur when a plant perceives a cold stimulus and ultimately leads to successful acclimation after a week of cold. Successful acclimation is defined as the ability of the plant to resume growth in the cold [33].

9.1 Plant Phenotype during Cold Acclimation

Plants show typical phenotypic responses to low suboptimal temperature acclimation [27, 40, 55]. Among the major responses, the most conspicuous at the phenotypic level is growth arrest. Whole *Arabidopsis* rosettes cease growth for about a week [21], and during this time plants adjust their molecular dynamics to formulate an appropriate response. Similarly, the root systems of the two plant models studied in this thesis, *Arabidopsis thaliana* and *Hordeum vulgare*, cease to increase dry weight when acclimated to suboptimal low temperature (Chapter 6 and Chapter 4, respectively). Growth retardation in *Arabidopsis* is due to continued cell elongation but reduced mitotic division [2]. Similarly, total protein content in the root system of barley seedlings is reduced upon acclimation to 4°C (Chapter 4), and because most of the dry weight is protein during germination, this confirms an inverse relationship between cold acclimation and

mitotic division, such that the root system of barley shows a similar response to temperatures of 4°C compared with *Arabidopsis* rosettes. In barley seedling root tips, relative growth rates calculated on the basis of dry weight fluctuate during the acclimation period (Chapter 7), suggesting that there are specific dynamics that determine how much protein is produced and how much weight is gained during acclimation. Thus, the most important phenotypic feature at the organism level of acclimated plants is the altered dynamics of biomass accumulation, which directly correlates with ribozyme function by virtue of its protein synthesis capacity.

9.2 Transcriptional Response of Translation-Related Genes during Cold Acclimation

Immediately upon sensing cold, plants trigger transcriptional responses that allow a series of molecular events to be initiated and lead to successful acclimation [25, 31, 32, 47, 56]. As described by Seki et al. (2002) [51], there are two main groups of plant transcriptional responses to cold. The first group contains transcripts that peak in expression 1-2 hours after the initial cold stimulus and set in motion the chain of events leading to acclimation. The second group peaks 10-12 hours after the initial cold stimulus and continues the events necessary to formulate an appropriate acclimation response. Protein-coding genes related to the ribosome in particular and protein biosynthesis in general are considered major hubs mediating the cold acclimation response [15], and are also differentially regulated during cold, the difference being that these transcripts are differentially regulated from the first to the seventh day of acclimation [21]. In this work, we have provided evidence to argue that ontology categories of translation-related genes respond differentially to cold and can be divided into two additional groups of important transcriptional cold responses (Chapter 6). Group three comprises transiently ribosome-associated proteins (RAPs), which include ribosome biogenesis factors (RBFs) and translation initiation factors (TIFs). Group three peaks in differential regulation one day after the initial cold stimulus and primarily includes protein-coding genes of nucleic acid binding and rRNA transcription and processing factors [16, 41, 45, 46]. Group four includes structural ribosomal proteins (rProteins) whose transcripts peak in differential regulation on day seven after the first stimulus. Transcriptional responses

of group four are quite unique in that they exhibit paralog-specific transcriptional dynamics that result in either up- or down-regulation of specific rProtein-encoding genes [35, 38]. This differential regulation suggests the potential functional divergence of rProtein paralogs [6] and structural heterogeneity of the ribosome that may be adjusted to different temperatures. The uncovered cold-transcriptional responses suggest that upregulation of ribosome biogenesis on day one triggers a later requirement for rProteins, which are transcriptionally regulated on day seven. Coincidentally, it takes seven days for plants to acclimate to the cold and resume growth. Thus, it seems likely that transcriptional rewiring of the ribosome biogenesis machinery and later rProtein-coding genes contributes to cold acclimation.

9.3 Ribosome Biogenesis as a Fundamental Process to Start Cold Acclimation

Transcriptomic changes suggest that plants have mechanisms to build new ribosomal complexes during and just before the end of the growth arrest phase that occurs during cold. This hypothesis stands to reason when we analyze the functional role of REIL proteins in plants [21, 48, 49]. REIL proteins are ribosome biogenesis factors that associate with immature 60S subunits to presumably mediate one of the late steps of ribosome biogenesis in the cytoplasm, like their yeast homolog Rei1 [22, 23, 39]. Removal of REIL proteins from plants results in a mutant that does not activate ribosome biogenesis only during cold acclimation and therefore does not successfully acclimate [11, 21]. Thus, ribosome complexes formed during cold acclimation specifically require REIL support to directly or indirectly activate their translational competence. Similarly, REIL mutants are unable to maintain rRNA processing and translate factors required at the very onset of cold acclimation to trigger the full transcriptional response [63]. Active ribosome biogenesis at the onset of cold acclimation may therefore be essential for the assembly of acclimated ribosomes capable of synthesizing the machinery required for rRNA processing and initiating the early transcriptional acclimation events that eventually lead to overcoming the growth arrest that occurs.

9.4 Origin and Spatial Constraints of Cold-Triggered Ribosome Heterogeneity

In eukaryotes, ribosome biogenesis is a sequential mechanism that begins in the nucleolus, continues in the nucleoplasm, and ends in the cytoplasm with the assembly of translationally competent ribosomes [62]. In plants, ribosome biogenesis exhibits many unique features [46, 60], but nonetheless the general process is fairly conserved given the universality of ribosomes and the protein biosynthesis process. In the stepwise process of ribosome biogenesis, rProteins are bound together to rRNA to aid assembly and provide stability to the process. Due to the modular nature of ribosomes, ribosomal regions are processed individually, which increases the likelihood that the rProteins corresponding to the region will be assembled and regulated together. For example, in yeast, removal of certain rProteins impairs certain rRNA processing steps, resulting in substoichiometry of rProteins and rRNA defects in their ribosomal domains [62]. Similarly, assembly of large mitochondrial ribosome subunits in yeast follows a hierarchical pattern of rProtein assembly in which protein groups are incorporated into ribosomes in a modular fashion [65]. Therefore, due to the ribosome assembly line, the rProtein substoichiometry that emerges during biogenesis may exhibit spatial dependencies that can be used to functionally characterize ribosome heterogeneity. Along the same lines, mechanisms that remodel ribosomal subunits as they transit between rounds of translation may also affect groups of neighbouring rProteins, and thus ribosomal regions, rather than specific rProteins individually.

To investigate cold-induced rProtein substoichiometry and its spatial extent, we used mathematical sophistication [36] in conjunction with cold-acclimated REIL knock-out genotypes to block ribosome biogenesis and find common rProtein abundance changes in ribosomal complexes of wild-type [38] plants. By pooling the results from *reil-dkos* and wild-type plants, we ensured that the revealed rProtein substoichiometry occurs mainly during ribosome biogenesis. In this context, we discovered that Arabidopsis ribosome biogenesis is likely to cause regional restructuring of the proteome around the polypeptide exit tunnel (PET) of ribosomes (Chapter 6). Importantly, Rei1, REIL homolog in yeast, inserts its C-terminus into the PET to check its integrity [22]. Therefore, such a checkpoint assay would be absolutely useful for ribosomal particles that show significant

alterations exactly at the functional site of REIL. This discovery led us to hypothesize that, because of these spatial rearrangements, Arabidopsis requires REIL proteins only during cold to activate remodelled and potentially specialized ribosomes and make them translationally competent. To substantiate the potential of spatially-remodelled heterogeneous ribosomal complexes for actual specialization, we systematically assessed [35] and examined seminal publications in the ribosome specialization field to determine whether we could link ribosome specialization to modulation of ribosomal regions (Chapter 5). We used independent datasets in which yeast ribosome specialization was associated with structural changes in small ribosomal subunits (SSU) upon a change in carbon source from glucose to glycerol [53, 54]. We discovered that the induced changes were significantly restricted to a region near the mRNA, tRNA entry sites (Chapter 5). Thus, we were able to formulate testable hypotheses about how biased translation can occur at the SSU level in the yeast system, but, more importantly, we confirmed regional restructuring of ribosomal complexes as a mechanism for generating ribosome specialization.

9.5 Modulation of the Translational Machinery and Consequences for Protein Synthesis

The entire protein biosynthetic apparatus, i.e., the cellular machinery within two degrees of the translational hub [5], undergoes extensive and very specific restructuring during cold acclimation in plants (Chapters 4 and 6 [37, 38]). Thus, plants appear to rely on their ribosome physiology to respond appropriately to external stimuli [35] or at least to low suboptimal temperatures.

Total protein content in plants decreases during cold acclimation, which generally correlates with the accumulation of soluble amino acid pools, including proline (i.e., a known cold-responsive metabolite) [24]. We made a similar observation in acclimated barley root tips (Chapter 7). Even though total protein decreases, cold acclimation triggers synthesis of specific proteins in plants [42]. In our system, rProteins and more generally proteins that form macromolecular complexes are accumulated and newly synthesized during cold (Chapter 4 and Chapter 7). The dynamics of rProtein synthesis and accumulation appear to be quite controlled in our barley system, all rProteins reduce their

ribosome-bound abundances, which means that fewer competent ribosomes are formed and, on the contrary, we found an excess of free rProteins that likely awaits to be assembled either in the cytoplasm, nucleus, or nucleolus (Chapters 4 and 7). Linked to the increased availability of free rProteins, ribosome biogenesis factors and complexes are accumulated during cold (Chapters 4 and 7) presumably to compensate for the relative absence of competent 40S and 60S subunits. Interestingly, of the preribosomal complexes that are accumulated during cold, only the SSU processome contains newly synthesized protein components (Chapter 7). The SSU processome forms a large macromolecular assembly that partitions the maturation events of pre-60S and pre-40S ribosomal particles and enables the stepwise progression of maturation of pre-40S ribosomal particles [3, 43, 44]. Thus, novel components of the SSU processome suggest cold-induced variations in 40S subunit composition and processing. Translation initiation factors (TIF) and pre-initiation/initiation complexes (i.e., 43S and 48S) are also accumulated during cold (Chapters 4 and 7), and this suggests that the limiting step for translation is the availability or binding of 60S complexes. However, the ratio of 40S to 60S assembled rProtein is not altered during cold relative to control temperature, implying that there are as many 60S subunits as 40S, but the former do not associate with every 48S initiation complex. This apparent selectivity performed by 60S-competent subunits results in the accumulation of translation initiation complexes. All TIF complexes are accumulated during cold due to protein synthesis (Chapter 7), and in *Escherichia coli*, as we report in barley, cold acclimation also triggers *de novo* synthesis and accumulation of initiation factors [7]. The accumulation of specific initiation factors can confer selectivity to ribosomes through their association with specific transcripts [10, 20, 26, 59].

At the structural level, Arabidopsis and barley ribosomes change when plants acclimate to low temperatures. The cold-induced changes are accumulation or depletion of specific rProtein paralogs from ribosomal pools (Chapters 6 and 7). Thus, in some cases ribosomes may have an excess of rProteins due to promiscuous or alternative binding events (e.g. [1]), whereas in other cases holes in ribosomal structures may result from the absence of the appropriate proteins [8]. The phenomenon of accumulating structurally heterogeneous ribosomal populations with respect to their rProtein paralog compositions is referred to as induced rProtein substoichiometry. In metazoans, rProtein substoichiometry is associated with functional aspects of translation that regulate cellular fate by shaping the proteome [17, 18]. For instance, in mammalian embryonic stem

cells, the presence or absence of rProteins in ribosomal populations confers the ability to ribosomes for preferential translation of specific transcripts [52]. Similarly, preferential use of rProtein paralogs can confer ribosome selectivity in terms of translational output [19, 28, 34, 50, 64]. Paralog number and stoichiometry are specially relevant in plants due to the increased number of paralog genes encoding each ribosomal protein. We found two main types of ribosome structure remodelling in plants during cold. The first, common to both plant systems, is rProtein substoichiometry around the polypeptide exit tunnel (PET). The PET rProteome restructuring is of the subtractive kind [8], that is, proteins that are no longer part of the ribosome structure at the ribosomal population level. This aspect of cold-induced ribosomal heterogeneity is very likely linked to the function of REIL, and probably leads to the observed cold-induced increase in synthesis of the cellular machinery needed to cope with misfolded or aggregated proteins, which are regarded as the signature of a defective PET (Chapter 7). Second, both subunits in the barley system accumulate rProteins around relevant inter-subunit bridges during cold acclimation, suggesting that the dynamics of subunit association may be changed during cold. Interestingly, we demonstrated that a limiting factor for cold-translation is in fact 60S - 48S joining and found that the newly synthesized initiation factors during cold, forming 43S and 48S pre-initiation complexes, have been linked to non-canonical mRNA binding as well as subunit anchoring in higher metazoans. The observation of accumulated pre-initiation/initiation complexes together with this aspect of triggered cold heterogeneity suggests that selective translation may be mediated by altered and preferential 60S association with specific initiation complexes (Chapter 7).

We used ^{15}N labelling to track the dynamics of protein synthesis and showed that cold-triggered rProtein substoichiometry originates in part from newly synthesized rProteins and in part from recycled and pre-existing rProteins, suggesting that ribosomes can adapt without requiring an entire ribosome biogenesis cycle. Similarly, in mammalian neuronal cells with long dendritic prominences, canonical ribosome biogenesis can be overridden, and ribosomes can preferentially translate specific rProtein paralog transcripts and assemble them on the fly to conserve resources and efficiently adapt to translational demands [13]. Therefore, this aspect highlights how potentially dynamic ribosome remodelling can be to preserve the cellular economy, and taken together with the induced structural adaptations that we report, may be part of the functional mechanisms that actively shape the cellular proteome to adapt to cold temperatures.

9.6 Proteome Shifts and Other Triggered Mechanisms during Cold Acclimation Suggesting Ribosome Specialization

Equally important pieces of evidence for ribosome specialization in our plant systems come from several independent cold acclimation experiments conducted in both *Arabidopsis* (Chapters 2 and 6) and barley (Chapters 4 and 7). First, altered ribosomal compositions during cold appear to be the canon in both species, with only a subset of the total rProtein paralog universe being differentially regulated or differentially accumulating at the transcriptome or proteome level. Second, evidence suggests that transcriptional control during cold in both plant systems relies on alternative splicing mechanisms [9] (Chapter 4), which, building on previous hypotheses, appears to be a level of translational control that relies entirely on the SSU. On the other hand, the large ribosomal subunits (LSU) are undergoing a restructuring of the PET, which is increasingly viewed as a sensitive sensor that shapes the proteome by closely monitoring polypeptide production during protein translation [57, 58, 61]. Accordingly, proteome shifts in our systems indicate that biased translation may be occurring during cold acclimation in plants (Chapters 4, 7, and 8). For example, at the total protein level, individual proteins accumulate in the proliferative tissue of barley roots during cold (Chapters 4 and 7). The accumulated proteins were found in all ontology categories directly related to protein biosynthesis. Similarly, the whole root was enriched in protein cold markers such as COR/LEA proteins and glutathione, S-glutathionylation-related enzymes (Chapter 4). At the level of multiprotein complexes, there was also cold-specific enrichment of translation-related complexes, whereas there was additional ontology enrichment of S-glutathionylation-related enzymes, ER-Golgi, nuclear, and cell cycle multiprotein complexes (Chapter 7). These shifts were examined using ^{15}N as a tool to distinguish between lack of degradation and *de novo* protein synthesis, and we found that more than 50% of the accumulated complexes and their protein components were newly synthesized. Thus, many of these proteome shifts are caused by cold ribosomes synthesizing the correct proteins by either active or passive selection. Ultimately, our labelling strategy confirmed that the translation of certain proteins is functional, as the newly synthesized proteoforms enter active protein pools. In addition, we report the precise composition of the newly synthesized acclimated ribosomes, allowing us to

link the altered average ribosome composition to potentially biased protein translation. A mechanistic link between altered ribosome structures and biased translation remains the grand challenge of the ribosome specialization field [4] and based on the evidence gathered in this thesis, we propose that plant 60S subunits may be able to select which 48S initiation complex to bind and thus which transcript to translate during cold acclimation.

9.7 Functional Aspects Linking Translational Regulation to Cold-Proteome Shifts

Ribosome specialization as a mechanism to enhance cold acclimation in plants, as in other organisms, requires evidence of functional ribosome heterogeneity that can exert translational control by directly translating specific transcripts [17], ultimately leading to proteome shifts that successfully acclimate plants to cold. In this work, we sought to gain functional insights into the translational reprogramming events that occur at the onset and during the first week of acclimation of plants to suboptimal low temperatures. The main mechanistic goal of this work was to establish a link between PET rearrangements and functional ribosome heterogeneity. Three distinct layers of results were generated to make a compelling case for ribosome specialization that occurs during cold and enhances acclimation by synthesizing a cold-specific proteome.

9.7.1 uL30 Ribosomal Protein Family: On the Origin of PET Rearrangements

T-DNA mutant lines of the rProtein family uL30 or RPL7 were obtained and characterized (Chapter 8 & Appendix B). This rProtein family is encoded by four paralog genes in Arabidopsis, which all show interesting cold-dynamics that suggest their involvement in triggered ribosome heterogeneity. The ribosome-bound paralogs (by proteome abundance) are B and C, whereas A and D are not bound to ribosomes or are too scarce in cytosolic complexes for us to detect the abundance of their peptides. The rare paralogs have a more pronounced phenotype when plants are germinated in selective plates than the abundant ones (Chapter 8), and a coding sequence alignment (CDS) of the uL30 paralogs from yeast and Arabidopsis shows that the dominant isoforms have diverged

the most compared with yeast (Chapter 6). Thus, the A and D paralogs could better preserve the rProtein functions known from yeast. The role of uL30 during ribosome biogenesis in yeast has been explained as an early step of pre-rRNA processing in the nucleolus [14]. Therefore, we aimed to test the functions of these proteins during ribosome biogenesis in Arabidopsis by complementing the mutant lines with tagged versions of the uL30 proteins (this part of the project is being pursued in collaboration with graduate student Dione Gentry-Torfer using the tools compiled in Appendix A). Importantly, deletion of both uL30 copies in yeast results in rearrangements of rProteins around the PET [30], and our own data suggest that uL30 is removed from polysomes upon cold in Arabidopsis (Chapter 6), implying a testable mechanistic link between the absence of uL30, PET rearrangements, and the need for REIL. Thus, the next steps will include testing the localization of the paralogs, the rProtein compositions of the complemented mutant lines as well as the non-complemented ones to verify that the rProteome is indeed reprogrammed around the PET when uL30 is absent.

9.7.2 REIL 60S Maturation Factor: On the Need For PET Quality Control

Following the chain of events, the detected changes in PET processing and composition could lead to the requirement of a specific maturation factor, i.e. REIL, for quality control of the 60S subunits before they become translationally active. Consequently, if the PET is not properly controlled during cold, it will impair ribosome biogenesis [11] and lead to impaired translation of CBF protein factors required for successful acclimation [63]. Hence, if altered PET is one of the structural requirements for cold-specialized ribosomes, then REIL proteins would be the active enhancers of the observed functional effects that cold-remodelled ribosomes ultimately cause. Regarding the physiological effects of cold-remodelled ribosomes, as outlined in Chapter 7, we can currently conclude that there is an accumulation and preferential synthesis of the CCT complex as well as several heat shock proteins during cold, suggesting protein aggregation, which is the major signature of a defective PET. Thus, this aspect highlights the physiological importance of PET, its assembly, and function during cold acclimation in plants. Future research is needed to uncover the involvement of REIL in this process and understand the physiological role of an altered PET during cold acclimation in plants. For example, understanding the impact that the absence of REIL has on ribosome composition, its

origin, and the functionality of proteome shifts. We are currently creating a dataset of relative abundances and fractional synthesis rates of ribosome-bound proteins in acclimated *reil-dkos* to elucidate this. In addition, we will calculate proteome-wide fractional synthesis rates in *reil-dkos* to determine the extent to which the observed translational control (Chapter 8) is caused by REIL-matured ribosomes.

9.7.3 Polysomes: On the Accumulation of Translating Ribosomes and Their Control of Translation

One week after the first cold stimulus, *Arabidopsis* wild-type plants accumulate actively translating polysomes compared with plants grown at optimal or suboptimal high temperatures (Chapter 8). Polysomes are multiple 80S ribosomal complexes involved in the translation of a single mRNA and are held in a specific conformational state by the addition of cycloheximide to the extraction buffers. Therefore, polysomes typically exhibit various oligomeric states, ranging from short disomes consisting of two 80S elongation-competent ribosomes to many 80S elongating ribosomes in the same mRNA chain. The accumulation of polysomes suggests that more protein biosynthesis occurs during the cold period than at optimal temperature, thereby implying that ribosomes formed during the cold period are efficiently equipped to cope with low temperatures. In addition to polysome accumulation, cold ribosomes are exceptionally good at controlling translation. We monitored translational control using Ribo-Seq, a technology that allows us to determine the translational efficiency of any transcript based on its baseline RNA-Seq quantity [29]. Using Ribo-Seq, we report that cold ribosomes are indeed selective and that this selectivity is impaired in cold-acclimated ribosomes of *reil-dkos* (Chapter 8). The main differential effect is directly related to a lower translation of transcripts encoding proteins from mitochondria and chloroplasts, suggesting that the mutants are deficient in energy production and that this may be one of the reasons why they cannot resume growth during cold. Finally, using ^{15}N labelling in our barley model, we found that cold remodelled ribosomes produce a functional proteome shift because they are able to incorporate labelled amino acids into the active protein pools. The ribozyme-mediated proteome shift suggests that 60S subunits may be able to select which 48S initiation complex to bind in order to selectively translate a cold proteome. Further experiments are needed to demonstrate conclusively what part of the proteome shift

may be caused by this apparent mechanism of selectivity and what part is indirectly controlled by transcript recruiting mechanisms.

9.8 Conclusions, Working Model and Outlook

In this thesis, we succeeded in finding optimal physiological conditions to study ribosome heterogeneity during cold acclimation in plants. For this purpose, we used root systems of acclimated plants to enrich our ribosome preparations with cytosolic ribosomes. At the same time, we analyzed protein synthesis on barley root meristems as a means of enriching translational dynamics during cold acclimation. Using these systems, we found that plant ribosomes are heterogeneous during cold and this heterogeneity relates to ribosome-bound proteins and arises in a controlled region-specific manner. More specifically, during ribosome biogenesis in cold, there is a restructuring of the proteome surrounding the PET, which appears to be depleted by the cold ribosome population. At the same time, a factor thought to control tunnel integrity is necessary for acclimation, namely the REIL factor, and thus the depletion of the rProteome could indicate increased fragility or even defective PET structure during cold. Second, an assembled elongation-competent 80S monosome establishes contact points between proteins of its 60S and 40S subunits, these protein binding sites between ribosomal subunits are apparently remodeled during cold in plants, which aligns with potential translational control at the level of translation initiation. Thus, we hypothesize that regional remodelling may be a mechanism of ribosome specialization used by plants during cold acclimation. With this idea in mind, we tested different metazoan models of rProtein-dependent ribosome specialization and discovered that ribosome specialization, as has been defined for yeast, may occur as regional restructuring of ribosomes rather than modulation of individual, unrelated proteins. Consequently, when we check the dynamics of protein synthesis in our barley and Arabidopsis systems during cold, results suggest that ribozyme-catalyzed protein synthesis is selective during cold and the translational output reaches active protein pools, supporting the notion of ribosome specialization in cold. An exemplary result of consistent and functional selective translation is the protein components of the small subunit processome, which are under ribosome biogenesis-dependent translational control in cold-acclimated Arabidopsis and preferentially translated in proliferative barley

root tissue during cold. The full model summarizing the sequence of translational events during cold acclimation in plants is shown in Figure 9.1.

Future work should aim to uncover fully functional mechanisms that modulate protein translation during cold acclimation. First, it is of particular importance to determine what fraction of the translational control that occurs during cold is mediated directly or indirectly by a reprogrammed ribosome structure. For example, cold triggers transcription factor-mediated regulation of many genes via known regulons, and thus a search for cis-regulatory elements in the non-coding genomic regions from those genes under translational control will be important to understand what part of the control derives directly from transcriptional regulation. Similarly, since alternative splicing appears to be a transcript-recruiting force for cold translation, one could use a tagged-PYM construct [12] (Chapter 4) to find the subset of transcripts that are likely to be translated via this shuttle, and in this way find out which part of the translational control is directly related to altered ribosomal structures. Second, the T-DNA insertion lines generated should be used to elucidate the origin of the PET rearrangements and possibly answer why REIL proteins are only required during cold. In addition, next steps could include tagging of recombinant uL30 proteins and complementation of the mutant lines to perform pull-down assays, purify cold polysomes, describe their composition, and sequence the footprints associated with them. In this way, altered ribosomal compositions could be associated with biased translation. Third, ^{15}N labeling combined with polysome profiling of *reil-dkos* can create maps of ribosome synthesis and composition in the cold that are dependent on REIL, clarifying whether REIL-matured ribosomes are the specialized complexes that enhance acclimation. Only then can the altered ribosome biogenesis-dependent rProtein compositions be linked to biases in the transition from transcript to active protein pools. Finally, rProtein network analyses should be extended to describe the spatial dynamics of rProtein synthesis in the context of their modular assembly during ribosome biogenesis. In terms of future prospects, given the diversity of technologies developed, this project provides a methodological framework for detecting ribosome specialization during cold acclimation in plants.

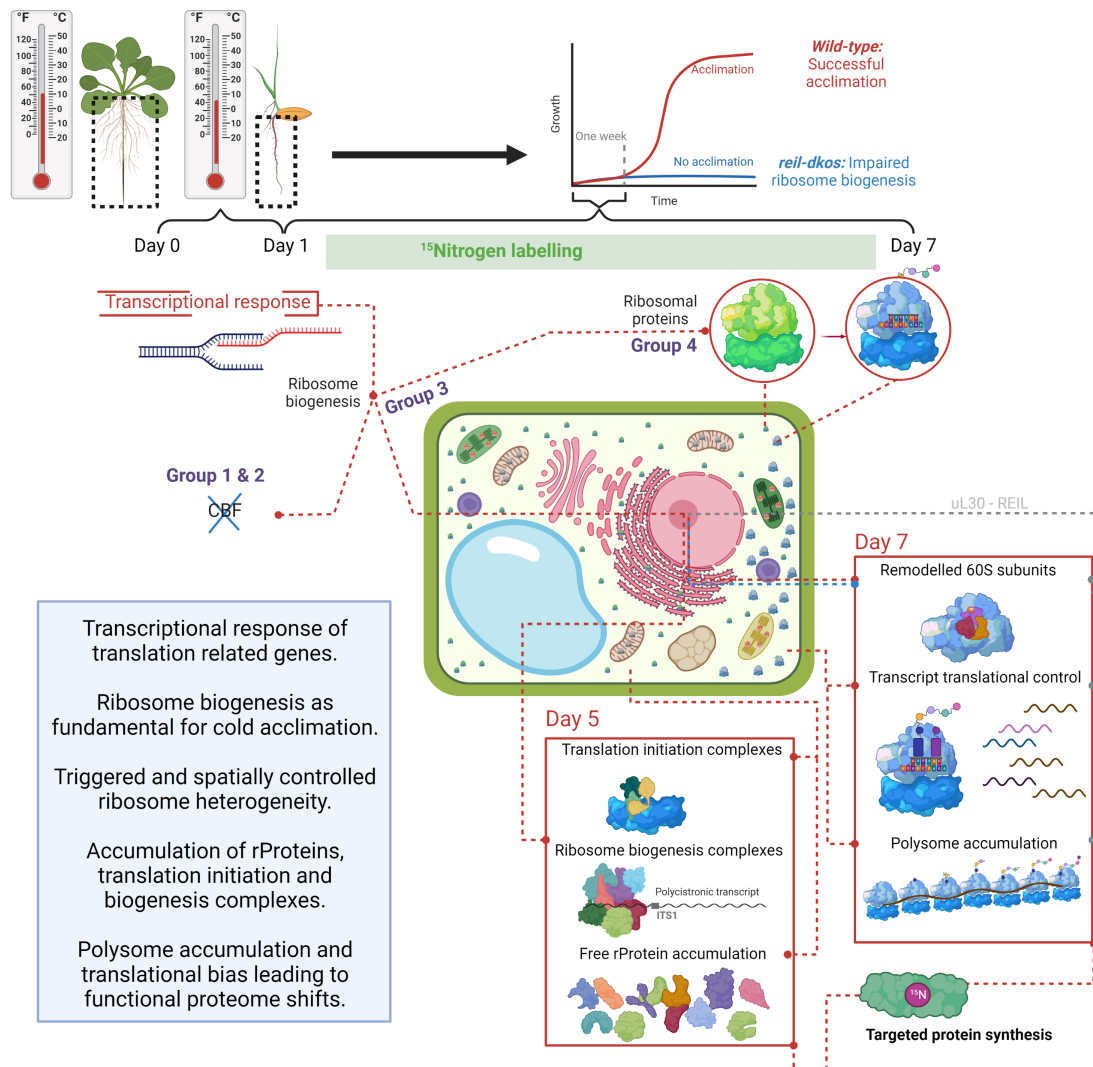


FIGURE 9.1: Proposal for a mechanistic model of the translational processes triggered when plants perceive cold, enabling them to adapt successfully to low suboptimal temperatures. The model summarises the main findings obtained in this thesis. First, ribosome biogenesis factors and ribosomal proteins form groups 3 and 4 of the transcriptional cold responses, which peak in differential expression after one day and one week of cold acclimation, respectively. Second, ribosome biogenesis is fundamental to successful acclimation. Third, plants trigger ribosome heterogeneity in a controlled manner, leading to spatial changes around the polypeptide exit tunnel in the large 60S subunits, alternative processing of the small 40S subunits and potential altered inter-subunit binding. Fourth, the assembly of heterogeneous ribosome complexes occurs in part during ribosome biogenesis using existing and newly synthesised protein components; this last point opens the possibility of on-the-run ribosome remodelling. Fifth, during the acclimation phase, there is a simultaneous accumulation of ribosome biogenesis and translation initiation complexes, as well as an accumulation of free ribosomal proteins in the cell, which indicate that competent ribosomes are built during acclimation and suggest 60S-mediated 48S complex selection. Finally, at the end of the acclimation period, actively translating and heterogeneous polysomes accumulate, translating subsets of transcripts and causing an effective proteome shift that leads to wild-type plants resuming growth after one week of cold. Conversely, the disruption of ribosome biogenesis leads to plants that cannot acclimate. Red dotted lines represent the part of the model that are sufficiently justified by the evidence found and the grey dotted lines represent parts of the model that require future research. The figure was created with [BioRender](#) and exported under a paid subscription.

Bibliography

- [1] Jean Paul Armache, Andreas M. Anger, Viter Márquez, Sibylle Franckenberg, Thomas Fröhlich, Elizabeth Villa, Otto Berninghausen, Michael Thomm, Georg J. Arnold, Roland Beckmann, and Daniel N. Wilson. Promiscuous behaviour of archaeal ribosomal proteins: Implications for eukaryotic ribosome evolution. *Nucleic Acids Research*, 41:1284–1293, 2013. ISSN 03051048. doi: 10.1093/nar/gks1259.
- [2] Mohammad A. Ashraf and Abidur Rahman. Cold stress response in arabidopsis thaliana is mediated by gnom arf-gef. *Plant Journal*, 97:500–516, 2019. ISSN 1365313X. doi: 10.1111/tpj.14137.
- [3] Jonas Barandun, Malik Chaker-Margot, Mirjam Hunziker, Kelly R. Molloy, Brian T. Chait, and Sebastian Klinge. The complete structure of the small-subunit processome. *Nature Structural and Molecular Biology*, 24:944–953, 2017. ISSN 15459985. doi: 10.1038/nsmb.3472.
- [4] Maria Barna, Katrin Karbstein, David Tollervey, Davide Ruggero, Gloria Brar, Eric Lieberman Greer, and Jonathan D. Dinman. The promises and pitfalls of specialized ribosomes. *Molecular Cell - Voices*, 82, 2022.
- [5] Jessica C. Bowman, Anton S. Petrov, Moran Frenkel-Pinter, Petar I. Penev, and Loren Dean Williams. Root of the tree: The significance, evolution, and origins of the ribosome. *Chemical Reviews*, 120:4848–4878, 2020. ISSN 15206890. doi: 10.1021/acs.chemrev.9b00742.
- [6] Ingo Braasch, Julien Bobe, Yann Guiguen, and John H. Postlethwait. Reply to: 'subfunctionalization versus neofunctionalization after whole-genome duplication'. *Nature Genetics*, 50:910–911, 2018. ISSN 15461718. doi: 10.1038/s41588-018-0163-3.
- [7] Anna Brandi, Lolita Piersimoni, Naser Aliye Feto, Roberto Spurio, Jean Hervé Alix, Frank Schmidt, and Claudio O. Gualerzi. Translation initiation factor if2 contributes to ribosome assembly and maturation during cold adaptation. *Nucleic Acids Research*, 47:4652–4662, 2019. ISSN 13624962. doi: 10.1093/nar/gkz188.
- [8] Joseph W. Briggs and Jonathan D. Dinman. Subtractional heterogeneity: A crucial step toward defining specialized ribosomes. *Molecular Cell*, 67:3–4, 2017. ISSN 10974164. doi: 10.1016/j.molcel.2017.06.022.

- [9] Cristiane P.G. Calixto, Wenbin Guo, Allan B. James, Nikoleta A. Tzioutziou, Juan Carlos Entizne, Paige E. Panter, Heather Knight, Hugh G. Nimmo, Runxuan Zhang, and John W.S. Brown. Rapid and dynamic alternative splicing impacts the arabidopsis cold response transcriptome. *Plant Cell*, 30:1424–1444, 2018. ISSN 1532298X. doi: 10.1105/tpc.18.00177.
- [10] Sandrine Caron, Martine Charon, Elisabeth Cramer, Nahum Sonenberg, and Isabelle Dusanter-Fourt. Selective modification of eukaryotic initiation factor 4f (eif4f) at the onset of cell differentiation: Recruitment of eif4gii and long-lasting phosphorylation of eif4e. *Molecular and Cellular Biology*, 24:4920–4928, 2004. ISSN 0270-7306. doi: 10.1128/mcb.24.11.4920-4928.2004.
- [11] Bo Eng Cheong, Olga Beine-Golovchuk, Michal Gorka, William Wing Ho Ho, Federico Martinez-Seidel, Alexandre Augusto Pereira Firmino, Aleksandra Skiryecz, Ute Roessner, and Joachim Kopka. Arabidopsis rei-like proteins activate ribosome biogenesis during cold acclimation. *Scientific Reports*, 11:1–25, 2021. ISSN 20452322. doi: 10.1038/s41598-021-81610-z.
- [12] Michael D. Diem, Chia C. Chan, Ihab Younis, and Gideon Dreyfuss. Pym binds the cytoplasmic exon-junction complex and ribosomes to enhance translation of spliced mrnas. *Nature Structural and Molecular Biology*, pages 1173–1179, 2007. ISSN 15459993. doi: 10.1038/nsmb1321.
- [13] Claudia M. Fusco, Kristina Desch, Aline R. Dörrbaum, Mantian Wang, Anja Staab, Ivy C.W. Chan, Eleanor Vail, Veronica Villeri, Julian D. Langer, and Erin M. Schuman. Neuronal ribosomes exhibit dynamic and context-dependent exchange of ribosomal proteins. *Nature Communications*, 12:1–14, 2021. ISSN 20411723. doi: 10.1038/s41467-021-26365-x.
- [14] Olivier Gadal, Daniela Strauss, Elisabeth Petfalski, Pierre Emmanuel Gleizes, Nicole Gas, David Tollervey, and Ed Hurt. Rlp7p is associated with 60s preribosomes, restricted to the granular component of the nucleolus, and required for pre-rrna processing. *Journal of Cell Biology*, 157:941–951, 2002. ISSN 00219525. doi: 10.1083/jcb.200111039.
- [15] Antoni Garcia-Molina, Tatjana Kleine, Kevin Schneider, Timo Mühlhaus, Martin Lehmann, and Dario Leister. Translational components contribute to acclimation

- responses to high light, heat, and cold in arabidopsis. *iScience*, 23:101331, 2020. ISSN 25890042. doi: 10.1016/j.isci.2020.101331.
- [16] Lisa Gasse, Dirk Flemming, and Ed Hurt. Coordinated ribosomal its2 rna processing by the las1 complex integrating endonuclease, polynucleotide kinase, and exonuclease activities. *Molecular Cell*, 60:808–815, 2015. ISSN 10974164. doi: 10.1016/j.molcel.2015.10.021.
- [17] David M. Gay, Anders H. Lund, and Martin D. Jansson. Translational control through ribosome heterogeneity and functional specialization. *Trends in Biochemical Sciences*, 47:66–81, 2022. ISSN 13624326. doi: 10.1016/j.tibs.2021.07.001.
- [18] Naomi R. Genuth and Maria Barna. The discovery of ribosome heterogeneity and its implications for gene regulation and organismal life. *Molecular Cell*, 71:364–374, 2018. ISSN 10974164. doi: 10.1016/j.molcel.2018.07.018.
- [19] Jeffrey E. Gerst. Pimp my ribosome: Ribosomal protein paralogs specify translational control. *Trends in Genetics*, 34:832–845, 2018. ISSN 13624555. doi: 10.1016/j.tig.2018.08.004.
- [20] Anna Maria Giuliodori, Anna Brandi, Claudio O. Gualerzi, and Cynthia L. Pon. Preferential translation of cold-shock mrnas during cold adaptation. *Rna*, 10:265–276, 2004. ISSN 13558382. doi: 10.1261/rna.5164904.
- [21] Olga Beine Golovchuk, Alexandre Augusto Pereira Firmino, Adrianna Dabrowska, Stefanie Schmidt, Alexander Erban, Dirk Walther, Ellen Zuther, Dirk K. Hinch, and Joachim Kopka. Plant temperature acclimation and growth rely on cytosolic ribosome biogenesis factor homologs. *Plant Physiology*, 176:2251–2276, 2018. ISSN 15322548. doi: 10.1104/pp.17.01448.
- [22] Basil J. Greber. Mechanistic insight into eukaryotic 60s ribosomal subunit biogenesis by cryo-electron microscopy. *Rna*, 22:1643–1662, 2016. ISSN 14699001. doi: 10.1261/rna.057927.116.
- [23] Basil J. Greber, Daniel Boehringer, Christian Montellese, and Nenad Ban. Cryo-em structures of arx1 and maturation factors rei1 and jjj1 bound to the 60s ribosomal subunit. *Nature Structural and Molecular Biology*, 19:1228–1233, 2012. ISSN 15459993. doi: 10.1038/nsmb.2425.

- [24] F. Hadi and M. P. Fuller. Effect of the cold acclimation on proline and protein contents in cauliflower clones. *Proceedings of the Nutrition Society*, 69, 2010. ISSN 0029-6651. doi: 10.1017/s0029665110001412.
- [25] Matthew A. Hannah, Arnd G. Heyer, and Dirk K. Hinch. A global survey of gene regulation during cold acclimation in *arabidopsis thaliana*. *PLoS Genetics*, 1: 0179–0196, 2005. ISSN 15537390. doi: 10.1371/journal.pgen.0010026.
- [26] Peiqi Hao, Jiaojiao Yu, Richard Ward, Yin Liu, Qiao Hao, Su An, and Tianrui Xu. Eukaryotic translation initiation factors as promising targets in cancer therapy. *Cell Communication and Signaling*, 18:1–20, 2020. ISSN 1478811X. doi: 10.1186/s12964-020-00607-9.
- [27] Dirk K. Hinch and Ellen Zuther. Introduction: Plant cold acclimation and winter survival, 2020. ISSN 19406029.
- [28] Tayah Hopes, Karl Norris, Michaela Agapiou, Charley G.P. McCarthy, Philip A. Lewis, Mary J. O’Connell, Juan Fontana, and Julie L. Aspden. Ribosome heterogeneity in *drosophila melanogaster* gonads through paralog-switching. *Nucleic Acids Research*, 50:2240–2257, 2022. ISSN 13624962. doi: 10.1093/nar/gkab606.
- [29] Nicholas T. Ingolia, Gloria A. Brar, Silvia Rouskin, Anna M. McGeachy, and Jonathan S. Weissman. The ribosome profiling strategy for monitoring translation in vivo by deep sequencing of ribosome-protected mrna fragments. *Nature Protocols*, 7:1534–1550, 2012. ISSN 17542189. doi: 10.1038/nprot.2012.086.
- [30] Jelena Jakovljevic, Uli Ohmayer, Michael Gamalinda, Jason Talkish, Lisa Alexander, Jan Linnemann, Philipp Milkereit, and John L. Woolford. Ribosomal proteins 17 and 18 function in concert with six a3 assembly factors to propagate assembly of domains i and ii of 25s rna in yeast 60s ribosomal subunits. *Rna*, 18:1805–1822, 2012. ISSN 13558382. doi: 10.1261/rna.032540.112.
- [31] Joachim Kilian, Dion Whitehead, Jakub Horak, Dierk Wanke, Stefan Weinl, Oliver Batistic, Cecilia D’Angelo, Erich Bornberg-Bauer, Jörg Kudla, and Klaus Harter. The atgenexpress global stress expression data set: Protocols, evaluation and model data analysis of uv-b light, drought and cold stress responses. *Plant Journal*, 50: 347–363, 2007. ISSN 09607412. doi: 10.1111/j.1365-313X.2007.03052.x.

- [32] Byeong Ha Lee, David A. Henderson, and Jian Kang Zhu. The arabidopsis cold-responsive transcriptome and its regulation by ice1. *Plant Cell*, 17:3155–3175, 2005. ISSN 10404651. doi: 10.1105/tpc.105.035568.
- [33] Jacob Levitt. *Responses of Plants to Environmental Stresses Vol. 1: Chilling, freezing, and high temperature stresses*, volume 1. Academic Press, 1980.
- [34] Catherine M. Mageeney and Vassie C. Ware. Specialized erpl22 paralogue-specific ribosomes regulate specific mrna translation in spermatogenesis in drosophila melanogaster. *Molecular Biology of the Cell*, 30:2240–2253, 2019. ISSN 19394586. doi: 10.1091/mbc.E19-02-0086.
- [35] Federico Martinez-Seidel, Olga Beine-Golovchuk, Yin Chen Hsieh, and Joachim Kopka. Systematic review of plant ribosome heterogeneity and specialization. *Frontiers in Plant Science*, 11:948, 2020. ISSN 1664462X. doi: 10.3389/fpls.2020.00948.
- [36] Federico Martinez-Seidel, Yin Chen Hsieh, Dirk Walther, Joachim Kopka, and Alexandre Augusto Pereira Firmino. Cosnet i : Complexome-structural network interpreter used to study spatial enrichment in metazoan ribosomes. *BMC Bioinformatics*, 22:605, 2021. ISSN 14712105. doi: 10.1186/s12859-021-04510-z.
- [37] Federico Martinez-Seidel, Pipob Suwanhaikasem, Shuai Nie, Michael G. Leeming, Alexandre Augusto Pereira Firmino, Nicholas A. Williamson, Joachim Kopka, Ute Roessner, and Berin A. Boughton. Membrane-enriched proteomics link ribosome accumulation and proteome reprogramming with cold acclimation in barley root meristems. *Frontiers in Plant Science*, 12:656683, 2021. ISSN 1664462X. doi: 10.3389/fpls.2021.656683.
- [38] Federico Martinez-Seidel, Olga Beine-golovchuk, Yin Chen Hsieh, Kheloud El Eshrakly, Michal Gorka, Bo Eng Cheong, Erika V. Jimenez-posada, Dirk Walther, Aleksandra Skirycz, Ute Roessner, Joachim Kopka, and Alexandre Augusto Pereira Firmino. Spatially enriched paralog rearrangements argue functionally diverse ribosomes arise during cold acclimation in arabidopsis. *International Journal of Molecular Sciences*, 22:6160, 2021. ISSN 14220067. doi: 10.3390/ijms22116160.
- [39] Alison E. Meyer, Lindsey A. Hoover, and Elizabeth A. Craig. The cytosolic j-protein, jjj1, and reil function in the removal of the pre-60 s subunit factor arx1.

- Journal of Biological Chemistry*, 285:961–968, 2010. ISSN 00219258. doi: 10.1074/jbc.M109.038349.
- [40] Adam J Middleton, Barbara Vanderbeld, Melissa Bredow, Heather Tomalty, Peter L Davies, and Virginia K Walker. Plant cold acclimation, 2014.
- [41] Sandra Missbach, Benjamin L. Weis, Roman Martin, Stefan Simm, Markus T. Bohnsack, and Enrico Schleiff. 40s ribosome biogenesis co-factors are essential for gametophyte and embryo development. *PLoS ONE*, 8:e54084, 2013. ISSN 19326203. doi: 10.1371/journal.pone.0054084.
- [42] Shyam S. Mohapatra, Ronald J. Poole, and Rajinder S. Dhindsa. Cold acclimation, freezing resistance and protein synthesis in alfalfa (*medicago satival. cv. saranac*). *Journal of Experimental Botany*, 38:1697–1703, 1987. ISSN 00220957. doi: 10.1093/jxb/38.10.1697.
- [43] Edward B. Mougey, Marina O’Reilly, Yvonne Osheim, Oscar L. Miller, Ann Beyer, and Barbara Sollner-Webb. The terminal balls characteristic of eukaryotic rna transcription units in chromatin spreads are rna processing complexes. *Genes and Development*, 7:1609–1619, 1993. ISSN 08909369. doi: 10.1101/gad.7.8.1609.
- [44] Yvonne N. Osheim, Sarah L. French, Kristin M. Keck, Erica A. Champion, Krasimir Spasov, François Dragon, Susan J. Baserga, and Ann L. Beyer. Pre-18s ribosomal rna is structurally compacted into the ssu processome prior to being cleaved from nascent transcripts in *saccharomyces cerevisiae*. *Molecular Cell*, 16:943–954, 2004. ISSN 10972765. doi: 10.1016/j.molcel.2004.11.031.
- [45] Denise Palm, Stefan Simm, Katrin Darm, Benjamin L. Weis, Maike Ruprecht, Enrico Schleiff, and Christian Scharf. Proteome distribution between nucleoplasm and nucleolus and its relation to ribosome biogenesis in *arabidopsis thaliana*. *RNA Biology*, pages 441–454, 2016. ISSN 15558584. doi: 10.1080/15476286.2016.1154252.
- [46] Denise Palm, Deniz Streit, Thiruvenkadam Shanmugam, Benjamin L. Weis, Maike Ruprecht, Stefan Simm, and Enrico Schleiff. Plant-specific ribosome biogenesis factors in *arabidopsis thaliana* with essential function in rna processing. *Nucleic Acids Research*, 47:1880–1895, 2019. ISSN 13624962. doi: 10.1093/nar/gky1261.

- [47] Hail Z. Rihan, Mohammed Al-Issawi, and Michael P. Fuller. Advances in physiological and molecular aspects of plant cold tolerance. *Journal of Plant Interactions*, 12:143–157, 2017. ISSN 17429153. doi: 10.1080/17429145.2017.1308568.
- [48] Stefanie Schmidt, Frederik Dethloff, Olga Beine-Golovchuk, and Joachim Kopka. The reil1 and reil2 proteins of arabidopsis thaliana are required for leaf growth in the cold. *Plant Physiology*, 163:1623–1639, 2013. ISSN 00320889. doi: 10.1104/pp.113.223925.
- [49] Stefanie Schmidt, Frederik Dethloff, Olga Beine-Golovchuk, and Joachim Kopka. Reil proteins of arabidopsis thaliana interact in yeast-2-hybrid assays with homologs of the yeast rlp24, rpl24a, rlp24b, arx1, and jjj1 proteins. *Plant Signaling and Behavior*, 9:e28224, 2014. ISSN 15592324. doi: 10.4161/psb.28224.
- [50] Nadav Segev and Jeffrey E. Gerst. Specialized ribosomes and specific ribosomal protein paralogs control translation of mitochondrial proteins. *Journal of Cell Biology*, 217:117–126, 2018. ISSN 15408140. doi: 10.1083/jcb.201706059.
- [51] Motoaki Seki, Mari Narusaka, Junko Ishida, Tokihiko Nanjo, Miki Fujita, Youko Oono, Asako Kamiya, Maiko Nakajima, Akiko Enju, Tetsuya Sakurai, Masakazu Satou, Kenji Akiyama, Teruaki Taji, Kazuko Yamaguchi-Shinozaki, Piero Carninci, Jun Kawai, Yoshihide Hayashizaki, and Kazuo Shinozaki. Monitoring the expression profiles of 7000 arabidopsis genes under drought, cold and high-salinity stresses using a full-length cdna microarray. *Plant Journal*, 31:279–292, 2002. ISSN 09607412. doi: 10.1046/j.1365-313X.2002.01359.x.
- [52] Zhen Shi, Kotaro Fujii, Kyle M. Kovary, Naomi R. Genuth, Hannes L. Röst, Mary N. Teruel, and Maria Barna. Heterogeneous ribosomes preferentially translate distinct subpools of mrnas genome-wide. *Molecular Cell*, 67:71–83, 2017. ISSN 10974164. doi: 10.1016/j.molcel.2017.05.021.
- [53] Nikolai Slavov, Stefan Semrau, Edoardo Airoldi, Bogdan Budnik, and Alexander van Oudenaarden. Differential stoichiometry among core ribosomal proteins. *Cell Reports*, 13:865–873, 2015. ISSN 22111247. doi: 10.1016/j.celrep.2015.09.056.
- [54] Ming Sun, Bingxin Shen, Wen Li, Parimal Samir, Christopher M. Browne, Andrew J. Link, and Joachim Frank. A time-resolved cryo-em study of saccharomyces cerevisiae 80s ribosome protein composition in response to a change in

- carbon source. *Proteomics*, 21:2000125, 2021. ISSN 16159861. doi: 10.1002/pmic.202000125.
- [55] Michael F. Thomashow. Plant cold acclimation: Freezing tolerance genes and regulatory mechanisms. *Annual Review of Plant Biology*, pages 571–599, 1999. ISSN 15435008. doi: 10.1146/annurev.arplant.50.1.571.
- [56] Jonathan T. Vogel, Daniel G. Zarka, Heather A. Van Buskirk, Sarah G. Fowler, and Michael F. Thomashow. Roles of the *cbf2* and *zat12* transcription factors in configuring the low temperature transcriptome of arabidopsis. *Plant Journal*, 41: 195–211, 2005. ISSN 09607412. doi: 10.1111/j.1365-313X.2004.02288.x.
- [57] Nora Vázquez-Laslop and Alexander S. Mankin. Picky nascent peptides do not talk to foreign ribosomes. *Proceedings of the National Academy of Sciences*, pages 5931–5932, 2011. ISSN 00278424. doi: 10.1073/pnas.1103011108.
- [58] Nora Vázquez-Laslop and Alexander S. Mankin. How macrolide antibiotics work. *Trends in Biochemical Sciences*, pages 668–684, 2018. ISSN 13624326. doi: 10.1016/j.tibs.2018.06.011.
- [59] Susan Wagner, Anna Herrmannová, Vladislava Hronová, Stanislava Gunišová, Nee-lam D. Sen, Ross D. Hannan, Alan G. Hinnebusch, Nikolay E. Shirokikh, Thomas Preiss, and Leoš Shivaya Valášek. Selective translation complex profiling reveals staged initiation and co-translational assembly of initiation factor complexes. *Molecular Cell*, 79:546–560, 2020. ISSN 10974164. doi: 10.1016/j.molcel.2020.06.004.
- [60] Benjamin L. Weis, Jelena Kovacevic, Sandra Missbach, and Enrico Schleiff. Plant-specific features of ribosome biogenesis. *Trends in Plant Science*, 20:729–740, 2015. ISSN 13601385. doi: 10.1016/j.tplants.2015.07.003.
- [61] Daniel N. Wilson, Stefan Arenz, and Roland Beckmann. Translation regulation via nascent polypeptide-mediated ribosome stalling. *Current Opinion in Structural Biology*, pages 123–133, 2016. ISSN 1879033X. doi: 10.1016/j.sbi.2016.01.008.
- [62] John L. Woolford and Susan J. Baserga. Ribosome biogenesis in the yeast *saccharomyces cerevisiae*. *Genetics*, 195:643–681, 2013. ISSN 00166731. doi: 10.1534/genetics.113.153197.

-
- [63] Hasi Yu, Xiangfeng Kong, Huan Huang, Wenwu Wu, Junghoon Park, Dae Jin Yun, Byeong ha Lee, Huazhong Shi, and Jian Kang Zhu. Stch4/reil2 confers cold stress tolerance in arabidopsis by promoting rna processing and cbf protein translation. *Cell Reports*, 30:229–242, 2020. ISSN 22111247. doi: 10.1016/j.celrep.2019.12.012.
- [64] Peilin Yu, Shengyi Wang, Chengying Ma, Xian Luo, Zhihao Xing, Xingui Wu, Rosemary K. Clyne, and Gwo-Jiunn Hwang. Affirmation of distinctive ribosomal protein paralogue-specific ribosomes. *SSRN Electronic Journal*, page 3334430, 2019. ISSN 1556-5068. doi: 10.2139/ssrn.3334430.
- [65] Rui Zeng, Erin Smith, and Antoni Barrientos. Yeast mitoribosome large subunit assembly proceeds by hierarchical incorporation of protein clusters and modules on the inner membrane. *Cell Metabolism*, 27:645–656, 2018. ISSN 19327420. doi: 10.1016/j.cmet.2018.01.012.

SciVal Author Metrics

Researcher Overview Report - Martinez-Seidel, Federico 2

Martinez-Seidel, Federico 2017 to >2022

Overall research performance

Entity: Martinez-Seidel, Federico · Year range: 2017 to 2023 · Data source: Scopus, up to 14 Dec 2022

14

Scholarly Output 

71.4% Open Access

1.22

Field-Weighted Citation Impact 

129

Citation Count 

9.2

Citations per Publication  *h*-index

6

4

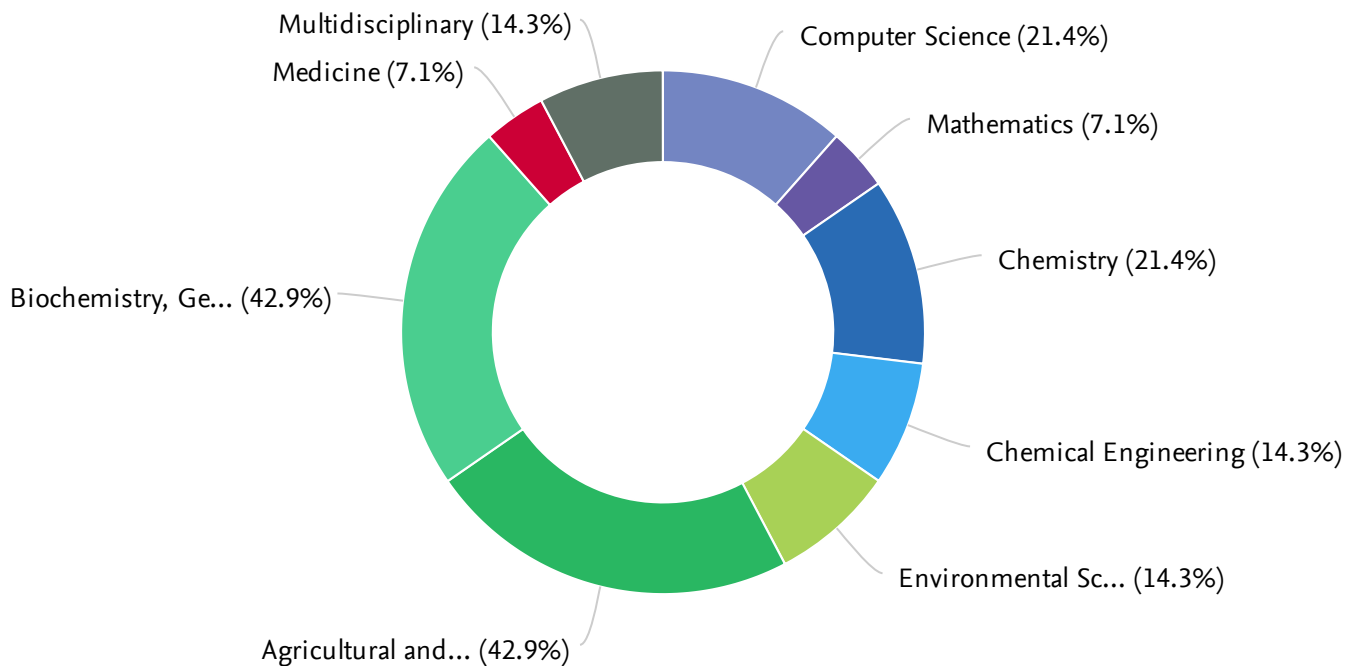
*h*5-index

This analysis provides an overall metrics summary of the researcher. The snowflake means the metrics have been calculated using the Snowball Metrics methodology.

Note: for researchers with a small scholarly output, please beware of highly cited publications which may skew the FWCI.

Publication share by Subject Area

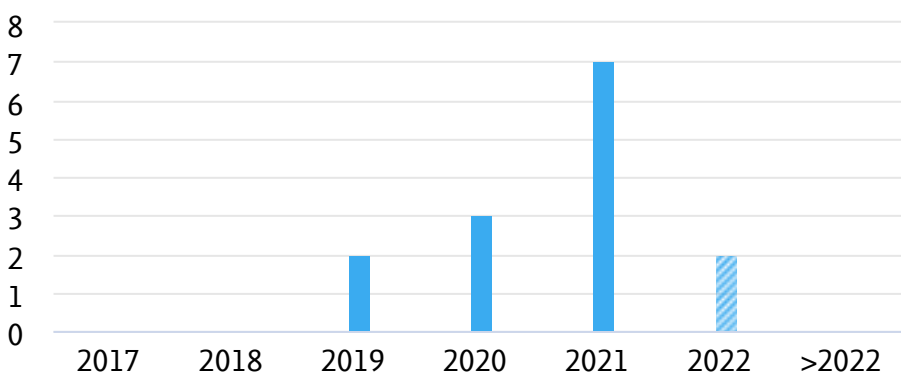
Entity: Martinez-Seidel, Federico · Year range: 2017 to 2023 · Data source: Scopus, up to 14 Dec 2022



This gives an overview of the Subject Areas in which the researcher is publishing and is based upon the high level All Science Journal Classification (ASJC). These Subject Areas are assigned to all articles via the journals in which they are published. Please note, that an article can belong to more than one ASJC.

Scholarly Output

Entity: Martinez-Seidel, Federico · Year range: 2017 to 2023 · Data source: Scopus, up to 14 Dec 2022



14

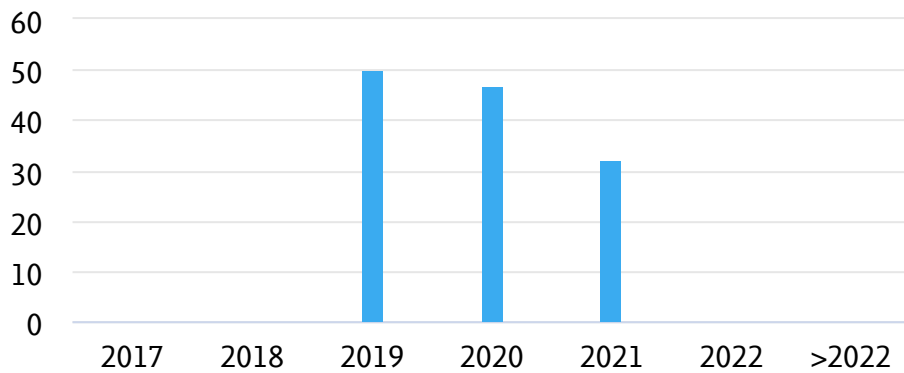
number of publications by authors of Martinez-Seidel, Federico

▨ Incomplete year

Scholarly Output indicates the prolificacy of the researcher: how many publications does the researcher have indexed in Scopus during the time period?

Citation Count

Entity: Martinez-Seidel, Federico · Year range: 2017 to 2023 · Data source: Scopus, up to 14 Dec 2022



129

number of citations received by publications of Martinez-Seidel, Federico

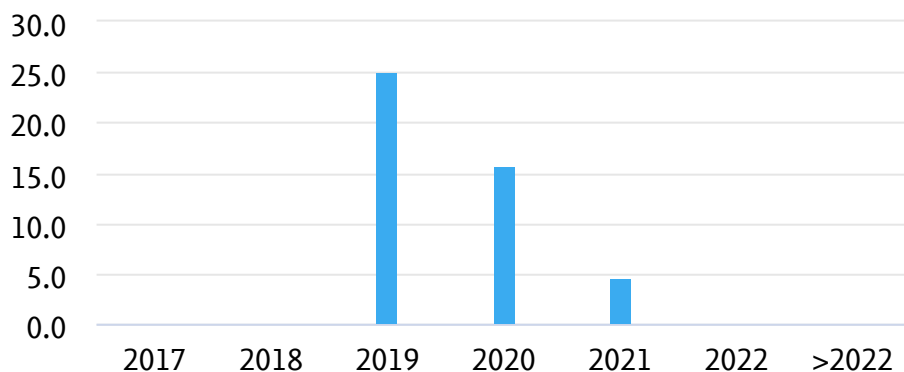
▨ Incomplete year

Citation count indicates the total citation impact of the researcher: how many citations have this researcher's publications received? The years are always the years in which items were published, and do not refer to the years in which citations were received.

Note: some subject areas cite publications more often than others.

Citations per Publication

Entity: Martinez-Seidel, Federico · Year range: 2017 to 2023 · Data source: Scopus, up to 14 Dec 2022



9.2

average number of citations per publication of Martinez-Seidel, Federico

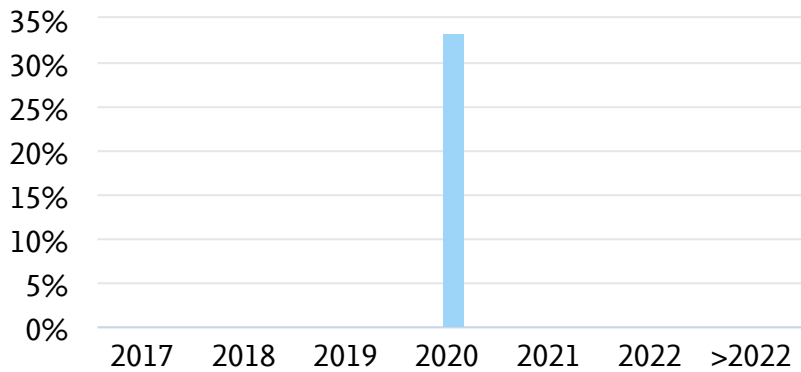
▨ Incomplete year

Citations per Publication indicates the average citation impact of each of a researcher's publications: how many citations have this researcher's publications received on average? The years are always the years in which items were published, and do not refer to the years in which citations were received.

Outputs in Top 10% Citation Percentiles (field-weighted)

Entity: Martinez-Seidel, Federico · Year range: 2017 to 2023 · Data source: Scopus, up to 14 Dec 2022

Share of publications of Martinez-Seidel, Federico that are among the most cited publications worldwide
field-weighted



1 (7.1%)

number of publications in the top 10% most cited publications worldwide

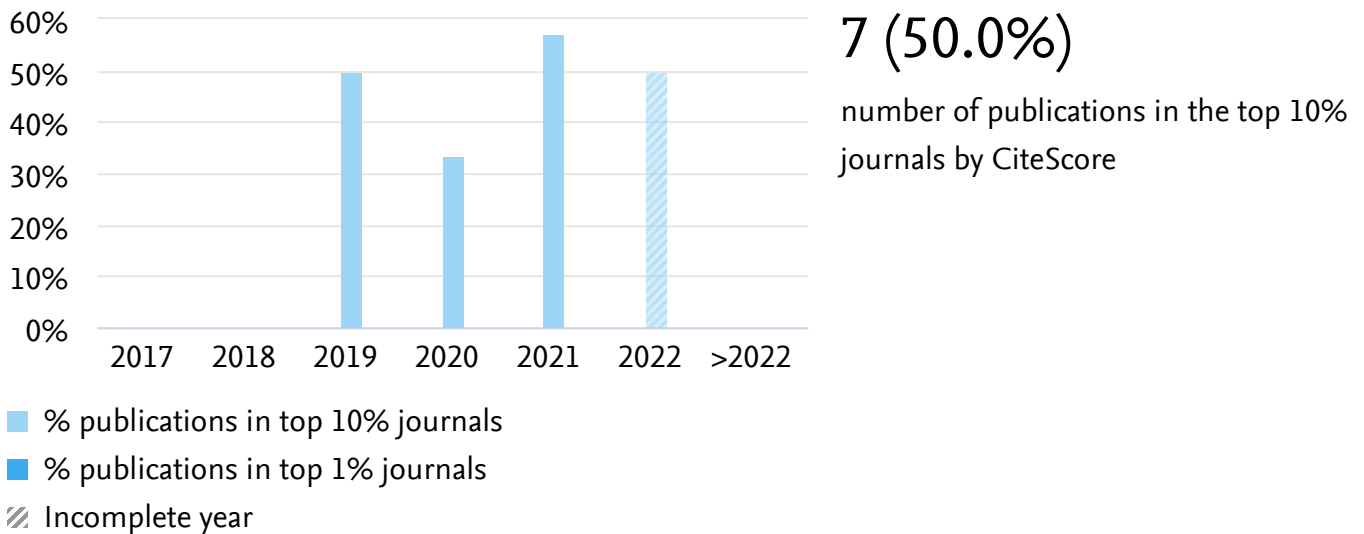
- % publications in top 10% most cited
- % publications in top 1% most cited
- ▨ Incomplete year

Outputs in Top Citation Percentiles indicates the extent to which a researcher's publications are present in the top 10% most-cited percentiles within Scopus. This number is then field-weighted to normalize for differences in subject area citation patterns.

Publications in Top Journal Percentiles by CiteScore Percentile

Entity: Martinez-Seidel, Federico · Year range: 2017 to 2023 · Data source: Scopus, up to 14 Dec 2022

Share of publications of Martinez-Seidel, Federico that are in the top journals by CiteScore Percentile

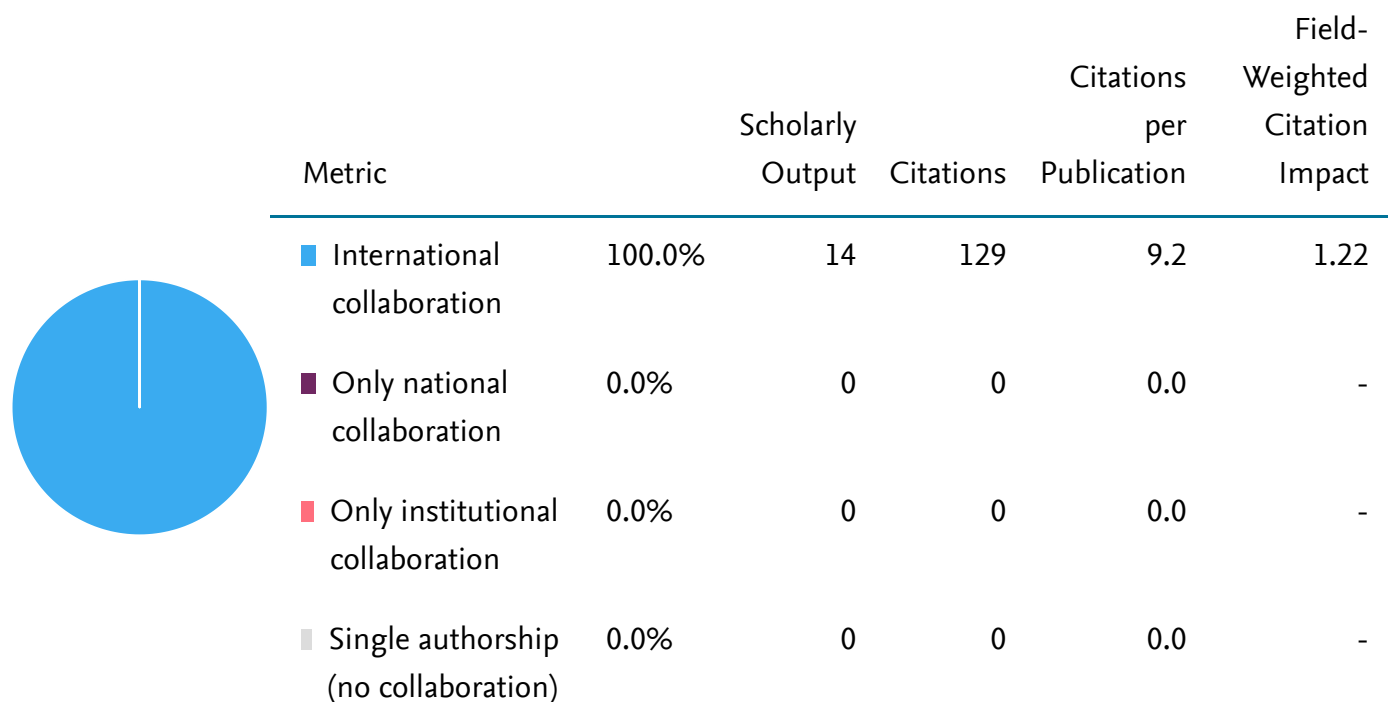


Publications in Top Journal Percentiles indicates the extent to which the researcher's publications are present in the most-cited journals in Scopus by CiteScore percentile. The percentage thresholds are taken directly from the CiteScore Percentile values that are calculated by Scopus. A journal receives a CiteScore Percentile for each ASJC in which it's categorized. SciVal always uses the highest relevant CiteScore Percentile, which is dictated by the subject area filter.

Collaboration

Entity: Martinez-Seidel, Federico · Year range: 2017 to 2023 · Data source: Scopus, up to 14 Dec 2022

Scholarly Output of Martinez-Seidel, Federico, by amount of international, national and institutional collaboration



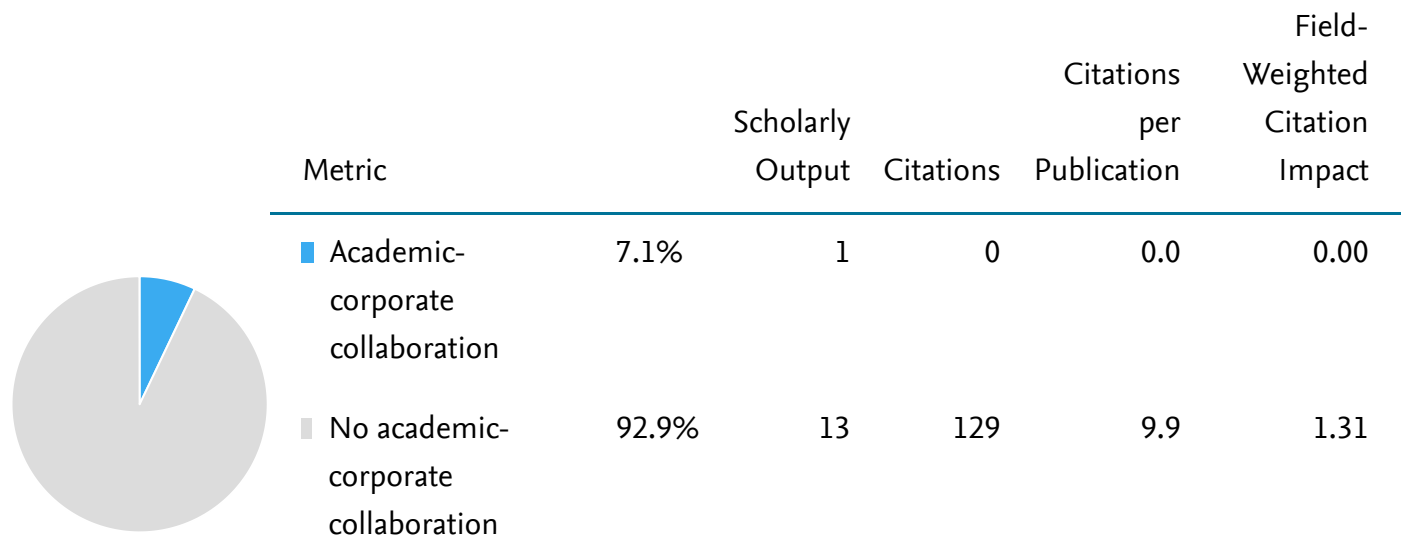
Indicates the extent to which the researcher's publications have international, national, or institutional co-authorship, and single authorship. A publication is assigned a single collaboration type.

Note: for collaboration types with a small scholarly output, please beware of highly cited publications which may skew the FWCI.

Academic-Corporate Collaboration

Entity: Martinez-Seidel, Federico · Year range: 2017 to 2023 · Data source: Scopus, up to 14 Dec 2022

Scholarly Output of Martinez-Seidel, Federico with both academic and corporate author affiliations



Academic-Corporate Collaboration indicates the degree of collaboration between academic and corporate affiliations: to what extent are this researcher's publications co-authored across the academic and corporate, or industrial, sectors?

A publication either exhibits academic-corporate collaboration, or it does not. This assignment is made based on the organization-type with which Scopus tags each affiliation.

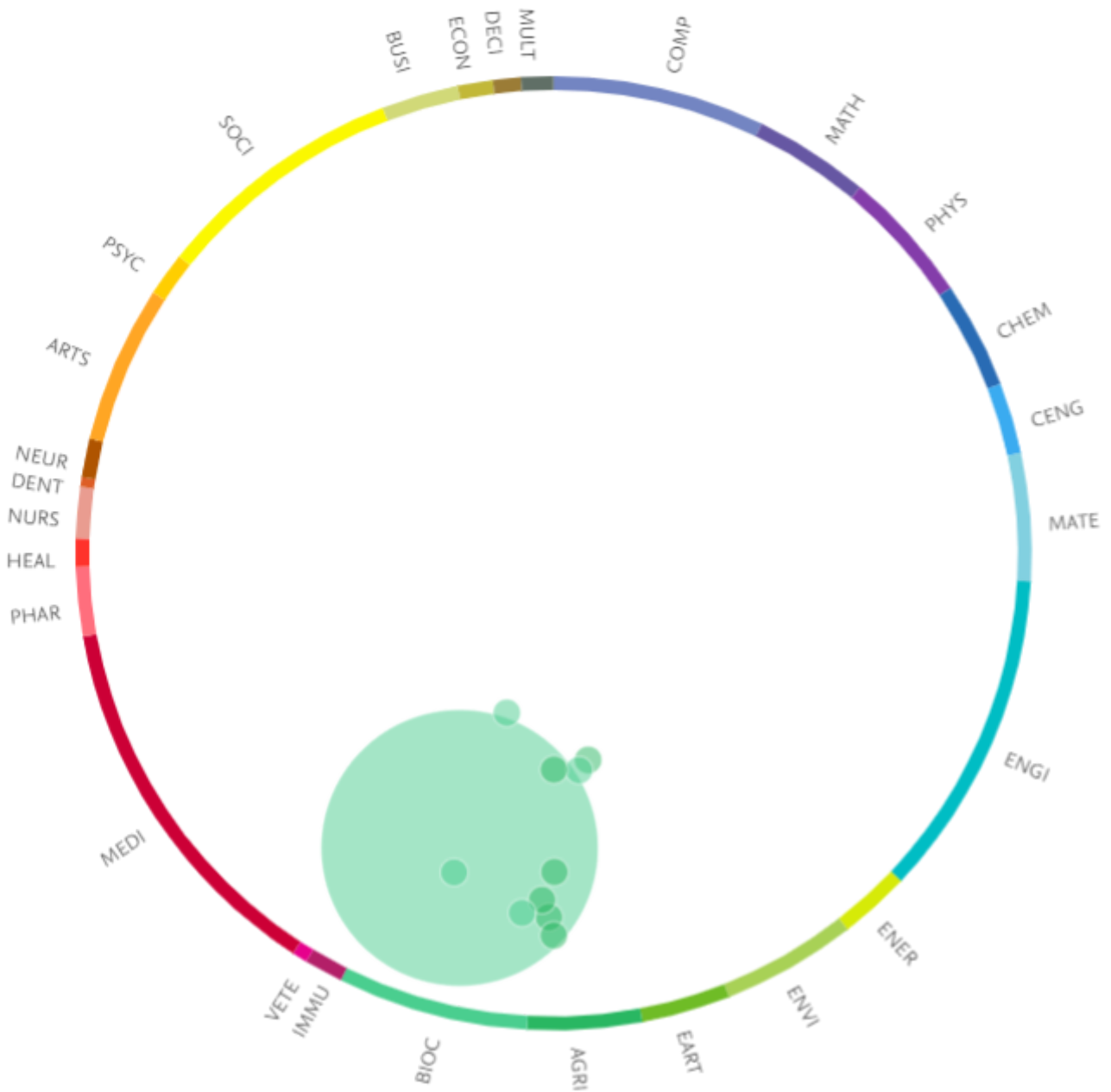
Note: for collaboration types with a small scholarly output, please beware of highly cited publications which may skew the FWCI.

Topics

Entity: Martinez-Seidel, Federico · Year range: 2017 to 2023 · Data source: Scopus, up to 14 Dec 2022

○ ○ ○ Bubble size: Scholarly Output of this Researcher

○ Bubble position is based on dominant ASJC categories.













Topics

COMP	Computer Science	PHAR	Pharmacology, Toxicology and Pharmaceutics
MATH	Mathematics	HEAL	Health Professions
PHYS	Physics and Astronomy	NURS	Nursing
CHEM	Chemistry	DENT	Dentistry
CENG	Chemical Engineering	NEUR	Neuroscience
MATE	Materials Science	ARTS	Arts and Humanities
ENGI	Engineering	PSYC	Psychology
ENER	Energy	SOCI	Social Sciences
ENVI	Environmental Science	BUSI	Business, Management and Accounting
EART	Earth and Planetary Sciences	ECON	Economics, Econometrics and Finance
AGRI	Agricultural and Biological Sciences	DECI	Decision Sciences
BIOC	Biochemistry, Genetics and Molecular Biology	MULT	Multidisciplinary
IMMU	Immunology and Microbiology		
VETE	Veterinary		
MEDI	Medicine		

A Topic is a collection of articles focused on a common intellectual research problem. There are 96,000 Topics in SciVal that are created by analyzing citation links between articles in Scopus - where there is a strong link a Topic is formed. This chart shows the Topics in which the researcher has published. To learn more, search for Topic Prominence in Science in the SciVal Support Hub.

Topics

Entity: Martinez-Seidel, Federico · Year range: 2017 to 2023 · Data source: Scopus, up to 14 Dec 2022

Topic	By this Researcher		Worldwide
	Scholarly Output	Field-Weighted Citation Impact	Prominence percentile
Small Nucleolar RNA; Biogenesis; Ribosomes T.4355	4	0.91	94.908 
Biomarkers; Hippuric Acid; Proton Magnetic Resonance Spectroscopy T.1027	1	0.00	99.492 
Cold Tolerance; Cold-Shock Response; Gene T.2867	1	2.31	98.637 
Purple Acid Phosphatase; Starvation; Root Hairs T.4191	1	1.15	97.641 
Embryo; Araucaria Angustifolia; Picea Abies T.8209	1	0.46	85.848 
Allergens; Food Allergies; Amandin T.9770	1	0.00	94.738 
Fruit; Solanum Pennellii; Methylheptenone T.10907	1	2.01	94.914 
Arabidopsis; Phosphatidic Acids; Diacylglycerol Kinase T.12409	1	0.00	91.324 
Ribosomal Protein S15A; Cell Division; Large Ribosomal Subunit T.19865	1	1.18	72.115 
Metabolomics; Sugar Phosphates; Liquid Chromatography-Mass Spectrometry T.23418	1	4.04	79.932 

A Topic is a collection of articles focused on a common intellectual research problem. There are 96,000 Topics in SciVal that are created by analyzing citation links between articles in Scopus - where there is a strong link a Topic is formed. This table shows the Topics in which the researcher has published, along with some metrics about each Topic. To learn more, search for Topic Prominence in Science in the SciVal Support Hub.

Appendix A

Molecular Cloning

Primer design	2
Plant growth	2
Purification of plant total RNA (QIAGEN protocol, modified)	2
First-Strand cDNA Synthesis (Thermo Fisher protocol, modified)	4
Plant DNA extraction (QIAGEN protocol, modified)	6
PCR to amplify a gene of interest (Thermo Fisher Protocol, modified)	7
Agarose gel electrophoresis	8
Gel purification to isolate DNA (QIAGEN protocol, modified)	9
Ligation of amplicon into entry vector (SD/D/TOPO) (Thermo Fisher Protocol, modified)	11
Transformation into <i>Escherichia coli</i>	11
Reproduce positive transformants	13
Isolate plasmid DNA from broth (QIAGEN protocol, modified)	14
Restriction enzyme digestion of plasmids – agarose gel electrophoresis	15
Sanger sequencing and glycerol stock	15
LR Recombination Reaction	16
Chemically competent cells	18
Electrocompetent cells	18
Electroporation	19
Colony PCR to analyze positive transformants	20
Agroinfiltration	21
Floral dipping	22

This document has been jointly assembled by Federico Martinez-Seidel and Dione Gentry-Torfer. The information has been compiled from the respective kits that are referenced in the section titles and is meant to be a procedural guideline adapted to the necessities of our laboratory that can be used by any researcher interested in using these methodologies.

Primer design

The design of the PCR primers to amplify the gene of interest is critical for expression. To enable directional cloning the forward primer must contain the sequence CACC at the 5' end of the primer. D-TOPO vectors have complementary overhang sequence GTGG. When designing the reverse primer, it must not be complementary to GTGG to ensure directional cloning product.

Plant growth

Arabidopsis thaliana accession Columbia-0 or mutant genotype seeds were planted on soil and grown in long-day conditions 16 h/8 h (day/night) at 22 °C/18 °C in a controlled climate chamber. These plants were subsequently used for RNA and DNA extraction assays.

Nicotiana benthamiana seeds were planted on soil and grown for 3-4 weeks in long-day conditions 16hs/8hs (day/night) at 22 °C in a controlled climate chamber. Early emerging flowers were cut out to preserve healthy leaves. These plants were subsequently used for Agroinfiltration.

Purification of plant total RNA (QIAGEN protocol, modified)

Materials

- *Arabidopsis thaliana*
- RNeasy® Plant Mini Kit (QIAGEN, Düsseldorf, Germany)
- RNase-Free DNase Set (QIAGEN, Düsseldorf, Germany)
- 2 ml and 1.5 ml microcentrifuge tubes (Eppendorf, Hamburg, Germany)
- Pipette and tips (Eppendorf, Hamburg, Germany)
- β-Mercaptoethanol (β-ME)
- Ethanol
- Liquid nitrogen
- Mortar and pestle (Morgan Advanced Materials, Windsor, UK)
- Vortex (IKA, Staufen, Germany)
- Centrifuge (Eppendorf, Hamburg, Germany)
- Thermomixer (Eppendorf, Hamburg, Germany)
- NanoDrop™ (One/OneC Microvolume UV-Vis Spectrophotometer (Thermo Fisher Scientific, Waltham, MA, USA))

Considerations

- Process a maximum amount of 1 Arabidopsis leaf (~ 30 mg) by immediately flash-freezing the tissue in liquid nitrogen and determining the starting material by weighing the tissue without allowing the tissue to thaw during handling prior to disruption in Buffer RLT.
- Perform all steps of the procedure at room temperature and quickly.
- Perform all centrifugation steps at 20–25 °C in a standard microcentrifuge.
- Add 10 µL β-Mercaptoethanol (β-ME) per 1 ml Buffer RLT before use in a fume hood.
- Before using for the first time, add 4 volumes of ethanol (96–100%) to buffer RPE to obtain a working solution.

Method:

1. Determine the amount of plant material (no more than 100 mg) by weighing the tissue.
2. Immediately place the weighed tissue in liquid nitrogen, and grind thoroughly with a mortar and pestle. Decant tissue powder and liquid nitrogen into an RNase-free, liquid-nitrogen-cooled, 2 ml microcentrifuge tube. Allow the liquid nitrogen to evaporate, but not allowing the tissue to thaw.
3. Add 450 µl of Buffer RLT to a maximum of 100 mg tissue powder, vortex vigorously and incubate 1–3 min at 56 °C to help to disrupt the tissue.
4. Transfer the lysate to a QIAshredder spin column, placed in a 2 ml collection tube, and centrifuge for 2 min at full speed. Carefully transferred the supernatant of the flow-through to a new microcentrifuge tube without disturbing the cell-debris pellet in the collection tube.
5. Add 0.5 volume of ethanol (96–100%) to the cleared lysate, and mix immediately by pipetting.
6. Transfer the sample (usually 650 µl) to a RNeasy spin column (pink) placed in a 2 ml collection tube and centrifuge for 15 s at 8000 x g (10,000 rpm). Discard the flow-through.
7. Add 700 µl Buffer RW1 to the RNeasy spin column and centrifuge for 15 s at 8000 x g (10,000 rpm) to wash the spin column membrane. Discard the flow-through.
8. Add 500 µl Buffer RPE to the RNeasy spin column and centrifuge for 15 s at 8000 x g (10,000 rpm) to wash the spin column membrane. Discard the flow-through and repeat this step.
9. Place the RNeasy spin column in a new 1.5 ml collection tube and add 30–50 µl RNase-free water directly to the spin column membrane and centrifuge for 1 min at 8000 x g (10,000 rpm) to elute the RNA.
10. Measure DNA concentration with a NanoDrop using ddH₂O as blank and record the concentration on the tube and store at -20 °C.

First-Strand cDNA Synthesis (Thermo Fisher protocol, modified)

Materials:

- SuperScript™ II Reverse Transcriptase (Thermo Fisher Scientific, Waltham, MA, USA)
- Oligo(dT)₁₂₋₁₈ Primer (Thermo Fisher Scientific, Waltham, MA, USA)
- 5X First-Strand Buffer (250 mM Tris-HCl, pH 8.3, RT; 375 mM KCl; 15 mM MgCl₂)
- DTT (100 mM)
- Storage Buffer (20 mM Tris-HCl (pH 7.5), 100 mM NaCl, 0.1 mM EDTA, 1 mM DTT, 0.01% (v/v) NP-40, 50% (v/v) glycerol)
- 2 ml and 1.5 ml microcentrifuge tubes (Eppendorf, Hamburg, Germany)
- Pipette and tips (Eppendorf, Hamburg, Germany)
- Sterile ddH₂O
- Ice
- Centrifuge (Eppendorf, Hamburg, Germany)
- Thermomixer (Eppendorf, Hamburg, Germany)
- NanoDrop™ (One/OneC Microvolume UV-Vis Spectrophotometer (Thermo Fisher Scientific, Waltham, MA, USA))

Method:

A 20 µL reaction volume can be used for 1 ng to 5 µg of total RNA or 1–500 ng of mRNA.

1. Add the following components to a nuclease-free microcentrifuge tube:

Premix1 per sample:

- | | |
|---|--|
| - Oligo(dT) (500 µg/mL) or
[50–250 ng random primers or
2 pmole gene-specific primer (GSP)] | 1 µL |
| - 1 ng to 5 µg total RNA | x µL |
| - 1 µL dNTP Mix (10 mM each) | 1 µL |
| - Sterile, ddH ₂ O | (w/o RNaseOUT) to 14 µL
(w RNaseOUT) to 13 µL |

2. Heat mixture to 65 °C for 5 min and quick chill on ice. Collect the contents of the tube by brief centrifugation and add:

Premix2 per sample:

- | | |
|---------------------------------------|------|
| - 5X First-Strand Buffer | 4 µL |
| - 0.1M DTT | 2 µL |
| - RNaseOUT™ (40 units/µL) (optional)* | 1 µL |

NOTE: RNaseOUT™ (Cat. No. 10777-019) is required if using <50 ng starting RNA.

3. Mix contents of the tube gently. If you are using oligo (dT)₁₂₋₁₈ or GSP, incubate at 42°C for 2 min. If you are using random primers, incubate at 25°C for 2 min.
4. Add 1 µL (200 units) of SuperScript™ II RT and mix by pipetting gently up and down.
NOTE: If you are using less than 1 ng of RNA, reduce the amount of SuperScript™ II RT to 0.25 µL (50 units) and add sterile, distilled water to a 20 µL final volume.
NOTE: If you are using random primers, incubate tube at 25°C for 10 min.
5. Incubate at 42°C for 50 min.
6. Inactivate the reaction by heating at 70°C for 15 min.
7. **[Optional]** First-Strand cDNA Synthesis Using SuperScript™ II RT, Continued. The cDNA can now be used as a template for amplification in PCR. However, amplification of some PCR targets (>1 kb) may require the removal of RNA complementary to the cDNA. To remove RNA complementary to the cDNA, add 1 µL (2 units) of *E. coli* RNase H and incubate at 37°C for 20 min.
8. Measure DNA concentration with a NanoDrop using ddH₂O as blank and record the concentration on the tube and store at -20 °C.

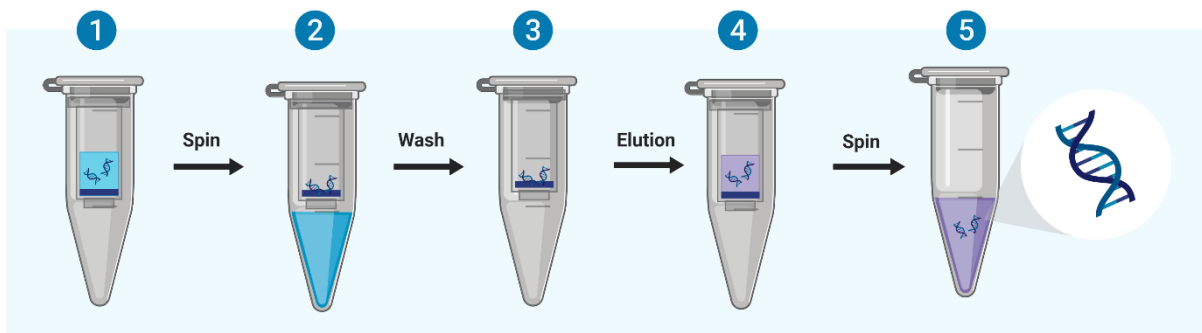
Plant DNA extraction (QIAGEN protocol, modified)

Materials:

- DNeasy® Plant Mini Kit (QIAGEN, Düsseldorf, Germany)
- Centrifuge (Eppendorf, Hamburg, Germany)
- Water Bath 1003 (Gesellschaft für Labortechnik, Burgwedel, Germany)
- 2 ml and 1.5 ml microcentrifuge tubes (Eppendorf, Hamburg, Germany)
- Pipette and tips (Eppendorf, Hamburg, Germany)
- Sterile ddH₂O
- Ice
- Liquid nitrogen
- Ethanol
- Scissors
- NanoDrop™ (One/OneC Microvolume UV-Vis Spectrophotometer (Thermo Fisher Scientific, Waltham, MA, USA))

Considerations

- Perform all centrifugation steps at room temperature (15–25°C).
- If necessary, re-dissolve any precipitates in Buffer AP1 and Buffer AW1 concentrates.
- Add ethanol to Buffer AW1 and Buffer AW2 concentrates.
- Preheat a water bath to 65°C.



Method:

1. Cut a piece of the youngest leaf (no more than 0.5 mm²~ 20 mg) and place it in a liquid nitrogen frozen tube
 - a. Label the tube and the plant accordingly
 - b. Clean scissors with a tissue between WT and mutant
2. Grind leaves with pestle/tip frozen in liquid nitrogen.
3. Add 400 µL Buffer AP1 and 4 µL RNase A. Vortex and incubate for 10 min at 65°C. Invert the tube 2–3 times during incubation.

NOTE: Do not mix Buffer AP1 and RNase A before use.
4. Add 130 µL Buffer P3. Mix and incubate for 5 min on ice.
5. Recommended: Centrifuge the lysate for 5 min at 20,000 x g (14,000 rpm).

6. Pipet the lysate into a QIAshredder spin column placed in a 2 ml collection tube. Centrifuge for 2 min at 20,000 x g.
7. Transfer the flow-through (500 µL) into a new tube without disturbing the pellet if present. Add 1.5 volumes of Buffer AW1 (750 µL), and mix by pipetting.
8. Transfer 650 µL of the mixture into a DNeasy Mini spin column placed in a 2 ml collection tube. Centrifuge for 1 min at ≥ 6000 x g (8000 rpm). Discard the flow-through. Repeat this step with the remaining sample.
9. Add 500 µL Buffer AW2, and centrifuge for 1 min at ≥ 6000 x g. Discard the flow-through.
10. Add another 500 µL Buffer AW2. Centrifuge for 2 min at 20,000 x g.
NOTE: Remove the spin column from the collection tube carefully so that the column does not come into contact with the flow-through.
11. Transfer the spin column to a new 1.5 ml or 2 ml microcentrifuge tube.
12. Add 25 µL ddH₂O for elution. Incubate for 5 min at room temperature (15–25 °C). Centrifuge for 1 min at 6000 x g.
13. Repeat step 12.
14. Measure DNA concentration with a NanoDrop using ddH₂O as blank and record the concentration on the tube and store at -20 °C.

PCR to amplify a gene of interest (Thermo Fisher Protocol, modified)

Materials:

- Phusion High-Fidelity DNA Polymerase (2 U/µL) (Thermo Fisher Scientific, Waltham, MA, USA)
- Template: Purified DNA or cDNA synthesized from purified mRNA
- Thermal cycler for PCR (Bio-Rad, Hercules, CA, USA)
- Pipette and tips (Eppendorf, Hamburg, Germany)
- PCR tubes 0.1 mL with flat caps (Nippon Genetics, Düren, Germany)
- ddH₂O
- Ice

Method:

1. Set up a 50 µL reaction in ice containing the following:

10 µL	Phusion HF 5x Buffer
5 µL	dNTPs (2 mM)
X µL	Template DNA (50 – 250 ng)
3 µL	Fwd primer (10 µM)
3 µL	Rev primer (10 µM)
0.5 µL	Phusion HF DNA Polymerase
Up to 50 µL	ddH ₂ O

2. Mix well by pipetting, give a quick spin and place tube on thermocycler.
3. Calculate times and temperatures according to your primers and gene size (colored in red in the table below)

Note: the CACC precursor part of the primers for the directional cloning does not need to be considered for the calculation of the annealing temperatures

4. Enter the following parameters in the thermocycler and start reaction (total duration around 1h50):

Temperature	Duration	Step	
98 °C	30 s	Initial denaturation	
98 °C	10 s	Denaturation	} 35X cycles
55-69 °C	30 s	Annealing	
72 °C	30 s/kb	Extension	
72 °C	10 min	Final extension	
4 °C		Hold	

Considerations:

- Initial denaturation at 98°C for 1.3 min is enough. Longer initial denaturation can be used for difficult templates such as GC-rich sequences or for colony PCR to extract the DNA from the cells.
- Annealing is based on the melting temperature (T_m) of the primer pair. Annealing temperatures can be optimized by doing a temperature gradient PCR starting 5°C below the calculated T_m . Use online T_m calculator tool from ThermoFisher.
- Time for elongation/extension depends on amplicon length, generally genomic DNA = 30s/Kb; cDNA = 30-40s/Kb

Agarose gel electrophoresis

Materials:

- Casting tray
- Well combs
- Electrophoresis system (Bio-Rad, Hercules, CA, USA)
- 1 kb DNA Hyper ladder (Thermo Fisher Scientific, Waltham, MA, USA)
- 1% Agarose gel
- TAE 1X
- PCR product
- 6X DNA Gel Loading Dye (New England Biolabs®, Ipswich, MA, USA)
- Molecular Imager GelDoc™ XR+ (Bio-Rad, Hercules, CA, USA)

Tris-acetate-EDTA (TAE) 50X stock running buffer

- 242 g Tris base in ddH₂O
- 57.1 mL glacial acetic acid
- 100 mL 0.5 EDTA, pH 8.0
- Adjust to 1 L with ddH₂O

TAE 1X working solution

- 25 mL 50X TAE
- Adjust to 1 L with ddH₂O

1% Agarose gel

- 1% SeaKem® LE Agarose (Lonza, Basel, Switzerland)
- 1X TAE buffer
- Microwave for 1-3 min until agarose has completely dissolved
- Let the bottle cool until it can be touched for 30 s
- Per each 100 mL agarose gel solution add 5 µL RedSafe™ Nucleic Acid Staining solution (iNtRON Biotechnology, Burlington, MA, USA)

Method:

1. Choose a size of casting tray and well comb depending on how many samples and µL per sample you have. Put the comb in the tray before you pour your gel.
2. Prepare 1% agarose gel and pour in casting tray slowly to avoid bubbles. You can pop them or push them to the sides with a pipette tip.
3. Wait 15-30 min for the gel to solidify. Remove well comb and place the gel into the gel box. Fill box with 1x TAE buffer until the gel is completely soaked.
4. Add 6x buffer to each PCR product. The loading buffer will help your PCR product sink into the well and it will stain your PCR product to watch it as it migrates through the gel.
5. Load 6 µL of 1 kb ladder into the first lane of the gel.
6. Load your samples into the wells of the gel. Don't pinch the pocket, load from top and have the tip in the middle of the pocket.
7. Run gel at 130 volts 25 min for a full gel run – rapid separation. For better band resolution use less volts and longer time. For example, 80 volts for ~ 60 min for half gel run and better band resolution.
NOTE: The DNA will run towards the positive (red) electrode, because it is negatively charged.
8. Turn off power and carefully remove the gel from the gel box.
9. Visualize your DNA fragments with the UV light using a molecular imager. Try to take a quick picture, you don't want the UV to mutate your DNA.

Gel purification to isolate DNA (QIAGEN protocol, modified)

This protocol is designed to extract and purify DNA of 70 bp to 10 kb from standard or low-melt agarose gels in TAE or TBE buffer using the QIAquick Gel Extraction Kit or the QIAquick PCR & Gel Cleanup Kit. Up to 400 mg agarose can be processed per spin column. These kits can also be used for DNA cleanup from enzymatic reactions. For DNA cleanup from enzymatic reactions using this protocol, add 3 volumes of Buffer QG and 1 volume of isopropanol to the reaction, mix, and then proceed with step 6 of the protocol. Alternatively, use the MinElute Reaction Cleanup Kit.

Materials:

- QIAquick® Gel Extraction Kit (QIAGEN, Düsseldorf, Germany)
- Sharp scalpel
- Isopropanol
- Molecular Imager GelDoc™ XR+ (Bio-Rad, Hercules, CA, USA)
- Microcentrifuge tubes, 2 ml (Eppendorf, Hamburg, Germany)
- Digital scale
- Thermomixer (Eppendorf, Hamburg, Germany)
- Vortex (IKA, Staufen, Germany)
- Centrifuge (Eppendorf, Hamburg, Germany)
- NanoDrop™ (One/OneC Microvolume UV-Vis Spectrophotometer (Thermo Fisher Scientific, Waltham, MA, USA))

Important points before starting

- The yellow color of Buffer QG indicates a pH ≤ 7.5 .
- Add ethanol (96–100%) to Buffer PE before use (see bottle label for volume).
- All centrifugation steps are carried out at 17,900 x g (13,000 rpm) in a conventional table-top microcentrifuge at room temperature (15–25 °C).

Method:

1. Weigh and label the tubes in which you will store your gel pieces, in order to have the precise weight of the gel fragment.
2. Excise the DNA fragment from the agarose gel with a clean, sharp scalpel using UV light to spot the fragment of interest.
NOTE: Minimize the size of the gel slice by removing extra agarose.
3. Add the gel slices into the weighted, labelled colorless tubes. Add 3 volumes of Buffer QG to 1 volume of gel.
NOTE: For example, add 300 μL of Buffer QG to each 100 mg of gel. For >2% agarose gels, add 6 volumes of Buffer QG.
4. Incubate at 50°C for 10 min or until the gel slice has completely dissolved. To help dissolve gel, mix by vortexing the tube every 2–3 min during the incubation.
IMPORTANT: Solubilize agarose completely. For >2% gels, increase incubation time.
5. After the gel slice has dissolved completely, check that the color of the mixture is yellow (similar to Buffer QG without dissolved agarose).
NOTE: If the color of the mixture is orange or violet, add 10 μL of 3 M sodium acetate, pH 5.0, and mix. The color of the mixture will turn to yellow.
6. Add 1 gel volume of isopropanol to the sample and mix. For example, if the agarose gel slice is 100 mg, add 100 μL isopropanol.
7. Place a QIAquick spin column in a provided 2 ml collection tube.
8. To bind DNA, apply the sample to the QIAquick column, and then centrifuge for 1 minute. The maximum volume of the column reservoir is 720 μL . For sample volumes >720 μL , load the remainder and spin again.
9. Discard flow-through and place QIAquick column back into the same collection tube.

10. Recommended: Add 0.5 ml of Buffer QG to QIAquick column and centrifuge for 1 minute.
11. To wash, add 0.75 ml of Buffer PE into the QIAquick column let the column stand 2–5 min and centrifuge for 1 minute.
12. Discard the flow-through and centrifuge the QIAquick column for an additional 1 minute at 17,900 x g (13,000 rpm).
13. Place QIAquick column into a clean 1.5 ml microcentrifuge tube.
14. To elute DNA, add 50 µL of ddH₂O (pH 7.0–8.5) to the center of the QIAquick membrane, let the column stand for 1 min and then centrifuge the column for 1 min.
15. Measure 1 µL for double stranded DNA content in a NanoDrop and store at –20 °C.

Ligation of amplicon into entry vector (SD/D/TOPO) (Thermo Fisher Protocol, modified)

Materials:

- pENTR™/SD/D-TOPO™ Cloning Kit (Thermo Fisher Scientific, Waltham, MA, USA)
- Gel Purified amplicon
- ddH₂O
- 0.5 mL microcentrifuge tubes
- Ice

Method:

1. Add the following components into a 0.5 mL tube.

1µL	Salt solution (provided in the kit)
1-3µL	Gel-purified amplicon
1µL	Entry Vector (SD/D/TOPO)
6µL	Final volume with ddH ₂ O

2. Mix gently and incubate 10- 15 min at room temperature
3. Place the reaction on ice and proceed to transform into *E. coli*

Transformation into *Escherichia coli*

Materials (per sample):

- LB plates containing Kanamycin 50µg/mL
- Water Bath 1003 (Gesellschaft für Labortechnik, Burgwedel, Germany)
- SOC (Super Optimal Broth with Catabolite repression; supplied the pENTR™ SD/D-TOPO™ Cloning Kit)
- Ice
- Orbital Shaker 3017 (Gesellschaft für Labortechnik, Burgwedel, Germany)
- OneShot® TOP10 *E. coli* chemically competent cells (Thermo Fisher Scientific, Waltham, MA, USA)
- D/TOPO cloning or LR reaction

WARNING: competent cells are very susceptible. Take the cells out from -80°C and place them **immediately** on ice before use. If they will not be used, they **must** be disposed. Never take them back to -80 °C.

LB liquid media and solid media

Add the following reagents into a sterile glass bottle (Schott Duran®, Mitterteich, Germany) and autoclave

- 10 g tryptone
- 5 g yeast extract
- 10 g NaCl
- Top up with 0.8 L ddH₂O and adjust pH 7.0 using NaOH
- 15 g bacto agar (only for solid media)

Method:

1. Equilibrate a water bath to 42 °C
2. Warm the SOC Media to room temperature
3. Warm selective plates to 37 °C for 30 min
4. Thaw on ice 1 aliquot of competent cells (serves two samples 25µL and 25µL)
5. Take 25 µL of competent cells to a new tube and label accordingly.
6. Add 2 µL of the D-TOPO cloning reaction into half vial One Shot® chemically competent cells and mix gently (no vortex, no pipetting); flick with your finger not too hard.
7. Incubate on ice 30 min, longer is not a problem
8. Heat shock the cells for 50 s at 42 °C in water bath
9. Immediately transfer the tubes to ice for 2:30 min
10. Add 175 µL room temperature SOC Medium for a total of 200 µLs volume
11. Cap the tube tightly and shake horizontally at 200-220 rpm at 37 °C for 1 h
12. Spread 100 µL (half volume) into a pre-warmed selective plate; two pre-warmed plates per sample.
13. Pellet the remaining by centrifuging at 1000 x g, 1 min, discard the flow-through, resuspend the pellet in 50 µL SOC Media, and spread into another selective plate

14. Incubate overnight at 37 °C (the plates must be incubated upside down so that the bacteria do not grow inside the media but on the top), no parafilm is needed to close the plates

The colonies can be stored up to 2 weeks safely at 4 °C without compromising the transformants. Seal the plates with parafilm, low temperatures will prevent exponential growth and depletion of the antibiotic.

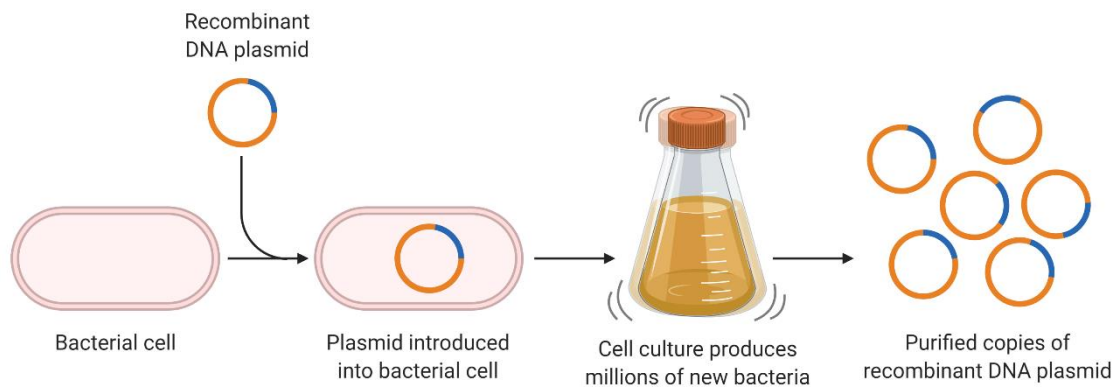
Reproduce positive transformants

Materials (per sample):

- LB liquid media supplemented with Kanamycin 50µg/mL
- Autoclaved tips
- 10 mL Glass tubes (autoclaved)
- Plates with LB agar supplemented with Kanamycin 50µg/mL

NOTE: LB liquid media containing antibiotics should be stored at 4°C and is good for one month

Method:



1. Aliquot 5 mL of LB liquid media containing 50 µg/mL Kanamycin in glass autoclaved tubes.
2. Pick a colony with an autoclaved pipette tip and submerge/throw the tip inside the tube and cap the tube allowing gas exchange.
3. Pick 3-10 transformed colonies per plate and culture them overnight in LB liquid media shaking at 220 rpm at 37°C.

NOTE: Usually the smaller colonies will contain your full-vector since the exogenous gene will make the bacteria grow slower.

IMPORTANT: Do not try to store broths at 4°C as a mean to store your transformants, because the bacteria will eject the plasmid rapidly. The broths must be used as soon as possible.

Isolate plasmid DNA from broth (QIAGEN protocol, modified)

Materials (per sample):

- Plasmid QIAprep Spin Miniprep Kit (QIAGEN, Düsseldorf, Germany)
- NanoDrop™ (One/OneC Microvolume UV-Vis Spectrophotometer (Thermo Fisher Scientific, Waltham, MA, USA))
- Liquid nitrogen
- Centrifuge
- 2 ml and 1.5 ml microcentrifuge tubes

1. Make glycerol stocks of all your broths: Gently mix 500µL of sterile 50% Glycerol with 500µL broth culture. Transfer the mixture to a cryo-vial (final concentration 25% Glycerol, label all details in the vial. Freeze in liquid nitrogen and store at -80°C).

NOTE: After 1 day of culture in the LB broth the bacteria will reach the stationary growth phase. At this point, make glycerol stocks of all your broths and after confirmation of your transformants (i.e., restriction enzyme digestion – agarose gel purification and Sanger sequencing) keep only the successful vials.

2. Proceed to isolate plasmid DNA from the rest of your broth (2 mL)

Considerations:

- **OPTIONAL:** Add LyseBlue reagent to Buffer P1 at a ratio of 1 to 1000.
- Add the provided RNase A solution to Buffer P1, mix, and store at 2–8°C.
- Add ethanol (96–100%) to Buffer PE before use (see bottle label for volume).
- All centrifugation steps are carried out at 13,000 rpm (~17,900 x g) in a conventional table-top microcentrifuge.

Method:

1. After taking 500 µL for the glycerol stocks, pellet the remaining volume of your bacterial overnight culture by centrifugation at 8000 rpm (3270 x g) for 10 min at room temperature (15–25 °C). Discard the supernatant.
2. Resuspend pelleted bacterial cells in 250 µL Buffer P1 and transfer to a microcentrifuge tube.
3. Add 250 µL Buffer P2 and mix thoroughly by inverting the tube 4–6 times until the solution becomes clear. Do not allow the lysis reaction to proceed for more than 5 min.
NOTE: If using LyseBlue reagent, the solution will turn blue.
4. Add 350 µL Buffer N3 and mix immediately and thoroughly by inverting the tube 4–6 times.
NOTE: If using LyseBlue reagent, the solution will turn colorless.
5. Centrifuge for 10 min.
6. Apply the supernatant from step 5 to the QIAprep spin column by decanting or pipetting. Centrifuge for 30–60 s and discard the flow-through.

7. Recommended: Wash the QIAprep spin column by adding 0.5 ml Buffer PB. Centrifuge for 30–60 s and discard the flow-through.
8. Wash the QIAprep spin column by adding 0.75 ml Buffer PE. Centrifuge for 30–60 s and discard the flow-through.
9. Centrifuge for 1 min to remove residual wash buffer.
10. Place the QIAprep column in a clean 1.5 ml microcentrifuge tube. To elute DNA, add 50 μ L ddH₂O to the center of the QIAprep spin column, let stand for 1 min, and centrifuge for 1 min.
11. Determine plasmid concentration in NanoDrop, label the tube and store at -20 °C.

Restriction enzyme digestion of plasmids – agarose gel electrophoresis

Materials (per sample, 20 μ L reaction):

2 μ L	CutSmart® Buffer
0.5 μ L	Restriction enzyme (MluI-HF)
2 μ L	Plasmid DNA (Usually ranges 50-100 ng/ μ L after mini prep)
Up to 15 μ L	ddH ₂ O

Enzyme capabilities: DNA: Enzyme ratio \rightarrow 1:2-10 \rightarrow 1000-5000 ng:1 μ L (i.e., 10 units)

Method:

1. Give a gentle mix by flicking the tube with your fingertip and incubate at 37 °C for 2h
2. Prepare agarose gel
3. Add 6X loading dye to each reaction
4. Load 10 μ L per sample on gel and 6 μ L of Hyper ladder 1kb in the first lane
5. Run at 100 V for 50 min and analyze gel under UV light with expected band sizes
6. If DNA content is very low, use higher exposition times to see all bands.

Sanger sequencing and glycerol stock

IMPORTANT!

After identifying the correct clone, send your construct for sanger sequencing to confirm that the gene is in the correct orientation, and that it does not contain point mutations due to the UV-light and other potentially harmful conditions along the way. After confirmation, be sure to keep the glycerol stocks stored safely at -80°C.

Materials:

Primers
ddH₂O
Pure Plasmid DNA
50% sterile Glycerol (0.22 μ M filtered or autoclaved)

Glycerol stock:

1. Inoculate positive transformant into LB/YEB liquid media with selective antibiotics and grow overnight at 37/28 °C, 200 rpm.
2. Prepare glycerol stocks for long term preservation of bacteria containing the vectors by mixing 1:1 sterile 50% glycerol and bacteria broth. Label accordingly.
3. Freeze in liquid nitrogen and store at -80 °C.

Sanger sequencing:

1. Design forward and reverse primers every 900 bp and order to a company that synthesizes oligos. Include the entire construct to confirm the cloning direction and the absence of important point mutations. Use a software, e.g., Benchling to design primers.

NOTE: For constructs in the D/TOPO vector backbone, you can use the kit provided M13 Fwd and Rev primers.

2. Primers are provided dry, which means you have to add the manufacturers recommended amount of ddH₂O to obtain a primer stock solution at 100 mM.
3. Prepare a working solution by diluting to 10 mM with ddH₂O.
4. Add the following components into a 1.5 mL microcentrifuge tube:

NOTE: Amounts and concentrations depend on the company you will send the samples to!

X µL (1 µg)	Pure plasmid DNA
2 µL	Primer (10 mM)
Up to 14 µL	ddH ₂ O

5. Make an alignment with the sequenced insert and the online vector template on Benchling to analyze potential fallbacks or successfully confirmed constructs.
6. Only keep the glycerol stocks that have been confirmed.

LR Recombination Reaction

The reaction is performed between an entry clone and the selected destination vector. The LR products are then transformed into competent *E. coli* hosts to select for an expression clone.

Materials:

- MluI-HF® (20.000 U/ml, restriction site: 5'-A[^]CGCGT, New England Biolabs, Ipswich, MA, USA)
- LR Clonase™ Enzyme Mix (Thermo Fisher Scientific, Waltham, MA, USA)
- TE Buffer, pH 8.0 (10 mM Tris, 1 mM EDTA)

IMPORTANT: To prevent D-TOPO vectors from transforming into the competent *E. coli* again (it could result in false positives since both vectors have the same antibiotic resistance marker), follow the next steps before performing the LR clonase reaction:

Method:

Digest D-TOPO plasmids with MluI HF[®] restriction enzyme or with another enzyme depending on the sequence compatibility. Make sure that it does not cut inside your insert and that includes the attL recombination sites.

1. Add the following components to 1.5 ml microcentrifuge tubes and mix gently:

1 µL	Restriction enzyme
100 ng (~5µL)	Plasmid DNA
2µL	CutSmart Buffer
Up to 20µL	ddH ₂ O

2. Incubate for 1-2 h at 37°C.
3. Inactivate enzyme at 65°C for 20 min.
4. **IMPORTANT:** To remove enzyme and salt traces purify the reaction by following the gel purification protocol.
5. Add the following components to 1.5 ml microcentrifuge tubes at room temperature and mix:

100-300 ng	(~ 7µL)	Entry clone (Transformed-digested D-TOPO)
300 ng	(~ 2µL)	Destination vector (pEarleyGate, pMDC99)
4 µL		5X LR Clonase reaction buffer
To 16 µL		TE Buffer

6. Take the LR Clonase from -80°C and thaw on ice (~ 2 min).
7. Vortex the LR Clonase briefly twice (2 s each time).
8. To each sample, add 4 µl of LR Clonase. Mix well by vortexing briefly twice (2 s each time).
Reminder: Return LR Clonase™ enzyme mix to -80°C immediately after use.

9. Incubate reactions at 25 °C for 1 h.

NOTE: For most applications, 1 h will yield a sufficient number of colonies for analysis. Depending on your needs, the length of the recombination reaction can be extended up to 18 h. For large plasmids (≥ 10 kb), longer incubation times (i.e. overnight incubation) will yield more colonies and are recommended.

10. Add 2 µL of the Proteinase K solution (600 U/ml) to each reaction. Incubate for 10 min at 37 °C.

NOTE: You may store the LR reaction at -20 °C for up to 1 week before transformation.

11. Proceed to transform a suitable *E. coli* host and select for expression clones following the section Transformation into *Escherichia coli*. Use 2 µL DNA from LR reaction (spin before) into 25 µL chemically competent cells.

Chemically competent cells

The protocol works for *E. coli* strains including DH5alpha, XL1 Blue, TOP10, ccdB survival™, and Stbl3™

Materials:

- CaCl₂ 50 mM (sterile)
- 50% glycerol (sterile)
- LB liquid media
- 1 cm pathlength optical glass cuvette (Eppendorf, Hamburg, Germany)
- Spectrometer (BioPhotometer 6131 (Eppendorf, Hamburg, Germany))
- Corning® centrifuge tubes (Merck, Darmstadt, Germany)
- Centrifuge for 4
- Ice
- Dry ice
- 0.5 ml microcentrifuge tubes

Method:

1. Dilute 1:50 in 100ml LB, grow until reaching an optical density of 0.5 – 0.8
IMPORTANT: Check the OD600 every 2 to 3 h until it reaches the desired value and collect when they are actively dividing (logarithmic growth) i.e.: OD600 from 0.3 to 0.5.
2. Centrifuge at 7000 rpm for 5 min
3. Discard supernatant, resuspend pellet in 50 ml CaCl₂ 50 mM (CaCl₂ is kept at 4 °C).
4. Incubate at 4 °C for 1 h
5. Centrifuge 15 min at 7000 rpm at 4°C
6. Discard supernatant, resuspend pellet in 9 ml CaCl₂ 50 mM + 1 ml glycerol 50%
7. Aliquot in 50 0.5 ml microcentrifuge tubes 200 µL each in dry ice and store at -80°C (do not freeze in liquid nitrogen), once thawed aliquots must be completely used and not re-stored.

Electrocompetent cells

Materials:

- YEB medium supplemented with Rifampicin and Gentamicin
- 10% glycerol solution (autoclave) (ice cold)
- ddH₂O (autoclave) (ice cold)
- Dry ice
- Liquid nitrogen
- 0.5 ml tubes (pre-chill in fridge)
- 50 ml tubes (pre-chill in fridge)
- Pipettes and tips
- Centrifuge for 50 ml tubes and for 4°C
- *Agrobacterium tumefaciens* GV3101

Method:

1. Inoculate 3 ml YEB media supplemented with Rifampicin and Gentamicin with 1 colony of *Agrobacterium* strain GV3101 in the morning and incubate at 28°C at 250 rpm for the rest of the day.
2. In the evening inoculate 3 x 150 ml YEB (containing the appropriate antibiotics) with 1 ml each of the culture grown throughout the day and incubate at 28 °C at 250 rpm until OD600 reaches 0.8 - 1.0 (This usually takes around 30 - 40 h).
3. Check OD600, and combine all 3 cultures once OD600 reaches 0.8-1.0
4. Chill culture by putting it on ice for 15 min and swirling it regularly.
NOTE: From here on everything needs to happen on ice or at 4°C!
5. Distribute culture into 8 x 50 ml tubes.
6. Pellet by centrifugation at 3500 x g for 20 min at 4°C.
7. Discard supernatant and resuspend each pellet in 10 ml ice cold H₂O.
8. Adjust volume to 50 ml each with ice cold H₂O.
9. Pellet cells by centrifugation at 3500 x g for 20 min at 4°C.
10. Discard supernatant and resuspend each pellet in 10 ml ice cold H₂O.
11. Combine solutions into 4 x 50 ml tubes and adjust to 50 ml with ice cold H₂O.
12. Pellet cells by centrifugation at 3500 x g for 20 min at 4°C.
13. Discard supernatant and resuspend each pellet in 10 ml ice cold H₂O.
14. Combine solutions into 2 x 50 ml tubes and adjust to 50 ml with ice cold H₂O.
15. Pellet cells by centrifugation at 3500 x g for 20 min at 4°C.
16. Discard supernatant and resuspend each pellet in 10 ml ice cold H₂O.
17. Combine solutions into 1 x 50 ml tubes and adjust to 50 ml with ice cold H₂O.
18. Pellet cells by centrifugation at 3500 x g for 20 min at 4°C. (Use a counterbalance tube)
19. Discard supernatant and resuspend pellet in 4.5 ml ice-cold 10% glycerol.
20. Dispense 50 µl aliquots into pre-chilled 0.5 ml tubes and flash freeze in dry ice or liquid nitrogen.
21. Store aliquots at -80°C until use.

Electroporation

Electroporate plasmids into *Agrobacterium* standard lab strain GV3101. Plasmid pUC19 can be used as positive control for transformation. GV3101 strain is resistant to rifampicin and gentamycin.

Materials:

- Electroporator 2510 (Eppendorf, Hamburg Germany)
- Orbital Shaker 3017 (Gesellschaft für Labortechnik, Burgwedel, Germany)
- MicroPulser Electroporation Cuvette, 0.1 cm gap (Bio-Rad, Hercules, CA, USA)
- YEB selective plates (rifampicin 10µg/ml, gentamycin 10µg/ml and Kanamycin 50µg/ml)

Per sample:

20 ng	Plasmid DNA
30 μ L	Electrocompetent <i>Agrobacteria</i> (Strain GV3101)
300 μ L	SOC Media

Method:

1. Prepare selective plates with YEB media supplemented antibiotics for GV3101
2. Pre-warm at 28 °C selective plates for 1 h
3. Place SOC media in a 37 °C water bath
4. Thaw electrocompetent cells on ice and place cuvettes on ice to chill them
5. Transfer 20 ng/ μ L (~1 μ L) of plasmid DNA at the bottom of an ice-cold electroporation cuvette.
6. Transfer 30 μ L of electrocompetent *Agrobacteria* on top of the plasmid DNA.
7. Incubate on ice for 10 min.
8. Set the electroporator to a voltage of 1800 and insert the cuvette into the cuvette holder. Give a double pulse with a time constant of 4.5 – 5.0 s.
9. Immediately after the pulse, add 200 μ L pre-warmed SOC media into the cuvette and transfer into a 2 mL microcentrifuge tube and cap tightly.
10. Incubate the cells at 28 °C for 2 h and shaking horizontally at 200 rpm in orbital shaker.
11. Spread 50 μ L incubated cells into pre-warmed YEB solid media selective plates supplemented with antibiotics. Centrifuge the remaining at 1000 x, 1 min, resuspend the pellet in 50 μ L SOC media and spread into another selective plate.
12. Incubate at 28 °C for 36 h.
13. Pick a single colony and reproduce it in YEB liquid media supplemented with antibiotics.
14. **IMPORTANT:** Prepare glycerol stocks for long term preservation of bacteria containing the confirmed vectors. Mix 1:1 sterile 50% glycerol and bacteria broth.

Colony PCR to analyze positive transformants

Primers: use a combination of the forward or reverse primer in your destination vector and a primer that hybridizes within your insert to confirm that all sequences are there (primers of the destination vector will do the trick; the same used for the Sanger sequencing).

1. Prepare a PCR Master Mix that contains the following reagents multiplied by the total amount of reactions/colonies to be analyzed:

Materials (per colony, 20 μ L reactions):

2 μ L	10x Buffer
0.5 - 1 μ L	dNTPs
1 μ L of 10 μ M	Fwd primer
1 μ L of 10 μ M	Rev primer
0.1 - 1 μ L	Polymerase

Up to 20µL ddH₂O

2. For each sample aliquot 20 µL of PCR Master Mix into 0.5 µL tube.
3. Pick 10-15 single colonies with a sterile pipette tip (templates) and make a patch with the same tip in a selective YEB plate to preserve the colonies for further analysis. Label accordingly.
4. Resuspend colonies individually into PCR wells containing the master mix (a very small amount is more than enough). Label accordingly and place reactions on thermocycler with the following conditions:

95°C	10 min	Initial denaturation (longer than normal to extract DNA from bacteria)
95°C	30 sec	Denaturation
50-68°C	30 sec	Annealing
72°C	15 sec/kb	Extension
72°C	5 min	Final extension

5. Run gel (agarose gel electrophoresis)

Agroinfiltration

Materials:

- 3 weeks old *N. benthamiana*
- Transformed *Agrobacteria* with plasmid of choice
- Sterile Erlenmeyer flask
- Orbital Shaker 3017 (Gesellschaft für Labortechnik, Burgwedel, Germany)
- YEB liquid media
- Rifampicin
- Gentamycin
- Spectrometer (BioPhotometer 6131 (Eppendorf, Hamburg, Germany))
- AS media: 10 mM MgCl₂, 10 mM MES-KOH, pH 5.6, 150 µM acetosyringone
- Sterile ddH₂O
- 1 ml Syringes

Method:

Agrobacteria preparation:

1. Pick a single colony of transformed *Agrobacteria* that contains the plasmid of choice.
2. Grow *Agrobacteria* overnight at 28 °C and 200 rpm in 5 ml YEB with rifampicin 50 µg/ml, gentamicin 20 µg/ml, and the specific antibiotic for the plasmid.
3. Use 200 µL of the overnight culture to inoculate 4.8 ml of fresh YEB-Rif, Gent, antibiotic media and grow for 4–5 h at 28 °C and 200 rpm to an OD of approximately 0.3–0.6.
4. Determine OD. Centrifuge at 3,000 × *g* for 15 min at 4 °C and wash the pellet twice with 5 ml of 4 °C cold water.

5. Resuspend either in 4 °C cold AS media for *Nicotiana* transformation. Adjust to a final OD of 0.1–0.2.
6. Incubate at least 1 h on ice before proceeding with the transformation steps

Infiltration:

1. Water plants 4–6 h prior infiltration.
2. Have the *Agrobacteria* ready
3. Use a 1 ml syringe to inject *Agrobacteria* suspension into the abaxial epidermis of a leaf. Label injected leaf with adhesive tape.
4. Infiltrate the third to fifth youngest leaves.
5. Return plants to the growth chamber after infiltration and ensure plants are well watered again.
6. Expression can be analyzed starting 36 h post-infiltration, depending on the promoter system used to drive expression of the constructs.

Floral dipping

Materials:

- Tips and pipette
- LB liquid media with antibiotics
- Erlenmeyer flasks (sterile)
- *Arabidopsis thaliana*
- Transformed *Agrobacteria*
- Orbital Shaker 3017 (Gesellschaft für Labortechnik, Burgwedel, Germany)
- vResuspension solution (5% sucrose solution + 500µL/L Silwett)
- 50 mL falcon tubes
- Centrifuge
- Tray with wet paper towels
- Plastic roll paper

Method:

1. Prepare LB liquid media supplemented with antibiotics and pour 25 mL into sterile Erlenmeyer flasks.
2. Inoculate the transformed *Agrobacteria* into the LB liquid media and incubate at 28 °C, 200 rpm for 48 h.
3. Select *Arabidopsis* plants with many recently opened flowers to be transformed (bacteria will penetrate through flowers).
4. Prepare the resuspension solution.
5. Harvest bacteria cells by centrifuging 10 min at 3500 RPM (slow speed recommended).
6. Discard supernatant and resuspend pellet in 35 mL resuspension solution in a 50 mL falcon tube by gently pipetting up and down.
7. Lay water-soaked paper towels in a tray.
8. Take the plant upside down and dip the flowers several times into the resuspension solution with the bacteria.

9. Place the plants horizontally in the tray.
10. Once all plants are in the tray, cover it with plastic roll paper or plastic cap overnight.
11. Stand the plants and place them in the green house/chamber and water regularly.
12. When the silicas are turning yellow stop watering and collect the seeds.

Appendix B

T-DNA Lines

COMPUTER PREP WORK.....	2
Identifying and ordering lines	2
Designing and ordering primers	2
Organisational Tips.....	3
LAB WORK	4
Step One — Plate Preparation	4
Step Two — Seed Surface Disinfestation.....	4
Step Three — Germination	5
Step Four — Pricking (Soil Transfer)	5
Step Five — Incubating	5
Step Six — Bagging.....	5
Step Seven — Cutting Plants (for drying).....	6
Step Eight — Harvesting seeds	6
DNA Extraction & Genotyping.....	7
PCR	8
Primers Preparation	8
Gel Electrophoresis.....	9
Genotyped and Confirmed Lines	11
Primers.....	11
uL30A.....	13
uL30B	14
uL30C.....	14
uL30D.....	15
Confirmation of multiple plants per line	15

This document has been jointly assembled by Federico Martinez-Seidel and Kheloud El Eshraky.

Computer Prep Work

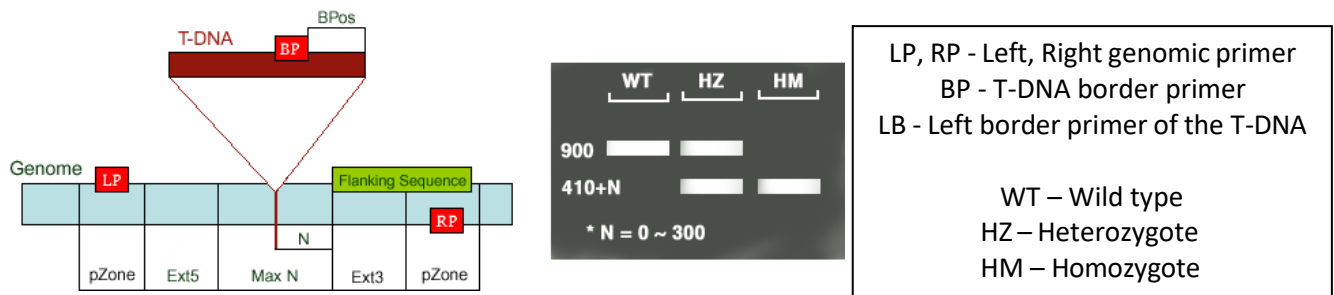
Identifying and ordering lines

- Have in hand the ATG codes of your genes of interest. For instance for a ribosomal protein family collect the ATG codes from all the paralogs in that family.
- For each ATG, identify the different T-DNA lines
 - o Go on TAIR's website <https://www.arabidopsis.org/>
 - o Search for gene of interest
 - o "Sequence Viewer" → "nucleotide seq viewer" → "Genes, T-DNA/Tn Insertions"
 - o Pick T-DNA lines that are inserted in the CDS (first exon is preferred, secondly UTR)
- Search for line availability on NASC website <http://arabidopsis.info/BasicForm>
- Check entry in ABRC, T-DNA lines with multiple unspecific insertions will be detailed there. All the NASC lines have an entry in ABRC.
- Import all relevant information to an Excel sheet (e.g: NASC stock #)
- Place order with NASC
 - o Proceed in NASC until needing the Purchase order number (ID number in the MPIMP system)
 - o Go to MPIMP homepage, service, admin, preorder list, create new. Get ID number, i.e., hidden_id.
 - o Insert hidden_id into NASC system and use Joachim's account when NASC asks for your details.
 - o Proceed to confirm payment by invoice.
 - o Invoice is sent to Joachim automatically, send an email to him in order to forward invoice to you.
 - o [you need an eProcurement account] Finally go to eProcurement and log in to create a new entry. Enter the free text shopping area and place your entry. Do not forget to attach the receipt in eProcurement.

Designing and ordering primers

- Design primers using Salk's website (<http://signal.salk.edu/tdnaprimers.2.html>) in order to ensure that amplicons are always of the same size and primers of the same annealing temperature. These two factors enable us to sow any line combination and genotype those with the same methodological parameters.
- Create primer order on Excel sheet for Eurofins <https://www.eurofins.com/genomic-services/our-services/dna-rna-oligonucleotides/>

1. Protocol for SALK T-DNA primer design



Images from © SIGNAL 2000-2010: <http://signal.salk.edu/tdnaprimers.2.html>

Organisational Tips

Create an Excel file with relevant gene information:

- Group name, ATG code, gene ID, alias, T-DNA line ID, NASC stock number, T-DNA location, marker used, marker concentration, vector used, background info, comments
- Example:

Group #	ATG_code	Gene_ID	Alias	Line_ID	Marker_used	Marker_conc	T-DNA_location	FOR/REV	Vector_name
uL30	1AT1G80750	uL30_RPL7A	uL30_rpl7a-1	SALK_134960C	Kanamycin	50 µg/L	First exon		pROK2
uL30	2AT1G80750	uL30_RPL7A	uL30_rpl7a-2	SALKSEQ_084392.1	Kanamycin	50 µg/L	First exon	rev	pROK2

Background	NASC_stock#	Phenotype	Status	Storage_location	Comment
Col-0	N664073	Wang, et al. (2017)			
Col-0	N584392		Seed production	CGWPhy13	

Once you have your T-DNA lines, you are ready to work with them.

But before sowing or taking any further steps, talk with the green team for a **pricking appointment** and **book space** for the plants in the following file:

X:\Service GREENTeam (“Space_request.xlsx” file → “Arabidopsis greenhouse request” sheet)

Arereservation_id	Study Id	Name of culture	AG_Agname	Area	Start (ddmmyyyy)	End (ddmmyyyy)	Remark	Location Id - ist
802		Federico Martinez Seidel	AG_Kopka	1.02	27.02.2020	01.03.2020	Seed production	CGW16h

Area calculation:

- 1 tray = 0.17m²
- 1 tray = 35 pots

Period for seed production: circa 2 months

Lab Work

Step One — Plate Preparation

1. Check the marker for each individual T-DNA line (different companies have different markers; i.e., antibiotics)
2. Marker concentration used in the media:

Kanamycin	BASTA (phosphinothricin)	Sulfadiazine
50 µg/L	20-25 µg/L	5.25 µg/L

NOTE: Kanamycin and BASTA (PPT) aliquots can be found in -20°C in EG, room 0.233

Sulfadiazine aliquots can be found in -20°C in our lab. Original sulfadiazine can be found in our lab.

To create concentrated stock Sulfadiazine solution (for 1L media)

- a) Measure 52.5 mg of Sulfadiazine
 - b) Top up with autoclaved ddH₂O to reach 10mL
 - c) Use a filter syringe inside clean bench to filter it from any impurities
 - d) Pipette 1 mL/Epi tube (use autoclaved 1,5 mL Epis)
 - e) Label each tube with corresponding concentration (5.25 mg/mL) and store in -20°C till further use
3. Go to media cabinet, take:
 - 0.5 MS Micro 6.8 Media (900mL)
 - 10% Sucrose (100mL)
 4. Heat the 0.5 MS Media in the microwave till completely melted
 5. In the down flow, add the 10% sucrose
 6. Allow to cool. Only add the antibiotics aliquot when the bottle can be touched for > 2mins
 7. Pipette 1mL of the antibiotics stock aliquot into the media and mix by inverting
 8. Slowly pour the media into plates (1L Media is enough for ≈ 10 big square plates or 20 small round ones)
 9. Allow media to cool and solidify in plates before using (or storing till further use)
Storage: Seal edges with Parafilm© and store in 4°C room till further use (recommended max storage of plates with antibiotics: up to 5 months)

Step Two — Seed Surface Disinfestation

In the lab:

1. Put aliquots from seed accessions in 1,5 ml Eppendorf tubes (do NOT take all seeds at once)
2. Add 995 µL EtOH (70%) + 5 µL Triton-x-100 per seed sample. **(WASH I)**
3. Mix for 20 minutes the tubes laying down horizontally taped to the surface of the thermomixer (800 RPM without heating, in thermomixer Eppendorf).
4. Spin samples at max speed for 2 minutes and remove supernatant,
5. Add 1ml 95 or 100% EtOH and shake for 10 minutes; spin down at max speed and go to down flow cabinet. **(WASH II)**

(Optional: Wash 6 times with sterile water, after last one leave water inside.)

Go to downflow cabinet

6. Pipette the seeds onto labelled (with pencil) autoclaved filters inside the downflow cabinet and wait until all the EtOH has evaporated
[alternatively: filter papers could be sterilised by submerging in 70% EtOH for circa 10 minutes, and then leaving to dry in downflow cabinet]
7. Sow the seeds in agar MS-media containing square petri dishes, by dropping a few seeds from the paper onto the plate. Make sure the plates are properly labelled with their corresponding line name.
8. Add a few WT seeds in a corner of each plate, mark this corner with an Edding© pen (this is done to ensure antibiotics are functioning and segregating the plants accordingly)
- 9. Each plate should be clearly labelled on the bottom.**

Step Three — Germination

Leave the plates to incubate for two weeks in one of the growing chambers (long day acclimation, such as K23 or K27) in the basement.

Notes regarding germination

Only seeds with T-DNA insertion will normally be able to grow on antibiotic-containing media. WT seeds will germinate, but then turn yellow as time progresses and growth is inhibited. Only transfer plants that are growing on the media. Preference should be given to “weird” or different looking seedlings, as they might be the homozygous plant. An average of 10 seedlings/line are preferred, to have an increase potential of having homo- or heterozygous plants.

In some cases, companies selling seeds mention that antibiotics marker could be “silenced” in T-DNA lines. This means that if none of the seeds germinate on the first try with antibiotic-containing media, the regular MS media should be used **without** antibiotics. This is only done if **NO Germination** occurs the first time.

Step Four — Pricking (Soil Transfer)

Performed by Green Team

For this step, make sure to make an appointment with Sven or anyone else from the Green Team for “pricking”. This is the process of taking out the seedlings from the plates and adding each individual plant to its own pot. For seed production, 8 cm pots (small size) are sufficient. This date should be 2 weeks after sowing the seeds.

Step Five — Incubating

Take pictures at regular intervals to document the development of each line, at regular conditions.

Step Six — Bagging

You will get an email when the plants are ready to be bagged.

Cover each plant with a paper bag, insert support rods and tie bottom with metal twist ties.

Label each tray with a paper with the following dates:

AG Kopka + your name

T: x (date of bagging)

F: x+2 weeks (date of watering)

E: x+4weeks (date of harvesting)

Step Seven — Cutting Plants (for drying)

Cut each plant from the base, ensuring the whole plant is inside the paper bag. Staple each bag shut with the plant label/identifier at the top. Use rubber band to group them together and leave them in the tray found in the green house. Green team takes it into K7 for drying (2 weeks).

Step Eight — Harvesting seeds

Prepare

- Sufficient amount of tubes/epis
- Sieves and accompanying metal bottom (found in the side room in green house) – sieve sizes 350 and 400 are reasonable, smaller sized sieves take longer
- Glass funnel
- Big tray filled with water (after use, dispose of water in autoclave soil box)
- Stickers – Either print new tube stickers (vertical barcode) or use the same sticker from the plant (horizontal barcode). I use the same sticker in order to avoid any mix-up.

Protocol

- Take bagged plants to the harvesting section in the green house
- Rub the paper bag of each plant to release all the seeds
- Cut out a corner and empty the seeds onto filter of choice
- Sieve the content to remove debris
- Deposit the seeds into their respective labelled tubes/epis using the glass funnel (glass tubes are better to avoid static problems)
- Properly clean out all the equipment used (sieve and bowls) between each sample with the airgun/compressor. Perform this step on top of the water bowl to avoid seed dispersal. This step is vital to avoid cross-contamination of the samples
- Dispose the rest of the plant material into an autoclaved bag. Soil is disposed in a special container found next to the sink.
- Store the seeds in our group's section in K8 (CGWPhy08: 15°C, 15% relative humidity)
- Make sure to label the box with all the relevant information (your name, line info, date of harvest ... etc)

DNA Extraction & Genotyping

Quick and Dirty Plant DNA extraction

Quick and dirty can be used at the initial stages to rapidly look for plants that contain the T-DNA insertion:

Sucrose 1M	
g	H ₂ O (mL)
0.5477	1.6
0.86	2.5
1.72	5

Sucrose extraction solution AKA "Magic Buffer"	5mL	7.5mL	10mL	15mL	20mL	30mL
H ₂ O	complete to	complete to	complete to	complete to	complete to	complete to
NaCl 5M	300 µL	450 µL	600 µL	900 µL	1.2 mL	1.8 mL
Sucrose 1M	1.5 mL	2.25 mL	3 mL	4.5 mL	6 mL	9 mL
Tris-HCl 1M pH7.5	250 µL	375 µL	500 µL	750 µL	1 mL	1.5 mL
Polyvinylpyrrolidone (PVP) (3%)(MW 40 kDa)	0.15 g	0.225 g	0.3 g	0.45 g	0.6 g	0.9 g

Prepare sucrose extraction solution from combining above solutions.

Note: PVP is optional to avoid oxidation of phenolic compounds (*it doesn't dissolve).

Phenolic compounds can inhibit PCR reactions.

Prepare the solutions and autoclave.

Sucrose 1M must be filtered instead.

Single Tubes

1. Pipette 200 µL of Sucrose extraction solution in a 2 mL epi.
2. Cut a little amount of leaf tissue (max 10 mg), preferably from the youngest leaf, and put inside the solution.
3. Insert retch ball into each tube, then use the retch mill to grind sample at max 1 min at room temperature. Alternatively, grind it with a pestle on ice.
4. Heat at 95-100°C for 10 minutes.
5. Centrifuge at 6000g for 30s and **put on ice.**
For PCR, DNA dilution of 20 times is used.
6. Pipette 19µL of autoclaved ddH₂O into 0.5 labelled epis.
7. Mix 1µL of supernatant (avoid debris) of the DNA solution into each epi.
8. Either put on ice to use immediately in PCR or store in -20°C.

96-Well plates

1. Design in excel your 96-samples array and mimic that in a trait in the greenhouse so that there is no need to keep track of which plant is where.
2. Add 750µL Magic Buffer and two metal beads 5mm to each microtube in the holding racks (the earliest pre-preparation is the night before, can be used to check oxidation of the metal beads).

3. Cut a small 25mm² piece of leaf (not bigger than the nail of the pinkie) and place in the buffer
4. Cover tubes with the provided collection caps and double check for even closure.
5. Retsch 2-4x for 1 min at 25 Hz in the Retsch Mill using the Qiagen plate adaptors (change the orientation of the metal covers each time) until the extract is light green. The leaf **MUST** be still visible and intact (too much grinding will inhibit the PCR – if small holes are visible that is OK).
6. Pipette with a 8-positions multi-pipette 25 -10 µL of extract into a storage plate (e.g., ABGene plate) and dilute with water with the same amount (2X), darker extracts can be diluted more.
7. Dispose the remaining extracts in the microtubes (caps do not close well so inverting the racks will make the liquid leak) and rescue the beads. Wash the beads with water and 70% EtOH overnight, let them standing in a tray overnight so that they are **PERFECTLY** dry before storing them in a FALCON tube.

DNeasy® Plant Mini Kit (QIAGEN protocol)

It is recommended to use the Kit (as detailed in Annex A of this thesis) to confirm the homozygous or heterozygous state of the plant lines.

PCR

After DNA extraction, measure DNA concentration with Nano Drop and perform the respective PCR.

The confirmatory PCR must have minimum 6 simultaneous reactions per mutant line:

1. Forward primer + T-DNA primer in **mutant** background.
2. Reverse primer + T-DNA primer in **mutant** background.
3. Forward primer + Reverse primer + T-DNA primer in **mutant** background.
4. Forward primer + Reverse primer in **mutant** background.
5. Forward primer + Reverse primer + T-DNA primer in **wild-type** background.
6. Forward primer + Reverse primer in **wild-type** background.

Primers Preparation

Primers Stock Solution 100µM
Primers Working Solution 10µM
DNA diluted 20x (1 µLDNA + 19 µL ddH ₂ O)

Materials and solutions

- 10x Dream Buffer
 - Dream *Taq* polymerase
 - dNTPs
- } (Transport on ice)
Found in 1.OG, in chemical room, fridge found at the end of the room
Need to take ice, labelled Epis, pipette, and tips
- 10µM Primers (Forward, reverse & LB)
 - DNA template of samples to be genotyped
 - PCR tubes
 - Autoclaved ddH₂O

Leave all chemicals on ice till used.

Method

1. According to amount of DNA template to be used (in this case 1 μ L is usually used), calculate the amount of ddH₂O to be added, so that the final volume per PCR tube is 10 μ L.
2. Pipette 1 μ L of 20x diluted DNA template into the PCR tube. Load DNA template into a 96-well plate.
3. Create MasterMixes, adding ddH₂O, buffer, dNTPs, primers and lastly, right before loading the master mixes into the 96 well-plates, the DreamTaq polymerase.
4. Pipette up and down to mix (do not vortex) – or mix by inverting.
5. Pipette 9 μ L of MasterMix into each PCR tube.
6. Select program on PCR machine.
7. Run PCR.

Reagent (Order)	Vol. 1 Rx. (μ L)	MasterMix (μ L) (X=no. of Rxs)
ddH ₂ O [1 MM]	5.7	= 5.7*X
10x Dream Buffer [2 MM]	1	= 1*X
dNTP (2mM) [3 MM]	1	= 1*X
DNA Template [6]	1	
Primer Fw (WS, 10 μ M) [4 MM]	0.4	
Primer Rv (WS, 10 μ M) [4 MM]	0.4	
Primer LB – depends on company (WS, 10 μ M) [4 MM]	0.4	
Dream Taq Polymerase [5 MM]	0.1	= 0.1*X
Total Volume	10	= Sum
Per Tube	7.8	

PCR Program

Temperature	Time	
94°C	5'	
94°C	30"	35 cycles
55°C	30"	
72°C	1'30"	
72°C	10'	
4°C	forever	

Duration of this PCR programme 01:42:30.

Either store PCR product in -20°C or load onto gel for electrophoresis immediately.

*Gel Electrophoresis**Materials*

- Agarose
- 1x TAE Buffer
- RedSafe

- PCR Product
- DNA Ladder

Procedure

- Measure 1% agarose and mix with 1x TAE Buffer.
- Heat in the microwave till dissolved completely (avoid overflow).
- Calculate volume of RedSafe and mix into slightly cooled gel. { see next for more details }
- Seal the edges of casting tray and prepare with desired number of combs/wells.
- Pour out the gel slowly into the casting tray, avoiding any bubbles. Pour until comb wells are covered but avoid over-filling. (If bubbles form, gently move to the side with a clean tip)
- Allow gel to cool down/solidify completely.
- Place the tray into the chamber filled with 1x TAE Buffer, make sure buffer covers the gel.
- Position the gel so that the wells are at the top, by the negative electrode.
- Load 8-20 μ L of PCR product into each well, in addition to 3-4 μ L of DNA ladder.
- After loading DNA, supply power (black -> red) [100 volt, around 45 mins for the big plate]
- Once the DNA has migrated enough, stop power.
{ this can be seen through the yellow tracking line, DNA is usually between yellow and blue line }
- Take tray on paper napkin to the picturing room.



Below are the expected results – according to SALK’s website



WT – Wild type
HZ – Heterozygote
HM – Homozygote

Keep homozygote and heterozygote lines, discard the rest.

Notes regarding gel preparation:

Volume of gel casting trays found in our lab:

- Small plate \approx 50mL Volume
- Medium plate \approx 100mL Volume
- Large plate \approx 160mL Volume

Calculate amount of RedSafe as follows:

(volume needed) x 20,000 = Final Volume

e.g. for small plate

0.0025 x 20,000 = 50mL

Gel Preparation Table

Gel tray Size	Small	Medium	Large
TAE(1x) Buffer	50mL	100mL	160mL
Agarose	0.5gm	1gm	1.6gm
RedSafe	2.5 μ L	5 μ L	8 μ L
Calculation	50mL/20,000= <u>0.0025 mL</u>	100/20,000 = <u>0.005 mL</u>	160/20,000= <u>0.008 mL</u>

TAE Buffer (1x)

20 mL TAE Buffer (50x) + 980 mL ddH₂O = 1L TAE Buffer (1x)

Genotyped and Confirmed Lines

Primers

#	Oligo Name	Sequence (5'->3')	Length
1	cc_AT3G13580_sgRNA1_For	ACCAGGTCTCAATTGGCTTTTCATTATCCGTATCCGTGTTTTAGAGCTAGAAATAGCAAG	60
2	cc_AT3G13580_sgRNA2_For	ACCAGGTCTCAATTGCTTATTTAACTCATTAGTAAGGTTTTAGAGCTAGAAATAGCAAG	60
3	cc_AT2G25210_sgRNA1_For	ACCAGGTCTCAATTGGATTCTCGTAGTTTGAATGATTGTTTTAGAGCTAGAAATAGCAAG	60
4	cc_AT3G02190_sgRNA1_For	ACCAGGTCTCAATTGGGCACTGGCGCCGTACCAAGCTGTTTTAGAGCTAGAAATAGCAAG	60
5	cc_AT3G05560_sgRNA1_For	ACCAGGTCTCAATTGACTTCAACATTGCTGAGAACGAGTTTTAGAGCTAGAAATAGCAAG	60
6	cc_AT3G13580_sgRNA1_Rev	TGGTGGTCTCTAAACAGACTGTTGTTCTCTGAGTCAGTCAATCTCTTAGTCGACTCTACC	59
7	cc_AT3G13580_sgRNA2_Rev	TGGTGGTCTCTAAACAGAAACAGGAGCTTGAGGCTGCCAATCTCTTAGTCGACTCTACC	59
8	cc_AT2G25210_sgRNA1_Rev	TGGTGGTCTCTAAACGATTTAGGGTTTCTCAGTGTTCATCTCTTAGTCGACTCTACC	59
9	cc_AT3G02190_sgRNA1_Rev	TGGTGGTCTCTAAACCTCTGTATCCTTTGTTCTATCTCAATCTCTTAGTCGACTCTACC	59
10	cc_AT3G05560_sgRNA1_Rev	TGGTGGTCTCTTACCATTGATTGTTCAAAGCCAAACCAATCTCTTAGTCGACTCTACC	59
11	uL30a_SALK_134960_F	TAAGGCTGCACCTTGAGAAGC	21
12	uL30a_SALKseq_084392_F	ATGATTGTGCATCCCTTTTGG	21
13	uL30a_SALKseq_62889_F	TTAGTCTGGTGGCAAAGTTG	21
14	uL30b_SAIL_1244_B01_F	CCTCTGGTGGTTAAGCTTTCC	21
15	uL30b_SALKseq_054635_F	TGAGCCCTATGTCACTTACGG	21

T-DNA Lines, Methods Compilation, FMS – KEE

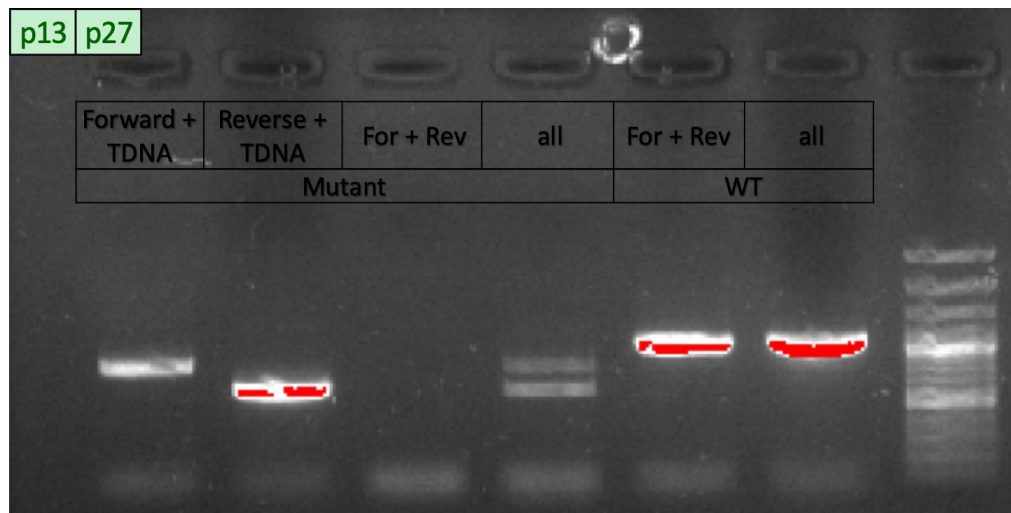
16	uL30c_SAIL_404_A06_F	CAAACACACAAGGAAACATCG	21
17	uL30_SALK_023212.42.90_F	TTTATCATTCTGATCCGTGGG	21
18	eL39_SALK_205605C_F	TCCCTTAGTGAACCTGTGTG	21
19	eL22a_GK_165G02_F	AAATCGCAAAGCCTTGAGAAG	21
20	eL22a_SALKseq_051552.0_F	ATTTGGGAAACCCATGAAGAG	21
21	eL22a_SAILseq_347_A04_F	AGCAAGGAGATTTGTGCTGAG	21
22	eL22b_GK_255C11_F	ATGGGCAAGTTTGAGTGTG	21
23	eL22c_SAIL_417_E10_F	TCGGATTTGTGATTATTCGG	21
24	eL22c_SALKseq_085507_F	ACATTGTACCAACCACCAACC	21
25	uL30a_SALK_134960_R	AACCTTAGGCTTCTCAATCG	21
26	uL30a_SALKseq_084392_R	TAAATTTGTTCCCTTTTCC	21
27	uL30a_SALKseq_62889_R	ATCATTCTTGCTGGTCACCAG	21
28	uL30b_SAIL_1244_B01_R	GCTCCACAGAGGTTAGTGTCG	21
29	uL30b_SALKseq_054635_R	TTTTAACCAACCAACCTCG	21
30	uL30c_SAIL_404_A06_R	GAACGAGTCCAACCTCACTGC	21
31	uL30_SALK_023212.42.90_R	ATTTCTAATGGATTGGTGGGC	21
32	eL39_SALK_205605C_R	TTTTCCGGTTAAAGGTAACCG	21
33	eL22a_GK_165G02_R	TGAGTCGGAACCACTCAATTC	21
34	eL22a_SALKseq_051552.0_R	TCAGAAGAACCAGATCGATG	21
35	eL22a_SAILseq_347_A04_R	CCACCAAAATCATACGACAGC	21
36	eL22b_GK_255C11_R	CAGACAAGCTCATCGTCTTC	21
37	eL22c_SAIL_417_E10_R	TCAACTGTACCAACCAACAAG	23
38	eL22c_SALKseq_085507_R	TCGGATTTGTGATTATTCGG	21
43	43_uL30d_SALK_114324_F	TAAGCCGGTTATTTTGTATCG	21
44	44_uL30d_SALK_133327_F	TTGGTTCACTAACTCTGTGATAG	26
45	45_eL39a_SAIL_140_D11_F	GATCGCAAGACTTCAAGATGG	21
47	47_eL39c_SALKseq_67765_F	GGCCTATTCCTACTGGATTC	21
48,49	48_49_uL3a-1/2_F	TTTCACGACAAAACCTTTTGCC	21
50	50_uL3a_SALK_019130C_F	CATCCCTTCTCTTCTTTG	21
51	51_uL3a_SALK_003794_F	TCTTCTTTGCGTGAATTCAC	21
52	52_uL3b_SALKseq_115704_F	TAAGAGGCTCTCAAGCTGG	21
54	54_uL3b_SALK_063314_F	CTCACAAGCTTCTGGTCAAGG	21
55	55_uL3b_GK-306C09_F	ATGAACACCAAGACAAGTCCG	21
56	56_rack1a_SALKseq_107_F	TCCACCAAAACACGAGAAATC	21
57	57_rack1a_SAIL_279_G02_F	TTTCGGCAGATGTACGTACTAC	22
58	58_rack1a_SALK_069083_F	TGTTGGTCTGTTATTGAAAATGTG	24
59	59_rack1b_rack1b-1_F	GAGACTCTGTCCGTATGGAG	21
60	60_rack1b_SAIL_413_B07_F	AGATTCTCCGGTAGCGAGATC	21
61	61_rack1b_SAIL_413_C07_F	GACCATCAGCTTCAGAGATGG	21
62	62_rack1b_WscDsLxHs031_F	TTCTCTGTTGCTGCACACAAC	21
63	63_rack1c_rack1c-1_F	CAGGGAGATGCTTTTGTGAG	21
64	64_rack1c_rack1c-2_F	TTAGGACTGAAGCAAAGCGAG	21
65	65_rack1c_SALK_015801_F	TAACACCATCTTCCACCAC	21
66,67	66_67_uL30d-1/2_R	CCTAGGAAATGGTCCACAAGTC	22
68	68_eL39a_SAIL_140_D11_R	AGGGAAAAGGTGCAATTTGAG	21

T-DNA Lines, Methods Compilation, FMS – KEE

70	70_el39c_SALKseq_67765_R	GGAAGGACTGGTCCTTCATTC	21
71	71_uL3a_SK14764_R	TCACTGATAAACCAACAACAACG	23
72	72_uL3a_GK-102F09_R	AAGACTCACCTTTCTCTGTG	22
73,74	73_74_uL3a-3/4_R	GCAATGGTACCACCATTGATC	21
75	75_uL3b_SALKseq_115704_R	AAAGGGCTGAAGCAGAAGAAG	21
77	77_uL3b_SALK_063314_R	TTGGTGTACCAAAGGAAAAG	21
78	78_uL3b_GK-306C09_R	TTCCAAGGAAAAGAGCTAGCC	21
79	79_rack1a_SALKseq_107_R	CTGAAGCAAAGAGCATGGATC	21
80	80_rack1a_SAIL_279_G02_R	CTGAATCTGACGCAGCTAACCC	21
81	81_rack1a_SALK_069083_R	GCCCATTTCCGATTTCTTATC	21
82	82_rack1b_rack1b-1_R	GATTTGGCTGAAGGGAAGAAG	21
83	83_rack1b_SAIL_413_B07_R	CACCAAAAACCCTTCCTAAGG	21
84	84_rack1b_SAIL_413_C07_R	TGATTCGTTCCGGTTTGAAAAG	21
85	85_rack1b_WscDsLxHs031_R	TCTCGGTAGAGTTCTCATGGG	21
86	86_rack1c-1_R	TGGTTGTGTGCTGCTACTGAG	21
87,88	87_88_rack1c-2/3_R	ACTGTGTGCTGTGCACCTCAC	21
89	2x_SALK_084392_F	TTTAGGGTTTTGAGTGGGGTC	21
90	5x_SALK_054635_F	TATTTAAGCCGGAAGCTCAGG	21
91	19x_SAIL_347_A04_F	CTGAATCATTCCGCAATATGC	21
92	55x_SALK_015801_F	TGGAAGATGCATAGGACAAATC	22
93	2x_SALK_084392_R	GTGTTGTTAATTGCGGATGG	21
94	5x_SALK_054635_R	GTTGTCTTCGAGACTTCGTGG	21
95	19x_SAIL_347_A04_R	AAAAATTCAAGTTATGTCATATGCG	25
96	55x_SALK_015801_R	TCAAGGAGAGGAACGATGATG	21

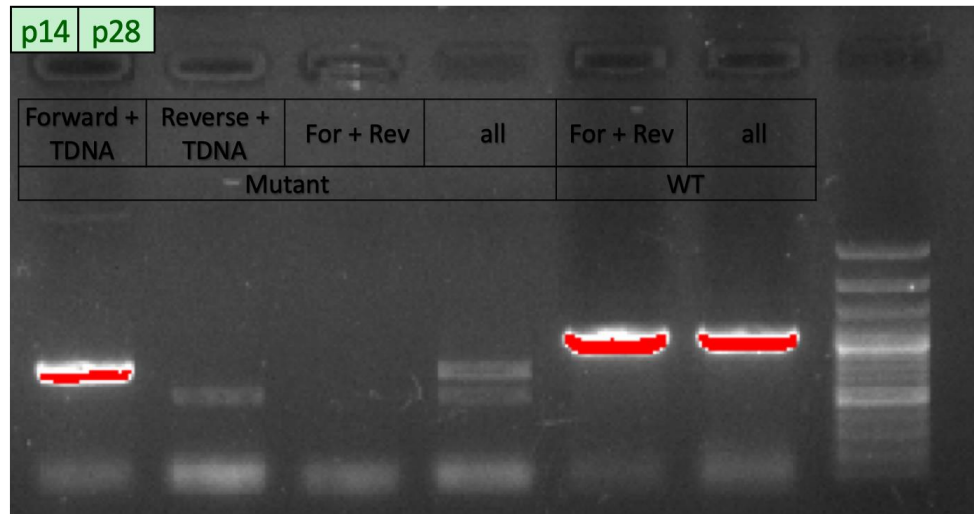
uL30A

L1 - uL30_rpl7a-1; Plant No. 419



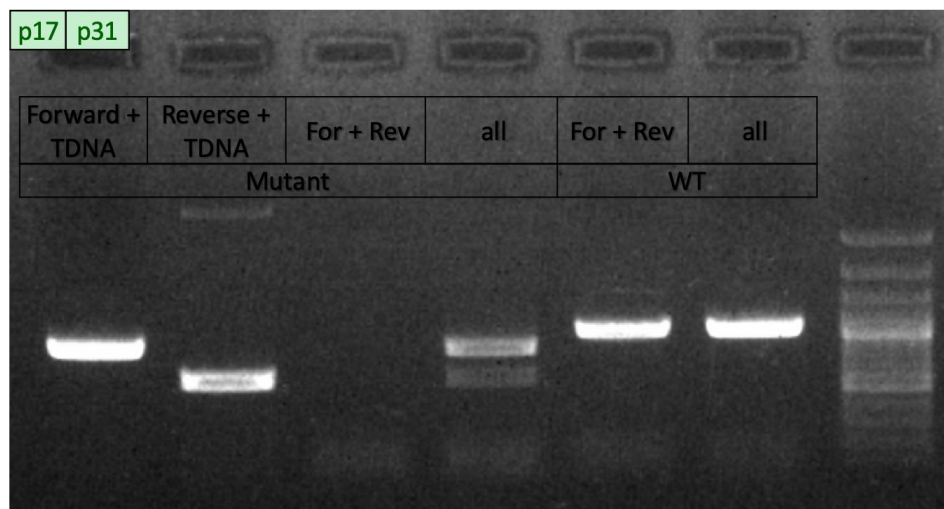
uL30B

L4 - uL30_rpl7b-1; Plant No. 321



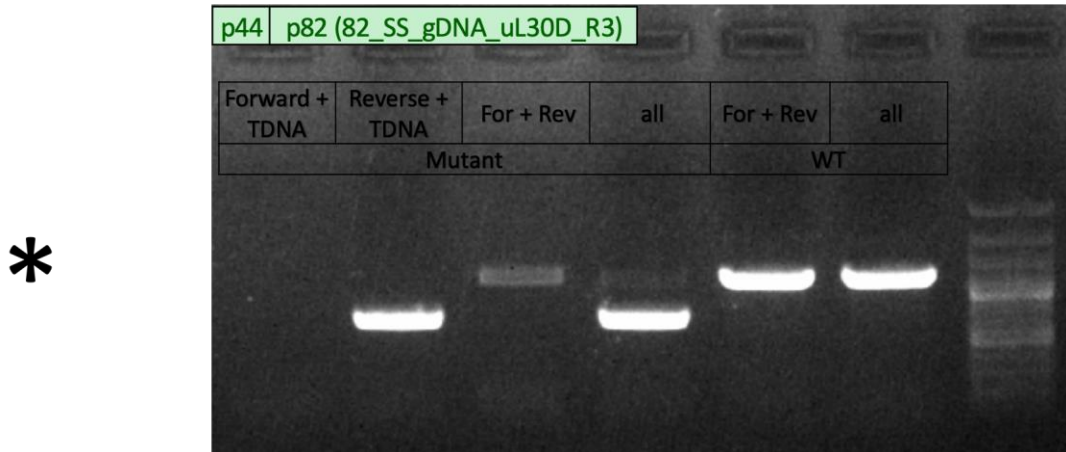
uL30C

L7 - uL30_rpl7c-2; Plant No. 282



uL30D

L8 - uL30_rpl7d-1; Plant No. 409 (heterozygous)



*heterozygous

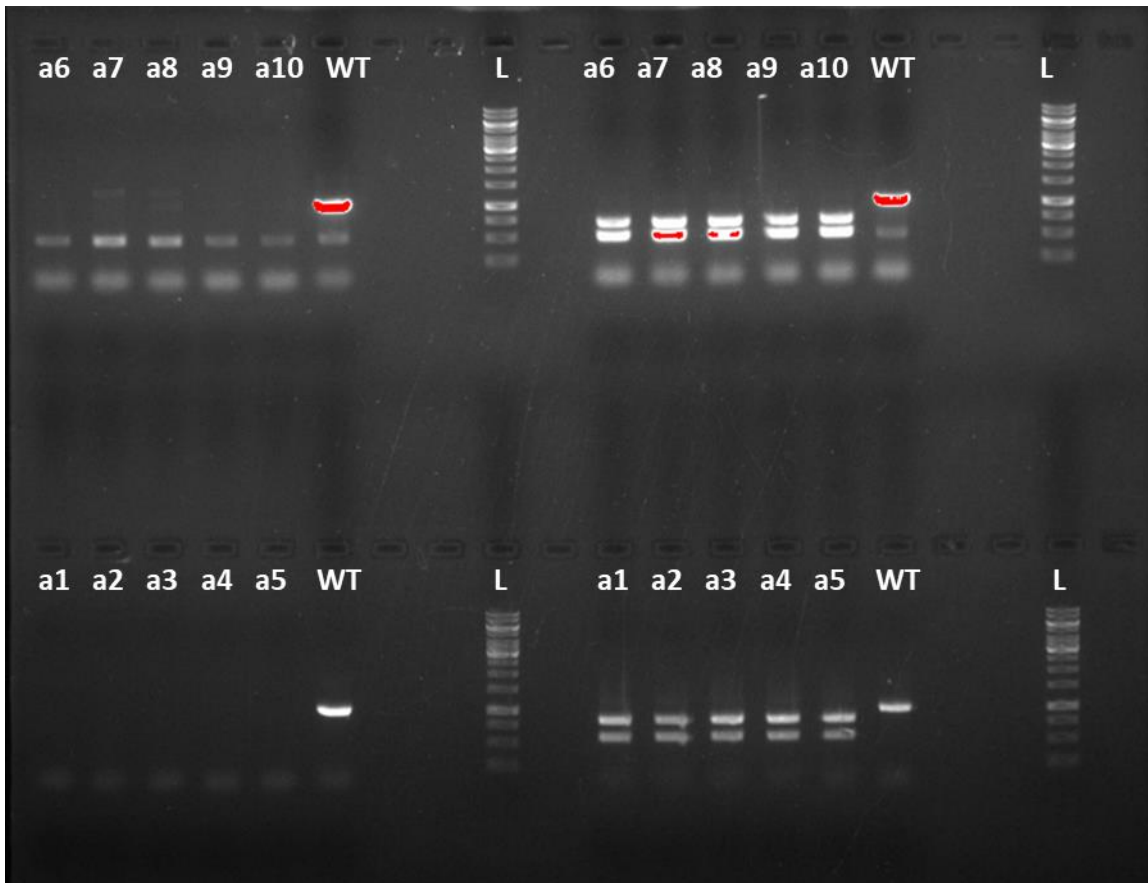
Confirmation of multiple plants per line

Reagent	Vol. 1 Rx. (μL)	MMX- WT MasterMix (μL) (X=no. of Rxs)	MMX' - HoZ or HeZ MasterMix (μL) (X=no. of Rxs)
ddH2O [1 MM]	5,7	57	57
10x Dream Buffer [2 MM]	1	10	10
dNTP (2mM) [3 MM]	1	10	10
DNA Template [6]	1		
Primer Fw (WS, 10μM) [5 MM]	0,4	4	4
Primer Rv (WS, 10μM) [5 MM]	0,4	4	4
Primer LB – depends on company (WS, 10μM) [5 MM]	0,4		4
Dream Taq Polymerase [4 MM]	0,1	1	1
Total Volume	10		

Line#	F	R	LB	MasterMix	Plant_ID_No.
L1 - uL30_rpl7a-1	p13	p27		MM1	B3 a37 - a41 (39)
L4 - uL30_rpl7b-1	p14	p28	Sail (p40)	MM2; MM2*	B1 a6 - a10; B3 a49 - a53
L7 - uL30_rpl7c-2	p17	p31	Salk (p39)	MM3	B1 a1 - a5
L8 - uL30_rpl7d-1	p44	p82 (82_SS_gDNA_uL30D_R3)	Salk (p39)	MM4; MM4*	B2 a13 - a17; B3 a43 - a47
WT					a11 -a12

uL30B and uL30C

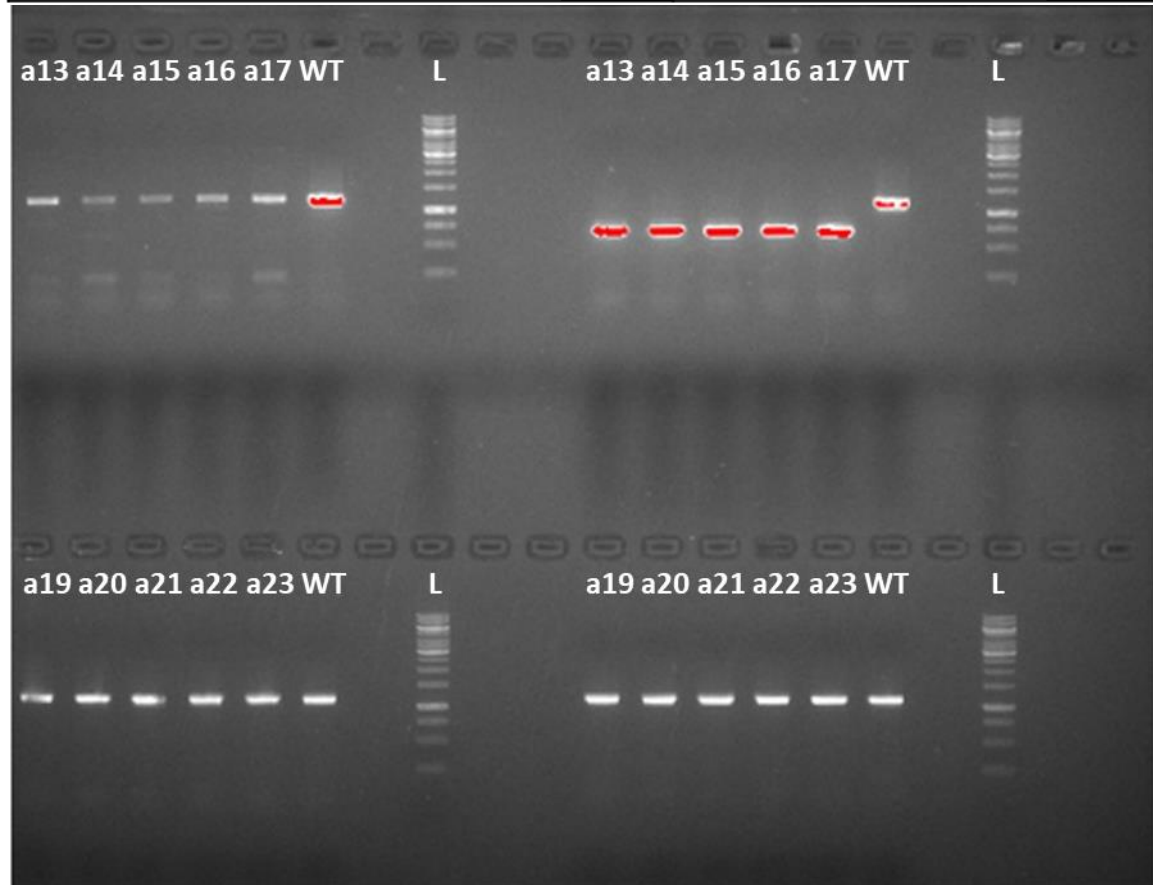
Batch 1: Gel													
2	2	2	2	2	WT	L	2'	2'	2'	2'	2'	WT	L
a6	a7	a8	a9	a10	a12		a6	a7	a8	a9	a10	a12	
HoZ	HoZ	HoZ	HoZ	HoZ			HoZ	HoZ	HoZ	HoZ	HoZ		
3	3	3	3	3	WT	L	3'	3'	3'	3'	3'	WT	L
a1	a2	a3	a4	a5	a12		a1	a2	a3	a4	a5	a12	
HoZ	HoZ	HoZ	HoZ	HoZ			HoZ	HoZ	HoZ	HoZ	HoZ		



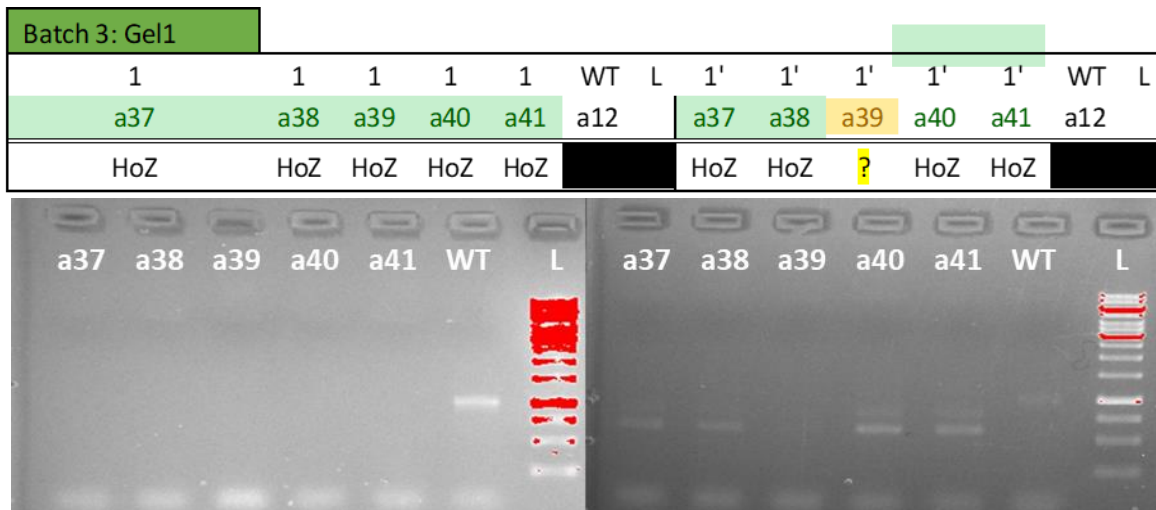
uL30D

Batch 2: Gel1

4	4	4	4	4	WT	L	4'	4'	4'	4'	4'	WT	L
a13	a14	a15	a16	a17	a12		a13	a14	a15	a16	a17	a12	
HeZ	HeZ	HeZ	HeZ	HeZ			HeZ	HeZ	HeZ	HeZ	HeZ		
5	5	5	5	5	WT	L	5'	5'	5'	5'	5'	WT	L
a19	a20	a21	a22	a23	a12		a19	a20	a21	a22	a23	a12	
?	?	?	?	?			?	?	?	?	?		



uL30A



Appendix C

Extended Methods

EXPERIMENTAL DESIGN	3
Growth chambers for hydroponics	3
EXP1: Labeling after ¹⁵N ammonium nitrate feeding	4
EXP2: Labeling after ¹⁵N amino acids feeding	5
Conditions and alternatives to consider	6
EXP2.1.2: Optimization of ribosomal shotgun proteomics	6
EXP2.1.3: Targeted double labelling and RP-turnover calculation	6
EXP2.1.4: Targeted N labelling (GLY-SER) and RP-turnover calculation	6
EXP2.1.5: Ammonium nitrate and potassium nitrate labelling in Hoagland medium	6
WET-LAB	7
Seeds management - Surface disinfestation	7
Seeds management – Sowing	7
MS-Medium for plant rearing	8
Hoagland solution for plant rearing	10
Tissue harvesting	13
Relative growth rate calculation	14
Metabolite extraction	15
Metabolite derivatization	16
Gas chromatography – time of flight – mass spectrometry	16
Gas chromatography – atmospheric pressure chemical ionization – mass spectrometry	17
Internal Standards	17
Total native protein concentration	17
Native extraction buffer	17
Nano drop protein content measurement	18

Extended Methods – FM-S

Western blot	18
Casting of SDS-PAGE gels (running or resolving gel 12%, stacking gel 5% polyacrylamide).	19
Loading of the proteins to SDS-PAGE gels: transfer the proteins into PVDF membrane and overnight block with 5% skim milk.	20
Binding the antibodies and visualizing the protein with the G-box.	21
¹⁵N Enrichment of Ribosomal Proteins (from Exp2_1_4)	22
Purification of Ribosomal Subunits	22
Measurement of Enriched Proteinogenic Amino Acids (GC-ToF-MS)	22
Label-assisted Ribosomal Proteomics	23
Measurement of Enriched Peptides (LC-MS/MS)	23
MALDI tissue imaging	24
Chemical cross-linking reaction in vivo	26
DRY-LAB	27
Data analysis of enrichments and labelled metabolite pools	27
Pre-processing of the chromatograms	27
TagFinder processing of ¹⁵ N Labelling experiments	27
Data mining for targeted compounds	33
TagFinder assisted annotation	33
Direct targeted search	34
Primary metabolites	34
N-containing compounds	34
Percentage of enrichment calculation using CORRECTOR	35
Data fixing assumptions	36
Statistical comparison of treatments	36
REFERENCES	39

Extended Methods – FM-S

All the materials, including their country of origin, used in this supplement have been detailed in the methods sections from the individual chapters embedded in this thesis except in Chapter 8, for which I report in this supplement each reagent comprehensively. Beyond Chapter 8, this supplement is meant just as a procedural step-by-step laboratory guideline to enhance reproducibility of all the methodologies used in this thesis.

Experimental design

Growth chambers for hydroponics

- Let the system (picture below) acclimate for one hour in the chamber before recording the temperature.
- Measure all growth chambers (e.g., phytotron 27th, Percival 06 and cold chamber)
- Use one of the hydroponic systems left from RGR to measure this so that the conditions are identical to those of the growing plants.

Example: Percival 06 set to 31°C and 40 μ E of light intensity for sterile cultivation is really at 30°C day night 16/8 hours, with an effective light intensity into our hydroponic systems of \sim 30 μ E:

System to measure temperature



Night Percival 06



Day Percival 06



EXP1: Labelling after ¹⁵N ammonium nitrate feeding

Arabidopsis thaliana Col-0 accession plants were grown until >1.10 morphological stage (Boyes, 2001) inside a phytotron at 20°C/18°C 16hours/8hours day/night cycle. The plants were grown in sterile glass containers with a metal mesh incorporated for support. The hydroponic reared plants were established in liquid MS medium where the solely nitrogen source was ammonium nitrate. The plants were transferred to containers where ammonium nitrate was labelled with ¹⁵N stable isotope after reaching the desired morphological stage. The experimental design consisted of three factors: Harvesting time (0, 1, 3, 7 days); fed solution (0; 0,5; 0,8 mM ¹⁵NH₄¹⁵NO₃ 98% Sigma Aldrich) and temperature treatment (20, 10 °C). The initial temperature was 20°C/18°C

day/night cycle. Three replicates were done per treatment. Per definition the plants collected at 0 hours were not replicated for the different feeding regimes and temperature treatments. Therefore 57 vials per tissue were collected, each vial containing the shoots or roots from 4 pseudo-replicated individuals.

EXP2: Labelling after ^{15}N amino acids feeding

Amino acids with known ^{15}N -abundance were used to boost enrichment of metabolite pools during the optimization of the enrichment methodology. Amino acids such as Alanine, aspartic acid, glutamic acid and phenylalanine with known isotopic abundances can be purchased; these monomers can also serve as internal standards. Amino acids were mixed with the feeding solution at known ratios. As with previous samples, harvested tissue was derivatized and analyzed with GC/MS.

Arabidopsis thaliana Col-0 accession plants were grown until before 1.10 morphological stage (Boyes, 2001) inside a phytotron at 20°C/18°C 16hours/8hours day/night cycle. The plants were grown in sterile glass containers with a metal mesh incorporated for support. The hydroponic reared plants were established in liquid MS medium where the solely nitrogen source was ammonium nitrate. The plants were transferred to containers where ^{15}N labelled amino acids were added at a concentration of 0.5mM in addition to non-labelled ammonium nitrate (The treatment designed as Mix contained 0.3mM of GLU instead of 0.5mM in both labelled and non labelled version); the transference was done after the plants reached the desired morphological stage and the labelling was done during three days before tissue harvesting. The experimental design consisted of these factors: fed solution, 8 levels (0,5 mM NH_4NO_3 + non-labelled Glutamate, Serine, Alanine or a mix of the 3; 0,5 mM NH_4NO_3 + labelled Glutamate, Serine, Alanine or a mix of the 3 [every time 0,5mM per amino acid]); temperature, 2 factors (20, 10 °C); one time regime (3 days). Three replicates were done per treatment. The tissue was collected in 20ml vials; each containing the shoots or roots from 8 pseudo-replicated individuals. 16 treatments * 3 replicates + 3 controls = 51 hydroponic systems each with 9 plants; 0,25 L per glass container; 18 L of medium in total.

The design was based on the results obtained from the soluble amino acid pool analysis. The previous experimental design consisted of three factors: Harvesting time (0, 1, 3, 7 days); fed solution (0; 0,5; 0,8 mM $^{15}\text{NH}_4^{15}\text{NO}_3$ [98% Sigma Aldrich]) and temperature treatment (20, 10 °C). According to our results, time 3 and 7, as well as concentrations 0,5mM and 0,8mM did not show significant differences in the percentage of enrichment but in both cases significant enrichment was found. Pragmatically it made more sense to use time point 3 (days) and feeding regime with 0.5 mM concentration of labelled ammonium nitrate. Three factors were tested: Organ (Shoot and root), Temperature (10, 20 °C) and Ribosomal subunit.

Conditions and alternatives to consider

- When harvesting the tissue, the roots were washed with non-labelled medium in order to wash out the ^{15}N labelled amino acids that were still outside the roots, since these labelled amino acids would be considered contamination in the results.

EXP2.1.2: Optimization of ribosomal shotgun proteomics

36 hydroponic systems were harvested, 3 pools of 12 hydroponic systems each were considered a biological replicate. This procedure allowed us to have enough tissue for repeated technical replicates and potential failure, which was the ideal situation enabling the optimization of the shotgun proteomics experimental protocol.

EXP2.1.3: Targeted double labelling and RP-turnover calculation

54 hydroponic systems were harvested, three temperatures were tested (i.e. 10°C, 20°C, 30°C). Half of the samples were treated as a control (i.e. non-labelled amino acid was added to the media in the same concentration as the treatment) and half were labelled with ^{15}N -SER+ ^{13}C -GLY [0.05 mM]. Three biological replicates per treatment consisting of the root tissues of 3 pooled hydroponic systems. This procedure allowed us to get enough tissue to perform the following analyses: Enrichment dynamics in the soluble amino acid fraction, label incorporation in total ribosomal protein fractions after hydrolysis and labelled-assisted shotgun proteomics of ribosomal fractions; the tissue needed was 60mg, 100mg and 100mg respectively.

In parallel 24 hydroponic systems were used to calculate the relative growth rate of our treated vs non-treated plants. This variable allowed us in addition to the protein content to calculate protein turnover at the individual RP level.

EXP2.1.4: Targeted N labelling (GLY-SER) and RP-turnover calculation

Same as 2.1.3, but label was introduced as amino acids in ammonium nitrate free MS media, plants were grown until shifting in ammonium nitrate containing media.

EXP2.1.5: Ammonium nitrate and potassium nitrate labelling in Hoagland medium

Same as 2.1.3, but label was introduced in 6 mM KNO_3 , 0.5 mM NH_4NO_3 .

Wet-Lab

Seeds management - Surface disinfestation

1. Put aliquots from seed accessions in 1.5 ml Eppendorf tubes.
2. Add 995 μ L EtOH (70%) + 5 μ L Triton-x-100 per seed sample.
3. Mix for 20 minutes the tubes laying down horizontally taped to the surface of the thermomixer (800 RPM with no T° in thermomixer Eppendorf).
4. Spin samples at max speed for 2 minutes and remove supernatant,
5. Add 1ml 95 or 100% EtOH and shake for 10 minutes; spin down at max speed and go to down flow cabinet.
6. Wash 6 times with sterile water, after last one leave water inside.
7. If needed imbibe seeds overnight in water under complete darkness.
8. Otherwise, pour the seeds into autoclaved filters inside the down flow cabinet and wait until all the EtOH residues + H₂O has dried out for manual sowing
9. Sow the seeds in agar MS-media containing square petri dishes (more than 12*12 per dish), sow allowing an even amount of agar between seeds because you will transfer them later with agar to the hydroponic systems.
10. Stratification: store the petri dishes for five days covered with aluminium foil at 4°C.

Seeds management – Sowing


1. Put a metallic mesh circular cut with bent corners inside a glass container and autoclave.
2. Prepare liquid MS medium, Micro 8.0, Sucrose 2.
3. Pour the medium inside the glass containers until it is in contact with the metallic mesh. Procedure must be done inside a sterile down-flow cabinet.
4. Place pieces of MS agar medium on top of the mesh. 1 piece per desired plant. Place seeds on top of the agar pile.
5. Use sterile tools to manipulate seeds inside the down-flow cabinet.
6. Transfer glass containers into desired phytotron with pre-set conditions until desired physiological stage.
7. Label bash with your name, Group name, Name abbreviation (if used on culture), Date, GMO name, LIMS construct ID.

Extended Methods – FM-S

MS-Medium for plant rearing

pH 5.7-5.8 Murashige & Skoog Medium No.4 (Micro and Macro elements, NH₄NO₃-Free).

Composition

Micro Elements	mg/l	μM
CoCl ₂ .6H ₂ O	0.025	0.11
CuSO ₄ .5H ₂ O	0.025	0.1
FeNa-EDTA	36.7	100
H ₃ BO ₃	6.2	100.27
KI	0.83	5
MnSO ₄ .H ₂ O	16.9	100
Na ₂ MoO ₄ .2H ₂ O	0.25	1.03
		
ZnSO ₄ .7H ₂ O	8.6	29.91
Macro Elements	mg/l	mM
CaCl ₂	332.02	2.99
KH ₂ PO ₄	170	1.25
KNO ₃	1900	18.79
MgSO ₄	180.54	1.5

Materials and Constituents

Constituent Amount (gr)	Final Volume (mL)					
	5000	4000	3000	2000	1000	500
MS	22	17.6	13.2	8.8	4.4	2.2
MES	2.5	2	1.5	1	0.5	0.25
Saccharose	100	80	60	40	20	10
<i>Micro Agar*</i>	40	32	24	16	8	4

*Only for sowing seeds, petri dishes.

Beaker, magnetic stirrer, pH-Meter, Balance.

Preparation of Solution:

- Dissolve all constituents in a large Beaker or Erlenmeyer with a magnetic stirrer;
- To use the pH-meter: Verify calibration; Adjust pH at 5.7-5.8 with addition of KOH (10%); Autoclave;
- Store at 4°C until used, Organic solutions in general are recommended to not be stored more than 2 weeks.

References: Schlesier, B., Bréton, F. & Mock, HP. Plant Mol Biol Rep (2003) 21: 449.
<https://doi.org/10.1007/BF02772594>.

Examples of Amino Acid Supplementation

Compound	g/mol	g/mmol	g/ 0.5 mmol	mg per 0,5 mmol
Glutamate L	148.1200	0.1481	0.0741	74.0600
Glycine L(3x ¹³ C)	77.0500	0.0771	0.0385	38.5250
Serine L	106.0900	0.1061	0.0530	53.0450
Proline L	116.1200	0.1161	0.0581	58.0600
Alanine L	90.0900	0.0901	0.0450	45.0450
Valine L	118.1400	0.1181	0.0591	59.0700
Glutamate NL	185.2000	0.1852	0.0926	92.6000
Glycine NL	75.0600	0.0751	0.0375	37.5300
Serine NL	105.0900	0.1051	0.0525	52.5450
Alanine NL	89.0900	0.0891	0.0445	44.5450

Extended Methods – FM-S

	Final Volume (mL) [0.5 mM]				
Compound (mg)	5000	4000	3000	2000	1000
Glutamate L	370.30	296.24	222.18	148.12	74.06
Glycine L(3x ¹³ C)	192.63	154.10	115.58	77.05	38.53
Serine L	265.23	212.18	159.14	106.09	53.05
Proline L	290.30	232.24	174.18	116.12	58.06
Alanine L	225.23	180.18	135.14	90.09	45.05
Glutamate NL	463.00	370.40	277.80	185.20	92.60
Glycine NL	187.65	150.12	112.59	75.06	37.53
Serine NL	262.73	210.18	157.64	105.09	52.55
Alanine NL	222.73	178.18	133.64	89.09	44.55

Hoagland solution for plant rearing

Title: Procedure for the preparation of Hoagland’s nutrient solution for hydroponic studies

Reference: Hoagland and Arnon, 1950

Citation: Hoagland, D.R. and D.I. Arnon. 1950. The water culture method for growing plant without soil. California Agri. Exp. Sta. Cir. No. 347. University of California Berkley Press, CA., pp: 347.

Reagents: See table given below Procedures:

Stock Solution

- Take 6 plastic bottles and wash them thoroughly. Label each bottle from 1 to 6 or as desired (as shown in column 1 of the table)
- Prepare molar solution of macro-nutrients and mM solutions for micro-nutrients by dissolving the quantity given in the “Amount required for SS” column
- Put each nutrient stock solution in a separate bottle. All macro-nutrients will be combined in one bottle. Do not mix unless needed because it would precipitate quickly 4. Store in a refrigerator at 4°C

Extended Methods – FM-S

These calculations are per litter basis. To calculate a different molarity, you will need to recalculate the given quantities

Working solution:

- Take one litter of water (tap or distilled) in an open container
- Use the given quantity of stock solution from each bottle as shown in “Volume of stock solution per litter of final solution” of the table e.g. you would need 6 ml of KNO₃ from bottle 1 per litter of water
- If you wish to prepare the half strength Hoagland’s nutrient solution, simply double the quantity of tap water (i.e. 2 L) OR use half quantity of stock (e.g. 3 ml of KNO₃ per litter)

Precautions:

For stock solution:

- Preferably, use laboratory grade salts to prepare stock solutions. Commercial grade salts precipitate and yields poor results.
- Keep each stock solutions in a separate bottle and do not mix before use
- Keep the stock bottles air locked/tightly sealed
- Never mix concentrated stock solutions before use
- Never use STOCK solution if you observe any precipitation in the stock bottle
- The shelf life of stock solution is about 6 months unless any precipitation occurs earlier.

For working solution:

- Freshly prepare working solution just before use by mixing the given quantity as shown in tables below.
- Never apply working solution if any precipitation is observed in the dilution container.
- Never store the working solution more than 3 days.
- Check the pH of working solution, and if necessary adjust to pH 5.8 to 6.3 with 1M KOH or HCl. If you do not want to change the K concentration then you can use NaOH but it will add Na.
- pH of nutrient solution: Depending on the nature of growing media, the pH of nutrient solution is altered over-time (mostly turns acidic). For example, in sand it goes acidic over a week or so. It may cause alterations in nutrient availability that is observed as leaf chlorosis. It is suggested to periodically replace the nutrient solution by completely draining by tap/distilled water once a week and replace with fresh nutrient solution.

Tip: If precipitation occur during addition of stock solutions to water, try adding MgSO₄ at end (Bottle number 4)

Non-Labelled

Table of Elemental Concentration in Stock and Working Solutions

Sr. #	Macronutrients (M)	M. Wt.	M of SS	Amount required for SS	Volume of Stock solution per litter of final solution	Element
1	KNO ₃	101.1	1	101.1	6 mL/L of water	K, N
2	Ca(NO ₃) ₂ .4H ₂ O	236.16	1	236.16	4 mL/L of water	Ca, N
3	(NH ₄) ₂ PO ₄	115.08	1	115.08	2 mL/L of water	N, P
4	MgSO ₄ .7H ₂ O	246.49	1	246.49	1 mL/L of water	Mg, S
5	Micronutrients (mM)	(all in one bottle)			1 mL/L of water	
	KCl	74.55	50	3.7275		K, Cl
	H ₃ BO ₃	61.84	25	1.546		B
	MnSO ₄ .H ₂ O	169.01	2	0.33802		Mn, S
	ZnSO ₄ .7H ₂ O	289.55	2	0.5791		Zn, S
	CuSO ₄ .5H ₂ O	249.71	0.5	0.124855		Cu, S
	H ₂ MoO ₄ (85% MoO ₃)	161.97	0.5	0.080985		Mo
6	Fe-EDTA	346.08	20	6.9216	1 mL/L of water	Fe

The composition is altered for Labelled medium → the calcium source is calcium phosphate that is only soluble in extreme acid (approx. 6M HCL), hence this was the first nutrient added to the medium. Afterwards pH was set to 5.8 and the other nutrients were added. For the non-labelled version ammonium carbonate had to be used instead of ammonium nitrate, this addition did not alter the pH of the medium.

Tissue harvesting

The tissue was harvested and instantly frozen in liquid nitrogen. The plants were divided in shoot and root tissue. Each sample represented a pool from n plants reared inside the same container (i.e., pseudo-replicates). The samples formed crystals due to the MS growth medium present while harvesting the tissue. Samples were grounded with mortar and pestle, preventing temperature to rise. The samples were kept during the entire time in liquid nitrogen. Subsequently the samples were weighted. 60 or 100 mg per sample were deposited in a labelled 2ml Eppendorf vial. Samples were stored at -80°C.

The metabolites were extracted from the samples. After centrifugation the supernatant was used for primary metabolome and soluble amino acids analysis; the pellet was reserved at -20 °C for protein hydrolysis and total proteinogenic amino acid analysis if necessary. The proteinogenic amino acids were analyzed after enrichment of the soluble fractions was confirmed, especially soluble amino acids. Enrichment would be an indication of possible label incorporation into internal pools and peptides.

Harvesting:

1. Harvest first the non-labelled samples (NL) to prevent contaminations from stable isotopes in the controls.
2. There are three temperature chambers:
 - a. Phytotron 27 at 20°C/18°C
 - b. Percival # 6 at 30°C/30°C
 - c. Cold chamber at 10°C/10°C
3. Each chamber contains 12 labelled and 12 non-labelled hydroponic systems to harvest
4. **One** biological replicate is pooled plants from three (3) hydroponic systems and hence there are 4 labelled and 4 non-labelled biological replicates per temperature.
5. Harvest shoots and roots separately, making sure to have paired tissue in the vials.
6. In the end you will need 16 harvesting tubes per temperature; 48 in total.
7. Harvesting procedure:
 - a. Take all the material to phytotron 27 in a trolley
 - b. Cover a styropor box with a layer of aluminium foil and a carton grid that is able to hold the size of the tubes (it is in our [2.217] lab below the sink)
 - c. Fill your box with liquid nitrogen and wait until cold; then place the open vials in the holes of the carton grid.
 - d. Take one hydroponic system at a time out of the traits were the plants are growing and place it in the trolley.
 - e. Remove the glass cap and with a pincet grab one plant, with your spare hand grab the shoots and tighten with the pincet in the root area until removing.

- f. Place first the roots rapidly in the vials and only then the shoots (roots must be harvested as rapid as possible because they are our main biological target)
 - i. If roots are labelled wash them in non-labelled spared Hoagland medium (pour in one glass jar, the medium is in the 4°C room).
 - ii. If the roots are non-labelled freeze them directly after removing.
 - g. Only take one hydroponic system at a time.
 - h. Take the trolley always next to the growing chambers in order to prevent additional stresses caused by moving the plants too much.
8. In the end, the 48 tubes that have remained in liquid nitrogen the whole time will be transferred to carton boxes and stored at -80°C.
 9. Pour a bit of liquid nitrogen into the boxes before taking out the vials to prevent rising of temperature while you fill the boxes with vials.
 10. **Never** put liquid nitrogen inside the vials while harvesting or they will explode when you take them out.

Relative growth rate calculation

A Sartorius BP210S balance was used for weighing everything. Plants were withdrawn from the hydroponic system. Roots were dried with filter paper three times in a short time period (26 seconds) and the agar bits were removed as thoroughly as possible without compromising the timing of the weighting. After dried, the plants were immediately placed inside wax-layered bags (i.e. oven-compatible tissue) and weighted. The difference between the empty “room ambient” bags weight and the full ones represents the fresh weight. Subsequently the bags were dried at 70°C for three days. After dried, the bags were taken out from the oven in a desiccator full of silica to prevent hydration. The bags were left 1 hour inside the desiccator in order to stabilize the temperature. The bags were subsequently weighed in the same balance. The difference between the empty “dry ambient” bags and the full ones represents the dry weight. Room ambient is defined as the weight of the bag immediately before starting the harvesting of the tissue. Dry ambient is defined as the weight of the bag after one day of drying at 70°C completely empty (this must be done before everything since after drying the plant tissue will stick to the bag walls). In order for the weights to be reproducible, the balance should be placed in the measuring area one day before weighting in order for the inner components of the scale to be temperature adjusted. Similarly, when taking bags out of the oven, they need to remain inside the desiccator approximately one hour until temperature equilibrates to room temperature. Small-scale metal objects were used to build a calibration graph in order to determine the reproducibility of the weights in different locations. The empty bags should be folded before weighting. Small imperceptible movements of the empty bags will not allow the weight to settle; instead, it will decrease for long time lapses increasing to unfeasible the waiting task.

Validation of fresh weight to calculate legitimate RGRs in our system: In order to validate FW after our treatment induction the ratios between FW and DW must remain constant. Otherwise, dry weight must be always used as input when aiming RGR calculation since DW is directly related to ribosome function.

Metabolite extraction

1. Sample plant material in 2ml Eppendorf tubes (round bottom-shaped). Define the exact mass of plant sample (60mg +/- 5 mg fresh weight for leaves or shoots); document the fresh weight of each sample. Shock-freeze each sample in liquid N₂ before determination of sample mass. Sample empty micro vials and use for non-sample controls. Make sure to include a set of non-treated control samples in order to screen for relative changes of metabolite levels. Provide 8 – 16 samples of each condition to be analysed. Do replications at the level of individual plants. Pooling of samples from a set of plants and replicate analyses of this pool is possible but less informative.
2. Homogenize with a Retschball mill, 3 min at 15 Hz of vibrational frequency. Take care that sample remains frozen.
3. Generate PreMix from steps 4-6 and aliquot 360µL of PreMix.
4. Add 300µL 100% Methanol, pre-cooled to -20°C, vortex. Most enzymatic activity stops.
5. Add 30µL stock nonadecanoic acid methylester (2mg/ml Stock in CHCl₃) for quantitative internal standardization of the lipid phase. Or in its absence, supplement premix with 30µL chlorophorm
6. Add 30µL of a pre-mixture made from sorbitol (used for quantitative internal standardization for the polar phase), d4-alanine, D- (-)-isoascorbic acid and any stable isotope labelled internal standard of special interest, vortex. The internal standards may also be included in the methanol solvent used for extraction (refer to 3). (Concentrations: sorbitol 0,2mg/ml in MeOH, d4-Alanine (2,3,3,3) 1mg/ml in H₂O). Or in their absence add 30µL more of methanol.
7. Shake 15 minutes at 70°C, 1000 RPM in a thermomixer. After approximately 1 minute of incubation, open the micro vials for a short moment to relieve the build-up of gas pressure. Let cool down samples to room temperature.
8. Add 200µL of CHCl₃.
9. Shake 5 minutes at 37 °C at 1000 RPM in a thermomixer.
10. Add 400µL H₂O, vortex.
11. Centrifuge 5 minutes at 20,800 rcf.
12. Transfer two 160µL-aliquot from the upper polar phase to 1.5ml tapered Eppendorff-tubes.
13. Dry in the SpeedVac overnight, without heating.
14. Store samples, backups and pellets at -20 °C

In case doing the extraction within several batches/days, prepare each day the amount of non-sample controls corresponding to biological replicates.

Metabolite derivatization

1. Protocol started in the morning, so that the GC-TOF-MS could be started at midday.
2. Make sure that the reference and treated samples are stored in the same bag at -20°C. When processing bags from the freezer wait for temperature equilibration and remove moisture before opening the bag.
3. Prepare one empty vial with all solutions as wash.
4. Additional QC-K (Blank tubes with extraction procedure) and MM (multimix 100 metabolites as standards) calibration mix.
5. Add 40 µL Methoxyaminhydrochlorid {e.g. 5mg/ml 4-dimethylaminopyridine [15mg DMAP] + 40mg/ml MeOX [120mg]} and solve in 3ml pyridine} to the dried aliquot and vortex after each step.
6. Shake 1.5h at 30°C (950 RPM in Thermomixer Eppendorf)
7. **OPTIONAL:** Add 10µL of alkan-mixture to the polar phase (stored at -20°C, pre-heat solution for 5 minutes at 70°C in the heating block).
8. **OPTIONAL:** Add 70 µL BSTFA or MTBSTFA. Vortex.
9. **DEFAULT:** premix alkane-mix with silylation reagent. First add BSTFA or MTBSTFA and then alkane-mix. In case of premix preparation, add 80 µL to each sample.
10. Shake 30 minutes at 37°C (950 RPM in Thermomixer Eppendorf).
11. Spin down 5 minutes at 20,800 rcf.
12. Transfer 80 µL into GC sample vials.
13. The trimethylsilyl amino acid derivatives (TMS) are then injected into the GC-TOF-MS.

Gas chromatography – time of flight – mass spectrometry

After tissue harvesting, metabolite extraction and subsequent derivatization is performed. Samples are then injected to the GC-TOF-MS.

1. Metabolic inactivation: shock-frozen in liquid nitrogen.
2. Extraction: Water: chloroform (2:1; v/v) 15 min at 70°C
3. Derivatization: MeOX 90 minutes at 30°C; TMS 30 minutes at 37°C.
4. Gas chromatograph: Agilent GC 6890
5. Separation: **Column:** 5% phenyl- 95% dimethylpolysiloxane, 30 meters + 10 meters pre-column, ID: 0.25 mm, DF: 0.25 µm, 5PDM VF-5ms (Varian, Darmstadt, Germany); **Program:** isothermal 1 minute 70°C, ramp 9°C/minute, isothermal 5 minutes 350°C; **Flow:** Helium, 0,6mL/minute; **Injection:** 1µL, splitless, 230°C; **Transfer:** 250°C; **Ion source:** 250°C
6. Detector: Pegasus III TOF mass spectrometer; mass to charge ratio (m/z) range = 70-600; 20 scans per second.
7. Retention index standards: Alkane mix; C₁₀, C₁₂, C₁₅, C₁₈, C₁₉, C₂₂, C₂₈, C₃₂, C₃₆.
8. Deconvolution using ChromaTOF: offset “just above noise”; smoothing set at 20; peak width set at 6; signal to noise ratio (S/N) set at 2.

Extended Methods – FM-S

9. The samples were measured first splitless and then in split 30 modes in order to increase the accuracy of the data mining methods.

Gas chromatography – atmospheric pressure chemical ionization – mass spectrometry

All the technical conditions were the same as previously published data (Erban et al., 2020; Strehmel et al., 2014).

1. Metabolic inactivation: shock-frozen in liquid nitrogen.
2. Extraction: Water: chloroform (2:1; v/v) 15 min at 70°C
3. Derivatization: MeOX 90 minutes at 30°C; TMS 30 minutes at 37°C.
4. Gas chromatograph: Agilent 7890A GC
5. Detector: microTOF-Q II hybrid quadrupole time-of-flight mass spectrometer (Bruker Daltonics) equipped with a multipurpose APCI source (Bruker Daltonics).
6. Retention index standards: Alkane mix; C₁₀, C₁₂, C₁₅, C₁₈, C₁₉, C₂₂, C₂₈, C₃₂, C₃₆.

Amino acid mix was injected as standard in different concentrations as well as biological samples. Exact masses were used to confirm the structural information of mass tags. The mass tags confirmed were those used for enrichment quantitation. Therefore, a library hit with the Golm metabolome database brought important information into the picture such as: number of trimethylsilyl groups, most common dissociation patterns, molecular weight, expected retention index. Additional to structural confirmation APCI data was used to confirm the uniqueness of the mass tags or the presence of contamination due to co-elution and hence ambiguity of mass tags.

Internal Standards

¹³C-Sorbitol was used during this research as quantitative internal standard of the polar phase.

Alkanes were used during this research as retention index internal standards. N-alkanes C₁₀ to C₃₆ were used (decane, dodecane, pentadecane, octadecane, nonadecane, docosane, octacosane, dotriacontane, hexatriacontane).

Total native protein concentration

Native extraction buffer

- 50mM Tris/HCl (pH 7.4)
- 10% (w/v) glycerol
- 150 mM KCl
- 5mM DTT
- Protease inhibitor cocktail (10µl in 1ml of extraction buffer) tablets contain 500µl and serve up to 50ml
- 1% DM (n-Dodecyl-β-D-Maltoside) [optional]

Extended Methods – FM-S

Procedure: Add 0.05 tween 20 as detergent and incubate for 10 minutes your plant extracts, then proceed with an adequate protein content analysis.

Nano drop protein content measurement

- Select the type of measurement you would like to do (Nucleic Acid, Protein...). It could be that you will be asked "Load the last Workbook...." . Select NO if you would not use the workbook of the measurement before.
- The next step is the "Wavelength verification". Remove the Kim Wipe before.
- Then make the Blank
- After the first measurement, you will be asked to specify where you would like to store the results. Beside the local disk, you can also select your exchange group folder. If you do not create a filename and store it the program asks you after every measurement to store the measurement.
- You can print out your results. Canon1North is the selected printer
- If you would like to export your results please go select "Report" and export as "*.tsv" file. This allows importing your results into an Excel sheet. In the "*.xml" (second option) the commas/points in the values will be ignored.
- When you finished your measurement, clean the optic and close the program.

Western blot

The starting material come from fractionated and purified ribosomes.

Instructions for resuspending the protein and filling the 10 wells of the SDS-PAGE gel:

- First well is for the pre-stained marker (6 μ L).
- 8 wells for samples (20 μ L of protein extraction buffer + 6 μ L of protein loading buffer [blue solution])
- Final well for crude protein control (100mg + 500 μ L protein extraction buffer, incubated in ice for 20 minutes, centrifuged at 20,800 rcf for 10 minutes at 4°C and then take 20 μ L of supernatant and add 6 μ L of protein loading buffer [blue solution]).

Casting of SDS-PAGE gels (running or resolving gel 12%, stacking gel 5% polyacrylamide).

Resolving gel for SDS-PAGE	
Resolving gel	
12%	50ml
H ₂ O	16,5
30% acrylamide mix	20
1.5 M TRIS (pH 8.8)	12,5
10% SDS	0,5
10% ammonium persulfate	0,5
TEMED	0,02

Taken from literature (Harlow D., 1988).

- Add only 10% ammonium persulfate and TEMED into the gel mixture when you want to start polymerizing it.
- Mix well, put aside the mixture remain after pouring the gel into the racks to see the degree of polymerization.
- Structural explanation: grey foam on the bottom of plastic transparent scaffolds. Green plastic racks secured with bottom facing the foams, two pieces of glass secured inside the green plastic racks, the gel goes inside the two pieces of glass. Remember to put the pieces of glass parallel in order to avoid leaking of liquid gel before polymerization.
- Add slowly a small layer of water to the top of the gel in order to prevent bubble formation and to homogenize the topography of the gel.
- Let polymerize for more than 30 minutes. Then pour away the water upper layer and dry the gel with sterile filter paper.

Stacking gel for SDS-PAGE

Stacking gel	
5%	10ml
H ₂ O	6,8
30% acrylamide mix	1,7
1.5 M TRIS (pH 8.8)	1,25
10% SDS	0,1
10% ammonium persulfate	0,1
TEMED	0,01

Taken from literature (Harlow D., 1988).

- Pour the stacking gel until the end part of the lower glass piece and insert the comb to create the gel wells (10 well combs).
- After polymerization, store the gels in wet tissue to prevent dehydration at 4°C (not more than one-week time). When ready to use the gels, slowly remove the comb and fill the wells with 1X SDS buffer in parallel to prevent vacuum force from filling the empty spaces with gel.

Loading of the proteins to SDS-PAGE gels: transfer the proteins into PVDF membrane and overnight block with 5% skim milk.

- Mix well with pipette to ensure protein solubilisation after each addition.
- Denature the protein at 95°C for 8 minutes before loading into the wells.
- Before loading fill with 1X SDS buffer to cover the inner part of the tank.
- After loading, fill the whole tank until the marked boundary.
- Run at 200 Volts for 60 minutes (no mA).
- Scratch out the SDS-PAGE gels and soak in water before transferring to PVDF.
- Construct sandwiches for the transferring to PVDF membranes: cut the PVDF and soak in MeOH for 10 minutes; the sandwich has a black and a transparent side, open it and put one whitish sponge at each side, followed by 4 layers of chromatography paper in the black side and 3 in the white side, put the soaked PVDF in the white side and the gel on top of it and then close the sandwich. The whole process must be done with the

Extended Methods – FM-S

sandwiches embedded in transferring buffer (for 2L: 400mL MeOH + 200mL 10X-SDS and then top up with distilled water).

- Put the sandwiches inside the respective racks, black side of the sandwich to the black side of the rack.
- Add transferring buffer to the marked boundary (3.5 L for 3 tanks or 6 gels)
- The transfer has to be done in a cold room because of the temperature increase.
- Place a magnetic stirrer on the bottom of the tanks and stir slowly while transferring.
- Run at 100 Volts, 350 mA for 40 minutes.
- Take out the membrane and block them in petri dishes filled with 5% skim milk (5g in 100mL TBST 0,1% [for 6 gels 400mL needed]) at 4°C, shaking gently at 23 rpm overnight.
- TBST: 100mL TBS Buffer, 1mL Tween 20 and top up to 1L with water.
- TBS Buffer: 87,7gr NaCl, 100ml 1M Tris (pH=7.5) and top up to 1L with water.
- Tris: Tris-HCL, MW=158 g/mol (pH ~ 4.8); Tris-base, MW=121.14 g/mol (pH ~ 10.8). The pH values are obtained when prepared 1 Molar solution.

Binding the antibodies and visualizing the protein with the G-box.

- Primary antibodies: RPS7 and RPS14 (30S), RPL2 and RPL32 (50S). 30S and 50S ribosomal subunits are specifically plastidic. Dilute the antibodies to a 1:3000 ratio with TBST 0.1% buffer. Final volume in 50mLs tube should be 50. Keep at 4°C.
- Take out the membrane from skim milk (recycle the skim milk), and wash the membranes 5 times, each time 5-10 minutes with TBST 0,1% buffer and shake fast at room temperature in between washing steps.
- Remove the last wash of TBST; pour the primary antibody into the petri dishes in order to bind it to the protein. Incubate at 4°C, 23 rpm for 2 hours.
- Recycle the primary antibody. Wash the membranes 5 times, each time 5-10 minutes with TBST 0.1% buffer and shake slow (faster than 23 rpm) at room temperature in between washing steps.
- Remove the last TBST wash. Bind the secondary antibody (polyclonal rabbit IgG [take 30µL of IgG + 300mL skim milk = 1:10000 ratio])
- Incubate at 4°C for 1 hour
- Take out the membrane from skim milk-antibody solution (recycle the solution), and wash the membranes 5 times, each time 5-10 minutes with TBST 0,1% buffer and shake fast at room temperature in between washing steps.
- Bring to the G-box to take images of the PVDF membranes (ground floor [pre-book the machine, unless introduced to the machine we need supervision]). Remove washing solution from petri dishes; soak membranes with staining solution for 1 minute making sure the entire membrane is embedded.
- Save file and analyse.

¹⁵N Enrichment of Ribosomal Proteins (from Exp2_1_4)

These samples were used to elaborate the proof of concept of labelled ribosomal proteins reproduced in Chapter 8.

Purification of Ribosomal Subunits

We purified ribosomal complexes according to previously reported methods (Firmino et al., 2020; Kawaguchi et al., 2003) with minor modifications. In brief, ribosome extraction buffer (Kawaguchi et al., 2003; Reynoso et al., 2015) was modified to (0.2 M TRIS hydrochloride, pH 9.0; 0.2 M KCl; 0.025 M EGTA, pH 8.0; 0.035 M MgCl₂*6H₂O; 1% PTE; 1% Detergent mix- Brij-35, Tween 20, Triton X-100, Igepal CA 630; 0.15 mM Chloramphenicol; 0.18 mM Cyclohexamide; 5 mM DTT; 1 mM PMSF; 1X Protease inhibitor cocktail (Sigma cat. No. P9599)) and used to lyse membranes and purify ribosome complexes from frozen tissue powder. The extracted ribosome complexes were loaded onto sterile ultracentrifuge Thinwall Polyallomer tubes (344059, Beckman Coulter, Brea, California, United States) that were previously filled with sucrose gradients prepared from 15% - 60% (w/v) stock solutions. Ultracentrifugation lasted 14.5 h at 33,000 x g using an Optima LM-80 XP ultracentrifuge and SW 41 Ti rotor (Beckman Coulter, Brea, California, United States). The ribosome complexes separated according to their sedimentation coefficient (Lebowitz et al., 2009) into 40S, 60S, 80S and low-oligomeric polysomal complexes that were monitored at 254 nm wavelength absorbance. A programmable density gradient fractionation system was used (Teledyne Isco Inc, NE 68504, United States) to obtain individual ~ 250µL fractions. Baseline and blank samples were used to normalize the absorbance axis of the chromatograms; ensuring the comparability of run-profiles. The normalized chromatogram graphs were used to select fractions of approximately 250 µL for further processing. The resulting fractions were loaded onto regenerated Amicon cellulose membranes (Ultra-0.5, 3 kDa cutoff, Merck, Kenilworth, New Jersey, United States). The filter units were washed iteratively with 500 µL of 0.04 M Tris-HCL buffer (pH 8.4) 0.2 M KCl and 0.1 M MgCl₂. The cleaned fractions were either TCA-precipitated, DTT-reduced, IAA-alkylated and trypsin-digested by filter aided sample preparation (FASP) (Erde et al., 2014; Swart et al., 2018) for LC-MS/MS of the enriched peptides or hydrolyzed and derivatized in order to measure the proteinogenic amino acids through GC-TOF-MS.

Measurement of Enriched Proteinogenic Amino Acids (GC-ToF-MS)

Proteins were precipitated using 1015 µL of a 3:1:2 methanol - chloroform - water solution. Samples were then centrifuged at 20,800 rcf for 90 minutes at 4°C and 600µL MeOH were added. After careful mixing samples were centrifuged again at 20,800 rcf for 120 minutes at 4°C. Pellets were re-suspended in approximately 1ml 6N HCl and incubated at 95°C for 24 hours. Afterwards hydrolysed samples were incubated at 105°C under a nitrogen stream (alternatively-air stream) until the samples were completely dry. To analyze the proteinogenic amino acids, dried samples were re-suspended in 150µL water, vortexed for 30 seconds and centrifuged at max speed for 30 seconds. Technical replicates of 60µL were transferred to sample vials and dried in a SpeedVac overnight at room temperature. Derivatization and sample measurements were performed identically to the previously described procedure.

Label-assisted Ribosomal Proteomics

TCA was added to a final concentration of 10% - 15% to the cleaned fractions in order to induce protein precipitation. Samples were then left for 1 h on ice and then centrifuged 30 min at 20,800 rcf. Samples were then washed with one volume of cold acetone 100% three times and the final pellet air-dried. The resulting pellet was re-suspended in 50 μ L of Elution Buffer (6M Urea, 2M Thiourea, 50mM Hepes pH 8), sonicated 10 seconds, vortexed 10 seconds and centrifuged 10 min at 20,800 rcf twice, pH was measured to ensure that all TCA was removed. Protein content was quantified using a simplified Coomassie Brilliant Blue assay. Briefly, 2 μ L drops of each sample were laid in filter paper and the paper was soaked in staining solution (Coomassie Brilliant Blue R250 0.25 g, Glacial acetic acid 10 ml, etOH: H₂O (1: 1 v/v) 90 ml). Subsequently rinsed with destaining solution (same as staining solution, but without the Coomassie R250 dye powder).

200 μ g of protein were loaded in 100 μ l elution Buffer to filter columns (2:1) and Spun down at 10000 rcf at 4°C, for 5 min. 100 μ l of elution Buffer were added to the filter and centrifugation was carried at 14000 rcf for 40 min at room temperature. 50 μ l 10 mM DTT in elution Buffer were added to the filter and centrifugation carried at 14000 rcf after 30 min at RT. 50 μ l 27 mM iodoacetamide in elution Buffer were added to the filter, the reaction stood in the dark mixing at 600 rpm in a thermomixer for 1 min and incubated without mixing for 5 min followed by centrifugation at 14000 rcf for 30min at RT. Finally, 100 μ l of Elution Buffer were added to the filter and centrifugation was carried at 14000 rcf for 40min at room temperature. The filters were transferred to a new collection tube and protein content was calculated as before. Protease digestion was performed using 100 μ l of trypsin solution in 100 mM AMBIC (Ammonium Bicarbonate) at a ratio of 1:25 protease:protein content for 14hs at 37°C. The reaction was then centrifuged at 14000 rcf for 40min at room temperature. 50 μ l of 0.5 M NaCl were added and centrifuged once more at 14000 rcf for 20min at room temperature. Finally, the reaction was quenched by adding TFA to a final concentration of 1%. Tryptic peptides were cleaned using Oasis solid-phase extraction (SPE) cartridges (Waters Co., United States). Briefly, columns were washed with 1 ml 100% methanol, followed by 1 ml 80% acetonitrile, 0.1% TFA in water and equilibrated with 2x 1 ml 0.1% TFA in water. Samples were dissolved in 0.1% TFA (600 μ l), pH was checked, and samples loaded onto the column. Tubes were washed with 200 μ l 0.1% TFA and this solution loaded onto the column. The column with the bound peptides was washed again with 2x 1 ml 0.1% TFA. Finally, the cleaned peptides were eluted with 800 μ l 60% acetonitrile, 0.1% TFA. The peptides were dried in a SpeedVac and stored at -80°C until measurement.

Measurement of Enriched Peptides (LC-MS/MS)

Dried peptides were resuspended in loading buffer (3% ACN, 0.1 % FA) and measured with Q Exactive HF (Thermo Fisher Scientific) coupled to a reverse-phase nano liquid chromatography ACQUITY UPLC M-Class system (Waters). The gradient ramped from 3.2% ACN to 25% ACN over 32 min, then up to 35% ACN in 5 min and up to 90% ACN over 2 min, followed by a 3 min washout with 90% ACN. Data were acquired in data dependent mode, where the top 12 most intense ions were fragmented per full scan. Full scans were acquired at a resolution of 120,000, with an AGC target 3e6, maximum injection time 50 ms, scan range 350 to 1500 m/. Each MS2 scan was recorded at a resolution of 30,000 with an AGC target of 1e5, maximum injection time 100 ms,

Extended Methods – FM-S

isolation window 1.2 m/z, normalized collision energy 27 and the dynamic exclusion of 30 sec. Charge states of 1 and ≥ 7 were excluded from the measurement.

MALDI tissue imaging

Solution preparation

- Ammonium bicarbonate (ABC) solution (400mM)
 - o 1.58g of ABC in 50mL of MilliQ water. Mix well until solids are completely dissolved.
- Ammonium bicarbonate solution (80mM)
 - o 2mL of 400mM ABC in 8mL of MilliQ water.
- TCEP solution (10mM)
 - o 100uL of 0.5M TCEP to 4.9mL of 80mM ABC
- Iodoacetamide (55mM) – Keep in dark and make it immediately before use
 - o Dissolve 9.3mg of iodoacetamide in 132 μ L of 80mM ABC (i.e., 375mM IAA)
 - o Take 117.4 μ L of iodoacetamide (375mM) in 682.6uL of 80mM ABC
 - o Take 400uL of 55mM iodoacetamide to pipette
- 95% Ethanol, 0.1% TFA
 - o 47.5mL of 100% Ethanol to 2.5mL of water, add 50uL TFA
- Trypsin (25ng/ μ L) – make immediately before use
 - o Add 800uL of 80mM ABC to 20 μ g vial of trypsin or protease
- HCCA matrix

Fresh Frozen tissue slides preparation

1. Warm up slide with finger for 10-15 seconds; ensure tissue section is completely thawed.
2. Immerse slide in 100% xylene for 3 minutes.
3. Immerse slide in 100% ethanol for 1 minute.
4. Immerse slide in 95% ethanol for 1 minute.

Extended Methods – FM-S

5. Immerse slide in 70% ethanol for 1 minute.
6. Immerse slide in MilliQ for 1 minute.
7. Leave the slide to dry before dehydrate it in desiccator for 15 minutes.

Set up HTX sprayer

1. Change to trypsin nozzle
2. Spray settings:
 - a. Gas pressure @ 10psi
 - b. Nozzle temperature @ 30°C
 - c. Nozzle height @40mm
 - d. Syringe pump as pump device (1.8mL/hr)
 - e. Velocity @ 750mm/min
 - f. Track spacing @ 2mm
 - g. Passes @ 10
3. Ensure there's hot water to maintain high humidity in the sprayer

Reduction step using TCEP

1. Use the glass pipette to pipette 400uL of 10mM TCEP into sprayer.
2. Run TM-Sprayer program with setting set above.
3. Incubate for 30 minutes to ensure efficient reduction.
4. Use methanol to clean the column and nozzle.

Alkylation step

1. Turn off light in HTX! IAA is sensitive to light. Try to keep covered with foil after spraying.
2. Load 800uL of iodoacetamide into the spray system using glass pipette.
3. Use the same spray settings but spray passes to 8 passes.
4. After visualising spray has hit tissue cover chamber window with foil to keep slide in the dark.
5. Leave to run and incubate for 30 minutes to induce alkylation.
6. Use methanol to clean the column and nozzle.
7. Immerse slide in 50mL tube of ethanol+TFA to remove excess TCEP and iodoacetamide.
8. Place in desiccator for 15 minutes and allow to dry.

Trypsin or protease spray

1. Nozzle is flushed with 80mM ABC before and after the run. Load 800uL of 25µg/µL trypsin into the TM-sprayer.
2. Use the settings stated before but change no. of passes to 8.

Extended Methods – FM-S

3. Incubate for 1 hour at 50°C. Slide is left on top of potassium sulphate to maintain humidity.
4. Place in desiccator for 10 minutes to dry,

Matrix spray

1. Spray setting:
 - a. Gas pressure @ 10psi
 - b. Velocity @ 950mm/min
 - c. Track spacing @ 3mm
 - d. Temperature @ 75°C
 - e. No. of passes @6
2. LC pump setting
 - a. Flow rate @1.2mL/min
 - b. Concentration: Methanol 70% Water 30%
3. Change nozzle to matrix nozzle
4. Before pumping in matrix solution, the pump system is flushed with 7mL of 70% ethanol.
5. Start the run.
6. Dry in desiccator for 15-20 minutes before MALDI run.
7. Flush the system with 70% ethanol and set LC pump setting to 1mL/min during flushing then leave it on 0.5mL/min.

Chemical cross-linking reaction in vivo

Use for stabilizing ribosomes and their interactors inside plant cell. Chemically properties: Formaldehyde is supposed to have a higher reactivity with amine groups, and it can fix some of the proteins and reduce the mobility of proteins in living cells. Sucrose and NaCl stabilize cells preventing them from breaking; sodium phosphate buffer is used in cytology for tissue fixation.

Procedure

- Harvest whole plant rosette into 25ml ice-cold MC buffer (100 mM sucrose, 10 mM sodium phosphate buffer pH 7, 50 mM NaCl) containing different concentrations of formaldehyde 0.1 %; 0.5%; 1% and control MC buffer w/o formaldehyde.
- Perform infiltration of plant tissue on ice two times for 5 min (with a mix step in-between) using 24 mbar vacuum conditions.
- Stop the crosslinking reaction by adding 2.5 ml of 1.25 M glycine with vacuum infiltration for 5 min.
- Wash plant tissue 3 times with ice-cold MC buffer w/o formaldehyde. Dry plants on paper towels and freeze in liquid nitrogen.
- Prepare plant tissue for ribosomal extraction procedure.

Dry-Lab

Data analysis of enrichments and labelled metabolite pools

The workflow for data analysis during this research entails: Baseline correction of the raw chromatogram files; Pre-processing of the chromatograms for increasing data matrices quality (internal standard usage, data synchronization and so on); targeted manual annotation of N containing mass tags; NIA correction; % of enrichment calculation and finally statistical comparison by regression where single mass tags represent variables and multiple regressors represent treatments.

Pre-processing of the chromatograms

Each file is constructed with a code to specify its history: e.g. 17013gx-1, year: 2017; day: 13th of the current year; g: code of the equipment (GC-TOF-EI-MS); x: code for the experimenter; -1 batch number. Before importing the chromatograms in Tagfinder the raw data was baseline corrected using ChromaTof software tool.

AMDIS and MS Search are open source software that enabled chromatogram visualization and putative identification of peaks, in the NIST webpage there are plenty versions that can be downloaded for free, plus demo libraries. These tools were used to open the chromatograms and explore them; as well as to establish the retention times for the alkane internal standards needed for the TagFinder processing of the chromatograms detailed in the next section.

TagFinder processing of ¹⁵N Labelling experiments

1. **Verify that your sample list matches your netCDF files** (the important thing is that all .netCDFs are listed; it is not important if the sample list has more information), and verify that all your netCDF files contain information by opening them in AMDIS; if they do not contain information remove them from the data folder.
2. **To begin with, the .netCDF files that result from baseline correction must be converted into .txt files.** Open TagFinder, create a new workspace (TagFinder/Create Workspace/Time scale=2; low mass=70; high mass= 600; Select output path [m/z 70600_Splitmode_organ_abs#]/create). Now convert your .netCDF files (Tools/Peak finder/**Files**/Add [look for your files and select them]/select output path [create a directory for your txt files inside your workspace folder named "txt_Files"]/**PeakFinder**/Smooth Width Apex Finder =5 [to establish peak zenith]; Low Intensity Threshold [to include noise] =1; check on merge peaks with a Max Merging Time Width of 0.05/ ok). Now you should have .txt files in your output path.

3. **Now importing your peak lists (.txt files).** Traditionally a signal to noise ratio of 2 is allowed, normal noise values after baseline correction range around 75, therefore the signal threshold is adjusted to 150. On the other hand, for the enrichment quantitation, the small peaks that usually represent NIA must be taken into account, because these small mass tags could contain the nitrogen enrichments. Therefore, the chromatograms are not noise subtracted after the baseline correction. This implies that the m/z ratio range of 70-600 units used for scanning all the primary metabolome must be divided into several ranges in individual workspaces in TagFinder in order to be able to import the chromatograms without exceeding the limiting memory capacity of java. This happens when the whole information load exceeds 2 gigabytes (the allowed file size of java). In one of our exemplary cases two work spaces were created for Splitless root or shoot and 4 workspaces were created for split30 Root&Shoot; additionally you must create a workspace of m/z = 85 in order to adjust the internal standards ranges. Create the indicated workspaces (TagFinder/Create Workspace/Time scale=2; [Splitless_low mass=70 or 301, high mass=300 or 600; Split30_low mass=70, 151, 301 or 451, high mass=150, 300, 450 or 600; plus in all cases one workspace with low and high mass =85]; Select output path/create).
4. **Import the txt files into the 85 m/z ratio work space** (TagFinder/Import Peak Lists/ Low Intensity Threshold [to include noise] =1; Start Time=0.0; End Time=100000; Click on files and locate your .txt files [in your txt files directory located in your workspace] click open/ok).
5. **Now set sample groups in 85m/z workspace.** This is to have all your data properly labelled and to arrange it in order of treatment and not on randomized order as during GC-MS (Samples/ Set Sample Groups/ Sample Groups.../locate your sample list file/open/Select sample name column [Rawname]/ok/Select group names column [Samptext]{these names are used in MPIMP-GOLM }/ ok/ Apply/ Exit).
6. **Now use the retention index standards to align the chromatograms** (only needed to perform on the 85 m/z because it will contain all your internal standards). Start with the file named "rt search peak picking.txt" inside your TagFinder folder/ Standards and templates for optimization/ copy it inside your 85m/z ratio folder in your workspace/ open it in excel. The file has 5 columns. Name: analyte; Spectrum_text: m/z and intensity; Int_Scale: factor for spectrum_text; Time_index: the relative time the absolute timepoints will be used for (RetentionIndex) MIN_RT: retention time in seconds -10; MAX_RT: retention time in seconds +10. Retrieve the RT values by opening one of the chromatograms file in AMDIS and looking for the internal standards, in this case alkanes, look for the masses: 71, 85, 99; remove the total ion count, click on the middle of each peak and copy and paste the values into excel; from c10 till c36; these values are in minutes, so first multiply by 60 to turn them into seconds and finally adjust MIN and

MAX_RT by subtracting and adding 10 seconds to your values respectively; after that copy and paste MIN and MAX_RT parameters as only values on the respective columns and delete your calculations. Save your "rt search peak picking.txt" file as a txt. **Open the file in the TagFinder** (RI Calculation/ Time Standard Finder [this action opens a menu on your lower window]/ Time Standards/ Open Time Standard List/ locate your "rt search peak picking.txt" file/open/[down below there are three directories: Time Standards, Results, RI method] Go to RI method/ Init RI Method/[back to Time Standards] Right click in each internal standard/ Run Time Standard Finder [if more or less values than needed are found, adjust the values under the column "intensity scale" or "low, high RT" for each particular standard in order to get matches in all chromatograms]/ Results [if more hits are found than needed, you can manually select your results. In the upper window you have your results, in the lower window the uncertainties, choose the right hit base on the RT values to match your upper results, right click on the selected hit and move it to results; do the same with all the uncertainties]/ select all values in your upper window/ right click on selection/ Send to RI method [do this with each standard] [note: when a Retention Time standard; usually C10; is absent from some chromatograms, remove it from your list/ Time Standards/ Remove Time Standard Query/ back to RI Method and Init Ri method again]/ **Save the Time Standards and the RI method in the same directory of your workspace** /RI method/ Save RI method/ choose your workspace/ rename as RI Method_tissue_splitmode)

7. **Perform a time index correlation to check the quality of the chromatography.** Open the saved RI method file in excel. It offers 4 columns. Open the file named as "RT – correlation _to _corroborate _chromatography _splitmode _organ.xlsx" it is located in Templates folder. Correlate each retention index standard with its two neighbours. (e.g. c12 with c10 and c15) by copying and pasting the values into the respective columns. Check with a graph whether the relation is direct and linear that represents a good quality of chromatography.
8. If no errors are found repeat step 4 and 5 for all your workspaces **after step 5 come back to this point.** Open your RI method in each workspace (RI Calculation/ Time Index calculator/ yes/ look for your RI saved file/ Open).
9. Now we will optimize our Time Scan width parameter in order to have synchronized mass tags. Import m/z ratio 70-600 with intensity of 150 (open the original workspace [which should be m/z ratio of 70-600] and import txt files with Low intensity Threshold of 150 to avoid noise (TagFinder/Import Peak Lists/Low Intensity Threshold [to avoid noise] =150; Start Time=0.0; End Time=100000; Click on files and locate your .txt files click open/ok). **Open your RI method** (RI Calculation/ Time Index calculator/ yes/ look for your RI saved file/ Open). **Set samples groups** (Samples/ Set Sample Groups/ Sample Groups.../locate your sample list file/open/Select sample name column [Rawname]/ok/Select group

names column [Samptext]{these names are used in MPIMP-GOLM }/ ok/ Apply/ Exit). **Setup TagFinder** (TagFinder/ Setup/ **Tag Scanning/ Time Scanner/** Time Scan width = 0.5 [initial value, it needs to be optimized]; Gliding Median Group Count =1; Min Fragment Intensity =150; everything else unchecked/*Tag Gen Filter/* check Tag Mass [74-146;150600. In order to filter out the non-specific masses from trimethylsilylation agent] the rest remains unchecked/*Intensity Calculator/ Simple/* Intensity Aggregation =MAX_INTENSITY. Everything else unchecked/Extended/uncheck everything/**Tag Correlation** and **Clustering** skip/**Tag Output/ Files/**Tag Output File =select path and change the default file-name for something identifiable by you [e.g. tags_Splitmode_Organ_abs150.tab]; Sample Annotation File =select again your sample list file; Compound translation file =no file selected/ *Tag Output/* Replace Missing Intensity Values by = do not put anything here; check Scan for Tags Only; everything else unchecked/ Apply). Now generate the Tags.Tab file in order to optimize the synchronization of targeted masses as explained below)

10. Run

11. Open your output file with any software that reads .tab. Look for putative masses of known compounds that have big peaks in your chromatograms to check if the masses are synchronized in the same tag or if you have to increase the Time Scan Width from 0.5. In a typical primary metabolome assessment we check the following:

Compounds used for time scan width optimization

RT Index	Representative Mass	Name
1265	299	Phosphoric Acid
1480	245	Malate
1804	273	Citrate
1856/1865	307	Fructose Main product/ Byproduct
1880/1900	160	Glucose Main product/ Byproduct
1918	323	¹³ C U-Sorbitol
2080	318/507	Myo-Inositol
2626	361	Sucrose

Your second column represents tag masses, look for the targeted masses by filtering on this column and subsequently filter by the first column Tag_Time_index to identify the masses. All the peaks will have an interval of appearance in chromatograms due to shifting; use this interval to determine the minimum Time Scan Width you need to use in order to merge a single compound on the same tag (F and G columns; Tag_Lo_time and Tag_High_Time) when the values are not synchronized in the same row. Alternatively generate your own list depending on your biological conditions and experimental objectives. Scan every compound on the list and then Setup TagFinder with the new Time Scan width, i.e. the largest one needed to merge signals from the same compounds and at the same time the smallest one possible to prevent merging of neighbouring signals belonging to different compounds. Now close the excel sheet and Run TagFinder again (rewrite the results on the same file and check synchronization again in all compounds). Time Scan Width for our samples: (Olga-Split30-120 samples = (2.5-learning week) 0.5; Federico-Splitless-Shoot 60 samples = learning trial: (3.5-learning week) 1.59; Bo Eng-Splitless-Root 60 samples = (1.5-learning week) 2.55.)

12. Now with an optimized data matrix you need to run the TagFinder for each m/z ratio workspace. In order to later combine the results and perform correlation analyses. Setup TagFinder (TagFinder/Setup/**Tag Scanning/Time Scanner/** Time Scan width = shoot_splitless_1.59 (3.5), shoot&root_split30_0.5 (2.5) or root_splitless_2.55 (1.5) in our case [optimized values]; Gliding Median Group Count =1; Min Fragment Intensity =150 [In these case all noise was imported but we do not want noise between adjacent peaks]; everything else unchecked/*Tag Gen Filter/* check Tag Mass =74-146; 150-600 [In order to filter out the non-specific masses from trimethylsylation agent]; check Sample Count =5 [prevents peaks that appear in less than 5 chromatograms to disturb our results] the rest remains unchecked/*Intensity Calculator/ Simple/* Intensity Aggregation =MAX_INTENSITY. Everything else unchecked/Extended/uncheck everything/**Tag Correlation** and **Clustering** skip/**Tag Output/ Files/**Tag Output File =select path and change the default file-name for something identifiable by you [e.g. tags_Splitmode_Organ_abs1_massrange.tab]; Sample Annotation File =select again your sample list file; Compound translation file =no file selected/ *Tag Output/* Replace Missing Intensity Values by =NA; check Scan for Tags Only; everything else unchecked [this parameter deactivates correlation since for doing it we first need to merge our resulting files]/ Apply)
13. Run TagFinder for all the workspaces.
14. Now you should have several .tab files in your output directories. Open the output and merge them to ensure that the masses between 70-600 are inside the file (check the B column named as "tag_mass"). Renumber the sequence on the "Tag_ID" column in order

to avoid the breaks from the merging of the origin files (since all of them started from 0 in the first place). Save the new file as a tab file in the same directory.

15. Perform the correlation in TagFinder. (Tools/ External Tools/ Select Jar File/ look for “tagtools4.1.jar” and open/ look for tag2D.Tag2D and run/ **Tag2D**/ Modulation Time =0.00001 [this is a smaller number than the scan rate]; Time Variation (Second Axis) =0.00001 [this is a smaller number than the scan rate]; Tag Input File =select your merged file; Tag output file =select the directory for your correlated file and rename (add correlated at the end); uncheck apply clustering/ **Tag Correlation**/ Correlation Method =Pearson; Maximum Tag Distance =0.2 [1-R²]; Cor Significance Level =SIG_0001; check IQR Check Pair Ratios.; Maximum IQR Pair Ratio Distance =0.05; Minimum Number of Sample Pairs =5; Min Sample Group Pair Count =0.0/ **Clustering**/ Core Adjacency Option =SAME_CORE; Min Core Option =INPUT_VALUE; Min Core Value =0; uncheck Check Score Limit/ok)
16. Select your correlated file and perform manual identification of compounds with the library help. (Tools/ External Tools/ targetfinder.TargetFinderPanel/ unfold your new window/ go to **Targets**/ File/ open target list/ find and open your library [for N containing compounds use the 15N library, for non N-containing compounds use the 1% std.dev library]/*Find Targets*/ Load Tag File/ find and open your correlation result file/ *Find targets*/ Setup Target Finder/ Target Sample Mode =ALL_SAMPLES; Mass Selection Mode =ALL_MASSES; Group By =TIME_GROUP; Min Matching Fragment Count =3; Min Match Value =2/ ok/ **Targets**/ select all compounds in the target window/ *Find Targets*/ Find Targets/ now your results must be in the **Match Results** tab/ **Match Results**/ on top of your analytes tab there is a small button with a blue “a” and red “z” with a downward pointer, click on it and remove the tag category “Time Expected” from the list and click ok/go to the Time Groups_Cluster Tab and start manual annotation group by group/ check the match compounds/ to finalize go back to the **Targets** tab/ *Results*/ Export to TAB file/ this is your ultimate data matrix to perform statistics.

Data mining for targeted compounds

Each amino acid mass spectra was dissected in order to select the most abundant mass tags that would be used as representative for the compounds. Subsequently the atomic composition of the selected mass tags was annotated; those mass tags that included nitrogen and were relatively abundant were annotated as potential candidates, examples are depicted in the following table:

Example of mass tags selected as potential descriptors of targeted metabolites

Identifier	a ₀	Formula
M000015_A138001-101-xxx_NA_1,352.85_TRUE_VAR5_ALK_Serine_(3TMS)	204	C8H22O1N1S0Si2
M000015_A138001-101-xxx_NA_1,352.85_TRUE_VAR5_ALK_Serine_(3TMS)	218	C8H20O2N1S0Si2
M000015_A138001-101-xxx_NA_1,352.85_TRUE_VAR5_ALK_Serine_(3TMS)	278	C10H28O2N1S0Si3
M000015_A138001-101-xxx_NA_1,352.85_TRUE_VAR5_ALK_Serine_(3TMS)	306	C11H28O3N1S0Si3
M000031_A133001-101-xxx_NA_1,302.68_TRUE_VAR5_ALK_Glycine_(3TMS)	174	C7H20O0N1S0Si2
M000031_A133001-101-xxx_NA_1,302.68_TRUE_VAR5_ALK_Glycine_(3TMS)	248	C9H26O1N1S0Si3
M000031_A133001-101-xxx_NA_1,302.68_TRUE_VAR5_ALK_Glycine_(3TMS)	276	C10H26O2N1S0Si3
M000036_A163001-101-xxx_NA_1,614.59_TRUE_VAR5_ALK_Glutamic_acid_(3TMS)	246	C10H24O2N1S0Si2
M000036_A163001-101-xxx_NA_1,614.59_TRUE_VAR5_ALK_Glutamic_acid_(3TMS)	348	C13H30O4N1S0Si3
M000036_A163001-101-xxx_NA_1,614.59_TRUE_VAR5_ALK_Glutamic_acid_(3TMS)	363	C14H33O4N1S0Si3

TagFinder assisted annotation

A targeted search of the aforementioned mass tags was done in TagFinder and the results were exported to a excel datasheet for further analysis (this approach requires the user to create a previous library in order to mine for the desired mass tags in TagFinder). In the results tab several filters were applied in order to get the real mass tags and not contamination that looked similar:

1. Column B was filtered only for “True Is” Selection Tag (column B represents the confirmation check in TagFinder while doing manual annotation of compounds).
2. Then each compound was selected by filtering in the F column “Name Analyte”.
3. If more mass tags that expected appeared the M column “Tag_Time_Index” was used to determine the real mass tags by comparing to the retention index of the Golm metabolome database.
4. The result was a list of mass tags ranging from a₀ [i.e. representative fragmented mass of the X compound] plus a₁ [i.e. representative fragmented mass plus one Dalton from enrichment of the X compound].
5. In order to confirm that the mass tags belonged to the same compound a correlation of each a₍₀₊₁₎ + b₍₀₊₁₎ summation is made. During a non-labelled experiment, the a₀ to a₁ ratio is constant, but since labelling is differential among plants, these two masses would no longer have a constant ratio during a labelling experiment. A fraction of a₀ would turn into

Extended Methods – FM-S

a_1 after the labelling with ^{15}N . Nevertheless the ratio between mass tags is always constant; hence to correct for the labelled fraction both tags a_0 and a_1 have to be summated.

6. When a correlation was found among mass tags these were taken as good descriptors for the X compound. Therefore, these mass tags were further used for the quantitation of enrichment percentages.

Direct targeted search

Alternatively, mass tags were directly retrieved from the .tabs file generated in the step 15 of the TagFinder workflow. Mass tags were found according to their mass to charge ratio, the second criterion was the matching RI with the Golm metabolome database. After identification each mass tag (a_0) and its found NIA peaks (a_1, a_2, \dots, a_i) were retrieved to a new file and the same correlation procedure as before was followed.

Primary metabolites

For the assessment of the primary metabolome changes due to introduced experimental stress (i.e. Temperature and/or ^{15}N), the natural isotopic abundance correction was not needed. A mere comparison between treatments was enough, hence non-corrected metabolite pools were normalized and transformed as follows:

1. Non-corrected metabolite pools ($a_0 \sum (0:4)$) were obtained.
2. The pools were normalized to the pool ($a_0 \sum (0:4)$) of ^{13}C Sorbitol internal standard (mass 323 RT = 1918).
3. The values were normalized by dividing them to the initial fresh weight of the samples.
4. Maximum scaling was done in order to allow a better comparison of treatments; statistics could be made at this point.
5. Alternatively, the data was median centred to deal with outliers and log 10 transformation was applied; nevertheless, these two last transformations yield negative values which could be problematic during GLM statistical analyses.
6. At last because excel finds number errors when dividing 0 by a constant, those errors were replaced by zero.
7. The data was used to perform statistics as described in the following section.

N-containing compounds

Those mass tags selected for enrichment analyses in nitrogen containing compounds must exhibit:

1. Good correlation of the mass tags metabolite pools (i.e. of $a_0 \sum (0:4)$ is correlated to $b_0 \sum (0:4)$), usually a strong indicator that two mass tags belong to the same compound is when one correlates both metabolite pools and the r^2 value is larger than 0.99; In this case a correlation was made for each $a_0 \sum (0:4)$ and $b_0 \sum (0:4)$ pair.

2. Uniqueness in the mass spectra across monoisotopic and NIA peaks. For example, 116 is an abundant mass tag of L-Asparagine after EI ionization and its structure is easily predicted. Nevertheless, 117 occurs in low probability as a dissociation residue of the compound. Hence the first isotopomer of 116 mass tag is contaminated by the 117 occurring after EI ionization. Thus, if uncontaminated, the abundances of any peak isotopologs should decrease from a_0 to a_4 as expected by the NIA, this is a chemical formula accuracy indicator for each mass tag.
3. Whenever possible the best mass tags in which to calculate the percentage of enrichment of amino acid compounds are the molecular weight (MW) mass tag, the MW – CH₃ and the MW-CH₃-C=O. Plus the structural information is easy to obtain.

The resulting mass tags were directly inputted to CORRECTOR for NIA correction, subsequent percentage of enrichment and metabolite pool calculations.

Percentage of enrichment calculation using CORRECTOR

The corrector software is designed for NIA correction, detailed usage is published (Huege et al., 2014). The software can handle ¹³C and ¹⁵N labelling experiments. Most amino acids have a single N and therefore positional labelling is not as important as with C labelling experiments; hence the analysis is simpler. A targeted approach was used in order to extract the representative mass tags from selected amino acids as shown in the previous section. Afterwards a library file was created in order to target results to specific mass tags.

1. CORRECTOR must be installed and used using Abacus (i.e. a Linux server) platform.
[cd{change directory}; ls{shows directory path}; dir{shows directory components};
./{run.exe}].
2. cd winhome; cd corrector_n15; now you are inside corrector
3. Command to run CORRECTOR in Linux terminal= ./corrector10a_64.exe -igz 0
input_file.txt output1.txt output2.txt
4. Corrector10a_64.exe = software file.
5. -igz = 0 [integer number always] this feature enables the user to ignore a selected number [integer] of null or negative higher mass isotopologs as expected due to the NIA for the enrichment calculation. The software starts counting nulls and negatives (atom percentages) after the main mass tag. Using 0 as integer prevents contamination from other coeluting mass tags to damage our results.
6. input_file.txt = Linux does not accept spaces in compounds names in the first column, the names from the Golm metabolome database have empty spaces, make sure to replace them by a _
7. output1.txt = Corrected metabolite pools
8. output2.txt = Enrichment percentages
9. Inside the corrconfig.cfg file: number_of_additional_peaks = 4; this indicates CORRECTOR to use the subsequent 4 peaks to perform the NIA correction of the first; Column R:

Extended Methods – FM-S

atomtype7_(non-backbone) = N to indicate the atom which could be labelled, number_of_atoms_of_atomtype7 = 1 or 2 for amino acids to indicate the number of atoms that could be labelled per mass tag. The column named “sum_of_all_atoms_of_in_the_fragment” must contain the summation of all atoms including the potentially labelled additions, if not the CORRECTOR will not do the calculation accurately.

The corrected abundances from experimentally obtained values serve as a proxy to establish changes in pool sizes of the respective amino acids; taking into account that the extracted, derivatized and measured fraction of compounds is representative of the pool sizes. The sum of the corrected abundances of all isotopologs for each mass tag was taken as the corrected metabolite pool. All calculations were highly correlated when compared to IsoCorrectoR (Heinrich et al., 2018) or IsoCor (Millard et al., 2019). Each of the software can be used for different purposes and depending on the format of the original dataset

Data fixing assumptions

The enrichment percentages and the metabolite pools were used for the subsequent statistical analyses. When the values obtained from CORRECTOR were outside physiological boundaries (negative [-%] or positive [X>100%] outliers) or 0%, these were transformed into 0,0001 for the sake of statistical comparisons. In case of systematic outliers across compounds, these were simply deleted from the data set. The corrected metabolite pools were transformed with natural logarithm (Ln) in order to reduce the orders of magnitude; this was necessary to avoid statistical artefacts when introducing the metabolite pool predictor.

Statistical comparison of treatments

Statistics were performed in R. The statistical model for analyzing the targeted retrieved enrichment percentages and/or metabolite pools (corrected or non-corrected) was a generalized linear model (GLM) with an inverse link function that belonged to the Gamma regression family as for the N-containing compounds; for the transformed pools, a Gaussian distribution was enough; since the transformations done were equivalent to perform a GLM of the Binomial family with a logit link function; therefore the resulting data were lognormal distributed. The mean function enables the relationship between the predictor and the mean of the distribution function.

Logit Link function: $X\beta = L_{10}(\mu/1-\mu)$ [in our case median centred due to outliers]

Inverse Link function: $X\beta = \mu^{-1}$

Extended Methods – FM-S

Model: $y = \beta_0 + \beta_1X_1 + \beta_2X_2 + \beta_3X_3 + \beta_4X_4 + \beta_5X_5 + \beta_6X_1 * X_4 + \beta_7X_2 * X_4 + \beta_8X_3 * X_4 + \epsilon_{ijk} \rightarrow$

$\epsilon_{ijk} \sim N.$

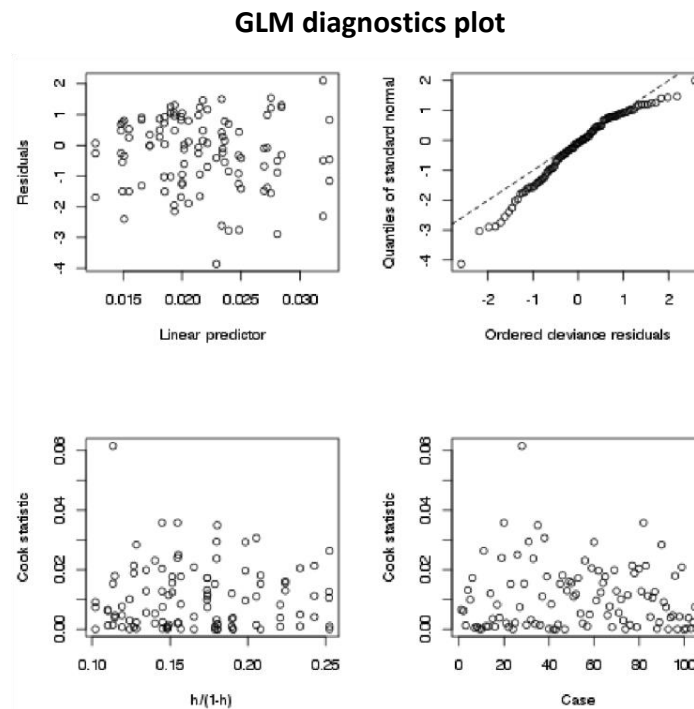
The dependent variables were: Enrichment percentage and non-corrected metabolite pool. The predictors were: Temperature [β_1X_1]; Organ [β_2X_2]; Labelling Time [β_3X_3]; Label concentration [β_4X_4]. In addition the interactions between Label concentration and the other factors were introduced [$\beta_6X_1 * X_4 + \beta_7X_2 * X_4 + \beta_8X_3 * X_4$]. Robust posthoc tests were made in order to avoid Type I and II Error; namely Tukey HSD test that is robust and allows high number of paired observations. One random variable was added as a predictor for the enrichment percentages. The variable was the natural logarithm of the metabolite pool [β_5X_5]; the null hypothesis in this case was that the metabolite pool did not influence the labelling; the alternative hypothesis is that it did.

The Cullen and Frey graph test basal to develop the RandoDiStats R package, which used it in order to check the distribution that best fits our data. In every case the data was described as beta distributed. Therefore, the closest regression family was the Gamma. Furthermore, the ratio between residual deviance and residual degrees of freedom was closest to one when the Gamma family was used, which means that the adjustment was the most reasonable in comparison with the other distributions. CORRECTOR software adjusts to zero all missing values. In order for the Gamma regression to be performed, the zeros had to be converted into any real number > 0 .

In order to test the strong assumptions that GLM does concerning the data. Four plots indicating the GLM diagnostics were done per analysis.

1. Independence of data points: can only be assured with good experimental design.
2. Normal distribution of the residuals: only stringent for Gaussian distributions.
3. Correct specification of the variance structure: Homoscedasticity is no longer assumed with GLM; the variance is a function of the mean and varies with the predictors (i.e. the heteroscedasticity takes a specific form).
4. Linear relationship between the response and the linear predictor: the y's should be linearly related to the predictors.

The following are the four diagnostic plots used for testing model assumptions:



Example: randomized data from 0 to 100. Top left = residuals plot; top right = residuals vs fitted plot; bottom left = cook statistic for high leverage data points; bottom right = cook statistic ordered according to treatments.

1. The top-left graph (homogeneity of the variance and the linear relation): Residuals should be distributed evenly around 0.
2. The top-right graph (normal distribution of the residuals): Extremely stringent for Gaussian distribution more relaxed for the other families.
3. The bottom-left graph (Cook statistic): identify points with high leverage on the dataset; the left bottom square is where all data points should be, those in other compartments are high leverage points. If the compartments don't show the leverage is well distributed among data points.
4. The bottom-right graph (Cook statistic): identify points with high leverage on the dataset. In this case the leverage value is plotted against the sample number. This allows identifying to which part of our data the high leverage points belong.

References

- Boyes, D. C. (2001). Growth Stage-Based Phenotypic Analysis of Arabidopsis: A Model for High Throughput Functional Genomics in Plants. *Plant Cell* 13, 1499–1510. doi:10.1105/tpc.13.7.1499.
- Erban, A., Martinez-Seidel, F., Rajarathinam, Y., Dethloff, F., Orf, I., Fehrle, I., et al. (2020). “Multiplexed Profiling and Data Processing Methods to Identify Temperature-Regulated Primary Metabolites Using Gas Chromatography Coupled to Mass Spectrometry,” in *Methods in Molecular Biology*, eds. D. K. Hinch and E. Zuther (New York, NY: Springer US), 203–239. doi:10.1007/978-1-0716-0660-5_15.
- Erde, J., Loo, R. R. O., and Loo, J. A. (2014). Enhanced FASP (eFASP) to increase proteome coverage and sample recovery for quantitative proteomic experiments. *J. Proteome Res.* 13, 1885–1895. doi:10.1021/pr4010019.
- Firmino, A. A. P., Gorka, M., Graf, A., Skiryecz, A., Martinez-Seidel, F., Zander, K., et al. (2020). Separation and paired proteome profiling of plant chloroplast and cytoplasmic ribosomes. *Plants* 9, 1–29. doi:10.3390/plants9070892.
- Harlow D., E. L. (1988). A laboratory manual. *Cold Spring Harb. Lab. Press*, 28–29. doi:10.1016/0968-0004(89)90307-1.
- Heinrich, P., Kohler, C., Ellmann, L., Kuerner, P., Spang, R., Oefner, P. J., et al. (2018). Correcting for natural isotope abundance and tracer impurity in MS-, MS/MS- and high-resolution-multiple-tracer-data from stable isotope labeling experiments with IsoCorrectoR. *Sci. Rep.* 8. doi:10.1038/s41598-018-36293-4.
- Huege, J., Goetze, J., Dethloff, F., Junker, B., and Kopka, J. (2014). Quantification of stable isotope label in metabolites via mass spectrometry. *Methods Mol. Biol.* 1056, 213–223. doi:10.1007/978-1-62703-592-7_20.
- Kawaguchi, R., Williams, A. J., Bray, E. A., and Bailey-Serres, J. (2003). Water-deficit-induced translational control in *Nicotiana tabacum*. *Plant, Cell Environ.* 26, 221–229. doi:10.1046/j.1365-3040.2003.00952.x.
- Lebowitz, J., Lewis, M. S., and Schuck, P. (2009). Modern analytical ultracentrifugation in protein science: A tutorial review. *Protein Sci.* 11, 2067–2079. doi:10.1110/ps.0207702.
- Millard, P., Delépine, B., Guionnet, M., Heuillet, M., Bellvert, F., Létisse, F., et al. (2019). IsoCor: Isotope correction for high-resolution MS labeling experiments. *Bioinformatics* 35, 4484–4487. doi:10.1093/bioinformatics/btz209.
- Reynoso, M. A., Juntawong, P., Lancia, M., Blanco, F. A., Bailey-Serres, J., and Zanetti, M. E. (2015). “Translating ribosome affinity purification (TRAP) followed by RNA sequencing technology (TRAP-SEQ) for quantitative assessment of plant translomes,” in *Plant Functional Genomics: Methods and Protocols: Second Edition*, 185–207. doi:10.1007/978-1-4939-2444-8_9.
- Strehmel, N., Kopka, J., Scheel, D., and Böttcher, C. (2014). Annotating unknown components from GC/EI-MS-based metabolite profiling experiments using GC/APCI(+)-QTOFMS. *Metabolomics* 10, 324–336. doi:10.1007/s11306-013-0569-y.
- Swart, C., Martínez-Jaime, S., Gorka, M., Zander, K., and Graf, A. (2018). Hit-Gel: Streamlining in-gel protein digestion for high-throughput proteomics experiments. *Sci. Rep.* 8, 8582.

Extended Methods – FM-S

doi:10.1038/s41598-018-26639-3.